

- i. HOST/GUEST COMPLEXES FOR ABSOLUTE STEREOCHEMICAL DETERMINATION OF ORGANIC MOLECULES;
- ii. TOTAL SYNTHESIS OF (–)-SALINOSPORAMIDE A;
- iii. STEREOCONTROLLED SPIROKETALIZATIONS, AND EFFORTS TOWARDS THE TOTAL SYNTHESIS OF OBTUSIN

By

Hadi Gholami

A DISSERTATION

Submitted to
Michigan State University
in partial fulfillment of the requirements
for the degree of

Chemistry – Doctor of Philosophy

2018

ABSTRACT

- i. HOST/GUEST COMPLEXES FOR ABSOLUTE STEREOCHEMICAL DETERMINATION OF ORGANIC MOLECULES;
- ii. TOTAL SYNTHESIS OF (–)-SALINOSPORAMIDE A;
- iii. STEREOCONTROLLED SPIROKETALIZATIONS, AND EFFORTS TOWARDS THE TOTAL SYNTHESIS OF OBTUSIN

By

Hadi Gholami

This dissertation consists of two parts. In the first part (Chapters I and II), the development of new molecular sensors for detection of asymmetry of organic molecules is disclosed. These sensors, also referred to as “host molecules”, are capable of forming stable complexes with chiral organic molecules. The design of the hosts are such that the point chirality of organic molecules is transferred into a helical twist of the molecular receptor, leading to axial chirality that can be detected as Exciton Coupled Circular Dichroism (ECCD). The absolute configuration of a few classes of organic molecules such as chiral monoamines, cyanohydrins, sulfoxides, phosphine oxides, and mono alcohols is assigned in a microscale, rapid and unambiguous manner.

In the second part of this thesis (Chapters III and IV), the development of new organic reactions and their further application towards the synthesis of natural products is discussed. In Chapter III, the successful completion of the total synthesis of (–)-Salinosporamide A is described. During the synthesis of this molecule, new reactions are developed that enabled the completion of this synthesis. In Chapter IV, the development of a halonium initiated spiroketalization and application of this methodology towards the total synthesis of Obtusin is disclosed. The enabling role of the protecting group on the

nucleophilic oxygen atom stands as a unique discovery that can improve the reaction outcome.

Dedicated to my beloved family for their love and support.

ACKNOWLEDGEMENTS

I would like to express my most sincere gratitude and appreciation to my Ph. D. advisor, Professor Babak Borhan, for his endless support, continuing encouragement, and kind guidance and advise. I cannot possibly be more thankful to him for welcoming me into his research group and providing me with the absolute freedom in thinking to enjoy the research that I was doing. I could not have asked for a better advisor and he for sure has exceeded my expectation.

I am greatly thankful to my committee member, Professor William Wulff, Professor James Jackson and Professor Milton Smith, for their helpful suggestions and comments and their support during the past few years.

I would like to thank all the members of the Borhan group for their invaluable help and support and friendship during my graduate school. I especially would like to thank Dr. Chrysoula Vasileiou for her limitless support and help. I am immensely thankful to Chrysoula for her patience in proofreading my dissertation and manuscripts. The past members of Borhan group, especially Dr. Kumar Ashtekar, Dr. Mercy Anyika, Dr. Arvind Jaganathan, Dr. Roozbeh Yousefi, and Dr. Elizabeth Santos are acknowledged for their encouragement, friendship and support during my graduate studies. I have had the pleasure and privilege of working with most of the current and former members of Borhan group, to that extend, I am thankful to all of them. I specially thank Jun and Debarshi for helping me with the spectroscopy projects and Yi, Saeedeh and Xinliang for working with

me on the synthetic projects. I am very thankful to all my talented undergraduate students, Olivia, Matt, Katie and Lindsey for helping me with the research.

I would like to extend my sincere gratitude to all my friends in the chemistry department for their support and encouragement. I felt welcome by all of them and they will be missed. I am especially thankful to Tayeb Kakeshpour for cheering me up whenever things get tough and my little friend, Mona Borhan for making Saturdays as a special day of week.

Saving the best for last, I have no word to describe how thankful I am to my wife, Mina who has been supporting me since the first day we have met. Her unconditional love and support have been my driving force in my daily life. I definitely would not be standing here if it was not because of her support and encouragements. She is my best friend and my better half. I wish I could live up to all her support. I would like to thank our families, specially our parents for their endless love and support. They have given me everything and have patiently supported me during my educations.

TABLE OF CONTENTS

LIST OF TABLES	x
LIST OF FIGURES	xii
KEY TO SYMBOLS AND ABBREVIATIONS	xxiv
Chapter I: Determination of absolute configuration of chiral organic molecules via exciton coupled circular dichroism	1
I-1 Introduction	2
I-2 Methods for the absolute stereochemical determination of chiral molecules	4
I-3 Application of chiroptical spectroscopy for determination of absolute configuration of chiral molecules	7
I-4 Chemical derivatization of chiral molecules with interacting chromophores for determination of absolute configuration	13
I-5 Porphyrin tweezers methodology: host:guest complex formation with chiral molecules for determination of absolute configuration	20
I-6 Design of a new host system for determination of absolute configuration of chiral molecules with one sites of attachment	26
I-7 Determination of the absolute configuration of chiral monoamines	31
I-8 Experimental section	38
I-8-1 Job's continuous plot analysis to determine complex stoichiometry	38
I-8-2 Synthesis of MAPOL I-31	40
REFERENCES	46
Chapter II: Determination of absolute configuration of chiral molecules (chiral cyanohydrins, sulfoxides, phosphine oxides and alcohols)	54
II-1 Determination of absolute configuration of chiral cyanohydrins	55
II-2 Determination of absolute configuration of chiral sulfoxides	76
II-3 Determination of absolute configuration of chiral phosphine Oxides	98
II-4 Tuning electronic properties of MAPOL scaffold	115
II-5 Experimental section	119
II-5-1 Materials and general instrumentations	119
II-5-2 Procedure for UV-vis and CD titration of Zn-MAPOL with chiral guest molecules (cyanohydrins, sulfoxides or phosphine oxides)	119

II-5-2-1	General procedure for UV-vis measurement.....	119
II-5-2-2	General procedure for CD measurement	120
II-5-3	Job's continuous plot analysis to determine the stoichiometry of complex between Zn-MAPOL and chiral guest molecules and binding constant measurements of the complex	121
II-5-4	Synthesis of the host systems.....	122
II-5-4-1	Synthesis of Zn-MAPOL	122
II-5-4-2	Synthesis of Zn-MAPOL-OMe II-40.....	123
II-5-4-3	Synthesis of F ₄ -Zn-MAPOL	124
II-5-4-4	Synthesis of F ₃₀ -Zn-MAPOL.....	127
II-5-5	Synthesis of chiral cyanohydrins	131
II-5-6	Synthesis of chiral sulfoxides	132
II-5-7	Conformational modeling studies	139
REFERENCES	140

Chapter III: Total synthesis of (–)-Salinosporamide A	147
III-1 Introduction	148
III-2 Proteasome Inhibition by Salinosporamide A	149
III-3 A survey of the previous total syntheses of Salinosporamide A .	150
III-4 Our synthetic approach towards the total synthesis of Salinosporamide A	153
III-5 Synthesis of Salinosporamide A	155
III-5-1 A Survey of anionic approaches for C-5 functionalization	159
III-5-2 Cationic approaches for C-5 functionalization.....	161
III-5-3 Radical based approaches for C-5 functionalization	164
III-5-4 Neutral based strategies for C-5 functionalization	167
III- 6 The total synthesis of (–)-Salinosporamide A	190
III- 7 Experimental section.....	197
III-7- 1 General remarks	197
III-7- 2 Total synthesis of (–)-Salinosporamide A	198
III-7- 3 Crystal data.....	229
III-7-3-1 Crystal data for III-91b (BB817C).....	229
III-7-3-2 Crystal data for (–)-III-25 (BB817D)	244
REFERENCES	259

Chapter IV: Diastereoselective halonium initiated spiroketalization; towards the total synthesis of Obtusin	267
IV- 1 Introduction; structural features of spiroketal moiety	268
IV- 2 Chemical synthesis of spiroketals	271
IV- 3 Development of halonium initiated spiroketalization	276
IV- 4 Development of mono and di-brominated spiroketalization reaction	280
IV- 5 Towards the total synthesis of Obtusin	291
IV-5- 1 Introduction	291

IV-5- 2	progress towards the total synthesis of Obtusin	293
IV- 6	Experimental section.....	308
IV-6-1	General remarks.....	308
IV-6-2	General procedure for bromo spiroketalization of THP-protected keto-alkenols	309
IV-6-3	General procedure for dibromo spiroketalization of THP-protected keto-alkenols	315
IV-6-4	Synthesis of ketones IV-116 to IV-121	321
IV-6-5	General procedure for synthesis of ketone IV-131 to IV-133	335
IV-6-6	Procedure for the synthesis of THP-protected keto alkenols IV-136	345
IV-7	Experimental data for the synthesis of Obtusin	347
REFERENCES	363

LIST OF TABLES

Table II-1:	Predicted and observed ECCD for cyanohydrins complexed with Zn-MAPOL	65
Table II-2:	Predicted and observed ECCD for sulfoxides complexed with ZnMAPOL	85
Table III-1:	Optimization of the C-H insertion reaction at the C-5 center	173
Table III-2:	Optimization of olefin cleavage towards installation of carbonyl on C-5	183
Table III-3:	Selective deprotection of the TBS ether in the presence of Boc protecting group.....	186
Table III-4:	Cardova's reported asymmetric aziridination of α,β -unsaturated aldehyde	191
Table III-5:	Fractional atomic coordinates ($\times 10^4$) and equivalent isotropic displacement parameters ($\text{\AA}^2 \times 10^3$) for III-91b . U_{eq} is defined as 1/3 of the trace of the orthogonalised U_{ij}	234
Table III-6:	Anisotropic displacement parameters ($\times 10^4$) III-91b . the anisotropic displacement factor exponent takes the form: $-2\pi^2[h^2a^{*2} \times U_{11} + \dots + 2hka^* \times b^* \times U_{12}]$	235
Table III-7:	Bond lengths in \AA for III-91b	237
Table III-8:	Bond angles in $^\circ$ for III-91b	239
Table III-9:	Hydrogen fractional atomic coordinates ($\times 10^4$) and equivalent isotropic displacement parameters ($\text{\AA}^2 \times 10^3$) for III-91b . U_{eq} is defined as 1/3 of the trace of the orthogonalised U_{ij}	241
Table III-10:	Fractional atomic coordinates ($\times 10^4$) and equivalent isotropic displacement parameters ($\text{\AA}^2 \times 10^3$) for (-)-III-25 . U_{eq} is defined as 1/3 of the trace of the orthogonalised U_{ij}	249
Table III-11:	Anisotropic Displacement Parameters ($\times 10^4$) (-)-III-25 . The anisotropic displacement factor exponent takes the form: $-2\pi^2[h^2a^{*2} \times U_{11} + \dots + 2hka^* \times b^* \times U_{12}]$	251

Table III-12: Bond lengths in Å for (–)-III-25	252
Table III-13: Bond angles in ° for (–)-III-25	254
Table III-14: Hydrogen fractional atomic coordinates ($\times 10^4$) and equivalent isotropic displacement parameters ($\text{\AA}^2 \times 10^3$) for (–)-III-25. U_{eq} is defined as 1/3 of the trace of the orthogonalised U_{ij}	256
Table III-15: Hydrogen bond information for (–)-III-25	258
Table IV-1: Substrate scope for halenium atom initiated diastereoselective spiroketalization	286
Table IV-2: Diastereoselective dibromo spiroketalization.....	289
Table IV-3: Bromo etherification of alcohol IV-86.....	296
Table IV-4: Bromo etherification of protected alcohol IV-101	301

LIST OF FIGURES

Figure I-1.	Representative enantiomers with drastically different biological activities .	3
Figure I-2.	Assignment of the absolute configuration of a secondary alcohol using Mosher method. Structure of the stable conformer that leads to the change in the chemical shift of the derivatized alcohol and the ^1H -NMR traces of both diastereomers, as well as the proposed mnemonic (dashed box) are demonstrated.....	5
Figure I-3.	a. Plane-polarized light composed of two circularly polarized components, <i>lcp</i> and <i>rcp</i> . As long as the phases of intensities of these two components remain the same, the resultant oscillating vector will be in the same plane and magnitude. b. If the <i>rcp</i> component become less intense (due to interaction with chiral media) the electric vector of light follows an elliptical path (elliptically polarized light, green oval). c. The degree of ellipticity is define as ψ , which is proportional to the circular dichroism. The rotation of ellipse (α) corresponds to optical rotation and ORD.....	8
Figure I-4.	Positive or negative CD spectra or Cotton effects	9
Figure I-5.	Schematic exciton band energy diagram of system with two interacting chromophores in various geometries. The ovals indicate chromophores with their electric dipole transition moments. The magnitude of the net electric dipole transition moments (μ_{net}) is deduced by employing a simple vector model analysis.	12
Figure I-6.	Schematic demonstration of two independently conjugated chromophores arranged in a helical twist. The electric dipole transition moments (blue line) are along the long axis of the benzoate moieties. The side view of interacting chromophores indicates clockwise or counter-clockwise arrangement of chromophores depending on the chirality of the diol. The clockwise helicity generates a positive ECCD spectrum (shown on tap right)	14
Figure I-7.	Dioxolane formation of chiral diols with I-6 leads to CD active complexes. The highlighted diastereomeric complexes (box) depict equilibrating dioxolanes that favor <i>M</i> conformation due to the chirality of the bound diol.	15

Figure I-8.	Development of an azepine probe (I-8) for sensing the absolute configuration of chiral carboxylic acids	16
Figure I-9.	Development of stereodynamic molecular probe I-10 for determination of enantiomeric composition and absolute configuration of chiral amino alcohols through imine formation.....	17
Figure I-10.	Structure of propeller-like Cu(II) complex with chirality on the backbone of one of the quinoline based ligand	18
Figure I-11.	Induced helical twist of the achiral quinoline based ligand on Cu(II) due to stereochemistry of the bound amino acid (methionine)	19
Figure I-12.	Structure of a copper based molecular probe for sensing the chirality of carboxylic acids.....	19
Figure I-13.	Stereodynamic assembly of chiral alcohol with <i>in situ</i> generated iminium I-19 into a trigonal bipyramidal scaffold leading to <i>P</i> or <i>M</i> helicities depending on the chirality of alcohol	20
Figure I-14.	(a) Structure of C ₅ -TPP tweezer; (b) model for complexation of chiral diamine with C ₅ -TPP tweezer (a bidentate coordination of diamines with the porphyrin tweezer leads to an observed helical twist); (c) Experimentally measured ECCD signal and proposed model for the preferred helical twist (left), counter-clockwise arrangement of interacting dipole transition moments leads to a negative ECCD signal.	22
Figure I-15.	Frontier orbital energy and charges of zinc porphyrins. Bonding affinity of <i>iso</i> -propanol and <i>iso</i> -propylamine with Zn-TPP-monoester and Zn-TPFP-monoester as analogues of Zn-TPP tweezer and Zn-TPFP tweezer (dashed box depicts structure of C ₅ -Zn-TPFP tweezer).	24
Figure I-16.	Pictorial representation of functional group families with methods for assignment of their stereochemistry. Chiral molecules with single site are derivatized with a carrier to form a bidentate guest molecule (left panel) prior to complex formation with tweezers; Structure of host systems, with various linker size as well as tuned steric and electronic profiles that enables determination of absolute configuration of the latter functionalities are shown at the bottom of this figure.....	25
Figure I-17.	Rational design of a new host system capable of sensing chirality of molecules with one site of attachment. Linker modification and change in the binding paradigm are notable adjustments.....	27

Figure I-18. Structure of newly designed host system. Biphenyl back bone, capable of adopting <i>P</i> or <i>M</i> helicity, renders equilibrating atropisomers. Upon introduction of chiral guest, that rests in the highlighted binding sites, one of the helicities become more prominent leading to the corresponding ECCD signal.....	28
Figure I-19. Successful synthesis of MAPOL I-31	29
Figure I-20. Complexation of MAPOL with chiral monoamine II-37S leads to a strong ECCD signal with a negative sign.....	31
Figure I-21. ¹ H-NMR spectra of titration of MAPOL 1 with <i>S</i> -(+)-1-cyclohexylethylamine I-37S . Highlighted with blue indicates the changes in the chemical shift of the methyl group of the amine substrate and the red area shows the changes in the chemical shift of the MAPOL backbone upon complexation with amine I-37S	33
Figure I-22. Job's continuous plot of MAPOL I-31 with I-37S : following the changes in chemical shift of MAPOL at 7.55 ppm (left) and chemical shift of amine I-37S at 0.99 ppm	34
Figure I-23. a) Complexation of I-37S with MAPOL leads to a strong negative ECCD signal. b) Binding of amine I-37S , with the <i>P</i> -helicity of MAPOL leads to steric clash of the methyl group with the porphyrin ring. Thus, positive ECCD with I-37S bound to MAPOL is not anticipated. c) The same binding of I-37S with the <i>M</i> -helicity of MAPOL places the medium size methyl group in the most sterically available position. This favorable arrangement leads to the anticipated positive ECCD spectrum	35
Figure II-1. Synthetic utility of cyanohydrin moiety	55
Figure II-2. Mosher's method determination of absolute configuration of chiral cyanohydrins.....	56
Figure II-3. Application of chiral solvating agents for determining the absolute configuration of chiral cyanohydrins	58
Figure II-4. Porphyrin tweezers and their envisioned complexation with chiral cyanohydrins for determination of absolute configuration	59
Figure II-5. Structure of MAPOL and potential modifications to improve binding interaction	60

Figure II-6. UV-vis spectra of Zn-MAPOL (1 μ M) in different solvents at room temperature	61
Figure II-7. ECCD spectra of Zn-MAPOL complexed with (<i>R</i>)-2-hydroxy-2-(<i>o</i> -tolyl) acetonitrile II-6R	62
Figure II-8. ECCD spectra of Zn-MAPOL (1 μ M) complexed with (<i>R</i>)-2-hydroxy-2-(<i>o</i> -tolyl) acetonitrile II-6R (50 equivalents) in different solvents at 0 $^{\circ}$ C.....	63
Figure II-9. ECCD spectra of Zn-MAPOL complexed with (<i>R</i>)-2-hydroxy-2-(<i>o</i> -tolyl) acetonitrile II-6R (50 equivalents) at different temperatures.....	64
Figure II-10. UV-vis spectra of Zn-MAPOL complexed with (<i>R</i>)-2-hydroxy-2-(<i>o</i> -tolyl) acetonitrile II-9R	67
Figure II-11. Jobs' plot of Zn-MAPOL with (<i>R</i>)-4-methylmandelonitrile II-9R absorbance at 410 nm	68
Figure II-12. Quenching the ECCD signal of II-6R in complex with Zn-MAPOL by addition of methanol	70
Figure II-13. Quenching the ECCD signal of II-6R in complex with Zn-MAPOL by addition of acetonitrile (MeCN).....	71
Figure II-14. a) Bidentate binding of II-6R , with the <i>P</i> -helicity of Zn-MAPOL, places the large aryl group in the most sterically available position. This favorable arrangement leads to the anticipated positive ECCD spectrum. b) Complexation of 5R with Zn-MAPOL leads to a strong positive ECCD signal. c) The same bidentate binding with the <i>M</i> -helicity leads to steric clash of the large aryl group with the porphyrin ring. Thus, negative ECCD with II-6R bound to Zn-MAPOL is not anticipated.....	72
Figure II-15. Side and top view of geometry optimized (DFT-B3LYP/6-31G*) complex of II-10R bound to Zn-MAPOL. The model shows the bulky <i>t</i> -butyl group in the open quadrant, the hydrogen bonding of the alcohol with the biphenol core, and the interaction of the cyano group with the metal center. The optimized geometry predicts a positive ECCD, as observed	73
Figure II-16. ECCD spectra of Zn-MAPOL (1 μ M) complexed with 4-chloromandelonitrile II-7 (50 equiv) at different enantio excess (left). The plot of ECCD amplitude versus % <i>ee</i>	75
Figure II-17. Example of bioactive drugs with chirality at the sulfur atom	76

Figure II-18. Chemical modification and derivatization of chiral sulfoxides for determination of absolute configuration.....	77
Figure II-19. ECCD spectrum of Zn-MAPOL (1 μ M) complexed with (<i>R</i>)- <i>p</i> -tolyl vinyl sulfoxide II-20R (50 equiv) in hexane at 0 $^{\circ}$ C	79
Figure II-20. UV-vis spectra of Zn-MAPOL (1 μ M) and Zn-MAPOL complexed with (<i>R</i>)- <i>p</i> -tolyl vinyl sulfoxide II-20R (50 equiv) in different solvents at 0 $^{\circ}$ C (solvents that yield ECCD signal).....	79
Figure II-21. UV-vis spectra of Zn-MAPOL (1 μ M) and Zn-MAPOL complexed with (<i>R</i>)- <i>p</i> -tolyl vinyl sulfoxide II-20R (50 equiv) in different solvents at 0 $^{\circ}$ C (solvents that do not yield ECCD signal).....	80
Figure II-22. ECCD spectra of Zn-MAPOL (1 μ M) complexed with (<i>R</i>)- <i>p</i> -tolyl vinyl sulfoxide II-20R (50 equiv) in different solvents at 0 $^{\circ}$ C	81
Figure II-23. ECCD spectra of Zn-MAPOL (1 μ M) complexed with (<i>R</i>)- <i>p</i> -tolyl vinyl sulfoxide II-20R (50 equiv) in different solvents at 0 $^{\circ}$ C	82
Figure II-24. ECCD spectra of Zn-MAPOL (1 μ M) complexed with (<i>R</i>)- <i>p</i> -tolyl vinyl sulfoxide II-20R at 0 $^{\circ}$ C in hexane	82
Figure II-25. UV-vis spectral change upon titration of Zn-MAPOL (1 μ M) with (<i>R</i>)- <i>p</i> -tolyl vinyl sulfoxide II-20R at 0 $^{\circ}$ C in hexane	83
Figure II-26. Job's plot of Zn-MAPOL with (<i>S</i>)- <i>p</i> -tolyl vinyl sulfoxide II-20R absorbance at 409 nm.....	84
Figure II-27. Change in the absorbance at 409 nm for evaluating K_{assoc} upon titration of Zn-MAPOL (1 μ M) with (<i>R</i>)- <i>p</i> -tolyl vinyl sulfoxide II-20R at 0 $^{\circ}$ C	84
Figure II-28. ECCD spectra of Zn-MAPOL-OMe (1 μ M) complexed with (<i>R</i>)- <i>p</i> -tolyl vinyl sulfoxide II-20R at 0 $^{\circ}$ C in hexane	88
Figure II-29. X-ray crystal structure of Zn-TPP in complex with dimethyl sulfoxide (hydrogens are omitted for clarity)	89
Figure II-30. a) Bidentate binding of II-20R , with the <i>P</i> -helicity of Zn-MAPOL, places the large aryl group in the most sterically available position. This favorable arrangement leads to the anticipated positive ECCD spectrum. b) Complexation of II-20R with Zn-MAPOL leads to a strong positive ECCD signal. c) The same bidentate binding with the <i>M</i> -helicity leads to steric	

clash of the large aryl group with the porphyrin ring. Thus, negative ECCD with II-20R bound to Zn-MAPOL is not anticipated.....	90
Figure II-31. Energy minimized (B3LYP/6-31G*) structures of the <i>P</i> and <i>M</i> helical Zn-MAPOL complexed with II-22R . The length of the substituents, measured as L_1 and L_2 , dictate the preferred helicity of the host system. The shorter L_2 of the phenyl group leads to smaller steric interactions with the porphyrin ring that is not bound to the sulfoxide	91
Figure II-32. Sterioml L parameter (total length of the substituent along the primary bond axis) and the measure length (L_1 , length of substituent to the furthest heavy atom) are illustrated for 1,2-dimethylpropyl group	92
Figure II-33. Negative ECCD spectrum obtained with Zn-MAPOL complexed with 50 equivalents of (<i>S</i>)- <i>p</i> -toluene sulfinamide II-29S at 0 °C in hexane	94
Figure II-34. UV-vis spectral change upon titration of Zn-MAPOL (1 μ M) with (<i>S</i>)- <i>p</i> -toluene sulfinamide S- II-29S at 0 °C in hexane	94
Figure II-35. Change in the absorbance at 409 nm for evaluating K_{assoc} upon titration of Zn-MAPOL (1 μ M) with (<i>S</i>)- <i>p</i> -toluene sulfinamide II-29S at 0 °C	95
Figure II-36. X-ray crystal structure of Zn-TPP complexed with sulfinamide II-34S (hydrogens are omitted for clarity)	96
Figure II-37. Complexation of esomeprazole (50 μ M) with Zn-MAPOL (1 μ M) yields a positive ECCD spectrum, correctly predicting the <i>S</i> stereochemistry of the molecule. The assignment is based on considering the benzimidazole side chain as the larger substituent (longer linear length as compared to the pyridyl side chain)	97
Figure II-38. ECCD spectra of Zn-MAPOL-OMe (1 μ M) complexed with (<i>R</i>)-methyl phenyl propyl phosphine oxide II-30R at 0 °C in hexane	99
Figure II-39. ECCD spectra of Zn-MAPOL-OMe (1 μ M) complexed with (<i>S</i>)-methyl-phenyl-propyl phosphine oxide II-30S at 0 °C in hexane	100
Figure II-40. UV-vis spectral change upon titration of Zn-MAPOL (1 μ M) with (<i>R</i>)-methyl-phenyl-propyl phosphine oxide II-30R	100
Figure II-41. Change in the absorbance at 409 nm for evaluating K_{assoc} upon titration of Zn-MAPOL (1 μ M) with (<i>R</i>)-methyl-phenyl-propyl phosphine oxide II-30R	101

Figure II-42. Structures of Sofosbuvir and <i>epi</i> -Sofosbuvir	104
Figure II-43. ECCD spectra of <i>epi</i> -Sofosbuvir (1 equiv) complexed with ZnMAPOL (1 μ M) in hexane at room temperature, DCM was added	105
Figure II-44. ECCD spectra of <i>epi</i> -Sofosbuvir (1 equiv) complexed with ZnMAPOL (1 μ M) in hexane at room temperature, NO dichloromethane was added (a), 40 μ L dichloromethane was added (b) and 100 μ L dichloromethane was added (c).....	106
Figure II-45. ECCD spectra of Sofosbuvir (1 equiv) complexed with ZnMAPOL (1 μ M) in hexane at room temperature, DCM was added	107
Figure II-46. ECCD spectra of Sofosbuvir complexed with ZnMAPOL (1 μ M) in dichloromethane	108
Figure II-47. ECCD spectra of <i>epi</i> -Sofosbuvir complexed with ZnMAPOL (1 μ M) in dichloromethane at 0 $^{\circ}$ C	109
Figure II-48. ECCD spectra of <i>epi</i> -Sofosbuvir complexed with ZnMAPOL (1 μ M) in chloroform at 0 $^{\circ}$ C	110
Figure II-49. ECCD spectra of Sofosbuvir complexed with ZnMAPOL (1 μ M) in chloroform at 0 $^{\circ}$ C	110
Figure II-50. ECCD spectra of Sofosbuvir (50 equiv) complexed with ZnMAPOL (1 μ M) in dichloromethane at 0 $^{\circ}$ C, effect of addition of acetone	111
Figure II-51. ECCD spectra of <i>epi</i> -Sofosbuvir (50 equiv) complexed with ZnMAPOL (1 μ M) in dichloromethane at 0 $^{\circ}$ C, effect of addition of acetone	112
Figure II-52. Coordination and the working model of Sofosbuvir complexed with ZnMAPOL. <i>P</i> -helicity is favored and positive ECCD signal was observed	113
Figure II-53. Coordination and the working model of <i>epi</i> -Sofosbuvir complexed with ZnMAPOL. <i>M</i> -helicity is favored and negative ECCD signal was observed	114
Figure II-54. Structural features of F ₆ -backbone	115
Figure II-55. Structure and UV-vis spectrum of F ₄ -MAPOL II-32 (1 μ M solution) in hexane at room temperature.	116

Figure II-56. Structure and UV-vis spectrum of F ₃₀ -Zn-MAPOL II-34 (1 μM solution) in hexane at room temperature.	117
Figure II-57. ECCD spectrum of F ₃₀ -Zn-MAPOL (1 μM) complexed with (<i>R</i>)-1-phenylethanol II-33R (100 equiv) in hexane at 0 °C	118
Figure III-1. Structure of Salinosporamide A and its closely related natural products	149
Figure III-2. Proposed inhibitory mechanism of Salinosporamide A in the proteasome active site	150
Figure III-3. First total synthesis of Salinosporamide A with the highlighted Baylis-Hillman cyclization as the key reaction of the synthesis	151
Figure III-4. Danishefsky's total synthesis of Salinosporamide A.....	151
Figure III-5. Biosynthetically inspired total syntheses of Salinosporamide A	152
Figure III-6. Conia-Ene type reaction to assemble the core of Salinosporamide A... ..	153
Figure III-7. Our developed methodology that give access to pyrrolidinone core and its exploitation for the synthesis of Salinosporamide A	154
Figure III-8. Synthesis of aziridine-alcohol III-25 for implementation of the tandem aza/Payne/hydroamination reaction	156
Figure III-9. Tandem aza/Payne/hydroamination and selective epoxide opening, access to decorated 2-pyrrolidinone core	157
Figure III-10. Installation of the carbon side chain on C-3 and deprotection of the amide moiety of the 2-pyrrolidinone core	158
Figure III-11. Functionalization of C-5, an anionic route	160
Figure III-12. Anionic functionalization of C-5 and the challenges facing this strategy	161
Figure III-13. Cationic approaches towards C-5 functionalization.....	162
Figure III-14. Functionalization of C-5, a radical initiated oxidative strategy	163
Figure III-15. Radical based strategies towards installation of functional group at C-5	165

Figure III-16. General reactivity profile in comparison to the direct C-H functionalization; controlling factor in the C-H insertion reactions	168
Figure III-17. Application of C-H insertion strategy in the total synthesis of natural products and complex molecules	169
Figure III-18. Functionalization at C-5 center employing metal mediated decomposition of α -diazocarbonyl, a C-H insertion strategy	171
Figure III-19. Envisioned functionalities to deliver the active carbene to the C-5 center for the C-H insertion reaction	172
Figure III-20. Installation of the carbonyl moiety on the C-5 center	176
Figure III-21. Selective oxidative cleavage of the terminal olefin	177
Figure III-22. Oxidative cleavage of the internal olefin, β -lactone ring formation	178
Figure III-23. Oxidative cleavage of the internal olefin towards deprotection of the pyrrolidinone nitrogen	179
Figure III-24. Strategies for the removal of the group on the pyrrolidinone nitrogen... ..	180
Figure III-25. An envisioned enone moiety for the facile removal of the group on the pyrrolidinone nitrogen after oxidative cleavage of the internal olefin	181
Figure III-26. Synthesis of the envisioned enone core and its X-ray crystal structure	182
Figure III-27. Access to the advanced bicyclic core III-94b , similar to Fukuyama's intermediate towards Salinosporamide A	185
Figure III-28. Completion of the racemic synthesis of Salinosporamide A	188
Figure III-29. Synthesis of α,β -unsaturated aldehyde III-107 for implementation of the asymmetric aziridination reaction	192
Figure III-30. Asymmetric aziridination of α,β -unsaturated aldehyde, access to aziridine-alcohol (-)-III-25	193
Figure III-31. Total synthesis of (-)-Salinosporamide A	195
Figure III-32. X-ray structure of III-91b (view 1)	232

Figure III-33. X-ray structure of III-91b (view 2).....	233
Figure III-34. X-ray structure of (-)-III-25 (view 1)	248
Figure III-35: The Model has Chirality at C1 (Chiral SPGR) S Verify; The Model has Chirality at C2 (Chiral SPGR) S Verify; The Model has Chirality at C3 (Chiral SPGR) S Verify	248
Figure III-36: The following hydrogen bonding interactions with a maximum D-D distance of 2.9 Å and a minimum angle of 120 ° are present in (-)-III-25 : O1–O3: 2.865 Å	249
Figure IV-1. Spiroketal moiety embedded in the structure of natural products.....	268
Figure IV-2. Anomeric effect, principle and structural requirements.....	269
Figure IV-3. The anomeric arrangements in 6,5- and 6,6-spiroketal frameworks	270
Figure IV-4. Different approaches to access the spiroketal moiety	272
Figure IV-5. List's approach to access spiroketal moiety in an enantioselective fashion	273
Figure IV-6. Nagorny's approach to access the spiroketal in an enantioselective fashion	274
Figure IV-7. Carreira's approach to access spiroketal in an enantioselective fashion	275
Figure IV-8. Examples of halogenated natural products. The halogenated spiroketals are highlighted in blue.....	276
Figure IV-9. Some of the developed methodologies by our group in the field of halofunctionalization of olefins	277
Figure IV-10. Experimental validation of the halonium affinity (HalA)	278
Figure IV-11. The effect of nucleophile on the olefin halofunctionalization, demonstration of nucleophile-assisted alkene activation (NAAA)	279
Figure IV-12. Our approach to access halogenated spiroketals.....	280
Figure IV-13. Bromo spiroketalization of ketone tethered to an unprotected alcohol .	281

Figure IV-14. X-ray crystal structure of macrocyclic IV-45	282
Figure IV-15. Bromo spiroketalization of ketone with a protected tethered alcohol....	283
Figure IV-16. Computed HalA values for ketone bearing different groups	284
Figure IV-17. X-ray crystal structure of product IV-54 and NOESY of IV-45	285
Figure IV-18. Synthesis of 5,6- and 5,5-spiroketals.....	287
Figure IV-19. Dibromospiroketal formation by excluding ethanol from the reaction mixture	288
Figure IV-20. X-ray crystal structure of dibromo-spiroketal IV-67	290
Figure IV-21. Structure of Obtusin and its proposed biogenesis	291
Figure IV-22. Retrosynthetic approach to access Obtusin featuring dibromo-spiroketalization and bromo-etherification steps.....	292
Figure IV-23. Installation of the <i>cis</i> olefin, access to epoxy alcohol IV-91	294
Figure IV-24. Installation of the ketone surrogate, towards bromo-etherification reaction	295
Figure IV-25. Assignment of the relative stereochemistry of the diastereomers IV-96 and IV-97	297
Figure IV-26. On the origin of the diastereoselectivity leading to IV-87 and IV-88	299
Figure IV-27. Rational design to improve the diastereoselectivity of the bromo-etherification reaction.....	300
Figure IV-28. Comparison of the bromo-etherification with and without protection group on the nucleophilic oxygen	303
Figure IV-29. Direct addition of alkyl lithium to the nitrile moiety towards installation of the ketone functionality	304
Figure IV-30. Approaches to improve the efficiency of the conversion of nitrile to ketone	305

Figure IV-31. A different approach to convert epoxy alcohol IV-90 to advanced intermediate IV-109	306
--	------------

KEY TO SYMBOLS AND ABBREVIATIONS

Å	angstrom
cm ⁻¹	wavenumber
M	molar
mM	millimolar
mg	milligram
mmol	millimole
>	larger than
<	less than
CHCl ₃	chloroform
DMF	dimethylformamide
ESI	electrospray ionization
Et ₃ N	triethylamine
EtOAc	ethyl acetate
HOMO	highest occupied molecular orbital
HRMS	high resolution mass spectrometry
LUMO	lowest unoccupied molecular orbital
mp	melting point
mbar	millibarr
MgSO ₄	magnesium sulfate
NaOH	sodium hydroxide

NMR	nuclear magnetic resonance
IR	infrared
α	angle of rotation
$[\alpha]_D$	specific rotation
Å	angstrom
A	CD amplitude
ACN	acetonitrile
AcOH	acetic acid
Ar	aromatic
$\text{BF}_3 \cdot \text{OEt}_2$	boron trifluoride diethyl ether
BINOL	1,1'-Bi-2-naphthol
Bn	benzyl
BnBr	benzyl bromide
BnCl	benzyl chloride
CD	circular dichroism
CE	Cotton effect
cm	centimeter
d	doublet
DCM	dichloromethane
DDQ	2,3-dichloro-5,6-dicyano-1,4-benzoquinone
DET	diethyl tartrate
DFT	density functional theory

DIPT	diisobutylaluminum hydride
DMAP	4-diaminopyridine
DMF	N,N-dimethylformamide
<i>ee</i>	enantiomeric excess
Et ₃ N	triethylamine
ϵ	molar absorption coefficient
ECCD	Exciton Coupled Circular Dichroism
Et ₂ O	diethyl ether
EtOAc	ethyl acetate
eq	equivalents
g	gram(s)
h	hour(s)
HPLC	high pressure liquid chromatography
Hz	hertz
<i>i</i> Pr	isopropyl
IR	infrared
<i>J</i>	NMR coupling constant
K _{assoc}	association constant
LAH	lithium aluminum hydride
m	magnetic dipole transition moment
m	multiplet
<i>m</i> CPBA	3-chloroperoxybenzoic acid

MeOH	methanol
min	minute
μg	micro gram
MHz	megahertz
M	molar
μM	micro molar
MS	mass spectrometry
m/z	mass to charge ratio
n	refractive index
NaOH	sodium hydroxide
nm	nanometer
NMR	nuclear magnetic resonance
ORD	optical rotatory dispersion
PCC	pyridinium chlorochromate
Ph	phenyl
PMB	para-methoxybenzyl
q	quartet
R	rotational strength
s	singlet
rt	room temperature
t	triplet
TBAF	tetrabutylammonium fluoride

TBS	<i>tert</i> -butyl dimethylsilyl
TFA	trifluoroacetic acid
THF	tetrahydrofuran
UV-vis	ultraviolet-visible spectroscopy
TPP-tz	5-(4-carboxyphenyl)-10,15,20-triphenylporphyrin tweezer
Zn-TPP	zinc tetraphenylporphyrin
Zn-TPP-tz	zinc 5-(4-carboxyphenyl)-10,15,20- triphenylporphyrin tweezer
Zn-TPFP	zinc 5-(4-carboxyphenyl)-10,15,20-tri(pentafluorophenyl)porphyrin tweezer
Zn(OAc) ₂	zinc acetate
<i>lcp</i>	left circularly polarized light
<i>rcp</i>	right circularly polarized light
VCD	vibrational circular dichroism
ECD	electronic circular dichroism
<i>edtm</i> , μ	electric dipole transition moment
UV	ultraviolet spectroscopy
InCl ₃	indium(III) chloride
TFA	trifluoroacetic acid
BBr ₃	boron tribromide
$\Delta\delta$	difference in chemical shift
CDCl ₃	deuterated chloroform
X	mole fraction
TMEDA	tetramethylethylenediamine

NH ₄ Cl	ammonium chloride
TLC	thine layer chromatography
Na ₂ SO ₄	sodium sulfate
CH ₂ Cl ₂	dichloromethane
NH ₄ HCO ₃	ammonium bicarbonate
MPA	methoxyphenyl acetic acid
equiv	equivalents
CaH ₂	calcium hydride
THF	tetrahydrofuran
EtOH	ethanol
SeO ₂	Selenium dioxide
^t BuOOH	<i>tert</i> -butyl hydroperoxide
NBS	N-bromosuccinimide
DMP	Dess-Martin periodinane
DMS	dimethyl sulfide
MgBr ₂	magnesium bromide
AIBN	2,2'-azobis(2-methylpropionitrile)
DBU	1,8-diazabicyclo(5.4.0)undec-7-ene
<i>dr</i>	diastereomeric ratio
PPh ₃	triphenylphosphine
TMSCHN ₂	trimethylsilyldiazomethane
LDA	lithium diisopropylamide

CrO ₃	chromium trioxide
TsCl	4-toluenesulfonyl chloride
NaI	sodium iodide
KO ^t Bu	potassium <i>tert</i> -butoxide
HCl	hydrochloric acid
NaHMDS	sodium bis(trimethylsilyl)amide
KHMDS	potassium bis(trimethylsilyl)amide
MMPP	magnesium monoperoxyphthalate
Boc	<i>tert</i> -butyloxycarbonyl
TBSCl	<i>tert</i> -Butyldimethylsilyl chloride
KOH	potassium hydroxide
NaOAc	sodium acetate
DMSO	dimethyl sulfoxide
Me ₃ SOI	trimethylsulfoxonium iodide
OsO ₄	osmium tetroxide
CSA	camphorsulfonic acid
ZnCl ₂	zinc chloride
Me ₃ Al	trimethylaluminium
Ph ₃ PCl ₂	triphenylphosphine dichloride
BOPCl	bis(2-oxo-3-oxazolidinyl) phosphinic chloride
NAAA	nucleophile assisted alkene activation
n.a.	not applicable

n.d.	not determined
Na ₂ SO ₄	sodium sulfate
NaH	sodium hydride
HalA	halenium affinity
MOM	methoxymethyl acetal
TES	triethylsilane
PMB	4-methoxybenzyl ether
TBDMH	1,3-dibromo-5,5-dimethylhydantoin
DCDMH	1,3-dichloro-5,5-dimethylhydantoin
NOSEY	nuclear Overhauser effect spectroscopy
THP	tetrahydropyran
BF ₃ •Et ₂ O	boron trifluoride diethyl etherate
TBCO	2,4,4,6-tetrabromo-2,5-cyclohexadienone
HMPA	hexamethylphosphoramide
nOe	nuclear Overhauser effect
TMSCl	trimethylsilyl chloride
TMS	trimethylsilyl
DHP	dihydropyran
^t BuLi	<i>tert</i> -butyllithium
ⁿ BuLi	<i>n</i> -butyllithium
PPTS	pyridinium <i>p</i> -toluenesulfonate
DIBAL-H	diisobutylaluminium hydride

**Chapter I: Determination of absolute configuration of chiral organic molecules
via exciton coupled circular dichroism**

I-1 Introduction

Life on earth, as we know it, is built with chiral scaffolds. From simple amino acids and sugars that are the foundation of biological life, to hormones, antibiotics, natural products, etc., all are examples of chiral objects. Chirality has been the subject of ongoing research in different branches of science, and understanding of chirality and its impact on chemistry and life has intrigued scientists since the introduction of this concept over a century ago.¹

A chiral molecule is capable of existing in two enantiomeric states. Enantiomers refer to non-superimposable, yet mirror images of a structure. Much akin to the left and right hand that are mirror images of each other but cannot be superimposed, a chiral molecule cannot be superimposed on its mirror image either. At the molecular level, a structure is chiral if there are no elements of symmetry. When a molecule is chiral, there are two different ways to arrange the atoms.

The two enantiomers of a molecule can have different behaviors as they interact with an asymmetric environment such as the active site of a receptor. One of the areas where the different actions of the two enantiomers is significantly important is when these molecules interact with a living organism such as the human body.³ As such, the different enantiomers of a chiral molecule can have different taste or smell due to their different interactions with the sensory receptors. For instance, the two enantiomers of mercaptohexanal, despite their similar physical and chemical characteristics have different smells (Figure I-1). The *S* enantiomer has a fruity odor while the *R* enantiomer has a pungent sulfur smell. Another example where chirality has led to different

properties, is observed in limonene. (*R*)-Limonene is the isomer that is found in orange and is the origin of its smell. The *S* enantiomer of this compound is the fragrant ingredient of lemon (Figure I-1). The impact of stereochemistry is far more pronounced when chirality is embedded in pharmaceutical products. Different enantiomers of a drug can interact differently with the chiral environment of a living organisms. Therefore, the mirror image of an active drug molecule can have devastatingly deleterious effects.¹

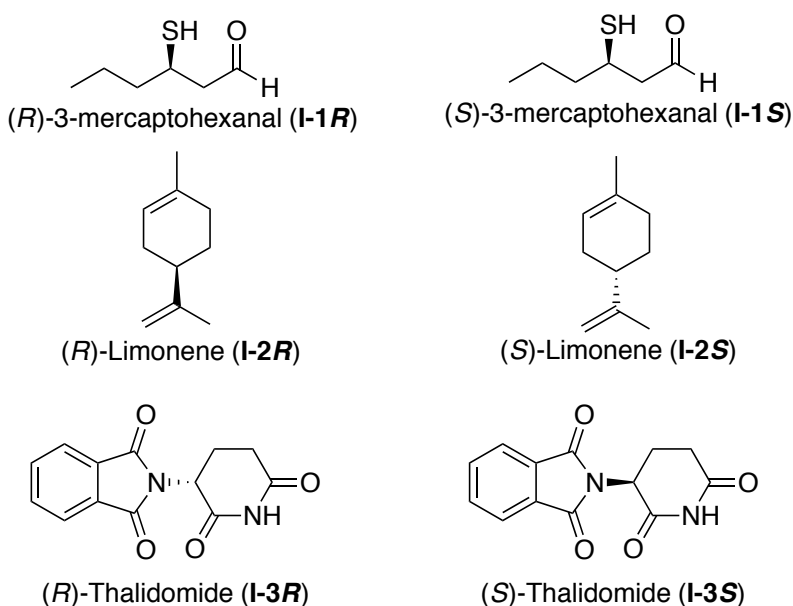


Figure I-1. Representative enantiomers with drastically different biological activities.

Thalidomide is an example where the two enantiomers lay at the two opposite ends of the spectrum with regards to the human health (Figure I-1). While the *R* enantiomer has antiemetic properties, the *S* enantiomer causes fetal abnormalities in infants. In 1960s, this drug was used as its racemic mixture and when it was prescribed to pregnant women, causing terrible birth defects for some babies.⁴ Catastrophic events such as this case and many other instances, have led to strict regulations with respect to the effect of the each enantiomers of a drug molecule. Currently, chiral drugs are only

approved as a single enantiomer, which makes the determination of absolute stereochemistry of a molecule an important task. Thus, introducing simple, efficient and reliable techniques for the assignment of absolute configuration of chiral molecule are in high demand.

Moreover, the assignment of stereochemistry is central to the progress of chemistry in any of its sub-disciplines that require the use of molecule for function, whether it is a pharmaceutical agent, synthetic intermediate, identification of new natural products, etc. The aim of our research program is to develop methodologies that could be used for the absolute stereochemical determination of chiral compounds. The goals are to provide simple, rapid, efficient, and non-ambiguous procedures for establishing the stereochemistry of chiral centers.

I-2 Methods for the absolute stereochemical determination of chiral molecules

Assignment of stereochemistry is crucial to the progress of chemistry in any of its sub-disciplines that require the use of molecules for function, whether it is pharmaceutical agent, synthetic intermediate, identification of new natural products, etc. To this end, many different approaches have been reported to establish the absolute configuration of chiral molecules. One of the most widely utilized techniques for this purpose is Mosher ester analysis of chiral molecules.⁵⁻⁹ According to this method, enantiomeric structures are derivatized with a chiral aryl carboxylic acids, with known configuration, to form two diastereomers. Derivatization can be performed on chiral molecules that contain hydroxyl and amine functionalities to form the corresponding

ester or amide derivatives. NMR analysis of the diastereomeric derivatives can lead to the elucidation of absolute configuration of the derivatized molecule. The anisotropic effect of the aryl substituents on the derivatization agent (aryl carboxylic acid) causes changes in the chemical shift of the substituents on the chiral target molecule. Interpretation of the changes in the chemical shifts can lead to determination of absolute configuration of the target molecule. There are a few assumptions that need to be taken into consideration before utilizing Mosher ester analysis for determination of absolute configuration.

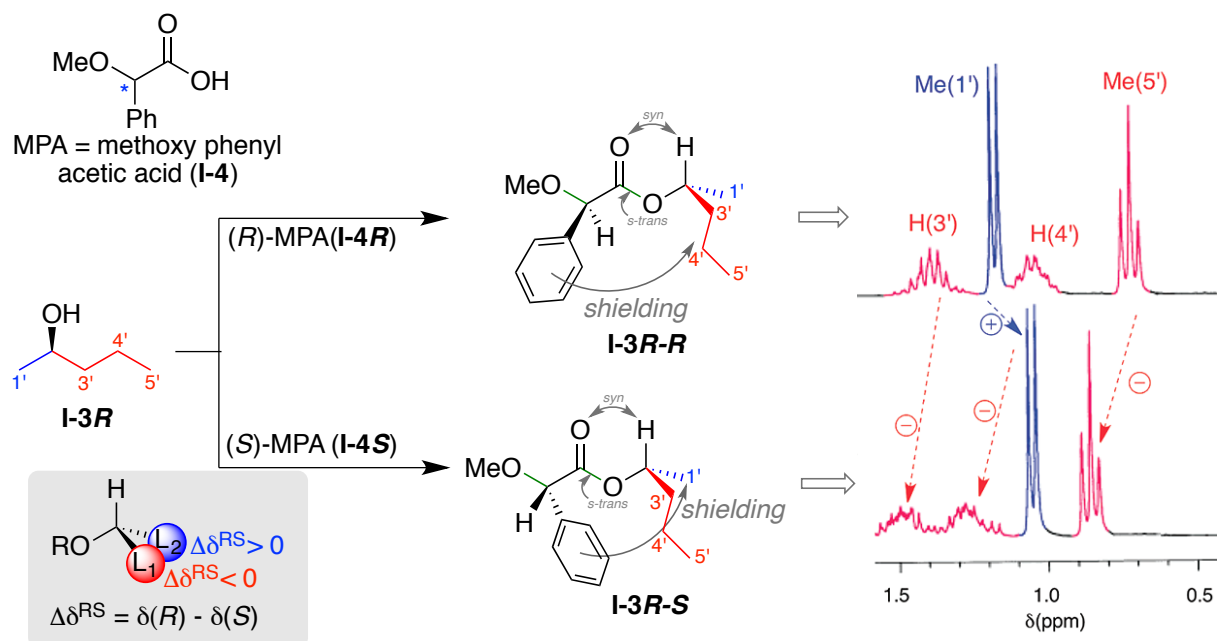


Figure I-2. Assignment of the absolute configuration of a secondary alcohol using Mosher method. Structure of the stable conformer that leads to the change in the chemical shift of the derivatized alcohol and the ^1H -NMR traces of both diastereomers, as well as the proposed mnemonic (dashed box) are demonstrated.

As illustrated in Figure I-2, structural features of Mosher ester *i.e.* the *s-trans* conformation of the ester group, the *syn* alignment of the ester carbonyl with the smallest group on the chiral center as well as the *anti-periplanar* alignment of methoxy

C-O bond with ester C-O bond are crucial in order to conceive meaningful results from changes in the chemical shifts. Deviation from any of these assumptions causes discrepancies on the results of Mosher ester analysis.⁸⁻⁹ Although this method has been extensively used for determination of absolute configuration, the requirement of milligram quantity of chiral sample for chemical derivatization and the uncertainty observed in some of the results are the limitations of this method. Furthermore, Mosher ester analysis can only be performed on molecules that contain a single derivatization group.

Another NMR based technique that can be used for the determination of absolute configuration is application of chiral solvating agents. In this method, the chiral solvating agent, non-covalently interacts with the target molecule and the anisotropic effect of the solvating agent on the substituents of the target molecule can be informational towards determination of the absolute configuration. Elimination of chemical reaction can be considered as advantage of these techniques as compared with the Mosher methods. However, lack of predictability and ambiguous results are by far the most notable limitations associated with the aforementioned methods for determination of the absolute configuration of chiral molecules.¹⁰⁻¹¹

On the other end of the spectrum, X-ray crystallographic techniques present a different solution to this issue. X-ray structure can provide unambiguous determination of the absolute configuration of asymmetry. The necessity of high quality single crystal hampers the application of this technique as a routine procedure for determination of absolute configuration. Nonetheless, X-ray structure elucidation is one of the most

powerful techniques for determination of the relative stereochemistry of organic molecules.

I-3 Application of chiroptical spectroscopy for determination of absolute configuration of chiral molecules

Interaction between plane polarized light and chiral molecules (chiroptical spectroscopy) is one of the earliest observations made with asymmetric molecules. Chiroptical data, as a unique physical property of chiral molecules, are measured as early as mid-nineteenth century.¹ Light waves consist of electric and magnetic vectors that oscillate perpendicular to one another and to the direction of the propagation of light. Unpolarized light in which the light waves propagate in all directions is the characteristic of most of the ordinary light sources. If an unpolarized light passes through a polarizing filter only small fraction of light waves which oscillate in parallel with the direction of the filter can make it through, thus leading to linearly polarized light (Figure I-3-a). Linearly polarized light is comprised of two circularly polarized light components *i.e.* left circularly polarized light (*lcp*) and right circularly polarized light (*rcp*). The phase and intensity of *lcp* and *rcp* components of light are the same, thus the projection of their combined amplitudes yields a straight line perpendicular to the propagation axis of light.^{1, 12}

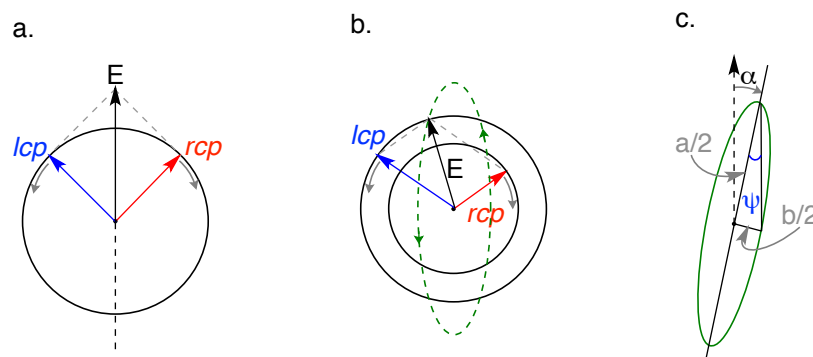


Figure I-3. **a.** Plane-polarized light composed of two circularly polarized components, *lcp* and *rcp*. As long as the phases of intensities of these two components remain the same, the resultant oscillating vector will be in the same plane and magnitude. **b.** If the *rcp* component become less intense (due to interaction with chiral media) the electric vector of light follows an elliptical path (elliptically polarized light, green oval). **c.** The degree of ellipticity is define as ψ , which is proportional to the circular dichroism. The rotation of ellipse (α) corresponds to optical rotation and ORD.

When polarized light passes through an achiral or racemic solution, the characteristics of the right and left components of light, such as velocity and absorbance, undergo changes to the same extent. As a result, the oscillating plan of polarized light remains unchanged. On the other hand, when light passes through an absorbing optically active substance, the velocity and absorbance of the *lcp* and *rcp* components of incident polarized light undergo changes with different extents, leading to a Cotton effect that is named after the French scientist, Amie Cotton. Measurement of alteration of velocity of left and right components of light results in Optical Rotatory Dispersion.¹³ Optical rotatory dispersion is based on the difference in the reflective indices of the two components of light, thus it can be recorded over all wavelengths. A derivative of ORD that is commonly utilized by scientists is specific optical rotation ($[\alpha]_D$) that is indicative of the optical activity at a specific wavelength. Sodium D-line (589 nm) is the wavelength commonly used as reference of optical rotation leading to $[\alpha]_D$.

Furthermore, these two components of light are absorbed by chiral media to a different extent due to difference in absorption coefficient of *lcp* and *rcp*, $\epsilon_L \neq \epsilon_R$. The difference $\Delta\epsilon \equiv \epsilon_L - \epsilon_R$ is called *Circular Dichroism* (CD). Recording differences in the absorption of *lcp* and *rcp* over wavelengths that the molecule absorbs light leads to a CD spectrum. CD spectra are similar to UV-vis spectra with the major difference that UV-vis is always a positive curve whereas the CD spectrum can be positive or negative depending on the chirality of the sample (Figure I-4).

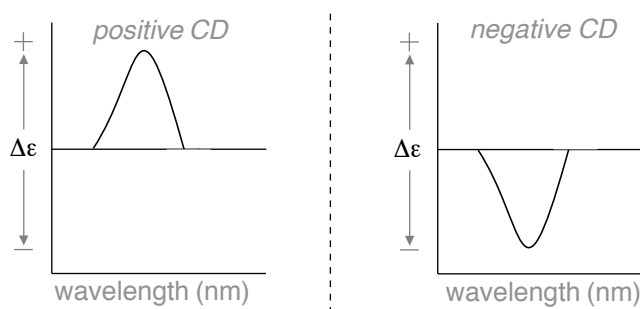


Figure I-4. Positive or negative CD spectra or Cotton effects.

This unique property based on the interaction of polarized light with a chiral compound that leads to two distinct parameters,¹³ ORD and CD, has found increasing usage in the assignment of absolute configuration. It should be noted that ORD can be observed in all wavelengths since the technique originates from changes in refractive indices of *lcp* and *rcp*. On the other hand, CD can only be observed in the wavelengths that the molecule exhibits absorption.

The application of chiroptical spectroscopy for determination of absolute configuration of chiral molecules is one of the most widely utilized methods. Measuring optical rotation can provide an empirical method for determination of absolute configuration. Comparison of the measured optical rotation (α_D) with the reported value

for the exact same compound can give access to the absolute configuration of a molecule. Nonetheless, if the optical rotation of a molecule is not known, measurement of $[\alpha]_D$ cannot give any information with respect to the absolute configuration of a given compound.

With recent advancements in computational modeling, optical rotation of a chiral molecule can be calculated and upon comparison with the measured value a platform for determination of the absolute stereochemistry can be exploited.¹⁴⁻¹⁶ Optical rotatory dispersion¹³ is another tool that can be utilized for determination of absolute stereochemistry.¹⁷⁻¹⁹ This method needs to be paired with computationally extracted ORD spectra in order to provide a reference spectrum for comparison with the experimentally measure ORD. Flexibility of molecular structure and presence of close lying conformers can complicate the computational analysis and applicability of this technique.

Another area where chiroptical techniques are utilized extensively for determination of chirality is application of methods based on circular dichroism (CD) spectroscopy.²⁰ Among various aspects of circular dichroism spectroscopy, vibrational circular dichroism (VCD), based on absorption at the infrared region and electronic circular dichroism (ECD) for absorption at UV-Vis region have found widespread applications in assignment of the absolute configuration of chiral molecules. In the case of VCD, the experimental spectrum of the target molecule must be compared with the calculated VCD spectra for both of the enantiomers.²¹⁻²⁵ This technique has shown promising utility for determination of chirality if the calculated spectra are performed with high-level

quantum chemical calculation. Due to weak absorption in VCD spectroscopy, long acquisition time and concentrated samples (large sample size) are usually required to access reliable results.

Electronic CD (ECD) originates from electronic transition in the UV-vis region within a chiral framework upon interaction with polarized light. Much akin to VCD spectroscopy, this method can be merged with computational techniques to exploit a comparative tool for the assignment of absolute configuration. A unique variant of this technique is the Exciton Coupled Circular Dichroism (ECCD) pioneered by Harada and Nakanishi in 1980s.²⁶⁻²⁷ ECCD utilizes the excited state coupling of two or more close-lying and strongly absorbing chromophores embedded in the structure of a chiral molecule. Presence of similar chromophores or chromophores with close UV-vis absorption profiles is crucial for a strong exciton couplet. These chromophores can pre-exist or be introduced into the chiral molecules via derivatization. For ECCD to arise, the electric dipole transition moments of the close by chromophores should interact with each other, that would lead in a splitting of the excited state energies. An electric dipole transition moment (*edtm*, μ) can be described for each transition. The *edtm* for each transition defines the net displacement of charge during the transition.¹² In most common systems that utilize ECCD, two chromophores are interacting with each other. In this paradigm, the transition dipoles can have in-phase or out-of-phase arrangements that result in two exciton states. The splitting energy of the two states ($2V_{12}$) is referred to as Davydov or exciton splitting (Figure I-5). The relative arrangements of the interacting chromophores determine the magnitude and the energy of splitting. For

systems with two chromophores, a face-to-face, head-to-tail or oblique arrangement of dipoles can be described. In the face-to-face arrangement, interaction of the two chromophores leads to increase in the excitation state energy due to electrostatic attraction and repulsion, as a results a blue shift in absorption is predicted (Figure I-5-a).

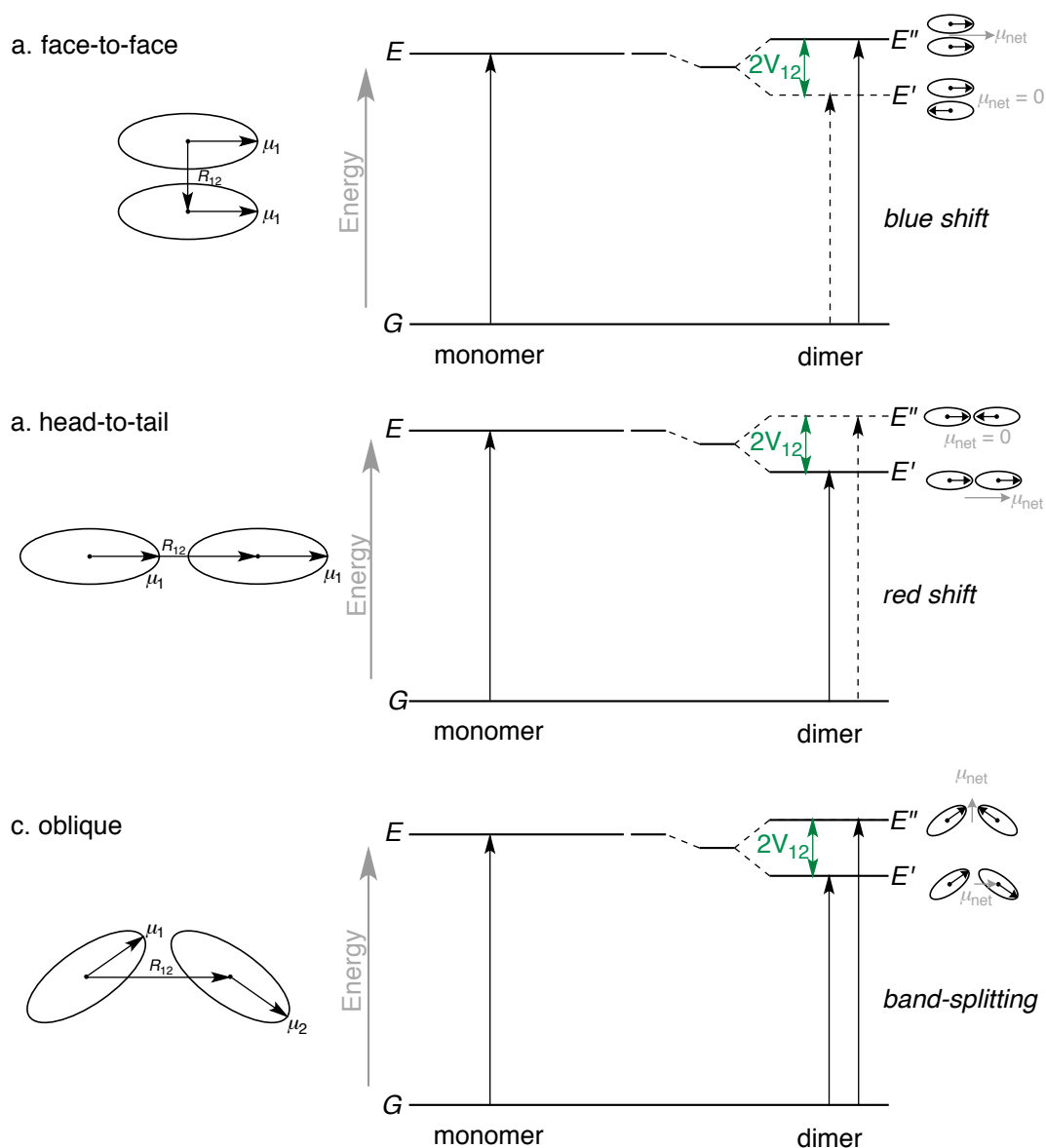


Figure I-5. Schematic exciton band energy diagram of system with two interacting chromophores in various geometries. The ovals indicate chromophores with their electric dipole transition moments. The magnitude of the net electric dipole transition moments (μ_{net}) is deduced by employing a simple vector model analysis.

This arrangement is also referred to as *H-aggregation*. In the case of head-to-tail arrangement (also known as *J-aggregation*) a red shift in absorption is expected since the electronic transition to the excited state with higher energy is dipole forbidden (Figure I-5-b). As illustrated in Figure I-5-c, if the two chromophores have an oblique arrangement, absorption to both of the excitation states will take place and a splitting of the absorption band into two components will be observed.¹² This arrangement is the most general type of aggregation of chromophore that is observed commonly for interacting chromophores and can provide useful information with regards to molecular chirality.

I-4 Chemical derivatization of chiral molecules with interacting chromophores for determination of absolute configuration

The coupling of asymmetrically disposed chromophores leads to an interpretable signal which is the direct consequence of the helicity of the coupling transitions of the two chromophores. Since not every chiral compound has asymmetrically arranged strong absorbing chromophores in their skeleton, enormous efforts have been directed towards design and introduction of interacting chromophores in chiral molecules. One of the early approaches was to derivatize chiral molecules with two chromophores for the purpose of absolute stereochemical determination.

In this regards, derivatization of chiral diols with 4-substituted benzoate as chromophores was envisioned (Figure I-6).²⁸ The stereochemistry of the derivatized diol dictates the relative arrangement of the newly installed benzoate chromophores. 1,2-

diol derivatized with 4-substituted benzoate demonstrates the oblique alignment of interacting chromophore in a helical arrangement (Figure I-6). Coupling of the *edtm* of the benzoate chromophores (indicated with blue solid lines) leads to the observed bisignate CD spectrum.

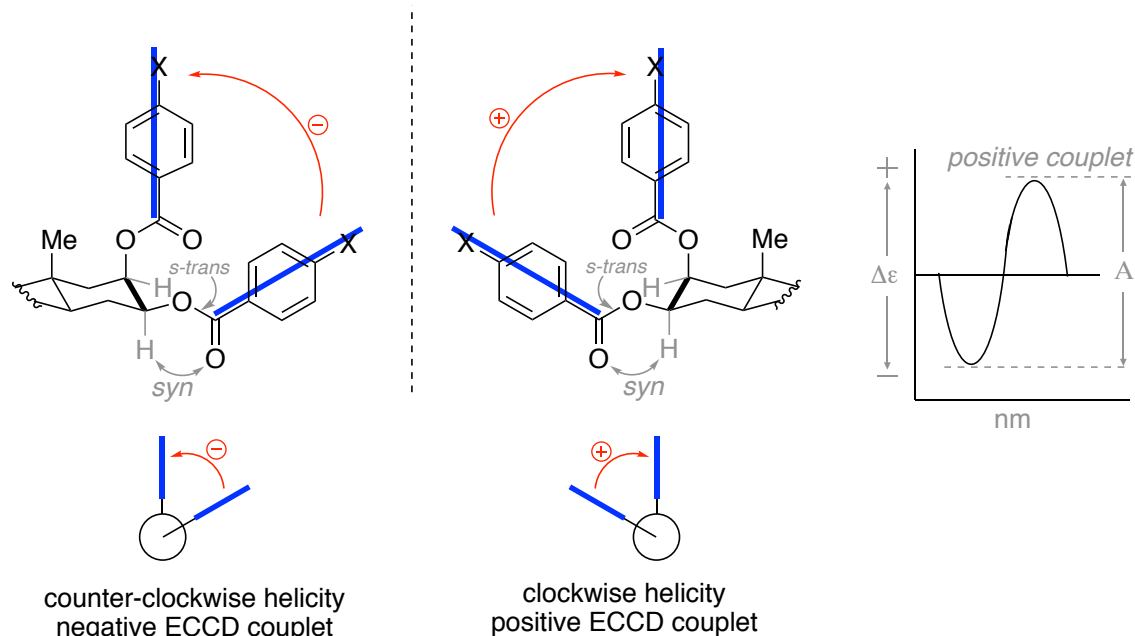


Figure I-6. Schematic demonstration of two independently conjugated chromophores arranged in a helical twist. The electric dipole transition moments (blue line) are along the long axis of the benzoate moieties. The side view of interacting chromophores indicates clockwise or counter-clockwise arrangement of chromophores depending on the chirality of the diol. The clockwise helicity generates a positive ECCD spectrum (shown on top right).

The sign of the ECCD spectrum is denoted as positive if the positive peak of the couplet appears at higher wavelength (as shown in Figure I-6) or negative if the negative couplet appears at higher wavelength. The sign of the ECCD spectrum is the direct demonstration of the helicity of the interacting chromophores, which in turn originates from the absolute configuration of the chiral diol. Thus, a clockwise helicity of

interacting chromophores leads to a positive ECCD signal and counterclockwise helicity generates a negative ECCD spectrum, thus enabling a none-empirical determination of the orientation of chromophores.^{12, 26-27}

Another approach for installation of chromophores into chiral molecules for determination of the absolute configuration has been reported by Rosini and coworkers.²⁹⁻³⁰ They utilized a bridged biphenyl system bearing a ketal moiety to form spiro dioxolanes with chiral 1,2- and 1,3-diols (Figure I-7). In this manner, the chirality of the diol induces axial chirality into the backbone of the bridge biphenyl system and leads to the appropriate ECCD response. The CD signal can be directly correlated into the absolute configuration of the derivatized diol. This method reveals a simple procedure for introducing absorbing chromophore into UV transparent diols in order to observe predictable CD signals that give access to the absolute stereochemical

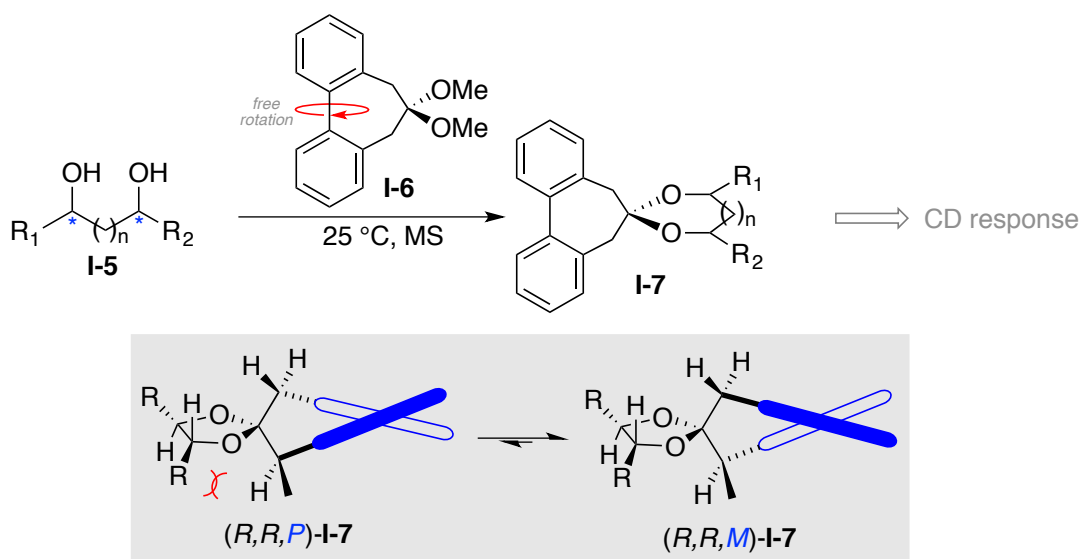


Figure I-7. Dioxolane formation of chiral diols with **I-6** leads to CD active complexes. The highlighted diastereomeric complexes (box) depict equilibrating dioxolanes that favor *M* conformation due to the chirality of the bound diol.

determination.

This backbone has been modified to be applicable for derivatization of chiral carboxylic acids (Figure I-8).^{2, 31} In the same paradigm, the chirality of the carboxylic acid induces a twist into the biaryl backbone of the azepine **I-18** that leads to the observed CD signal. Figure I-8 (box) highlights the most stable conformation of the derivatized acid that features co-planarity of the smallest group on the chiral acid with the methyl moiety of the azepine in order to minimize 1,3- strain. *P* helicity is more stable for the shown configuration due to alleviation of steric repulsion between the large group on the chiral center and the azepine.

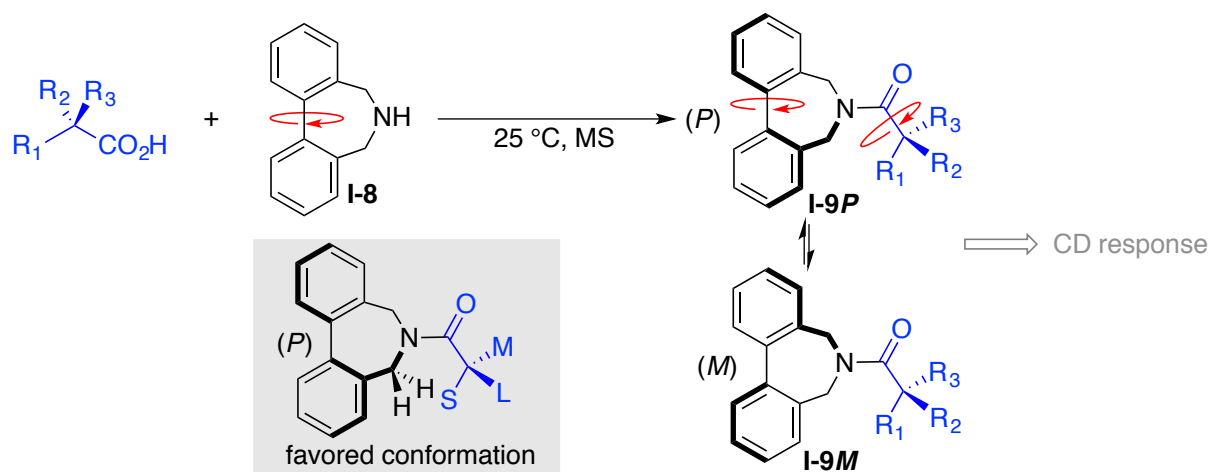


Figure I-8. Development of an azepine probe (**I-8**) for sensing the absolute configuration of chiral carboxylic acids.

In another elegant design, Wolf and coworkers introduced triaryl **I-10** as a molecular probe for determination of the absolute configuration of amino alcohols (Figure I-9).³²⁻³⁶ This foldamer features two cofacial salicylaldehyde rings on a naphthalene backbone. They have shown that salicylaldehyde rings can freely rotate around the C-C bond of the naphthalene ring leading to C_2 -symmetric *M,M*-**I-10** and *P,P*-**I-10** rotamers that

interconvert through the meso form. Schiff base formation of the aldehyde moieties on the sensor's backbone with chiral amino alcohols would result in a population imbalance between the *M,M* and *P,P* rotamers. The rotamer with minimized steric repulsion will be dominating and generates the corresponding CD signal. The intensity and sign of the CD signal can be used to elucidate the absolute configuration of the bound chiral molecules as well as the enantiomeric excess of the sample.

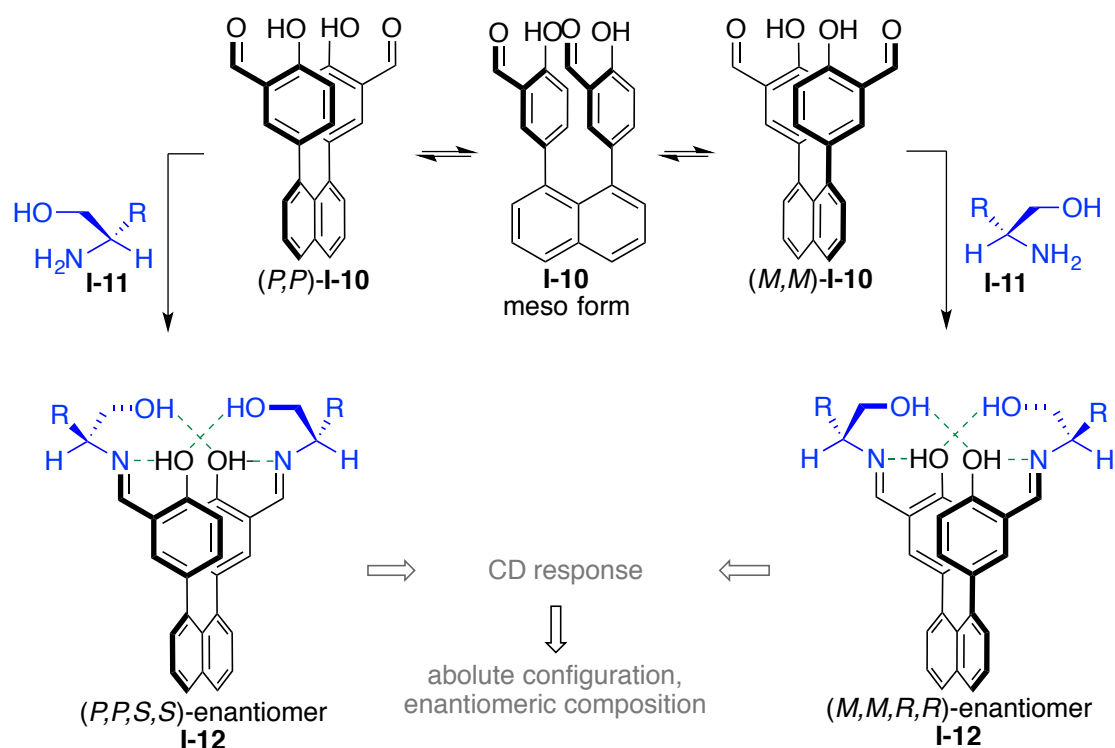


Figure I-9. Development of stereodynamic molecular probe **I-10** for determination of enantiomeric composition and absolute configuration of chiral amino alcohols through imine formation.

Another example that utilizes three interacting chromophores for the determination of the absolute configuration of chiral molecules is reported by Canary and coworkers (Figure I-10). They take advantage of complexation of Zn(II) and Cu(II) with quinoline based ligands to arrange the chromophores around the metal center.

The chirality on linker to one of the quinoline ligands controls the helical arrangement of the ligands around metal center leading to a strong CD signal. In a similar manner, the helical twist of quinoline based ligands around Cu(II) is controlled by the stereochemistry of chiral methionine (Figure I-11).³⁷⁻³⁹ The *R* amino acid induces a *P* twist the ligands and generates positive CD couplet. On the other hand, the *S* enantiomer leads to *M* twist and a negative ECCD signal as output.

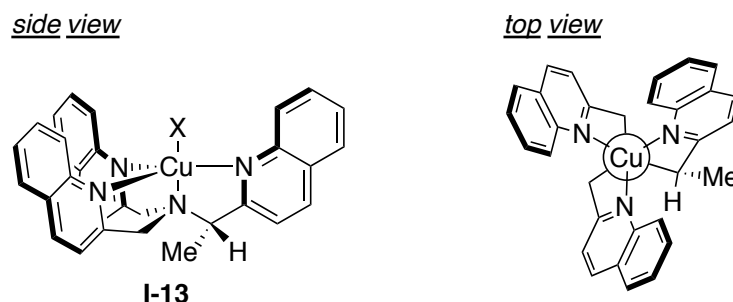


Figure I-10. Structure of propeller-like Cu(II) complex with chirality on the backbone of one of the quinoline based ligand.

Alternatively, in order to access a stereo-dynamic system, an achiral ligand can be used as a chromophore and chiral molecules can be introduced to the complex through ligand exchange with water molecule on the copper complex (Figure I-12).⁴⁰⁻⁴¹ The chirality of the new coming ligand (chiral carboxylic acid) then dictates the helicity of the interacting chromophores. The helical twist of the ligands provides strong ECCD signal that is consequence of the absolute configuration of the bound chiral carboxylic acid.

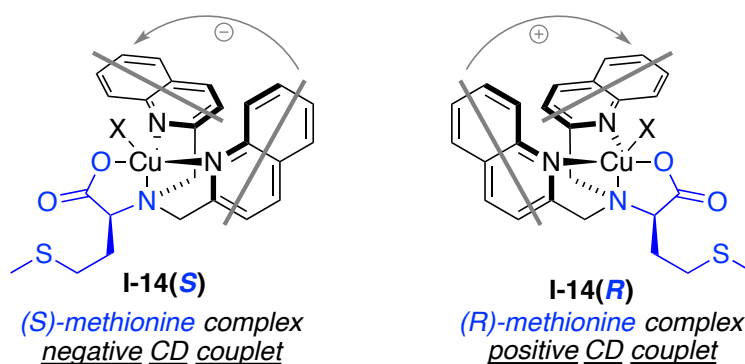


Figure I-11. Induced helical twist of the achiral quinoline based ligand on Cu(II) due to stereochemistry of the bound amino acid (methionine).

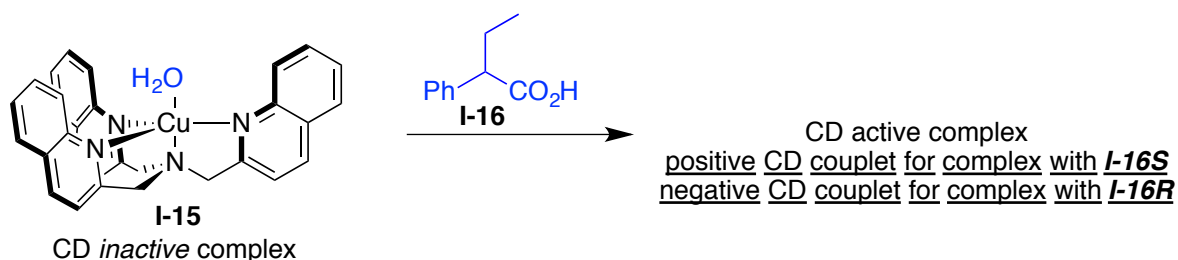


Figure I-12. Structure of a copper based molecular probe for sensing the chirality of carboxylic acids.

In another elegant strategy, Anslyn and coworkers described a dynamic covalent assembly between pyridine-2-carboxaldehyde, di(2-picolyl)amine, a chiral alcohol and zinc triflate that proceeds via an activated iminium intermediate **I-19** (Figure I-13).⁴²⁻⁴⁴ The chirality of the alcohol determines the chirality of the newly formed N,O-acetal center in **I-20** and consequently the helical twist of the pyridine ligands is the outcome of the latter stereo-induction.

This multi-component association gives access to stereochemical determination as well as estimation of the enantiomeric excess of the chiral secondary alcohols.

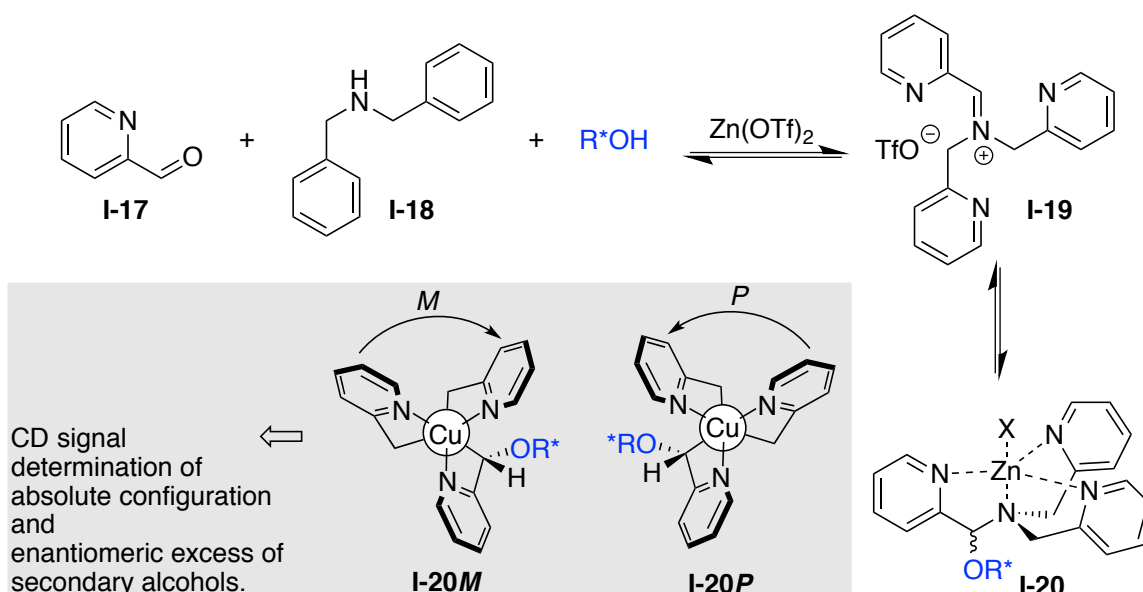


Figure I-13. Stereodynamic assembly of chiral alcohol with *in situ* generated iminium **I-19** into a trigonal bipyramidal scaffold leading to *P* or *M* helicities depending on the chirality of alcohol.

I-5 Porphyrin tweezers methodology: host:guest complex formation with chiral molecules for determination of absolute configuration

Another strategy that is applicable for organic compounds that lack the presence of two strongly absorbing chromophores is host-guest complex formation of the chiral organic molecule (guest) and an achiral system containing two or more chromophores (host). In this approach, chiral molecules are not necessarily chemically derivatized with the chromophoric host systems, yet their chirality is transferred to interacting chromophores of the host system through metal coordination. The porphyrin tweezers methodology pioneered by Nakanishi and co-workers is one of the most utilized host system that has been applied to the assignment of absolute configuration of different families of organic molecules.⁴⁵ In this approach, porphyrins as unique chromophores form host-guest complexes with chiral organic molecules. In the complex formation

event, the chirality of the bound organic compound leads to a helical twist of the porphyrin tweezer resulting in a detectable ECCD signal. The sign of the ECCD signal can be non-empirically correlated to the helical twist of the interacting porphyrin chromophores. As illustrated in Figure I-14, the host guest complexation of diamine **I-22**, with stereogenic center on one of the amine groups with porphyrin tweezer **I-21** gives rise to the latter helical arrangement of the two porphyrins. In order to minimize the steric repulsion of the complex, the porphyrin bound to the stereogenic nitrogen slides towards the small group on the chiral center and moves away from the larger group on this carbon.

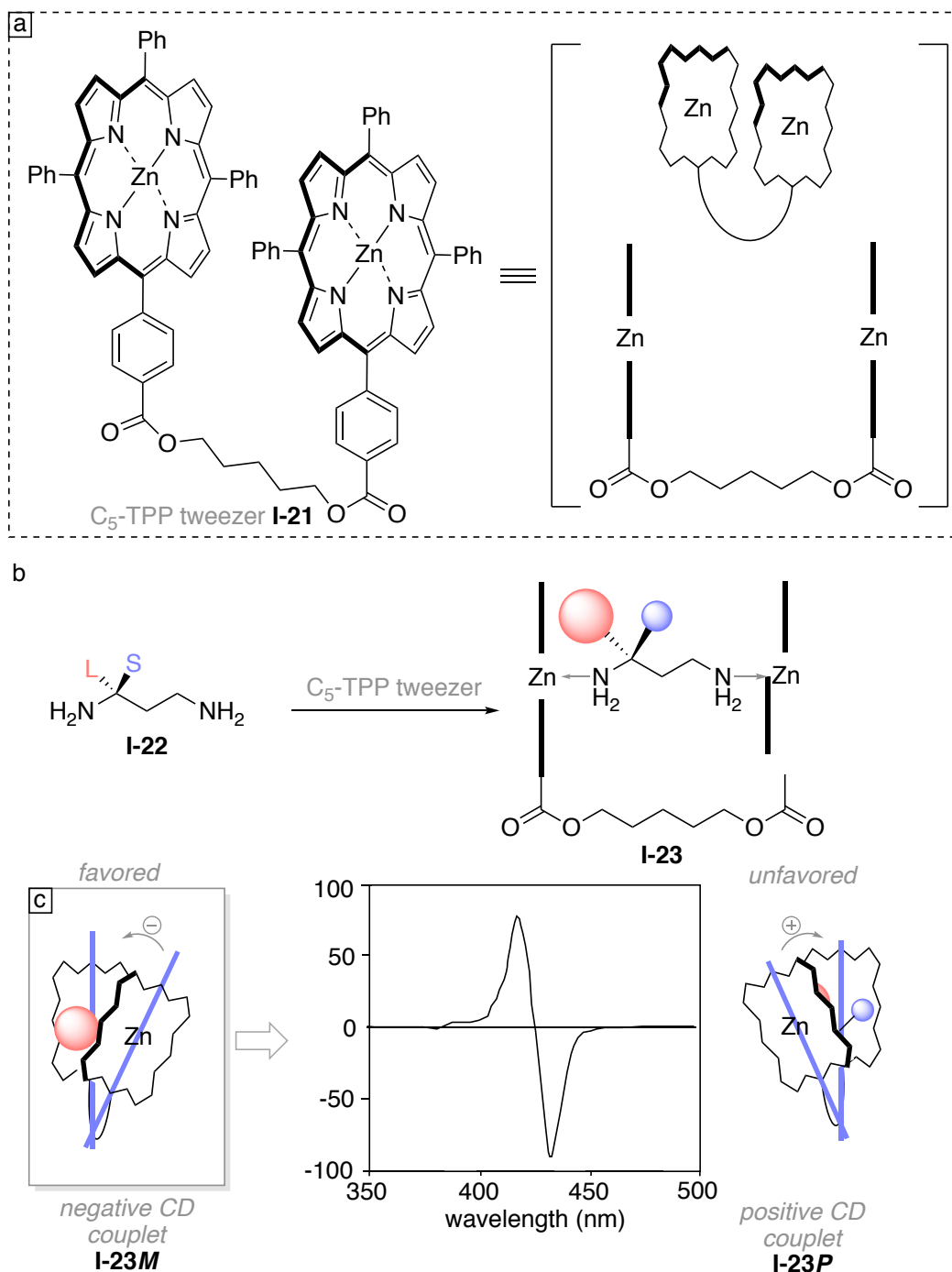


Figure I-14. (a) Structure of C_5 -TPP tweezer; (b) model for complexation of chiral diamine with C_5 -TPP tweezer (a bidentate coordination of diamines with the porphyrin tweezer leads to the observed helical twist); (c) Experimentally measured ECD signal and proposed model for the preferred helical twist (left), counter-clockwise arrangement of interacting dipole transition moments leads to a negative ECD signal.

The latter arrangement leads to a counter-clockwise helical twist, and a negative ECCD signal for this complex is predicted. The tweezer methodology is competent to report the chirality of host molecules with two bonding sites. This ECCD based approach has been applied to the absolute stereochemical deamination of a wide range of compound including polyols,⁴⁶ carbohydrates,⁴⁷⁻⁴⁹ quinuclidines,⁵⁰⁻⁵¹ amines,⁵²⁻⁵³ amino acids amino alcohols,^{38, 54} and hydroxyl acids.⁵⁵⁻⁵⁶

The requirement of two coordinating sites on the guest molecules preclude complex formation of the porphyrin tweezers with chiral molecules with only one binding site such as chiral mono-alcohol, mono-amines, carboxylic acids, etc. Nonetheless, this issue has been circumvented to some extent via derivatization of the chiral mono dentate molecules with a carrier that provides a second coordinating site. Following this approach, chiral alcohols, amines and carboxylic acids can be converted to their corresponding ester or amide derivatives prior to complexation with the porphyrin tweezer.⁵⁷⁻⁶¹ The zinc centered porphyrin is Lewis acidic enough for coordination with amine containing chiral molecules, however hydroxyl groups suffer from low binding affinity for complex formation with the zinc porphyrin. Our group has included significant modifications to the porphyrin tweezer methodology, providing a platform for sensing the chirality of chiral molecules with hydroxyl groups as coordinating site. The Lewis acidity of the zinc center was greatly improved by employing perfluorinated phenyl rings substituted on the porphyrin meso positions. Zn-TPFP **I-26** porphyrin tweezer is capable of ECCD active complex formation with chiral 1,2-diols,⁶² epoxy alcohols⁶³ and distal diols⁶⁴ for absolute stereochemical determination (Figure I-16). The computed HOMO

and LUMO energies of zinc-tetraphenyl porphyrin (Zn-TPP) and zincated perfluorinatedphenyl porphyrin (Zn-TPFP) confirmed the increased Lewis acidity of the metallocenter in the fluorinated porphyrin tweezer system as compared to the zinc in the non-fluorinated host systems (Figure I-15). These computational data were corroborated with experimentally measured binding constants for complexation of alcohols and amines with zinc porphyrins of various electronic profiles. The measured binding constants for Zn-TPFP are roughly 40 times higher than that for Zn-TPP for complexation with amines or alcohols (Figure I-15).⁶²

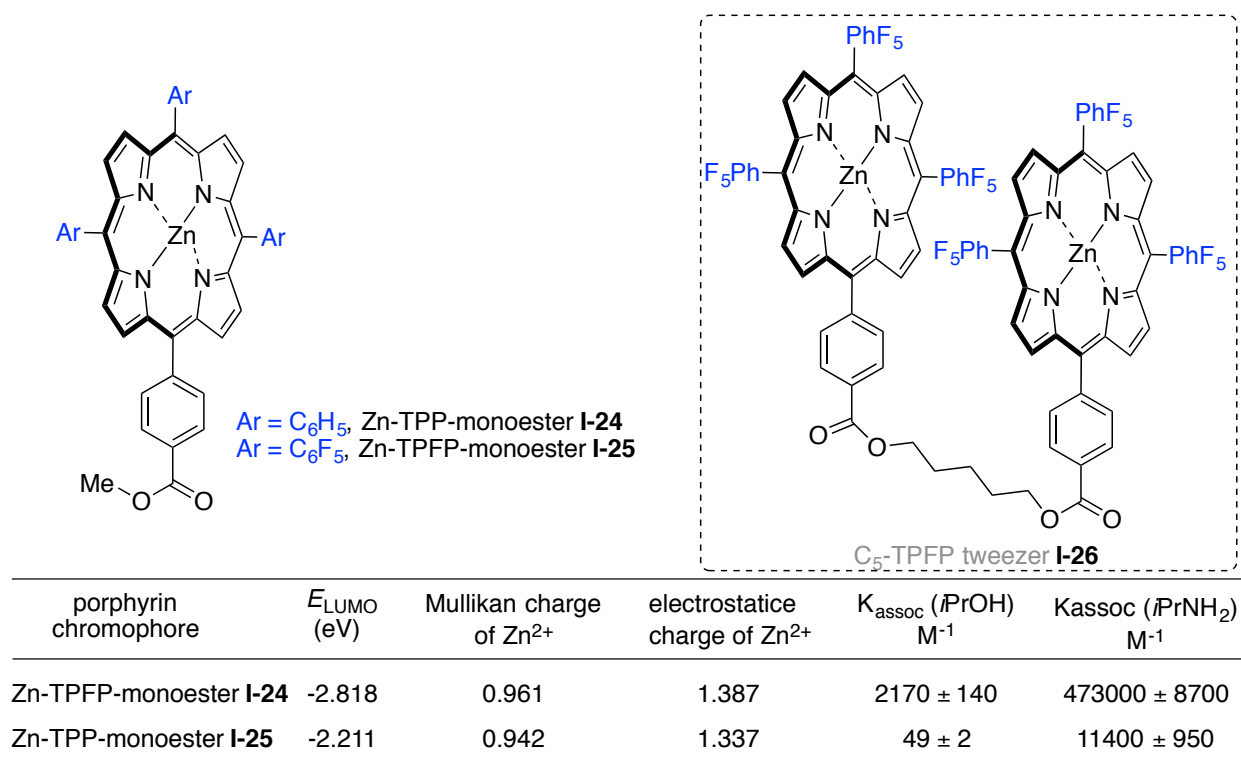


Figure I-15. Frontier orbital energy and charges of zinc porphyrins. Bonding affinity of *iso*-propanol and *iso*-propylamine with Zn-TPP-monoester and Zn-TPFP-monoester as analogues of Zn-TPP tweezer and Zn-TPFP tweezer (dashed box depicts structure of C5-Zn-TPFP tweezer).

The development of TPFP tweezer methodology provided a unique platform for assignment of absolute configuration of many classes of organic molecules. The

following pictorial summary illustrates our major contributions to this area (Figure I-16).⁶²⁻⁶⁷

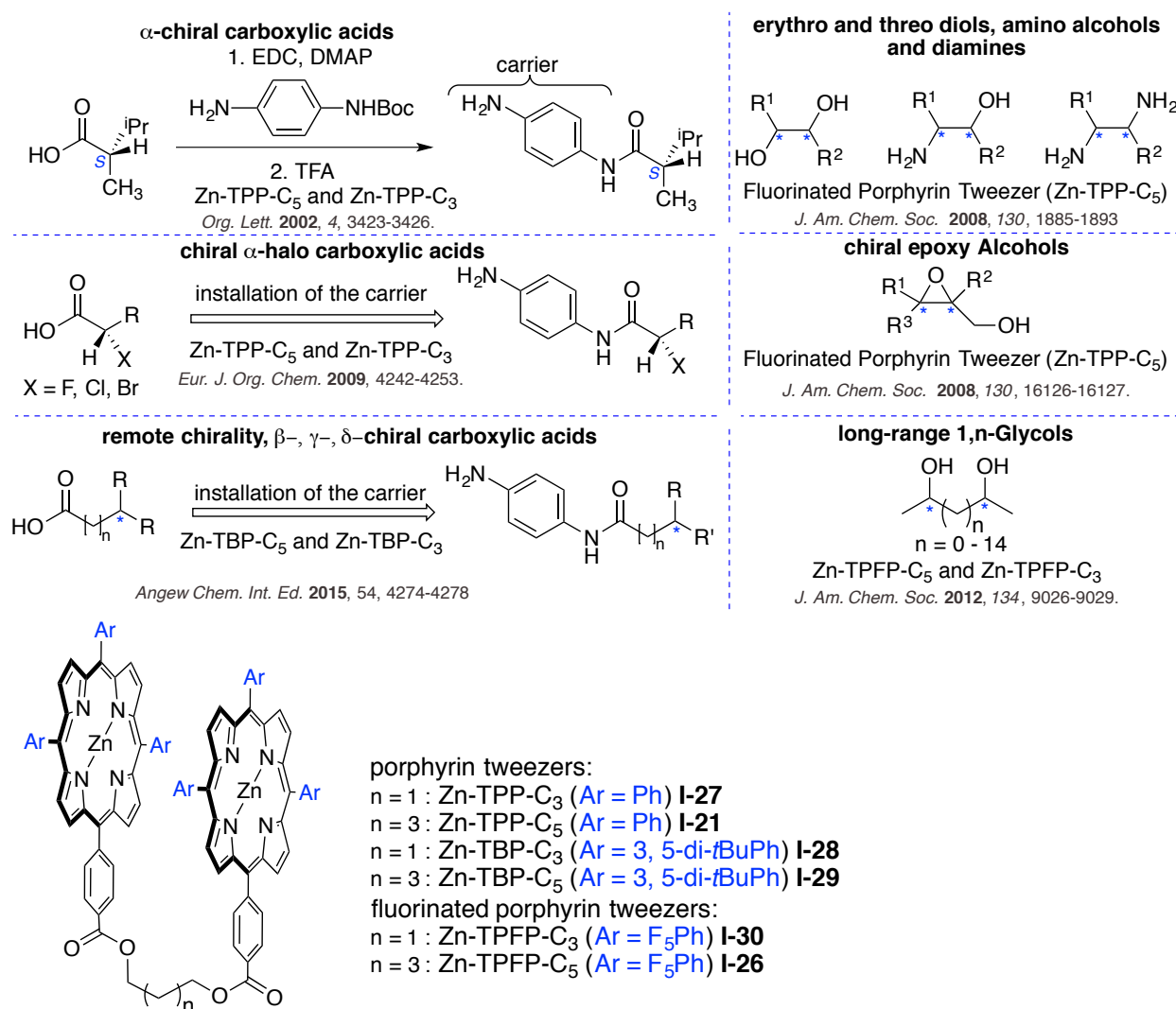


Figure I-16. Pictorial representation of functional group families with methods for assignment of their stereochemistry. Chiral molecules with single site are derivatized with a carrier to form a bidentate guest molecule (left panel) prior to complex formation with tweezers; Structure of host systems, with various linker size as well as tuned steric and electronic profiles that enables determination of absolute configuration of the latter functionalities are shown at the bottom of this figure.

Modifications of porphyrin tweezer, in terms of electronic modulation of the host system as well as steric adjustments and linker size variations, have led to successful

application of this methodology for the determination of the absolute configuration of the represented functionalities. Nevertheless, the major limitation associated with the porphyrin tweezer methodology, as illustrated in Figure I-16, is the prerequisite of needing two coordinating sites on the chiral molecule to induce a helical arrangement of the interacting porphyrin chromophores. Designing a host system that eliminate the requirement of two binding site that limits the application of this methodology, became our group's focus.

I-6 Design of a new host system for determination of absolute configuration of chiral molecules with one sites of attachment

As described above, application of the porphyrin tweezers methodology, with all its potential, is limited to molecules with two coordination sites. If a molecule with sing site of attachment is to be analyzed via porphyrin tweezers, a drivatization step is necessary that implement a second binding site in order to derive the complex formation. As derivatization is not desirable it also cannot be implemented to many classes of molecules with one site of attachment. We set out to design a new host system to remedy this shortcoming. The envisioned host system should be capable of forming ECCD active complexes with chiral molecules with only one site of attachment without the necessity for derivatization.

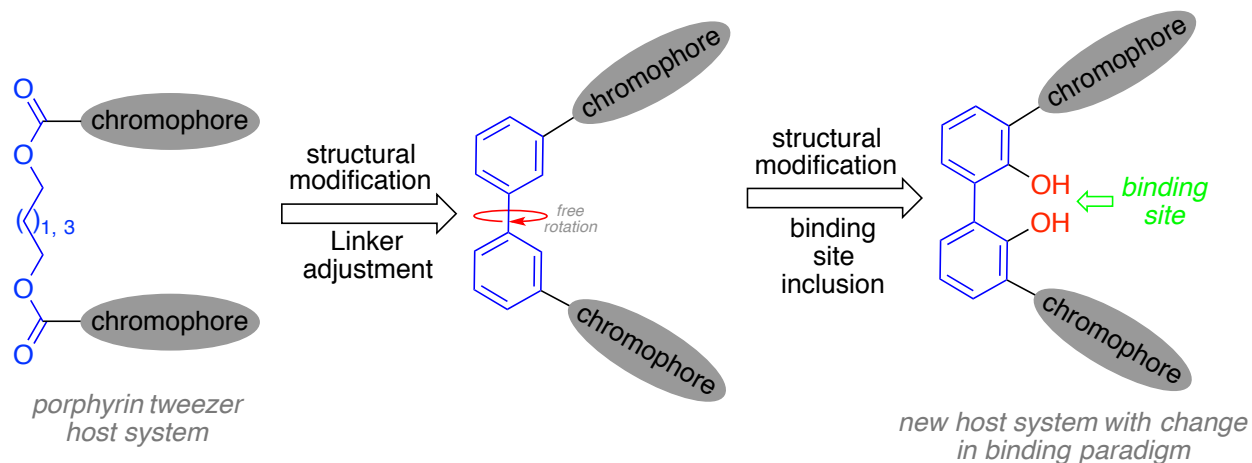


Figure I-17. Rational design of a new host system capable of sensing chirality of molecules with one site of attachment. Linker modification and change in the binding paradigm are notable adjustments.

Approaching this problem from a rational design perspective, we realized that the porphyrin tweezer methodology with its flexible linker (alkyl chain as linker) necessitates the concurrent coordination of two sites from a guest molecule to the metalloporphyrin in order to induce helical twist and generate CD active complexes. Our approach was to design a molecular framework that places the porphyrin moieties in a face-to-face arrangement even in the absence of a chiral molecule. As such, the envisioned system would be helical, but racemic, and can adopt either *P* or *M* helicity. The chiral molecule would then solely be responsible to induce a preference over the existing and equilibrating helicities (Figure I-17).

To this end, a 2,2'-biphenol functionality was envisioned as a backbone for the interacting chromophoric porphyrin rings (Figure I-17). 2,2'-Biphenol systems can exist as equal *P* and *M* atropisomers due to the free rotation around the bi-aryl C-C bond (in the absence of bulky substituent at the 6,6' positions). In this hypothetical design the porphyrin ring would be placed on the 3,3' position of the biphenol core. The free

rotation along the axial chirality of the biphenyl moiety leads to equally populated *P* and *M* atropisomers.⁶⁸ The *P* atrop-isomer leads to a clockwise helical twist of the chromophoric porphyrin rings, yielding to a positive ECCD signal, while a negative ECCD signal originates from the *M* helicity. In the absence of a chiral guest, the host molecule is ECCD silent since the population of the equilibrating helical twists (*P* and *M*) leading to opposite ECCD signals is equal. Upon introduction of a chiral molecule that can form a stable complex with the host system, an imbalance in the population of the *P* and *M* helicities is anticipated. As a result, the interaction between the host system and a chiral molecule, the point chirality of the chiral guest molecule is transferred to the axial chirality of the host system. Thus, the favored atrop-isomer with higher population will result in a ECCD signal.

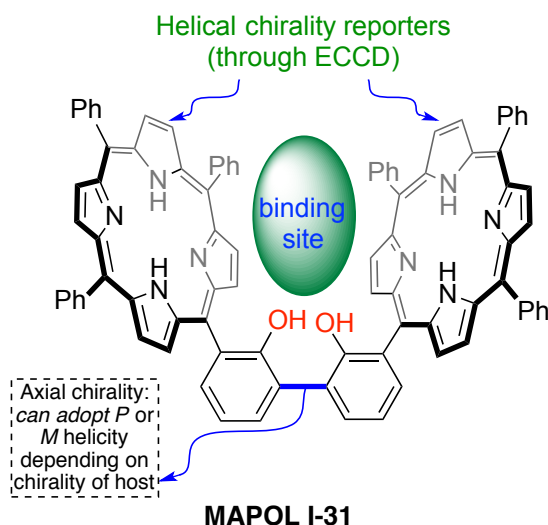


Figure I-18. Structure of newly designed host system. Biphenyl back bone, capable of adopting *P* or *M* helicity, renders equilibrating atropisomers. Upon introduction of chiral guest, that rests in the highlighted binding sites, one of the helicities become more prominent leading to the corresponding ECCD signal.

MAPOL (**I-31**)⁶⁸ was envisioned as the potential host molecule able to deliver on the latter prerequisites (Figure I-18). The synthesis of this molecule was the first challenge to overcome. Typically, synthesis of mono-porphyrin compounds proceeds with average yield of 10-20%. For our target molecule with two porphyrin rings embedded in the structure of the host system, the theoretical yield was not expected to be high. Many different routes for the synthesis of MAPOL were screened. Eventually a disconnective approach was chosen to forge the porphyrin moieties.

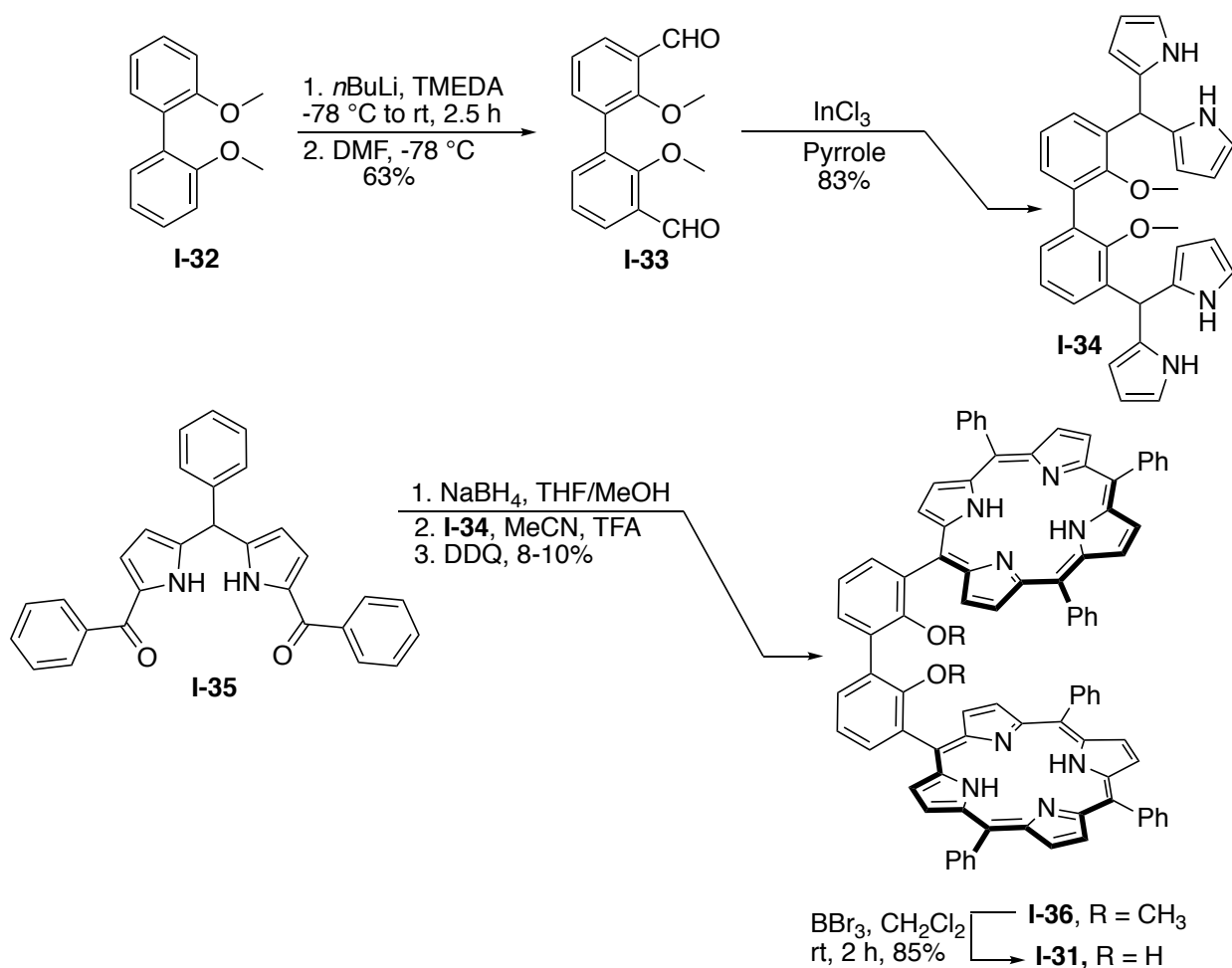


Figure I-19. Successful synthesis of MAPOL **I-31**.

As depicted in Figure I-18, the synthesis of MAPOL commenced with commercially available 2,2'-bisphenol **I-32** that was underwent a directed ortho formylation leading to the bisaldehyde **I-33**. Condensation of this bisaldehyde with pyrrole in the presence of InCl_3 led to the formation of dipyrromethane derivative **I-34**. To prepared the other half of the porphyrin rings, benzaldehyde was condensed with pyrrole followed by dibenzylation to give **I-35**. These two components (**I-34** and **I-35**) were married together through a 2+2 porphyrin formation reaction. Diketone **I-35** was reduced to its corresponding diol that was directly reacted with dipyrromethane **I-34** in the presence of TFA as a Lewis acid in acetonitrile. Oxidation of the condensed product with DDQ furnished the porphyrin ring to yield **I-36**. The dimethyl MAPOL **I-36** was readily isolated in a relatively good yield of ~10% considering two porphyrin rings were assembled in one step. The ease of isolation was the major advantage of this synthesis. Since the only possible porphyrin in this reaction is the expected product, the higher order oligomers were easily removed form organic products with a simple filtration. MAPOL was obtained via demethylation of **I-36** in the presence of BBr_3 .

I-7 Determination of the absolute configuration of chiral monoamines

With MAPOL in hand, we set out to test the applicability of this host system with chiral monoamines as proof of concept. The classical porphyrin tweezers were incompetent to form an ECCD active complex with monoamines due to lack of a second binding element. In this newly designed host system a change in the binding paradigm was implemented. As such, MAPOL, bearing a biphenol core, was envisioned to form a hydrogen bond network with the amino group of chiral monoamines. This binding mode places the chiral carbon in the center of the host molecule, forcing interactions with the pseudo face-to-face arranged porphyrins. Two diastereomeric complexes are thus possible, where the fixed chirality of chiral amine (*R* or *S*) induces the flexible axial chirality of the host system (*P* or *M*).

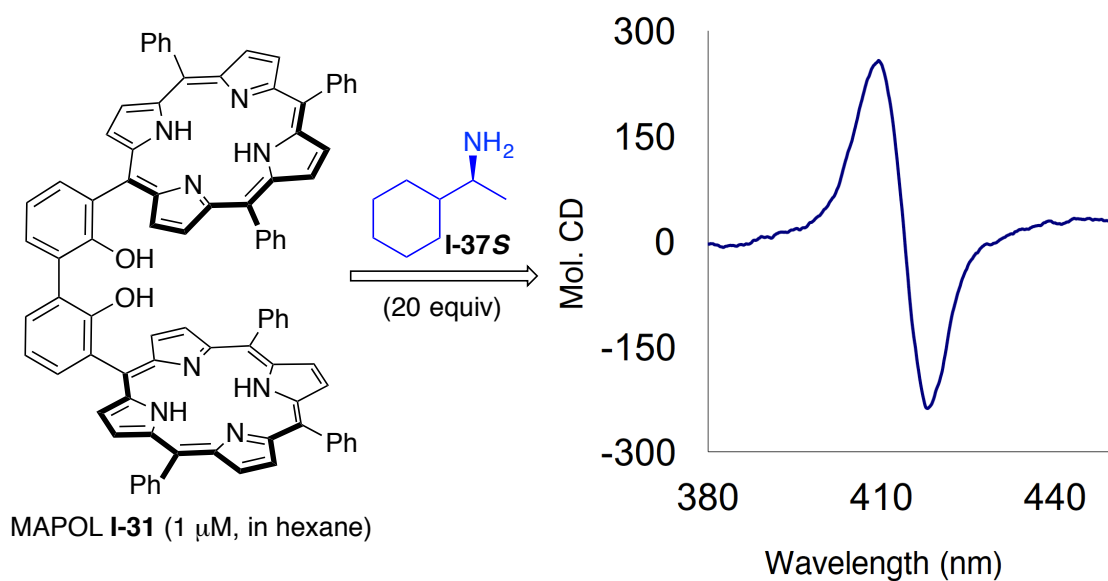


Figure I-20. Complexation of MAPOL with chiral monoamine **I-37S** leads to a strong ECCD signal with a negative sign.

The equilibrating diastereomers are expected to have different energies, with the more stable complex that has alleviated steric strain, having a higher population. The observed ECCD signal would be the result of the higher populated helicity. With this hypothetical analogy, chiral amine **II-37S** was complex with MAPOL in hexane (Figure I-20). Gratifyingly, the complex was CD active and produced a negative ECCD signal. The generation of ECCD signal confirms the formation of a stable chiral host:guest complex. To further verify the complex formation between chiral amine and MAPOL, the complexation was followed by ^1H -NMR. Addition of amine **I-37S** to MAPOL in chloroform showed dramatic changes in the chemical shift of the guest molecule along with notable changes of the protons on the host molecule. In brief, protons on the chiral amine **I-37S** undergo significant up field shifts at a lower host:guest ratio (Figure I-21). Upon increasing the host:guest ratio, the chemical shifts of the amine protons increase towards those of the free amine. At low equivalents of free amine, most of the guest molecules are in the cavity of MAPOL, thus experiencing strong anisotropic effect of the porphyrin rings that results in up-field shift of the amine's proton resonances. At higher equivalents of the amine however, the chemical shifts are the average chemical shift of the bound and free amine. The region highlighted with blue background indicates the changes in the chemical shifts of the methyl group on the chiral amine **I-37S**. This methyl group in the free amine appears at ~ 1.0 ppm, while in the 1:4 complexation ratio with MAPOL (0.25 equiv) is located at ~ 0.0 ppm.

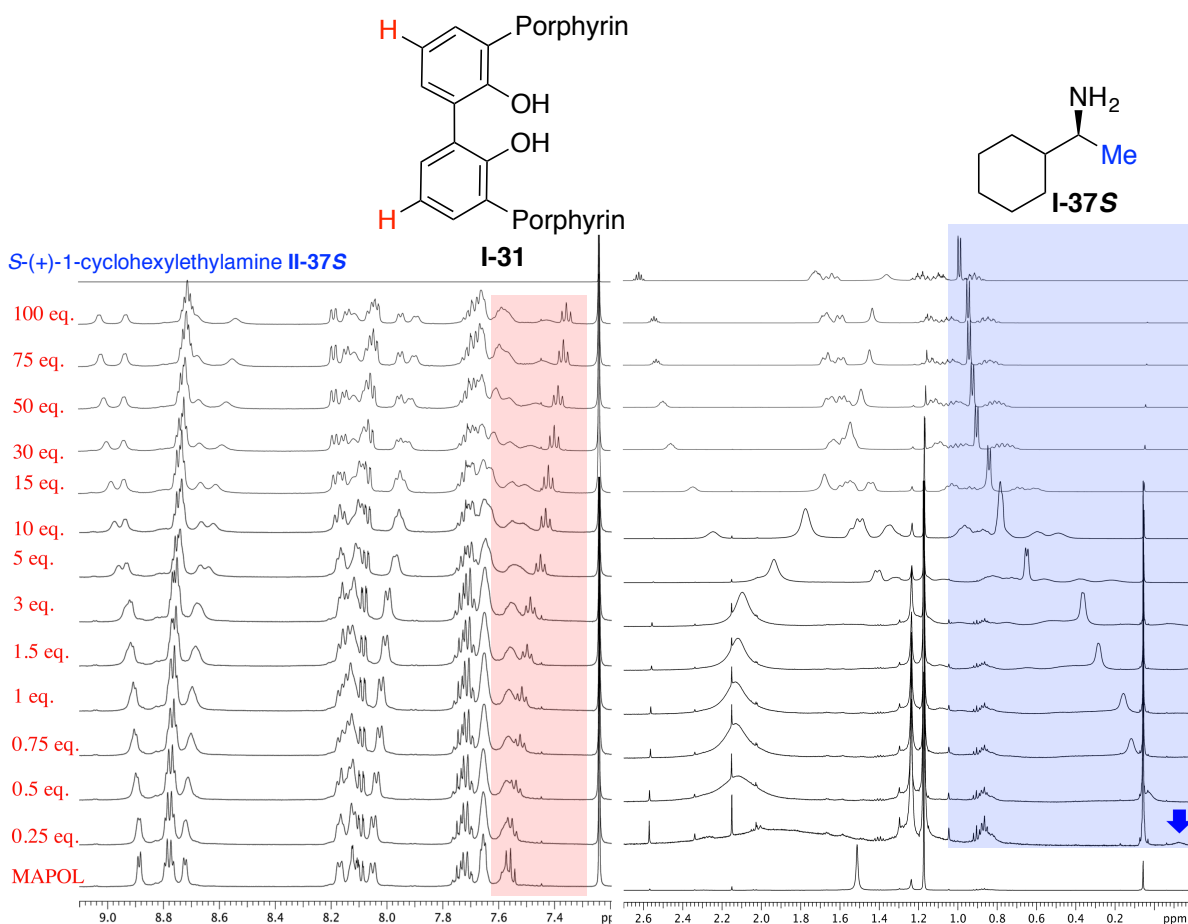


Figure I-21. ^1H -NMR spectra of titration of MAPOL **1** with *S*-(+)-1-cyclohexylethylamine **I-37S**. Highlighted with blue indicates the changes in the chemical shift of the methyl group of the amine substrate and the red area shows the changes in the chemical shift of the MAPOL backbone upon complexation with amine **I-37S**.

Job's plot analysis of the changes in the chemical shift of both amine and MAPOL as function of the equivalents of added amine clearly indicates a 1:1 stoichiometry of the complex (Figure I-21). The fact that following the chemical shift changes of either MAPOL **I-31** or amine **I-37S** in the ^1H -NMR titration leads to the same binding stoichiometry is self-consistent and supports the proposed binding paradigm.

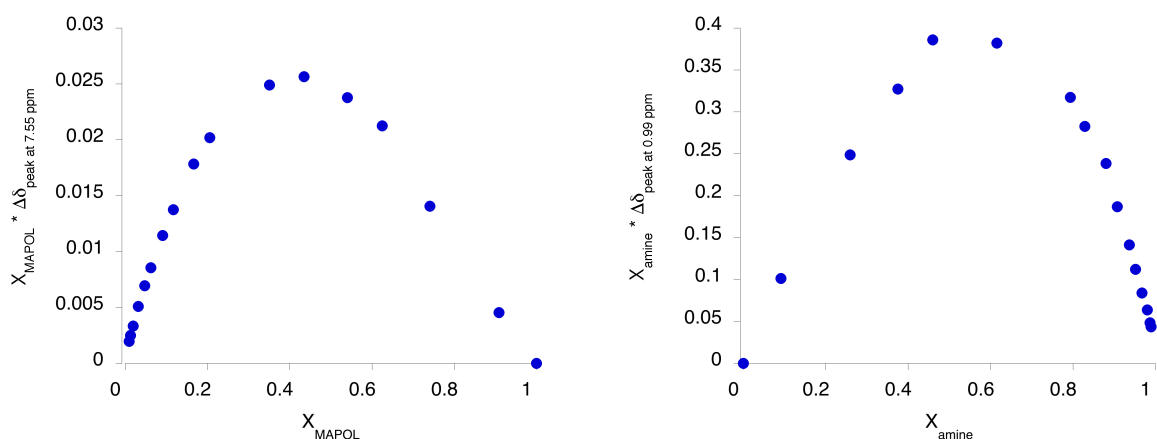


Figure I-22. Job's continuous plot of MAPOL **I-31** with **I-37S**: following the changes in chemical shift of MAPOL at 7.55 ppm (left) and chemical shift of amine **I-37S** at 0.99 ppm.

The generality of the host system for complex formation with a variety of chiral monoamines was tested. Of note is the opposite ECCD signals for enantiomeric amines that points to the fact that one enantiomer of the guest molecule favors *M* helicity and the opposite enantiomer favors *P* helicity. To correlate the chirality of the bound amine with the helicity of the preferred atrop-isomer of MAPOL, the following mnemonic is proposed. The binding element that derives the complex formation is hydrogen bonding between amine group of the guest molecule and the hydroxyl groups of the host system. This binding paradigm forces the amine group to point towards the center of MAPOL and places the stereogenic carbon in the cavity of MAPOL. Minimization of the steric repulsion between groups on the asymmetric carbon and the porphyrin rings were thought to be the determinant factor for the preferred helicity. In Figure I-22, the *S* enantiomer of chiral amine **I-37S** is complexed with MAPOL. The groups attached to the chiral center have different sizes. These groups can be generally classified as small (hydrogen), medium (methyl) and large (cyclohexyl) based on their relative size.

A-value (or other steric parameters) can be used for assignment of the relative size of the substituents. In the case of chiral monoamines with MAPOL we sorted the substituents on the stereogenic center based on their A-values. Both possible stereogenic complexes of the chiral amine with MAPOL (*S-M* and *S-P* diastereomeric complexes) will be considered for relative stability (Figure I-23, b versus c). Among the substituents attached to the chiral center, the cyclohexyl group is the most sterically demanding group, thus occupying the most sterically accessible position. Due to the tetrahedral geometry of the chiral carbon, the remaining two groups (medium and small) will be projected towards specific quadrants.

Considering the *P* helicity, the medium group points towards one of the porphyrin rings, while in the *M* helicity the smaller group is placed in the same position. This simple analysis reveals that the *M* helicity is more stable than *P* helicity. As a result, the sign of the ECCD signal is expected for this favored complex. Indeed, the experimental measurements corroborated the negative ECCD signal. The same analogy can be utilized for all of the amines, with the measured ECCD signal in full agreement with the predicted sign obtained from the proposed mnemonic. Furthermore, the measurements are in micro scale regime and assessment of absolute configuration can be obtained in minutes, which adds to the practicality of this technique.

In summary, we have designed a new host system that can give access to the absolute configuration of chiral monoamines in a non-empirical, micro scale and rapid fashion. In this new design, chiral monoamines form complexes with MAPOL as the host system through hydrogen bonding. Metal-free porphyrin rings act solely as

chromophores and reporter of helicity as opposed to the porphyrin tweezers methodology where the porphyrin rings are in fact the binding site as well as the interacting chromophores. This design holds promises to deliver methods for assignment of absolute configuration of other mono-dentate chiral molecules.

I-8 Experimental section

1-8-1 Job's continuous plot analysis to determine complex stoichiometry

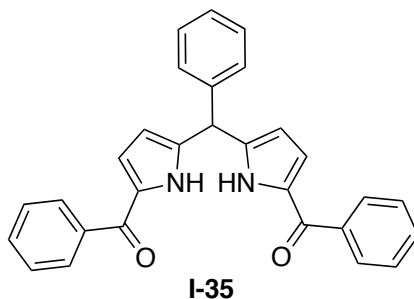
The complex stoichiometry for the host-guest complexes were determined through ^1H -NMR titration of MAPOL (host) with chiral amines *S*-(+)-1-cyclohexylethylamine **I-37S** as the guest molecule. The following describes the experimental detail for binding titration of **I-37S** with MAPOL. Upon complexation of amine **I-37S** with MAPOL, ^1H -NMR spectra of MAPOL as well as amine undergoes changes in chemical shift ($\Delta\delta$) due to the large anisotropic effect of the porphyrin rings. These changes in chemical shifts can be used as a read-out for determining the composition of host:guest complexation in solution.

For titration, MAPOL (5.0 mg, 0.004 mmol) was dissolved in CDCl_3 (1 mL), and the NMR spectrum was recorded (*tert*-butyl methyl ether was used as internal standard). Following this, 0.1, 0.25, 0.5, 0.75, 1, 1.5, 2, 3, 4, 5, ... up to 100 equivalents of amine [dissolved in CDCl_3 (0.1M amine stock solution for up to 2 equivalents and 1M amine stock solution for 3 equivalents and above)] was added to the NMR tube; the NMR spectra was recorded after each addition.

Job's plot based on changes in chemical shift of MAPOL ($\Delta\delta_{\text{MAPOL}}$), was obtained with respect to changes in chemical shift ($\Delta\delta$) of one of the MAPOL protons (peak at 7.55 ppm). The molar fraction of MAPOL (X_{MAPOL}) was multiplied by the changes in ^1H -NMR chemical shift of MAPOL ($\Delta\delta_{\text{MAPOL}}$) for each titration data point. The resulting value was plotted against the molar fraction of MAPOL. Peaking at 0.5 mol fraction corresponds to a 1:1 host:guest complex.

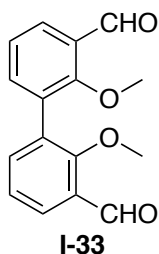
Alternatively, Job's plot analysis based on the chemical shift changes of the amine ($\Delta\delta_{\text{amine}}$) was pursued. The chemical shift changes of the methyl peak (doublet centered at 0.99 ppm) of amine **I-37S**, was chosen for analysis. Changes in chemical shift of the methyl ($\Delta\delta_{\text{amine}}$) was multiplied the by mole fraction of amine (X_{amine}) at each titration data point and the result was plotted against the mole fraction of amine (X_{amine}).

I-8-2 Synthesis of MAPOL I-31:



1,9-Bis(benzoyl)-5-phenyldipyrromethane I-35 was prepared according to previously reported procedures.⁶⁹

¹H-NMR (CDCl₃, 500 MHz); δ 5.66 (s, 1H), 5.98 (m, 1H), 6.58 (m, 2H), 7.32 (t, J = 7.5 Hz, 1H), 7.38 (t, J = 7.5 Hz, 6H), 7.48 (m, 4H), 7.76 (d, J = 7.5 Hz, 4H), 11.12 (br 2H) ppm. ¹³C-NMR (CDCl₃, 125 MHz); δ 44.9, 111.2, 120.9, 127.3, 127.9, 128.7, 128.8, 129.6, 130.9, 131.5, 138.1, 140.3, 141.2, 184.4. TOF MS ES+ (C₂₉H₂₂N₂O₂): Calc. [M + H]⁺: 431.1760, Found [M + H]⁺: 431.1757.

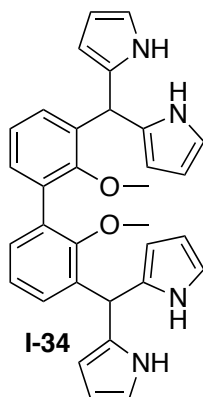


Synthesis of 2,2'-dimethoxy-[1,1'-biphenyl]-3,3'-dicarbaldehyde I-33:

Freshly distilled ether (85 mL) was added to a flame-dried round bottom flask equipped with a magnetic stirring bar, and cooled to -78 °C. To this flask was added 2,2'-dimethoxy-biphenyl **I-32** (3.0 g, 14.0 mmol), *n*-BuLi (2.5 M solution in hexane, 16.8

mL, 42 mmol, 3.0 equiv) and TMEDA (4.8 mL, 42 mmol, 3.0 equiv) dropwise. The reaction mixture was kept at -78 °C for 5 min, and then allowed to warm to room temperature, and stirred for an additional 2.5 h. The solution was once again cooled to -78 °C, and DMF (6.2 mL, 80 mmol) was added slowly over a 10 min period. The reaction mixture was allowed to warm to room temperature, and was immediately quenched with aqueous NH₄Cl solution. The organic layer was extracted with dichloromethane, and solvents were removed under reduced pressure. The crude mixture was purified by column chromatography (silica gel, 10% - 15% EtOAc in hexane) to give **I-33** (2.4 g, 63%) as a white solid.

¹H-NMR (CDCl₃, 300 MHz); δ 3.56 (s, 6H), 7.30 (t J = 7.5, 2H), 7.61 (dd, J_1 = 7.0 Hz J_2 = 1.5 Hz, 2H), 7.89 (dd, J_1 = 7.5 Hz J_2 = 1.5 Hz, 2H), 10.43 (s, 2H). ¹³C-NMR (CDCl₃, 75 MHz); δ 63.1, 124.4, 128.7, 129.5, 131.5, 137.5, 160.9, 189.8. TOF MS ES+ (C₁₆H₁₄O₄): Calc. [M + H]⁺: 271.0970, Found [M + H]⁺: 271.0967.

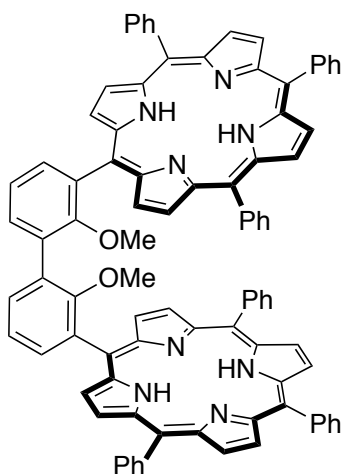


Synthesis of 2,2'-dimethoxy-3,3'-dipyrromethane-1,1'-biphenyl **I-34**:

Following a standard procedure,⁷⁰ bis-aldehyde **I-33** (0.54 g, 2.0 mmol) was dissolved in pyrrole (27.0 mL, 400 mmol). After degassing with a stream of argon for 10

min, InCl_3 (0.40 mmol, 88 mg) was added. The mixture was stirred for 1.5 h at room temperature under atmosphere of argon. The reaction was quenched by addition of NaOH (480 mg, 12.0 mmol) with stirring for an additional 45 min. The reaction mixture was filtered by a Buchner funnel to remove insoluble byproducts. The excess pyrrole was recovered using vacuum distillation. The viscous residue was triturated with hexanes (2 x 15 mL), and the volatiles were evaporated using rotary evaporator. The resultant yellow solid was subjected to column chromatography (hexanes/dichloromethane/ethyl acetate = 7:2:1). The product was isolated as a light yellow solid (840 mg, 83%).

^1H -NMR (500 MHz, CDCl_3); δ 2.97 (s, 3H), 5.79 (s, 2H), 5.89 (m, 4H), 6.11 (dd, $J_1 = 6.0$ Hz, $J_2 = 3.0$ Hz, 4H), 6.67 (m, 4H), 7.08 (dd, $J_1 = 8.0$ Hz, $J_2 = 7.0$ Hz, 2H), 7.15 (dd, $J_1 = 8.0$ Hz, $J_2 = 2.0$ Hz, 2H), 7.27 (dd, $J_1 = 7.0$ Hz, $J_2 = 2.0$ Hz, 2H), 8.27 (br, 4H, NH). ^{13}C -NMR (125 MHz, CDCl_3); δ 155.1, 136.1, 132.1, 130.4, 129.3, 124.0, 116.8, 108.3, 106.8, 60.4, 39.0. TOF MS ES^+ ($\text{C}_{32}\text{H}_{30}\text{N}_4\text{O}_2$): Calc. $[\text{M} + \text{H}]^+$: 503.2447, Found $[\text{M} + \text{H}]^+$: 503.2444.



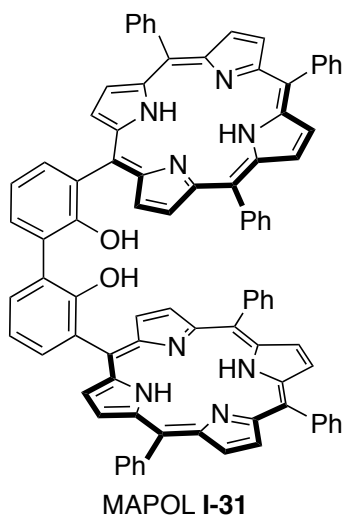
Methoxy-MAPOL **I-36**

Synthesis of Methoxy-MAPOL **I-36**:

Following a standard procedure,⁷¹ to a solution of freshly prepared 1,9-bis(benzoyl)-5-phenyldipyrromethane **I-35** (0.43 g, 1.0 mmol) in dry THF/methanol (10:1, 44 mL) was added NaBH₄ (766 mg, 20.0 mmol) in several portions. After completion of the reduction (TLC 40% EtOAc/Hexanes), saturated NH₄Cl (70 mL) and CH₂Cl₂ (130 mL) were added to the reaction mixture. The organic layer was separated, washed twice with water, dried (Na₂SO₄), and placed in a 1000-mL round-bottomed flask. Removal of the solvent by rotary evaporation under vacuum yielded the dicarbinol as a foamlike yellow solid. To this crude product, dipyrromethane **I-34** (0.23 g, 0.50 mmol) and acetonitrile (400 mL) were added, and the mixture was stirred to achieve a homogeneous yellow solution. TFA (0.93 mL, 12.2 mmol) was added with rapid stirring. After 5 min, DDQ (0.67 g, 3.7 mmol) was added. After stirring for 1 h at room temperature, triethylamine (1.69 mL, 12.2 mmol) was added, and the entire reaction mixture was filtered through a pad of alumina (4 x 8 cm) and washed with CH₂Cl₂ (~ 500 mL) until the eluant was no longer colored. The resulting porphyrin solution was concentrated, redissolved in CH₂Cl₂ (50

mL), and passed through a pad of silica (4 x 8 cm) with CH₂Cl₂ to remove nonporphyrinic pigments. The purple fractions were combined and concentrated to give a purple solid. Precipitation from CH₂Cl₂/methanol gave the pure product **I-36** (62 mg, 9.6%).

¹H-NMR (500 MHz, CDCl₃); δ -2.68 (br, 4H), 3.07 (s, 6H), 7.64 (dd, *J*₁ = 8.0 Hz, *J*₂ = 7.0 Hz, 2H), 7.70-7.85 (m, 18 H), 8.16-8.20 (m, 4H), 8.25-8.31 (m, 12H), 8.93 (m, 12H), 9.08 (m, 4H). ¹³C-NMR (CDCl₃); δ 61.1, 115.9, 120.0, 120.4, 122.0, 126.62, 126.66, 127.6, 127.7, 132.0, 132.3, 134.4, 134.5, 135.3, 135.9, 142.0, 142.2, 158.2. TOF MS ES⁺ (C₉₀H₆₂N₈O₂): Calc. [M + H]⁺: 1287.5074, Found [M + H]⁺: 1287.5117.



Synthesis of MAPOL I-31:

To a sample of methoxy MAPOL **I-36** (50 mg, 0.038 mmol) in dry methylene chloride (100 mL) was added BBr₃ (1.0 M solution in dichloromethane, 0.2 mmol, 0.2 mL) drop-wise under atmosphere of argon at 0 °C. The reaction was stirred at room temperature for 2 h before it was quenched with saturated solution of ammonium

bicarbonate (NH_4HCO_3). The reaction was extracted with methylene chloride, dried (Na_2SO_4), passed through a pad of silica and solvent removed to give a purple solid, which was purified further by precipitation from $\text{CH}_2\text{Cl}_2/\text{MeOH}$ to give the pure MAPOL **I-31** (42 mg, 85%).

^1H -NMR (500 MHz, CDCl_3); δ -2.78 (br, 4H, NH), 6.12 (s, 2H, OH), 7.57 (m, 6H), 7.66 (m, 8H), 7.70-7.75 (m, 6H), 8.06 (d, $J = 7.0$ Hz, 4H), 8.10-8.13 (m, 8H), 8.18 (d, $J = 7.0$ Hz, 4H), 8.74 (d, $J = 4.5$ Hz, 4H), 8.78-8.81 (dd, $J_1 = 11.5$ Hz, $J_2 = 4.5$ Hz), 8.91 (d, $J = 4.5$ Hz, 4H). ^{13}C -NMR (125 MHz, CDCl_3); δ 112.7, 120.2, 120.3, 120.8, 125.8, 126.6, 126.6, 127.6, 127.7, 129.7, 132.7, 134.5, 134.9, 141.8, 142.0, 152.7; IR (film) 3319, 2924, 2853, 1716, 1473, 1441, 1350, 1219, 1176, 1072, 966, 800, 731. TOF MS ES^+ ($\text{C}_{88}\text{H}_{58}\text{N}_8\text{O}_2$): Calc. $[\text{M} + \text{H}]^+$: 1259.4761, Found $[\text{M} + \text{H}]^+$: 1259.4816.

REFERENCES

REFERENCES

1. Berova, N. N., K.; Woody, R., *Circular Dichroism Principles and Applications*. Wiley-VCH: 2000.
2. Dutot, L.; Wright, K.; Wakselman, M.; Mazaleyrat, J. P.; Peggion, C.; De Zotti, M.; Formaggio, F.; Toniolo, C., Central-to-axial chirality transfer and induced circular dichroism in 6,7-dihydro-5H-dibenz[c,e]azepine derivatives of alpha- and beta-amino esters. *Tetrahedron Letters* **2008**, 49 (21), 3475-3479.
3. Lu, H.; Kobayashi, N., Optically Active Porphyrin and Phthalocyanine Systems. *Chemical Reviews* **2016**, 116 (10), 6184-6261.
4. Thomson, W., Kelvin's Baltimore Lectures and Modern Theoretical Physics. Historical and Philosophical Perspectives. *MIT Press*.
5. Dale, J. A.; Dull, D. L.; Mosher, H. S., .alpha.-Methoxy-.alpha.-trifluoromethylphenylacetic acid, a versatile reagent for the determination of enantiomeric composition of alcohols and amines. *The Journal of Organic Chemistry* **1969**, 34 (9), 2543-2549.
6. Dale, J. A.; Mosher, H. S., Nuclear magnetic resonance nonequivalence of diastereomeric esters of .alpha.-substituted phenylacetic acids for the determination of stereochemical purity. *Journal of the American Chemical Society* **1968**, 90 (14), 3732-3738.
7. Dale, J. A.; Mosher, H. S., Nuclear magnetic resonance enantiomer regents. Configurational correlations via nuclear magnetic resonance chemical shifts of diastereomeric mandelate, O-methylmandelate, and .alpha.-methoxy-.alpha.-trifluoromethylphenylacetate (MTPA) esters. *Journal of the American Chemical Society* **1973**, 95 (2), 512-519.
8. Seco, J. M.; Quiñoá, E.; Riguera, R., The Assignment of Absolute Configuration by NMR. *Chemical Reviews* **2004**, 104 (1), 17-118.
9. Seco, J. M.; Quiñoá, E.; Riguera, R., Assignment of the Absolute Configuration of Polyfunctional Compounds by NMR Using Chiral Derivatizing Agents. *Chemical Reviews* **2012**, 112 (8), 4603-4641.
10. Wenzel, T. J.; Wilcox, J. D., Chiral reagents for the determination of enantiomeric excess and absolute configuration using NMR spectroscopy. *Chirality* **2003**, 15 (3), 256-270.

11. Yang, L.; Wenzel, T.; Williamson, R. T.; Christensen, M.; Schafer, W.; Welch, C. J., Expedited Selection of NMR Chiral Solvating Agents for Determination of Enantiopurity. *ACS Central Science* **2016**, 2 (5), 332-340.
12. Kobayashi, N. M., A.; Mack, J., *Circular Dichroism and Magnetic Circular Dichroism Spectroscopy for Organic Chemists*. Royal Society of Chemistry: 2012.
13. Wezenberg, S. J.; Salassa, G.; Escudero-Adan, E. C.; Benet-Buchholz, J.; Kleij, A. W., Effective Chirogenesis in a Bis(metallosalphen) Complex through Host-Guest Binding with Carboxylic Acids. *Angew. Chem., Int. Ed.* **2011**, 50 (3), 713-716, S713/1-S713/25.
14. Kondru, R. K.; Wipf, P.; Beratan, D. N., Theory-Assisted Determination of Absolute Stereochemistry for Complex Natural Products via Computation of Molar Rotation Angles. *Journal of the American Chemical Society* **1998**, 120 (9), 2204-2205.
15. Kondru, R. K.; Wipf, P.; Beratan, D. N., Atomic Contributions to the Optical Rotation Angle as a Quantitative Probe of Molecular Chirality. *Science* **1998**, 282 (5397), 2247.
16. Ribe, S.; Kondru, R. K.; Beratan, D. N.; Wipf, P., Optical Rotation Computation, Total Synthesis, and Stereochemistry Assignment of the Marine Natural Product Pitiamide A. *Journal of the American Chemical Society* **2000**, 122 (19), 4608-4617.
17. Giorgio, E.; Roje, M.; Tanaka, K.; Hamersak, Z.; Sunjic, V.; Nakanishi, K.; Rosini, C.; Berova, N., Determination of the absolute configuration of flexible molecules by ab initio ORD calculations: A case study with cytoxazones and isocytoxazones. *Journal of Organic Chemistry* **2005**, 70 (17), 6557-6563.
18. Giorgio, E.; Viglione, R. G.; Rosini, C., Assignment of the absolute configuration of large molecules by ab initio calculation of the rotatory power within a small basis set scheme: the case of some biologically active natural products. *Tetrahedron-Asymmetr* **2004**, 15 (13), 1979-1986.
19. Giorgio, E.; Viglione, R. G.; Zanasi, R.; Rosini, C., Ab initio calculation of optical rotatory dispersion (ORD) curves: A simple and reliable approach to the assignment of the molecular absolute configuration. *Journal of the American Chemical Society* **2004**, 126 (40), 12968-12976.
20. Hembury, G. A.; Borovkov, V. V.; Inoue, Y., Chirality-sensing supramolecular systems. *Chemical Reviews* **2008**, 108 (1), 1-73.
21. Devlin, F. J.; Stephens, P. J.; Besse, P., Are the absolute configurations of 2-(1-hydroxyethyl)-chromen-4-one and its 6-bromo derivative determined by X-ray crystallography correct? A vibrational circular dichroism study of their acetate derivatives. *Tetrahedron-Asymmetr* **2005**, 16 (8), 1557-1566.

22. Devlin, F. J.; Stephens, P. J.; Cheeseman, J. R.; Frisch, M. J., Prediction of vibrational circular dichroism spectra using density functional theory: Camphor and fenchone. *Journal of the American Chemical Society* **1996**, *118* (26), 6327-6328.
23. Stephens, P. J.; Aamouche, A.; Devlin, F. J.; Superchi, S.; Donnoli, M. I.; Rosini, C., Determination of absolute configuration using vibrational circular dichroism spectroscopy: The chiral sulfoxide 1-(2-methylnaphthyl) methyl sulfoxide. *Journal of Organic Chemistry* **2001**, *66* (11), 3671-3677.
24. Stephens, P. J.; Devlin, F. J.; Cheeseman, J. R.; Frisch, M. J., Calculation of optical rotation using density functional theory. *J Phys Chem A* **2001**, *105* (22), 5356-5371.
25. Nafie, L. A.; Keiderling, T. A.; Stephens, P. J., Vibrational Circular-Dichroism. *Journal of the American Chemical Society* **1976**, *98* (10), 2715-2723.
26. Harada, N. N., K., *Circular Dichroic Spectroscopy: Exciton Coupling in Organic Stereochemistry*. University Science Books: Mill Valley, CA, 1983.
27. Nakanishi, K. B., N., *The Exciton Chirality Method*. VCH Publishers: New York, 1994.
28. Nakanishi, K.; Kuroyanagi, M.; Nambu, H.; Oltz, E. M.; Takeda, R.; Verdine, G. L.; Zask, A., Recent Applications of Circular-Dichroism to Structural Problems, Especially Oligosaccharide Structures. *Pure Appl Chem* **1984**, *56* (8), 1031-1048.
29. Superchi, S.; Casarini, D.; Laurita, A.; Bavoso, A.; Rosini, C., Induction of a preferred twist in a biphenyl core by stereogenic centers: A novel approach to the absolute configuration of 1,2-and 1,3-diols. *Angew Chem Int Edit* **2001**, *40* (2), 451-454.
30. Tartaglia, S.; Padula, D.; Scafato, P.; Chiummiento, L.; Rosini, C., A chemical/computational approach to the determination of absolute configuration of flexible and transparent molecules: Aliphatic diols as a case study. *Journal of Organic Chemistry* **2008**, *73* (13), 4865-4873.
31. Superchi, S.; Bisaccia, R.; Casarini, D.; Laurita, A.; Rosini, C., Flexible biphenyl chromophore as a circular dichroism probe for assignment of the absolute configuration of carboxylic acids. *Journal of the American Chemical Society* **2006**, *128* (21), 6893-6902.
32. Ghosn, M. W.; Wolf, C., Chiral Amplification with a Stereodynamic Triaryl Probe: Assignment of the Absolute Configuration and Enantiomeric Excess of Amino Alcohols. *Journal of the American Chemical Society* **2009**, *131* (45), 16360-+.

33. Ghosn, M. W.; Wolf, C., Synthesis, Conformational Stability, and Asymmetric Transformation of Atropisomeric 1,8-Bisphenolnaphthalenes. *Journal of Organic Chemistry* **2011**, *76* (10), 3888-3897.
34. Ghosn, M. W.; Wolf, C., Enantioselective recognition of amines with an atropisomeric 1,8-bisphenolnaphthalene. *Tetrahedron* **2011**, *67* (36), 6799-6803.
35. Ghosn, M. W.; Wolf, C., Enantioselective CD analysis of amino acids based on chiral amplification with a stereodynamic probe. *Tetrahedron* **2010**, *66* (23), 3989-3994.
36. Wolf, C.; Bentley, K. W., Chirality sensing using stereodynamic probes with distinct electronic circular dichroism output. *Chemical Society Reviews* **2013**, *42* (12), 5408-5424.
37. Barcena, H. S.; Holmes, A. E.; Zahn, S.; Canary, J. W., Redox inversion of helicity in propeller-shaped molecules derived from S-methyl cysteine and methioninol. *Organic Letters* **2003**, *5* (5), 709-711.
38. Zahn, S.; Canary, J. W., Absolute configurations of N,N-dialkyl alpha-amino acids and beta-amino alcohols from exciton-coupled circular dichroism spectra of Cu(II) complexes. *Organic Letters* **1999**, *1* (6), 861-864.
39. Zahn, S.; Canary, J. W., Electron-induced inversion of helical chirality in copper complexes of N,N-dialkylmethionines. *Science* **2000**, *288* (5470), 1404-1407.
40. Joyce, L. A.; Maynor, M. S.; Dagna, J. M.; da Cruz, G. M.; Lynch, V. M.; Canary, J. W.; Anslyn, E. V., A Simple Method for the Determination of Enantiomeric Excess and identity of Chiral Carboxylic Acids. *Journal of the American Chemical Society* **2011**, *133* (34), 13746-13752.
41. Joyce, L. A.; Canary, J. W.; Anslyn, E. V., Enantio- and Chemoselective Differentiation of Protected alpha-Amino Acids and beta-Homoamino Acids with a Single Copper(II) Host. *Chem-Eur J* **2012**, *18* (26), 8064-8069.
42. You, L.; Berman, J. S.; Anslyn, E. V., Dynamic multi-component covalent assembly for the reversible binding of secondary alcohols and chirality sensing. *Nature Chemistry* **2011**, *3* (12), 943-948.
43. You, L.; Pescitelli, G.; Anslyn, E. V.; Di Bari, L., An Exciton-Coupled Circular Dichroism Protocol for the Determination of Identity, Chirality, and Enantiomeric Excess of Chiral Secondary Alcohols. *Journal of the American Chemical Society* **2012**, *134* (16), 7117-7125.
44. You, L.; Berman, J. S.; Lucksanawichien, A.; Anslyn, E. V., Correlating Sterics Parameters and Diastereomeric Ratio Values for a Multicomponent Assembly To

Predict Exciton-Coupled Circular Dichroism Intensity and Thereby Enantiomeric Excess of Chiral Secondary Alcohols. *Journal of the American Chemical Society* **2012**, *134* (16), 7126-7134.

45. Huang, X.; Rickman, B. H.; Borhan, B.; Berova, N.; Nakanishi, K., Zinc porphyrin tweezer in host-guest complexation: determination of absolute configurations of diamines, amino acids, and amino alcohols by circular dichroism. *J. Am. Chem. Soc.* **1998**, *120* (24), 6185-6186.
46. Rele, D.; Zhao, N.; Nakanishi, K.; Berova, N., Acyclic 1,2-/1,3-mixed pentols. Synthesis and general trends in bichromophoric exciton coupled circular dichroic spectra. *Tetrahedron* **1996**, *52* (8), 2759-2776.
47. Wiesler, W. T.; Nakanishi, K., Relative and Absolute Configurational Assignments of Acyclic Polyols by Circular-Dichroism .1. Rationale for a Simple Procedure Based on the Exciton Chirality Method. *Journal of the American Chemical Society* **1989**, *111* (26), 9205-9213.
48. Zhao, N.; Zhou, P.; Berova, N.; Nakanishi, K., Combined synthetic CD strategy for the preparation and configurational assignments of model acyclic 1,3-polyols with a 1,2-diol terminal. *Chirality* **1995**, *7* (8), 636-651.
49. Mizuno, T.; Yamamoto, M.; Takeuchi, M.; Shinkai, S., Sugar 'chirality' sensing using a 'prochiral' salen-Co(II) complex. *Tetrahedron* **2000**, *56* (34), 6193-6198.
50. Zhao, N.; Kumar, N.; Neuenschwander, K.; Nakanishi, K.; Berova, N., Quaternary Ammonium-Salts as Chromophores for Exciton-Coupled Circular-Dichroism - Absolute-Configuration of Hypocholesterolemic Quinuclidines. *Journal of the American Chemical Society* **1995**, *117* (29), 7844-7845.
51. Zhao, N.; Berova, N.; Nakanishi, K.; Rohmer, M.; Mougnot, P.; Jurgens, U. J., Structures of two bacteriohopanoids with acyclic pentol side-chains from the cyanobacterium Nostoc PCC 6720. *Tetrahedron* **1996**, *52* (8), 2777-2788.
52. Skowronek, P.; Gawronski, J., A simple circular dichroism method for the determination of the absolute configuration of allylic amines. *Tetrahedron Letters* **2000**, *41* (16), 2975-2977.
53. Skowronek, P.; Gawronski, J., Absolute configuration of alpha-phthalimido carboxylic acid derivatives from circular dichroism spectra. *Tetrahedron-Asymmetry* **1999**, *10* (23), 4585-4590.
54. Shiota, O.; Nakanishi, K.; Berova, N., Phytosphingosines - A facile synthesis and spectroscopic protocol for configurational assignment. *Tetrahedron* **1999**, *55* (48), 13643-13658.

55. Gimple, O.; Schreier, P.; Humpf, H. U., A new exciton-coupled circular dichroism method for assigning the absolute configuration in acyclic alpha- and beta-hydroxy carboxylic acids. *Tetrahedron-Asymmetr* **1997**, *8* (1), 11-14.
56. Rickman, B. H.; Matile, S.; Nakanishi, K.; Berova, N., A two-step chemical/chiroptical method for determining absolute configurations of alpha-hydroxy acids. *Tetrahedron* **1998**, *54* (20), 5041-5064.
57. Huang, X. F.; Borhan, B.; Rickman, B. H.; Nakanishi, K.; Berova, N., Zinc porphyrin tweezer in host-guest complexation: Determination of absolute configurations of primary monoamines by circular dichroism. *Chem-Eur J* **2000**, *6* (2), 216-224.
58. Huang, X. F.; Fujioka, N.; Pescitelli, G.; Koehn, F. E.; Williamson, R. T.; Nakanishi, K.; Berova, N., Absolute configurational assignments of secondary amines by CD-sensitive dimeric zinc porphyrin host. *Journal of the American Chemical Society* **2002**, *124* (35), 10320-10335.
59. Kurtan, T.; Nesnas, N.; Koehn, F. E.; Li, Y. Q.; Nakanishi, K.; Berova, N., Chiral recognition by CD-sensitive dimeric zinc porphyrin host. 2. Structural studies of host-guest complexes with chiral alcohol and monoamine conjugates. *Journal of the American Chemical Society* **2001**, *123* (25), 5974-5982.
60. Proni, G.; Pescitelli, G.; Huang, X. F.; Nakanishi, K.; Berova, N., Magnesium tetraarylporphyrin tweezer: A CD-sensitive host for absolute configurational assignments of alpha-chiral carboxylic acids. *Journal of the American Chemical Society* **2003**, *125* (42), 12914-12927.
61. Proni, G.; Pescitelli, G.; Huang, X. F.; Quraishi, N. Q.; Nakanishi, K.; Berova, N., Configurational assignment of alpha-chiral carboxylic acids by complexation to dimeric Zn-porphyrin: host-guest structure, chiral recognition and circular dichroism. *Chemical Communications* **2002**, (15), 1590-1591.
62. Li, X. Y.; Tanasova, M.; Vasileiou, C.; Borhan, B., Fluorinated porphyrin tweezer: A powerful reporter of absolute configuration for erythro and threo diols, amino alcohols, and diamines. *Journal of the American Chemical Society* **2008**, *130* (6), 1885-1893.
63. Li, X. Y.; Borhan, B., Prompt Determination of Absolute Configuration for Epoxy Alcohols via Exciton Chirality Protocol. *Journal of the American Chemical Society* **2008**, *130* (48), 16126-+.
64. Li, X. Y.; Burrell, C. E.; Staples, R. J.; Borhan, B., Absolute Configuration for 1,n-Glycols: A Nonempirical Approach to Long-Range Stereochemical Determination. *Journal of the American Chemical Society* **2012**, *134* (22), 9026-9029.

65. Tanasova, M.; Yang, Q. F.; Olmsted, C. C.; Vasileiou, C.; Li, X. Y.; Anyika, M.; Borhan, B., An Unusual Conformation of alpha-Haloamides Due to Cooperative Binding with Zincated Porphyrins. *European Journal of Organic Chemistry* **2009**, (25), 4242-4253.
66. Tanasova, M.; Anyika, M.; Borhan, B., Sensing Remote Chirality: Stereochemical Determination of beta-, gamma-, and delta-Chiral Carboxylic Acids. *Angew Chem Int Edit* **2015**, 54 (14), 4274-4278.
67. Yang, Q.; Olmsted, C.; Borhan, B., Absolute Stereochemical Determination of Chiral Carboxylic Acids. *Organic Letters* **2002**, 4 (20), 3423-3426.
68. Anyika, M.; Gholami, H.; Ashtekar, K. D.; Acho, R.; Borhan, B., Point-to-Axial Chirality Transfer—A New Probe for “Sensing” the Absolute Configurations of Monoamines. *Journal of the American Chemical Society* **2014**, 136 (2), 550-553.
69. Geier, G. R.; Chick, J. F. B.; Callinan, J. B.; Reid, C. G.; Auguscinski, W. P., A Survey of Acid Catalysis and Oxidation Conditions in the Two-Step, One-Flask Synthesis of Meso-Substituted Corroles via Dipyrromethanedicarbinols and Pyrrole. *The Journal of Organic Chemistry* **2004**, 69 (12), 4159-4169.
70. Laha, J. K.; Dhanalekshmi, S.; Taniguchi, M.; Ambroise, A.; Lindsey, J. S., A scalable synthesis of meso-substituted dipyrromethanes. *Org Process Res Dev* **2003**, 7 (6), 799-812.
71. Rao, P. D.; Dhanalekshmi, S.; Littler, B. J.; Lindsey, J. S., Rational syntheses of porphyrins bearing up to four different meso substituents. *Journal of Organic Chemistry* **2000**, 65 (22), 7323-7344.

Chapter II: Determination of absolute configuration of chiral molecules (chiral cyanohydrins, sulfoxides, phosphine oxides and alcohols)

II-1 Determination of absolute configuration of chiral cyanohydrins

With the successful utilization of MAPOL for determining the absolute configuration of chiral monoamines,¹ we sought to expand the applicability of this host system to determine the absolute configuration of other functionalities. Specifically, we set out to target functionalities that chiroptical techniques, specifically porphyrin tweezers methodologies, have failed to provide a robust and reliable means for determination of absolute configuration. For this purpose, chiral cyanohydrins were selected as a target functionality. Chiral cyanohydrins are versatile intermediates in organic synthesis since they can be easily converted into a variety of other chiral functional groups such as α -

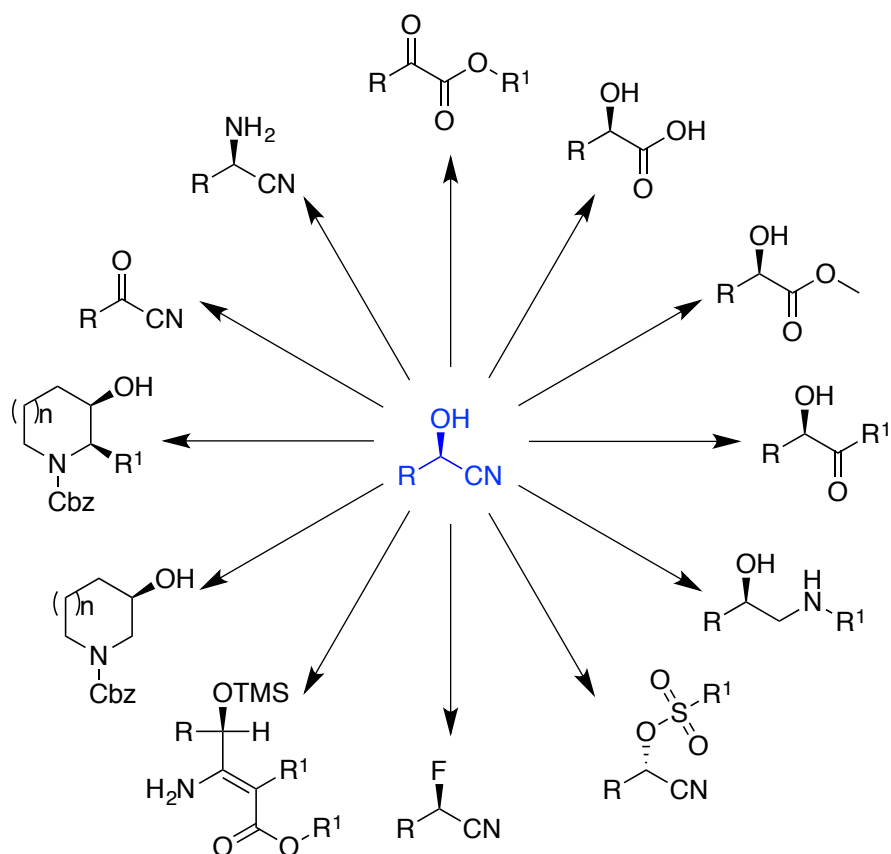
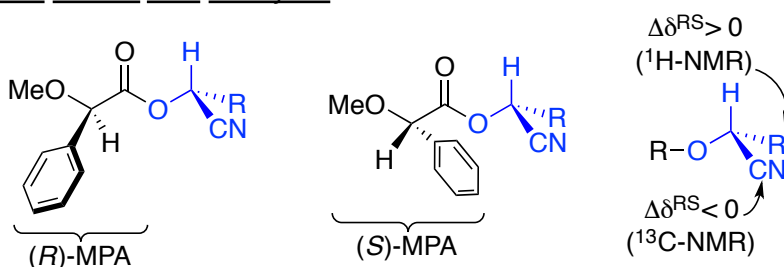


Figure II-1. Synthetic utility of cyanohydrin moiety.

hydroxyacids, α -hydroxyketones, hydroxyamines, α -aminonitriles, and α -hydroxy esters (Figure II-1).³⁻⁴

Chiral cyanohydrins can be readily accessed through asymmetric addition of cyanide to aldehydes and ketones. Over the past few decades many different catalytic systems have been reported for the synthesis of this chiral moiety. Despite enormous advancements in the synthesis of chiral cyanohydrins, a direct, general and practical method for the absolute stereochemical determination of this functionality is lacking. The current state of the art in the determination of absolute configuration of chiral cyanohydrins is based on NMR analysis of their diastereomeric Mosher ester derivatives.⁵⁻⁸ Following typical assumptions in the Mosher ester analysis, models for the most stable conformer of the diastereomeric derivatives are utilized to explain the chemical shift changes and provide a route for the assignment of stereochemistry. For cyanohydrins derived from aldehydes, the co-planarity of the hydrogen atom on the chiral carbon with the carbonyl group of the Mosher ester is the key feature in the proposed

a. Cyanohydrins derived from aldehydes



b. Cyanohydrins derived from ketones

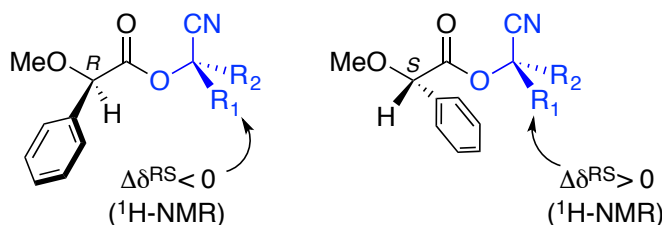


Figure II-2. Mosher's method determination of absolute configuration of chiral cyanohydrins.

model. With this alignment and the Mosher method assumption of *anti*-alignment of the methoxy group and the C-O ester bond of the MPA acid, the groups on the chiral carbon either will eclipse the phenyl group of the Mosher ester or be on the opposite face. The anisotropic effect of the phenyl group results in shielding of the nuclei that are eclipsed (Figure II-2). Interpretation of the shielding or deshielding of the substituent provides the absolute configuration of the chiral cyanohydrin center. In this particular case the effect of the Mosher ester on the ^1H -NMR of the group attached to the cyanohydrin center as well as the changes on the ^{13}C -NMR of the nitrile group are used for assignment of absolute configuration. The same analogy can be used for cyanohydrins derived from ketones. In these substrates, upon derivatization with Mosher acid, the nitrile group as the smallest group on the stereogenic carbon, will be co-planar with the ester carbonyl. In cyanohydrins derived from ketones, change in the ^1H -NMR of both substituents attached to the chiral center will be used as a probe for the determination of absolute configuration. These techniques rely heavily on predicting conformational distribution of populations that affect the resultant NMR spectra.

Another NMR-based approach for determining the absolute configuration of chiral cyanohydrins is the use of chiral solvating agents.⁹⁻¹⁰ Chiral solvating agents function non-covalently, *i.e.* via hydrogen bonding, interact with chiral cyanohydrins. Similar to Mosher ester analysis, the anisotropic effect of the substituents on the chiral solvating agent causes a shift in the ^1H -NMR of the groups on the chiral cyanohydrin. The absolute configuration of cyanohydrins can be assessed utilizing the proposed models (Figure II-3). The advantage of chiral solvating agents over Mosher method is the elimination of the

derivatization step. Nonetheless, the non-covalent interaction between solvating agent and the guest molecule can complicate the results as the nature of interactions is heavily depending on the structure of the target molecule, solvent composition, temperature, etc.

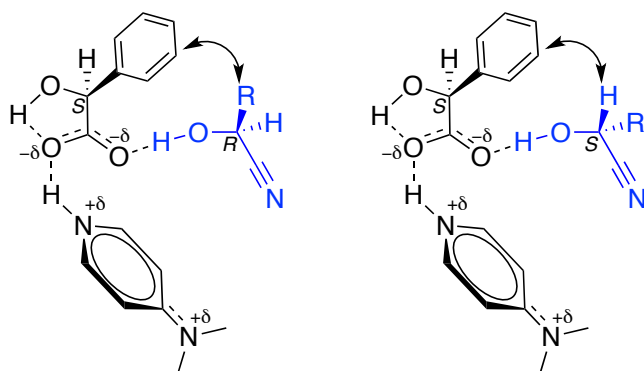


Figure II-3. Application of chiral solvating agents for determining the absolute configuration of chiral cyanohydrins.

On the other hand, chiroptical techniques, despite their intrinsic sensitivity to asymmetry as well as their propensity for rapid and micro-scale analysis, have not provided a routine method for the analysis of this functional group. The main shortcoming in this area has been devising a host system that can form stable and ECCD active complexes with chiral cyanohydrins. We set out to remedy the shortcoming in this area utilizing our MAPOL-based host:guest complexation methodology. This host system is capable of sensing the chiral information from the bound guest molecules and function as a reporter of chirality. Our goal was set to sense the absolute configuration of chiral cyanohydrins in a reliable, predictable and readable fashion. In addition, we planned to take advantage of the high sensitivity of the chiroptical techniques to devise a rapid, microscale and non-empirical methodology for assignment of absolute configuration of cyanohydrins.

At first glance, the cyanohydrin moiety has two potential binding sites, the hydroxyl and the nitrile groups, that are located on the chiral carbon with tetrahedral geometry. Our initial approach was to exploit both of these potential binding sites to drive a complex formation with perfluorinated porphyrin tweezers. As such, porphyrin tweezers such as C3-Zn-TPFP-tz (**II-1**) and C5-Zn-TPFP-tz (**II-2**)¹¹ were complexed with the synthesized chiral cyanohydrin **II-6R** (Figure II-4).

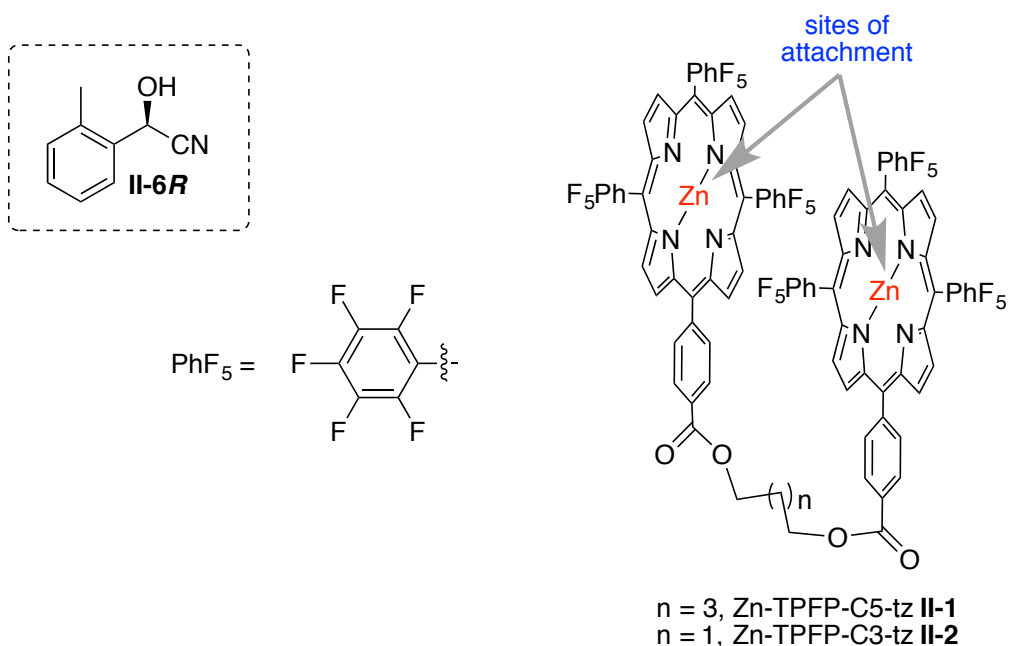


Figure II-4. Porphyrin tweezers and their envisioned complexation with chiral cyanohydrins for determination of absolute configuration.

Not surprisingly, under various complexation conditions, no ECCD signal was observed. This can be attributed to multiple reasons, with employing chiral cyanohydrins as a bidentate guest molecule. The fact that both of the coordinating sites (nitrile and hydroxyl group) are located on the same tetrahedral carbon might preclude concurrent coordination of both groups to the zinc of the host system. Furthermore, Zn-TPFP porphyrins are Lewis acidic enough for coordination of oxygen based nucleophiles,

via introducing electron-withdrawing groups (EWG) on the backbone of MAPOL could potentially facilitate hydrogen bonding interaction by generating more acidic hydroxyl groups. However, as it will be discussed in detail in section II-4, MAPOL with fluorinated backbone proved to be incompetent for complex formation with alcohols.

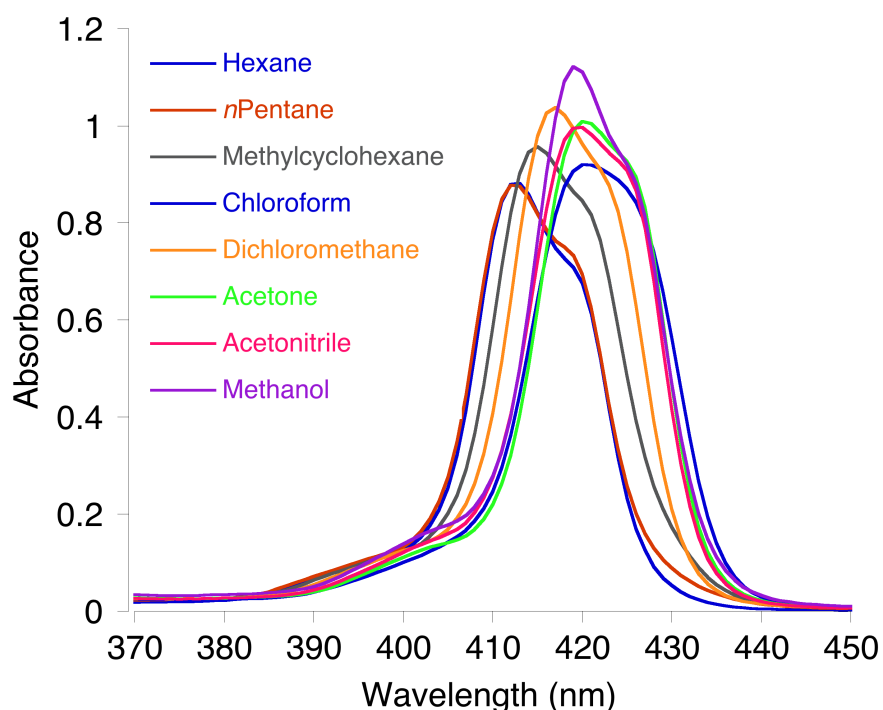


Figure II-6. UV-vis spectra of Zn-MAPOL (1 μ M) in different solvents at room temperature.

Alternately, porphyrin rings in MAPOL can be potentially utilized as binding sites for complex formation with chiral cyanohydrins. We sought inclusion of metal in these porphyrin rings in order to provide additional coordinating sites to enable ECCD active complex formation with chiral cyanohydrins. MAPOL was zincated with zinc acetate to form Zn-MAPOL (**II-4**) and the presence of zinc at the center of the porphyrin ring was confirmed using ^1H NMR (disappearance of pyrrolic NH peaks).

Zn-MAPOL has a strong UV absorption with λ_{max} at 413 nm in hexanes. Figure II-6 illustrates the UV spectra of Zn-MAPOL in different solvents. A solution of Zn-MAPOL in

hexane was complexed with chiral cyanohydrin **II-6R**. Gratifyingly, strong ECCD signal was observed (Figure II-7). ECCD titration of Zn-MAPOL with different equivalents of cyanohydrin **II-6R** revealed that the amplitude of ECCD signals increases with higher equivalents of cyanohydrins. Saturation of the signal was observed at around 300 equivalents of cyanohydrin (Figure II-7, right).

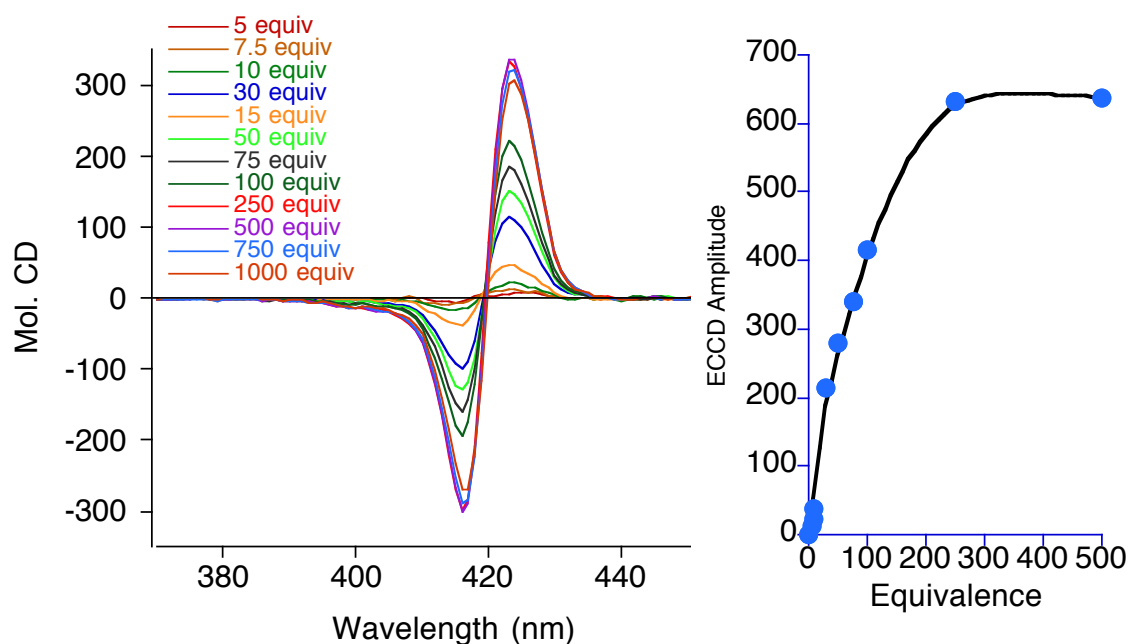


Figure II-7. ECCD spectra of Zn-MAPOL complexed with (*R*)-2-hydroxy-2-(*o*-tolyl)acetonitrile **II-6R**.

The ECCD signal can be detected after addition of 5 equivalents of chiral cyanohydrin. This accounts for less than 1 μg of cyanohydrin that is required for determination of its absolute configuration. Furthermore, the method eliminates preparative chemistries and ECCD signal can be obtained in minutes.

Traditionally, hexane has been utilized as the solvent of choice for host:guest complex formation and ECCD measurements using the porphyrin tweezers methodology. The low polarity of hexane and other nonpolar solvents minimizes solvent-solute

interactions and consequently facilitates the host:guest complex formation. Indeed, only non-polar solvents result in formation of ECCD active complex of cyanohydrin and Zn-MAPOL (Figure II-8). The complex of Zn-MAPOL and cyanohydrin **II-6R** in hexane and pentane yield high ECCD amplitudes, while signal with lower intensity was observed when methyl cyclohexane was used as solvent. Nonetheless, ECCD signal was not observed in polar solvents such as dichloromethane, acetone, methanol, etc.

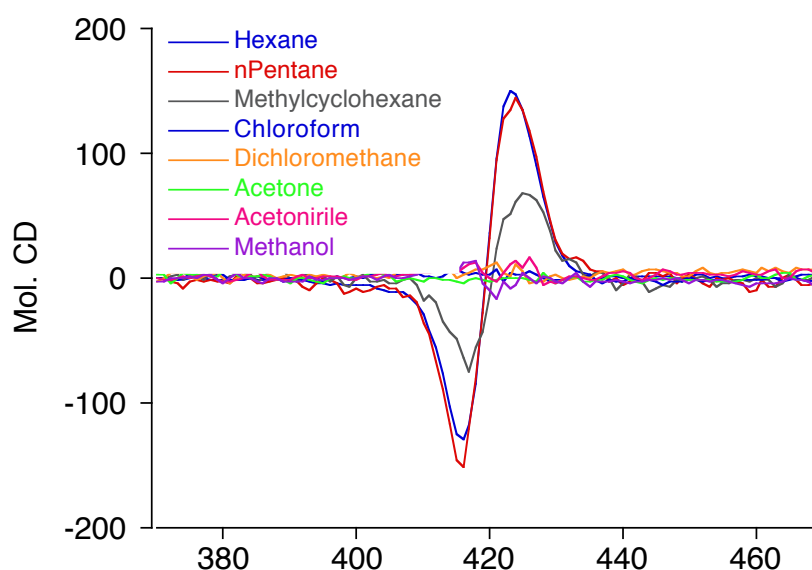


Figure II-8. ECCD spectra of Zn-MAPOL (1 μ M) complexed with (*R*)-2-hydroxy-2-(*o*-tolyl)acetonitrile **II-6R** (50 equivalents) in different solvents at 0 $^{\circ}$ C

The solvent-solute interaction can be observed in the UV spectrum of Zn-MAPOL in different solvents (Figure II-6). Zn-MAPOL in hexane and pentane has similar UV-vis spectra with λ_{max} at 413 nm. In more polar solvents, the UV-vis spectrum of Zn-MAPOL red shifts, along with increase in the absorption. This can be due to coordination to the zinc centered porphyrin or conformational changes of the host system.

The ECCD of the host:guest complex is sensitive to the temperature of CD measurement. Stronger ECCD signals (higher amplitude of the signal) were observed at

lower temperatures. Upon increasing temperature, the intensity of the ECCD signal decreases, and above 40 °C the system becomes ECCD silent (Figure II-9). The trend shows a decay in the signal amplitude as a function of temperature. The decrease in the ECCD signal can be explained considering the fact that the low energy differences between the equilibrating diastereomeric atrop-isomers can be overcome at higher temperatures.

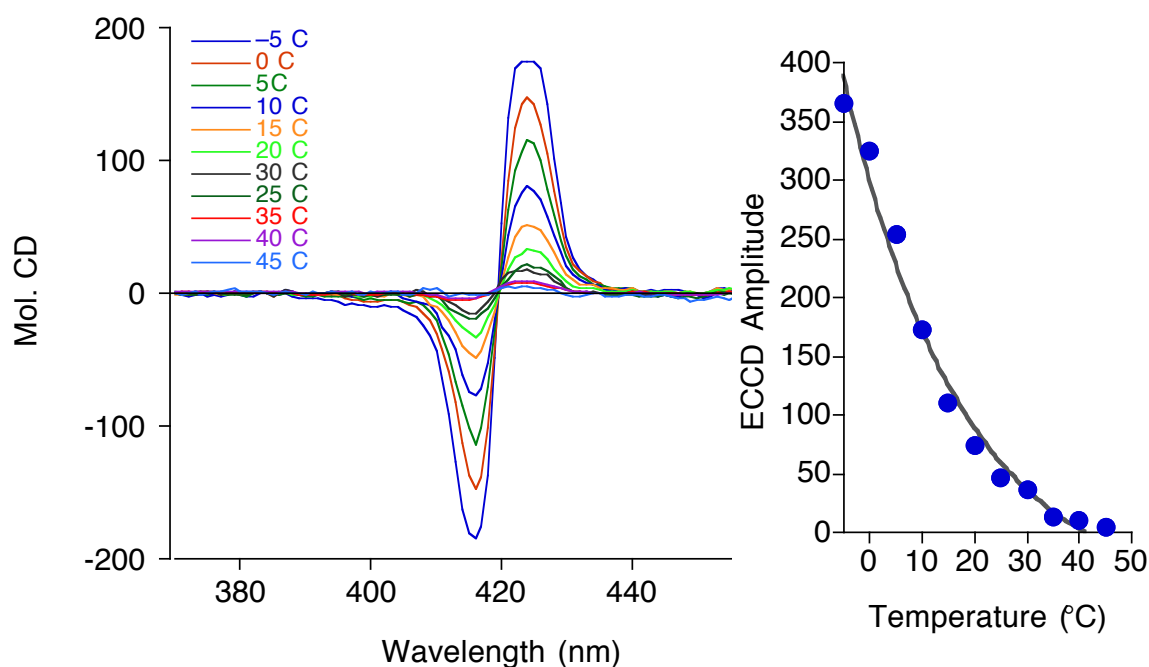


Figure II-9. ECCD spectra of Zn-MAPOL complexed with (*R*)-2-hydroxy-2-(*o*-tolyl) acetonitrile **II-6R** (50 equivalents) at different temperatures.

Next, we turn our attention to the generality of the method for complex formation with different chiral cyanohydrins. A diverse set of chiral cyanohydrins was synthesized following reported procedures.¹²⁻¹⁵ Hexane was used as solvent and ECCD measurements were performed at 0 °C with 1 μ M Zn-MAPOL and 50 equivalents of chiral

cyanohydrins. As depicted in Table II-1, all surveyed cyanohydrins, derived from both aldehydes and ketones, gave strong ECCD signals.

Table II-1. Predicted and observed ECCD for cyanohydrins complexed with Zn-MAPOL.

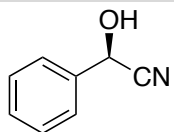
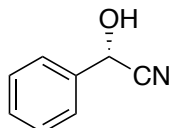
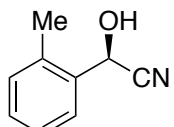
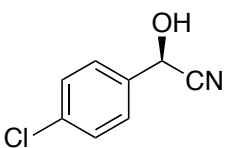
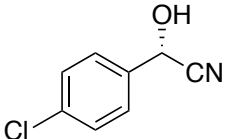
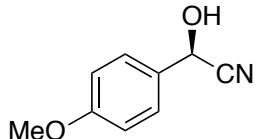
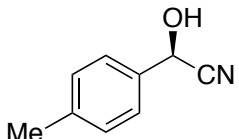
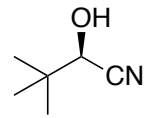
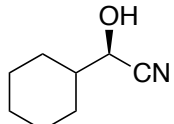
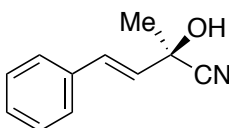
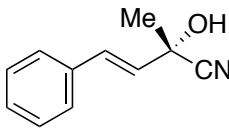
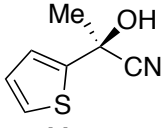
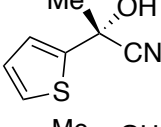
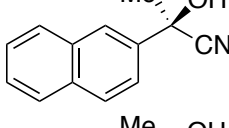
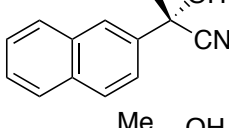
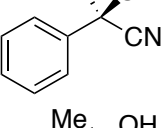
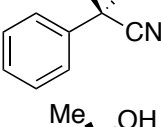
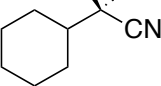
entry ^a	sulfoxide	Pred.	λ nm ($\Delta\epsilon$)	A/A_{corr} ^c	
1		II-5R	pos	424, +142 415, -101	+243/+282
2		II-5S	neg	424, -14 414, +25	-39/-278
3		II-6R	pos	423, +151 416, -130	+281/+312
4		II-7R	pos	423, +97 414, -107	+204/+211
5		II-7S	neg	423, -51 414, +55	-106/-200
6		II-8R	pos	423, + 124 415, -85	+209/+214
7		II-9R	pos	423, +92 415, -93	+185/+190
8		II-10R	pos	425, +43 416, -23	+66/+150
9		II-11R	pos	424, +99 415, -97	+196/+242

Table II-1 (cont'd)

entry ^a	sulfoxide	Pred.	λ nm ($\Delta\epsilon$)	A/A_{corr} ^c	
10		II-12S	pos	424, +46 415, -56	+102/+112
11		II-12S	neg	425, -54 415, +39	-93/-109
12		II-13S	pos	425, +49 415, -29	+78/+96
13		II-13R	neg	423, -45 414, +42	-87/-98
14		II-14R	pos	425, +42 416, -23	+65/+75
15		II-14S	neg	425, -32 414, +39	-71/-76
16		II-15R	pos	425, +45 415, -30	+75/+95
17		II-15S	neg	425, +44 416, -42	-86/-97
18		II-16R	pos	425, +28 418, -38	+66/+146

[a] All CD measurements were performed with 1 μM Zn-MAPOL in hexane at 0 $^{\circ}\text{C}$; 50 equiv of cyanohydrin were used to record the data. [b] Corrected amplitude based on the *ee* of the cyanohydrins. [c] For ketones, 2 μM Zn-MAPOL was used for analysis. [d] Due to the low *ee* of the substrate, 100 equiv was used for complexation.

Of note are the enantiomers that give opposite signals with comparable amplitude when the enantiopurity of the cyanohydrin sample is taken into account ($A_{\text{corr.}}$). Furthermore, the amplitude of the ECCD signal of cyanohydrins derived from aldehydes is generally higher than that of cyanohydrins derived from ketones. A better stereo-differentiation of substituents on the chiral center (hydrogen versus R group) or stronger binding interaction (less steric repulsion) is most probably responsible for the higher ECCD amplitude of cyanohydrins derived from aldehydes. Furthermore, since the predicted sign arises from the relative size of the substituents on the chiral center, thus the predicted sign of ECCD signal is independent of the assignment of configuration (*R* or *S*). The *R/S* assignment is derived from Cahn-Ingold-Prelog rules that only considers the atomic number of substituents.

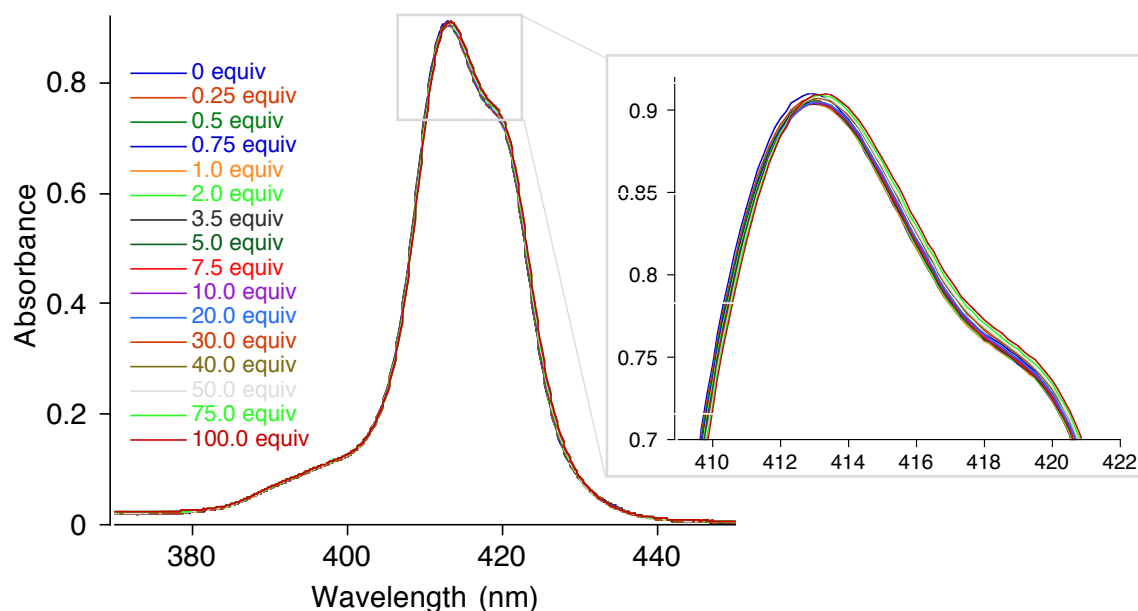


Figure II-10. UV-vis spectra of Zn-MAPOL complexed with (*R*)-2-hydroxy-2-(*o*-tolyl)-acetonitrile **II-9R**.

In Table II-1 we report the ECCD amplitude at 50 equivalents (50 μ M) of added cyanohydrins. It should be noted that the signal could be observed at lower equivalents. Generally, aldehyde derived cyanohydrins give clear signal at around 5-10 equivalents while for the ketone derived cyanohydrins 10-20 equivalents of the guest molecule is required to have a reliable signal.

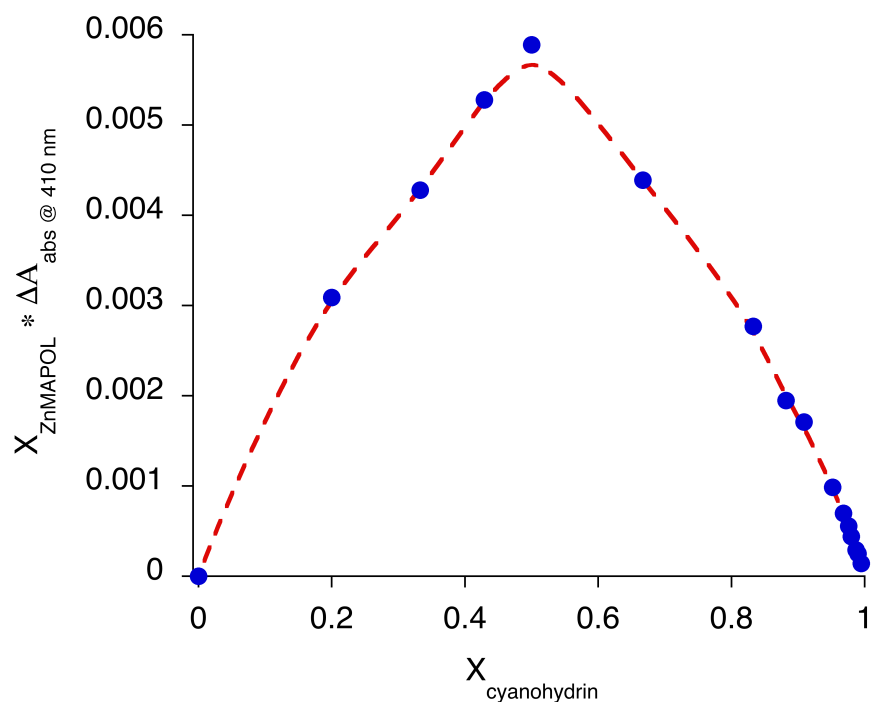


Figure II-11. Job's plot of Zn-MAPOL with (*R*)-4-methylmandelonitrile **II-9R** absorbance at 410 nm.

The stoichiometry of the complex between cyanohydrins and Zn-MAPOL was determined employing Job's plot analysis. Job's plot was derived by following the changes in the UV-vis absorption (at 410 nm) of the complex upon increasing the equivalents of cyanohydrin (Figure II-11). A peak at 0.5 mole fraction of cyanohydrin is indicative of 1:1 host/guest complex formation.

With this working methodology in hand, we sought to propose a binding model that can provide a mean for prediction of the sign of ECCD signals, enabling a solution for the

determination of absolute configuration of cyanohydrins. As such, we required a better understanding of the bonding paradigm involved in the complex formation between cyanohydrins and Zn-MAPOL. Both components of the complex (Zn-MAPOL and cyanohydrin) are capable of forming a bidentate interaction. Zn-MAPOL consists of hydrogen bonding elements (via hydroxyl groups) and coordination interaction (via the zinc centered porphyrin rings).

Cyanohydrins, on the other hand, have hydroxyl group and nitrile moiety that both can be potentially involved in the hydrogen bonding or coordination interactions. A dual bonding host system was required to give rise to the observed ECCD signal. As discussed at the beginning of this chapter, MAPOL with only the hydrogen bonding element failed to produce an ECCD active complex with chiral cyanohydrins. Furthermore, weakening the hydrogen bonding capability of the host system, by replacing the hydroxyl groups of the host (Zn-MAPOL) with methoxy groups (Zn-MAPOL-OMe), failed to produce consistent ECCD signals with chiral cyanohydrins. Nonetheless, some of the chiral cyanohydrins did yield ECCD signals upon complexation with Zn-MAPOL-OMe, however the intensity of the signals was low. It should be noted that Zn-MAPOL-OMe can still act as hydrogen bond acceptor through the oxygen atoms and similar bonding regime as Zn-MAPOL can be anticipated. As a result, generation of ECCD active complex between some of the cyanohydrins and this host system is not unexpected.

In order to delineate the effect of each of the binding elements on the generation of host:guest complex, the chiroptical behavior of the ECCD active complex of cyanohydrin **II-6R** (50 equiv) with Zn-MAPOL in the presence of binding competitors was interrogated. The objectives were to introduce molecules that have similar binding moieties as cyanohydrins to the ECCD active complex and follow the effects on the ECCD signal. Acetonitrile was used to compete with the nitrile group of cyanohydrins and methanol was used as competitor of the hydroxyl group of cyanohydrins. These were added to the ECCD active **II-6R**:Zn-MAPOL complex individually. The amplitude of the signal decreases upon addition of these bonding competitors and complete eradication of the ECCD signal was observed at around 2000 equivalent of methanol (Figure II-12) and 4000 equivalents of acetonitrile (Figure II-13). It can be noted that the decay of the signal is much faster when methanol is added to the ECCD active complex as compared to

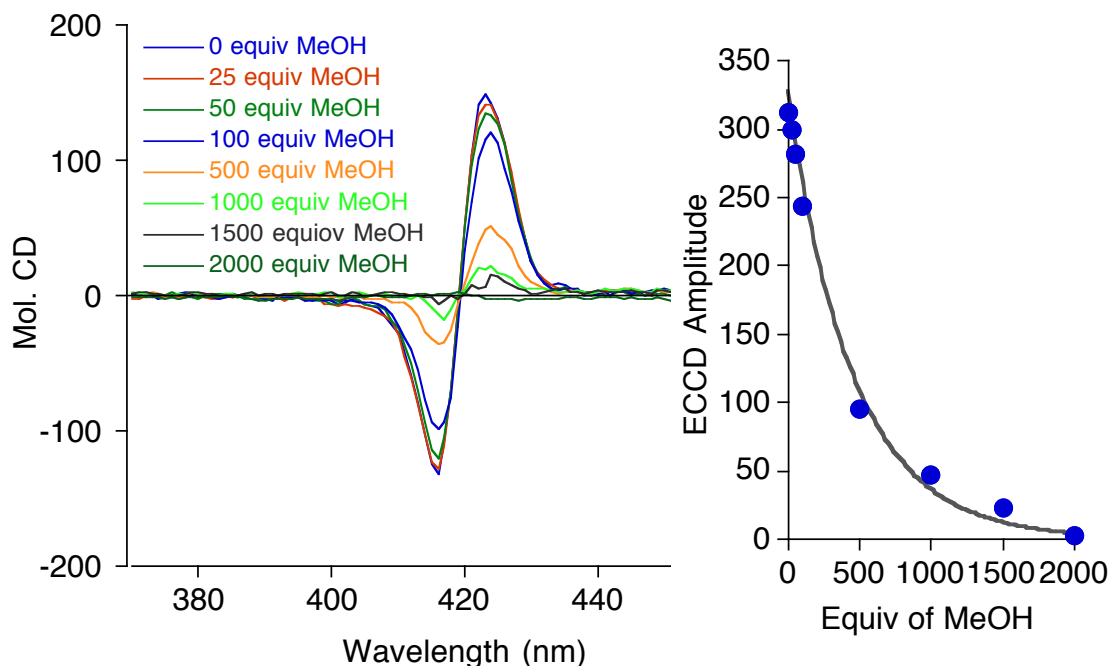


Figure II-12. Quenching the ECCD signal of **II-6R** in complex with Zn-MAPOL by addition of methanol.

addition of acetonitrile. This can potentially indicate that the hydroxyl group of cyanohydrin is the main binding element in the complex formation and disrupting this bonding element has a more profound effect on the strength of the ECCD signal.

Additionally, chemical intuition suggests that hydroxyl groups are better hydrogen bonding donors and acceptors than nitrile groups. We envisioned the bonding paradigm in which the hydroxyl group of the cyanohydrin is involved in hydrogen bonding with the biphenol core while the nitrile is coordinated with the metallo center.

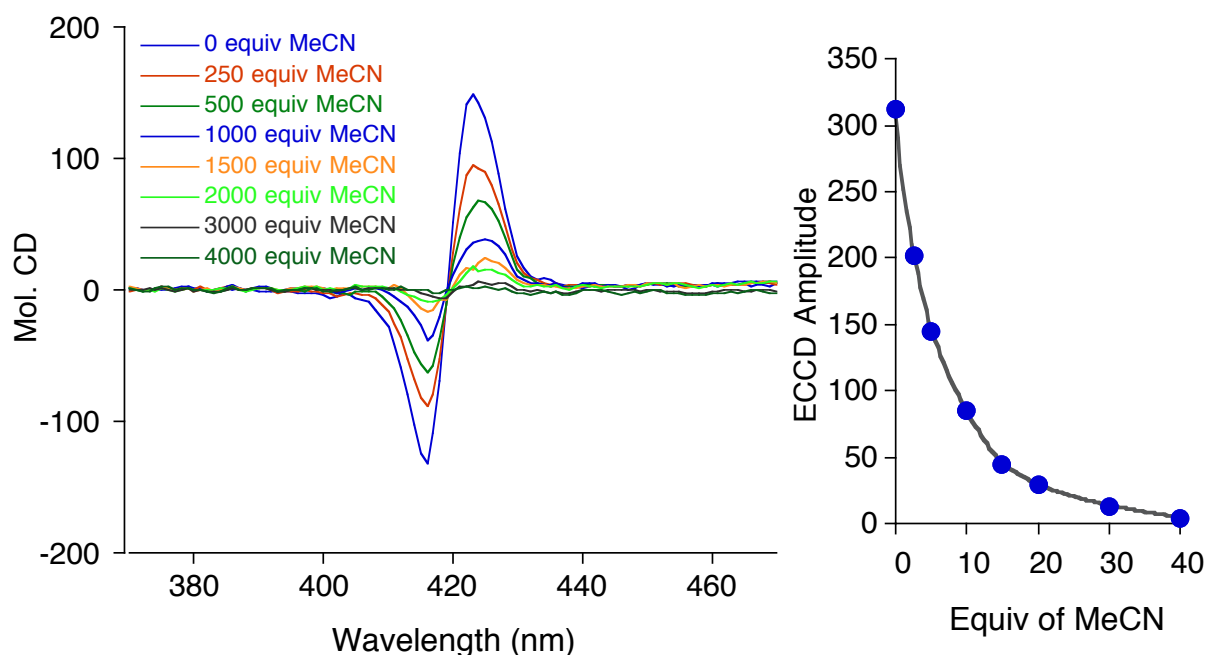


Figure II-13. Quenching the ECCD signal of **II-6R** in complex with Zn-MAPOL by addition of acetonitrile (MeCN).

With this proposed binding mode, the following mnemonic is presented (Figure II-14). Hydroxyl group of cyanohydrin is pointing towards the center of Zn-MAPOL to form a hydrogen-bonding network with the backbone of the host system. The nitrile group concurrently points towards the zinc in the center of one of the porphyrin rings. These two

binding interactions place the chiral tetrahedral carbon in the center of the host system and the induction of point chirality of cyanohydrin to the axial chirality of the host system can take place.

Much akin to the discussion that was presented for complexation of chiral amine with MAPOL, minimization of steric repulsion is the determinant factor that leads to the preferred helicity. As shown in Figure II-14, in the *R*, *M* complex the larger group (Ar) based on A-value as the operating steric parameter,¹⁶ is in the sterically congested position. The repulsion between the porphyrin ring and the aryl group causes this complex to be less favorable. On the other hand, in the *R*, *P* complex, the large substituent on the chiral center is positioned in the open quadrant and the smaller group (hydrogen) is

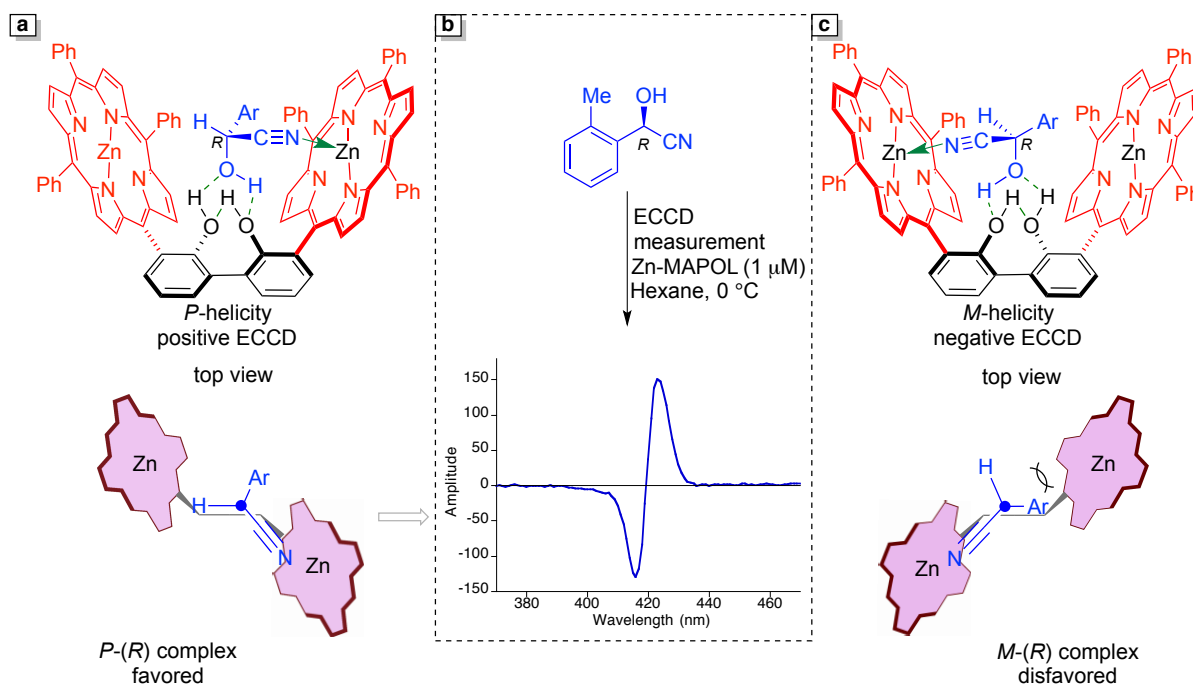


Figure II-14. a) Bidentate binding of **II-6R**, with the *P*-helicity of Zn-MAPOL, places the large aryl group in the most sterically available position. This favorable arrangement leads to the anticipated positive ECCD spectrum. b) Complexation of **5R** with Zn-MAPOL leads to a strong positive ECCD signal. c) The same bidentate binding with the *M*-helicity leads to steric clash of the large aryl group with the porphyrin ring. Thus, negative ECCD with **II-6R** bound to Zn-MAPOL is not anticipated.

placed in close proximity of the porphyrin ring. One would expect this complex to be more stable.

Since the helicity of this complex (*P*) generates a clockwise twist of the interacting chromophores, a positive ECCD signal is expected. Indeed, the experimental measurement confirmed the positive sign of the ECCD signal. The same analogy can be used for cyanohydrins in Table II-1 and the predicted ECCD signals are in agreement with the experimental ECCD signals. This working model can be used to determine the absolute configuration of chiral cyanohydrin with only considering the relative size of the substituents on the chiral carbon. The relative size of the substituents is used to determine the preferred helicity. A-values as thermodynamic steric parameters, are used as a general guiding tool for assignment of relative size (small versus large) of substituents on the chiral carbon.

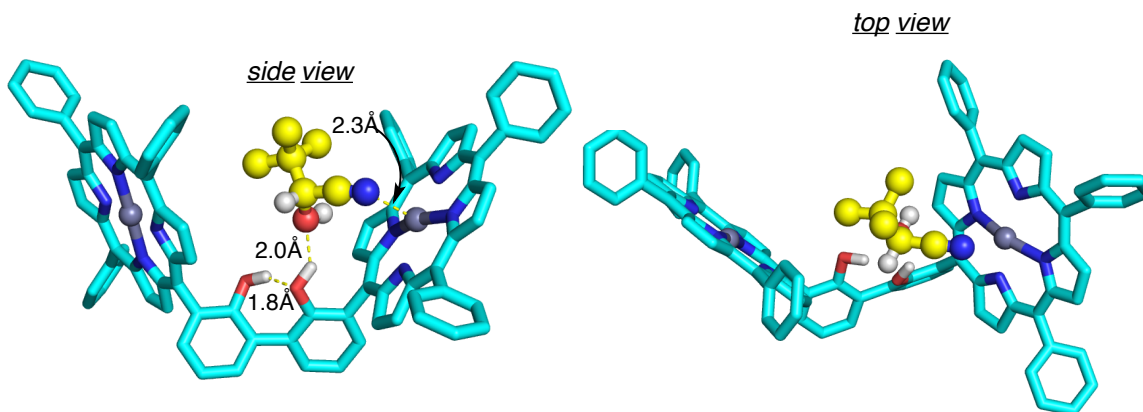


Figure II-15. Side and top view of geometry optimized (DFT-B3LYP/6-31G^{*}) complex of **II-10R** bound to Zn-MAPOL. The model shows the bulky t-butyl group in the open quadrant, the hydrogen bonding of the alcohol with the biphenol core, and the interaction of the cyano group with the metal center. The optimized geometry predicts a positive ECCD, as observed.

Figure II-15 illustrates an energy minimized model for **II-10R** bound to Zn-MAPOL in the proposed orientation that leads to the observed ECCD. Of note are the structural features such as the ordinary bond angles and lengths for hydrogen bonding and coordination to the metallocenter that corroborate the proposed model in Figure II-15.

In addition to the application of the technique for determination of the absolute configuration of chiral cyanohydrins, the method can be utilized for determining the enantiopurity of the cyanohydrin sample. The amplitude of ECCD signal is linearly correlated to the enantiopurity of the chiral samples. This in fact is one of the most important properties of chiroptical techniques that enables analysis of samples that are not necessarily enantio-pure. The diastereomeric complexes arising from two enantiomers of a molecule that are bound to the host system would have opposite ECCD signals and the excess enantiomer would lead to the observed signal. Samples with low enantio-purity can be an issue if Mosher ester or any other techniques are used for determination of the absolute configuration. In those techniques, sample with low *ee* would lead to the generation of diastereomers that need to be separated before analysis and it can complicate the assignment of configuration. We further take advantage of this unique property of chiroptical techniques to assess the enantio purity of the cyanohydrin sample. To this end, a standard curve was derived from correlating the ECCD amplitude with the enantiopurity of the cyanohydrin samples (Figure II-16). A linear fit with high regression ($R^2 = 0.998$) was accessed upon complexation of cyanohydrin **II-7** with Zn-MAPOL. The derived standard curve could be used to measure the *ee* of unknown samples.

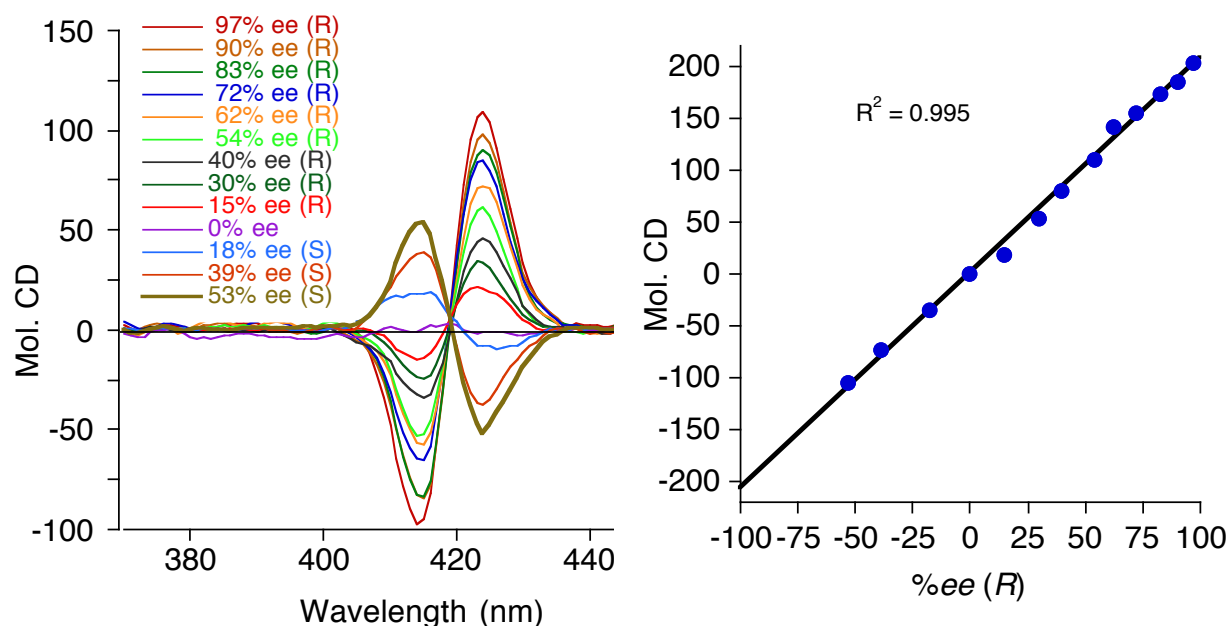


Figure II-16. ECCD spectra of Zn-MAPOL (1 μM) complexed with 4-chloromandelonitrile **II-7** (50 equiv) at different enantio excess (left). The plot of ECCD amplitude versus %ee.

In summary, we report on the use of a new host system for the absolute stereochemical determination of cyanohydrins in a non-empirical fashion. This constitutes the first direct methodology that enables a reliable and rapid assignment for the absolute stereochemistry of cyanohydrins. This is a microscale method that requires no derivatization and yields the results in a matter of minutes. The stereochemistry is reliably extracted from the CD spectra by assuming hydrogen bonding of the alcohol to the biphenol core, coordination of the cyano group with the zincated porphyrin, and minimizing steric interactions by placing the large group in the most unhindered quadrant.

II-2 Determination of absolute configuration of chiral sulfoxides

The ubiquitous nature of the chiral carbon atom, in every facet of science as it relates to the structure of an organic molecule, has led to tremendous activity for assigning its absolute stereochemistry. The chiral sulfur atom has enjoyed much less attention, although one can argue it is no less important. In its oxide form, the sulfur atom can be asymmetric, with similarly profound impact on its chemical and spectroscopic characteristics, as well as its biological activity. From a substantial list of biologically active sulfoxide containing molecules,¹⁷ Nexium® (one of the world's highest selling drugs), oxisurane, and armodafinil are examples of important pharmaceuticals that share the same commonality; the sulfoxide is the only asymmetric center in these molecules (Figure II-17).¹⁸⁻¹⁹

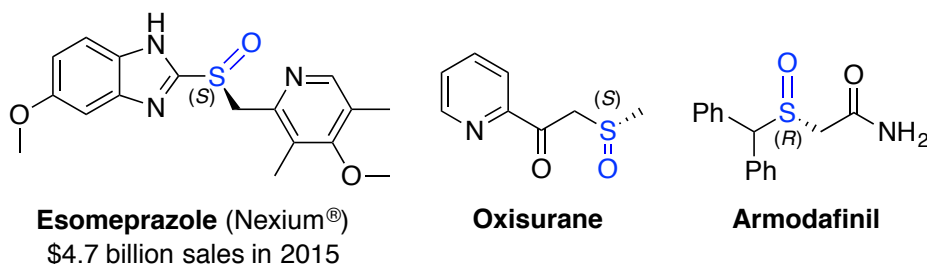


Figure II-17. Example of bioactive drugs with chirality at the sulfur atom.

Chiral sulfoxides as ligands and auxiliaries are also important contributors in asymmetric synthesis, and are used often in both academic and industrial settings.²⁰⁻²² The importance of this functionality necessitates a robust, reliable, efficient, preferably micro-scale and direct method for the assignment of absolute configuration. Nonetheless, the structural features of sulfoxides (lack of a suitable derivatizing site) has posed a challenge to port over the prototypical procedures used for the absolute stereochemical

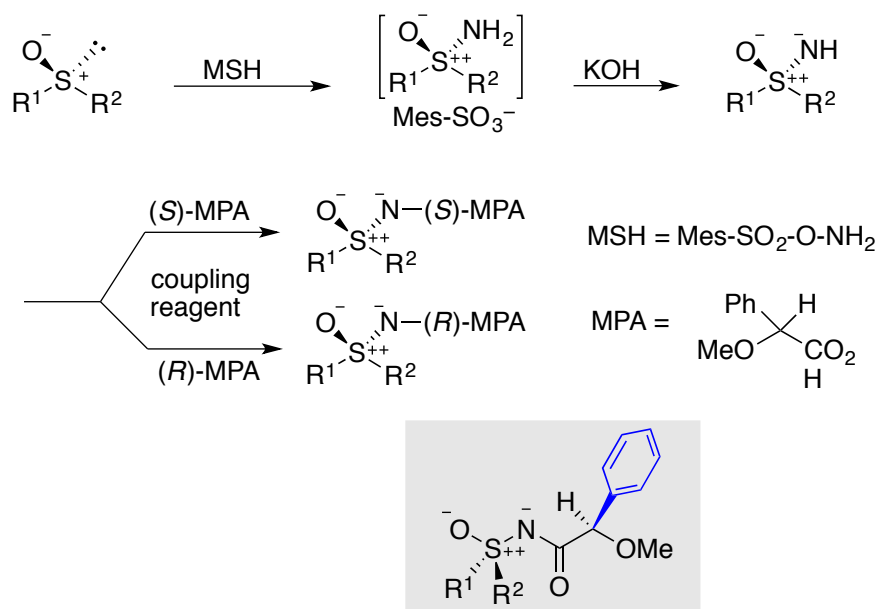


Figure II-18. Chemical modification and derivatization of chiral sulfoxides for determination of absolute configuration.

assignment of carbon substituted functionalities. A modified Mosher ester analysis was an early attempt in this regard. Typical ester derivatization of the sulfoxide oxygen results in racemization on the chiral sulfur. Yabuuchi and Kusumi circumvented this problem via an initial oxidation of the sulfoxide to generate corresponding iminosulfanone, which was then derivatized as its MPA-amide (Figure II-18).²³ NMR analysis of the Mosher ester derivative employing the proposed mnemonic (Figure II-18, shadow box) could lead to assignment of stereochemistry on the chiral sulfur. Limited use of chiral solvating agents for NMR analysis has been reported, although this strategy has not delivered a comprehensive solution.²⁴⁻²⁶ An electronic CD method to address aryl sulfoxides has been reported by Rosini and coworkers.²⁴ Alternatively, the most successful chiroptical technique for determination of absolute configuration of sulfoxides has been vibrational circular dichroism (VCD),²⁷⁻³¹ although this has not yet become a routine and common methodology for the synthetic community.

Our goal was to develop a simple and micro-scale procedure that enables the facile determination of the absolute stereochemistry of chiral sulfoxides using Exciton Coupled Circular Dichroism (ECCD). As previously discussed, our approach to this problem originates from our interest in utilizing host systems capable of adopting either the *P* or *M* helicity as the consequence of predictable interactions of a bound chiral guest molecule. The host:guest interactions are such that the point chirality of the guest is translated to the axial chirality of the host, which in turn leads to an observable ECCD signal. To this end, we envisioned the use of our recently developed host molecule, MAPOL **II-3**,¹ as a receptor that binds sulfoxides. Our constraints for success were to develop a methodology that is sensitive, highly reproducible, and operationally simple for chemists not necessarily versed in spectroscopic techniques. Herein, we demonstrate the utility of Zn-MAPOL **II-4**³² to address a long-standing problem in the assignment of absolute stereochemistry of chiral sulfoxides with the specific goals addressed above.

Although sulfoxides have putatively two sites of coordination (the oxygen atom and the sulfur lone pair), the geometric constraints of the host system would preclude bidentate binding. We first hypothesized that sulfoxides could bind via hydrogen bonding to the biphenol, and thus provide a mechanism for interaction with MAPOL. Nonetheless, binding of a number of chiral sulfoxides with MAPOL failed to produce a discernable ECCD signal. We had also envisioned the possibility of a different binding paradigm with the zincated analogue of MAPOL (Zn-MAPOL). One could propose chiral sulfoxides putatively coordinate to the zinc center of the porphyrin ring. Gratifyingly, complexation of

model sulfoxide **II-20R** with Zn-MAPOL led to a strong ECCD signal centered on the Soret band (420 nm) of the host system (Figure II-19).

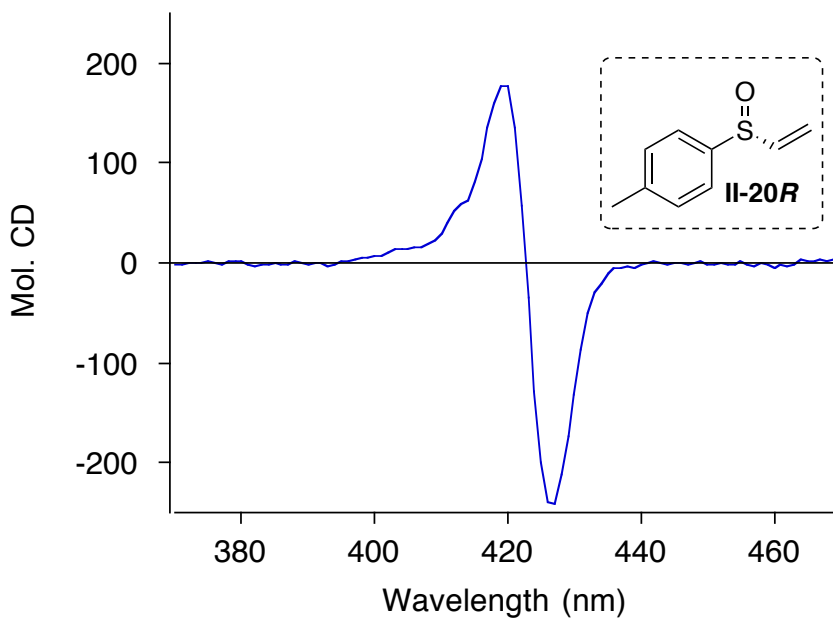


Figure II-19. ECCD spectrum of Zn-MAPOL (1 μ M) complexed with (*R*)-*p*-tolyl vinyl sulfoxide **II-20R** (50 equiv) in hexane at 0 °C.

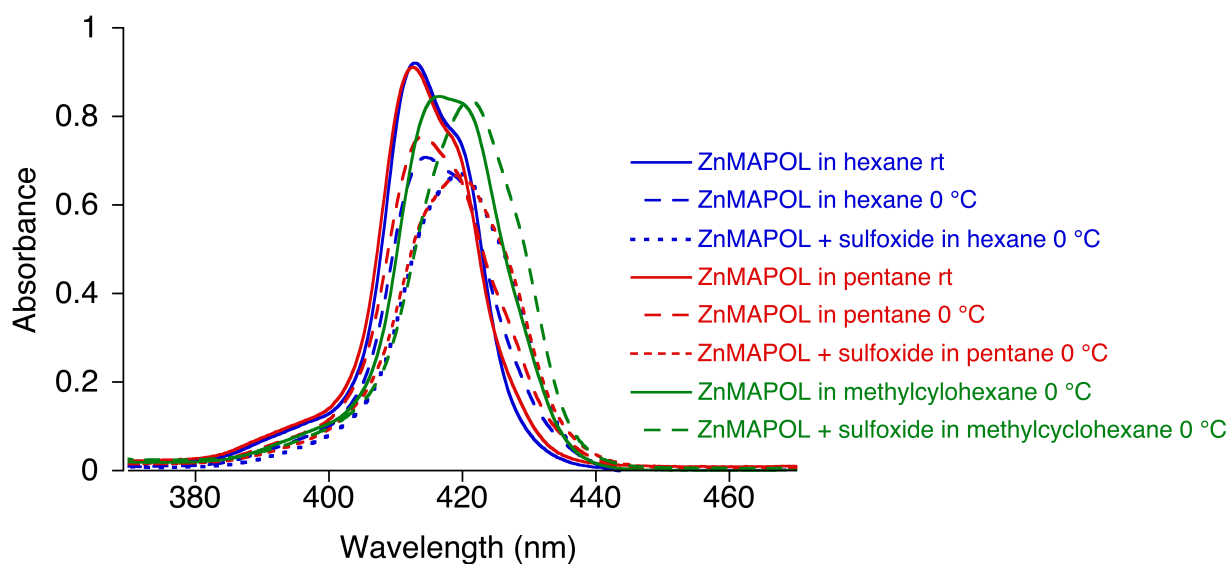


Figure II-20. UV-vis spectra of Zn-MAPOL (1 μ M) and Zn-MAPOL complexed with (*R*)-*p*-tolyl vinyl sulfoxide **II-20R** (50 equiv) in different solvents at 0 °C (solvents that yield ECCD signal).

As depicted in Figure II-22, when nonpolar solvents (hexane, pentane and methyl cyclohexane) were used for complex formation of **II-20R** with Zn-MAPOL, strong ECCD signals were observed. On the other hand, polar solvents failed to give any detectable ECCD signal for **II-20R**:Zn-MAPOL complex (Figure II-22). The UV-Vis spectra of **II-20R**:ZnMAPOL complex in different solvents also revealed complex formation between sulfoxide **II-20R** and Zn-MAPOL.

The UV-Vis spectra in solvents that the complex yield ECCD signal, show characteristic red shift upon addition of sulfoxide to Zn-MAPOL solution (Figure II-20). In sharp contrast, in solvents that the complex was ECCD silent, addition of sulfoxide did not change the UV spectrum (Figure II-21). It can be summarized that in the case of polar solvents, the interaction between the solvent and the host system out competes the interaction between the sulfoxide and Zn-MAPOL.

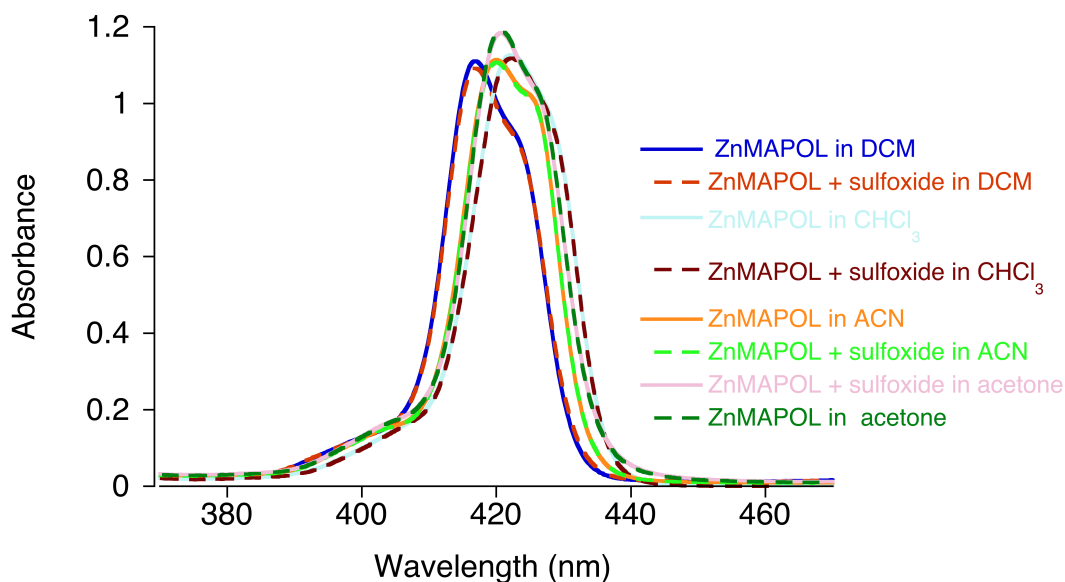


Figure II-21. UV-vis spectra of Zn-MAPOL (1 μ M) and Zn-MAPOL complexed with (*R*)-*p*-tolyl vinyl sulfoxide **II-20R** (50 equiv) in different solvents at 0 $^{\circ}$ C (solvents that do not yield ECCD signal).

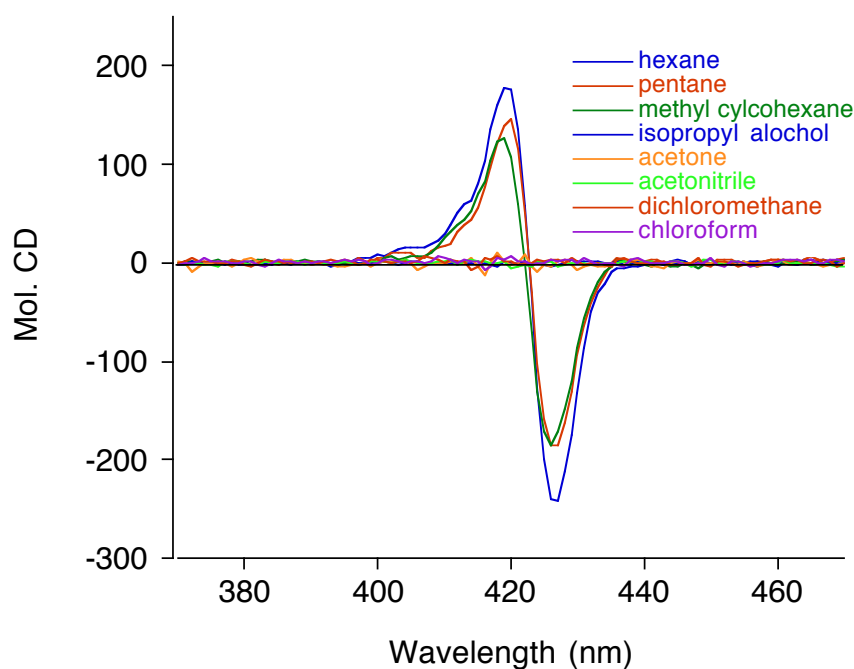


Figure II-22. ECCD spectra of Zn-MAPOL (1 μ M) complexed with (*R*)-*p*-tolyl vinyl sulfoxide **II-20R** (50 equiv) in different solvents at 0 $^{\circ}$ C.

In addition, the **II-20R**:Zn-MAPOL showed the expected temperature dependence for the observed signal (Figure II-23). At lower temperatures the ECCD amplitude is higher, and at above 40 $^{\circ}$ C the ECCD signal was not observed. Interestingly, upon lowering the temperature the ECCD signal can be restored. The latter observation consistent the fact that at the lower temperatures the energy difference between diastereomeric rotomers is more pronounced, thus leading to a larger population difference. Next, the dependence of the ECCD amplitude to the equivalents of sulfoxide was investigated (Figure II-24). ECCD signal can be observed upon addition of 5 equivalents of sulfoxide to Zn-MAPOL. Increasing the equivalents of sulfoxide increases the ECCD amplitude while preserving the sign of the ECCD signal, reaching saturation at 100 equivalents in most cases.

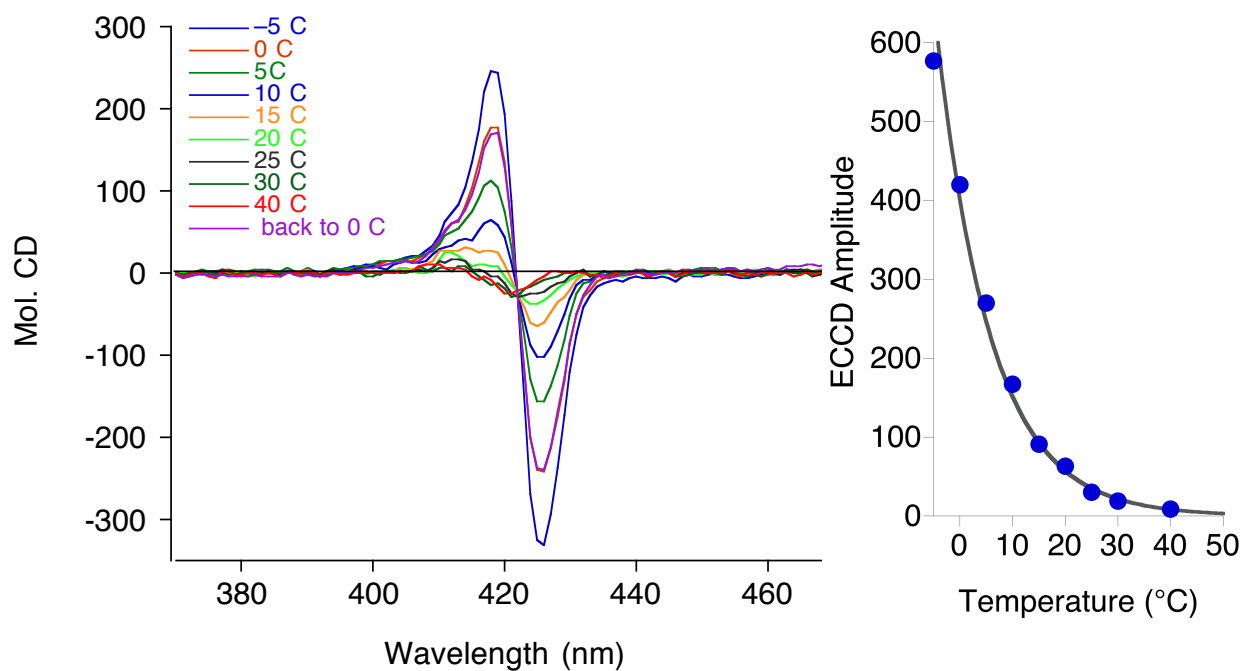


Figure II-23. ECCD spectra of Zn-MAPOL (1 μ M) complexed with (*R*)-*p*-tolyl vinyl sulfoxide **II-20R** (50 equiv) in different solvents at 0 °C.

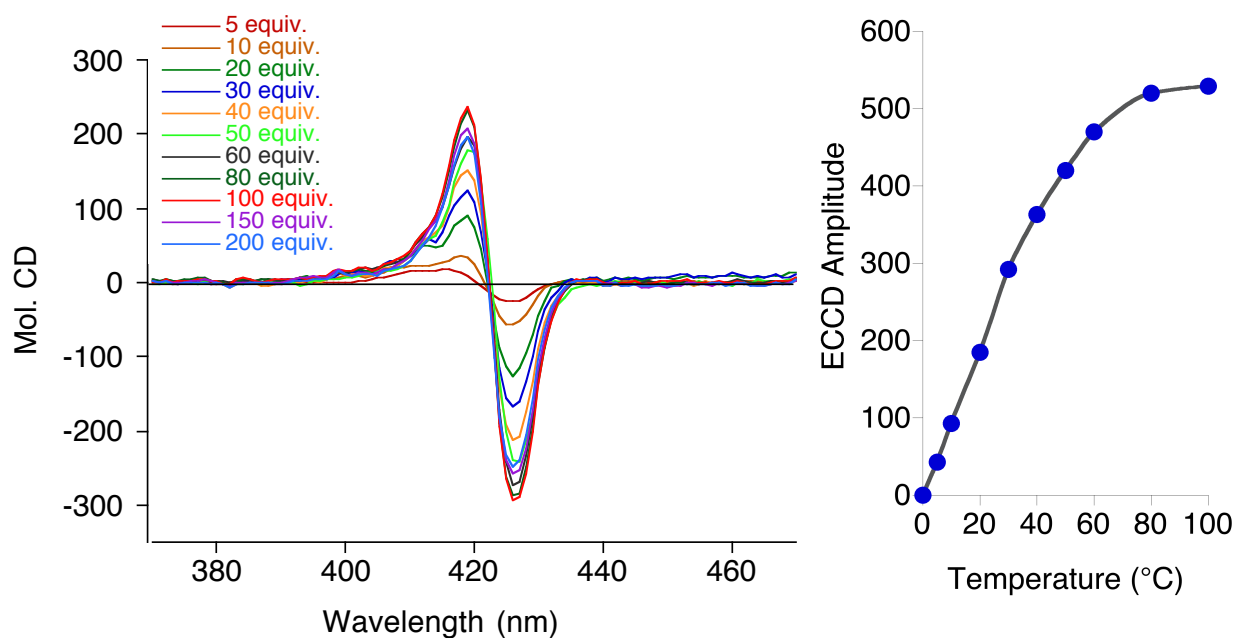


Figure II-24. ECCD spectra of Zn-MAPOL (1 μ M) complexed with (*R*)-*p*-tolyl vinyl sulfoxide **II-20R** at 0 °C in hexane.

The saturation of the ECCD amplitude is due to the fact that the host:guest complexation is a dynamic process, while the ECCD amplitude is proportional to the population of the bound complex that is favored by a larger excess of the sulfoxide. As illustrated in Figure II-25, the binding affinity can be measured at 409 nm upon addition of sulfoxide to the solution of Zn-MAPOL (1 μM). K_{assoc} of the complex is measured in excess of $14,500 \text{ M}^{-1}$ (Figure II-27). Furthermore, the stoichiometry of the complex between sulfoxide and Zn-MAPOL is extracted from the UV titration spectra. Job's plot analysis indicates a 1:1 stoichiometry of the complex as evident from the maxima obtained at 0.5 mole fraction (Figure II-26).

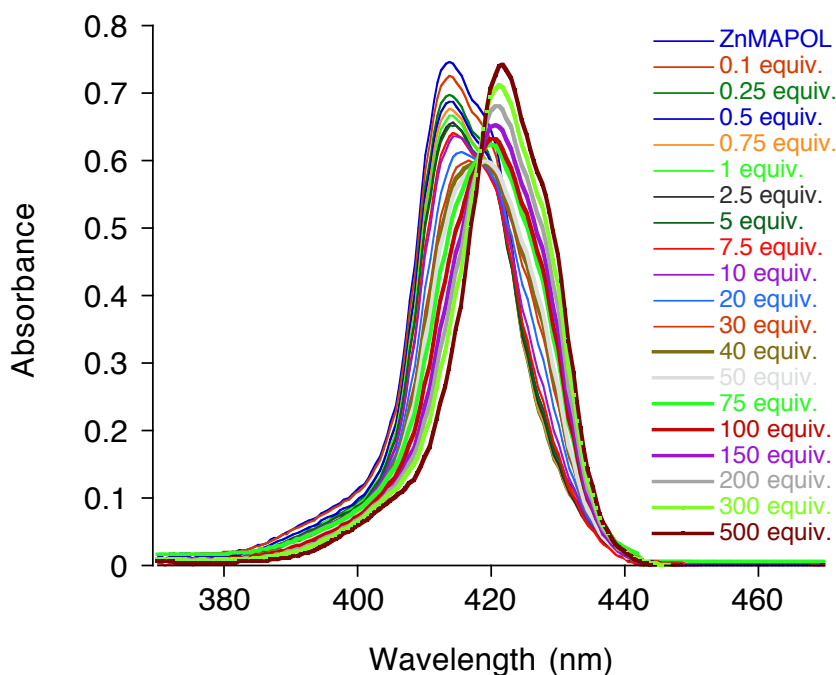


Figure II-25. UV-vis spectral change upon titration of Zn-MAPOL (1 μM) with (*R*)-p-tolyl vinyl sulfoxide **II-20R** at 0 °C in hexane.

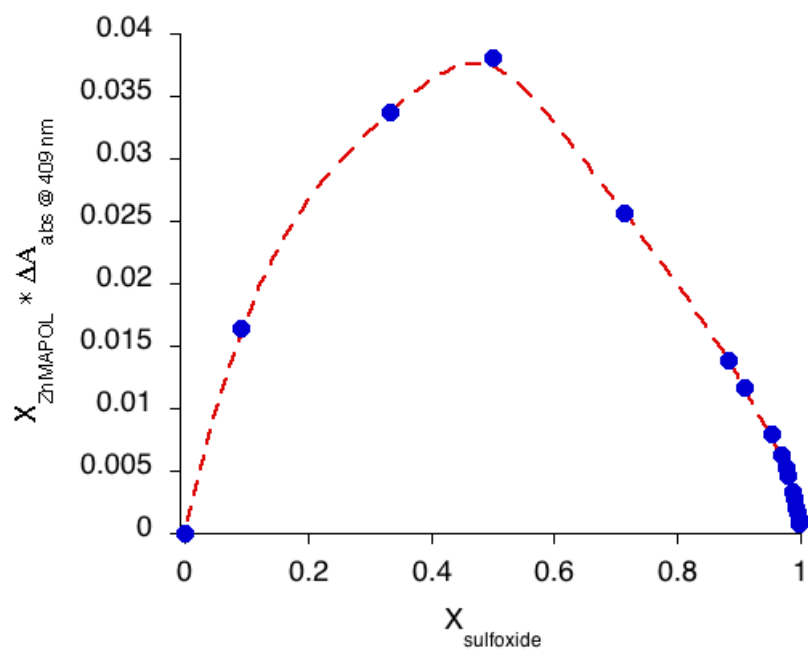


Figure II-26. Job's plot of Zn-MAPOL with (*S*)-*p*-tolyl vinyl sulfoxide **II-20R** absorbance at 409 nm.

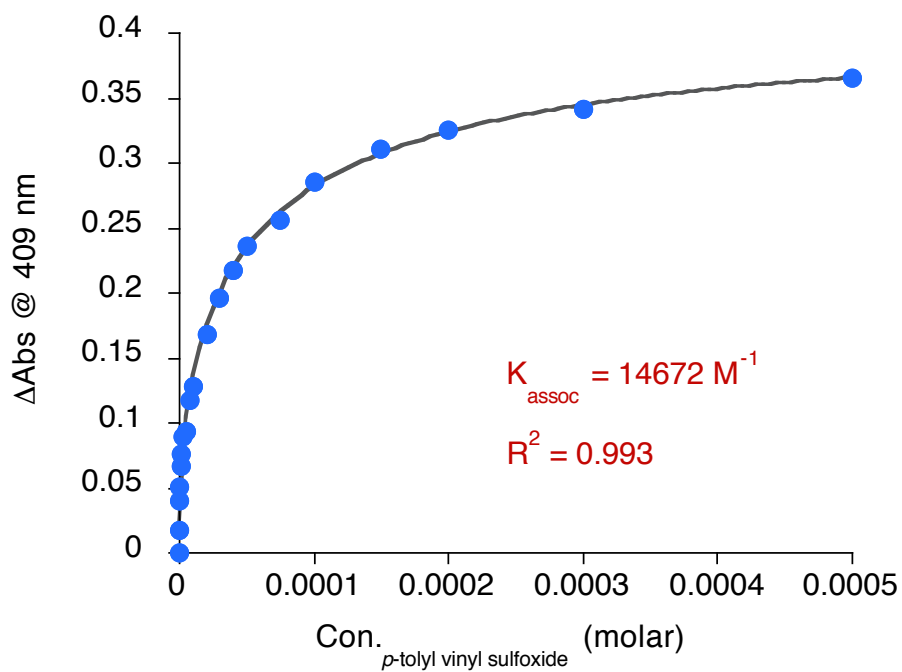


Figure II-27. Change in the absorbance at 409 nm for evaluating K_{assoc} upon titration of Zn-MAPOL (1 μM) with (*R*)-*p*-tolyl vinyl sulfoxide **II-20R** at 0 °C.

With the initial results in hand, a number of chiral sulfoxides, with various alkyl and aryl substituents were synthesized via previously reported procedures (Table II-2).^{29, 33-37} Using a standard protocol (1 μ M Zn-MAPOL and 50 equivalents of sulfoxide dissolved in hexane), strong ECCD signals were obtained for host/guest complexes in all cases. Not surprisingly, enantiomers yield ECCD signals with opposite sign albeit with equal intensities when correction for enantiopurity is applied (A_{corr}).

Table II-2. Predicted and observed ECCD for sulfoxides complexed with ZnMAPOL.

entry ^a	sulfoxide		$L_1(\text{\AA})/L_2(\text{\AA})^b$	Pred.	λ nm ($\Delta\epsilon$)	A/A_{corr}^c
1		II-17R	4.6/1.8	neg	426, -166 418, +173	-339/-365
2		II-17S	4.6/1.8	pos	425, +168 416, -116	+284/+351
3		II-18R	6.1/1.8	neg	427, -252 419, +219	-471/-611
4		II-18S	6.1/1.8	pos	427, +199 419, -137	+336/+589
5		II-19R	6.1/2.7	neg	427, -248 419, +240	-488/-574
6		II-19S	6.1/2.7	pos	427, + 218 419, -135	+353/+588
7		II-20R	6.1/2.7	neg	427, -241 419, +178	-419/-445

Table II-2 (cont'd)

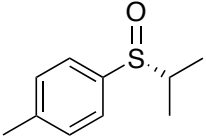
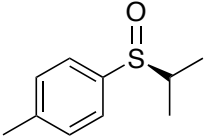
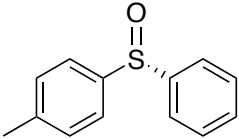
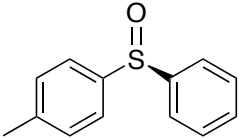
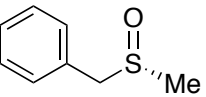
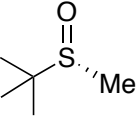
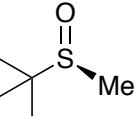
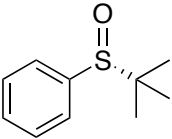
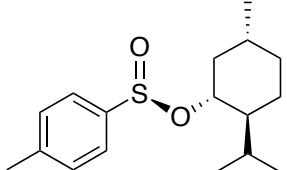
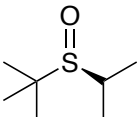
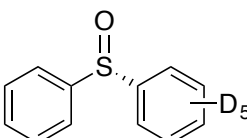
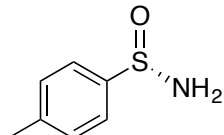
entry ^a	sulfoxide		L ₁ (Å)/L ₂ (Å) ^b	Pred.	λ nm (Δε)	A/A _{corr} ^c
8		II-21<i>R</i>	6.1/2.8	neg	428, -259 420, +140	-399/-463
9		II-21<i>S</i>	6.1/2.8	pos	427, +154 419, -84	+238/+456
10		II-22<i>R</i>	6.1/4.6	neg	428, -299 420, +262	-561/-738
11		II-22<i>S</i>	6.1/4.6	pos	428, +257 419, -201	+458/+750
12		II-23<i>R</i>	5.3/1.8	neg	426, -97 418, +81	-178/-212
13		II-24<i>R</i>	2.8/1.8	neg	426, -168 418, +137	-305/-406
14		II-24<i>S</i>	2.8/1.8	pos	426, +122 418, -155	+277/+420
15		II-25<i>R</i>	4.6/2.8	neg	428, -270 419, +155	-425/-559
16		II-26<i>S</i>	6.1/5.8	pos	425, +48 417, -29	+77 ^d
17		II-27<i>S</i>	2.8/2.8	pos	426, +65 420, -30	+95/+271
18		II-28<i>S</i>	2.8/2.8	pos	425, +17 417, -9	+26 ^d

Table II-2 (cont'd)

entry ^a	sulfoxide	L ₁ (Å)/L ₂ (Å) ^b	Pred.	λ nm (Δε)	A/A _{corr} ^c	
19		II-29S	6.1/1.6	neg	426, -709 418, +624	-1333 ^d

[a] Zn-MAPOL (1 μM) and 50 equivalents of the sulfoxide were dissolved in hexane, and CD measurements were performed at 0 °C. [b] L₁ and L₂ correspond to the substituents on the left and right hand side of the structures as drawn, respectively. [c] A_{corr} values are calculated by dividing the measured A by the %ee. [d] These samples were enantiomerically pure.

Deriving a simple mnemonic for correlating the sign of the observed ECCD spectrum to the absolute stereochemistry at the sulfur center requires a structurally detailed picture of the geometric constraints that lead to the observed helicities reported in Table II-2. To begin, it is important to point out a number of facts: 1. Zincation of the porphyrin rings was obligatory to observe ECCD with bound chiral sulfoxides. 2. The bis-methoxylated Zn-MAPOL (Zn-MAPOL-OMe) did yield ECCD signals of the same sign, albeit with reduced amplitudes, thus suggesting that coordination to the zinc center is the main binding interaction responsible for induced helicity. Figure II-27 illustrates, the CD titration of sulfoxide **II-20R** with Zn-MAPOL-OMe. The sign of the ECCD signal is same as when this substrate is complexed with Zn-MAPOL (Figure II-19) however the amplitudes of signals are lower at any given equivalents of sulfoxide. 3. Hard-soft binding principles dictate the tendency for sulfoxides to coordinate to metals either through oxygen or sulfur. Oxygen atom binding to metal centers is most often observed as a result of its greater polarization, and thus higher electron density. Soft metals (late transition metals such as platinum) tend to coordinate to sulfur, while harder metals prefer oxygen as the coordinating site.²² Fortuitously, the crystal structure of Zn-TPP in complex with dimethyl sulfoxide with Zn-

TPP is reported and indeed reveals the anticipated coordination of oxygen to the zinc center.³⁸ Furthermore, we obtained a high resolution crystal structure of Zn-TPP in complex with dimethyl sulfoxide that confirms the coordination of oxygen atom of sulfoxide to the zinc center of the porphyrin (Figure II-28). Unfortunately, countless efforts to obtain crystal structure of Zn-MAPOL or its analogue with or without bound substrate were unsuccessful. The latter three points argue strongly for the coordination of the sulfoxide oxygen atom to the metallated porphyrin.

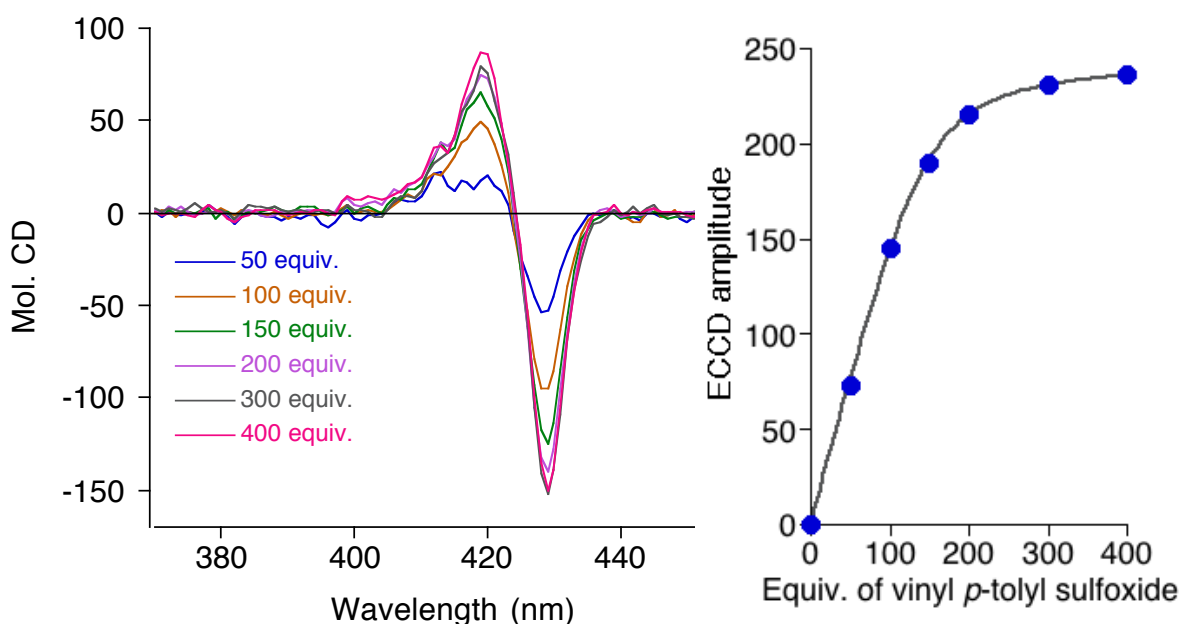


Figure II-28. ECCD spectra of Zn-MAPOL-OMe (1 μ M) complexed with (*R*)-*p*-tolyl vinyl sulfoxide **II-20R** at 0 $^{\circ}$ C in hexane.

Figure II-29 depicts our proposed mode of binding and conformational arrangements that lead to the preferred helicity and consequently the observed ECCD. This was derived based on the constraints and observations about complexation described above. Coordination of the oxygen atom lone pairs of the sulfoxide with the metalloporphyrin occurs in a manner to minimize steric interactions. The geometry of the sulfoxide, in

particular the lone pair orbital bound to Zn^{2+} , necessitates the projection of one of the sulfur atom substituents towards the bound porphyrin ring. This is apparent from the crystal structure of DMSO bound to Zn-TPP with a Zn-O-S bond angle of 128° . Of the three substituents on the sulfur atom, the lone pair presumably would be the least sterically intrusive group, and thus would occupy this space. Our own high resolution crystal structure of DMSO, bound to Zn-TPP, also demonstrates the same conformational preference, with the lone pair pointing towards the plane of the porphyrin ring (Figure II-29).

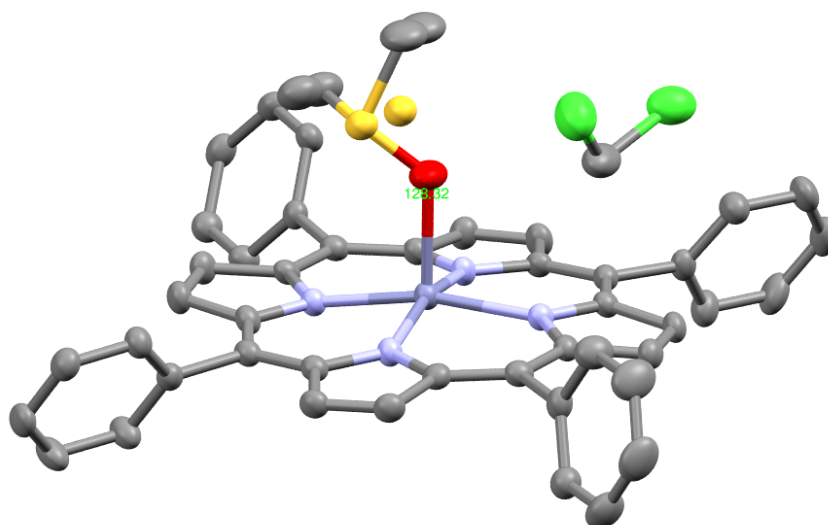


Figure II-29. X-ray crystal structure of Zn-TPP in complex with dimethyl sulfoxide (hydrogens are omitted for clarity).

As illustrated with substrate **II-20R** in Figure II-30, the next choice would be to minimize steric interactions of the two remaining groups as they project outwards from the center of the porphyrin ring they are bound to, by placing the largest group, in this case the aryl substituent, in the least sterically demanding space. Considering both *P* and *M* helicities of the host, the *M*-(*R*) complex orients the aryl group away from the

second porphyrin ring, while in the *P*-(*R*) complex, the aryl group suffers from larger, undesired interactions. One would thus suggest that the *M* helicity is energetically favored. The prediction based on this model leads to a negative induced helicity in Zn-MAPOL, which indeed fits the observed ECCD spectrum for **II-20R** bound to Zn-MAPOL. This simple mnemonic predicts the correct ECCD for all substrates listed in Table II-2.

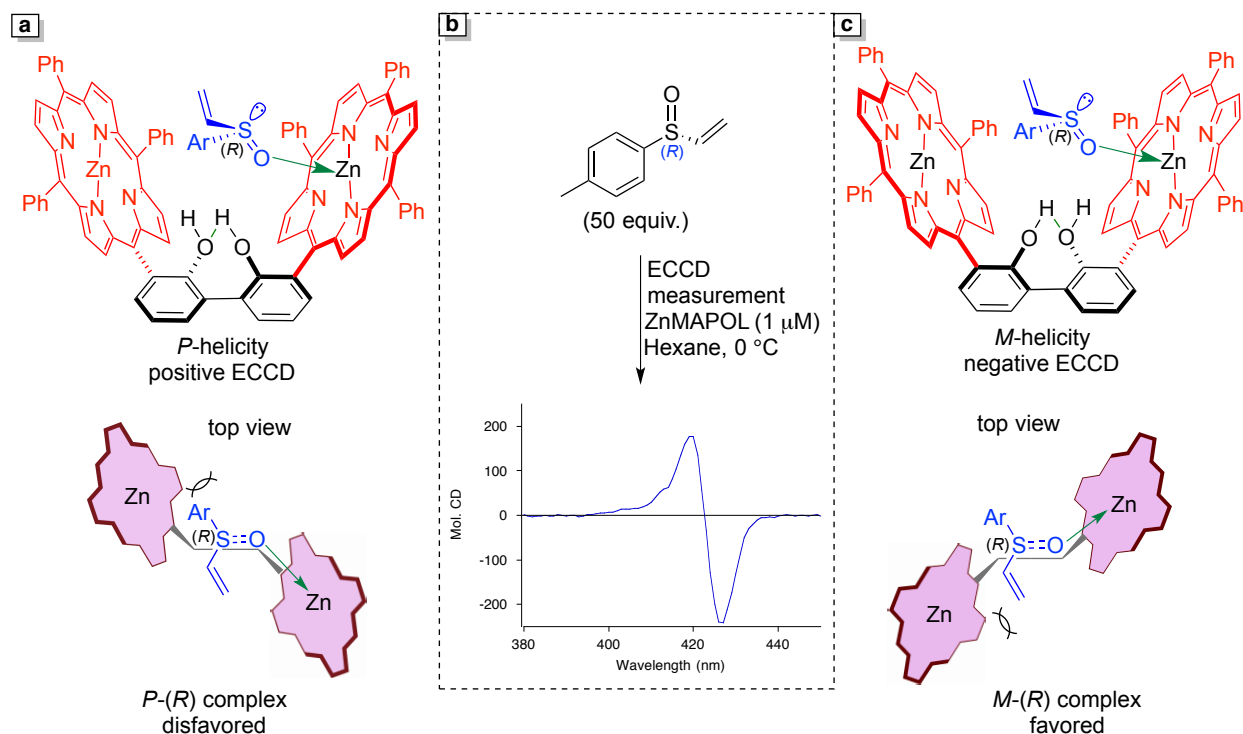


Figure II-30. a) Bidentate binding of **II-20R**, with the *P*-helicity of Zn-MAPOL, places the large aryl group in the most sterically available position. This favorable arrangement leads to the anticipated positive ECCD spectrum. b) Complexation of **II-20R** with Zn-MAPOL leads to a strong positive ECCD signal. c) The same bidentate binding with the *M*-helicity leads to steric clash of the large aryl group with the porphyrin ring. Thus, negative ECCD with **II-20R** bound to Zn-MAPOL is not anticipated.

The critical choice to be made for applying the latter mnemonic rests with determining which of the two groups attached to the asymmetric sulfur is larger. In systems described previously (amines and cyanohydrins), A-values, a thermodynamic measure of steric size, were used as determinants of size. A careful analysis of the data in Table II-2,

specifically, correlation of the strength of the ECCD signal with the difference in steric size of the substituents, suggests that A-values alone are not sufficient to rationalize the data. For example, although the A-values of phenyl and 4-Me-Ph are expectedly similar, the ECCD observed for **II-22** (Table II-2, entries 10 and 11) is unexpectedly large ($A_{\text{corr}} = -738$). The greatest difference between the latter two substituents is in their length, i.e., measuring the distance L_1 from the sulfur atom to the furthest heavy atom on 4-Me-Ph is 6.1 Å, while L_2 , measured from the sulfur atom to the furthest heavy atom on Ph is 4.6 Å (Figure II-31). The geometry dictated by the coordination of the sulfoxide with the zincated porphyrin projects the two substituents towards the plane of the opposite porphyrin ring. Thus, the difference in length of the two substituents is more significant than their bulk, leading to a larger *P/M* population difference.

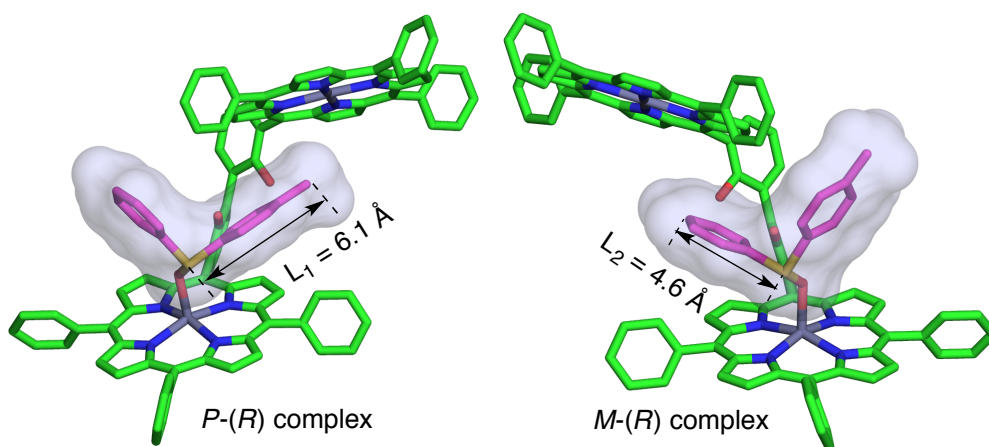


Figure II-31. Energy minimized (B3LYP/6-31G*) structures of the *P* and *M* helical Zn-MAPOL complexed with **II-22R**. The length of the substituents, measured as L_1 and L_2 , dictate the preferred helicity of the host system. The shorter L_2 of the phenyl group leads to smaller steric interactions with the porphyrin ring that is not bound to the sulfoxide.

As depicted in Figure II-31, the length of the substituents is measured in an analogous fashion to the *L* parameter for sterimol analysis (Figure II-32).³⁹⁻⁴² A note of caution is

warranted; the latter criterion applies only if the length of the substituent can be predicted in a reasonable manner. In cases such as flexible long chain alkyl groups, where a number of different energetically close lying conformations can be present, the prediction for length can be difficult, and thus, could lead to erroneous predictions.



Figure II-32. Sterimol L parameter (total length of the substituent along the primary bond axis) and the measure length (L_1 , length of substituent to the furthest heavy atom) are illustrated for 1,2-dimethylpropyl group.

Prioritization of the longer group over the shorter substituent, as described above, leads to a predictable assignment of absolute stereochemistry for all substrates listed in Table II-2. Note that the table lists L_1 and L_2 values for each substituent, which are used to derive the predicted sign of the ECCD spectrum. The most striking example that validates the use of length, as the primary consideration to distinguish the relative size of the substituents on the sulfur center is the ECCD obtained with **II-25R** (Table II-2, entry 15). Considering A-values, one would expect the opposite sign for the ECCD spectrum as the *t*-butyl group has a larger A-value (>4.5) than the phenyl substituent (3.0). Nonetheless, the length of the phenyl group is longer (4.6 Å for Ph, 2.8 Å for *t*-butyl), thus dictating the population difference that leads to the observed negative ECCD. In cases where the measured L is identical for both groups, then A-values are used as the secondary consideration to decide size priority. An example of this is **II-27S**, where L_1 and L_2 for *t*-butyl and iso-propyl are the same, yet the A-value for *t*-butyl (>4.5) is

substantially larger than the A-value for iso-propyl (2.15). Considering that the A-value is a predictor of 'volume', it stands to reason that when the lengths of the substituents are the same, the volume of the substituents can exert a stereodefining role. Indeed, the predicted positive ECCD is observed experimentally (Table 1, entry 17). Notably, the same analysis can be used for the absolute determination of **II-28S**. The slightly larger per-deuterated benzene ring leads to the anticipated ECCD signal, albeit in small amplitude, reflective of the slightly larger volume of the perdeuterated phenyl vs. phenyl. Nonetheless, the latter observation demonstrates the sensitivity of the current system. The size difference of phenyl versus perdeuterated phenyl is very minimal. Deuterium with A-value of 0.006 is assumed to be slightly larger than hydrogen (A-value of 0.000). In a seminal analysis Dunitz and Ibberson have studied the molecular volume of C_6H_6 versus C_6D_6 in the crystal structure at different temperature.⁴³ They realized that at lower temperatures benzene is slightly larger than deuterated benzene due to stronger vibrations of C–H versus C–D. However, at temperature above 170 K deuterated benzene occupies more space than C_6H_6 . The sulfinamide **II-29S** (Table II-2, entry 19) produced the largest ECCD amplitude upon complexation with ZnMAPOL. Figure II-33 demonstrates the ECCD titration of ZnMAPOL with sulfinamide **II-29S**. Much akin to sulfoxides, saturation of the ECCD amplitude was observed at about 100 equivalents of sulfinamide (Figure II-33, right). Strong ECCD amplitude observed for sulfinamide in complex with Zn-MAPOL can be indicative of high binding affinity of this moiety as compared to sulfoxides. Binding affinity of sulfinamide in complex formation with Zn-

MAPOL was measured by following the changes in the UV-Vis spectra of Zn-MAPOL upon addition of different equivalents of sulfinamide (Figure II-34).

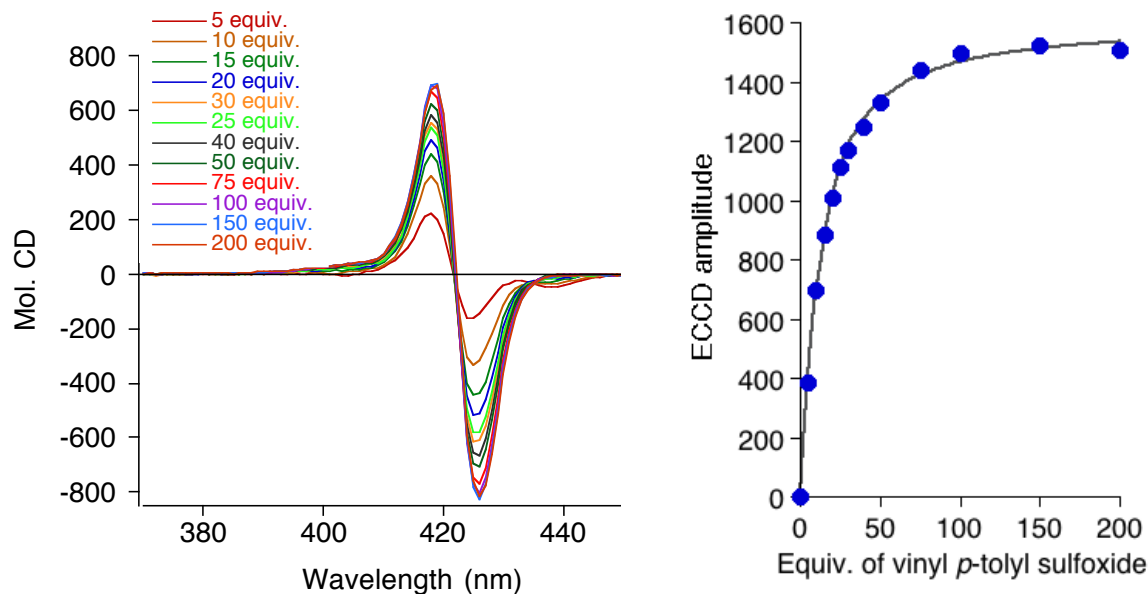


Figure II-33. Negative ECCD spectrum obtained with Zn-MAPOL complexed with 50 equivalents of (*S*)-*p*-toluene sulfinamide **II-29S** at 0 °C in hexane.

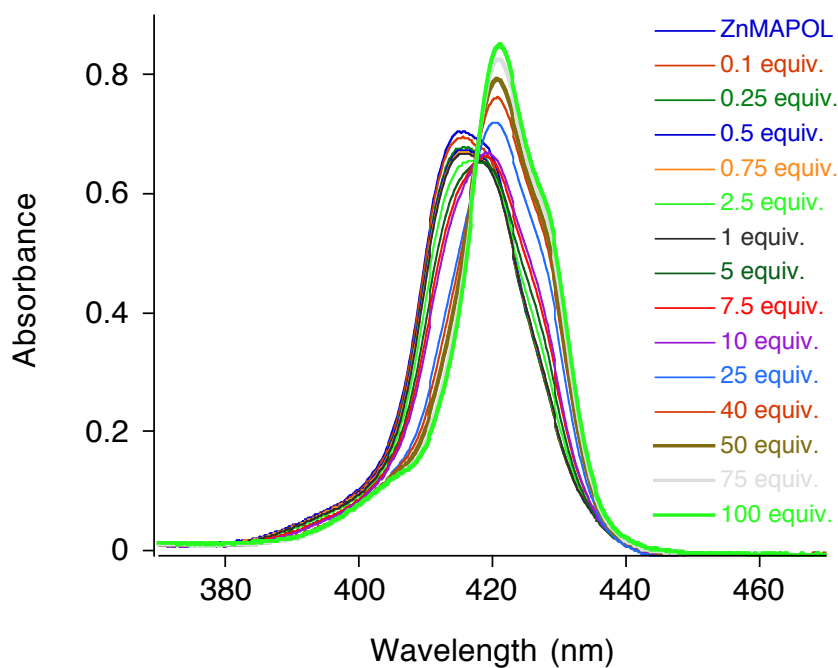


Figure II-34. UV spectral change upon titration of Zn-MAPOL (1 μ M) with (*S*)-*p*-toluene sulfinamide **S-II-29S** at 0 °C in hexane.

A superior binding affinity ($K_d = 35,236 \text{ M}^{-1}$) was measured that can presumably be indicative of the highly polarized nature of sulfur–oxygen bond (Figure II-35).

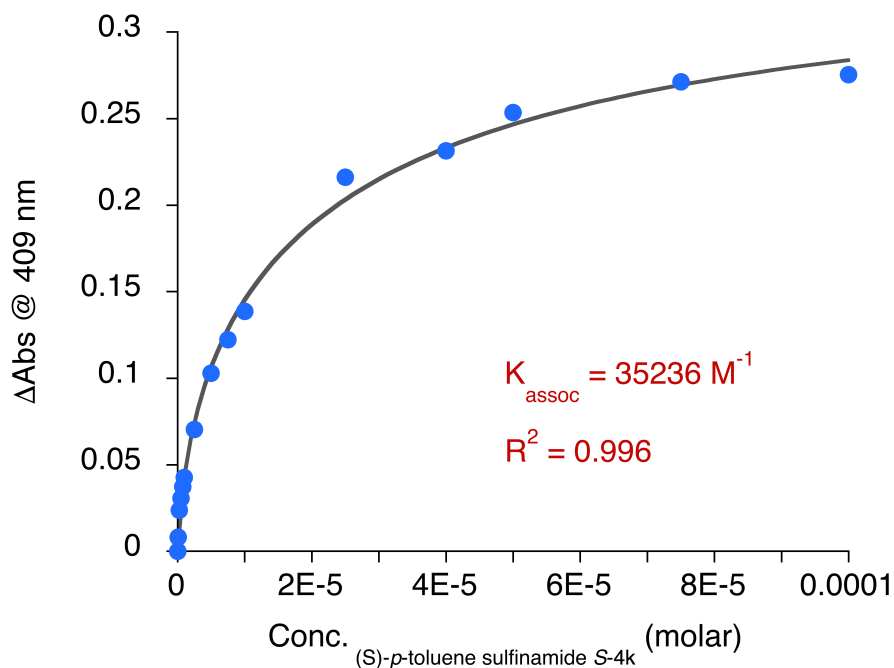


Figure II-35. Change in the absorbance at 409 nm for evaluating K_{assoc} upon titration of Zn-MAPOL (1 μM) with (*S*)-*p*-toluene sulfinamide **II-29S** at 0 °C.

In the sulfinamide substrate there is an $-\text{NH}_2$ group that can coordinate to the zinc center and potentially change the binding mode for complex formation. The crystal structure of sulfinamide **II-34S** with Zn-TPP provides clear evidence for the anticipated binding of the oxygen atom of this substrate to the metallocenter (Figure II-36).

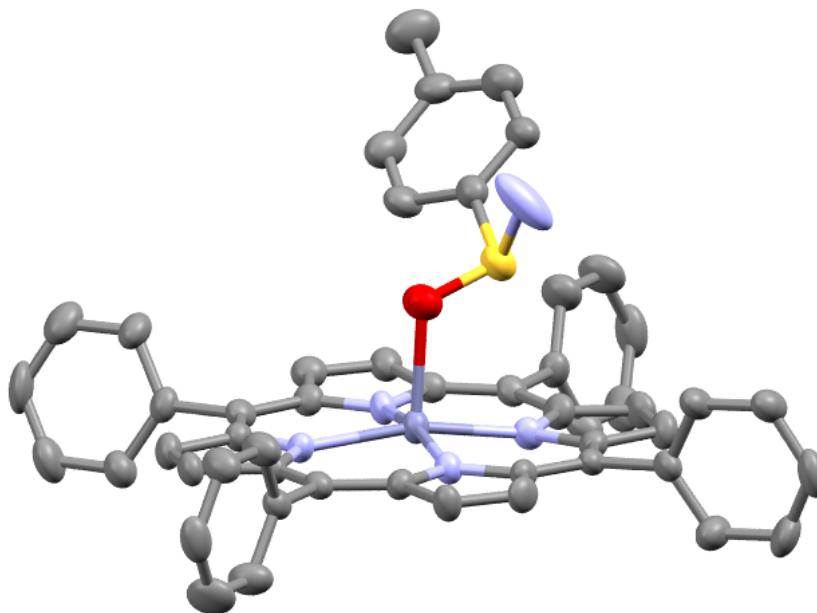


Figure II-36. X-ray crystal structure of Zn-TPP complexed with sulfinamide **II-34S** (hydrogens are omitted for clarity).

Having demonstrated the efficacy of the methodology with a variety of chiral sulfoxides, we next challenged the system with a more complex molecular structure containing ancillary groups that could alter or abolish coordination of the sulfoxide moiety with the metalloporphyrin. To address the latter concern, esomeprazole (Nexium[®]), a highly effective proton pump inhibitor, with a number of potential coordinating functional groups was complexed with Zn-MAPOL (Figure II-37). Gratifyingly, a positive ECCD was observed, consistent with what was expected, considering the longer benzo-imidazole substituent as the determinant for helicity.

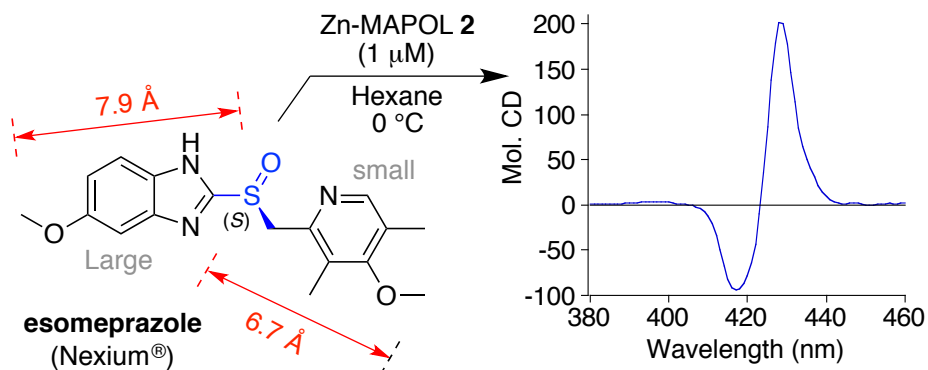


Figure II-37. Complexation of esomeprazole (50 μM) with Zn-MAPOL (1 μM) yields a positive ECD spectrum, correctly predicting the *S* stereochemistry of the molecule. The assignment is based on considering the benzoimidazole side chain as the larger substituent (longer linear length as compared to the pyridyl side chain).

In summary, we have reported the first direct chiroptical method for the absolute stereochemical determination of chiral sulfoxides without the need for derivatizations or chemical transformations. The procedure is reliable, requiring only microgram quantity of chiral sulfoxides. Furthermore, the absolute stereochemistry is derived in a matter of minutes, with an operationally simple method that is amenable for researchers with little experience in chiroptical techniques. The mnemonic for correlating the observed ECD sign to the actual stereochemistry at the sulfur center is straightforward, requiring the operator to only make a choice on the relative length and size of the substituents attached to the sulfur center.

II-3 Determination of absolute configuration of chiral phosphine oxides

With the successful demonstration of Zn-MAPOL as a molecular receptor for the determination of absolute configuration of chiral sulfoxides, we were interested to further expand the utility of this host system for other functionalities. In this regards, we envisioned application of Zn-MAPOL for determination of absolute configuration of phosphine oxides as close analogues of chiral sulfoxides. The lack of a reliable methodology to detect the absolute configuration of chiral phosphine oxides was our motivation to pursue the feasibility of complex formation of phosphine oxide with our newly designed host system for the purpose of sensing the chirality on the chiral phosphorus atom. Current state of the art for determination of absolute configuration of chiral phosphine oxide is heavily reliant on X-ray crystallography. Nonetheless, application of VCD for determination of absolute configuration *tert*-butyl-1-(2-methylnaphthyl) phosphine oxide is reported.⁴⁴ Chiral phosphine oxides are widely used in transition metal chemistry as ligands.⁴⁵⁻⁴⁶ Upon reduction, phosphine oxides can be converted into chiral phosphines which are equally important as chiral phosphine oxides. Additionally, chiral phosphine oxide moiety can be found in a number of pharmaceutically important products. Our goal was to leverage the inherent sensitivity of chiroptical techniques utilizing our host system to devise a methodology that can lead to the absolute stereochemical determination of chiral phosphine oxides in a rapid, micro-scale, derivatization-free and non-empirical fashion.

Mr. Debarshi Chakraborty (Borhan group, MSU) has synthesized a diverse set of chiral phosphine oxides utilizing reported procedures.⁴⁷⁻⁵⁰ Complex formation between

various phosphine oxides and Zn-MAPOL, utilizing the optimized condition for complexation of sulfoxides, leads to detectable and reliable ECCD signals. As an example, the ECCD signal of (*R*)-methyl phenyl propyl phosphine oxide with Zn-MAPOL is shown (Figure II-38).

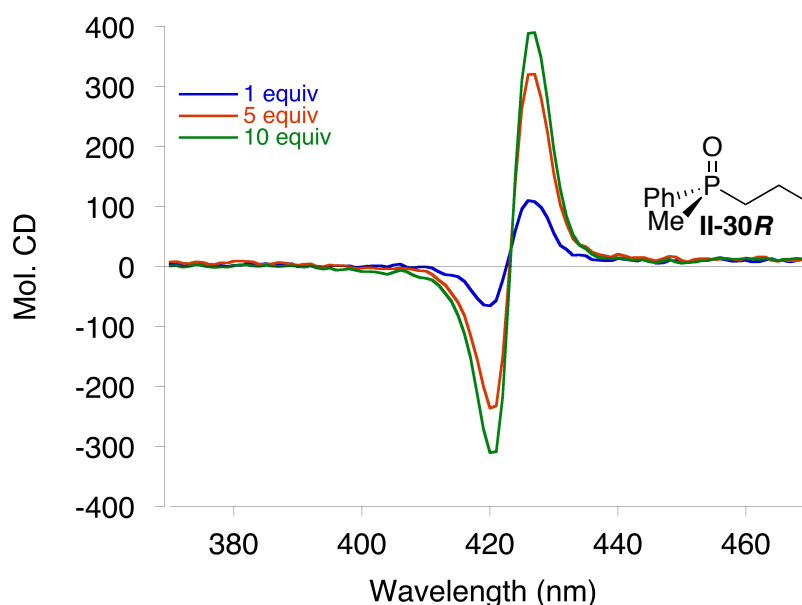


Figure II-38. ECCD spectra of Zn-MAPOL-OMe (1 μ M) complexed with (*R*)-methyl phenyl propyl phosphine oxide **II-30R** at 0 °C in hexane.

As expected, the enantiomer of this phosphine oxide leads to ECCD signal with opposite sign (Figure II-39). Interestingly, the observed amplitudes for ECCD of chiral phosphine oxides are generally higher than chiral sulfoxides.

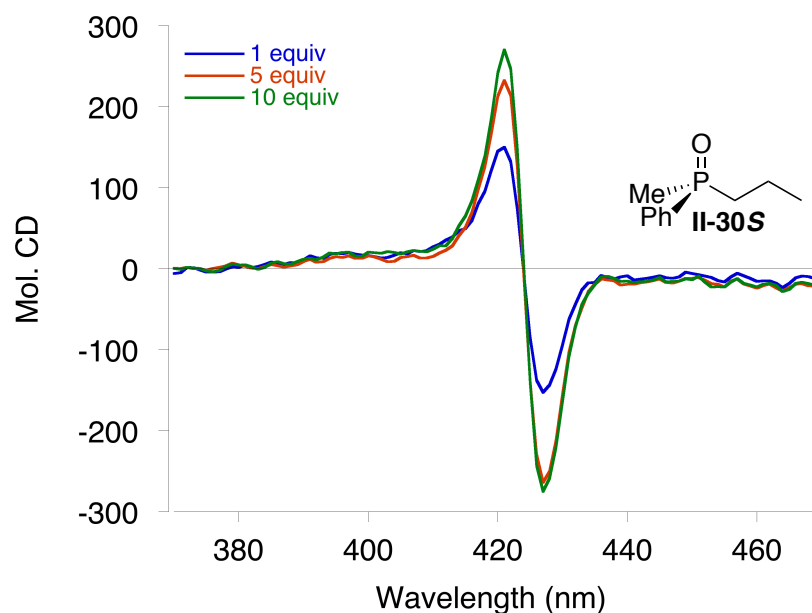


Figure II-39. ECD spectra of Zn-MAPOL-OMe (1 μ M) complexed with (*S*)-methyl-phenyl-propyl phosphine oxide **II-30S** at 0 $^{\circ}$ C in hexane.

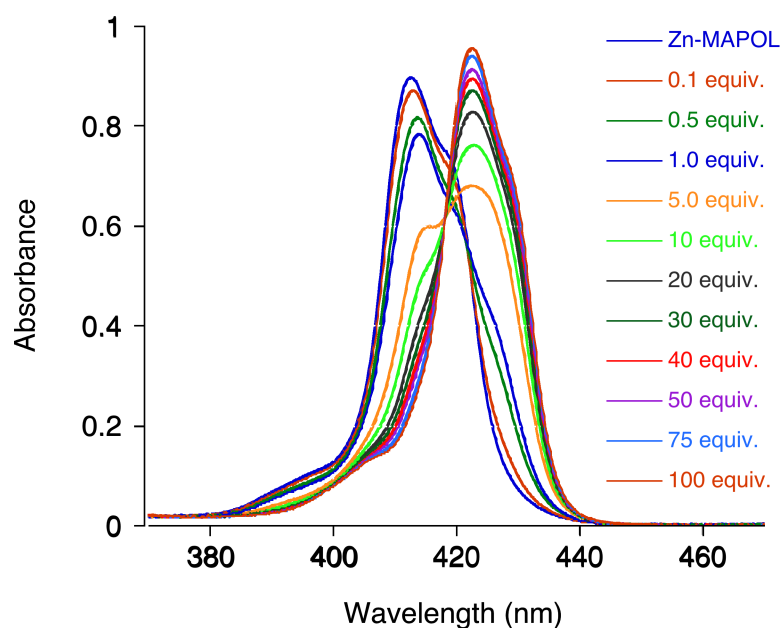


Figure II-40. UV-vis spectral change upon titration of Zn-MAPOL (1 μ M) with (*R*)-methyl-phenyl-propyl phosphine oxide **II-30R**.

The large amplitudes for phosphine oxides proved instrumental for our

measurements, since the ECD signals could be measured with as low as only one equivalent of phosphine oxide when complexed with Zn-MAPOL (1 μM). This set an extremely low detection limit that has enormous advantages for analysis of samples with limited available quantity. The exceptionally high intensity of the ECD signals finds its origin in high bonding affinity of phosphine oxides to Zn-MAPOL that is the result of the highly polarized phosphorous–oxygen bond. Binding affinity was measured following changes in the UV-vis absorption of Zn-MAPOL at 409 nm upon addition of chiral phosphine oxide (Figures II-40 and II-41). This bonding affinity is roughly twenty times higher than the affinity measured for sulfoxides.

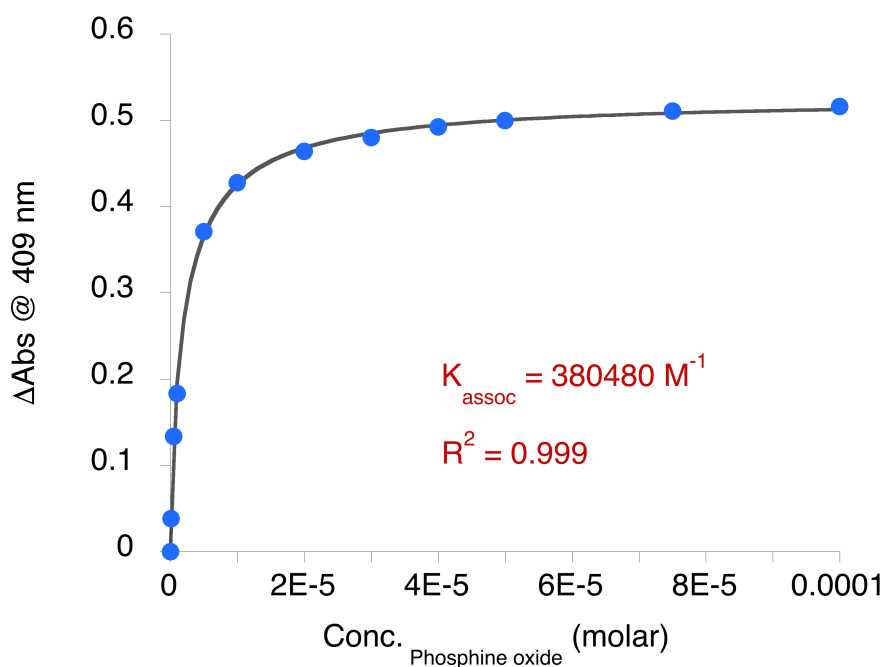


Figure II-41. Change in the absorbance at 409 nm for evaluating K_{assoc} upon titration of Zn-MAPOL (1 μM) with (*R*)-methyl-phenyl-propyl phosphine oxide **II-30R**.

We envisioned the binding interaction of chiral phosphine oxides with Zn-MAPOL to

be similar to what we proposed for chiral sulfoxides. As such, coordination of the highly polarized oxygen atom of P–O bond to the metalocentered porphyrin drives the complex formation and places the stereogenic phosphorus atom at the center of the host system. Minimization of steric repulsions dictates the preferred helicity that leads to the corresponding ECCD signal. In a similar arrangement of substituents on the chiral center as proposed for chiral sulfoxides, the smallest group on the phosphine oxide would point towards the bound porphyrin and the remaining medium and large groups project towards the second porphyrin ring. The relative size of medium and large substituents induce preference on the orientation of the second porphyrin ring, leading to the corresponding twist on the backbone of the host system. The preferred helicity is obtained such that the second porphyrin reside closer to the medium size group and further away from the larger group to minimize steric repulsion. The mnemonic shown in Figure II-52 and II-53 can be used to predict the sign of the ECCD signal by considering the relative size of the substituents on the chiral center.

As stated earlier, a large number of pharmaceutical products contain embedded chiral phosphine oxides in their skeleton. A research team from Merck Chemical Company showed interest in employing our Zn-MAPOL methodology to sense the absolute configuration of chiral phosphine oxides within drug molecules. They have recently reported a new methodology that gives access to a family of prodrugs with chiral phosphorous center in the form of phosphoramidates.⁵¹

Zn-MAPOL proved to be efficient for formation of ECCD active complexes with chiral phosphine oxides bearing carbon based substituents. We sought to verify the applicability

of our host molecule with complex systems that contain other coordinating sites and chiral centers along with a chiral phosphine oxide moiety. At the outset of this endeavor, we were interested in developing a reliable method that can be used by scientists at Merck for the determination of the absolute configuration of stereogenic phosphorous as part of pharmaceutical products. In this regards, determination of the absolute configuration of Sofosbuvir as a close analogue of most of pharmaceutical compounds containing stereogenic phosphorous was targeted (Figure II-42). Sofosbuvir is currently used for treatment of hepatitis C. This molecule has multiple chiral centers as well as different functionalities such as ester, amide, hydroxyl, etc. The only difference between the two stereoisomers of Sofosbuvir is the configuration on the stereogenic phosphorous atom. In an ideal scenario, the complex formation between the host system and these pseudo enantiomers (with regards to the phosphorous center) should yield ECCD signals with opposite sign. In this envisioned setting, the preference of the helical twists solely originates from the chirality on phosphorous and the substituents attached to this moiety.

Using hexane, the optimal solvent for most of our host:guest complex formations, both epimers of Sofosbuvir resulted in a positive ECCD signal, albeit with different intensities. The intensity of the ECCD signal for Sofosbuvir was higher than the ECCD signal for epi-Sofosbuvir. This observation was not unexpected, since these two epimers are diastereomers of one another.

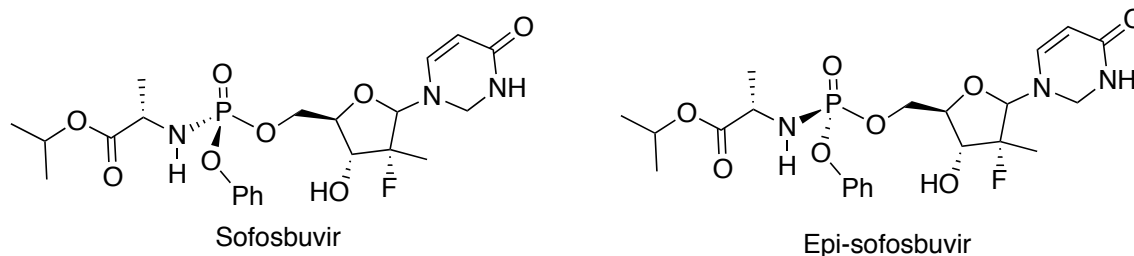


Figure II-42. Structures of Sofosbuvir and *epi*-Sofosbuvir.

We postulated that this inconsistency is the result of possible secondary interactions along with the primary coordination of the phosphorous oxygen moiety to the zinc centered porphyrin. These secondary interactions can exist as a result of hydrogen bonding or possibly coordination of heteroatoms of the substrate to the second zinc center. In other word, the two stereoisomers behave like two diastereomers (as they are) in complex formation with Zn-MAPOL and the opposite configuration on the phosphorous center is obscured by other parameters. Based on our previous findings with this host system, the phosphine oxide binding with zinc is the strongest interaction amongst other functionalities that are present in the molecule.

Our approach to this issue was to take advantage of the superior binding affinity of phosphine oxide in comparison to the other moieties and pursue strategies that weaken the overall interaction. We hypothesized that the weak interactions can be deteriorated or eliminated, while preserving the stronger interaction (phosphine oxide). In this manner, we investigated complex formation in the presence of different additives in order to weaken the putative secondary interactions that originate from other functionalities embedded in the molecule. It was noticed that different additives have a similar behavior, resulting in decreasing the ECCD intensity of both epimers.

Based on our previous investigations, the interaction between the host system and the guest molecule is maximized in hexane. As a result, the ECCD intensity in this is maximum for any given host-guest system. Hexane was chosen as solvent and the additives were used from their stock solutions in DCM. We noticed that after addition of about 50-100 equivalents of additive (butyl amine for instance) to the complex of Sofosbuvir and ZnMAPOL (1 μ M each), the ECCD signal of both epimers of Sofosbuvir decreases and the ECCD signal for epi-Sofosbuvir switches from positive to negative. We hypothesized that the additives either occupy the second zinc centered porphyrin or disrupt the possible hydrogen bonding network. As a result, the interaction between Sofosbuvir and ZnMAPOL becomes mono-dentate (as desired), thus the host/guest complex would follow the same mnemonic as a simple phosphine oxide substrate.

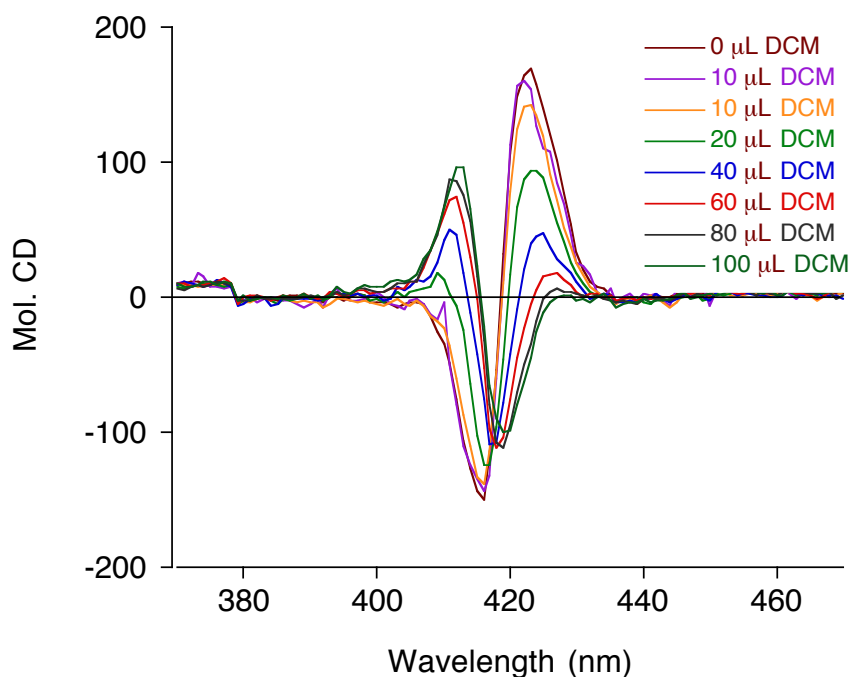


Figure II-43. ECCD spectra of epi-Sofosbuvir (1 equiv) complexed with ZnMAPOL (1 μ M) in hexane at room temperature, DCM was added.

The observed trend was similar for various additives. We realized that the effect is related to the change in solvent composition as opposed to the effect of additives (addition of DCM). Next, addition of DCM to a solution of Sofosbuvir and ZnMAPOL (1 μ M each) in hexane at room temperature was investigated (Figure II-43).

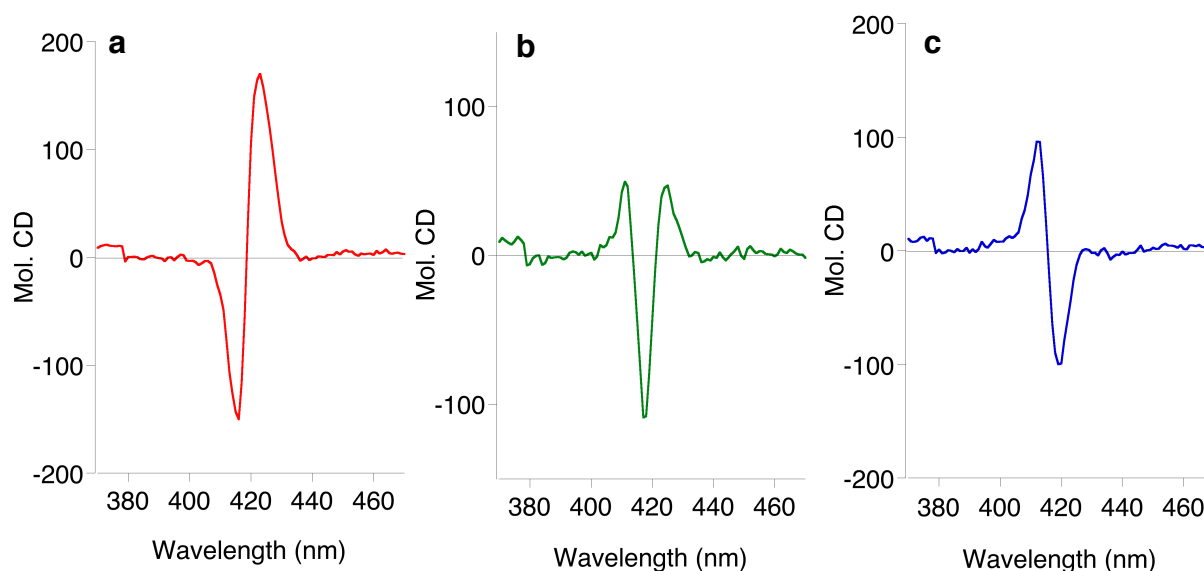


Figure II-44. ECD spectra of *epi*-Sofosbuvir (1 equiv) complexed with ZnMAPOL (1 μ M) in hexane at room temperature, NO dichloromethane was added (a), 40 μ L dichloromethane was added (b) and 100 μ L dichloromethane was added (c).

As observed before, the amplitude of the initial positive ECD signal of *epi*-Sofosbuvir in complex with ZnMAPOL (Figure II-44-a) decreased by addition of DCM. A clear switch in the ECD signal was observed upon addition of 40 μ L DCM to the complex in 1 mL hexane (Figure II-44-b) and followed by a clean negative signal after addition of 100 μ L of DCM (Figure II-44-c). Nevertheless, the ECD signal for Sofosbuvir showed a lower degree of dependence to the addition of DCM. After addition of 150 μ L DCM, the signal

decreased to ~80% of its initial intensity and the sign of the ECCD signal remained positive (Figure II-44).

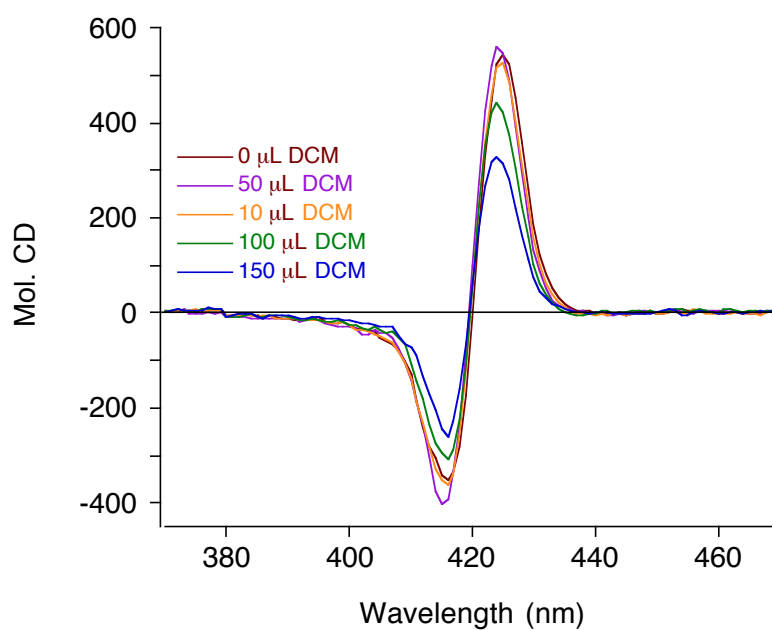


Figure II-45. ECCD spectra of Sofosbuvir (1 equiv) complexed with ZnMAPOL (1 μM) in hexane at room temperature, DCM was added.

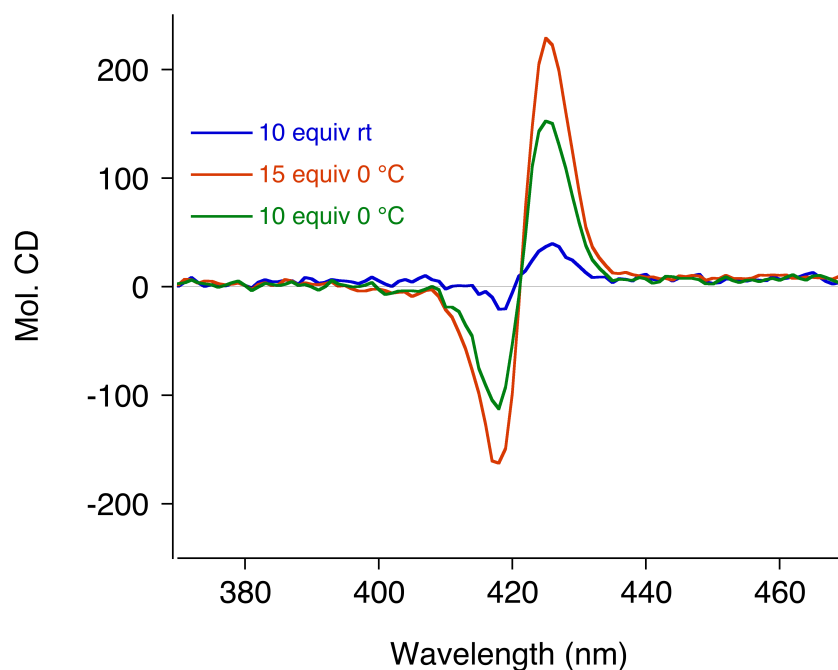


Figure II-46. ECCD spectra of Sofosbuvir complexed with ZnMAPOL (1 μ M) in dichloromethane.

Next we measured the ECCD spectra for both epimers of Sofosbuvir in DCM. Sofosbuvir (0.001 M in DCM) was added to a 1 μ M solution of ZnMAPOL in DCM at 0 °C. Addition of Sofosbuvir gave a positive ECCD signal (Figure II-45) while epi-Sofosbuvir produced a negative ECCD signal (Figure II-46). These data are consistent with the data in mixed hexane-DCM solvent system. Of note is the lower intensity of the ECCD signal in DCM, as compared to the signal for both epimers in hexane-DCM (compare Figures II-43 and II-45 to Figures II-46 and II-47).

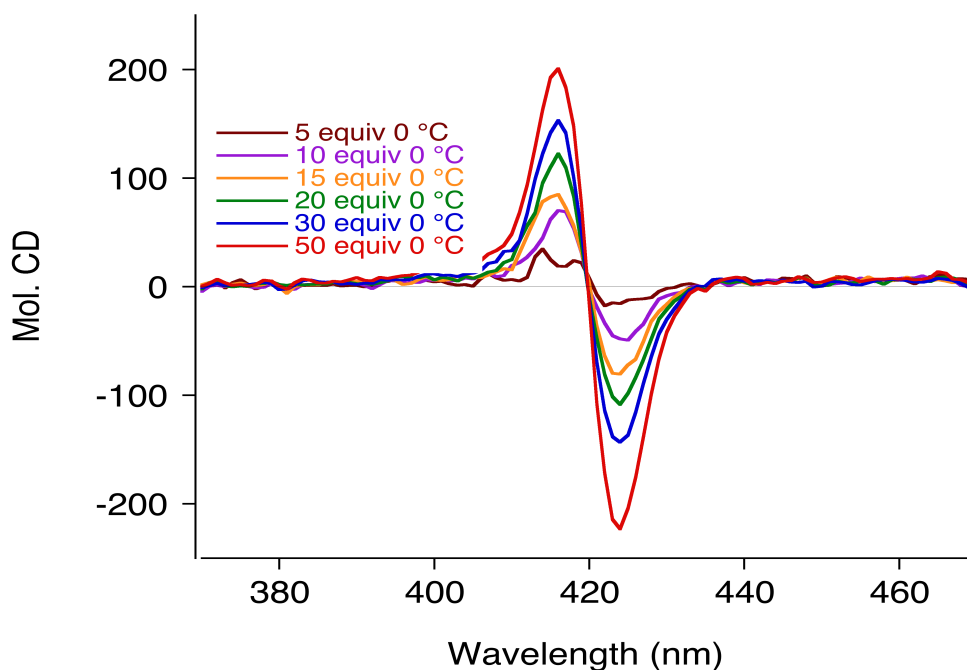


Figure II-47. ECCD spectra of *epi*-Sofosbuvir complexed with ZnMAPOL (1 μ M) in dichloromethane at 0 $^{\circ}$ C.

Furthermore, a variety of solvents were screened. Most of the solvents did not yield any detectable ECCD signal. However, chloroform gave similar results as to what was observed in DCM with slightly lower intensities for both epimers of Sofosbuvir (Figures II-48 and II-49). It should be noted that none of the previously studied functional groups form an ECCD active complex with porphyrin tweezers or MAPOL. Under this conditions other possible binding events were eradicated and the coordination of phosphine oxide was preserved, as it has by far the strongest interaction with the host system.

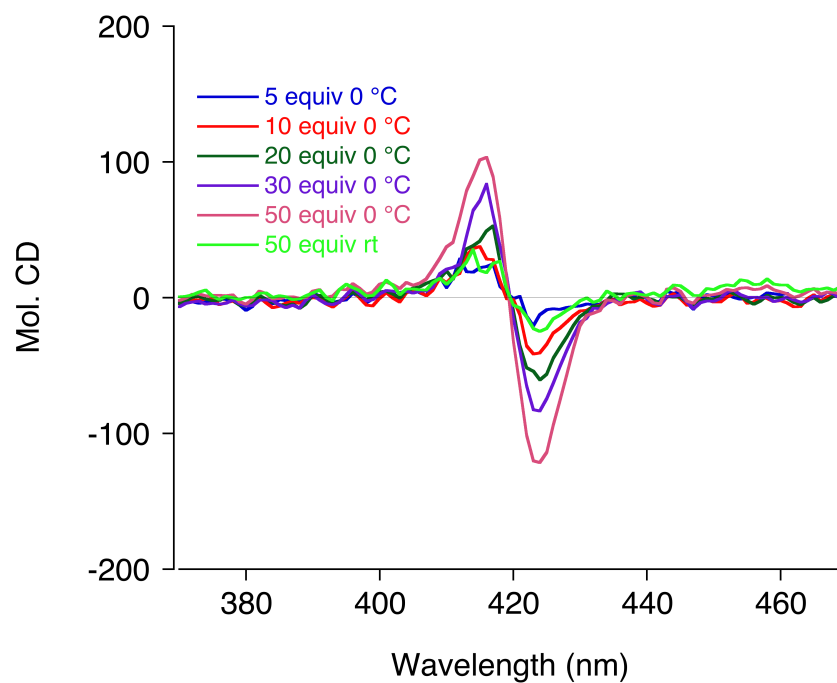


Figure II-48. ECCD spectra of *epi*-Sofosbuvir complexed with ZnMAPOL (1 μ M) in chloroform at 0 $^{\circ}$ C.

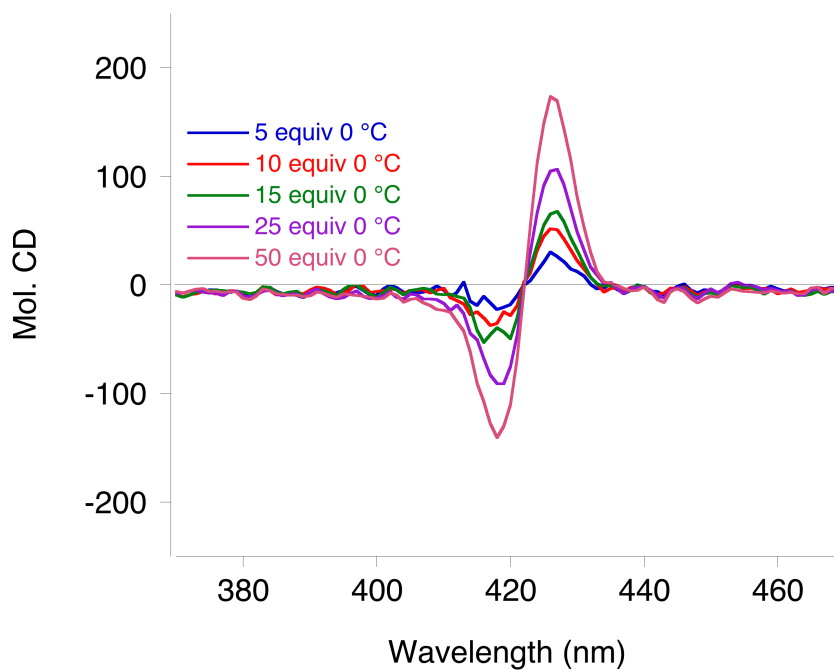


Figure II-49. ECCD spectra of Sofosbuvir complexed with ZnMAPOL (1 μ M) in chloroform at 0 $^{\circ}$ C.

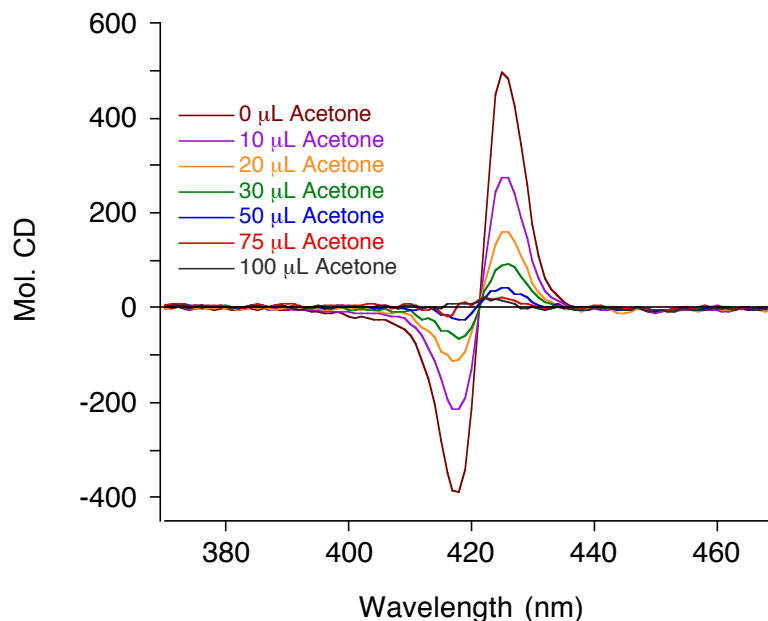


Figure II-50. ECCD spectra of Sofosbuvir (50 equiv) complexed with ZnMAPOL (1 μ M) in dichloromethane at 0 $^{\circ}$ C, effect of addition of acetone.

Since most chiral phosphine oxides embedded in pharmaceutical products are relatively polar, acetone is normally used to prepared the stock solution of these compounds. Thus, the effect of addition of acetone on the ECCD spectra of both epimers of Sofosbuvir was screened. To this end, to a solution of ZnMAPOL (1 μ M in DCM) Sofosbuvir (50 equiv) at 0 $^{\circ}$ C was added. CD spectra of the sample was collected after addition of 0,10, 20, 30, 50, 75 and 100 μ L acetone. Interestingly, addition of acetone resulted in a decrease of the intensity of the ECCD signal (Figure II-50). After 100 μ L of acetone the signal was completely lost. The same erosion of ECCD signal was observed for epi-Sofosbuvir upon addition of acetone (Figure II-51). As a result the stock solutions should be prepared in either DCM or chloroform.

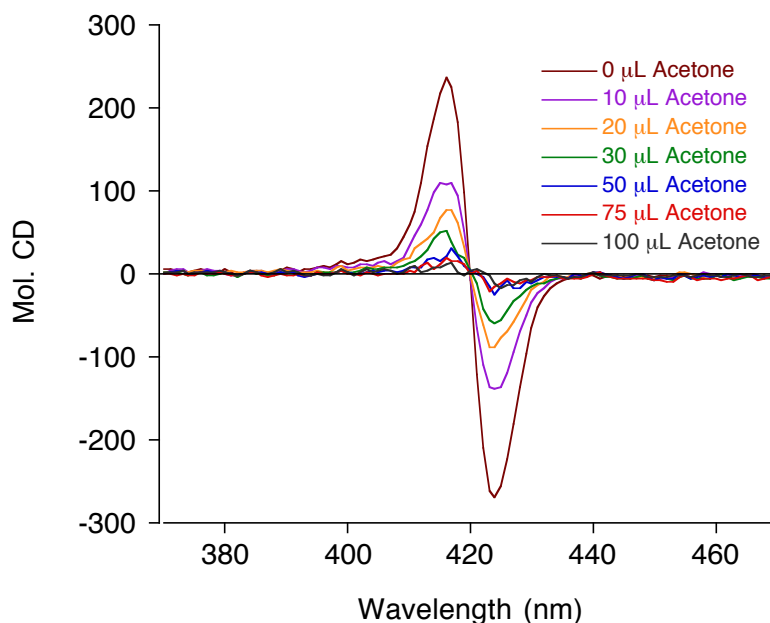


Figure II-51. ECCD spectra of *epi*-Sofosbuvir (50 equiv) complexed with ZnMAPOL (1 μ M) in dichloromethane at 0 $^{\circ}$ C, effect of addition of acetone.

To propose a working model, the relative sizes of the substituents on the phosphorous atom should be assigned. The O-phenyl is assigned as the smallest group, the substituent on the nitrogen atom as the medium size group and the uracil group as the largest group. Upon binding of the oxygen atom to the zinc, the smallest group (O-phenyl) on the phosphorous atom points towards the bound porphyrin. The remaining medium and large substituents project toward the second porphyrin ring. For the Sofosbuvir the *P*-helicity is favored as the large group is positioned away from the second porphyrin ring. This arrangement leads to a clockwise twist of the interacting chromophores, yielding a positive ECCD signal, which is in agreement with the measured spectrum (Figure II-52). Following the same analogy, *M*-helicity is preferred and as a result a negative ECCD signal is predicted for *epi*-Sofosbuvir, which is confirmed by the recorded ECCD signal (Figure II-53).

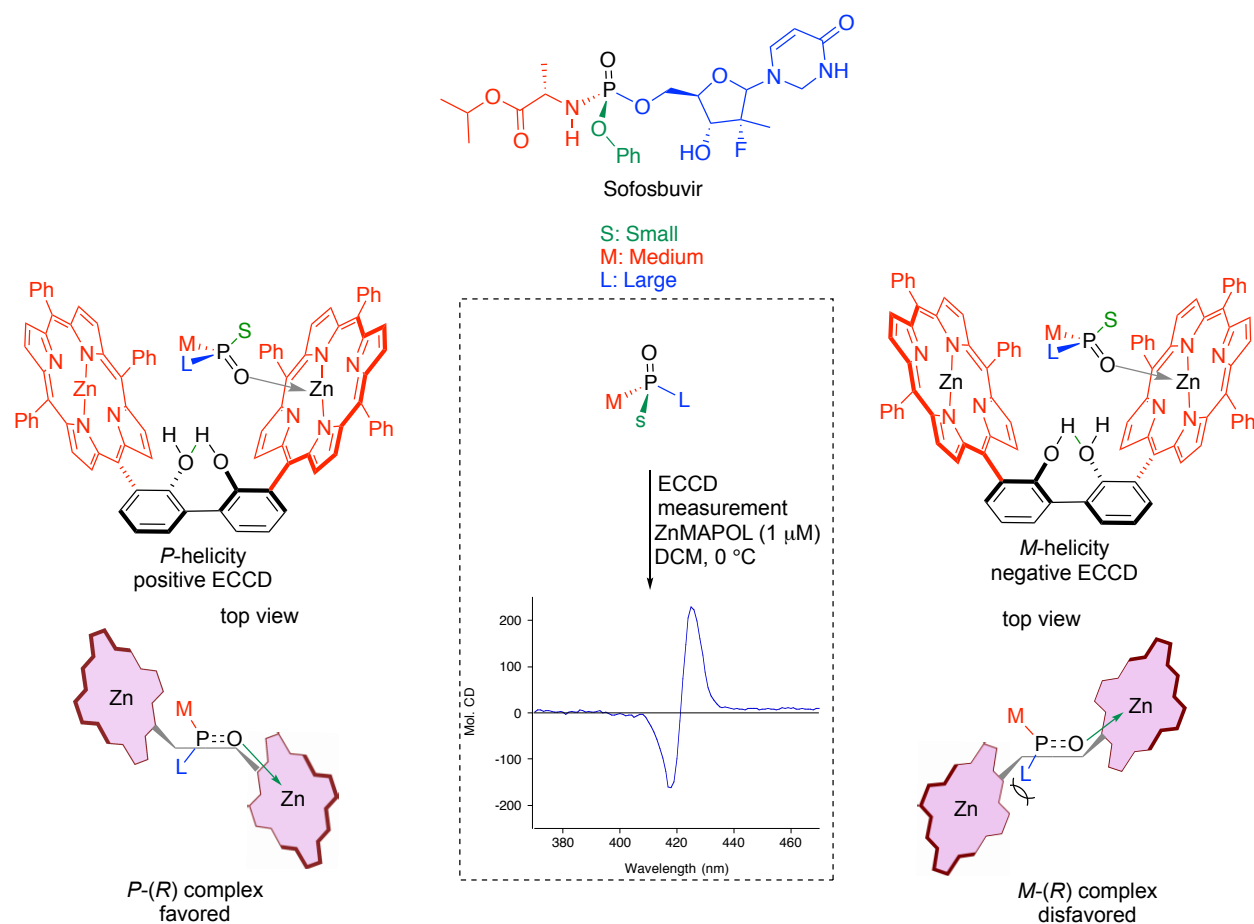


Figure II-52. Coordination and the working model of Sofosbuvir complexed with ZnMAPOL. *P*-helicity is favored and positive ECCD signal was observed.

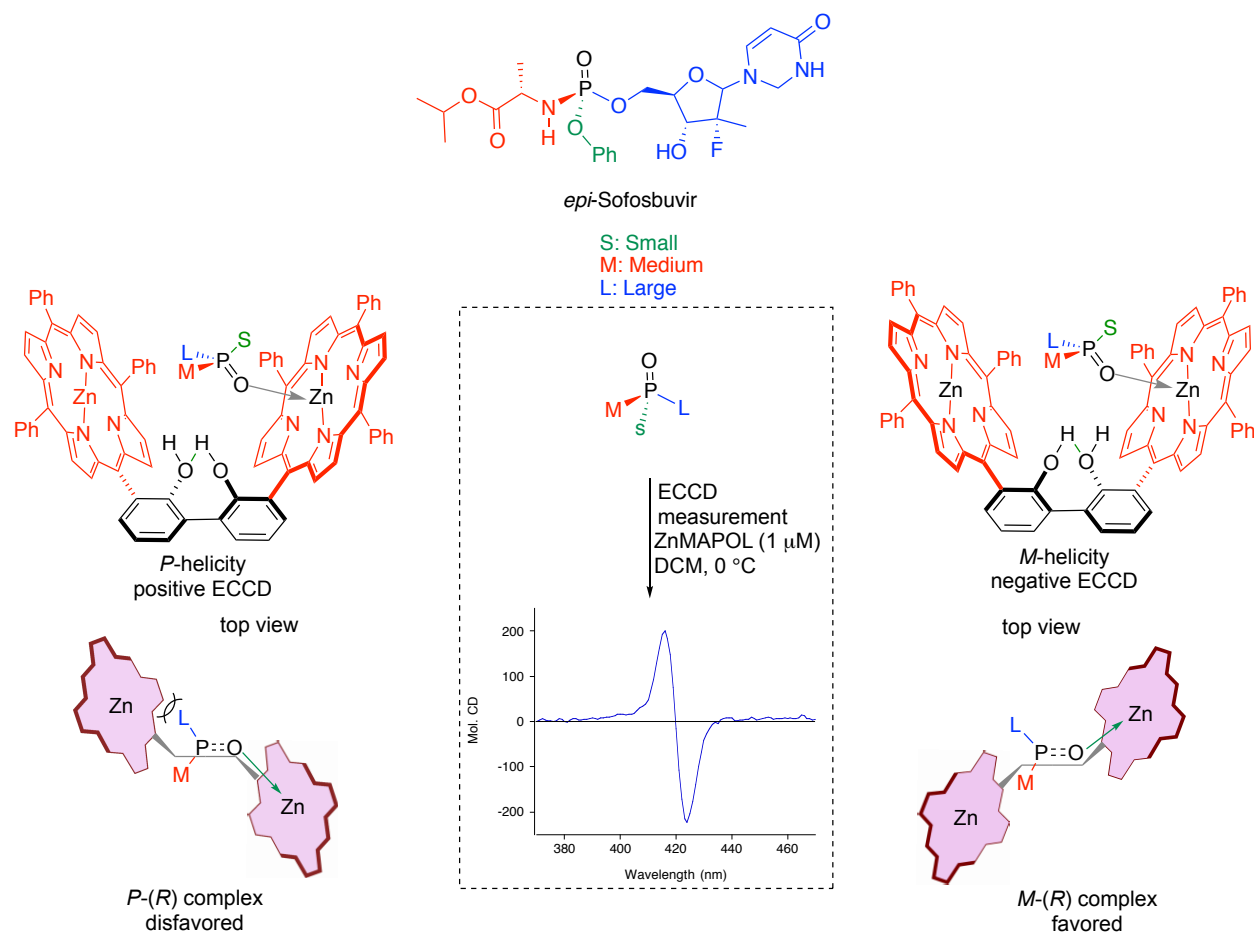


Figure II-53. Coordination and the working model of *epi*-Sofosbuvir complexed with ZnMAPOL *M*-helicity is favored and negative ECCD signal was observed.

II-4 Tuning electronic properties of MAPOL scaffold

MAPOL and its zincated analogue, Zn-MAPOL, are powerful hosts for the determination of absolute configuration of multiple functionalities. We sought to further investigate the binding capability of this scaffold by modulation of the electronic properties on the binding site. Namely, the hydrogen bonding affinity was thought to improve by placing fluorine atoms on the biphenol backbone. There are six hydrogens on the biphenyl moiety, and replacing them with fluorine atoms would result in more electron deficient aromatic rings that subsequently leads to more acidic hydroxyl groups. As a result, a stronger hydrogen binding network would be expected. Nonetheless, introducing fluorine in the 6,6' position of the host backbone results in elevating the rotational barrier of the diaryl bond, thus **II-31** was not a suitable backbone for host synthesis. We envisioned a backbone with only four fluorine atoms with hydrogens at 6,6' positioned to facilitate the free rotation along the diaryl bond (highlighted in bold, Figure II-54).

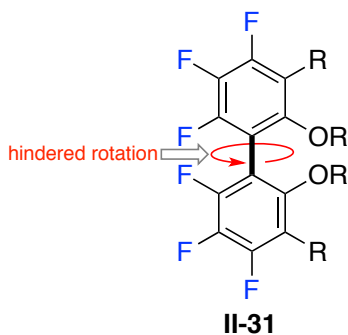


Figure II-54. Structural features of F₆-backbone.

The F4-MAPOL **II-32** was synthesized in a similar route described for MAPOL. We sought to utilize the improved hydrogen bonding affinity of this host system to form CD active complexes with alcohols as proof of concept. (*R*)-1-phenylethanol **II-33** as a model

alcohol was complexed with F₄-MAPOL, nonetheless the complex did not lead to an observable ECCD signal. This could be due to weak hydrogen bonding interaction between the host system and the alcohol or low energy difference of the diastereomeric rotomers. With this unsuccessful trial, we resorted to a different modification of the host system.

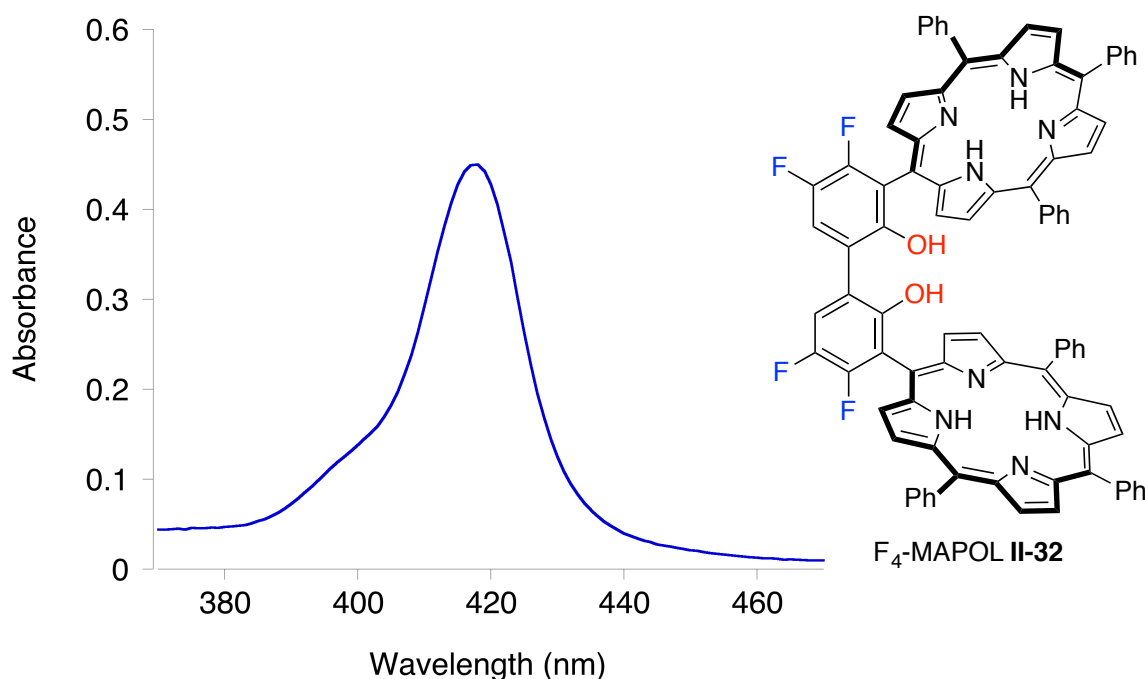


Figure II-55. Structure and UV-vis spectrum of F₄-MAPOL **II-32** (1 μ M solution) in hexane at room temperature.

Our previous studies with porphyrin tweezer system demonstrated that the high Lewis acidity of the zinc center on porphyrins is substantially influential to derive complex formation with alcohols. TPFP tweezers were successful in formation of ECCD active complexes with diols and epoxy alcohols. To this end, we pursued incorporation of fluorine atoms on the porphyrin ring in order to improve Lewis acidity on the zinc center. In analogy, F₃₀-Zn-MAPOL **II-34** was synthesized. This host system was complexed with

chiral (*R*)-1-phenylethanol. Gratifyingly, an ECCD signal was observed for this chiral alcohol in complex with F₃₀-Zn-MAPOL (Figure II-56). The latter modification presents a unique opportunity to further explore the applicability of this molecular receptor for molecules that lack the presence of strong coordinating sites. Further investigation into the generality of this methodology for determination of absolute configuration of chiral alcohols is ongoing.

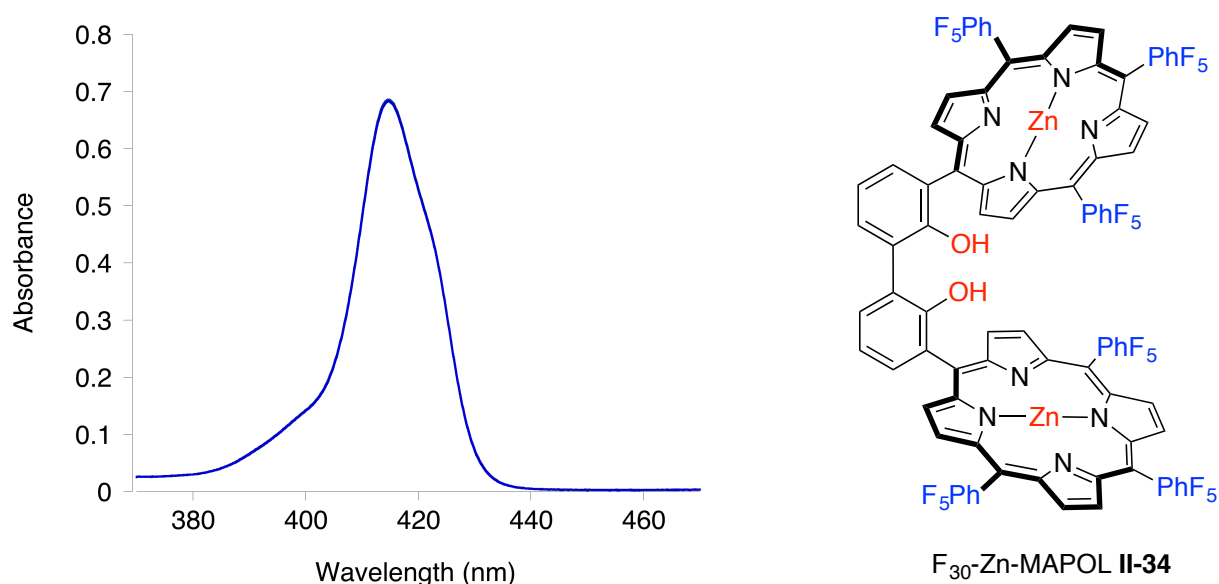


Figure II-56. Structure and UV-vis spectrum of F₃₀-Zn-MAPOL II-34 (1 μ M solution) in hexane at room temperature.

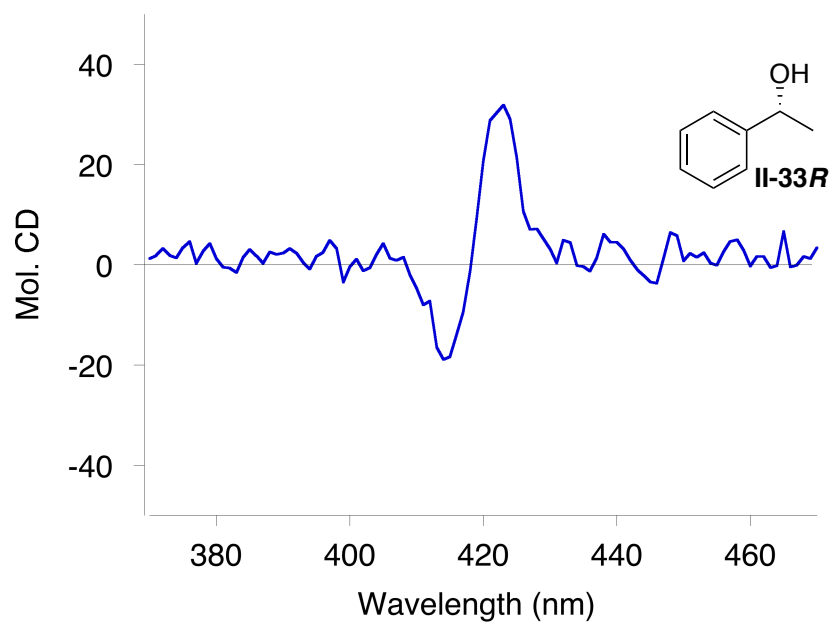


Figure II-57. ECCD spectrum of F_{30} -Zn-MAPOL (1 μ M) complexed with (*R*)-1-phenylethanol **II-33R** (100 equiv) in hexane at 0 °C.

II-5 Experimental section

II-5-1 Materials and general instrumentations

Anhydrous solvents used for CD measurements were purchased from Aldrich and were spectra grade. Unless otherwise mentioned, solvents were purified as follows. Toluene and CH_2Cl_2 were dried over CaH_2 whereas THF and Et_2O were dried over sodium (dryness was monitored by colorization of benzophenone ketyl radical); they were freshly distilled prior to use. NMR spectra were obtained using 500 MHz Varian NMR spectrometers and referenced using the residual ^1H peak from the deuterated solvent. Column chromatography was performed using Silicycle 60Å, 35-75 μm silica gel. Pre-coated 0.25 mm thick silica gel 60 F254 plates were used for analytical TLC and visualized using UV light, iodine, potassium permanganate stain, *p*-anisaldehyde stain or phosphomolybdic acid in EtOH stain. CD spectra were recorded on a JASCO J-810 spectropolarimeter, equipped with a temperature controller (Neslab 111) for low temperature studies, and are reported as Mol. CD / λ [nm]. UV-vis spectra were recorded on an Agilent, Cary 100 UV-visible spectrophotometer with scan rate of 100nm/min.

II-5-2 Procedure for UV-vis and CD titration of Zn-MAPOL with chiral guest molecules (cyanohydrins, sulfoxides or phosphine oxides)

II-5-2-1 General procedure for UV-vis measurement

Zn-MAPOL **II-4** (1 μL of a 0.001 M solution in anhydrous CH_2Cl_2) was added to hexane (> 95% *n*-Hexane) (1 mL) in a 1.0 cm UV-cell to obtain a 1 μM solution. The background spectrum was recorded from 350 nm to 500 nm with a scan rate of 100

nm/min. Chiral guest (1 up to 5000 equivalents) from a stock solution (in anhydrous dichloromethane) with different concentration was added as follows: For less than 20 equivalents a stock solution with concentration of 1 μM was used; A 0.01 M solution was used for up to 100 equivalents, a 0.1 M solution was used for up to 100 equivalents, and for more than 1000 equivalents if needed a 1 M solution was used. As a result, the maximum dilution of the spectroscopic sample was kept to less than 0.5% of the initial volume. The UV spectrum was measured after each addition. In order to compensate for the cyanohydrin contribution on the observed UV spectrum, same amount of cyanohydrin was added to the reference UV sample for each titration point.

II-5-2-2 General procedure for CD measurement

Zn-MAPOL (1 μL of a 0.01 M solution in anhydrous CH_2Cl_2) was added to hexane (> 95% *n*-Hexane) (1 mL) in a 1.0 cm CD cell (equipped with cooling water circulation) to obtain a 1 μM solution (for cyanohydrins derived from ketone (**11-15**) 2 μL Zn-MAPOL was used, resulting in a 2 μM solution for CD measurements). The background spectrum was recorded from 350 nm to 480 nm with a scan rate of 100 nm/min at 0 °C. Chiral guest (up to 1000 equivalents of a 0.01 M or 0.1 M solution in anhydrous CH_2Cl_2) was added into the prepared host solution to afford the host/guest complex. The CD spectra were measured immediately (10 accumulations). The resultant ECCD spectra recorded in millidegrees were normalized based on the host concentration (1 μM or 2 μM) to obtain the molecular CD (Mol. CD).

II-5-3 Job's continuous plot analysis to determine the stoichiometry of complex between Zn-MAPOL and chiral guest molecules and binding constant measurements of the complex

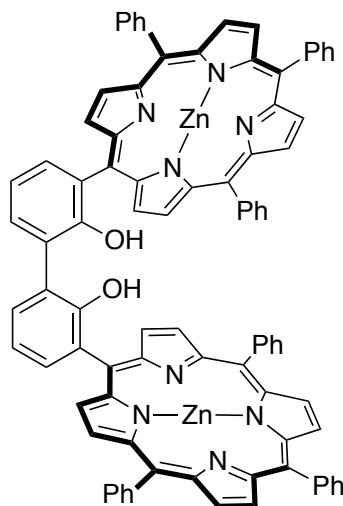
Job's plot analysis was achieved from changes in the UV-vis absorbance of Zn-MAPOL upon addition of chiral molecules according to the following procedure: To 1 mL of hexanes in a 1 cm cuvette, Zn-MAPOL (1 μ L of a 1 mM stock solution) was added. UV-vis spectrum was collected (350 nm-500 nm). To this Zn-MAPOL solution, chiral guest at (0.25, 0.5, 0.75, 1, 2, 5, 7.5, 10, 20, 30, 40, 50, and 75 equivalents) was added and UV-vis spectra (350 nm-500 nm) were recorded after each addition. Changes in the UV-vis absorbance (ΔA_{abs}) were calculated by subtracting the absorbance at each titration point from the absorbance of free Zn-MAPOL at 410 or 409 nm. The molar fraction of Zn-MAPOL ($X_{\text{Zn-MAPOL}}$) multiplied by the change in UV-vis absorbance (ΔA_{abs}) for each titration point was determined and was plotted against the molar fraction of Zn-MAPOL. Binding constants of the complex between Zn-MAPOL and chiral guest molecules were also extracted from changes in the UV-vis spectrum of host system upon addition of chiral guest molecules. Plotting the changes at 410 or 409 nm against the concentration of guest molecule lead to the corresponding curve that the K_{assoc} values were evaluated employing the following equation reported by Aida and co-workers:⁵²

$$\Delta \text{Abs} = (L(1 + K_{\text{assoc}}X + K_{\text{assoc}}A) - (L^2(K_{\text{assoc}}X + K_{\text{assoc}}A + 1)^2 - 4 K_{\text{assoc}}^2 AXL^2)^{0.5}) / 2K_{\text{assoc}}A$$

where X and A represent $[\text{Guest}]_{\text{total}}$ and $[\text{Host}]_{\text{total}}$, respectively; L denotes ΔAbs at 100% complexation; L and K_{assoc} are parameters.

II-5-4 Synthesis of the host systems

II-5-4-1 Synthesis of Zn-MAPOL



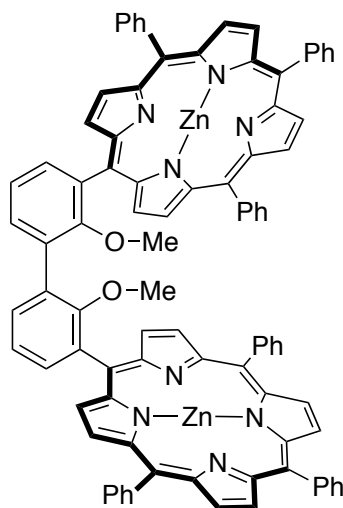
Zn-MAPOL II-4

Following a standard procedure, to a solution of MAPOL (12.6 mg, 0.010 mmol) in dry dichloromethane (2 mL) was added 5 drops of a saturated solution of zinc acetate $[\text{Zn}(\text{OAc})_2]$ in methanol (saturated solution of zinc acetate in methanol was prepared from a zinc acetate sample that was washed with dichloromethane, ethyl acetate, and diethyl ether successively, followed by drying under vacuum). Reaction was stirred at room temperature for 12 h. The reaction mixture was passed through a plug of celite. The filtrate was deposited on silica gel and place on a pipet column. DCM was used as eluent to deliver pure zincated MAPOL (Zn-MAPOL **3**) (12 mg, 86 %).

^1H -NMR (500 MHz, CDCl_3); δ 6.22 (s, 2H, OH), 7.56 (m, 6H), 7.64 (m, 8H), 7.68-7.74 (m, 6H), 8.02 (d, $J = 7.0$ Hz, 4H), 8.09-8.14 (m, 8H), 8.16-8.17 (m, 4H), 8.79 (d, $J = 4.0$ Hz, 4H), 8.85 (d, $J = 5.0$, 4H), 8.88 (d, $J = 4.0$ Hz, 4H), 8.96 (d, $J = 5.0$ Hz, 2H) ppm.

^{13}C -NMR (125 MHz, CDCl_3); δ 113.7, 120.3, 121.2, 125.8, 126.4, 126.5, 127.4, 127.5, 130.4, 131.2, 131.9, 132.0, 132.7, 134.2, 134.3, 134.8, 142.5, 142.6, 150.1, 150.2, 150.3, 150.4, 152.6 ppm.

II-5-4-2 Synthesis of Zn-MAPOL-OMe II-40



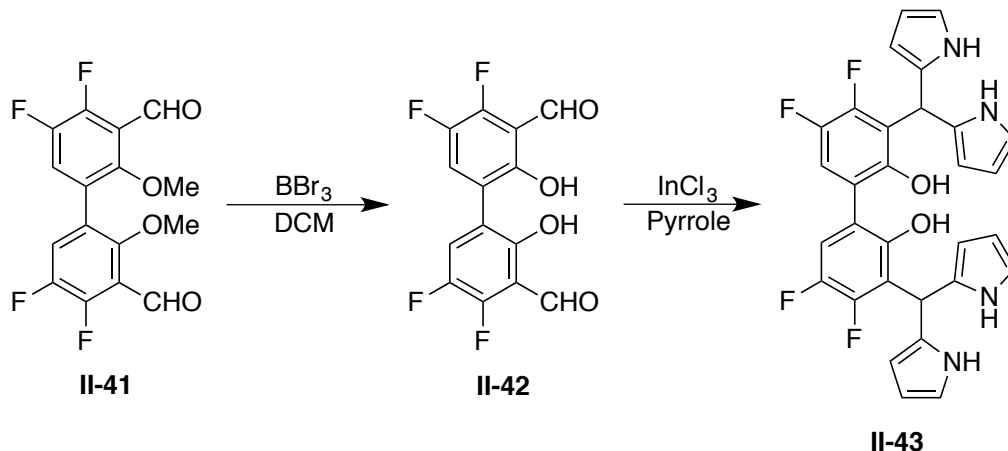
Zn-MAPOL-OMe II-35

MAPOL-OMe (10.0 mg, 0.008 mmol) was converted into Zn-MAPOL-OMe (10.0 mg, 90%) according to the procedure described for preparation of Zn-MAPOL II-4.

^1H -NMR (500 MHz, CDCl_3); δ 2.95 (s, 6H), 7.57 (dd, $J_1 = 8$ Hz, $J_2 = 7$ Hz, 2H), 7.66-7.76 (m, 18H), 8.10 (m, 4H), 8.15 (d, $J = 7$ Hz, 4H), 8.18 (d, $J = 5$ Hz, 6H), 8.22 (d, $J = 6$ Hz, 2H), 8.87 (m, 4H), 8.91 (m, 8H), 9.04 (m, 4H).

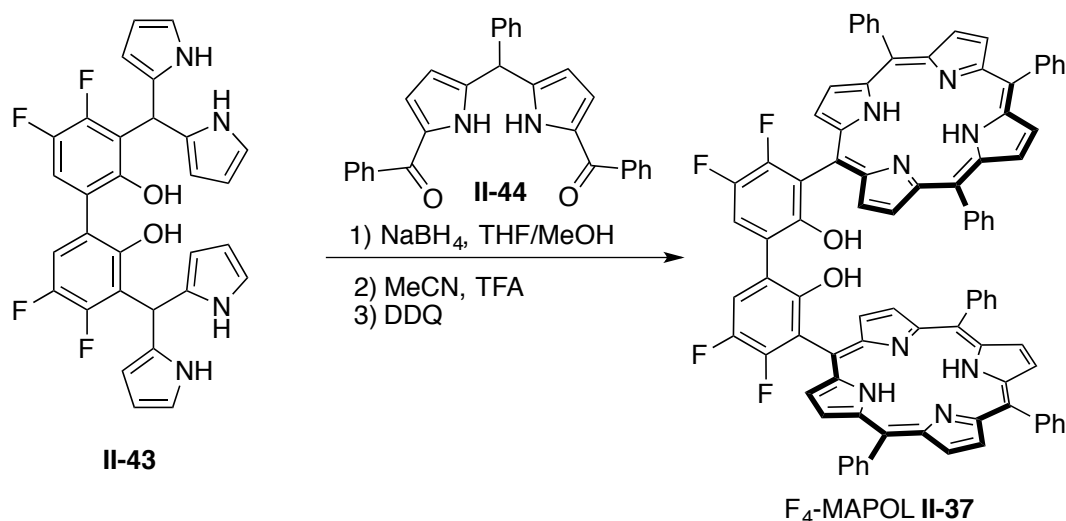
^{13}C -NMR (125 MHz, CDCl_3); δ 61.0, 116.8, 121.0, 121.3, 121.9, 126.4, 126.5, 127.4, 131.7, 131.8, 131.9, 132.1, 132.2, 134.3, 134.4, 135.5, 135.9, 142.7, 142.8, 150.0, 150.1, 150.2, 150.4, 158.2 ppm

II-5-4-3 Synthesis of F₄-Zn-MAPOL



Synthesis of F₄-Bisphenol-dipyrromethan **II-43:** To a sample of dimethoxy bisaldehyde **II-41** (0.34 g, 1.0 mmol) in dry methylene chloride (10 mL) was added BBr_3 [5.0 mmol, 5.0 mL (1.0 M solution in methylene chloride)] drop-wise under atmosphere of argon at 0 °C. The reaction was stirred at room temperature for 12 h before it was quenched with saturated solution of ammonium bicarbonate (NH_4HCO_3). The reaction was extracted with methylene chloride, dried (Na_2SO_4) and volatiles were removed. The crude was taken up in pyrrole (200 mmol, 14.0 mL). To this solution was added InCl_3 (0.1 equiv, 0.1 mmol) at room temperature under atmosphere of argon. Reaction was stirred at this temperature for 90 min. NaOH (0.3 g) was added to the reaction and stirring was continued for another hour. Reaction mixture was filtered; excess pyrrole was isolated by distillation 1 at 45-50 °C under vacuum (~0.1 torr). and crude product was purified by column chromatography (1:1 ethyl acetate/hexanes). 300 mg dipyrromethane product **II-43** was isolated, 54 % yield over two steps.

^1H NMR (500 MHz, CDCl_3) δ 8.39 (s, 4H, NH), 6.79 (m, 4H), 6.71 (m, 2H), 6.21 (m, 4H), 6.14 (m, 4H), 5.97 (s, 2H), 5.57 (s, 2H).

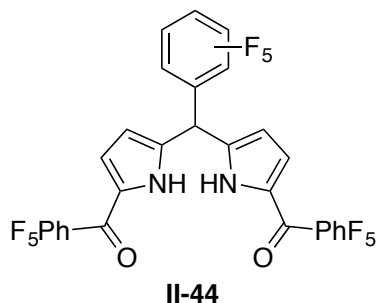


F₄-MAPOL II-37 was synthesized from **II-43** following the procedure described for the synthesis of MAPOL.¹ To a solution of freshly prepared 1,9-bis(benzoyl)-5-phenyldipyrromethane **II-44** (0.43 g, 1.0 mmol) in dry THF/methanol (10:1, 44 mL) was added NaBH₄ (0.766 g, 20.0 mmol) in several portions. After completion of the reduction (TLC 40% EtOAc/Hexanes), saturated NH₄Cl (70 mL) and CH₂Cl₂ (130 mL) were added to the reaction mixture. The organic layer was separated, washed twice with water, dried (Na₂SO₄), and placed in a 1000-mL round-bottomed flask. Removal of the solvent by rotary evaporation under vacuum yielded the dicarbinol as a foamlike yellow solid. To this crude product, dipyrromethane **II-43** (0.27 g, 0.5 mmol) and acetonitrile (400 mL) were added, and the mixture was stirred to achieve a homogeneous yellow solution. TFA (0.930 mL, 12.2 mmol) was added with rapid stirring. After 5 min, DDQ (0.67 g, 3.7 mmol) was added. After stirring for 1 h at room temperature, triethylamine (1.69 mL, 12.2 mmol) was added, and the entire reaction mixture was filtered through a pad of alumina (4 x 8 cm) and washed with CH₂Cl₂ (~ 500 mL) until the eluant was no longer colored. The

resulting porphyrin solution was concentrated, redissolved in CH₂Cl₂ (50 mL), and passed through a pad of silica (4 x 8 cm) with CH₂Cl₂ to remove nonporphyrinic pigments. The purple fractions were combined and concentrated to give a purple solid. Precipitation from CH₂Cl₂/methanol gave the pure product **II-37** (35 mg, 5.2% yield).

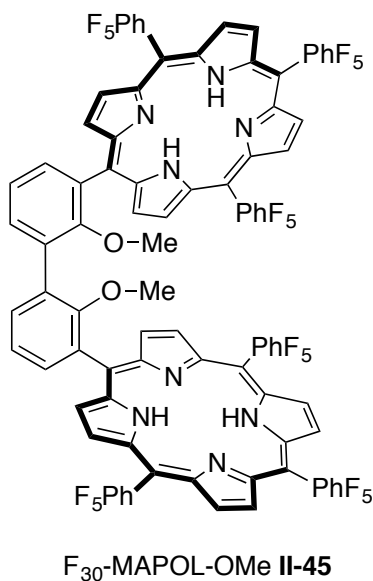
¹H NMR (500 MHz, CDCl₃) δ 9.06 (br, 4H), 9.2 (br, 4H), 8.89 (br, 8H), 8.25 (m, 12H), 7.81 (m, 20H), 7.55 (br, 2H), -2.61 (br, 4H).

II-5-4-4 Synthesis of F₃₀-Zn-MAPOL



(((perfluorophenyl)methylene)bis(1H-pyrrole-5,2-diyl))bis ((perfluorophenyl)methanone) II-44: This compound was synthesized according to previously reported procedures.⁵³

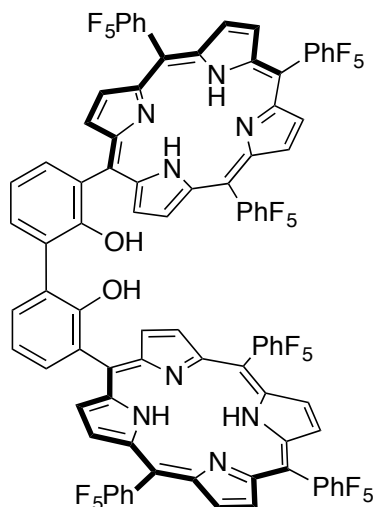
¹H NMR (500 MHz dms_o-d₆) δ 12.70 (s, 2H, NH), 6.87 (br, 2H), 6.03 (s, 1H), 6.01(br, 2H).



F₃₀-MAPOL-OMe II-45 was synthesized using F₃₀-diacyl dipyrromethan **II-44** following the standard procedure described for the synthesis of MAPOL.¹ To a solution of

freshly prepared F₃₀-diacyl dipyrromethan **II-44** (0.7 g, 1.0 mmol) in dry THF/methanol (10:1, 44 mL) was added NaBH₄ (0.766 g, 20.0 mmol) in several portions. After completion of the reduction (TLC 40% EtOAc/Hexanes), saturated NH₄Cl (70 mL) and CH₂Cl₂ (130 mL) were added to the reaction mixture. The organic layer was separated, washed twice with water, dried (Na₂SO₄), and placed in a 1000-mL round-bottomed flask. Removal of the solvent by rotary evaporation under vacuum yielded the dicarbinol as a foamlike yellow solid. To this crude product, dipyrromethane **I-34** (0.23 g, 0.50 mmol) and acetonitrile (400 mL) were added, and the mixture was stirred to achieve a homogeneous yellow solution. TFA (0.93 mL, 12.2 mmol) was added with rapid stirring. After 5 min, DDQ (0.67 g, 3.7 mmol) was added. After stirring for 1 h at room temperature, triethylamine (1.69 mL, 12.2 mmol) was added, and the entire reaction mixture was filtered through a pad of alumina (4 x 8 cm) and washed with CH₂Cl₂ (~ 500 mL) until the eluant was no longer colored. The resulting porphyrin solution was concentrated, redissolved in CH₂Cl₂ (50 mL), and passed through a pad of silica (4 x 8 cm) with CH₂Cl₂ to remove nonporphyrinic pigments. The purple fractions were combined and concentrated to give a purple solid. Precipitation from CH₂Cl₂/methanol gave the pure product **II-45** (20 mg, 2.1%).

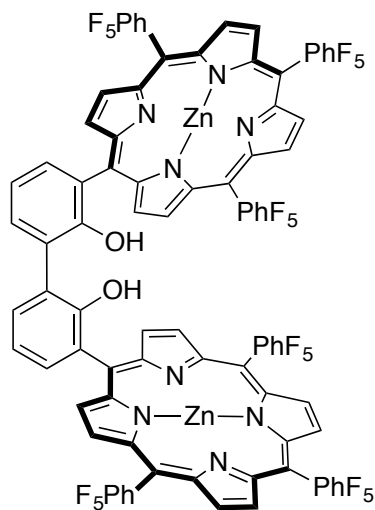
¹H NMR (500 MHz, CDCl₃) δ 9.17 (br, 4H), 8.96 (s, 8H), 8.84 (s, 4H), 8.14 (m, 4H), 7.66 (dd, *J*₁ = *J*₂ = 7.6 Hz, 2H), 2.97 (s, 6H), -2.81 (br, 4H).



F₃₀-MAPOL II-46

F₃₀-MAPOL II-46 Following the standard procedure described for the synthesis of MAPOL,¹ F₃₀-MAPOL-OMe was subjected demethylation of the methoxyl group through reaction with BBr₃. The crude was used in the next step without purification.

¹H NMR (500 MHz, CDCl₃) δ 9.03 (br, 4H), 8.88 (br, 8H), 8.70 (br, 4H), 8.19 (dd, *J* = 7.5, 1.8 Hz, 2H), 8.12 (dd, *J* = 7.5, 1.8 Hz, 2H), 7.63 (dd, *J* = 7.5 Hz, 2H), -2.91 (s, 4H).



F₃₀-Zn-MAPOL II-39

F₃₀-Zn-MAPOL II-39 was prepared from **F₃₀-MAPOL** (20 mg) following the procedure described for Zn-MAPOL³² synthesis. 15 mg pure product was prepared 71% yield over two steps.

¹H NMR (500 MHz, CDCl₃) δ 9.11 (d, *J* = 4.7 Hz, 4H), 8.92 (q, *J* = 4.7 Hz, 8H), 8.79 (d, *J* = 4.7 Hz, 4H), 8.20 (dd, *J* = 7.5, 1.7 Hz, 2H), 8.14 (dd, *J* = 7.5, 1.7 Hz, 2H), 7.65 (dd, *J*₁ = *J*₂ = 7.5 Hz, 1H), 6.14 (s, 2H, OH).

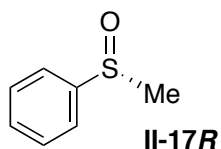
II-5-5 Synthesis of chiral cyanohydrins

Asymmetric silylated cyanohydrines derived from aldehydes and ketones were converted into their corresponding chiral cyanohydrins according to the reported procedure.¹⁴ Cyanohydrins **II-5R**,¹⁴ **II-5S**,¹² **II-6R**,¹⁴ **II-7S**,¹² **II-10R**,¹⁴ **II-11R**,¹⁴ **II-12R**,¹³ **II-12S**,¹³ **II-13R**,¹³ **II-13S**,¹³ **II-14R**,¹³ **II-14S**,¹³ **II-15R**,¹³ **II-15S**¹³ and **II-16R**¹⁵ were synthesized according to reported procedures.

Cyanohydrins derived from ketones: **II-12R**, **II-12S**, **II-13R**, **II-13S**, **II-14R**, **II-14S**, **II-15R**, **II-15S** were synthesized according to method D in the referenced study.¹³ *L*-Phenylglycine was applied as catalyst to access the *R* cyanohydrins and cyanohydrin with *S* configuration were synthesized using *R*-phenylglycine as chiral catalyst.

II-5-6 Synthesis of chiral sulfoxides

Chiral sulfoxides with known configuration on the stereogenic sulfur were synthesized according to reported procedures. Enantiomeric purity of the synthesized chiral sulfoxides was measured using optical rotation and comparison with the known literature values.



Methyl phenyl sulfoxide (**II-17R** and **II-17S**):

R enantiomer was synthesized according to the reported procedure.³⁵

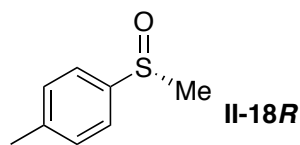
$[\alpha]_D = +138.8$ ($c = 2.0$, EtOH), $ee = 85\%$; Lit.³⁵ $+149$ ($c = 2.0$, EtOH);

S enantiomer was synthesized according to the reported procedure.³⁵

$[\alpha]_D = -116.5$ ($c = 1.0$, acetone), $ee = 81\%$; Lit.³⁵ -143 ($c = 1.0$, acetone);

^1H NMR (500 MHz CDCl_3) δ 7.74 – 7.54 (m, 2H), 7.54 – 7.46 (m, 3H), 2.70 (s, 3H). ^{13}C

NMR (126 MHz, CDCl_3) δ 145.55, 130.98, 129.30, 123.46, 123.42, 43.88.



Methyl *p*-tolyl sulfoxide (**II-18R** and **II-18S**):

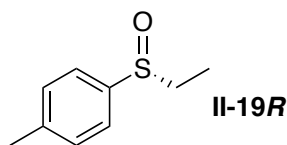
R enantiomer was synthesized according to the reported procedure.³⁷

$[\alpha]_D = +116$ ($c = 1.0$ ethanol), $ee = 77\%$; Lit.⁵⁴ $+151$ ($c = 1.0$, ethanol)

S enantiomer was synthesized according to the reported procedure.³³

$[\alpha]_D = -86$ ($C = 1.0$), $ee = 57\%$; Lit.⁵⁵ -150 ($c = 2.0$, acetone)

^1H NMR (500 MHz, CDCl_3) δ 7.61 – 7.44 (m, 2H), 7.37 – 7.28 (m, 2H), 2.69 (s, 3H), 2.40 (s, 3H). ^{13}C NMR (126 MHz, CDCl_3) δ 142.49, 141.49, 130.02, 123.52, 44.02, 21.41.



Ethyl *p*-tolyl sulfoxide (**II-19R** and **II-19S**):

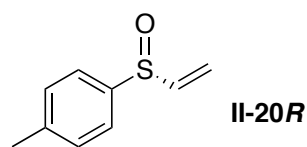
R enantiomer was synthesized according to the reported procedure.³⁷

$[\alpha]_D = +168$ ($c = 1.0$ acetone); Lit.⁵⁶ $+198$ ($c = 1.0$, acetone); $ee = 85\%$

S enantiomer was synthesized according to the reported procedure.³³

$[\alpha]_D = -119$ ($c = 1.0$ acetone); Lit.⁵⁷ -202 ($c = 1.0$, acetone); $ee = 60\%$

^1H NMR (500 MHz, CDCl_3) δ 7.59 – 7.38 (m, 2H), 7.37 – 7.25 (m, 2H), 2.85 (dq, $J = 13.2$, 7.4 Hz, 1H), 2.73 (dt, $J = 13.2$, 7.4 Hz, 1H), 2.39 (s, 3H), 1.16 (t, $J = 7.4$ Hz, 3H). ^{13}C NMR (126 MHz, CDCl_3) δ 141.34, 140.06, 129.81, 124.19, 50.35, 21.40, 6.04.



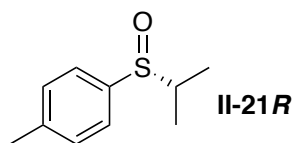
(*R*)-*p*-Tolyl vinyl sulfoxide (**II-20R**):

$[\alpha]_D = +376$ ($c = 1.0$, acetone) Lit.⁵⁸ $+400$ ($c = 1.0$, acetone); $ee = 94\%$

R enantiomer was synthesized according to the reported procedure.³⁷

^1H NMR (500 MHz, CDCl_3) δ 7.50-7.48 (m, 2H), 7.30-7.28 (m, 2H), 6.56 (dd, $J = 16.5$, 9.6 Hz, 1H), 6.17 (d, $J = 16.5$ Hz, 1H), 5.86 (d, $J = 9.6$ Hz, 1H), 2.39 (s, 3H).

^{13}C NMR (126 MHz, CDCl_3) δ 143.03, 141.87, 140.07, 130.13, 124.87, 120.38, 21.43.



i-Propyl *p*-tolyl sulfoxide (**II-21R** and **II-21S**):

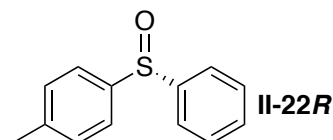
R enantiomer was synthesized according to the reported procedure.³⁷

$[\alpha]_D = +164$ ($c = 1.0$, acetone); Lit.³⁵ $+194$ ($c = 0.9$, acetone); $ee = 85\%$

S enantiomer was synthesized according to the reported procedure.³³

$[\alpha]_D = -101$ ($c = 1.0$, acetone); Lit.⁵⁹ -194 ($c = 1.0$, acetone); $ee = 52\%$

^1H NMR (500 MHz, CDCl_3) δ 7.51 – 7.38 (m, 2H), 7.31 – 7.27 (m, 2H), 2.78 (h, $J = 6.9$ Hz, 1H), 2.39 (s, 3H), 1.17 (d, $J = 6.9$ Hz, 3H), 1.12 (d, $J = 6.9$ Hz, 3H). ^{13}C NMR (126 MHz, CDCl_3) δ 141.36, 138.44, 129.55, 125.03, 54.50, 21.41, 15.71, 14.12.



Phenyl *p*-tolyl sulfoxide (**II-22R** and **II-22S**):

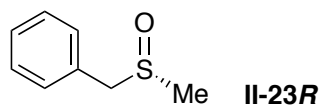
R enantiomer was synthesized according to the reported procedure.³⁷

$[\alpha]_D = +16.0$ ($c = 1.0$, acetone); Lit.⁶⁰ $+21$ ($c = 2.0$, acetone); $ee = 76\%$

S enantiomer was synthesized according to the reported procedure.³³

$[\alpha]_D = -12.6$ ($c = 1.0$, acetone); Lit.⁶⁰ -21 ($c = 2.0$, acetone); $ee = 61\%$

^1H NMR (500 MHz, CDCl_3) δ 7.61 – 7.59 (m, 2H), 7.51 – 7.49 (m, 2H), 7.44 – 7.38 (m, 3H), 7.26 – 7.22 (m, 3H), 2.34 (s, 3H). ^{13}C NMR (126 MHz, CDCl_3) δ 145.77, 142.44, 141.62, 130.85, 130.01, 129.23, 124.96, 124.66, 21.40.

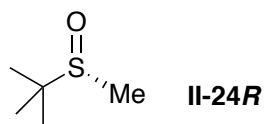


(*R*)-Benzyl methyl sulfoxide (**II-23R**):

R enantiomer was synthesized according to the reported procedure.³⁵

$[\alpha]_D = -88.1$ ($c = 1.0$, EtOH), $ee = 84\%$; Lit.³⁵(Fernandez, 1992 #22) -105 ($c = 6.0$, EtOH);

^1H NMR (500 MHz, CDCl_3) δ 7.38 – 7.32 (m, 3H), 7.30 – 7.25 (m, 2H), 4.04 (d, $J = 12.8$ Hz, 1H), 3.91 (d, $J = 12.8$ Hz, 1H), 2.43 (s, 3H). ^{13}C NMR (126 MHz, CDCl_3) δ 129.98, 129.61, 128.96, 128.41, 60.30, 37.26.



t-Butyl methyl sulfoxide (**II-24R** and **II-24S**):

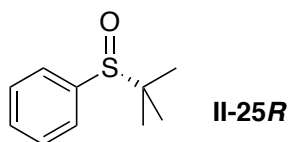
R enantiomer was synthesized according to the reported procedure.³⁵

$[\alpha]_D = -3.2$ ($c = 1.0$, acetone), $ee = 75\%$; Lit.³⁵ -4.3 ($c = 3.83$, acetone)

S enantiomer was synthesized according to the reported procedure.³⁵

$[\alpha]_D = +2.8$ ($c = 1.0$, acetone), $ee = 66\%$; Lit.³⁵ $+4.3$ ($c = 1.64$, acetone)

^1H NMR (500 MHz, CDCl_3) δ 2.33 (s, 3H), 1.20 (s, 9H). ^{13}C NMR (126 MHz, CDCl_3) δ 52.51, 31.50, 22.43.



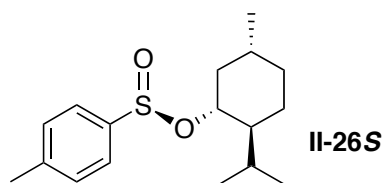
t-Butyl phenyl sulfoxide (**II-25R**):

R enantiomer was synthesized according to the reported procedure.³⁷

$[\alpha]_D = +123$ ($c = 1.0$, acetone); Lit.³⁷ $+161$ ($c = 1.0$, acetone); $ee = 76\%$

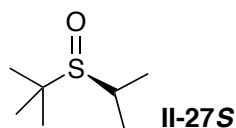
^1H NMR (500 MHz, CDCl_3) δ 7.66 – 7.53 (m, 2H), 7.50-7.47 (m, 3H), 1.17 (s, 9H). ^{13}C

NMR (126 MHz, CDCl_3) δ 139.98, 131.10, 128.33, 126.28, 55.74, 22.77.



(*S*)-Menthyl *p*-tolyl sulfoxide (**II-25S**).³³

^1H NMR (500 MHz, CDCl_3) δ 7.58 (d, $J = 8.3$ Hz, 2H), 7.30 (d, $J = 7.9$ Hz, 2H), 4.10 (td, $J = 10.8, 4.5$ Hz, 1H), 2.39 (s, 3H), 2.26 (dd, $J = 12.0, 3.1$ Hz, 1H), 2.17 – 2.06 (m, 1H), 1.66 (dt, $J = 12.0, 2.8$ Hz, 2H), 1.50 – 1.41 (m, 1H), 1.38 – 1.28 (m, 1H), 1.25 – 1.14 (m, 1H), 1.08 – 0.96 (m, 1H), 0.94 (d, $J = 6.5$ Hz, 3H), 0.90 – 0.78 (m, 4H), 0.69 (d, $J = 7.0$ Hz, 3H). ^{13}C NMR (126 MHz, CDCl_3) δ 143.07, 142.39, 129.58, 124.95, 80.10, 77.25, 77.00, 76.75, 47.81, 42.91, 33.98, 31.70, 25.18, 23.10, 22.06, 21.49, 20.83, 15.43.

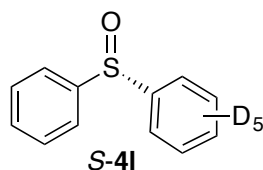


(*R*)-*t*-Butyl *i*-propyl sulfoxide (**II-27S**):

R enantiomer was synthesized according to the reported procedure.³⁷

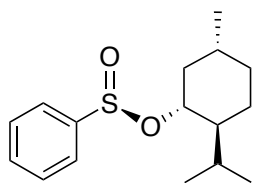
$ee = 35\%$ (HPLC, according to the reported method).

^1H NMR (500 MHz, CDCl_3) 2.85 (m, 1H), 1.29 (d, $J = 7.1$ Hz, 1H), 1.24 (s, 9H), 1.21 (d, $J = 7.0$ Hz, 1H). ^{13}C NMR (125 MHz, CDCl_3) δ 54.05, 44.45, 23.40, 20.43, 15.24.



(*S*)-Phenyl perdeuteriophenyl sulfoxide (**S-4I**)

S enantiomer was synthesized from following precursor according to the reported procedure.



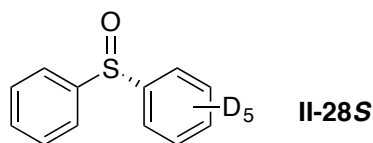
O-(1*R*,2*S*,5*R*)-(-)-menthyl-(*S*)-benzenesulfinate (-)-(S)

This compound was synthesized according to the reported procedure.²⁹ The diastereomeric mixture product was purified to the titled pure diastereomer according the procedure described by Herbrandson and Dickerson.⁶¹

$[\alpha]_D = -210$ ($c = 1.45$, acetone); Lit. -209.3 ($c = 1.45$, acetone)

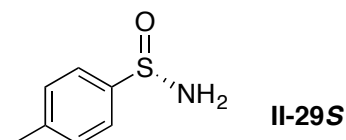
^1H NMR (500 MHz, CDCl_3) δ 7.77 – 7.66 (m, 2H), 7.56 – 7.46 (m, 3H), 4.12 (td, $J = 10.8$, 4.5 Hz, 1H), 2.31 – 2.23 (m, 1H), 2.13 – 2.07 (m, 1H), 1.71 – 1.64 (m, 2H), 1.53 – 1.43 (m, 1H), 1.38 – 1.30 (m, 1H), 1.22 (q, $J = 11.8$ Hz, 1H), 1.03 (m, 1H), 0.95 (d, $J = 6.6$ Hz, 3H), 0.85 (d, $J = 7.2$ Hz, 4H), 0.69 (d, $J = 6.9$ Hz, 3H).

^{13}C NMR (126 MHz, CDCl_3) δ 146.00, 131.84, 128.94, 125.01, 80.38, 47.82, 42.93, 33.96, 31.72, 25.19, 23.10, 22.06, 20.84, 15.42.



II-28S was synthesized from O-(1*R*,2*S*,5*R*)-(-)-menthyl-(*S*)-benzenesulfinate (-)-(*S*) (Shown above) according to the reported procedure.²⁹

^1H NMR (500 MHz, CDCl_3) δ 7.63 (dt, J = 7.6, 1.6 Hz, 2H), 7.48 – 7.29 (m, 3H). ^{13}C NMR (126 MHz, CDCl_3) δ 145.55 (s), 145.36 (s), 131.00, 130.49 (t, $J_{13\text{C}-\text{D}}$ = 24.7 Hz), 129.27 (s), 128.76 (t, $J_{13\text{C}-\text{D}}$ = 24.7 Hz), 124.72 (s), 124.33 (t, $J_{13\text{C}-\text{D}}$ = 24.7 Hz).



(*S*)-*p*-toluene sulfinamide **II-29S** was purchased from Sigma-Aldrich and was used as received.

II-5-7 Conformational modeling studies

Full optimizations on all conformations of the complexes studied were performed at the semi-empirical Parameterized Model (PM6) using the Spartan-14 software running on a Linux platform. The local minima were then subjected to geometry optimization at the B3LYP/6-31G* (gas phase) level of theory. Finally, the complex with the lowest conformational energy for Zn-MAPOL complexed with represented cyanohydrin or sulfoxide was subject to DFT geometry optimization (B3LYP/6-31G*, gas phase).

REFERENCES

REFERENCES

1. Anyika, M.; Gholami, H.; Ashtekar, K. D.; Acho, R.; Borhan, B., Point-to-Axial Chirality Transfer—A New Probe for “Sensing” the Absolute Configurations of Monoamines. *Journal of the American Chemical Society* **2014**, *136* (2), 550-553.
2. Dutot, L.; Wright, K.; Wakselman, M.; Mazaleyrat, J. P.; Peggion, C.; De Zotti, M.; Formaggio, F.; Toniolo, C., Central-to-axial chirality transfer and induced circular dichroism in 6,7-dihydro-5H-dibenz[c,e]azepine derivatives of alpha- and beta-amino esters. *Tetrahedron Letters* **2008**, *49* (21), 3475-3479.
3. Brunel, J.-M.; Holmes, I. P., Chemically Catalyzed Asymmetric Cyanohydrin Syntheses. *Angewandte Chemie International Edition* **2004**, *43* (21), 2752-2778.
4. Effenberger, F., Synthesis and Reactions of Optically Active Cyanohydrins. *Angewandte Chemie International Edition in English* **1994**, *33* (15-16), 1555-1564.
5. Louzao, I.; Garcia, R.; Seco, J. M.; Quinoa, E.; Riguera, R., Absolute Configuration of Ketone Cyanohydrins by H-1 NMR: The Special Case of Polar Substituted Tertiary Alcohols. *Organic Letters* **2009**, *11* (1), 53-56.
6. Louzao, I.; Seco, J. M.; Quinoa, E.; Riguera, R., The assignment of absolute configuration of cyanohydrins by NMR. *Chemical Communications* **2006**, (13), 1422-1424.
7. Louzao, I.; Seco, J. M.; Quinoa, E.; Riguera, R., The Use of a Single Derivative in the Configurational Assignment of Ketone Cyanohydrins. *European Journal of Organic Chemistry* **2010**, (34), 6520-6524.
8. Seco, J. M.; Quinoa, E.; Riguera, R., Assignment of the Absolute Configuration of Polyfunctional Compounds by NMR Using Chiral Derivatizing Agents. *Chemical Reviews* **2012**, *112* (8), 4603-4641.
9. Moon, L. S.; Jolly, R. S.; Kasetti, Y.; Bharatam, P. V., A new chiral shift reagent for the determination of enantiomeric excess and absolute configuration in cyanohydrins. *Chemical Communications* **2009**, (9), 1067-1069.
10. Moon, L. S.; Pal, M.; Kasetti, Y.; Bharatam, P. V.; Jolly, R. S., Chiral Solvating Agents for Cyanohydrins and Carboxylic Acids. *Journal of Organic Chemistry* **2010**, *75* (16), 5487-5498.
11. Li, X.; Tanasova, M.; Vasileiou, C.; Borhan, B., Fluorinated Porphyrin Tweezer: A Powerful Reporter of Absolute Configuration for erythro and threo Diols, Amino Alcohols, and Diamines. *J. Am. Chem. Soc.* **2008**, *130* (6), 1885-1893.

12. Hatano, M.; Ikeno, T.; Miyamoto, T.; Ishihara, K., Chiral Lithium Binaphtholate Aqua Complex as a Highly Effective Asymmetric Catalyst for Cyanohydrin Synthesis. *Journal of the American Chemical Society* **2005**, *127* (31), 10776-10777.
13. Liu, X.; Qin, B.; Zhou, X.; He, B.; Feng, X., Catalytic Asymmetric Cyanosilylation of Ketones by a Chiral Amino Acid Salt. *Journal of the American Chemical Society* **2005**, *127* (35), 12224-12225.
14. Ryu, D. H.; Corey, E. J., Highly Enantioselective Cyanosilylation of Aldehydes Catalyzed by a Chiral Oxazaborolidinium Ion. *Journal of the American Chemical Society* **2004**, *126* (26), 8106-8107.
15. Ryu, D. H.; Corey, E. J., Enantioselective Cyanosilylation of Ketones Catalyzed by a Chiral Oxazaborolidinium Ion. *Journal of the American Chemical Society* **2005**, *127* (15), 5384-5387.
16. Eilei, E. L.; Wilen, S. H., *In Stereochemistry of Organic Compounds*. New-York, 1994.
17. Fernández, I.; Khier, N., Recent Developments in the Synthesis and Utilization of Chiral Sulfoxides. *Chemical Reviews* **2003**, *103* (9), 3651-3706.
18. Bentley, R., Role of sulfur chirality in the chemical processes of biology. *Chemical Society Reviews* **2005**, *34* (7), 609-624.
19. Wojaczyńska, E.; Wojaczyński, J., Enantioselective Synthesis of Sulfoxides: 2000–2009. *Chemical Reviews* **2010**, *110* (7), 4303-4356.
20. Carreno, M. C., Applications of Sulfoxides to Asymmetric Synthesis of Biologically Active Compounds. *Chemical Reviews* **1995**, *95* (6), 1717-1760.
21. Pulis, A. P.; Procter, D. J., C–H Coupling Reactions Directed by Sulfoxides: Teaching an Old Functional Group New Tricks. *Angewandte Chemie International Edition* **2016**, *55* (34), 9842-9860.
22. Sipos, G.; Drinkel, E. E.; Dorta, R., The emergence of sulfoxides as efficient ligands in transition metal catalysis. *Chemical Society Reviews* **2015**, *44* (11), 3834-3860.
23. Yabuuchi, T.; Kusumi, T., NMR Spectroscopic Determination of the Absolute Configuration of Chiral Sulfoxides via N-(Methoxyphenylacetyl)sulfoximines. *Journal of the American Chemical Society* **1999**, *121* (45), 10646-10647.
24. Donnoli, M. I.; Superchi, S.; Rosini, C., Recent progress in application of spectroscopic methods for assigning absolute configuration of optically active sulfoxides. *Mini-Reviews in Organic Chemistry* **2006**, *3* (1), 77-92.

25. Buist, P. H.; Behrouzian, B.; MacIsaac, K. D.; Cassel, S.; Rollin, P.; Imberty, A.; Gautier, C.; Pérez, S.; Genix, P., Stereochemical analysis of d-glucopyranosyl-sulfoxides via a combined NMR, molecular modeling and X-ray crystallographic approach. *Tetrahedron: Asymmetry* **1999**, *10* (15), 2881-2889.
26. Yang, L.; Wenzel, T.; Williamson, R. T.; Christensen, M.; Schafer, W.; Welch, C. J., Expedited Selection of NMR Chiral Solvating Agents for Determination of Enantiopurity. *ACS Central Science* **2016**, *2* (5), 332-340.
27. Aamouche, A.; Devlin, F. J.; Stephens, P. J.; Drabowicz, J.; Bujnicki, B.; Mikołajczyk, M., Vibrational Circular Dichroism and Absolute Configuration of Chiral Sulfoxides: tert-Butyl Methyl Sulfoxide. *Chemistry – A European Journal* **2000**, *6* (24), 4479-4486.
28. Devlin, F. J.; Stephens, P. J.; Scafato, P.; Superchi, S.; Rosini, C., Determination of absolute configuration using vibrational circular dichroism spectroscopy: The chiral sulfoxide 1-thiochromanone S-oxide. *Chirality* **2002**, *14* (5), 400-406.
29. Drabowicz, J.; Zajac, A.; Lyzwa, P.; Stephens, P. J.; Pan, J.-J.; Devlin, F. J., Determination of the absolute configurations of isotopically chiral molecules using vibrational circular dichroism (VCD) spectroscopy: the isotopically chiral sulfoxide, perdeuteriophenyl-phenyl-sulfoxide. *Tetrahedron: Asymmetry* **2008**, *19* (3), 288-294.
30. Petrovic, A. G.; He, J.; Polavarapu, P. L.; Xiao, L. S.; Armstrong, D. W., Absolute configuration and predominant conformations of 1,1-dimethyl-2-phenylethyl phenyl sulfoxide. *Organic & Biomolecular Chemistry* **2005**, *3* (10), 1977-1981.
31. Stephens, P. J.; Aamouche, A.; Devlin, F. J.; Superchi, S.; Donnoli, M. I.; Rosini, C., Determination of Absolute Configuration Using Vibrational Circular Dichroism Spectroscopy: The Chiral Sulfoxide 1-(2-methylnaphthyl) Methyl Sulfoxide. *The Journal of Organic Chemistry* **2001**, *66* (11), 3671-3677.
32. Gholami, H.; Anyika, M.; Zhang, J.; Vasileiou, C.; Borhan, B., Host–Guest Assembly of a Molecular Reporter with Chiral Cyanohydrins for Assignment of Absolute Stereochemistry. *Chemistry – A European Journal* **2016**, *22* (27), 9235-9239.
33. Andersen, K. K., Synthesis of (+)-ethyl p-tolyl sulfoxide from (–)-menthyl (–)-p-toluenesulfinate. *Tetrahedron Letters* **1962**, *3* (3), 93-95.
34. Andersen, K. K.; Gaffield, W.; Papanikolaou, N. E.; Foley, J. W.; Perkins, R. I., Optically Active Sulfoxides. The Synthesis and Rotatory Dispersion of Some Diaryl Sulfoxides. *Journal of the American Chemical Society* **1964**, *86* (24), 5637-5646.
35. Fernandez, I.; Khiar, N.; Llera, J. M.; Alcudia, F., Asymmetric synthesis of alkane- and arenesulfinates of diacetone-D-glucose (DAG): an improved and general route

- to both enantiomerically pure sulfoxides. *The Journal of Organic Chemistry* **1992**, 57 (25), 6789-6796.
36. García Ruano, J. L.; Alemparte, C.; Aranda, M. T.; Zarzuelo, M. M., A General and Expeditious One-Pot Synthesis of Sulfoxides in High Optical Purity from Norephedrine-Derived Sulfamidites. *Organic Letters* **2003**, 5 (1), 75-78.
 37. Lu, B. Z.; Jin, F.; Zhang, Y.; Wu, X.; Wald, S. A.; Senanayake, C. H., New General Sulfinylating Process for Asymmetric Synthesis of Enantiopure Sulfinates and Sulfoxides. *Organic Letters* **2005**, 7 (8), 1465-1468.
 38. Vinodu, M.; Goldberg, I., A dimethyl sulfoxide/chloroform clathrate of (dimethyl sulfoxide)(tetraphenylporphyrinato)zinc(II). *Acta Crystallographica Section E* **2004**, 60 (5), m579-m581.
 39. Verloop, A., *IUPAC Pesticide Chemistry*. Pergamon: 1983; Vol. 1.
 40. Verloop, A. T., J., in *Biological Activity and Chemical Structure*. Elsevier: 1977.
 41. Verloop, A. T., J., in *QSAR in Drug Dosing and Toxicology* (ed. Hadzi. B. & Jerman-Blazic, B.). Elsevier: 1987; Vol. 97.
 42. Harper, K. C.; Bess, E. N.; Sigman, M. S., Multidimensional steric parameters in the analysis of asymmetric catalytic reactions. *Nat Chem* **2012**, 4 (5), 366-374.
 43. Dunitz, J. D.; Ibberson, R. M., Is Deuterium Always Smaller than Protium? *Angewandte Chemie International Edition* **2008**, 47 (22), 4208-4210.
 44. Wang, F.; Wang, Y.; Polavarapu, P. L.; Li, T.; Drabowicz, J.; Pietrusiewicz, K. M.; Zygo, K., Absolute Configuration of tert-Butyl-1-(2-methylnaphthyl)phosphine Oxide. *The Journal of Organic Chemistry* **2002**, 67 (18), 6539-6541.
 45. Dutartre, M.; Bayardon, J.; Juge, S., Applications and stereoselective syntheses of P-chirogenic phosphorus compounds. *Chemical Society Reviews* **2016**, 45 (20), 5771-5794.
 46. Dai, W.-M.; Yeung, K. K. Y.; Leung, W. H.; Haynes, R. K., Air-stable P-stereogenic secondary phosphine oxides as chiral monodentate ligands for asymmetric catalytic carbon-carbon bond formation. *Tetrahedron: Asymmetry* **2003**, 14 (18), 2821-2826.
 47. Camp, N. P.; Hawkins, P. C. D.; Hitchcock, P. B.; Gani, D., Synthesis of stereochemically defined phosphoramidate-containing peptides: Inhibitors for the HIV-1 proteinase. *Bioorganic & Medicinal Chemistry Letters* **1992**, 2 (9), 1047-1052.
 48. Camp, N. P.; Perrey, D. A.; Kinchington, D.; Hawkins, P. C. D.; Gani, D., Synthesis of peptide analogues containing phosphoramidate methyl ester functionality: HIV-1

- proteinase inhibitors possessing unique cell uptake properties. *Bioorganic & Medicinal Chemistry* **1995**, 3 (3), 297-312.
49. Copey, L.; Jean-Gérard, L.; Andrioletti, B.; Framery, E., Synthesis of P-stereogenic secondary phosphine oxides using α -d-glucosamine as a chiral precursor. *Tetrahedron Letters* **2016**, 57 (5), 543-545.
 50. Zhang, H.; Sun, Y.-M.; Zhao, Y.; Zhou, Z.-Y.; Wang, J.-P.; Xin, N.; Nie, S.-Z.; Zhao, C.-Q.; Han, L.-B., One-Pot Process That Efficiently Generates Single Stereoisomers of 1,3-Bisphosphinylpropanes Having Five Chiral Centers. *Organic Letters* **2015**, 17 (1), 142-145.
 51. DiRocco, D. A.; Ji, Y.; Sherer, E. C.; Klapars, A.; Reibarkh, M.; Dropinski, J.; Mathew, R.; Maligres, P.; Hyde, A. M.; Limanto, J.; Brunskill, A.; Ruck, R. T.; Campeau, L.-C.; Davies, I. W., A multifunctional catalyst that stereoselectively assembles prodrugs. *Science* **2017**, 356 (6336), 426.
 52. Shoji, Y.; Tashiro, K.; Aida, T., Sensing of Chiral Fullerenes by a Cyclic Host with an Asymmetrically Distorted π -Electronic Component. *Journal of the American Chemical Society* **2006**, 128 (33), 10690-10691.
 53. Geier, G. R.; Chick, J. F. B.; Callinan, J. B.; Reid, C. G.; Auguscinski, W. P., A Survey of Acid Catalysis and Oxidation Conditions in the Two-Step, One-Flask Synthesis of Meso-Substituted Corroles via Dipyrrromethanedicarbinols and Pyrrole. *The Journal of Organic Chemistry* **2004**, 69 (12), 4159-4169.
 54. Drago, C.; Caggiano, L.; Jackson, R. F. W., Vanadium-Catalyzed Sulfur Oxidation/Kinetic Resolution in the Synthesis of Enantiomerically Pure Alkyl Aryl Sulfoxides. *Angewandte Chemie International Edition* **2005**, 44 (44), 7221-7223.
 55. Wu, Y.; Liu, J.; Li, X.; Chan, A. S. C., Vanadium-Catalyzed Asymmetric Oxidation of Sulfides Using Schiff Base Ligands Derived from β -Amino Alcohols with Two Stereogenic Centers. *European Journal of Organic Chemistry* **2009**, 2009 (16), 2607-2610.
 56. Hoffmann, R. W.; Nell, P. G., α -Chloroalkylmagnesium Reagents of >90% ee by Sulfoxide/Magnesium Exchange. *Angewandte Chemie International Edition* **1999**, 38 (3), 338-340.
 57. Ogawa, S.; Furukawa, N., Regiospecific ortho lithiation of o-halophenyl p-tolyl sulfoxides and synthesis of meta-substituted optically active aryl alcohols. *The Journal of Organic Chemistry* **1991**, 56 (19), 5723-5726.
 58. Maignan, C.; Raphael, R. A., Investigation of a chiral masked ketene synthon synthesis of the (+)-(1r4r) and (-)-1s,4s enantiomers of dehydronorcamphor. *Tetrahedron* **1983**, 39 (20), 3245-3249.

59. Rayner, P. J.; O'Brien, P.; Horan, R. A. J., Preparation and Reactions of Enantiomerically Pure α -Functionalized Grignard Reagents. *Journal of the American Chemical Society* **2013**, *135* (21), 8071-8077.
60. Cardellicchio, C.; Fiandanese, V.; Naso, F.; Scilimati, A., Optically active sulfoxides by enantiospecific reactions of bromovinyl aryl sulfoxides with grignard reagents. *Tetrahedron Letters* **1992**, *33* (35), 5121-5124.
61. Herbrandson, H. F.; Dickerson, R. T., Derivatives of Aromatic Sulfinic Acids. III. Evidence for the Hydrogen Dichloride Ion from Epimerization Reactions¹. *Journal of the American Chemical Society* **1959**, *81* (15), 4102-4106.

Chapter III:
Total synthesis of (–)-*Salinosporamide A*

III-1 Introduction

In contrast to most fields, where researchers define the objectives of research, in the field of natural product synthesis the ultimate goal of a project is predefined by nature. Chemists, particularly organic chemists have aligned their research goals with nature's creatively designed molecules to pursue a few fundamental objectives: First, they try to provide a synthetic route that can give access to large quantity of naturally occurring molecules that in most cases are isolated in minute quantities. Secondly, nature has created these molecules through precise biochemical transformation, while organic chemists can exercise their creativity by developing new reactions and methodologies. Furthermore, inspired by the structure and chemical composition of natural compounds, a rich platform is available for drug discovery and formulation of new therapeutics and materials.¹

Starting with Wohler's total synthesis of urea, almost two centuries ago, chemical synthesis of naturally occurring molecules has led chemists to make important contributions in areas ranging from drug development to materials science. As one would expect, there are infinite number of possible syntheses for a natural product. Thus, these fascinating molecules have and will provide limitless source of inspiration for chemists. As a result, regardless of how many times a naturally occurring molecule has been targeted for chemical synthesis, they continue to fuel creativity in the field of chemistry.¹

One such molecule, which has proved to be a test bed for reaction discovery in the past few years, is *Salinosporamide A* (**III-1**, Figure III-1). This molecule with its intriguing chemical structure with multiple fascinating features has led to development of many new

methodologies that are not only utilized to access this molecule, but also continue to benefit the field in a broader scope. Salinosporamide A that is structurally related to Omuralide **III-3** and Lactacystin **III-4**,² was first isolated from a novel microbial source, *Salinispora* strains, by Fenical and co-worker in 2003.³ Since its isolation, the chemical synthesis of Salinosporamide A has been targeted by many research groups.⁴⁻⁵ Chemist's fascination with the synthesis of this compound lent itself to the presence of densely functionalized γ -lactone core with five contiguous stereocenters in this structure along with the unique biological properties of this compound. Salinosporamide A is a superbly effective proteasome inhibitor against many tumor cell lines.

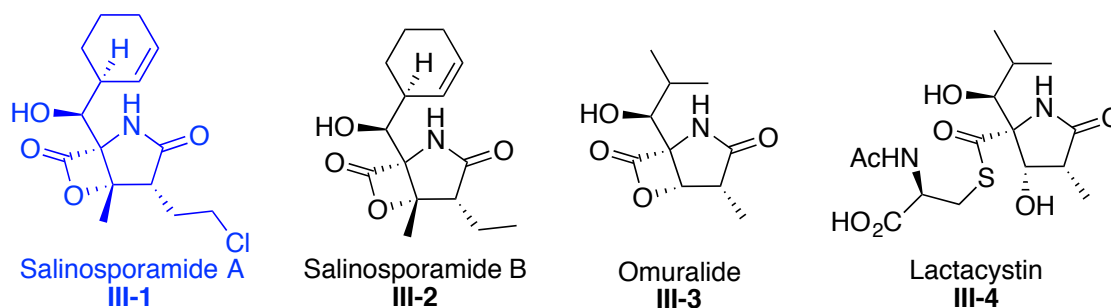


Figure III-1. Structure of Salinosporamide A and its closely related natural products.

III- 2 Proteasome inhibition by Salinosporamide A

The mode of action of Salinosporamide A, related to the inhibition of proteasome, has been studied using yeast 20S proteasome core in complex with the natural product. These investigations are empowered by the availability of the crystal structure of the Salinosporamide A in complex with 20S proteasome.⁶ The β -lactone moiety of Salinosporamide A (the chemical warhead of this compound) undergoes opening via attack originating from Thr1O γ residue (Figure III-2). The tertiary alcohol **III-5**, revealed

after the β -lactone opening event, further acts as a nucleophile to displace the chlorine atom and furnishes the substituted tetrahydrofuran ring **III-6**. The latter transformations

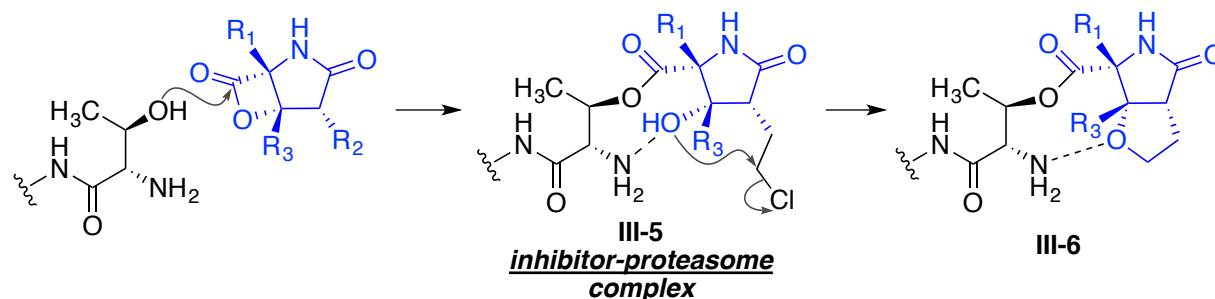


Figure III-2. Proposed inhibitory mechanism of Salinosporamide A in the proteasome active site.

exploit a nonreversible process that covalently links the compound with the proteasome. The high IC_{50} of Salinosporamide A, $2.6 K_{ass} (M^{-1}s^{-1})$ for chymotrypsin and $4.1 K_{ass} (M^{-1}s^{-1})$ for trypsin like proteasomes, indeed finds its origin in the latter strong complex formation with the proteasome active site.

III- 3 A survey of the previous total syntheses of Salinosporamide A

The highly captivating structural architecture of Salinosporamide A, along with its unique cytotoxicity profile has made this natural product an attractive synthetic target for many research groups in the past few years. Namely, five contiguous stereogenic centers along with a highly functionalized bicyclic framework provides a unique opportunity for reaction discovery and has fueled the inspiration of many chemists to assemble a diverse set of steps to give access to this molecule.⁴⁻⁵

After its isolation in 2003, Salinosporamide A was first synthesized by Corey's group in 2004.⁷ Their synthesis commenced with (*S*)-threonine methyl ester **III-7**, followed by an elegant set of chemical transformations that gave access to Salinosporamide A (Figure

III-3). The key reaction in their synthesis is a Baylis-Hillman cyclization reaction on **III-8** to assemble the 2-pyrrolidinone core **III-9**. Throughout their synthesis, they have developed many different reactions that are utilized and continue to be useful for researchers in the field.⁸

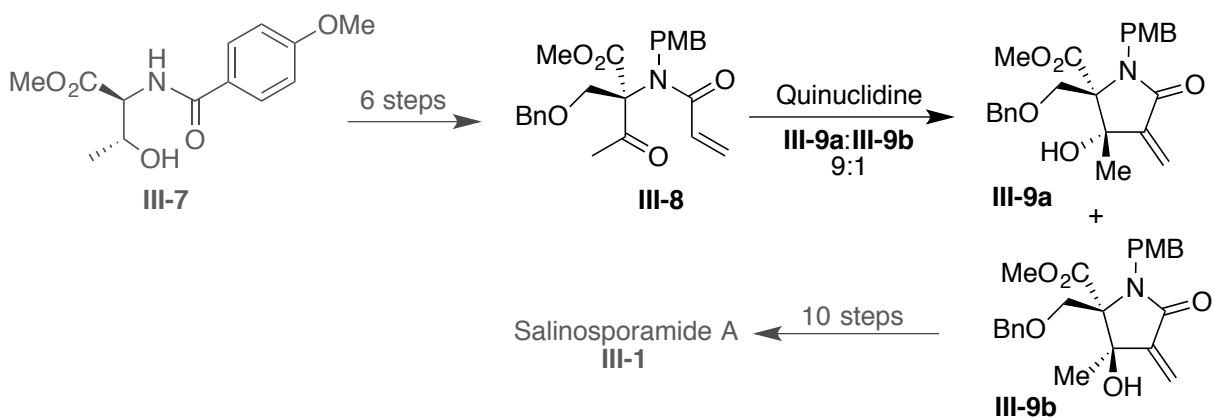


Figure III-3. First total synthesis of Salinosporamide A with the highlighted Baylis-Hillman cyclization as the key reaction of the synthesis.

The second total synthesis of Salinosporamide A is reported by Danishefsky's group in 2005 (Figure III-4).⁹ Their synthesis leveraged the stereo-defined face selectivity of pyroglutamate derivative **III-10** to introduce substituents on the 2-pyrrolidinone core leading to **III-11**, which is converted to the natural product in 23 steps.

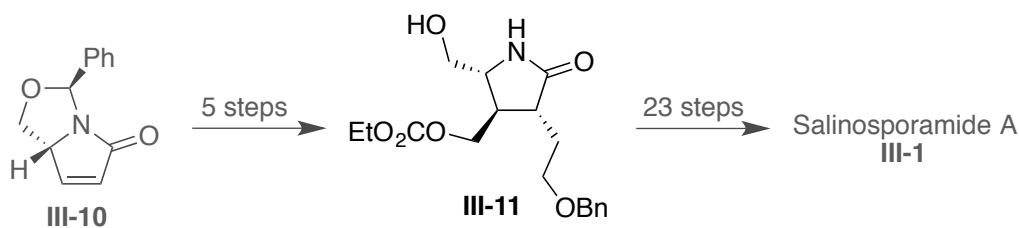
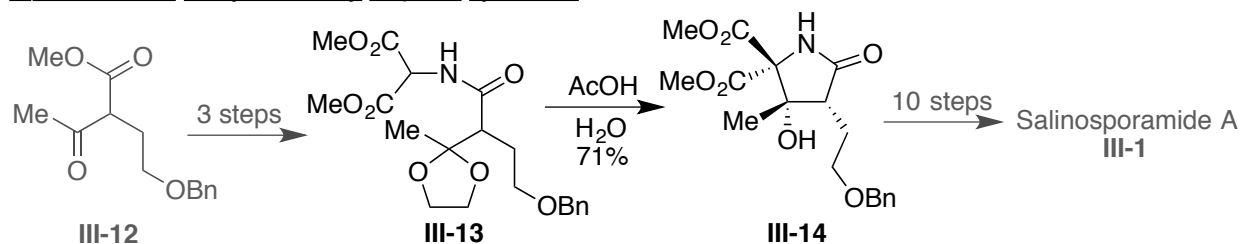


Figure III-4. Danishefsky's total synthesis of Salinosporamide A.

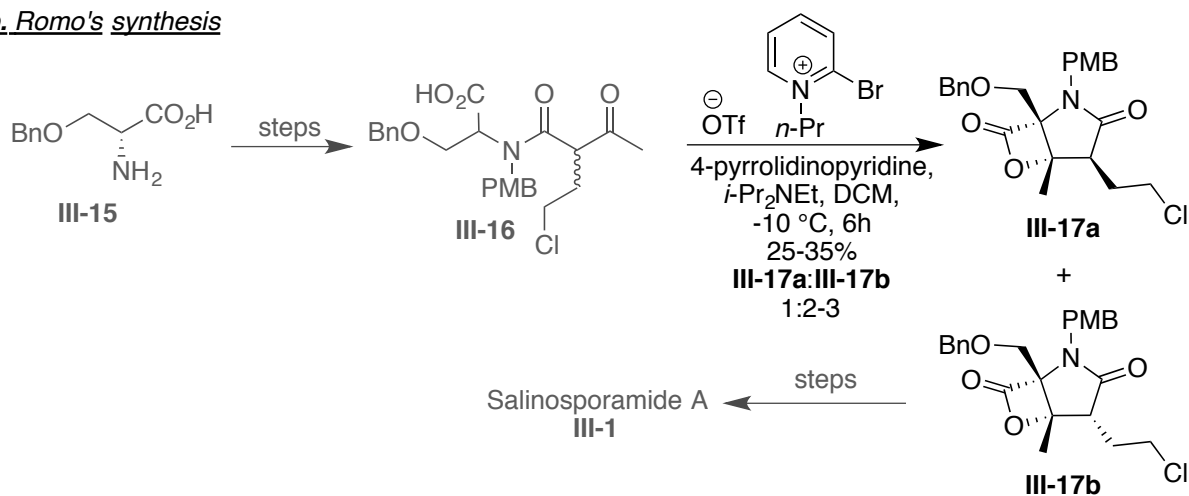
The first biosynthetically inspired synthesis of Salinosporamide A is reported by Pattenden and co-workers in 2006 (Figure III-4, a).¹⁰ The key transformation in their

synthesis is a nucleophilic attack of amidomalonate moiety in **III-13** into the tethered methyl ketone to furnish the substituted pyrrolidinone core **III-14**.

a. Pattenden's biosynthetically inspired synthesis



b. Romo's synthesis



c. Fukuyama's synthesis

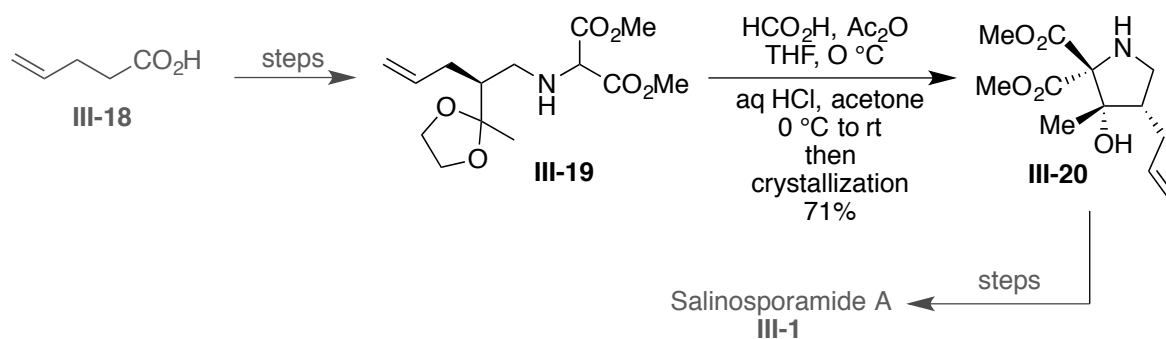


Figure III-5. Biosynthetically inspired total syntheses of Salinosporamide A.

This core (**III-14**) can eventually lead to the natural product with a few synthetic transformations. The latter biosynthetically inspired reaction of amidomalonate into methyl ketone has been utilized by many other research groups. Figure III-5, b and c,

highlights the reported total synthesis of Salinosporamide A by Romo¹¹⁻¹² and Fukuyama.¹³ They have used the biosynthetically inspired route to forge the pyrrolidine core towards the total synthesis of this molecule. In a similar manner, Hatakeyama and coworkers have utilized indium catalyzed Conia-Ene type reaction on **III-21** to install the pyrrolidinone core of the natural product **III-22** (Figure 6).¹⁴ A sequence of diastereoselective reactions ultimately converts **III-22** to Salinosporamide A. Additionally, many other total and formal syntheses of this natural product have also been reported in the past few years.^{15-20 21-22}

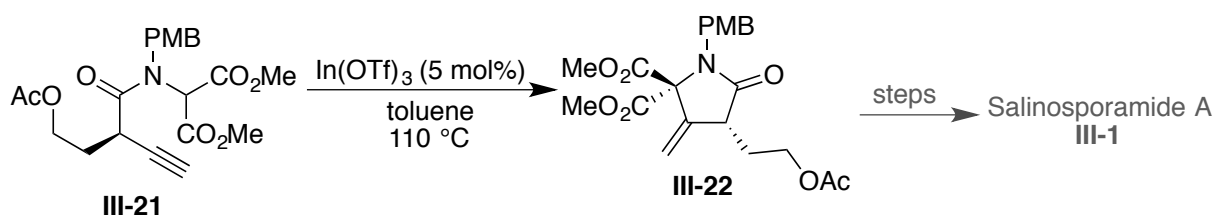


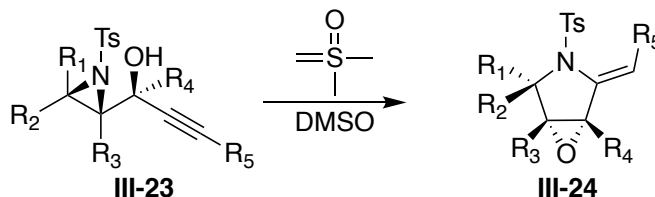
Figure III-6. Conia-Ene type reaction to assemble the core of Salinosporamide A.

III- 4 Our synthetic approach towards the total synthesis of Salinosporamide A

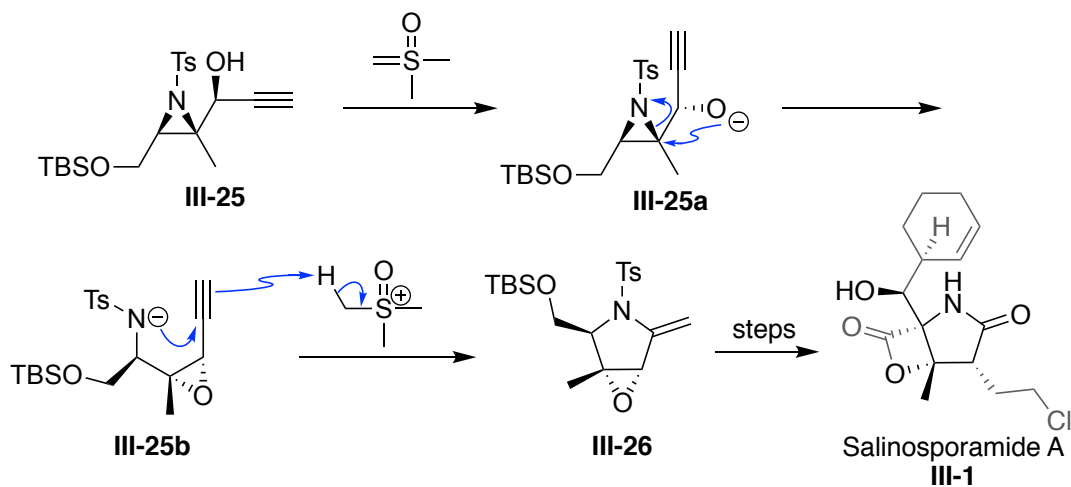
Our total synthesis of Salinosporamide A was initiated by Dr. Aman Kulshrestha, a former graduate student in our group.²³ Our synthetic approach stems from a methodology that was developed in our lab few years ago.²⁴ In this methodology, an aza-Payne/hydroamination rearrangement of aziridine alcohol **III-23** delivers the functionally decorated 2-pyrrolidinone core **III-24** that can serve as a versatile platform to give access to the skeleton of Salinosporamide A (Figure III-7, a). As illustrated in Figure III-7, b, deprotonation of aziridinalcohol **III-25** triggers the aza/Payne rearrangement via *anti* opening of the aziridine by the neighboring oxygen nucleophile, leading to the formation

of the corresponding epoxide **III-25b**. This action reveals a nitrogen anion that is stabilized by the tosyl group. The nucleophilic nitrogen consequently adds across the alkyne moiety, aided by protonation of the emerging vinyl anion, yielding the pyrrolidine core **III-26** (Figure III-7, b). We surmised that **III-26** can be utilized to access Salinosporamide A.

a. tandem aza-Payne/hydroamination reaction



b. access to the core of salinosporamide A through aza-Payne/hydroamination



c. our retrosynthetic approach for the synthesis of Salinosporamide A

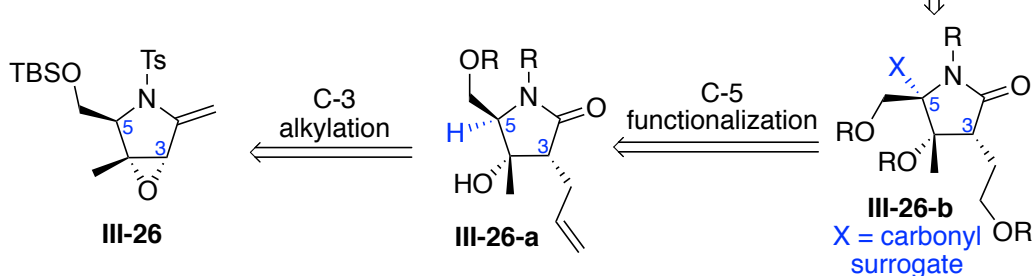


Figure III-7. Our developed methodology that give access to pyrrolidinone core and its exploitation for the synthesis of Salinosporamide A.

Our generalized retrosynthesis of Salinosporamide A is illustrated in Figure III-7, c. We envisioned an advanced intermediate such as **III-26b** that can be converted to the natural product in few steps. The carbonyl surrogate on **III-26b** is thought to be accessed via C-5 functionalization from **III-26a**. The epoxide moiety in **III-26** would provide a path for C-3 alkylation.

III- 5 Synthesis of Salinosporamide A

Our generalized retrosynthetic analysis illustrated in Figure III-7. Our synthesis commenced with the preparation of the appropriately functionalized aziridine alcohol **III-25** for the diastereoselective aza-Payne/hydroamination reaction (Figure III-8). Commercially available 3-methyl-2-butanol **III-27** was protected as its TBS ether followed by a selective allylic oxidation of the less sterically encumbered methyl group with SeO_2 and $t\text{BuOOH}$ that delivers allyl alcohol **III-28**. The allylic oxidation proceeded with partial over oxidation of the alcohol to the corresponding aldehyde, but reduction of the crude mixture delivers the **III-28** in excellent yield. Racemic aziridination of the allyl alcohol **III-28** with Chloramine-T in the presence of catalytic bromine source (NBS) gave access to aziridine alcohol **III-29**.²⁵ Dess-Martin periodinane oxidation of this alcohol yielded the corresponding aziridine aldehyde **III-30** with good yield from **III-27**. Following a methodology developed in our lab, addition of ethynyl magnesium bromide to the latter aldehyde **III-30** resulted in the formation of propargyl alcohol **III-25** with excellent yield and complete diastereoselectivity.²⁶ Access to **III-25** sets the stage for implementation of the key tandem aza-Payne/hydroamination reaction.

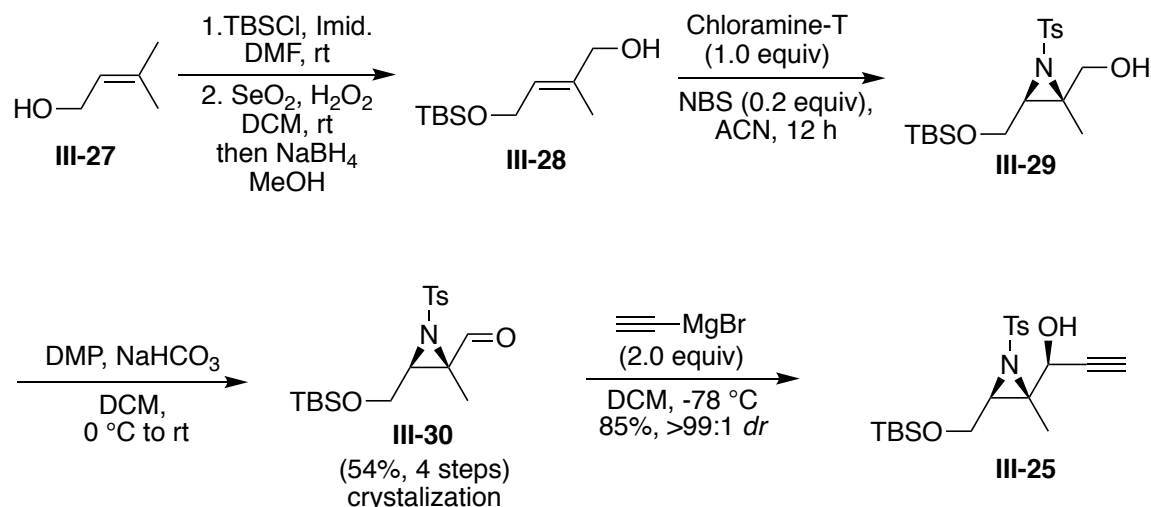


Figure III-8. Synthesis of aziridine-alcohol **III-25** for implementation of the tandem aza/Payne/hydroamination reaction.

Fortunately, the key tandem aza-Payne/hydroamination reaction on **III-25** took place with high yield and selectivity and afforded the corresponding N-Ts enamide **III-26**, which was used in the following step without purification (Figure III-9). Ozonolysis of the resultant enamide **III-26** followed by reductive work up of the ozonide complex utilizing dimethyl sulfide (DMS) leads to the 2-pyrrolidinone intermediate **III-31** in excellent yield, without the need for purification. The crude product from ozonolysis reaction was directly subjected to the following reaction.

C-3 in Salinosporamide A contains a side chain bearing a chlorine atom. Thus we envisioned that a regioselective opening of the epoxide **III-31** could give access to the appropriate moiety for installation of chloride at a later stage. In this paradigm, nucleophilic opening of epoxide with bromide was thought to be a suitable strategy, facilitating the installation of the carbon side chain on C-3. Treatment of crude epoxide **III-31** with MgBr₂ in dry diethyl ether at 0 °C leads to a highly regioselective opening of

the epoxide, affording bromohydrin **III-32**. The *anti*-opening of the epoxide with bromide and the regioselectivity of the reaction were confirmed based on X-ray crystal structure of this compound (Figure III-9). The reaction proved to be sensitive to the quality of MgBr_2 , requiring a freshly purchased MgBr_2 that was dried under vacuum overnight.

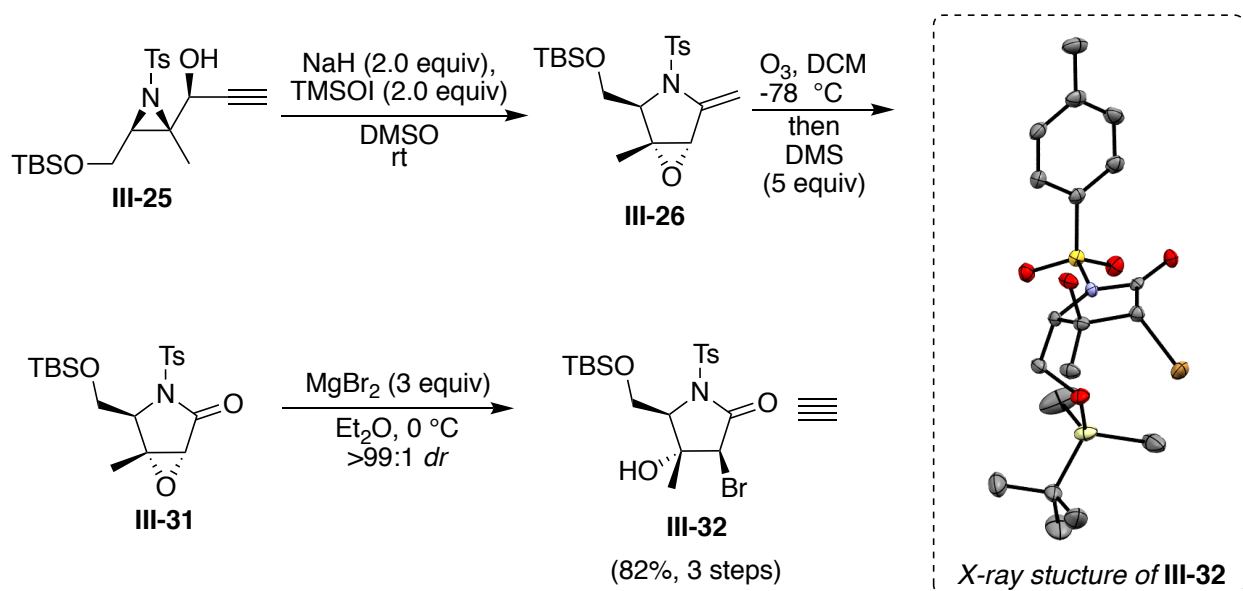
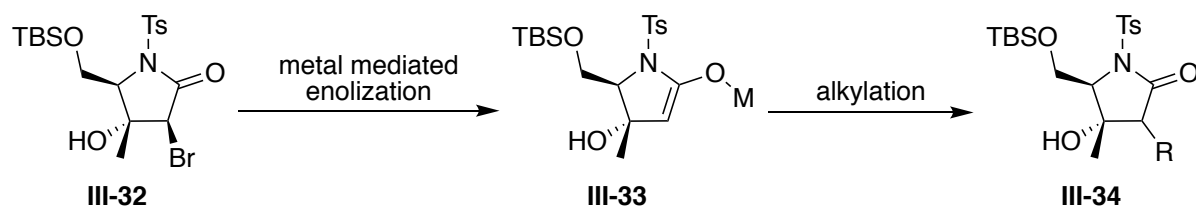


Figure III-9. tandem aza/Payne/hydroamination and selective epoxide opening, access to decorated 2-pyrrolidinone core.

We next turned our attention to the installation of the substituent on C-3. To this end, various metal catalyzed enolization/alkylation sequence of the α -bromo amide in **III-32** were envisioned (Figure III-10, a). However, undesired intramolecular displacement of the bromide by the tertiary hydroxyl group led to the formation of epoxide **III-31**, hampering the introduction of the alkyl group on C-3 under basic conditions. We then resorted to a radical mediated alkylation of α -bromo amide **III-32**. To that end, **III-32** was treated with allyl-tri-*n*-butyl stannane in the presence of AIBN as a radical initiator.

a. envisioned functionalization of C-3 through enolization



b. successful radical mediated side chain installation on C-3

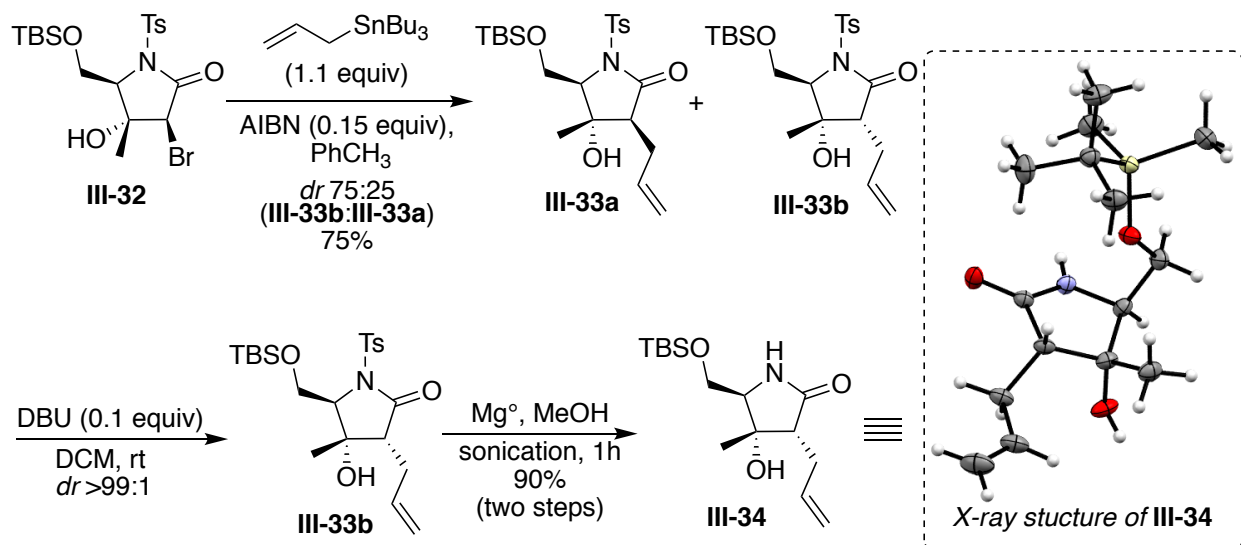


Figure III-10. Installation of the carbon side chain on C-3 and deprotection of the amide moiety of the 2-pyrrolidinone core.

The reaction delivers the α -allylated product **III-33** as a ~3:1 diastereomeric mixture. The presence of sterically intrusive substituents at C-4 and C-5 dictates the diastereomeric ratio of the allylation reaction on C-3. We leveraged the steric bias around C-3 to syphon the diastereomeric mixture (**III-33a** and **III-33b**) into pure diastereomer **III-33b**. Epimerization of C-3 in the presence of catalytic amount of DBU exclusively give access to the thermodynamic diastereomer **III-33b**. By having the substitution pattern on the C-3 and C-4 aligned with the skeleton of the natural product, manipulation of C-5 was tackled. In this vein, the tosyl protecting group was removed utilizing magnesium metal in

methanol with sonication, yielding **III-34** in high yield.²⁷ The X-ray crystal structure of **III-34** confirmed the relative stereochemistry of the substituents on the pyrrolidinone core (Figure III-10, dashed box). The reactions described above (from alcohol **III-27** to pyrrolidinone **III-34**) were developed by Dr. Aman Kulshrestha,²³ however these reaction were further optimized and performed on large scale as part of contributions of this thesis towards the total synthesis of Salinosporamide A.

The C-5 center in the natural product is a quaternary center bearing the β -lactone, thus installation of a carbonyl group on this carbon was targeted. We faced enormous issues with functionalization of this center. We envisioned utilization of anionic, cationic or radical based strategies to alkylate C-5. To pursue any of these strategies, the advance intermediate **III-34** or its analogues had to be modified accordingly. For instance, to implement anionic based approaches, C-5 must bear an acidic hydrogen, thus the carbinol carbon on C-5 was elaborated to a variety of carbonyl moieties. Below, we will discuss some of the anionic approaches that were pursued.

III-5- 1 A Survey of anionic approaches for C-5 functionalization

Anionic approaches, where C-5 acts a nucleophile, were pursued via functional group interconversion of the substituents on C-5 to expose an acidic α hydrogen for deprotonation. To this end, the oxidation state of the carbinol carbon on C-5 was adjusted to ester **III-37** or aldehyde **III-36** in order to facilitate deprotonation of this center (Figure III-11). Many different reaction strategies were tested with no success to functionalize this carbon to give **III-39**. In summary, there are two major challenges that preclude

functionalization of C-5 center under basic conditions. First, the presence of a tertiary alcohol on C-4 and its facile elimination assisted by the presence of acidic hydrogens on C-3, posed a major challenge for the latter functionalization. Secondly, the kinetic acidity of the C-3 proton prevents deprotonation of the more acidic, albeit sterically hindered, C-5 proton (Figures III-11 and III-12).

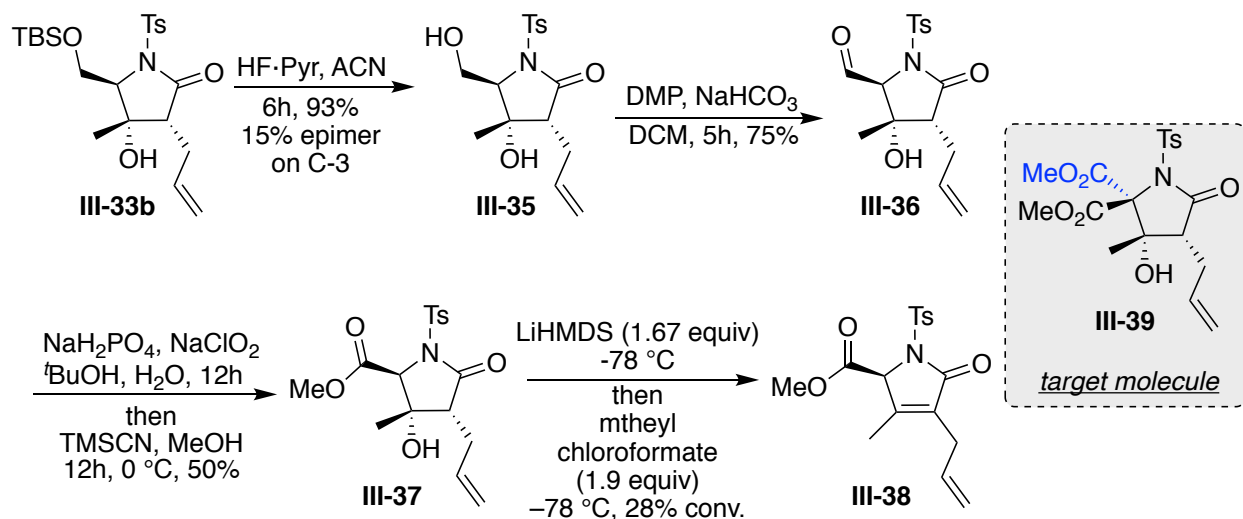
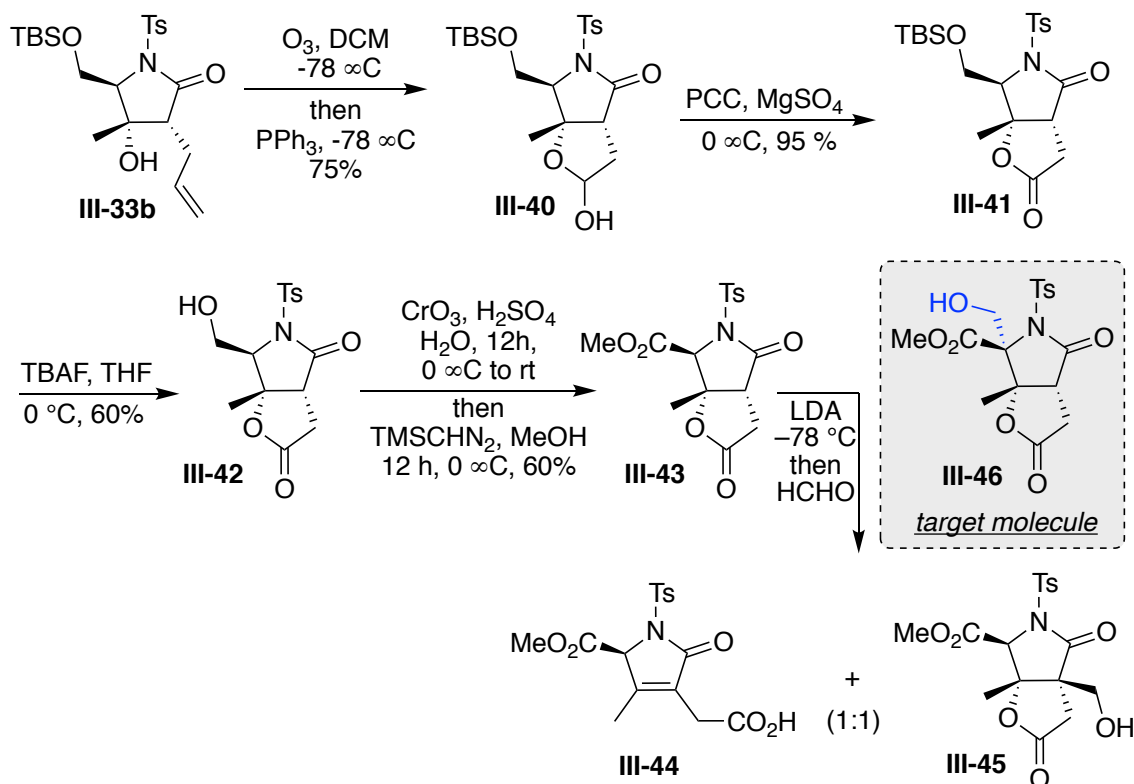


Figure III-11. Functionalization of C-5, an anionic route.

As a result, formation of many different side products such as dehydration, functionalization on C-3, retroaldol reaction and degradation of pyrrolidinone core are the unavoidable issues associated with the C-5 functionalization (Figures III-11 and III-12). To remedy this issue, a slight modification of the pyrrolidinone core was considered. In this respect, tertiary alcohol at C-4 was masked as a lactone in **III-41**. Nonetheless, this did not lead to the desired functionalization on C-5 under various conditions. As a small sample of the reactions that were investigated, formylation of the C-5 with LDA is illustrated in Figure III-12. Undesired deprotonation of C-3 leading to **III-45** and elimination to furnish **III-44** represent major side products that hampered functionalization at C-5.

These results point to the fact that deprotonation at C-3 is an issue, while deprotonation at C-5 suffers from unintended β -elimination, even with a hydroxide present at C-4 (Figure III-12).



The group on C-4 poses a challenge towards C-5 functionalization via anionic strategies; Elimination, retroaldol, etc. are the main culprits that impede further functionalization.

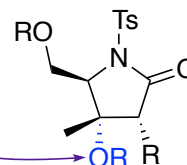


Figure III-12. Anionic functionalization of C-5 and the challenges facing this strategy.

III-5- 2 Cationic approaches for C-5 functionalization

In this strategy, C-5 was envisioned to act as an electrophilic center. To this end, the pyrrolidinone core must be modified to expose an enamide moiety such as **III-46** in which C-5 could act as an electrophilic center (Figure III-13). An envisioned strategy was the

epoxidation of **III-46** that can provide a path towards functionalization of C-5. One possible route could be acid mediated opening of epoxide in **III-47** and interception of the intermediate with cyanide (**III-48**), ultimately leading to functionalization of this center. Towards this goal, **III-33b** was deprotected under acidic conditions. The alcohol **III-49** was then subjected to dehydration condition with Burgess²⁸ and Grieco²⁹ reagents, however, enamide **III-46** was not obtained.

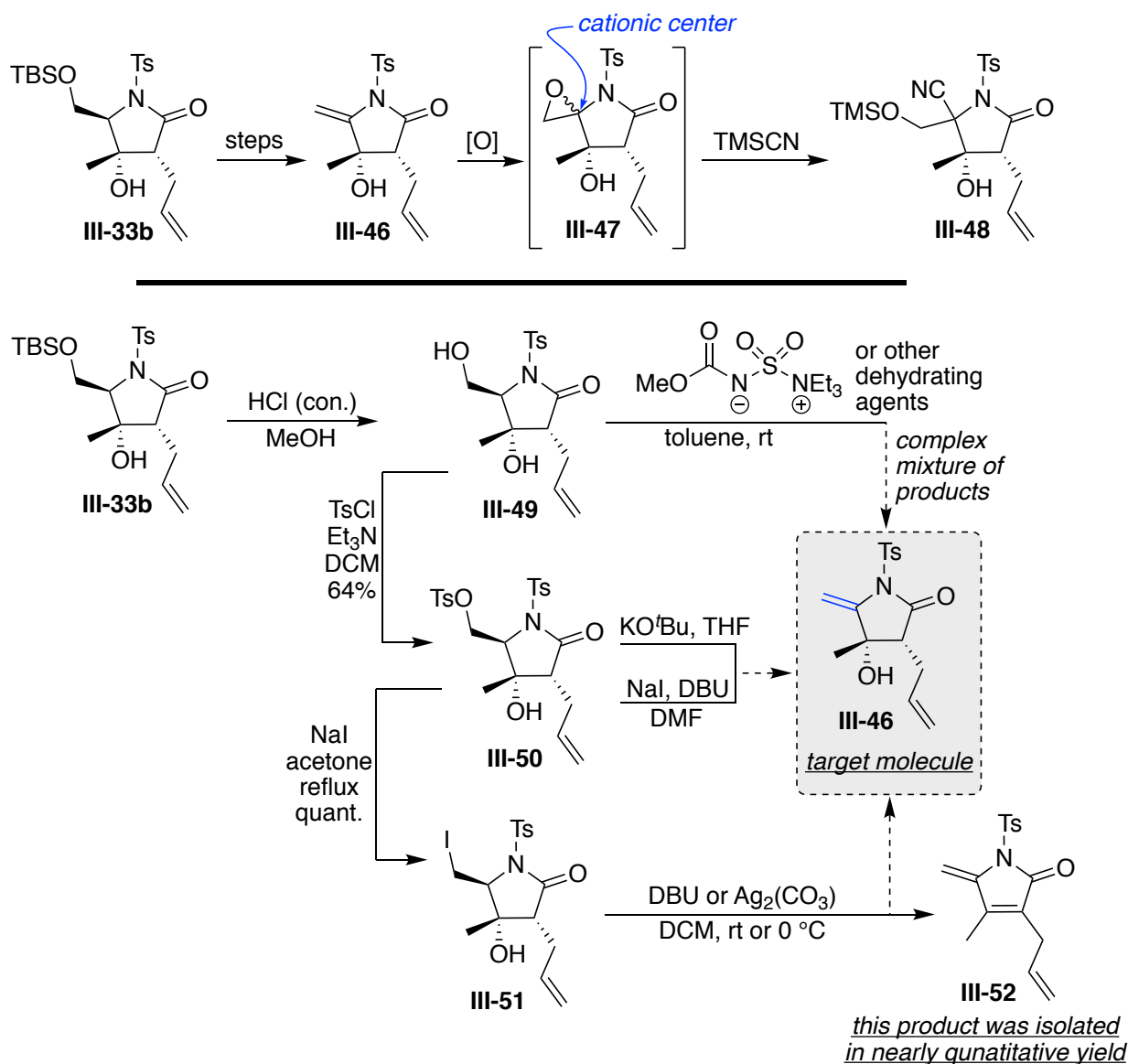
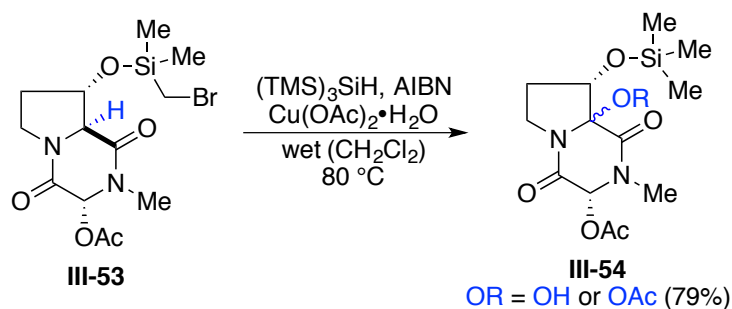


Figure III-13. Cationic approaches towards C-5 functionalization.

In most cases a complex reaction mixture of products was observed. In another approach, an indirect dehydration reaction was pursued. Conversion of alcohol **III-49** into a good leaving group followed by elimination was thought to deliver enamide **III-46**. Nonetheless, treatment of the tolylated analogue **III-50** under various basic condition did not lead to the desired elimination to form enamide **III-46**. In another route, the iodide analogue **III-51** was subjected to the elimination reaction.³⁰ Unfortunately, enamide **III-46** was not achieved, however, clean conversion of the iodide analogue to **III-52** was witnessed, demonstrating once again the facile dehydration of the tertiary alcohol at C-4 (Figure III-13). Reaction at lower temperatures or using different bases did not prevent the undesired elimination.

Overman's directed oxidation



Implementation of the directed oxidation

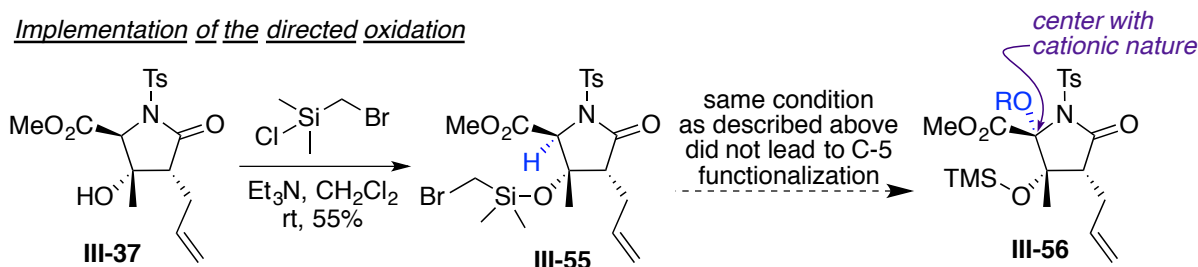


Figure III-14. Functionalization of C-5, a radical initiated oxidative strategy.

In a different approach, we were inspired by the radical chain oxidation reaction to functionalize the angular carbon on **III-53** to access **III-54** reported by Overman and coworkers.³¹ In this transformation, the generated radical results in the homolytic cleavage of the C–H bond, initiating the oxidation of this center that leads to the formation of the corresponding N,O-acetal **III-54**. It was envisioned that such a transformation could lead to oxidation at C-5 of **III-55**, which ultimately can deliver the intended alkylation of C-5. To this end, the tertiary alcohol in **III-37** was functionalized with (bromomethyl)-dimethylsilyl as a radical-translocating group leading to **III-55** (Figure III-14). Upon subjecting **III-55** to the reaction conditions described in the reported procedure,³¹ the desired functionalization/oxidation of C-5 was not observed and instead a complex mixture of products was generated. The lack of the angular geometry on C-5, as compared to the framework reported by Overman in structure **III-53**, could be a possible reason for the failure of the latter reaction.

III-5- 3 Radical based approaches for C-5 functionalization

Having failed to alkylated C-5 via anionic or cationic strategies, we envisioned a homolytic C–H cleavage to deliver the resulting radical intermediate that can be trapped by appropriate group, ultimately leading to the functionalization of this center. One of our early approaches was inspired by Overman's strategy that is outlined above.³¹ In this regard, **III-57** was envisioned to undergo translocation of the generated radical in **III-57a** to that of **III-57b** which in turn can be trapped by various functionalities such as alkyne moieties to give C-5 functionalized **III-58**.³² Nonetheless, we could not observe any

functionalization at the C-5 center under various conditions with different trapping groups. Removal of the bromide under radical condition and formation of a complex mixture of products was observed (Figure III-15).

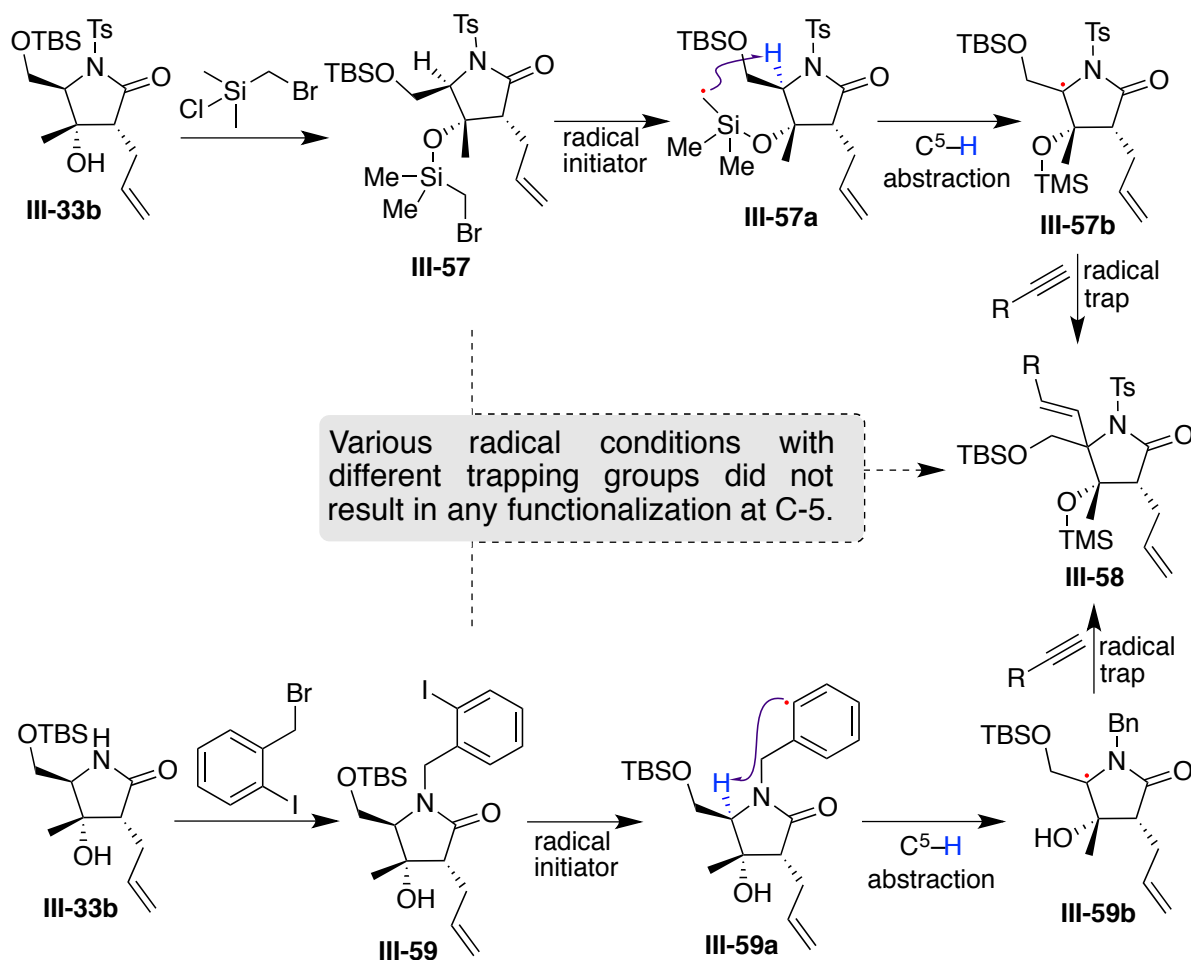


Figure III-15. Radical based strategies towards installation of functional group at C-5.

Alternatively, an aryl iodide was envisioned to deliver the radical on C-5 (Figure III-15). 2-Iodo benzyl was installed on the amide nitrogen of **III-33b** to deliver **III-59**.³³ Upon subjecting **III-59** to radical initiators it was speculated that the aryl radical **III-59a** generated from the homolytic cleavage of the iodo group, would undergo hydrogen abstraction from C-5 (6 six atoms away) to give access to the radical species on C-5 (**III-**

59b), which can be trapped by functionalities that can deliver a carbonyl group on this center. Nevertheless, subjecting **III-59** to radical mediated reaction conditions did not lead to the desired functionalization on C-5. Instead, a complex mixture of products was observed based on crude NMR analysis.

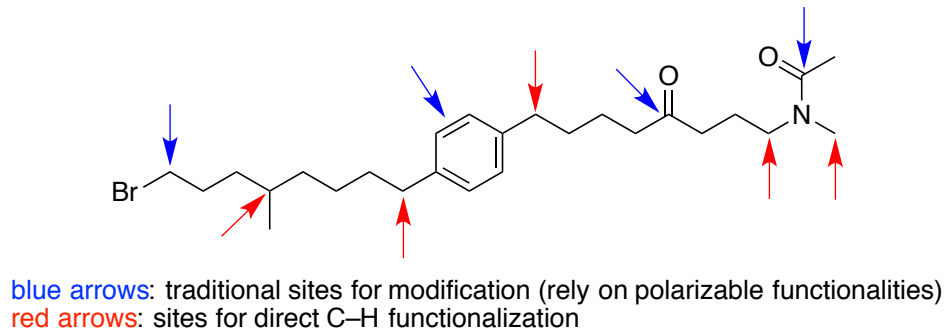
Having faced all the above mentioned unsuccessful efforts, and many other strategies that are not discussed here, to functionalize the C-5 center under anionic, cationic and radical conditions, we resorted to neutral based strategies for the latter functionalization.

III-5- 4 **Neutral based strategies for C-5 functionalization**

Since none of the charge or radical based strategies gave access to any functionalization of C-5, the effort resorted to approaches during which this center would stay neutral in order to prevent prevalent side reactions. Direct C–H functionalization can provide a route to avoid generating a reactive center at C-5.³⁴⁻³⁸ These types of reactions are orthogonal to the general reactivity of molecules that are driven by the polarization due to the presence of functionalities in the molecules or radical centers that are generated therein. As illustrated in Figure III-16, in the shown structure with multiple reactive sites, the blue arrows are indicative of sites that are reactive based on the polarization of the functional groups in the molecule while the red arrows point to the centers that are reactive towards direct C–H functionalization.³⁷⁻³⁸ One category of direct C–H functionalization is that of active carbene species that insert into carbon-hydrogen bonds, leading to functionalization at the centers highlighted red arrows in Figure (III-16). There are a few factors that control the reactivity of the hydrogen bond for C–H insertion reaction. Among those, the steric and electronic profiles are the most pronounced factors that determine the fate of the active carbene species.³⁷⁻³⁸ Less sterically hindered and more electron rich C–H bonds are more reactive for insertion reactions (Figure III-16, bottom). Nevertheless, extra factors such as conformational preferences and the distance between the reactive carbene and C–H bond can affect the course of an insertion reaction. In this regard, intramolecular C–H insertion reactions are generally preferred to take place on the hydrogen atoms that are six atoms away from the active carbene. Thus,

five membered ring products are expected in most cases where intramolecular C-H insertion reactions ensue.

a. sites of reaction based on functional groups vs C-H functionalization



a. controlling factor of C-H insertion

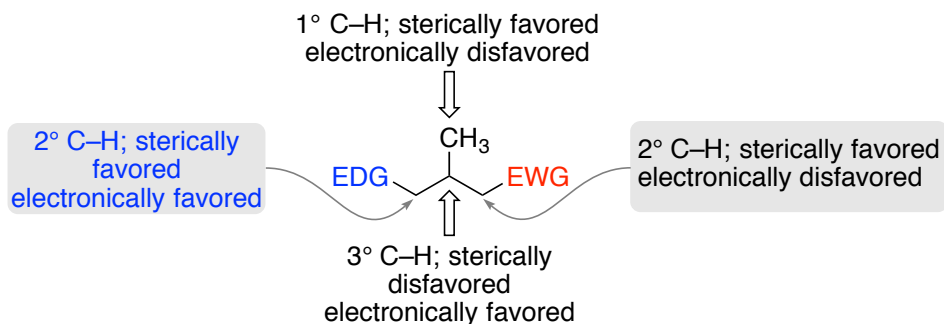
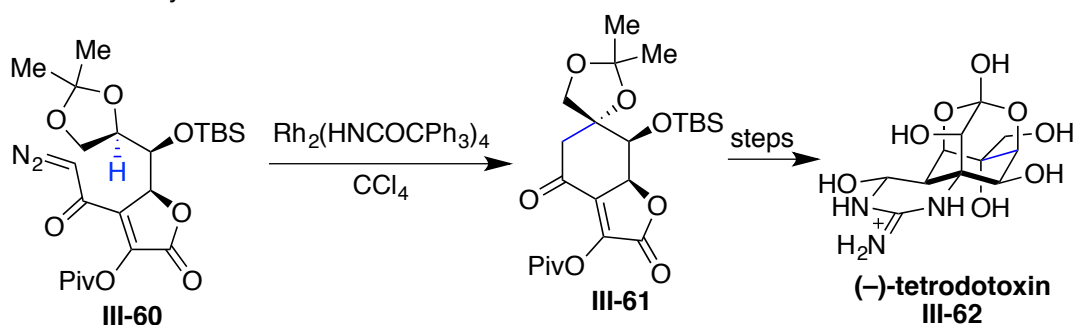


Figure III-16. General reactivity profile in comparison to the direct C-H functionalization; controlling factor in the C-H insertion reactions.

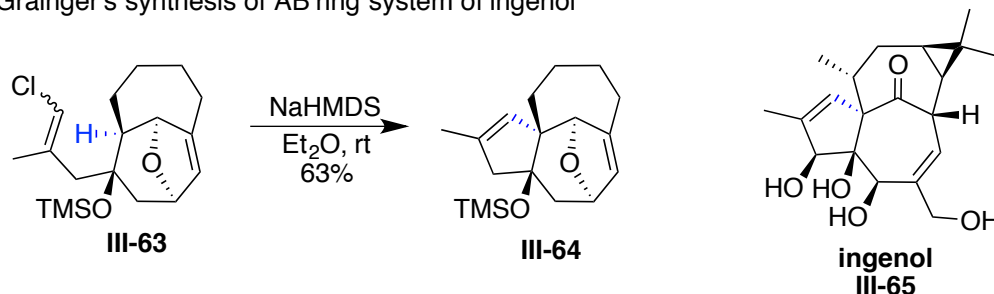
A survey of the reported procedures shows the frequent application of C-H insertion strategies to assemble the skeleton of natural products.^{34-35, 39} In general, there are two different types of motifs that provide carbene species for the latter functionalization. Reaction of diazo carbonyl compounds in the presence of transition metals⁴⁰ and deprotonation of vinyl halide followed by subsequent α elimination are common approaches to generate the carbene intermediate.⁴¹⁻⁴³

Du Bois and coworkers have employed the reaction of α -diazo carbonyl **III-60**, in the presence of a rhodium complex for intramolecular C-H insertion on the carbinol center to deliver **III-61**.³⁹ **III-61** is further elaborated to give access to (–)-tetrodotoxin **III-62** (Figure III-17, a). The use of vinyl halide for generating active carbenes for C–H insertion is well explored. As an example, depicted in Figure III-17b and c is the deprotonation of vinyl halides **III-63** and **III-66** to provide the corresponding carbene intermediates for subsequent insertion; the five membered ring products of the latter reaction are further used towards target complex skeletons.^{42–44}

a. Du Bois's synthesis of tetrodotoxin



b. Grainger's synthesis of AB ring system of ingenol



c. Wardro's synthesis of lactacystin

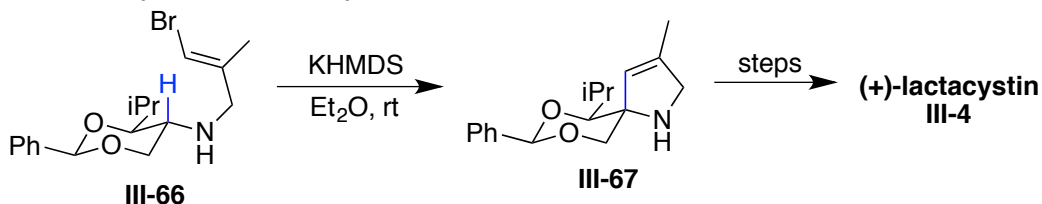


Figure III-17. Application of C-H insertion strategy in the total synthesis of natural products and complex molecules.

With the wealth of reports on the direct C–H insertion reactions, and the fact that most of the charge containing strategies failed to deliver C-5 functionalization for our synthesis, the idea was conceived of leveraging C-H insertion strategies to functionalize this center. The approach was to utilize one of the neighboring groups near C-5 as the handle to deliver the active carbene intermediate for insertion into the target C–H bond. It was envisioned that the amide moiety, or the tertiary alcohol on C-4, or the carbinol group on C-5 or the side chain on the C-3 can be utilized as an ancillary group to deliver the active carbene species for functionalization of the C-5 center. One of the early approaches was to utilize the substituents on C-3 to generate a carbene from α -diazo carbonyl (**III-72**) for C-5 functionalization (Figure III-18). The plan was to convert the advanced skeleton **III-71** into the α -diazo compound **III-72**. To this end, deprotection of the primary alcohol in **III-34** was carried out using HCl (2N aq.) in THF.⁴⁵ Diol protection of primary and tertiary alcohol in **III-68** gave the corresponding acetal product **III-69**. The allyl group on C-3 was then oxidized to carboxylic acid **III-71**, followed by acid chloride formation. As reported in the literature,⁴⁶ treatment of acid chlorides with (trimethylsilyl)diazomethane could give access to the α -diazo carbonyl compounds. In our case however, this reported methodology repeatedly failed to deliver the desire transformation to access **III-72**.

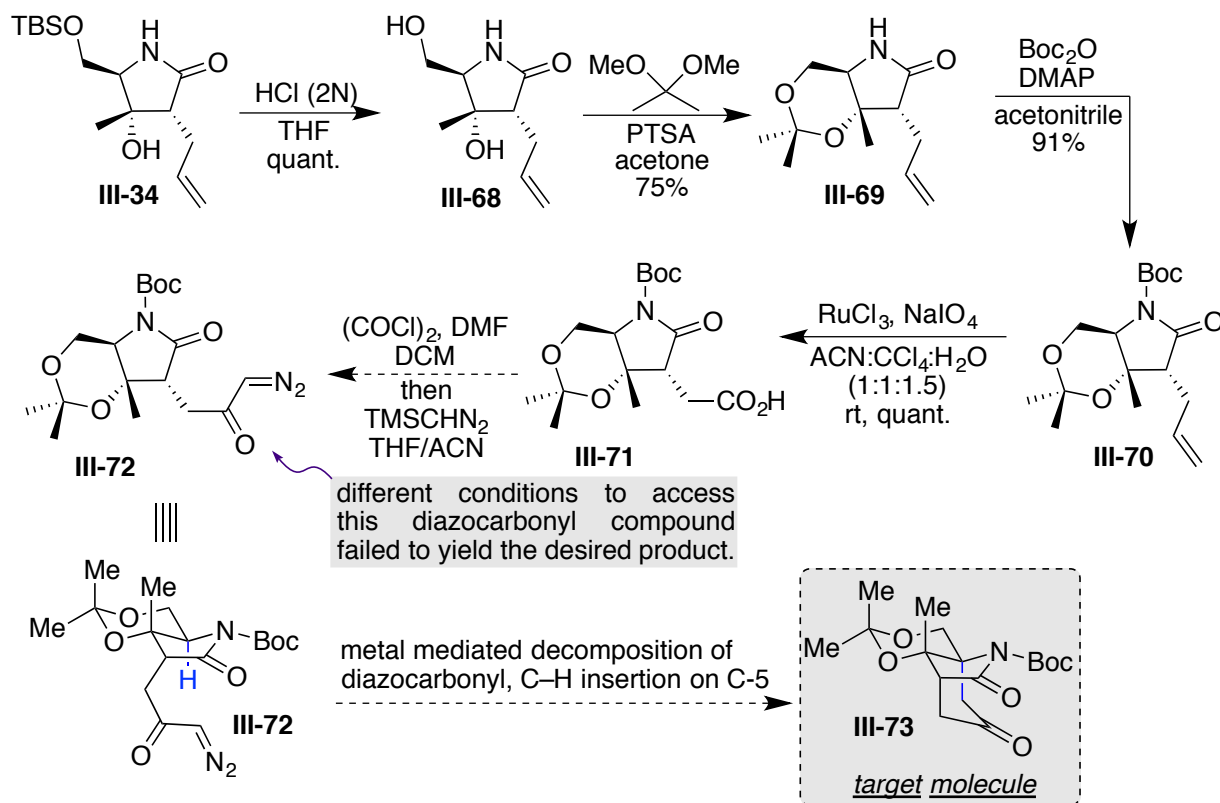
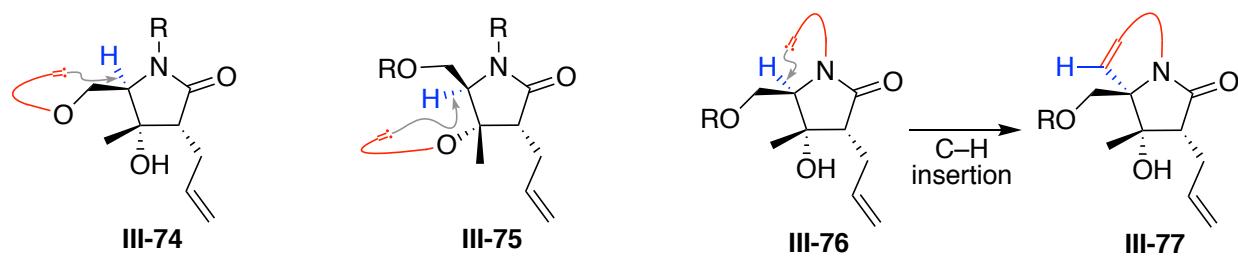


Figure III-18. Functionalization at C-5 center employing metal mediated decomposition of α -diazo carbonyl, a C-H insertion strategy.

Next we turned our attention to engage the tertiary alcohol on C-4, group on the C-5 or the amide nitrogen as a handle to deliver the carbene species. Many trials to use the tertiary alcohol as a handle for carbene insertion failed presumably due to the sterically congested hydroxyl group. Difficulties associated with the functionalization of this hindered alcohol precludes installation of any surrogates that would deliver the active carbene intermediate.

a. envisioned moieties to deliver carbene for C-5 functionalization



b. lactam nitrogen to deliver carbene for C-H insertion

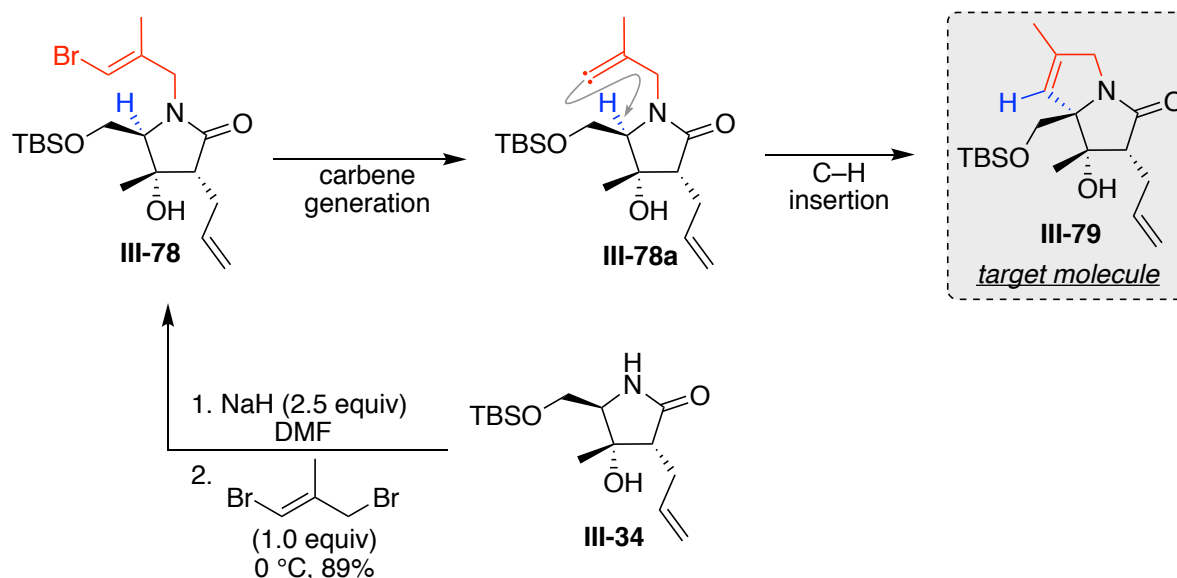
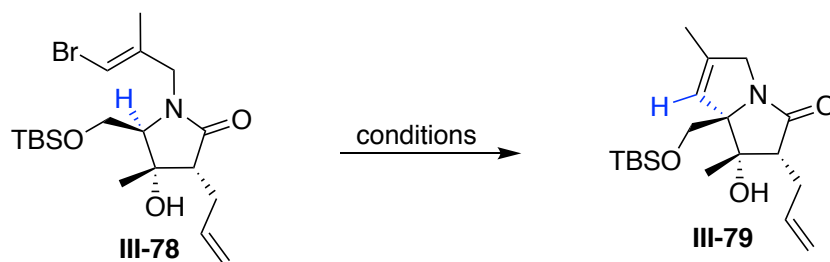


Figure III-19. Envisioned functionalities to deliver the active carbene to the C-5 center for the C-H insertion reaction.

The last resort was to install a carbene surrogate on the amide nitrogen (Figure III-19, a). The deprotected pyrrolidinone **III-34** was derivatized as the vinyl bromide **III-78** in high yield. This vinyl bromide was to be converted to the corresponding carbene upon deprotonation of the vinyl proton. We were optimistic that the carbene would only insert into the targeted C–H at C-5, since this bond is fairly electron rich and is in close proximity of the generated carbene (six atoms away) (Figure III-19, b). As such, conditions to

generate the requisite carbene **III-78a** from vinyl bromide **III-78** were examined (see Table III-1).

Table III-1: Optimization of the C-H insertion reaction at the C-5 center.



entry ^a	solvent	KHMDS (equiv) ^b	temp. (°C) ^c	time (hour)	conversion (%) ^d	yield (%) III-79/III-78
1	THF	3.0	−40 to 4	12	40	25/53
2 ^f	THF	6.0	−40 to rt	12	100	25/−
3	THF	5.0	−40 to rt	12	100	30/−
4	THF	2.0	−78 to −30	14	0	−/90
5 ^g	THF	5.0	−78 to rt	6	0	−/85
6	toluene	3.0	−78 to 0	12	60	27/30
7 ^h	toluene	3.0	−78 to 0	12	10	−/80
8	toluene	3.0	−40 to 0	12	100	33/−
9	toluene	2.0	−78 to 0	20	25	14/74
10	toluene	5.0	−40 to 0	4	100	43/−
11 ⁱ	toluene	5.0	−40 to 0	6	80	10/36
12	toluene	5.0	0 to rt	6	90	15/9
13	toluene	3.0	−78	15	85	53/13

Table III-1 (cont'd).

entry	solvent	KHMDS (equiv) ^b	temp. (°C) ^c	time (hour)	conversion (%) ^d	yield (%) III-79/III-78
14	toluene	3.0	−40 to −20	12	70	60/17
15	toluene	3.0	−40 to −20	3.5	87	58/14
16	toluene	5.0	−40 to −20	3.5	90	75/10
17	toluene	6.0	−40 to −20	3.5	90	71/10
18	toluene	3.0	−40 to −20	12	70	51/20
19	toluene	3.0	−40 to −20	1	75	50/25 ⁱ
20	toluene	3.0	−40 to −20	2	80	53/30 ⁱ
21 ^k	toluene	5.0	−40 to −20	3.5	90	73/10

[a] Reactions were performed on a 0.1 mmol scale. [b] KHMDS (0.5 M in toluene) was used. [c] The base was added at the first temperature and the reaction was stirred at the second temperature. [d] Conversions are estimated from ¹H-NMR using triphenylmethane as an internal standard. [e] Isolated yield unless otherwise noted. [f] KHMDS was added in two portions with 6-hour interval. [g] KHMDS (0.5 M in THF) was used. [h] LiHMDS (1.0 M in hexane) was used. [i] KHMDS was added over 45 minutes at −40 °C. [j] Yields are estimated from ¹H-NMR using triphenylmethane as internal standard. [k] Reaction was performed on a 1 mmol scale.

Vinyl bromide **III-78** was reacted with potassium bis(trimethylsilyl)amide (KHMDS, 0.5 M in toluene) under various conditions. To our delight, the C-H inserted product **III-79** was the only isolable product of the reaction along with the remaining starting material **III-78**. The reaction proved to be sensitive to multiple variables. Reaction time, equivalents of KHMDS, initial reaction temperature, and the temperature during the reaction progress were crucial for the optimal yield of the C–H inserted product. With THF as the solvent,

KHMDS as the base and the initial reaction temperature of $-40\text{ }^{\circ}\text{C}$ followed by stirring at $4\text{ }^{\circ}\text{C}$, only 40% conversion was observed based on ^1H NMR analysis of the crude mixture. In the same reaction, $\sim 25\%$ product formation was also observed based on ^1H NMR analysis (entry 1, Table 1). Increasing the temperature and the equivalents of the base leads to complete consumption of the vinyl bromide, however the yield of the product did not show significant improvement (entry 2-3, Table 1). To our surprise, KHMDS solution in THF instead of toluene did not give any product formation and complete recovery of the vinyl bromide was observed (entry 5, Table 1). Keeping this anomaly in mind, toluene was examined as the reaction solvent. Generally, the conversions and yields improved in comparison to reactions carried out in THF as solvent. Ultimately, we realized that at higher reaction temperatures, despite improved conversions, the yield of the product does not improve (entry 12, Table 1). It should be noted that both starting vinyl bromide and the product are prone to decomposition and side product formation due to the presence of hydroxyl group on C-4 and the acidic hydrogen on C-3. Thus, the reaction should give better results at lower temperatures. The reaction at $-78\text{ }^{\circ}\text{C}$ gave good conversion and moderate yield of the product (entry 13, Table 1). The mass balance of the reaction can be improved by further optimization. Using 5.0 equivalents of the base with an initial temperature of $-40\text{ }^{\circ}\text{C}$ and stirring at $-20\text{ }^{\circ}\text{C}$ for 3.5 hours followed by quenching at $-20\text{ }^{\circ}\text{C}$ gave the best conversion and yield of the product along with good mass balance (entry 16, Table 1). The reaction on a larger scale gave similar results with 73% yield of the desired product (83% brsm) (entry 21, Table 1).

With this methodology in place, the newly installed olefin on C-5 can be converted to carbonyl group through oxidative cleavage. Additionally, the terminal olefin side chain on C-3 must be oxidatively cleaved to provide the required functionality for installation of the chlorine atom. One of the early efforts was to oxidatively cleave both the terminal and internal double bonds in **III-79** in order to shorten the number of steps. It was hypothesized that the aldehyde obtained from the oxidation of the terminal olefin in **III-80** will be trapped as its hemiacetal **III-81** by the neighboring tertiary alcohol on C-4, opening an avenue for dissecting the bis-aldehyde product for following transformations (Figure III-20). Similar hemiacetal between the aldehyde on C-5 and the hydroxyl on C-4 in **III-82** would be less favored due to the smaller ring size. To this end, compound **III-80** was subjected to ozonolysis conditions. Unfortunately, a complex mixture of multiple products was observed. This outcome can be due to the fact that the aldehydes can undergo hemiacetal formation with the neighboring tertiary alcohol and the newly formed stereogenic acetal center exist as mixture of stereoisomers.

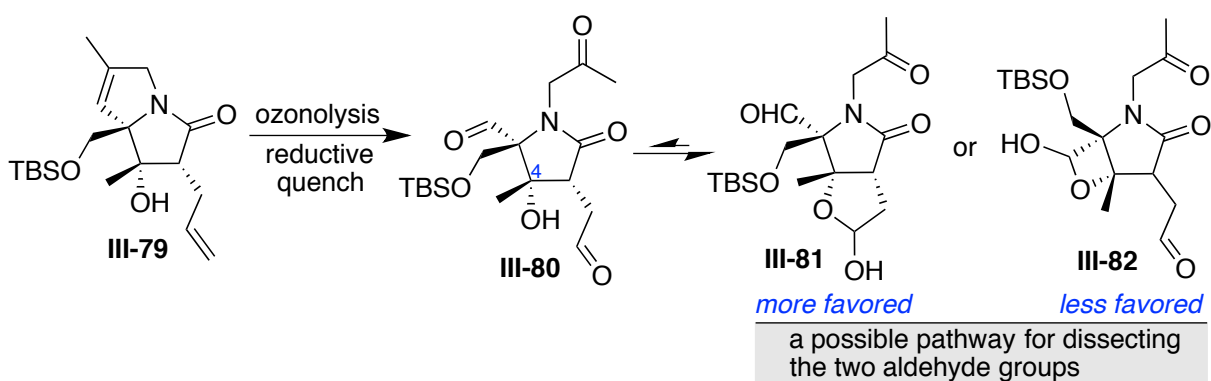


Figure III-20. Installation of the carbonyl moiety on the C-5 center.

To avoid this complication, a sequential oxidative cleavage of the olefin was pursued. We leverage the reactivity differences of the olefins to selectively cleave the terminal in the presence of the internal, tri-substituted double bond in **III-79**. Osmium tetroxide mediated oxidation led to selective cleavage of the terminal double bond and the resultant aldehyde was trapped as the hemiacetal by the neighboring tertiary alcohol leading to a diastereomeric mixture **III-83**. This diastereomeric mixture of hemiacetals can be reduced to the diol **III-84** or alternately they can be converted to the acetals **III-85a/b** via acid catalyzed reaction with methanol.

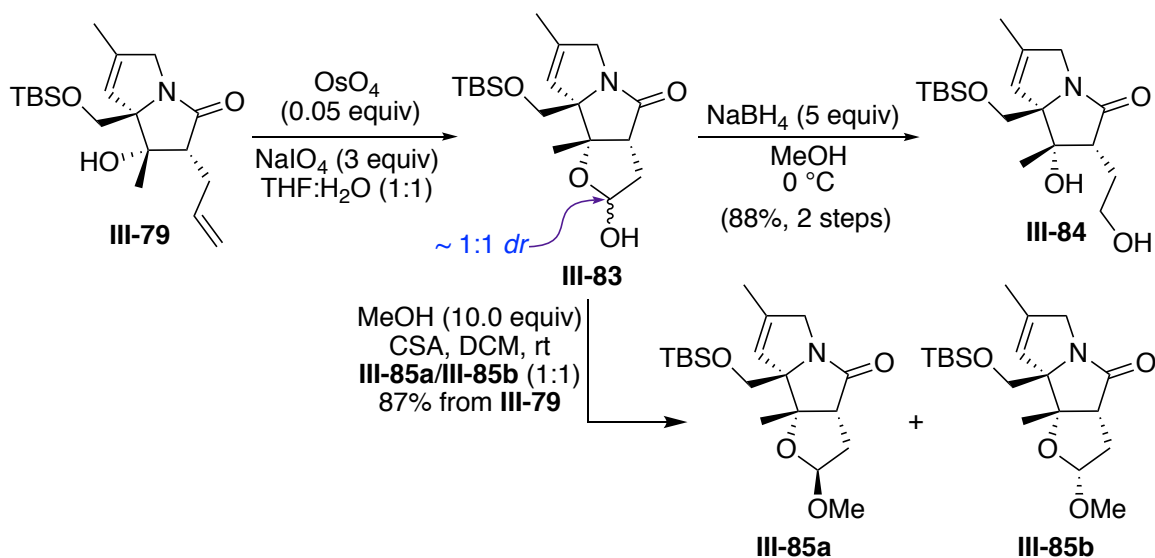


Figure III-21. Selective oxidative cleavage of the terminal olefin.

To our surprise, the acetal formation proceeded without any preferences for either diastereomers **III-85a** or **III-85b**. One would expect that the geometry of the bicyclic backbone would favor addition of methanol to the oxocarbenium intermediate, generated from reaction of **III-83** with acid, from the convex face leading to **III-85a** as the major product. Nevertheless, the results did not follow this hypothetical speculation. However,

this poor diastereoselectivity will not be an issue since the two diastereomers are separable via column chromatography, and furthermore, the stereochemistry of the acetal center is inconsequential since it will eventually be converted into a primary alcohol.

The cleavage of the internal olefin to install the carbonyl moiety at C-5 was the next target. It was envisioned that there could be multiple paths to complete the total synthesis of Salinosporamide from **III-84** or **III-85**. One approach is depicted in Figure III-22 and was the first to be explored. The internal olefin in **III-84** subjected to ozonolysis followed by oxidative workup. The resulting acid **III-86** was then used to form β -lactone **III-86** along with the conversion of the primary alcohol into a chloride to access the advanced intermediate **III-87** in 23% yield from **III-84**.⁷ From this point the removal of the group on the nitrogen and formation of the carbinol on C-5 in three steps would lead to completion of the synthesis of Salinosporamide A. Among the remaining four steps, the removal of the group on the nitrogen atom is the most untested and could pose a challenge for the completion of the synthesis. Thus, removal of this group on a more readily available analogue was first investigated.

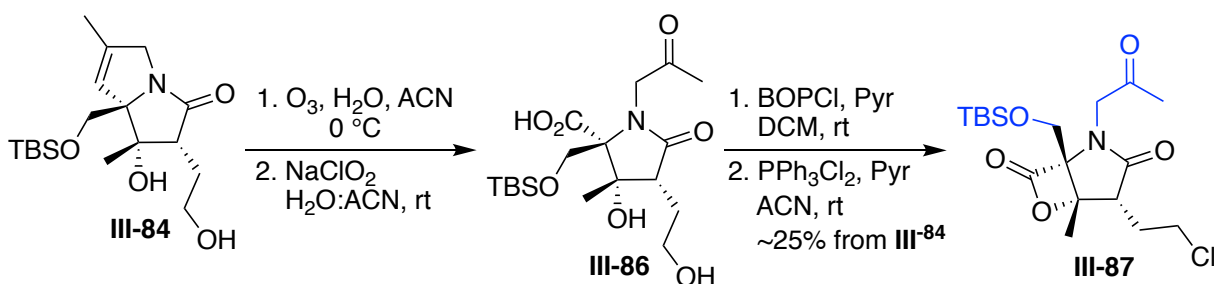


Figure III-22. Oxidative cleavage of the internal olefin, β -lactone ring formation.

Acetal **III-85** was anticipated to undergo oxidative cleavage to give methyl ester **III-88**. This ester is a simpler analogue of **III-87** for dealkylation studies of the nitrogen atom. Direct conversion of the olefin to methyl ester by ozonolysis in methanol followed by treatment of the reaction mixture with acetic anhydride failed to yield **III-88**.⁴⁷ Alternatively, a sequential ozonolysis/oxidation-esterification led to the formation of methyl ester **III-86** in good yield (Figure III-23).

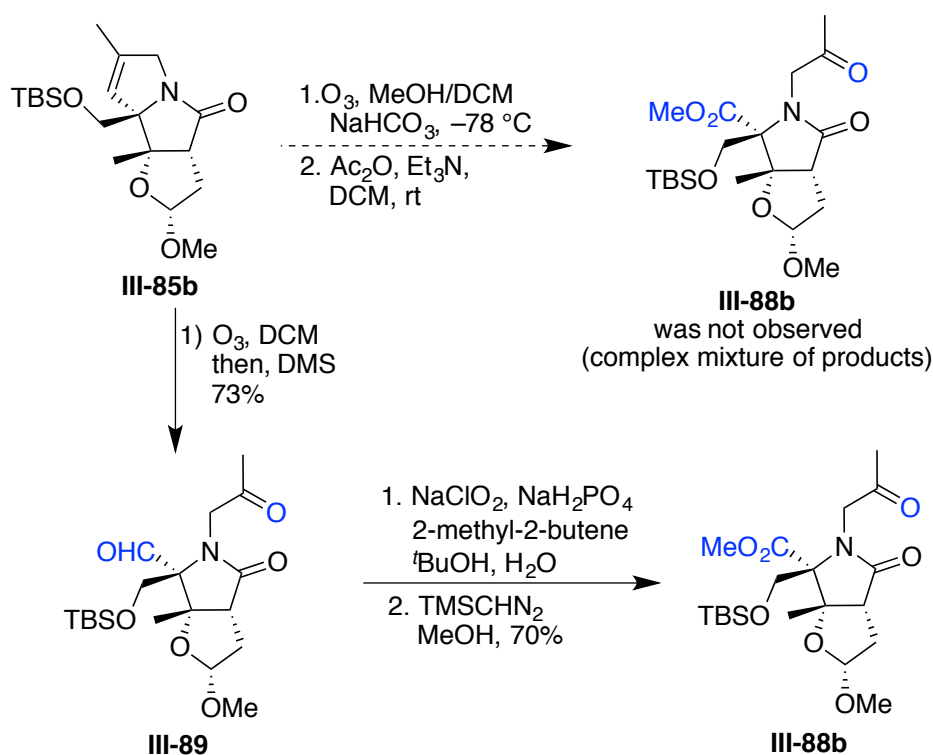


Figure III-23. Oxidative cleavage of the internal olefin towards deprotection of the pyrrolidinone nitrogen.

Our first trial to free the nitrogen atom in **III-88** was a radical mediated α -cleavage of the ketone utilizing samarium (II) iodide. This reagent is well known to cleave carbon heteroatom bonds on the alpha position of carbonyl compounds.⁴⁸⁻⁵² However, the

reaction proved incompetent for the cleavage of the group on the nitrogen in **III-86**. The reaction with samarium (II) iodide under various conditions only resulted in the recovery of the starting material **III-86** (Figure III-24). In another approach, we resorted to different strategies that convert the methyl ketone to a functionality that can be easily cleaved from the nitrogen atom.

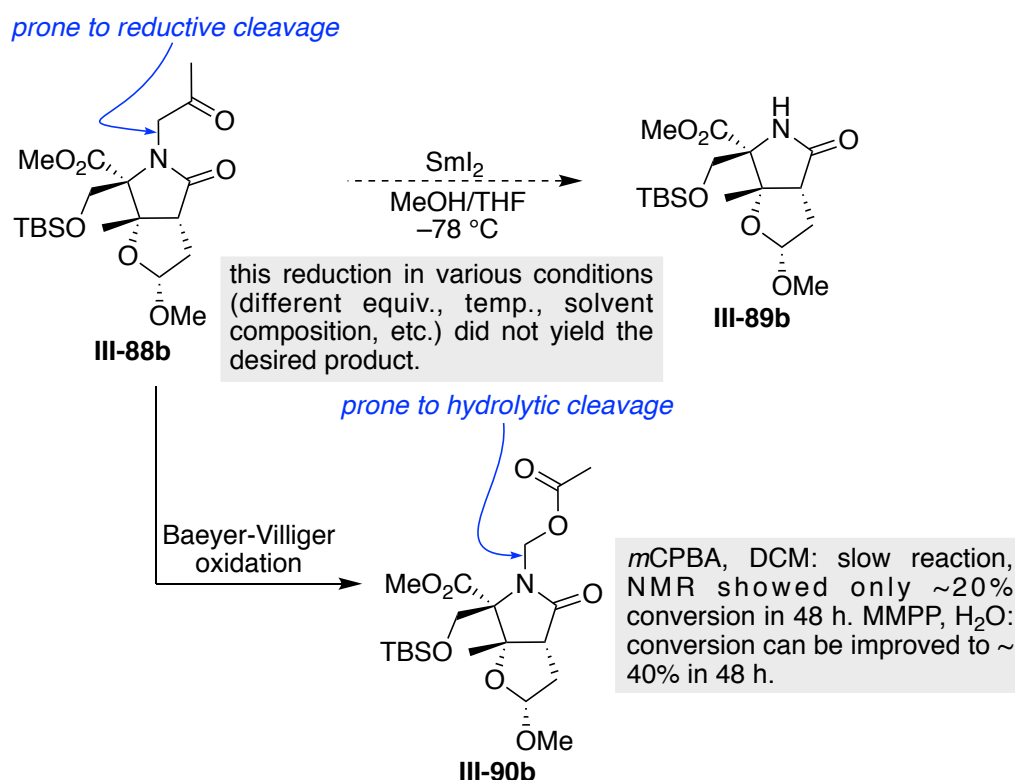


Figure III-24. Strategies for the removal of the group on the pyrrolidinone nitrogen.

In this regard, Baeyer-Villiger oxidation of **III-88** to give access to the acetate product **III-90** was performed. It is anticipated that this oxidation would occur next to the methylene group, leading to an acetate group that is prone to hydrolytic cleavage. After screening various oxidizing reagents known to perform the Baeyer-Villiger reaction, we realized that *meta*-chloroperbenzoic acid can give access to the desired product **III-90**, but only with

low conversion.⁵³ The reaction conversion can be improved to some extent utilizing magnesium monoperoxyphthalate (MMPP) in water.⁵⁴ However, complete conversion of the starting material was not achieved and the reaction in the presence of a multifold excess of the oxidant and elongated reaction time did not improve the results. Next, we envisioned modification of the olefin in **III-85** in such a way that the oxidation of the olefin would lead to a cleavable group remaining on the pyrrolidone nitrogen. To this end, oxidative cleavage of the enone in **III-91** was speculated to provide an intermediate that would be capable of being easily transformed to **III-93** (Figure III-25).

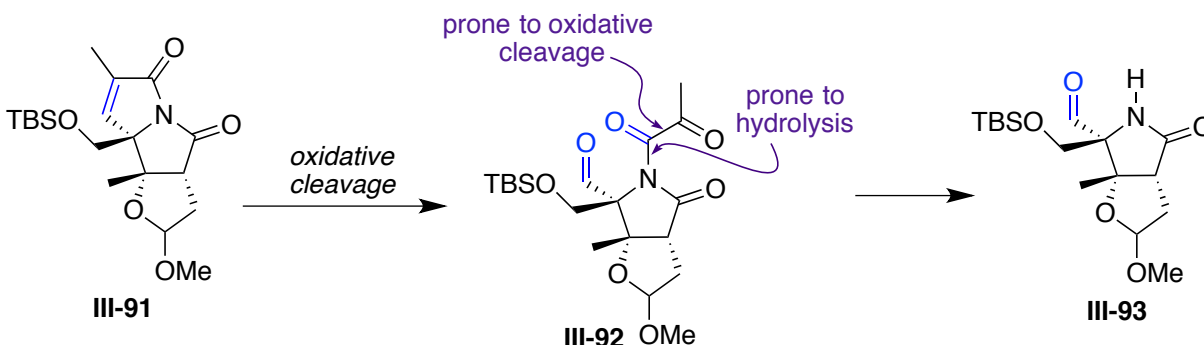


Figure III-25. An envisioned enone moiety for the facile removal of the group on the pyrrolidinone nitrogen after oxidative cleavage of the internal olefin.

The allylic methylene in **III-85** was oxidized to the corresponding carbonyl with CrO_3 and pyridine, yielding enone **III-91** in high yield.⁵⁵ The X-ray crystal structure of **III-91b** confirmed the structure as predicted (Figure III-26).

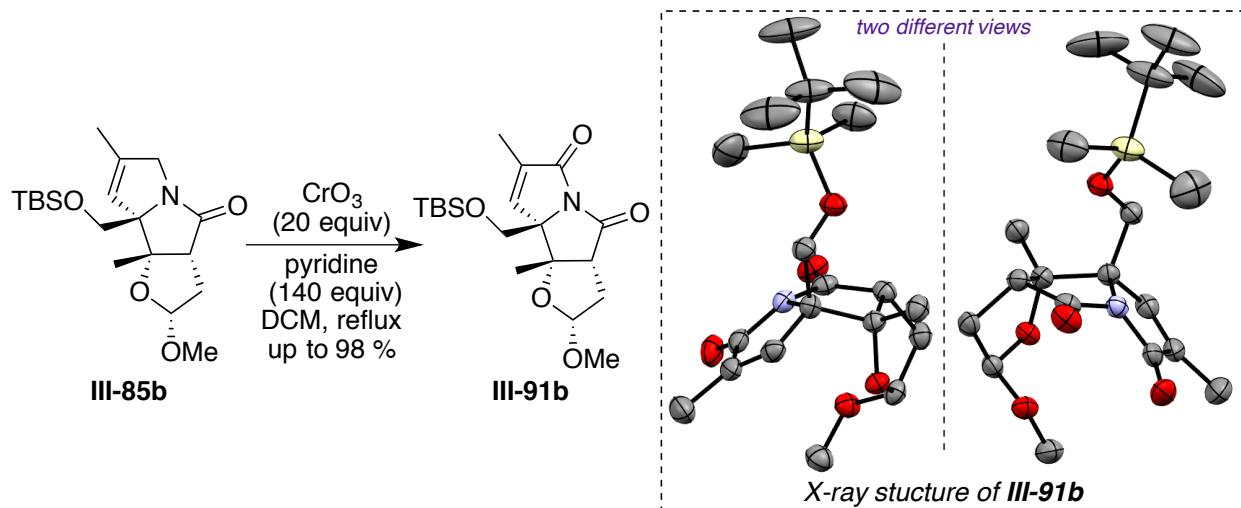
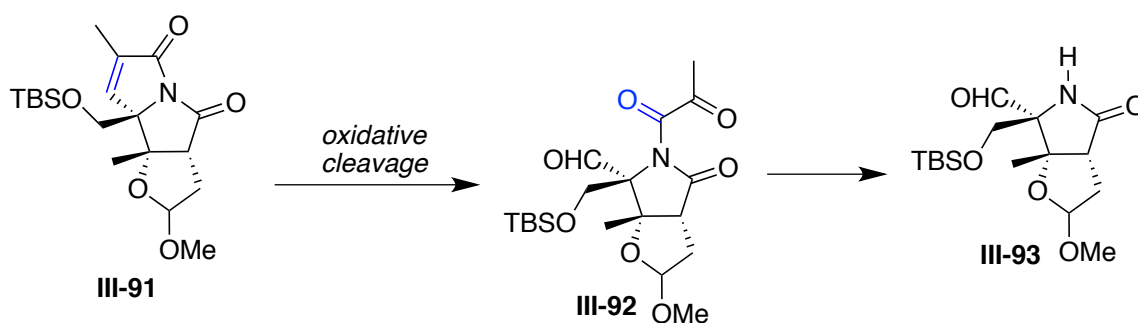


Figure III-26. Synthesis of the envisioned enone core and its X-ray crystal structure.

The oxidative cleavage of **III-91** proved challenging. A diverse set of oxidative conditions were tried with no success, indicating the low reactivity of the olefin. The low reactivity of this double bond for oxidation is not surprising since the olefin is conjugated. Furthermore, this olefin is hindered by the bicyclic framework, as well as the neighboring quaternary carbon. As listed in Table 2, most trials resulted in the recovery of the unsaturated imide **III-91**. Most of the metal mediated conditions failed to give access to the cleaved product.⁵⁶⁻⁵⁷ Ozonolysis, at low temperature after 30 minutes did not give any cleaved products. This strong oxidizing condition at higher temperatures resulted in a complex mixture of decomposed products (entry 7, Table 2). Generally, ozonolysis results in a blue solution, indicating the completion of the reaction and accumulation of excess unreacted ozone. As indicated in the entry 6 Table 2, ozonolysis reaction at $-78\text{ }^\circ\text{C}$ after 30 minutes (reaction was blue) leads to almost complete recovery of starting materials **III-91**. However, the presence of the blue color was misleading since with longer reaction time the formation of the cleaved products was observed.

Table III-2: Optimization of olefin cleavage towards installation of carbonyl on C-5.



entry	conditions	results (notes)
1	KMnO ₄ , 18-crown-6 then NaIO ₄ , LiOH	complex mixture of products
2	OsO ₄ , Oxone, DMF, rt	III-91 was recovered (>98%)
3	OsO ₄ , Oxone, DMF, 65 °C	III-91 was recovered (>98%)
4	RuCl ₃ , NaClO ₄	III-91 was recovered (>98%)
5	RuO ₂ , NaIO ₄ , EtOH/H ₂ O/TFA, rt	III-91 was recovered (>98%)
6	O ₃ , DCM, -78 °C, 30 minutes	III-91 was recovered (>98%)
7	O ₃ , acetone/H ₂ O (95:5), 0 °C	complex mixture of products
8	O ₃ , DCM, -78 °C, 90 minutes then DMS	40 conv. (III-92 : III-93 ~3:1) basic workup
9	O ₃ , DCM, -78 °C, 3-5 hours then DMS	90 conv. (III-92 85%, III-93 8%) acidic workup
10	O ₃ , MeOH, NaHCO ₃ , -78 °C, 3-5 hours then Ac ₂ O, Et ₃ N	complex mixture of products

After a number of these trials, the bubbling of ozone for 90 min into the DCM solution of **III-91** at $-78\text{ }^{\circ}\text{C}$ gave a ~40% conversion (entry 8, Table 2). Elongating the reaction time to 3 h led to >90% cleavage of **III-91** (entry 9, Table 2). Reductive workup of the ozonolysis reaction with dimethyl sulfide provide the desire aldehyde functionality on C-5. It was noted that the basic workup of the reaction leads to partial cleavage of the di-carbonyl on the pyrrolidone nitrogen delivering **III-93**. Nevertheless, when the reductive ozonolysis product was quenched with saturated ammonium chloride, the dicarbonyl product **III-92** was isolated. Formation of **III-93** under basic workup condition demonstrates the susceptibility of the dicarbonyl moiety on **III-92** for hydrolytic removal of this group from pyrrolidine nitrogen. Due to the ease of purification, dicarbonyl **III-92** was preferred over **III-93**. With aldehyde **III-92** in hand, we postulated the use of our methodology to convert the aldehyde to methyl ester from the Borhan laboratories by treatment of **III-92** with oxone in methanol (Figure III-27, top).⁵⁸⁻⁵⁹ Unfortunately, this condition did not result in the formation of methyl ester **III-89** (Figure III-27, top). In another approach, **III-92** was oxidized under Kraus-Pinnick conditions to deliver that corresponding carboxylic acid **III-94**. To our delight, the di-carbonyl on the imide nitrogen was removed under the basic conditions of the Kraus-Pinnick oxidation. This result is in agreement with the product distribution that was observed under basic work up of the ozonolysis reaction (entry 9, Table 2). The crude carboxylic acid **III-94** was directly converted to the methyl ester **III-89b** with trimethyldiazomethane in methanol in near quantitative yield, and was used in the following Boc-protection reaction without purification (Figure III-27).

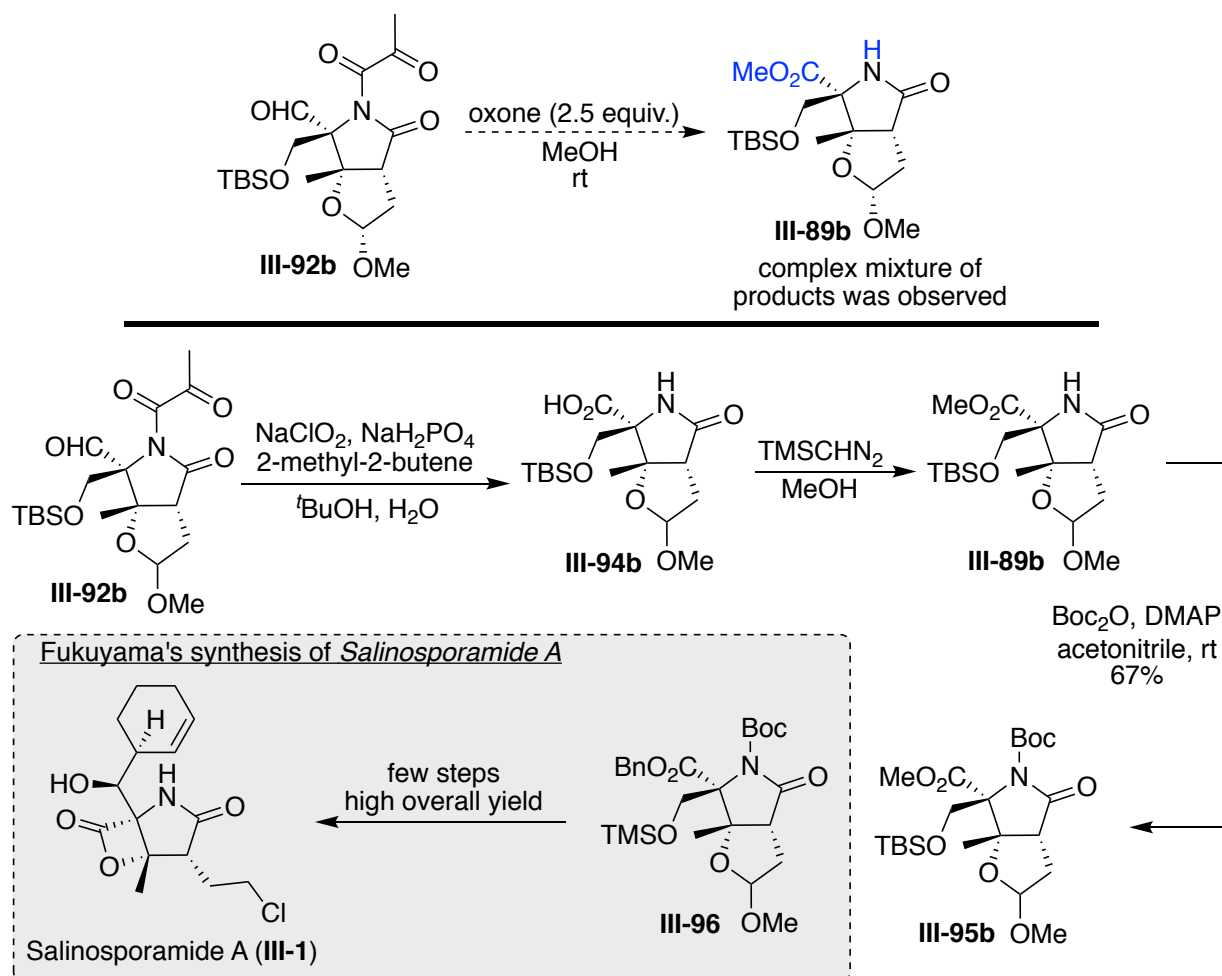
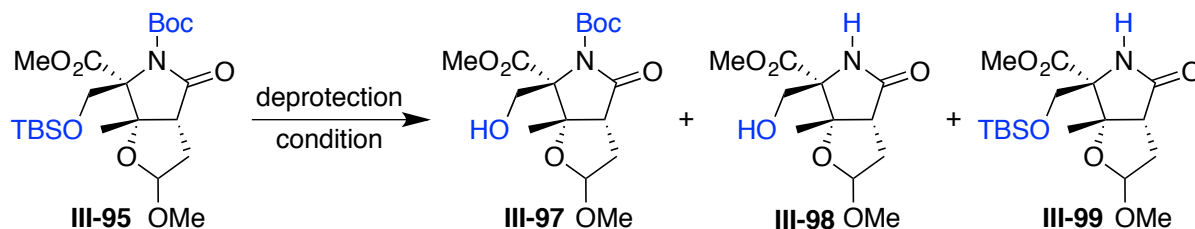


Figure III-27. Access to the advanced bicyclic core **III-94b**, similar to Fukuyama's intermediate towards Salinosporamide A.

The *tert*-butyloxycarbonyl protection of the crude amide **III-89b** was carried out following the reported protocol,¹³ leading to **III-95b** in good yield (67% over three steps). This advanced scaffold closely resembles **III-96**, an intermediate in Fukuyama and coworkers' synthesis of Salinosporamide A (Figure III-27, highlighted box). To that end, a selective de-protection of the TBS-ether in the presence of the Boc protecting group was pursued. It was realized that the Boc group is labile and is removed before TBS deprotection, thus leading to amide **III-99**.

Table III-3: Selective deprotection of the TBS ether in the presence of Boc protecting group.



entry ^a	solvent	reagent	condition	results (notes) ^b
1	MeOH	CSA (1.1 equiv)	0 °C, 3h	III-95 was recovered (>98%)
2	THF	HCl (2N)	0 °C to rt, 3h	III-95 was recovered (>98%)
3	MeOH	PTSA (1.1 equiv)	rt, 3h	III-98 was the major product (>80%)
4	MeOH	PTSA (1.1 equiv)	0 °C	~20 % conversion, III-99 as major product
5	THF	HF•Pyr	0 °C to rt, 3h	complex mixture of products
6	MeOH	AcCl	4 °C, 12h	~30 % conversion, III-98 as major product
7	AcOH:THF:H ₂ O (3:1:1)		0 °C	III-95 was recovered (>98%)
8	AcOH:THF:H ₂ O (3:1:1)		45 °C, 12h	III-95 was recovered (>98%)
9	HCO ₂ H:THF:H ₂ O (3:6:1)		rt	III-95 was recovered (>98%)
10	DCM	BF ₃ •Et ₂ O	rt	III-98 and III-99 (~2:1) as products

Table III-3 (cont'd)

entry	solvent	reagent	condition	results (notes) ^b
11	THF	TBAF (5.0 equiv)	0 °C to rt, 5h	complex mixture of products
12	MeOH	CCl ₄ , ultrasonication	40 °C, 2h	III-95 was recovered (>98%)
13	MeOH	PPTS (1.1 equiv)	rt, 2h	III-95 was recovered (>98%)
14	MeOH	H ₂ SO ₄	0 °C to rt, 2h	III-95 was recovered (>98%)
15	ACN	HF (aq)	0 °C to rt, 3h	~ 50% conv., III-99 as major product
16	EtOH	HCl (con.) 1%	0 °C to rt, 3h	III-95 was recovered (>98%)
17	DCM	Quinolinium fluorochromate	rt, 5h	III-95 was recovered (>98%)
18	THF	TBAF (5.0 equiv), CSA (5.0 equiv)	0 °C to rt, 3h	~ 20% conv., III-97 as major product
19	THF	TBAF (2.5 equiv), AcOH (7.5 equiv)	rt, 72h	~75% con., 60% III-97 was isolated
20	THF	TBAF (5.0 equiv), AcOH (10.0 equiv)	45 °C, 48h	>95% con., 85% III-97 was isolated

[a] Reaction were performed in a 0.1 mmol scale. [b] Yield and the ratio of the products were estimated based on ¹H-NMR analysis of the crude mixture.

As illustrated in Table 3, various reported conditions failed to give access to the de-protected alcohol **III-99**. The main problems were the removal of the Boc group yielding

III-99, or the concurrent removal of the TBS and Boc groups leading to **III-98**. Most of the reported acid catalyzed strategies to remove TBS either resulted in the recovery of **III-98**, or the dual deprotection of TBS and the Boc group. Ultimately, treatment of **III-95** with TBAF in the presence of acetic acid gave access to the desired product **III-97** in good yield (entry 20, Table 3).⁶⁰ Buffered reaction with acid was necessary to prevent removal of the Boc group or transposition of the Boc from the amide nitrogen to the alcohol on C-5. Deprotected alcohol **III-97** was readily oxidized to the aldehyde **III-100b** employing Dess–Martin periodinane in DCM. Following reported procedures, aldehyde **III-100b** was reacted with *in situ* generated cyclohexenyl zinc chloride at $-78\text{ }^{\circ}\text{C}$ to give access to the alcohol **III-101b** with complete stereochemical control in excellent yield.^{7, 13}

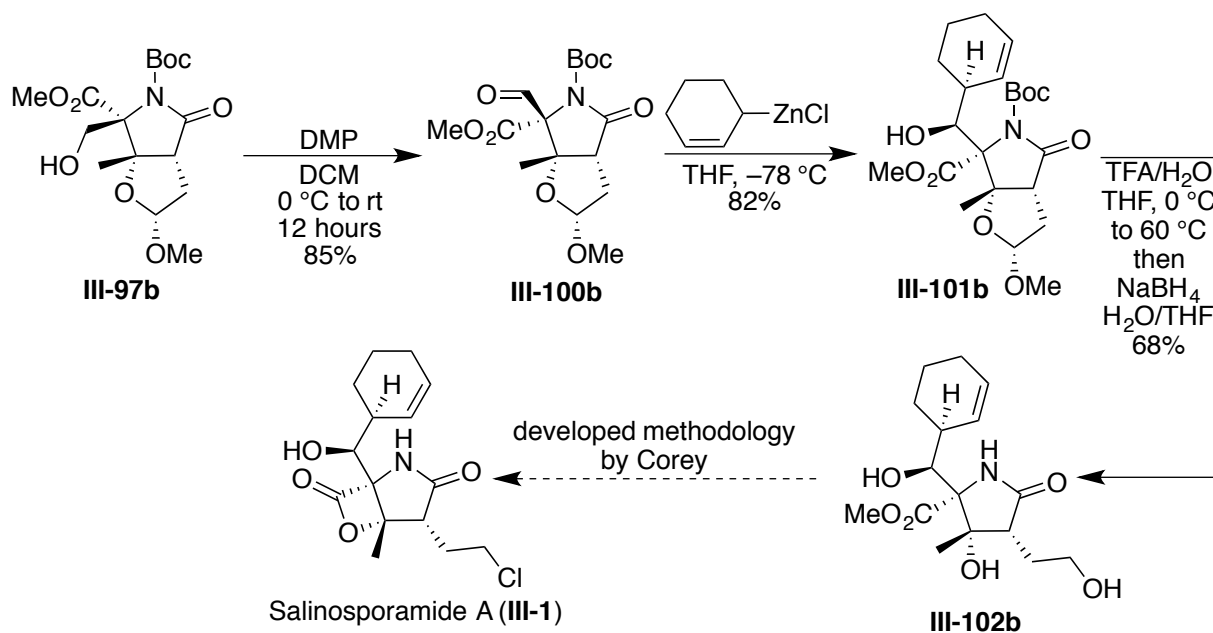


Figure III-28. Completion of the racemic synthesis of Salinosporamide A.

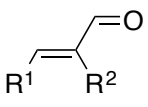
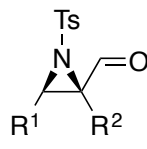
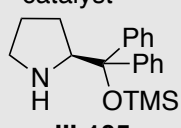
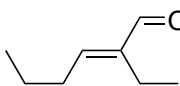
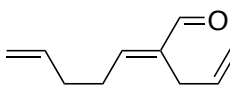
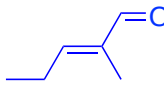
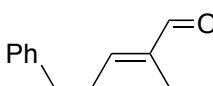
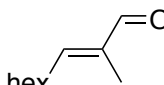
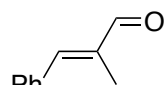
The Boc protecting group was removed with exposure to trifluoro acetic acid, resulting in the hydrolysis of the acetal group as well. The crude hemiacetal was treated with

NaBH₄, leading to diol **III-102b** in good yield.¹³ The advanced intermediate **III-102b** can be converted to Salinosporamide A following the procedure reported by Corey and co-workers.⁷ Having in hand the synthesis that leads to the racemic total synthesis of Salinosporamide A, we pursued the asymmetric synthesis of this molecule. The following section highlights our total synthesis of (–)-Salinosporamide A.

III- 6 The total synthesis of (–)-Salinosporamide A

After successful implementation of the racemic synthesis of Salinosporamide A, we sought to carry out the enantiopure synthesis of this natural product. The highly diastereoselective nature of the racemic synthetic route provides a routine strategy to implement the enantiopure synthesis. As such, we envisioned utilization of the enantiopure aziridine **III-30** followed by a sequence of diastereoselective reactions, as outlined above, to give access to (–)-Salinosporamide A. Asymmetric aziridination reactions have witnessed tremendous attention in the past few years.⁶¹⁻⁶² A highly enantioselective aziridination reaction that gives access to tri-substituted in gram scale was desirable as the starting point for the synthesis of (–)-Salinosporamide A. After a thorough survey of the reported protocols for the synthesis of tri-substituted aziridines,⁶³⁻⁶⁷ we chose to use the reported procedure by Cardova and co-workers.⁶⁷ They have used commercially available proline based chiral catalyst **III-105** to synthesize various tri-substituted aziridines from unsaturated aldehydes (Table 4). Fortunately, this reported procedure utilizes unsaturated aldehydes as starting materials and the resulting tosyl protected aziridines are the starting materials for our racemic synthetic route. Cardova and coworkers have demonstrated the applicability of their methodology for various substrates and the aziridine products are isolated in good yield and excellent enantiopurity (Table 4).⁶⁷ In particular, substrate **III-103c**, highlighted in Table 4 (entry 3), is similar to the unsaturated aldehyde **III-107**, requiring for the total synthesis of (–)-Salinosporamide A (Figure III-29).

Table III-4: Cardova's reported asymmetric aziridination of α,β -unsaturated aldehyde.

<div style="display: flex; align-items: center; justify-content: space-around;"> <div style="text-align: center;">  <p>III-103</p> </div> <div style="text-align: center;"> $\xrightarrow[\text{Toluene, rt}]{\text{cat. (20 mol\%) TsNHOTs (1.2 equiv) NaOAc (1.5 equiv)}}$ </div> <div style="text-align: center;">  <p>III-104</p> </div> <div style="border: 1px solid gray; padding: 5px; text-align: center;"> <p>catalyst</p>  <p>III-105</p> </div> </div>					
entry	aldehydes	<i>t</i> (hours)	yield (%)	<i>dr</i>	<i>ee</i> (%)
1	 III-103a	74	81	8:1	99
2	 III-103b	68	77	10:1	99
3	 III-103c	66	84	>25:1	99
4	 III-103e	72	79	>25:1	99
5	 III-103f	66	83	17:1	99
6	 III-103g	65	55	>25:1	98

Aldehyde **III-107** was synthesized to implement the asymmetric aziridination as the starting point for the synthesis of (–)-Salinosporamide A. For this purpose, protection of commercially available 2-methyl 2-butenol followed by a highly selective oxidation of the less sterically hindered allylic methyl group gives access to aldehyde **III-107** in high yield (Figure III-29).

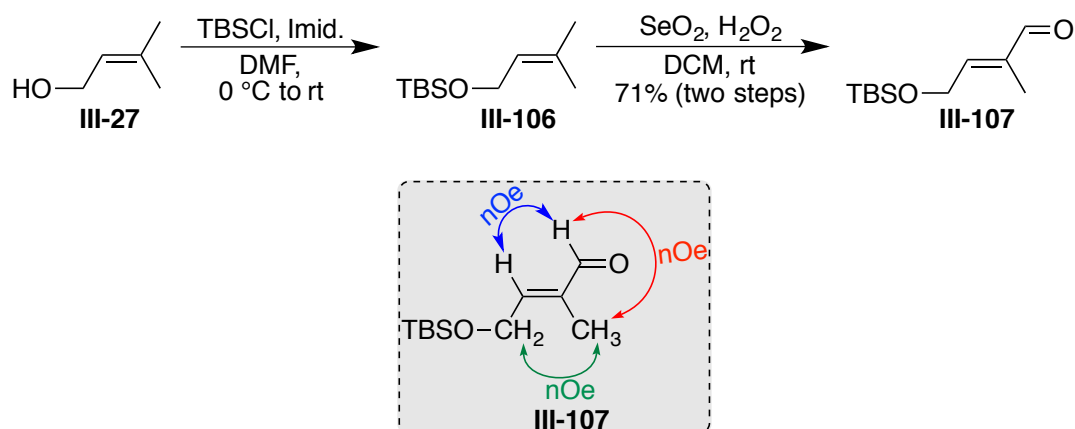


Figure III-29. Synthesis of α,β -unsaturated aldehyde **III-107** for implementation of the asymmetric aziridination reaction.

With aldehyde **III-107** in hand, the enantioselective aziridination reaction, following the procedure reported by Cardova,⁶⁷ was carried out. Fortunately, the aziridinal **(+)-III-30** was obtained in excellent yield and enantioselectivity (>98% ee). Asymmetric aziridination was carried out in 15 mmol scale (~5 g) without significant deterioration of the reaction efficiency. The reaction, in most cases, was completed within 12 h. To our surprise, decreasing the catalytic loading to 5 mol% (instead of the reported 20 mol%), showed only about 25% conversion of starting material in 24 h.

Chiral aziridine aldehyde **(+)-III-30** was reacted with ethynyl magnesium bromide at low temperature. Complete diastereoselective reaction was observed with excellent yield. The crystal structure of **(+)-III-25** confirmed the absolute configuration of the asymmetric centers (Figure III-30).

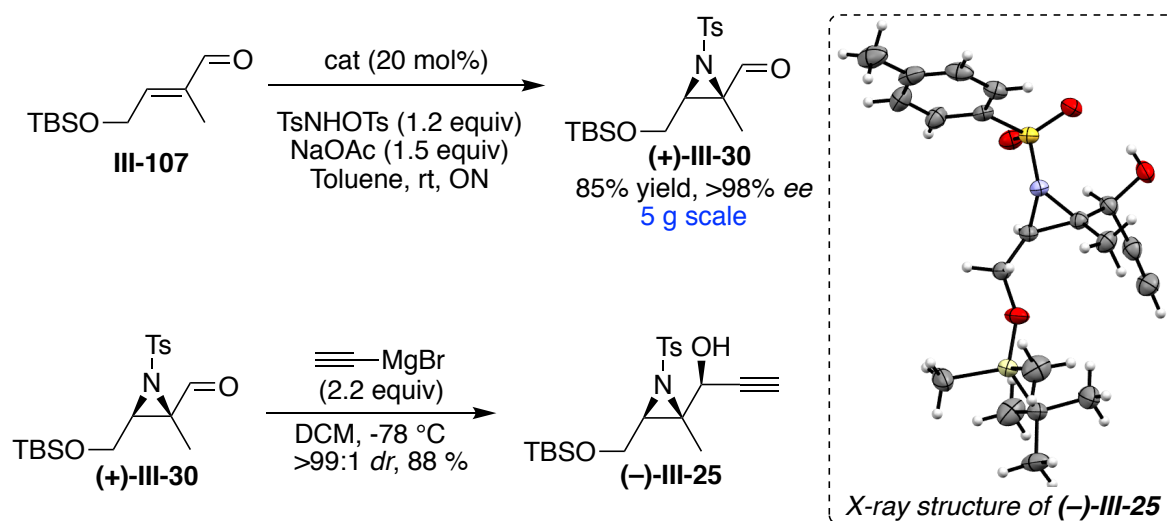


Figure III-30. Asymmetric aziridination of α,β -unsaturated aldehyde, access to aziridine-alcohol **(-)-III-25**.

Figure III-31 demonstrates the completion of the total synthesis of **(-)-Salinosporamide A**. The key tandem aza/Payne hydroamination reaction proceeded with high yield and the resultant enamide product was subjected to ozonolysis followed by the regio- and diastereoselective epoxide opening with MgBr_2 to deliver bromohydrin **(+)-III-32** in high yield over three steps. With bromohydrin **(+)-III-32** in hand, radical mediated functionalization of C-3 was pursued. Following the optimized methodology for the racemic synthesis, exposure of bromohydrin **(+)-III-32** to AIBN as a radical initiator followed by addition of *tri-n*-butyl allyl stannane in refluxing toluene, resulted in **(-)-III-33a/b** as a 3:1 mixture of diastereomers at C-3. This diastereomeric mixture was then epimerized to the thermodynamic product **(-)-III-33b** in the presence of catalytic DBU. The tosyl protecting group was removed with magnesium powder in methanol under sonication to deliver the pyrrolidinone **(-)-III-34**.

The amide nitrogen of the pyrrolidinone **(-)-III-34** was functionalized with vinyl bromide *en route* to the C-H insertion reaction. The C-H insertion took place in good yield delivering **(+)-III-79**. Oxidative cleavage of the terminal olefin followed by acetalization gave access to **III-85a** and **(-)-III-85b**. From this step the synthesis is shown for the beta diastereomer **III-85b**, same reactions sequence are carried out with **III-85a** with comparable results to that of **III-85b**. Oxidation of the internal olefin led to aldehyde **(-)-III-92b**. A sequence of Kraus-Pinnick oxidation, esterification of the resultant acid and Boc protection of the amide resulted in **(-)-III-95b**. The TBS group was removed in the presence of Boc protecting group and the resulting primary alcohol was oxidized to aldehyde **(-)-III-100b**. Following reported procedures,¹³ addition of cyclohexenyl zinc chloride to this aldehyde led to **(-)-III-101b** with complete stereochemical control for the newly formed stereocenters. Treatment of **(-)-III-101b** with TFA followed by sodium borohydride gave access to diol **(-)-III-102b**. The methyl ester in **(-)-III-102** was hydrolyzed with dimethylaluminium methyltellurolate and the resulting carboxylic acid was converted to the β -lactam **(-)-III-108**.^{2, 14} Completion of the synthesis was achieved by chlorination of the primary alcohol in **(-)-III-108** to yield **(-)-Salinosporamide A** (Figure III-31).^{7, 13} The NMRs and optical rotation of the synthesized **(-)-Salinosporamide A** was same as the reported data.

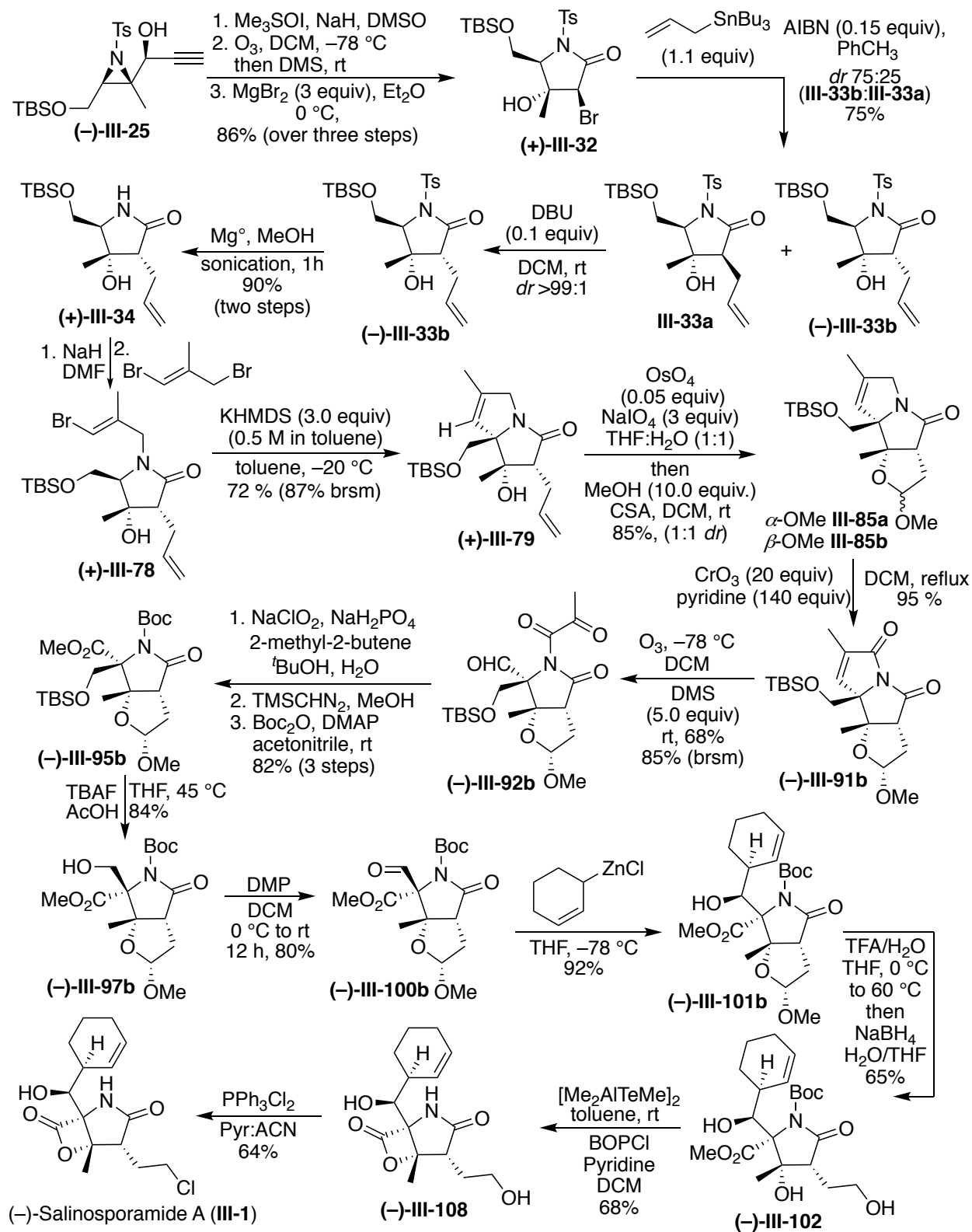


Figure III-31. Total synthesis of (-)-Salinosporamide A.

In summary, we report the asymmetric total synthesis of (–)-Salinosporamide A. Our synthesis highlights the development of a few key reactions that enabled us to access this natural product. The synthesis is built on a tandem aza/Payne reaction that gives access to the pyrrolidine core of the natural product. A C–H insertion reaction stands as one of the key reactions that facilitate a functionalization that most of the routine procedures failed to accomplish. Throughout the synthesis many selective reactions are developed that can be useful in the field.

III-7 Experimental section

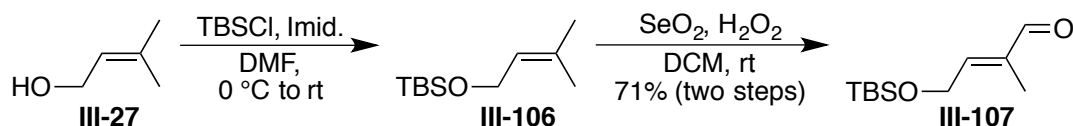
III-7-1 General remarks

Molecular sieves (4Å) were dried at 160 °C under 0.25 mtorr pressure prior to use. Unless otherwise mentioned, solvents were purified as follows. CHCl_3 (amylene stabilized) was purchased from Sigma Aldrich and incubated over 4Å MS for 48 h prior to use. Toluene and CH_2Cl_2 were dried over CaH_2 whereas THF and Et_2O were dried over sodium (dryness was monitored by colorization of benzophenone ketyl radical); they were freshly distilled prior to use. NMR spectra were obtained using a 500 MHz and 600 MHz Varian NMR spectrometers and referenced using the residual ^1H peak from the deuterated solvent. Waters 2795 (Alliance HT) instrument was used for HRMS 68 analysis with polyethylene glycol (PEG-400-600) as a reference.

Column chromatography was performed using Silicycle 60Å, 35-75 μm silica gel. Pre-coated 0.25 mm thick silica gel 60 F254 plates were used for analytical TLC and visualized using UV light, iodine, potassium permanganate stain, *p*-anisaldehyde stain or phosphomolybdic acid in EtOH stain.

III-7-2 Total synthesis of (–)-Salinosporamide A

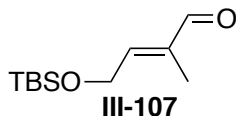
Synthesis of aldehyde III-107:



Synthesis of III-106: Commercially available 3-methyl-2-butenol **III-27** (12.0 g, 139 mmol) was dissolved in DMF (70 mL). To this solution imidazole (23.7 g, 348 mmol) and TBSCl (23.1 g, 153 mmol) were added at 0 °C. Reaction was stirred at room temperature for 5 h before it was quenched by addition of water (100 mL). The aqueous layer was extracted with ethyl acetate (3 x 100 mL). Combined organic layers were washed with brine (100 mL) and dried over sodium sulfate. Volatiles were removed under vacuum and the residue was used in the following step without purification. An analytical sample of the crude was passed through silica plug (ethyl acetate/hexane = 5%) to give pure compound (**III-106**) as a clear oil.

$^1\text{H-NMR}$ (500 MHz, CDCl_3) δ 5.30 (t, 1H, $J = 6.5$ Hz), 4.22 (d, 2H, $J = 6.5$ Hz), 1.68 (s, 3H), 1.60 (s, 3H), 0.90 (s, 9H), 0.07 (s, 6H);

$^{13}\text{C-NMR}$ (125 MHz, CDCl_3) δ 133.9, 124.9, 60.6, 26.4, 26.1, 18.8, 18.2, -4.7.



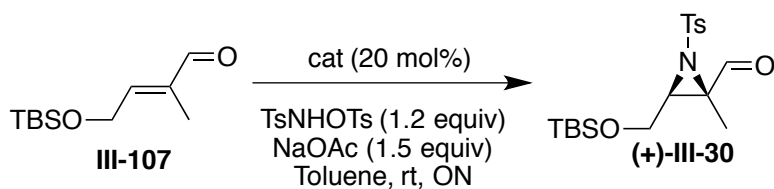
Synthesis of aldehyde 107: SeO_2 (9.0 g, 82 mmol, 1.0 equiv) was dissolved in DCM (200 mL) at room temperature. To this mixture was added $t\text{BuOOH}$ (70 wt.% in water,

30.0 mL, 217 mmol) dropwise at 0 °C. The reaction was stirred at this temperature for 30 min. To this mixture at 0 °C was added crude **III-106** (100 mmol) in DCM (100 mL) dropwise. The reaction mixture was stirred at room temperature for 15 h before it was quenched by addition of water (50 mL). The organic layer was separated and the aqueous layer was extracted with DCM (3 x 100 mL). The combined organic extract was washed with 10% KOH (4 x 50 mL), sat. NaHCO₃ (1 X 100 mL) and water (1 x 50 mL). The organic solvent was evaporated under reduced pressure. Crude aldehyde was purified on column chromatography (silica, ethyl acetate/hexane = 5%) to yield the pure aldehyde as a light yellow oil (15.2 g, 71.0 mmol, 71% yield).

¹H-NMR (500 MHz, CDCl₃) δ 9.40 (s, 1H), 6.50 (m, 1H), 4.48 (dq, *J* = 5.3, 1.2 Hz, 2H), 1.71 (q, *J* = 1.3 Hz, 3H), 0.90 (s, 9H), 0.08 (s, 6H).

¹³C-NMR (125 MHz, CDCl₃) δ 194.59, 153.16, 137.71, 60.48, 25.82, 18.28, 9.37, -5.30.

TOF MS ES⁺ (C₁₁H₂₃O₂Si): Calc. [M + H]⁺: 215.1467, Found [M + H]⁺: 215.1463.



Synthesis of Aziridine (+)-III-30: To a stirred solution of aldehyde **III-107** (3.2 g, 15 mmol, 1.0 equiv) in toluene (30 mL) were added (*S*)-(-)-α,α-diphenyl-2-pyrrolidinemethanol trimethylsilyl ether (1.0 g, 3.0 mmol, 0.2 equiv), 4-methyl-N-(tosyloxy)benzenesulfonamide (6.1 g, 18 mmol, 1.2 equiv) and NaOAc (1.8 g, 22 mmol, 1.5 equiv) at room temperature. The resulting reaction mixture was vigorously stirred at

room temperature for 12 h. After completion of the reaction, the insoluble salts were removed by filtration and the cake was washed with ethyl acetate. After removal of the volatiles the crude product was purified on silica column chromatography (ethyl acetate/hexane = 10%) yielding the aziridine product as light yellow oil (5.1 g, 12 mmol 88%). The enantiomeric excess was determined by HPLC analysis in comparison with racemic material (ODH-column, n-hexane/*i*PrOH = 98/2, 0.5 mL/min, 250 nm); R_T (major enantiomer) = 20.1 min, R_T (minor enantiomer) = 21.6 min.

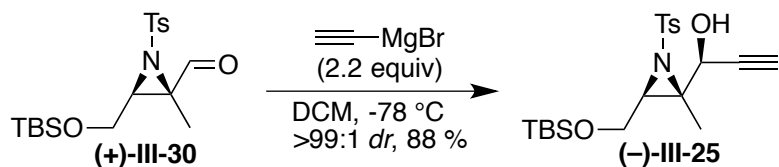
$ee = >98\%$

$[\alpha]_D^{23} = +31.0$ (c 1.0, CHCl_3).

$^1\text{H-NMR}$ (500 MHz, CDCl_3) δ 9.51 (s, 1H), 7.82 (d, $J = 8.4$ Hz, 2H), 7.31 (d, $J = 8.4$ Hz, 2H), 3.73 – 3.63 (m, 3H), 2.43 (s, 3H), 1.40 (s, 3H), 0.82 (s, 9H), -0.02 (s, 3H), -0.04 (s, 3H).

$^{13}\text{C-NMR}$ (125 MHz, CDCl_3) δ 194.50, 144.63, 136.20, 129.69, 127.51, 60.33, 56.80, 50.98, 25.68, 21.64, 18.16, 11.90, -5.51, -5.57.

TOF MS ES^+ ($\text{C}_{18}\text{H}_{30}\text{NO}_4\text{SSi}$): Calc. $[\text{M} + \text{H}]^+$: 384.1665, Found $[\text{M} + \text{H}]^+$: 384.1667.



Synthesis of aziridine alcohol III-25: To aldehyde **III-30** (5.0 g, 13 mmol, $>98\%$ ee) in dry DCM (100 mL), at $-78\text{ }^\circ\text{C}$ under argon was added ethynylmagnesium bromide (0.5 M in THF, 2.1 equiv, 27 mmol, 55 mL) dropwise. The reaction mixture was stirred at this

temperature and the reaction progress was monitored by TLC. After 30 min, TLC showed complete consumption of starting material. The reaction was quenched by addition of sat. ammonium chloride (50 mL) at $-78\text{ }^{\circ}\text{C}$. The reaction mixture was warmed up to room temperature. The organic layer was isolated and the aqueous layer was extracted with DCM (3 x 50 mL). The combined organic extract was washed with brine, dried over sodium sulfate, and concentrated under reduced pressure. The crude product was isolated by column chromatography (silica, ethyl acetate/hexane = 10%). Alcohol **III-25** was isolated as a white crystalline solid (4.7 g, 88 %, 11.5 mmol, *dr* >99:1).

mp = $82\text{--}84^{\circ}$

$[\alpha]_{\text{D}}^{23} = -11.0$ (*c* 1.0, CHCl_3).

$^1\text{H-NMR}$ (500 MHz, CDCl_3) δ 7.81 (d, *J* = 8.4 Hz, 2H), 7.29 (d, *J* = 8.4 Hz, 2H), 4.85 (dd, *J* = 3.6, 2.3 Hz, 1H), 3.67 (dd, *J* = 11.2, 5.3 Hz, 1H), 3.60 – 3.50 (m, 2H), 3.22 (dd, *J* = 6.8, 5.3 Hz, 1H), 2.50 (d, *J* = 2.3 Hz, 1H), 2.41 (s, 3H), 1.52 (s, 3H), 0.81 (s, 9H), -0.04 (s, 3H), -0.06 (s, 3H).

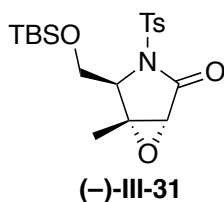
$^{13}\text{C-NMR}$ (125 MHz, CDCl_3) δ 144.28, 137.09, 129.56, 127.26, 80.32, 74.42, 65.25, 60.42, 58.16, 50.88, 25.68, 21.62, 18.11, 12.89, -5.52, -5.60.

TOF MS ES^+ ($\text{C}_{20}\text{H}_{32}\text{NO}_4\text{SSi}$): Calc. $[\text{M} + \text{H}]^+$: 410.1821, Found $[\text{M} + \text{H}]^+$: 410.1819.

2H), 3.39 (d, $J = 0.9$ Hz, 1H), 2.38 (s, 3H), 1.47 (s, 3H), 0.85 (s, 9H), 0.09 (s, 3H), 0.08 (s, 3H).

^{13}C -NMR (125 MHz, CDCl_3) δ 143.88, 142.74, 134.62, 129.22, 127.66, 98.50, 66.86, 63.92, 62.72, 62.35, 25.73, 21.64, 17.97, 14.24, -5.55, -5.68.

TOF MS ES^+ ($\text{C}_{20}\text{H}_{32}\text{NO}_4\text{SSi}$): Calc. $[\text{M} + \text{H}]^+$: 410.1821, Found $[\text{M} + \text{H}]^+$: 410.1837.



Synthesis of pyrrolidinone (-)-III-31: The crude enamide **(+)-III-26** (9.0 g, from the above reaction) was dissolved in anhydrous DCM (250 mL). Ozone gas was bubbled through this solution at -78 °C, until the reaction turn to a persistent dark blue color (approximately 30 min). At this point the, bubbling of ozone was ceased and the excess ozone was removed by bubbling nitrogen through the reaction -78 °C until the blue color disappeared. Dimethyl sulfide (DMS, 7 mL) was added to the mixture and the reaction was allowed to warm up to room temperature. Evaporation of the volatiles gave the crude product **(-)-III-31**, which was used in the next step without purification. An analytical sample of the crude was passed through a plug of silica (ethyl acetate/hexane = 10% to 20%) to afford pure **(-)-III-31** as a white solid.

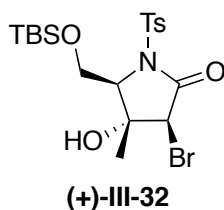
mp = 109 – 111 °

$[\alpha]_{\text{D}}^{23} = -62.0$ (c 1.0, CHCl_3).

$^1\text{H-NMR}$ (500 MHz, CDCl_3) δ 7.83 (d, $J = 8.1$ Hz, 2H), 7.29 (d, $J = 8.0$ Hz, 2H), 4.36 – 4.29 (m, 1H), 4.13 (dd, $J = 11.5, 2.5$ Hz, 1H), 3.88 (dt, $J = 11.5, 1.2$ Hz, 1H), 3.33 (s, 1H), 2.40 (s, 3H), 1.58 (s, 3H), 0.78 (s, 7H), 0.05 (s, 3H), -0.02 (s, 3H).

$^{13}\text{C-NMR}$ (125 MHz, CDCl_3) δ 169.09, 145.13, 135.23, 129.59, 128.05, 64.51, 61.36, 59.38, 57.35, 25.54, 21.67, 17.82, 13.51, -5.77, -5.85.

TOF MS ES^+ ($\text{C}_{19}\text{H}_{30}\text{NO}_5\text{SSi}$): Calc. $[\text{M} + \text{H}]^+$: 412.1614, Found $[\text{M} + \text{H}]^+$: 412.1624.



Synthesis of bromo alcohol (+)-III-32: To the crude epoxide (–)-III-31 from the above reaction (dried under vacuum overnight) under argon was added dry diethyl ether (300 mL) and the reaction flask was placed at 0 °C. Anhydrous MgBr_2 (dried overnight under vacuum, 3.0 equiv, 17 g) was added to the reaction in portions. The reaction was stirred at this temperature for 3 h, after which TLC showed complete consumption of the epoxide (–)-III-31. The reaction was quenched by slow addition of saturated ammonium chloride (100 mL) at 0 °C. The organic layer was separated and the aqueous layer was extracted with ethyl acetate (3 x 100 mL). The combined organic extract was washed with water and brine, then dried over sodium sulfate. Volatiles were evaporated and the crude product was purified with column chromatography (ethyl acetate/hexane = 10% to 20%). Pure product (+)-III-32 was isolated as a white solid (9.0 g, 18 mmol, 86% yield over 3 steps).

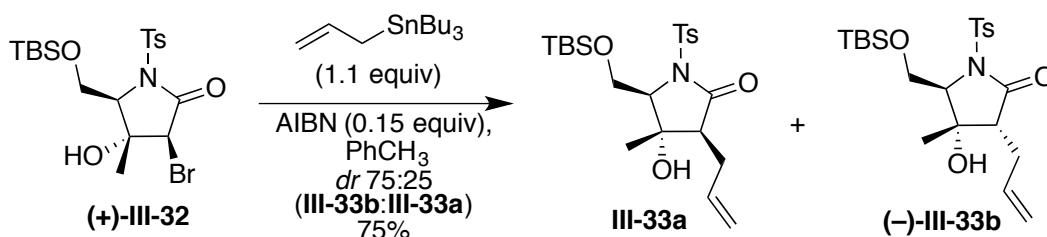
mp = 143–145°

$[\alpha]_{\text{D}}^{23} = +31.0$ (c 1.0, CHCl_3).

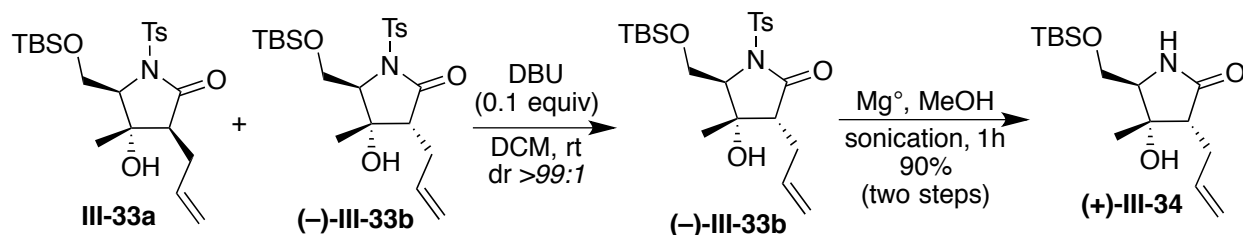
$^1\text{H-NMR}$ (500 MHz, CDCl_3) δ 7.90 (d, $J = 8.3$ Hz, 1H), 7.31 (d, $J = 8.1$ Hz, 1H), 4.20 – 4.11 (m, 1H), 3.96 (s, 0H), 2.41 (s, 1H), 1.61 (s, 1H), 0.90 (s, 3H), 0.13 (s, 1H), 0.10 (s, 1H).

$^{13}\text{C-NMR}$ (125 MHz, CDCl_3) δ 169.09, 145.13, 135.23, 129.59, 128.05, 64.52, 61.36, 59.38, 57.35, 25.54, 21.67, 17.82, 13.51, -5.77, -5.85.

TOF MS ES^+ ($\text{C}_{19}\text{H}_{31}\text{BrNO}_5\text{SSi}$): Calc. $[\text{M} + \text{H}]^+$: 492.0876, Found $[\text{M} + \text{H}]^+$: 492.0872.



Synthesis of III-33: Bromo pyrrolidinone (+)-III-32 (5.5 g, 11 mmol, 1.0 equiv) was dissolved in toluene (100 mL). The solution was degassed for 10 minutes at 100 °C under argon. AIBN (0.15 mmol, 1.65 mmol, 270 mg) was added to this mixture followed by addition of allyltributyl stannane (1.1 equiv, 12 mmol, 4.0 mL). The reaction mixture was heated to reflux for 3 h (TIC confirmed completion of the reaction). The solvent was evaporated (in a well ventilated hood) and the crude was purified via column chromatography (ethyl acetate/hexanes = 10 to 20%) yielding an inseparable mixture of distereomers as a 1:3 ratio of III-33a and III-33b (3.8 g, 8.3 mmol, 75% combined yield).



The distereomeric mixture of **III-33a** and **III-33b** (5.9 g, 13 mmol) was dissolved in dry DCM (150 mL) at room temperature and DBU (0.20 mL, 1.3 mmol, 0.10 equiv) was added. The reaction was stirred at room temperature for 5 h. Solvent was evaporated and the residue was used in the following step without further purification. An analytical sample of the crude was passed through a plug of silica (ethyl acetate/hexane = 20%) to give pure **(-)-III-33b** as a white solid.

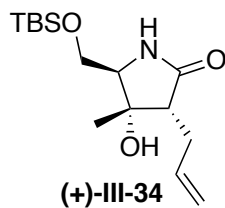
mp = 128–130°

$[\alpha]_{\text{D}}^{23} = -16.0$ (c 1.0, CHCl_3).

$^1\text{H-NMR}$ (500 MHz, CDCl_3) δ 7.93 – 7.88 (m, 2H), 7.28 (d, J = 8.1 Hz, 2H), 5.88 – 5.76 (m, 1H), 5.07 (dp, J = 16.9, 1.5 Hz, 1H), 5.00 (dq, J = 10.1, 1.3 Hz, 1H), 4.10 (ddd, J = 11.7, 2.9, 1.0 Hz, 1H), 4.00 (dd, J = 2.9, 1.5 Hz, 1H), 3.89 (dt, J = 11.7, 1.3 Hz, 1H), 2.84 (ddd, J = 6.8, 5.7, 1.0 Hz, 1H), 2.48 – 2.41 (m, 1H), 2.40 (s, 3H), 2.21 (dtd, J = 15.2, 8.2, 1.2 Hz, 1H), 1.62 (br, 1H), 1.45 (d, J = 1.1 Hz, 3H), 0.79 (d, J = 1.1 Hz, 9H), 0.06 (d, J = 1.0 Hz, 3H), 0.01 (d, J = 1.0 Hz, 3H).

$^{13}\text{C-NMR}$ (125 MHz, CDCl_3) δ 174.02, 144.74, 136.59, 135.89, 129.46, 128.14, 116.65, 77.06, 70.69, 62.11, 52.08, 27.95, 25.67, 22.38, 21.67, 17.94, -5.73, -5.90.

TOF MS ES^+ ($\text{C}_{22}\text{H}_{36}\text{NO}_5\text{SSi}$): Calc. $[\text{M} + \text{H}]^+$: 454.2083, Found $[\text{M} + \text{H}]^+$: 454.2087.



Synthesis of amide (+)-III-34: To the crude lactam **(-)-III-33b** (5.8 g) in methanol (100 mL) was added magnesium powder (5.0 equiv, 65 mmol 1.6 g). The solution was sonicated in an ultra-sonicator bath for 1 h to afford detosylated compound **(+)-III-34** (3.50 g, 11.7 mmol, 90% in two steps) as a white solid.

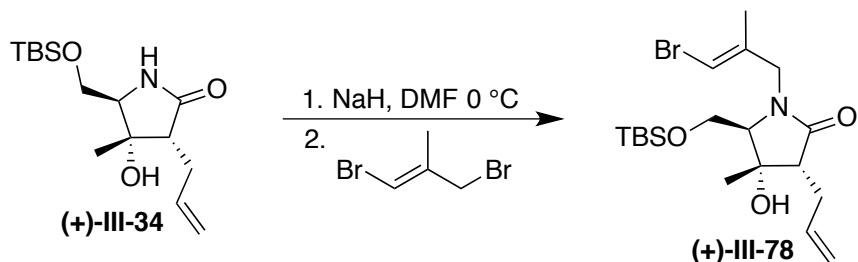
mp = 102–104°

$[\alpha]_D^{23} = +65.0$ (*c* 1.0, CHCl₃).

¹H-NMR (500 MHz, CDCl₃) δ 6.04 – 5.90 (m, 1H), 5.80 (br, 1H), 5.22 – 5.11 (d, *J* = 17.5 Hz, 1H), 5.09 – 5.03 (d, *J* = 11.5 Hz, 1H), 3.63 (dd, *J* = 10.6, 3.8 Hz, 1H), 3.59 (dd, *J* = 10.6, 5.4 Hz, 1H), 3.38 (ddd, *J* = 5.1, 3.8, 1.2 Hz, 1H), 2.57 (dddd, *J* = 11.8, 9.5, 7.9, 4.4 Hz, 1H), 2.47 – 2.35 (m, 2H), 1.37 (s, 3H), 0.86 (s, 10H), 0.03 (s, 3H), 0.03 (s, 3H).

¹³C-NMR (125 MHz, CDCl₃) δ 177.25, 137.34, 116.45, 77.57, 65.03, 62.75, 50.80, 28.80, 25.77, 23.06, 18.08, -5.57, -5.63.

TOF MS ES⁺ (C₁₅H₃₀NO₃Si): Calc. [M + H]⁺: 300.1995, Found [M + H]⁺: 300.1999.



Synthesis of vinyl bromide (+)-III-78: To a solution of amide **(+)-III-34** (2.4 g, 8.0 mmol, 1.0 equiv) in dry DMF (50 mL) at 0 °C was added sodium hydride (0.68 g, 17 mmol, 2.1 equiv). The reaction mixture was stirred at this temperature for 30 min before a solution of ally bromide⁶⁹ (1.79 g, 8.40 mmol, 1.05 equiv) in dry DMF (10 mL) was added dropwise. The reaction was stirred at 0 °C for 2 h, quenched by the addition of saturated NH₄Cl (50 mL) and the aqueous layer was extracted with ethyl acetate (3 x 10 mL). The combined organic extract was washed with brine (50 mL), dried over sodium sulfate and concentrated under reduced pressure. The crude product was purified by column chromatography (ethyl acetate/hexane = 20%), yielding pure product **(+)-III-78** as an off white solid (2.9 g, 85%).

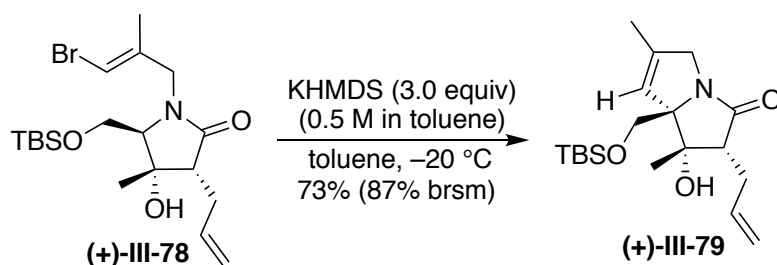
mp = 64–66°

$[\alpha]_D^{23} = +59.0$ (*c* 1.0, CHCl₃).

¹H-NMR (500 MHz, CDCl₃) δ 6.12 (q, *J* = 1.3 Hz, 1H), 5.96 (dddd, *J* = 17.1, 10.0, 8.5, 5.5 Hz, 1H), 5.15 (dq, *J* = 17.1, 1.7 Hz, 1H), 5.04 (dtd, *J* = 10.1, 1.8, 0.8 Hz, 1H), 4.45 – 4.38 (m, 1H), 3.73 – 3.63 (m, 2H), 3.42 (dt, *J* = 15.2, 1.0 Hz, 1H), 3.14 (t, *J* = 2.7 Hz, 1H), 2.63 (dddd, *J* = 14.7, 7.2, 3.6, 1.8 Hz, 1H), 2.59 – 2.54 (m, 1H), 2.41 – 2.31 (m, 1H), 1.76 – 1.73 (m, 3H), 1.62 (br, 1H), 1.43 (s, 3H), 0.84 (s, 9H), 0.02 (s, 3H), 0.01 (s, 3H).

¹³C-NMR (125 MHz, CDCl₃) δ 174.74, 137.73, 137.25, 116.28, 104.67, 76.76, 67.92, 59.10, 50.94, 46.29, 29.01, 25.73, 23.26, 17.96, 17.24, -5.63, -5.75.

TOF MS ES⁺ (C₁₉H₃₅BrNO₃Si): Calc. [M + H]⁺: 432.1570, Found [M + H]⁺: 432.1574.



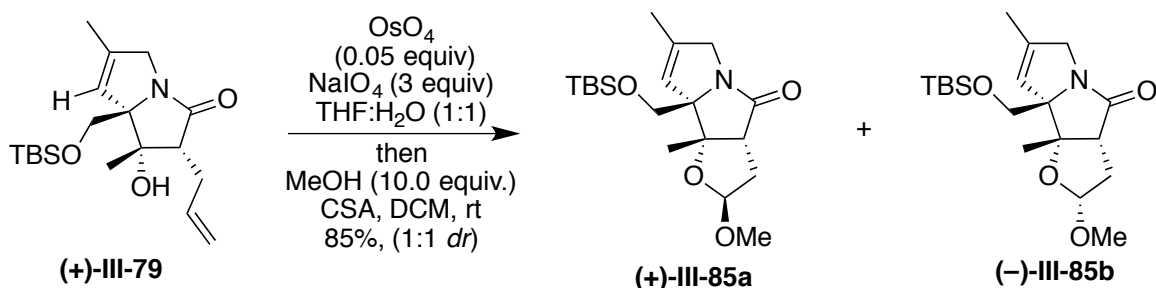
Synthesis of bicyclic (+)-III-79: To a solution of vinyl bromide **(+)-III-78** (0.43 g, 1.0 mmol, 1.0 equiv) in dry toluene (20 mL) at 40 °C was added KHMDS (0.5 M in toluene, 10 mL, 5.0 mmol, 5.0 equiv) dropwise. The reaction mixture was cooled to $-20\text{ }^{\circ}\text{C}$ and was stirred at this temperature for 3.5 h. The reaction was then quenched at this temperature with sat. NH_4Cl (20 mL). Reaction mixture was brought to room temperature and the organic layer was separated. The aqueous layer was extracted with ethyl acetate (3 x 20 mL). The combined organic layers were washed with brine (20 mL), dried over sodium sulfate and concentrated under reduced pressure. The crude product was purified on column chromatography (ethyl acetate/hexane = 20% to 40%). Pure product **(+)-III-79** was isolated as a light yellow oil (257 mg, 0.73 mmol, 73% yield).

$[\alpha]_{\text{D}}^{23} = +76.0$ (c 1.0, CHCl_3).

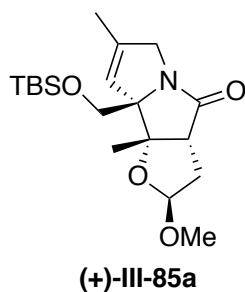
$^1\text{H-NMR}$ (500 MHz, CDCl_3) δ 5.97 (ddd, $J = 24.2, 9.4, 5.6$ Hz, 1H), 5.33 (s, 1H), 5.14 – 5.06 (m, 1H), 4.99 (d, $J = 10.1$ Hz, 1H), 4.27 (d, $J = 15.5$ Hz, 1H), 3.70 (d, $J = 10.7$ Hz, 1H), 3.66 – 3.59 (m, 1H), 3.49 (d, $J = 10.7$ Hz, 1H), 2.94 (t, $J = 6.7$ Hz, 1H), 2.57 – 2.48 (m, 1H), 2.34 – 2.24 (m, 1H), 1.81 (d, $J = 1.6$ Hz, 3H), 1.43 (s, 3H), 1.42 (br, 1H), 0.85 (d, $J = 0.9$ Hz, 9H), 0.01 (s, 3H), 0.00 (s, 3H).

$^{13}\text{C-NMR}$ (125 MHz, CDCl_3) δ 177.71, 142.49, 137.89, 120.33, 115.56, 83.34, 80.79, 65.17, 53.43, 53.29, 27.54, 25.73, 21.39, 18.08, 14.68, -5.59, -5.76.

TOF MS ES⁺ (C₁₉H₃₄NO₃Si): Calc. [M + H]⁺: 352.2308, Found [M + H]⁺: 352.2325.



Synthesis of III-85 a and b: To a solution of (+)-III-79 (3.0 mmol, 1.0 g, 1.0 equiv) in THF:H₂O (1:1, 60 mL) at room temperature was added OsO₄ (0.05 M solution in water, 3.0 mL, 0.15 mmol, 0.05 equiv). To this mixture sodium periodate (1.9 g, 9.0 mmol, 3.0 equiv) was added after 5 min (during which the reaction turns dark). The reaction mixture was stirred at room temperature for 1 h (reaction turns to a milky suspension) during which, TLC indicated complete consumption of starting material. The reaction was quenched by addition of sodium thiosulfate (10 mL, sat. sol.). The reaction mixture was transferred to separatory funnel and extracted with ethyl acetate (4 x 20 mL). The organic layers were combined, washed with brine (20 mL), dried over sodium sulfate and concentrated under reduced pressure. To the resulting diastereomeric hemiacetal mixture in DCM (150 mL) were added methanol (2.0 equiv, 6.0 mmol, 0.25 mL) and CSA (0.15 mmol, 35 mg, 0.05 equiv) at room temperature. The reaction mixture was stirred at this temperature for 12 h after which solvent was evaporated and the crude product was purified via column chromatography (silica, ethyl acetate/hexane = 20% to 40%). Two diastereomers were isolated in a 1:1 ratio with a combined yield of 85%.



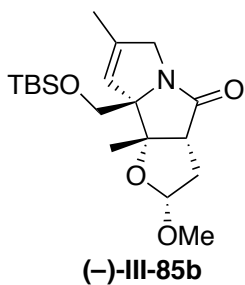
Data for the less polar diastereomer; (+)-III-85a: 450 mg, 1.22 mmol, 41% yield as a clear oil.

$[\alpha]_D^{23} = +48.0$ (c 1.0, CHCl_3).

$^1\text{H-NMR}$ (500 MHz, CDCl_3) δ 5.38 (q, $J = 1.5$ Hz, 1H), 4.90 (dd, $J = 6.3, 3.9$ Hz, 1H), 4.12 (d, $J = 15.3$ Hz, 1H), 3.70 (d, $J = 10.8$ Hz, 1H), 3.56 (ddt, $J = 15.3, 2.5, 1.2$ Hz, 1H), 3.36 (d, $J = 10.8$ Hz, 1H), 3.30 (s, 3H), 3.11 (d, $J = 8.6$ Hz, 1H), 2.71 (ddd, $J = 14.0, 6.2, 1.2$ Hz, 1H), 2.00 (ddd, $J = 14.0, 8.6, 3.9$ Hz, 1H), 1.77 (d, $J = 1.5$ Hz, 3H), 1.51 (s, 3H), 0.85 (s, 9H), 0.01 (s, 3H), -0.00 (s, 3H).

$^{13}\text{C-NMR}$ (125 MHz, CDCl_3) δ 177.68, 138.58, 121.30, 105.15, 89.60, 82.22, 65.32, 55.47, 54.60, 52.79, 34.33, 25.78, 19.59, 18.15, 14.76, -5.51, -5.78.

TOF MS ES^+ ($\text{C}_{19}\text{H}_{34}\text{NO}_4\text{Si}$): Calc. $[\text{M} + \text{H}]^+$: 368.2257, Found $[\text{M} + \text{H}]^+$: 368.2267.

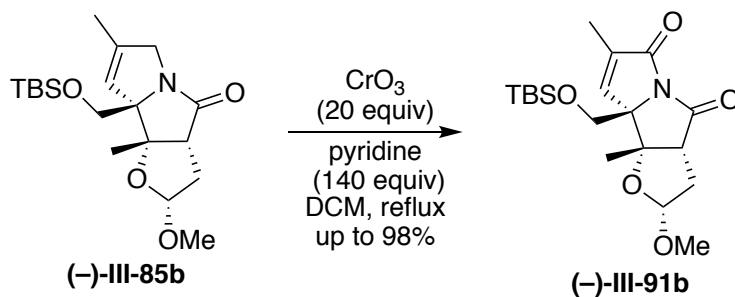


Data for the more polar diastereomer; (-)-III-85b: 480 mg, 1.30 mmol, 44% yield as a clear oil.

$[\alpha]_D^{23} = -77.0$ (c 1.0, CHCl_3).

$^1\text{H-NMR}$ (500 MHz, CDCl_3) δ 5.47 (q, $J = 1.8$ Hz, 1H), 4.88 (d, $J = 5.0$ Hz, 1H), 4.09 – 4.04 (m, 1H), 3.70 (d, $J = 10.7$ Hz, 1H), 3.68 – 3.63 (m, 1H), 3.37 (d, $J = 10.7$ Hz, 1H), 3.10 (s, 3H), 2.92 (d, $J = 8.0$ Hz, 1H), 2.43 (d, $J = 13.2$ Hz, 1H), 2.07 (ddd, $J = 13.2, 8.1, 5.0$ Hz, 1H), 1.77 (d, $J = 1.5$ Hz, 3H), 1.44 (s, 3H), 0.84 (s, 9H), 0.01 (s, 3H), 0.00 (s, 3H).
 $^{13}\text{C-NMR}$ (125 MHz, CDCl_3) δ 177.19, 138.58, 122.36, 104.16, 90.74, 83.16, 65.51, 54.26, 53.77, 53.66, 34.70, 25.76, 20.88, 18.09, 14.48, -5.51, -5.87.

TOF MS ES^+ ($\text{C}_{19}\text{H}_{34}\text{NO}_4\text{Si}$): Calc. $[\text{M} + \text{H}]^+$: 368.2257, Found $[\text{M} + \text{H}]^+$: 368.2267.



Synthesis of enone (-)-III-91b: To CrO_3 (22 mmol, 2.2 g, 20 equiv) in dry DCM (30 mL) at 0 °C was added pyridine (154 mmol, 12.4 mL, 140 equiv) dropwise under argon. The reaction mixture was stirred at this temperature for 10 min followed by stirring at room temperature for 30 min. To this mixture at 0 °C was added **(-)-III-85b** (1.1 mmol, 0.40 g, 1.0 equiv) in DCM (30 mL). the reaction mixture was refluxed for 24 h. After this period of time, the reaction mixture was cooled to room temperature and volatiles were removed under pressure. The residue was re-dissolved in ethyl acetate (100 mL) and the precipitates were removed by filtration through celite. The product was purified via column chromatography (silica, ethyl acetate/hexane = 20%), yielding **(-)-III-91b** as a white solid (305 mg, 0.8 mmol, 73%).

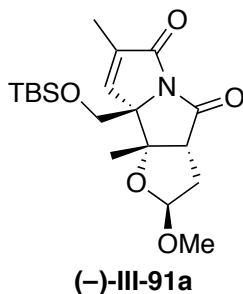
mp = 161–164°

$[\alpha]_D^{25} = -210.0$ (*c* 1.0, CHCl₃).

¹H-NMR (500 MHz, CDCl₃) δ 6.78 (q, *J* = 1.7 Hz, 1H), 4.87 (d, *J* = 4.8 Hz, 1H), 3.92 (d, *J* = 10.5 Hz, 1H), 3.39 (d, *J* = 10.5 Hz, 1H), 3.12 (d, *J* = 8.1 Hz, 1H), 3.05 (s, 2H), 2.46 (d, *J* = 13.2 Hz, 1H), 2.16 (ddd, *J* = 13.2, 8.1, 4.8 Hz, 1H), 1.89 (d, *J* = 1.7 Hz, 4H), 1.47 (s, 3H), 0.85 (s, 7H), 0.03 (s, 3H), 0.03 (s, 3H).

¹³C-NMR (125 MHz, CDCl₃) δ 172.51, 168.68, 141.31, 136.12, 104.01, 88.66, 76.41, 66.80, 56.73, 54.67, 35.61, 25.75, 20.42, 18.13, 11.13, -5.64, -5.92.

TOF MS ES⁺ (C₁₉H₃₂NO₇Si): Calc. [M + H]⁺: 382.2050, Found [M + H]⁺: 382.2060.



(-)-III-91a (282 mg, 0.74 mmol, 74% yield) was synthesized as an off white solid from **(+)-III-85a** (386 mg, 1.0 mmol), according to the procedure described above for the synthesis of **(-)-III-91b**.

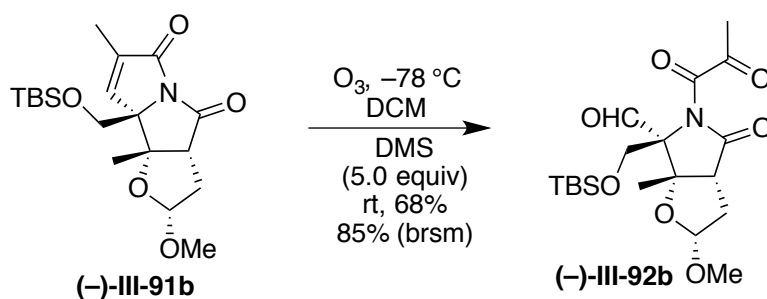
mp = 75–78°

$[\alpha]_D^{23} = -12.0$ (*c* 1.0, CHCl₃).

¹H-NMR (500 MHz, CDCl₃) δ 6.74 (q, *J* = 1.6 Hz, 1H), 4.89 (dd, *J* = 6.3, 4.0 Hz, 1H), 3.92 (d, *J* = 10.7 Hz, 1H), 3.39 (d, *J* = 10.7 Hz, 1H), 3.33 (d, *J* = 9.2 Hz, 1H), 3.29 (s, 3H), 2.71 (ddd, *J* = 14.3, 6.3, 1.1 Hz, 1H), 2.14 (ddd, *J* = 14.2, 9.0, 4.0 Hz, 1H), 1.88 (d, *J* = 1.6 Hz, 3H), 1.53 (s, 3H), 0.85 (s, 9H), 0.03 (s, 3H), 0.02 (s, 3H).

^{13}C -NMR (125 MHz, CDCl_3) δ 173.40, 169.09, 141.66, 136.15, 105.16, 87.18, 75.69, 66.48, 57.90, 55.76, 35.44, 25.72, 19.05, 18.14, 11.23, -5.64, -5.85.

TOF MS ES^+ ($\text{C}_{19}\text{H}_{32}\text{NO}_5\text{Si}$): Calc. $[\text{M} + \text{H}]^+$: 382.2050, Found $[\text{M} + \text{H}]^+$: 382.2051.



Synthesis of dicarbonyl (-)-III-92b: **(-)-III-91b** (0.25 g, 0.65 mmol) was dissolved in DCM (50 mL). To this mixture at $-78\text{ }^\circ\text{C}$ was bubbled ozone for 3 h. The excess ozone was removed via bubbling nitrogen at this temperature. To the reaction mixture was added dimethyl sulfide (0.25 mL, 3.3 mmol, 5.0 equiv) at $-78\text{ }^\circ\text{C}$. The reaction mixture was warmed up to room temperature and stirred for 3 h. Saturated aqueous ammonium chloride (20 mL) was added to the reaction mixture and the organic layer was separated. The aqueous layer was extracted with DCM (3 x 20 mL). Organic layers were combined, washed with brine (20 mL), dried over sodium sulfate and concentrated under reduced pressure. The crude product was purified via column chromatography (ethyl acetate/hexane = 10% to 20%) to give the pure product **(-)-III-92b** as an off white solid (180 mg, 0.44 mmol, 68% yield). Starting material **(-)-III-91b** (64 mg, 17%) was recovered.

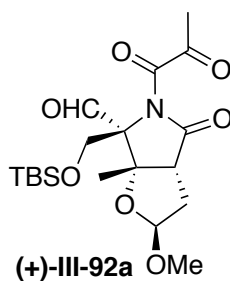
mp = $79\text{--}81^\circ$

$[\alpha]_{\text{D}}^{23} = -96.0$ (c 1.0, CHCl_3).

$^1\text{H-NMR}$ (500 MHz, CDCl_3) δ 9.50 (s, 1H), 4.99 (d, J = 4.7 Hz, 1H), 4.18 (d, J = 11.3 Hz, 1H), 4.11 (d, J = 11.4 Hz, 1H), 3.31 (s, 3H), 2.93 (dd, J = 8.2, 0.7 Hz, 1H), 2.45 (dd, J = 13.4, 0.7 Hz, 1H), 2.39 (s, 3H), 2.21 (ddd, J = 13.2, 8.2, 4.8 Hz, 1H), 1.42 (s, 3H), 0.83 (s, 9H), 0.04 (s, 3H), 0.02 (s, 3H).

$^{13}\text{C-NMR}$ (125 MHz, CDCl_3) δ 196.3, 193.8, 176.4, 168.2, 104.0, 89.8, 75.1, 60.1, 55.0, 51.3, 35.1, 26.2, 25.7, 25.6, 20.0, 17.9, -5.8, -5.9.

TOF MS ES^+ ($\text{C}_{19}\text{H}_{32}\text{NO}_7\text{Si}$): Calc. $[\text{M} + \text{H}]^+$: 414.1948, Found $[\text{M} + \text{H}]^+$: 414.1950.



(+)-III-92a (170 mg, 0.40 mmol, 82%) was synthesized from **(-)-III-91a** (191 mg, 0.50 mmol), as a white solid according to the procedure described above for the synthesis of **(+)-III-92b**.

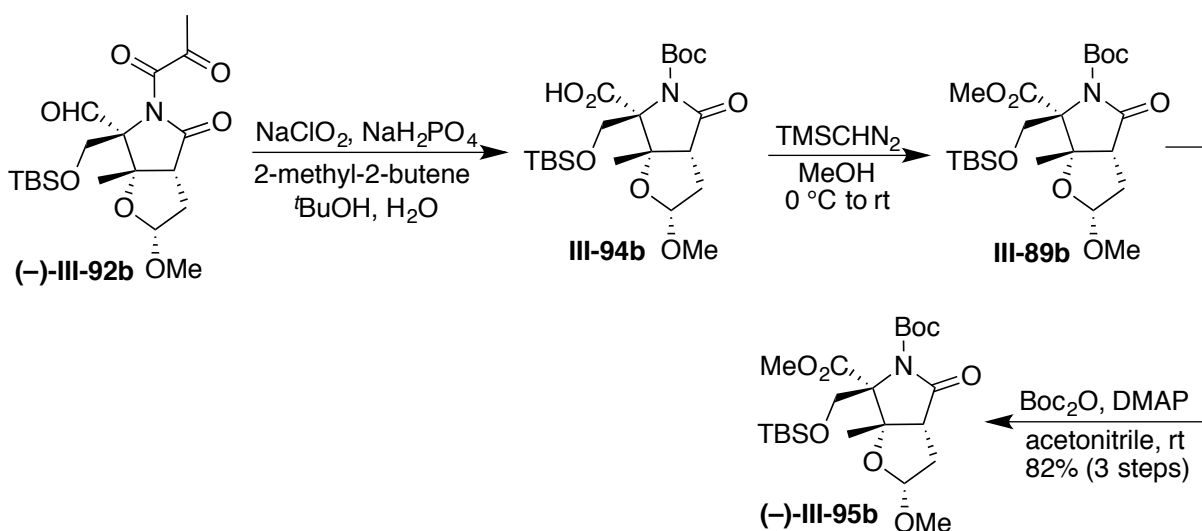
mp = 71–74°

$[\alpha]_{\text{D}}^{23} = +80.0$ (c 1.0, CHCl_3).

$^1\text{H-NMR}$ (500 MHz, CDCl_3) δ 9.47 (s, 1H), 5.10 – 5.03 (m, 2H), 4.18 (d, J = 11.4 Hz, 1H), 4.06 (d, J = 11.4 Hz, 1H), 3.30 (s, 3H), 3.09 (ddd, J = 9.5, 1.5, 0.8 Hz, 1H), 2.64 (ddd, J = 14.4, 6.2, 1.6 Hz, 1H), 2.40 (s, 3H), 2.25 (ddd, J = 14.4, 9.4, 3.8 Hz, 1H), 1.53 (s, 3H), 0.84 (s, 9H), 0.05 (s, 3H), 0.02 (s, 3H).

^{13}C -NMR (125 MHz, CDCl_3) δ 196.8, 193.9, 177.5, 168.4, 105.2, 89.8, 75.0, 59.4, 55.8, 52.7, 35.4, 26.3, 25.6, 19.0, 17.9, -5.8.

TOF MS ES^+ ($\text{C}_{19}\text{H}_{32}\text{NO}_7\text{Si}$): Calc. $[\text{M} + \text{H}]^+$: 414.1948, Found $[\text{M} + \text{H}]^+$: 414.1936.



Synthesis of (-)-III-95b: Dicarbonyl **(-)-III-92b** (0.17 g, 0.41 mmol, 1.0 equiv) was dissolved in *tert*-butyl alcohol (7 mL). To this solution at room temperature was added 2-methyl 2-butene (0.1 mL, 1.0 mmol) followed by addition of sodium chlorite (1.7 mmol, 3.5 mL of 0.5 M aqueous solution) and sodium phosphate mono basic (3.5 mmol, 3.5 mL of 1.0 M aqueous solution). The reaction was stirred at room temperature for 24 h. aqueous saturated NH_4Cl (10 mL) was added to the reaction mixture and the solution was transferred to a separatory funnel. The aqueous layer was extracted with ethyl acetate (5 x 20 mL). The combined organic extracts were dried over sodium sulfate, filtered and concentrated under reduced pressure. Crude acid **(-)-III-94b** was used in the following step without further purification.

The crude carboxylic acid **(-)-III-94b** was dissolved in methanol (10 mL). To this solution at 0 °C trimethylsilyl diazomethane (2.0 M in diethyl ether, 10 equiv, 4.0 mmol, 2.0 mL) was added dropwise under nitrogen. The reaction mixture was stirred for 12 h, during which the reaction mixture was allowed to warm up to room temperature. Aqueous NaHCO₃ (sat., 20 mL) was added to the reaction mixture and the aqueous layer was extracted with ethyl acetate (4 x 10 mL). The combined organic extracts were washed with brine (20 mL), dried over sodium sulfate and concentrated under reduced pressure. The resulting methyl ester **(-)-III-89b** was used in the next step without further purification.

The crude methyl ester **(-)-III-89b** was dissolved in dried acetonitrile (10 mL). To this mixture under nitrogen at 0 °C were added Boc-anhydride (0.72 g, 3.2 mmol, 8.0 equiv) and DMAP (49 mg, 0.4 mmol, 1.0 equiv). The reaction was stirred at 0 °C for another 5 h upon which, ¹H-NMR confirmed complete consumption of the starting material. Volatiles were removed under pressure and the residue was directly loaded on to a column (basified silica with Et₃N, ethyl acetate/hexane = 10% to 20% as eluent) to yield the Boc protected product **(-)-III-95b** as a light yellow oil (160 mg, 0.34 mmol, 82% yield from **(-)-III-92b**).

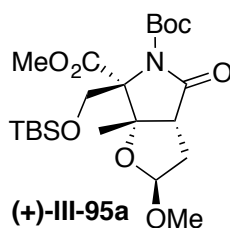
Data for **(-)-III-95b:**

$[\alpha]_D^{23} = -95.0$ (*c* 0.5, CHCl₃).

¹H-NMR (500 MHz, CDCl₃) δ 4.89 (d, *J* = 5.0, 1H), 4.37 (d, *J* = 10.8 Hz, 1H), 4.12 (d, *J* = 10.8 Hz, 1H), 3.74 (s, 3H), 3.21 (s, 3H), 2.76 (d, *J* = 8.1 Hz, 1H), 2.43 (d, *J* = 13.3 Hz, 1H), 2.16 (ddd, *J* = 13.3, 8.1, 5.0 Hz, 1H), 1.48 (s, 9H), 1.44 (s, 3H), 0.82 (s, 9H), 0.02 (s, 3H), -0.01 (s, 3H).

^{13}C -NMR (125 MHz, CDCl_3) δ 173.6, 167.6, 150.0, 103.9, 86.9, 82.9, 62.2, 55.0, 52.1, 51.6, 35.5, 28.2, 28.0, 25.7, 20.5, 18.0, -5.6, -5.8.

TOF MS ES^+ ($\text{C}_{22}\text{H}_{40}\text{NO}_8\text{Si}$): Calc. $[\text{M} + \text{H}]^+$: 474.2523, Found $[\text{M} + \text{H}]^+$: 474.2519.



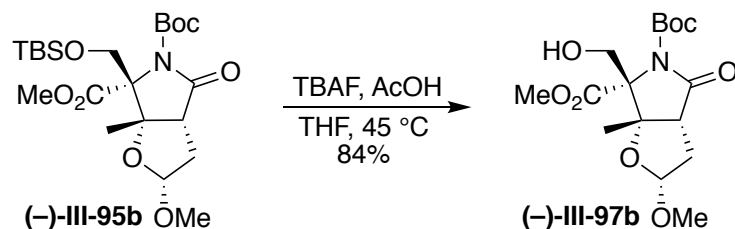
(+)-III-95a (120 mg, 0.25 mmol, 77%) was synthesized from the corresponding dicarbonyl **(+)-III-92a** (140 mg, 0.33 mmol) according to the procedure described above for the synthesis of **(-)-III-95b** as a light red colored oil.

$[\alpha]_{\text{D}}^{23} = +28.0$ (c 0.5, CHCl_3).

^1H -NMR (500 MHz, CDCl_3) δ 4.97 (dd, $J = 6.0, 4.3$ Hz, 1H), 4.30 (d, $J = 10.8$ Hz, 1H), 4.14 (d, $J = 10.8$ Hz, 1H), 3.71 (s, 3H), 3.26 (s, 3H), 2.90 (dd, $J = 9.3, 1.5$ Hz, 1H), 2.65 (ddd, $J = 14.0, 6.0, 1.5$ Hz, 1H), 2.15 (ddd, $J = 14.0, 9.3, 4.3$ Hz, 1H), 1.55 (s, 3H), 1.47 (s, 9H), 0.82 (s, 9H), 0.02 (s, 3H), 0.01 (s, 3H).

^{13}C -NMR (125 MHz, CDCl_3) δ 174.75, 167.76, 149.65, 105.10, 85.89, 83.45, 61.57, 55.61, 52.66, 52.01, 35.91, 27.99, 27.87, 25.65, 19.85, 17.94, -5.65, -5.71.

TOF MS ES^+ ($\text{C}_{22}\text{H}_{40}\text{NO}_8\text{Si}$): Calc. $[\text{M} + \text{H}]^+$: 474.2523, Found $[\text{M} + \text{H}]^+$: 474.2522.



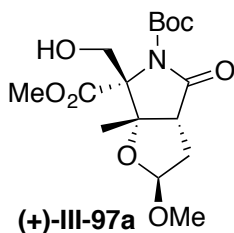
Synthesis of (-)-III-97b: To silyl protected alcohol **(-)-III-95b** (1.0 equiv, 0.30 mmol, 0.14 g) in dry THF (10 mL) under argon at 0 °C were added acetic acid (20.0 equiv, 6.00 mmol, 0.33 mL) and TBAF (1.0 M in THF, 10 equiv, 3.0 mmol, 3.0 mL) dropwise. The reaction mixture was placed in a pre-heated oil bath at 45 °C. The mixture was stirred at this temperature for 48 h, upon which TLC showed completion of reaction. The reaction mixture was cooled to room temperature and was quenched by the addition of sat. NaHCO₃ (10 mL). The aqueous layer was extracted with ethyl acetate (4 x 10 mL). The combined organic extract was washed with brine (10 mL), dried over sodium sulfate and concentrated under reduced pressure. The resulting crude product was purified on column chromatography (ethyl acetate/hexane = 50%) to yield the pure alcohol **(-)-III-97b** as a white sticky solid (90 mg, 0.25 mmol, 84%).

$[\alpha]_{\text{D}}^{23} = -115.0$ (*c* 1.0, CHCl₃).

¹H-NMR (500 MHz, CDCl₃) δ 4.89 (d, *J* = 4.9 Hz, 1H), 4.41 (d, *J* = 12.2 Hz, 1H), 4.11 (d, *J* = 12.2 Hz, 1H), 3.75 (s, 3H), 3.20 (s, 3H), 2.96 (d, *J* = 8.0 Hz, 1H), 2.40 (d, *J* = 13.2 Hz, 1H), 2.13 (ddd, *J* = 13.2, 8.0, 4.9 Hz, 1H), 1.98 (br, 1H), 1.48 (s, 12H).

¹³C-NMR (125 MHz, CDCl₃) δ 173.94, 167.42, 150.58, 103.89, 86.93, 83.62, 62.33, 55.00, 52.28, 51.21, 35.45, 27.98, 22.65, 20.73.

TOF MS ES⁺ (C₁₆H₂₆NO₈): Calc. $[M + H]^+$: 360.1658, Found $[M + H]^+$: 360.1671.



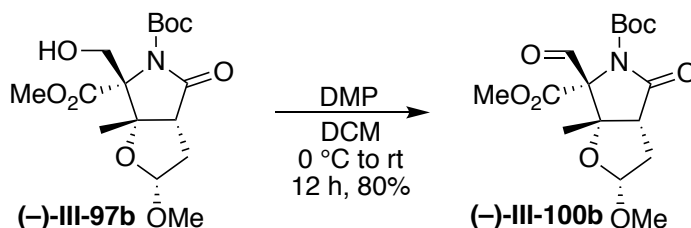
(+)-III-97a (61 mg, 0.17 mmol, 81%) was synthesized according to the procedure described above for the synthesis of **(-)-III-97b** as a white sticky solid.

$[\alpha]_D^{23} = +65.0$ (c 1.0, CHCl_3).

$^1\text{H-NMR}$ (500 MHz, CDCl_3) δ 5.03 – 4.96 (m, 1H), 4.38 (dd, $J = 11.9, 5.3$ Hz, 1H), 4.18 (dd, $J = 11.9, 6.3$ Hz, 1H), 3.74 (s, 3H), 3.28 (s, 3H), 3.01 (ddd, $J = 9.3, 1.6, 0.7$ Hz, 1H), 2.68 (ddd, $J = 14.1, 6.0, 1.6$ Hz, 1H), 2.18 (ddd, $J = 14.1, 9.3, 4.1$ Hz, 1H), 1.89 (br, 1H), 1.61 (s, 3H), 1.50 (s, 9H).

$^{13}\text{C-NMR}$ (125 MHz, CDCl_3) δ 174.86, 167.54, 150.03, 105.10, 86.00, 84.01, 61.48, 55.61, 52.46, 52.19, 35.79, 27.91, 27.63, 20.14.

TOF MS ES^+ ($\text{C}_{16}\text{H}_{26}\text{NO}_8$): Calc. $[\text{M} + \text{H}]^+$: 360.1658, Found $[\text{M} + \text{H}]^+$: 360.1671.



Synthesis of aldehyde (-)-III-100b: Alcohol **(-)-III-95b** (1.0 equiv, 0.24 mmol, 85 mg) was dissolved in dry DCM (5 mL). To this solution at 0 °C were added Dess-Martin periodinane (5.0 equiv, 1.1 mmol, 400 mg) and sodium bicarbonate (5.0 equiv, 1.1 mmol, 85 mg). The reaction mixture was allowed to warm up to room temperature and stirred

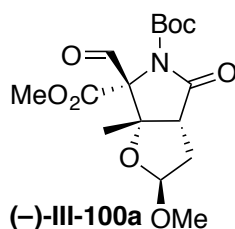
for 12 h. The reaction was quenched by addition of sodium thiosulfate (5 mL, sat.), sodium bicarbonate (5 mL, sat.) and water (5 mL). The mixture was extracted with DCM (4 x 10 mL). The combined organic extract was washed with brine, dried over sodium sulfate and concentrated under reduced pressure. The crude aldehyde was purified by column chromatography (silica, ethyl acetate/hexane = 20% to 50%) to yield pure aldehyde **(-)-III-100b** (68 mg, 0.19 mmol, 80%) as a white sticky gel.

$[\alpha]_D^{23} = -122.0$ (*c* 1.0, CHCl₃).

¹H-NMR (500 MHz, CDCl₃) δ 10.08 (s, 1H), 4.96 (d, *J* = 5.0 Hz, 1H), 3.89 (s, 3H), 3.23 (s, 3H), 2.82 (dd, *J* = 8.2, 0.7 Hz, 1H), 2.49 (dd, *J* = 13.4, 0.7 Hz, 1H), 2.16 (ddd, *J* = 13.4, 8.2, 5.0 Hz, 1H), 1.43 (s, 9H), 1.37 (s, 3H).

¹³C-NMR (125 MHz, CDCl₃) δ 196.8, 172.1, 166.7, 105.0, 84.4, 55.5, 52.8, 50.7, 34.8, 27.8, 21.5.

TOF MS ES⁺ (C₁₆H₂₄NO₈): Calc. [M + H]⁺: 358.1502, Found [M + H]⁺: 358.1504.



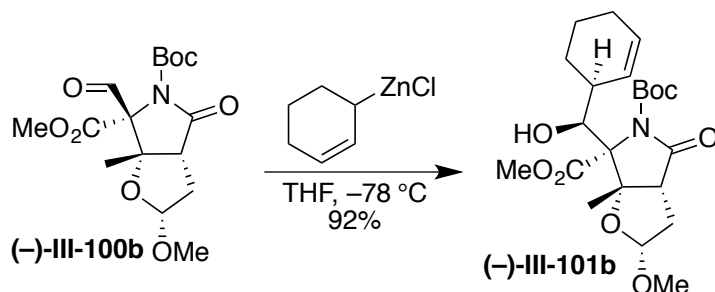
(-)-III-100a was synthesis according to the procedure described above for the synthesis of **(-)-III-100b**. 50 mg pure aldehyde was isolated (0.14 mmol, 85%) as a white gluey solid.

$[\alpha]_D^{23} = +48.0$ (*c* 1.0, CHCl₃).

$^1\text{H-NMR}$ (500 MHz, CDCl_3) δ 10.11 (s, 1H), 5.03 (dd, $J = 5.8, 3.9$ Hz, 1H), 3.87 (s, 3H), 3.32 (s, 3H), 2.99 (dd, $J = 9.5, 2.6$ Hz, 1H), 2.66 (ddd, $J = 14.0, 5.8, 2.6$ Hz, 1H), 2.20 (ddd, $J = 14.0, 9.5, 3.9$ Hz, 1H), 1.51 (s, 3H), 1.43 (s, 9H).

$^{13}\text{C-NMR}$ (125 MHz, CDCl_3) δ 196.3, 172.8, 166.4, 166.2, 106.1, 85.4, 84.7, 55.8, 52.7, 51.9, 35.4, 27.7, 21.6.

TOF MS ES^+ ($\text{C}_{16}\text{H}_{23}\text{NO}_8$): Calc. $[\text{M} + \text{H}]^+$: 358.1502, Found $[\text{M} + \text{H}]^+$: 358.1502.



Synthesis of (-)-III-101b: Following reported procedures.¹³ tributyl(2-cyclohexenyl)stannane (10 equiv, 1.8 mmol, 0.72 g) was dissolved in dry THF (2 mL). To this mixture at $-78\text{ }^\circ\text{C}$ under argon was added *n*-butyllithium (10 equiv, 1.8 mmol, 1.0 mL of 1.8 M sol. in hexane) dropwise. After stirring for 1 h at this temperature, to this mixture was added ZnCl_2 (10 equiv, 1.8 mmol, 1.8 mL of 1.0 M sol. in diethyl ether). The reaction mixture was stirred at $-78\text{ }^\circ\text{C}$ for another 30 min, after which aldehyde **(-)-III-100b** (1.0 equiv, 0.18 mmol, 65 mg) in dry THF (2 mL) was added dropwise. The reaction mixture was further stirred at this temperature for 5 h. Aqueous NH_4Cl (10 mL, sat.) was added at $-78\text{ }^\circ\text{C}$, the reaction mixture was warmed to room temperature and the organic layer was separated. The aqueous layer was extracted with ethyl acetate (3 x 10 mL). The combined organic extracts were washed with brine (10 mL), dried over sodium sulfate and concentrated

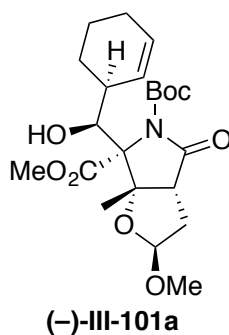
under reduced pressure. The crude product was purified by column chromatography (silica, ethyl acetate/hexane = 50%) yielding the pure product **(-)-III-101b** as a white foam (72 mg, 0.16 mmol, 92% yield).

$[\alpha]_D^{25} = -149.0$ (*c* 1.0, CHCl₃).

¹H-NMR (500 MHz, CDCl₃). δ 5.98 (dq, *J* = 10.7, 3.3, 2.6 Hz, 1H), 5.49 (dd, *J* = 10.7, 2.9 Hz, 1H), 4.90 (d, *J* = 4.8 Hz, 1H), 4.25 – 4.17 (m, 1H), 3.78 (s, 3H), 3.25 (s, 2H), 2.99 (d, *J* = 7.9 Hz, 1H), 2.93 (s, 1H), 2.44 (d, *J* = 13.1 Hz, 1H), 2.16 (ddd, *J* = 13.1, 7.9, 4.9 Hz, 1H), 1.98 (m, 2H), 1.84 (d, *J* = 6.9 Hz, 1H), 1.79 (td, *J* = 10.1, 9.5, 6.0 Hz, 1H), 1.75 – 1.67 (m, 1H), 1.56 (d, *J* = 8.8 Hz, 3H), 1.51 (s, 9H), 1.47 (s, 3H).

¹³C-NMR (125 MHz, CDCl₃) 175.47, 167.08, 150.43, 134.84, 125.17, 103.63, 89.17, 83.11, 76.02, 54.88, 51.94, 51.03, 37.84, 35.81, 30.23, 27.84, 25.07, 20.75, 20.66.

TOF MS ES⁺ (C₂₂H₃₄NO₈): Calc. $[M + H]^+$: 440.2284, Found $[M + H]^+$: 440.2286.



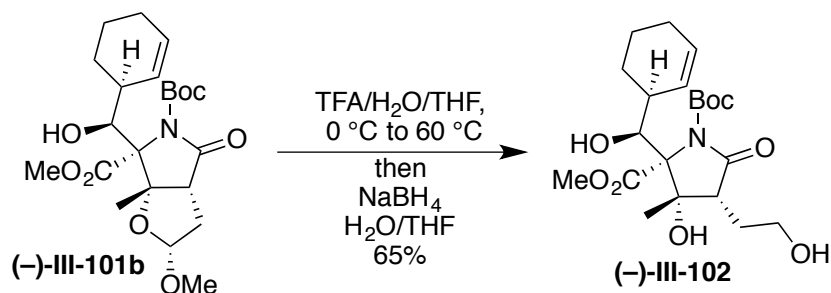
Synthesis of (-)-III-101a: **(-)-III-101a** was synthesized according to the procedure described above for the synthesis of **(-)-III-101b**. **(-)-III-101a** (51 mg, 0.12 mmol, 92% yield) was isolated as a white foam.

$[\alpha]_D^{23} = -10.0$ (*c* 1.0, CHCl₃).

$^1\text{H-NMR}$ (500 MHz, CDCl_3) δ 5.98 (ddt, $J = 10.0, 3.9, 1.9$ Hz, 1H), 5.44 (dd, $J = 10.0, 2.9$ Hz, 1H), 4.99 (dd, $J = 6.0, 4.5$ Hz, 1H), 4.25 (d, $J = 6.4$ Hz, 1H), 3.75 (s, 3H), 3.28 (s, 3H), 3.12 (d, $J = 9.1$ Hz, 1H), 2.90 (br, 1H), 2.65 (ddd, $J = 14.0, 6.0, 1.4$ Hz, 1H), 2.16 (ddd, $J = 14.0, 9.1, 4.5$ Hz, 1H), 1.98 (m, 2H), 1.88 – 1.68 (m, 4H), 1.60 (s, 3H), 1.57 – 1.53 (m, 2H), 1.49 (s, 9H).

$^{13}\text{C-NMR}$ (125 MHz, CDCl_3) δ 176.29, 167.18, 150.16, 134.62, 125.33, 104.88, 88.02, 83.85, 75.34, 55.60, 52.29, 51.88, 37.75, 36.05, 30.26, 27.77, 25.05, 20.82, 20.16.

TOF MS ES^+ ($\text{C}_{22}\text{H}_{34}\text{NO}_8$): Calc. $[\text{M} + \text{H}]^+$: 440.2284, Found $[\text{M} + \text{H}]^+$: 440.2282.



Synthesis of diol (–)-III-102: Following the reported procedures,¹³ to a solution of (–)-III-101b (1.0 equiv, 0.13 mmol, 60 mg) in distilled THF (0.5 mL) at 0 °C was added a mixture of trifluoroacetic acid and water (1:1, v:v, 2 mL) dropwise. The reaction flask was placed in a preheated oil bath at 60 °C and stirring was continued at this temperature for 2 h. To the mixture at 0 °C was added ice (1.0 g) and toluene (3 mL), and the volatiles were removed under vacuum at room temperature. During the concentration period, toluene was added to the mixture to keep the concentration of TFA low. The resulting residue was dissolved in distilled THF (1 mL) and water (1 mL). To this mixture at 0 °C was added sodium borohydride (25 mg, 0.65 mmol, 5.0 equiv) and the mixture was stirred

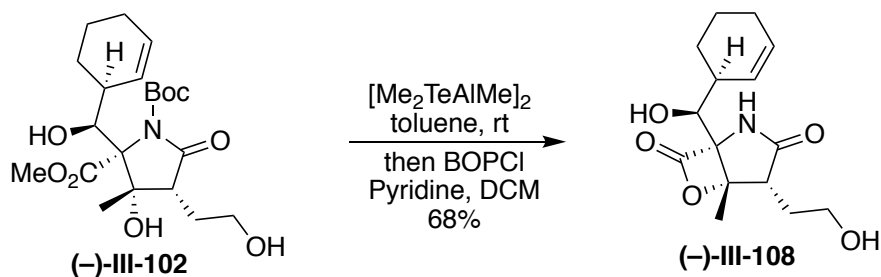
for 1 h. The reaction was quenched with saturated solution of ammonium chloride (5 mL) and the mixture was extracted with ethyl acetate (5 x 10 mL). The combined organic extracts were washed with brine, dried over sodium sulfate and concentrated under reduced pressure to give the crude product as a white solid. The crude product was purified on silica column chromatography (silica, ethyl acetate/hexane = 20% then methanol/ethyl acetate = 5%) to give **(-)-III-102** as a pure white solid (28 mg, 0.08 mmol, 65%).

$[\alpha]_D^{23} = -55.0$ (c 1.0, CHCl_3)

$^1\text{H-NMR}$ (500 MHz, CDCl_3). δ 8.37 (brs, 1H), 6.00 (m, 1H), 5.72 (m, 1H), 5.30 (brs, 1H), 4.10 – 4.03 (m, 1H), 3.80 (s, 3H), 3.78 – 3.72 (m, 2H), 3.70 – 3.65 (m, 1H), 2.83 (dd, $J = 9.8, 3.3$ Hz, 1H), 2.78 – 2.68 (m, 1H), 2.17 (d, $J = 7.2$ Hz, 1H), 1.97 (m, 3H), 1.90 (m, 2H), 1.60 – 1.70 (m, 2H), 1.52 (s, 3H).

$^{13}\text{C-NMR}$ (125 MHz, CDCl_3) δ 180.4, 172.5, 133.8, 124.1, 81.8, 79.4, 75.3, 61.9, 52.8, 51.2, 38.8, 28.0, 26.1, 24.8, 20.7, 19.6.

TOF MS ES^+ ($\text{C}_{16}\text{H}_{26}\text{NO}_6$): Calc. $[\text{M} + \text{H}]^+$: 328.1760, Found $[\text{M} + \text{H}]^+$: 328.1760.



Synthesis of β -lactone **(-)-III-108:** To a suspension of tellurium (0.72 g, 5.60 mmol) in toluene (2.5 mL) was added Me_3Al (2.0 M in toluene, 2.5 mL, 5.0 mmol). The mixture

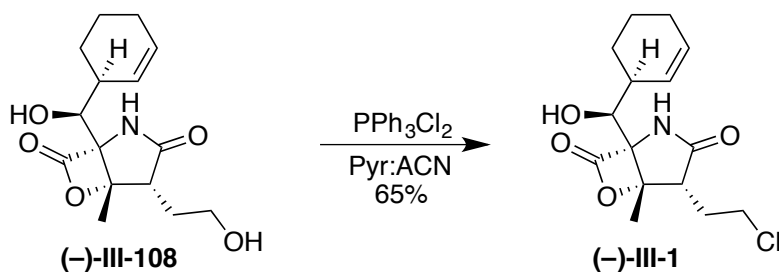
was refluxed for 6 h and cooled to room temperature. The resulting $[\text{Me}_2\text{AlTeMe}]_2$ (ca 0.8 M in toluene, 2.0 mL, 8.0 mmol, 10 equiv) was added to **(-)-III-102** (25.0 mg, 0.08 mmol). After stirring at room temperature for 12 h, the reaction mixture was diluted with ethyl acetate (5 mL). HCl (1.0 M, 3 mL) was added slowly to the mixture at 0 °C. The reaction mixture was further stirred at room temperature for 2 h. The acidified aqueous layer (pH = 1) was extracted with ethyl acetate/ethanol (20:1 v:v, 20 ml). The combined organic extracts were dried over sodium sulfate and concentrated under reduced pressure to yield the crude carboxylic acid as an off white solid, which was used in the following step without purification. To a solution of the carboxylic acid (20 mg) in dichloromethane (2 mL) were added pyridine (0.3 mL) and BOPCl (100 mg, 0.25 mmol), and the mixture was stirred at room temperature for 3.5 h. The reaction mixture was diluted with ethyl acetate (5 mL) and saturated NH_4Cl (5 mL). The organic layer was separated and the aqueous layer was extracted with ethyl acetate (4 x 5 mL). The combined organic extracts were washed with brine (5 mL), dried over sodium sulfate and concentrated under reduced pressure. The crude product was purified by column chromatography (silica, ethyl acetate/hexane = 20% to 50%) to give the β -lactone **(-)-III-108** (12.0 mg, 0.04 mmol, 68%) as a colorless solid:

$$[\alpha]_{\text{D}}^{23} = -72.0 \text{ (} c \text{ 0.5, MeOH)}$$

$^1\text{H-NMR}$ (500 MHz, pyridine- d_5) δ 10.60 (s, 1H), 6.46 (d, J = 10.3 Hz, 1H), 5.91 (ddd, J = 10.3, 4.9, 2.5 Hz, 1H), 5.08 (br, 2H), 4.30 (m, 2H), 4.20 (dt, J = 8.8, 6.4 Hz, 1H), 3.41 (t, J = 7.0 Hz, 1H), 2.90 (m, 1H), 2.56 (dq, J = 13.4, 7.0 Hz, 1H), 2.34 (dq, J = 13.3, 6.4 Hz, 3H), 2.19 (s, 3H), 1.99 – 1.90 (m, 2H), 1.74 (m, 2H), 1.40 (m, 1H).

^{13}C -NMR (125 MHz, pyridine- d_5) δ 178.66, 170.31, 129.40, 129.20, 87.49, 80.60, 71.48, 60.24, 46.76, 39.77, 29.62, 26.90, 25.78, 22.18, 20.76.

TOF MS ES⁺ ($\text{C}_{15}\text{H}_{22}\text{NO}_5$): Calc. $[\text{M} + \text{H}]^+$: 296.1498, Found $[\text{M} + \text{H}]^+$: 296.1497.



Synthesis of (–)-Salinosporamide A (–)-III-1: β -lactone (–)-III-108 (8.0 mg, 0.03 mmol) was dissolved in acetonitrile (0.5 mL) and anhydrous pyridine (0.5 mL) at room temperature under argon. To this solution was added Ph_3PCl_2 (5.00 equiv, 0.16 mmol, 55.0 mg), and stirring was continued for 3.5 h. The reaction was quenched by addition of water (5 mL) followed by addition of ethyl acetate (5 mL). The aqueous layer was extracted with ethyl acetate (4 x 5 mL), combined extracts were washed with brine (5 mL), dried over sodium sulfate and concentrated under reduced pressure. The crude product was purified by column chromatography (silica, ethyl acetate = 20% to 40%) to yield (–)-Salinosporamide A as a white solid (6.0 mg, 0.02 mmol, 64%).

$[\alpha]_{\text{D}}^{23} = -69.0$ (c 0.4, MeOH)

^1H -NMR (500 MHz, pyridine- d_5) δ 10.67 (s, 1H), 6.45 (d, $J = 10.3$ Hz, 1H), 5.91 (d, $J = 10.3$ Hz, 1H), 5.02 (br, 1H), 4.28 (t, $J = 9.1$ Hz, 1H), 4.21 – 4.11 (m, 1H), 4.05 (m, 1H), 3.21 (t, $J = 7.2$ Hz, 1H), 2.94 – 2.82 (m, 1H), 2.56 – 2.47 (m, 1H), 2.41 – 2.30 (m, 2H),

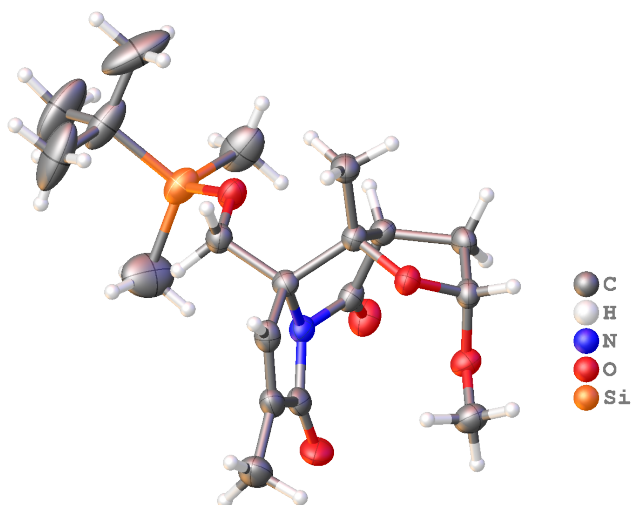
2.10 (d, $J = 2.3$ Hz, 3H), 1.99 – 1.90 (m, 2H), 1.72 (t, $J = 11.0$ Hz, 2H), 1.42 – 1.36 (m, 1H).

^{13}C -NMR (125 MHz, pyridine- d_5) δ 177.34, 169.84, 129.48, 129.09, 86.72, 80.76, 71.39, 46.57, 43.70, 39.73, 29.42, 26.87, 25.77, 22.14, 20.41.

TOF MS ES⁺ ($\text{C}_{15}\text{H}_{21}\text{ClNO}_4$): Calc. $[\text{M} + \text{H}]^+$: 314.1159, Found $[\text{M} + \text{H}]^+$: 314.1165.

III-7-3 Crystal data

III-7-3-1 Crystal data for III-91b (BB817C)



Experimental. Single colorless plate-shaped crystals of **III-91b (BB817C)** were used as received. A suitable crystal ($0.38 \times 0.15 \times 0.06$) mm³ was selected and mounted on a nylon loop with paratone oil on a Bruker APEX-II CCD diffractometer. The crystal was kept at $T = 173(2)$ K during data collection. Using **Olex2**,⁷⁰ the structure was solved with the **ShelXT**⁷¹ structure solution program, using the Intrinsic Phasing solution method. The model

Compound	BB817C
Formula	C ₁₉ H ₃₁ NO ₅ Si
$D_{calc.}/\text{g cm}^{-3}$	1.215
μ/mm^{-1}	0.140
Formula Weight	381.54
Color	colorless
Shape	plate
Size/mm ³	0.38×0.15×0.06
T/K	173(2)
Crystal System	triclinic
Space Group	<i>P</i> -1
$a/\text{\AA}$	7.1927(8)
$b/\text{\AA}$	7.5787(8)
$c/\text{\AA}$	21.102(2)
$\alpha/^\circ$	83.7720(10)
$\beta/^\circ$	82.5490(10)
$\gamma/^\circ$	66.3970(10)
$V/\text{\AA}^3$	1043.13(19)
<i>Z</i>	2

was refined with version of **XL**⁷¹ using Least Squares minimisation.

Crystal Data. C₁₉H₃₁NO₅Si, $M_r = 381.54$, triclinic, $P\bar{1}$ (No. 2), $a = 7.1927(8)$ Å, $b = 7.5787(8)$ Å, $c = 21.102(2)$ Å, $\alpha = 83.7720(10)^\circ$, $\beta = 82.5490(10)^\circ$, $\gamma = 66.3970(10)^\circ$, $V = 1043.13(19)$ Å³, $T = 173(2)$ K, $Z = 2$, $Z' = 1$, $\mu(\text{MoK}\alpha) = 0.140$, 15883 reflections measured, 4145 unique ($R_{int} = 0.0465$) which were used in all calculations. The final wR_2 was 0.1580 (all data) and R_1 was 0.0547 ($I > 2(I)$).

Z'	1
Wavelength/Å	0.710730
Radiation type	MoK α
$\Theta_{min}/^\circ$	1.950
$\Theta_{max}/^\circ$	26.142
Measured Refl.	15883
Independent Refl.	4145
Reflections Used	2893
R_{int}	0.0465
Parameters	243
Restraints	0
Largest Peak	0.743
Deepest Hole	-0.271
GooF	1.063
wR_2 (all data)	0.1580
wR_2	0.1404
R_1 (all data)	0.0796
R_1	0.0547

Structure Quality Indicators

Reflection: d min (Mo) 0.81 | I/σ 12.0 | Rint 4.65% | complete 100%

Refinement: Shift 0.000 | Max Peak 0.7 | Min Peak -0.3 | GooF 1.063

A colorless plate-shaped crystal with dimensions $0.38 \times 0.15 \times 0.06 \text{ mm}^3$ was mounted on a nylon loop with paratone oil. Data were collected using a Bruker APEX-II CCD diffractometer equipped with an Oxford Cryosystems low-temperature device, operating at $T = 173(2) \text{ K}$.

Data were measured using ω of -0.50° per frame for 299.34 s using MoK_α radiation (sealed tube, 50 kV, 40 mA). The total number of runs and images was based on the strategy calculation from the program **COSMO** (BRUKER, V1.61, 2009). The actually achieved resolution was $\Theta = 26.142$.

Cell parameters were retrieved using the **SAINT**⁷² software and refined using **SAINT**⁷² on 5215 reflections, 33% of the observed reflections. Data reduction was performed using the **SAINT**⁷² software which corrects for Lorentz polarisation. The final completeness is 99.90 out to 26.142 in Θ . A multi-scan absorption correction was performed using SADABS-2014/5 (Bruker,2014/5) was used for absorption correction. wR_2 ⁷³ was 0.0606 before and 0.0512 after correction. The Ratio of minimum to maximum transmission is 0.9066. The $\lambda/2$ correction factor is 0.00150. The absorption coefficient μ of this material is 0.140 mm^{-1} at this wavelength ($\lambda = 0.71073 \text{ \AA}$) and the minimum and maximum transmissions are 0.6757 and 0.7453. SADABS-2014/5 (Bruker,2014/5) was used for

absorption correction. wR_2^{73} was 0.0606 before and 0.0512 after correction. The Ratio of minimum to maximum transmission is 0.9066. The $\lambda/2$ correction factor is 0.00150.

The structure was solved in the space group $P-1$ (# 2) by Intrinsic Phasing using the **ShelXT**⁷¹ structure solution program. The structure was refined by Least Squares using version 2014/6 of **XL**⁷¹ incorporated in **Olex2**.⁷⁰ All non-hydrogen atoms were refined anisotropically. Hydrogen atom positions were calculated geometrically and refined using the riding model.

There is a single molecule in the asymmetric unit, which is represented by the reported sum formula. In other words: Z is 2 and Z' is 1.

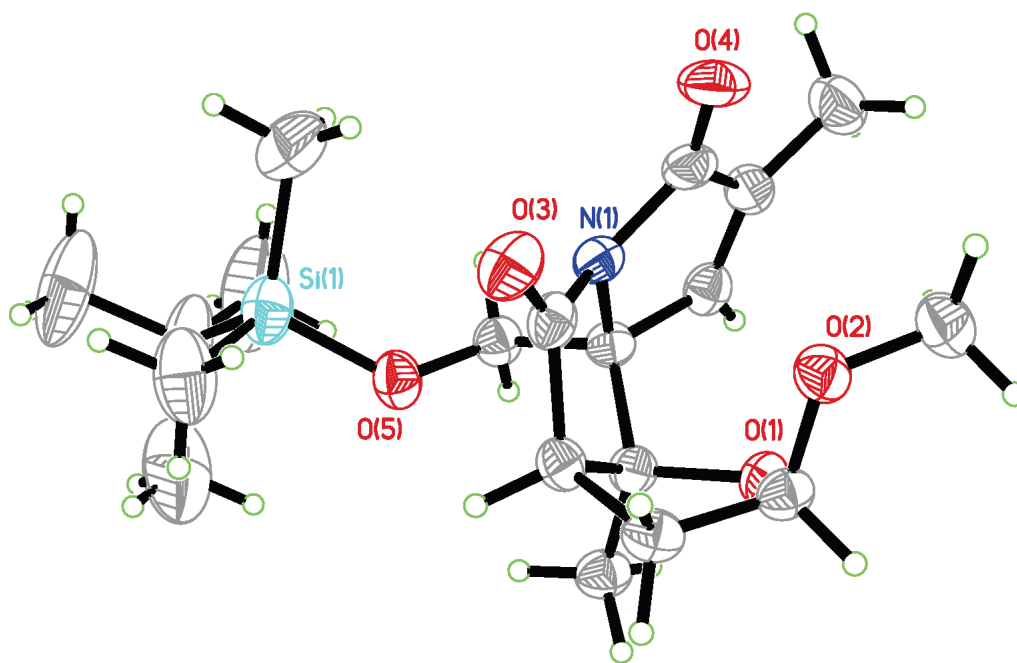


Figure III-32. X-ray structure of **III-91b** (view 1).

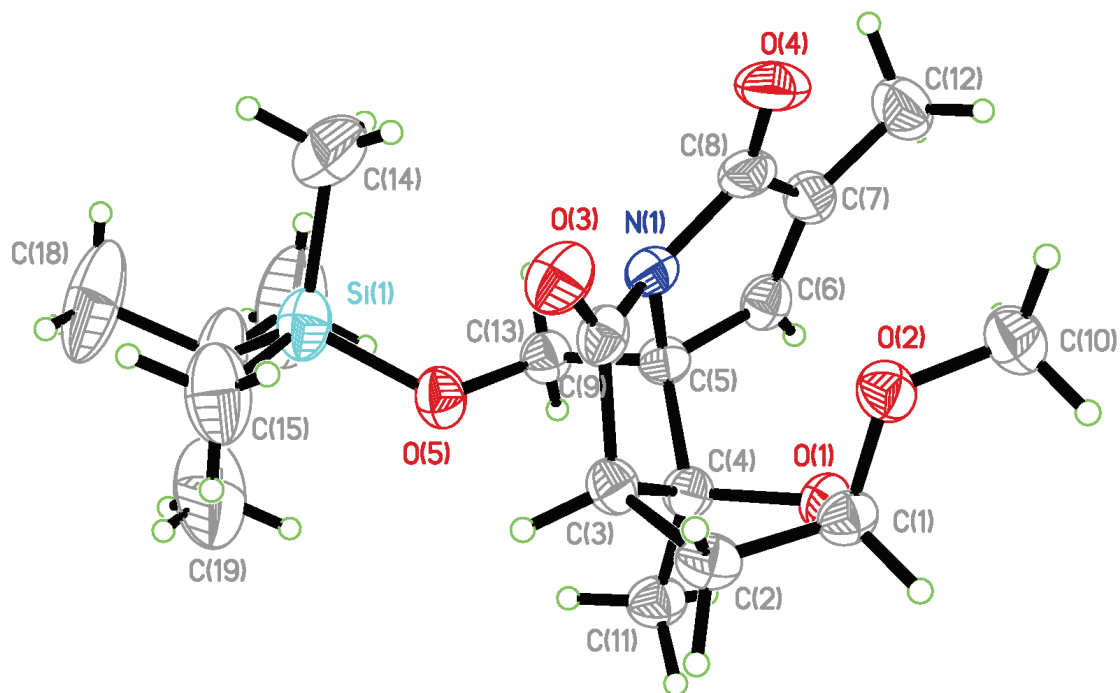


Figure III-33. X-ray structure of **III-91b** (view 2).

Table III-5: Fractional Atomic Coordinates ($\times 10^4$) and Equivalent Isotropic Displacement Parameters ($\text{\AA}^2 \times 10^3$) for **III-91b**. U_{eq} is defined as 1/3 of the trace of the orthogonalised U_{ij} .

Atom	x	y	z	U_{eq}
Si1	5874.7(11)	7679.7(12)	3600.4(3)	45.6(2)
O1	9017(2)	4166(2)	1153.2(7)	30.7(4)
O2	12240(2)	4302(2)	1025.7(7)	34.8(4)
O3	11576(2)	5871(2)	2472.6(8)	42.2(4)
O4	10562(3)	9004(2)	1330.2(9)	46.7(5)
O5	6037(2)	6652(2)	2936.2(7)	37.8(4)
N1	8731(3)	7323(2)	1907.3(9)	29.0(4)
C1	11146(3)	3114(3)	1188.5(11)	31.6(5)
C2	11416(3)	2408(3)	1882.7(11)	33.6(5)
C3	9658(3)	4025(3)	2229.3(11)	30.1(5)
C4	7955(3)	4652(3)	1783(1)	29.2(5)
C5	6991(3)	6884(3)	1800.4(10)	28.2(5)
C6	6290(3)	8085(3)	1199.8(11)	33.0(5)
C7	7428(4)	9081(3)	990.3(11)	35.5(6)
C8	9118(4)	8541(3)	1406.3(12)	34.4(5)
C9	10180(3)	5781(3)	2236.8(10)	31.1(5)
C10	12161(4)	5057(4)	378.5(12)	43.5(6)
C11	6461(3)	3687(3)	1921.4(12)	36.3(6)

Table III-5 (cont'd)

Atom	x	y	z	U_{eq}
C12	7228(4)	10534(4)	440.4(13)	50.7(7)
C13	5312(3)	7603(3)	2348.5(10)	32.9(5)
C14	6444(7)	9874(6)	3406.9(18)	81.9(11)
C15	7853(5)	5821(5)	4060.5(15)	70(1)
C16	3272(4)	8301(6)	4033.4(14)	68.6(10)
C17	1671(5)	9814(8)	3628.5(19)	107.9(17)
C18	3191(6)	9092(8)	4680.3(17)	106.1(17)
C19	2843(7)	6460(8)	4149.4(19)	110.5(17)

Table III-6: Anisotropic Displacement Parameters ($\times 10^4$) **III-91b**. The anisotropic displacement factor exponent takes the form: $-2\pi^2[h^2a^{*2} \times U_{11} + \dots + 2hka^* \times b^* \times U_{12}]$

Atom	U_{11}	U_{22}	U_{33}	U_{23}	U_{13}	U_{12}
Si1	39.2(4)	62.8(5)	35.3(4)	-9.3(3)	0.7(3)	-20.2(4)
O1	27.4(8)	32.2(8)	31.0(8)	-6.5(6)	-0.5(6)	-9.8(6)
O2	32.2(8)	39.4(9)	35.1(9)	-2.6(7)	-0.1(7)	-17.2(7)
O3	32.5(9)	51.5(11)	45.7(10)	-11.6(8)	-7.8(7)	-16.4(8)
O4	47.8(10)	36.7(9)	63.5(12)	-7.6(8)	6.6(9)	-27.3(8)
O5	37.0(9)	39.6(9)	30.4(9)	-2.1(7)	1.2(7)	-9.5(7)
N1	27.5(9)	28.1(9)	32.6(10)	-6.7(8)	-0.1(8)	-11.6(8)
C1	26.5(11)	27.4(11)	38.6(13)	-6.4(9)	-0.4(9)	-7.9(9)

Table III-6 (cont'd)

Atom	U_{11}	U_{22}	U_{33}	U_{23}	U_{13}	U_{12}
C2	27.2(11)	27.6(11)	42.3(14)	0.3(10)	-3.5(10)	-7.5(9)
C3	27.4(11)	32.3(12)	29.0(12)	-0.4(9)	-0.6(9)	-11.1(9)
C4	28.1(11)	28.4(11)	29.9(12)	-3.2(9)	0.1(9)	-10.2(9)
C5	25.5(11)	28.0(11)	32.0(12)	-2.3(9)	-3.3(9)	-11.3(9)
C6	31.7(12)	31.5(12)	31.6(12)	-4.6(10)	-4.7(9)	-6.9(10)
C7	40.0(13)	25.5(11)	34.5(13)	-3.3(10)	3.9(10)	-7.9(10)
C8	36.4(13)	23.9(11)	41.6(14)	-10.5(10)	6.3(10)	-11.5(10)
C9	26.2(11)	37.8(13)	28.9(12)	-8.8(10)	2.0(9)	-11.9(10)
C10	42.3(14)	47.5(15)	39.8(14)	0.8(11)	2.9(11)	-19.7(12)
C11	32.9(12)	33.5(12)	44.6(14)	-5.6(10)	-0.1(10)	-15.4(10)
C12	59.6(17)	40.1(14)	45.2(16)	5.2(12)	2.4(13)	-16.2(13)
C13	30.8(12)	31.9(12)	32.5(12)	-3.1(10)	-1.3(10)	-8.8(10)
C14	113(3)	93(3)	68(2)	-23(2)	-6(2)	-67(2)
C15	53.0(18)	103(3)	46.4(18)	1.4(17)	-11.8(14)	-22.4(18)
C16	39.0(16)	125(3)	40.6(17)	-28.9(18)	6.0(13)	-28.1(18)
C17	42.7(19)	167(4)	76(3)	-39(3)	2.4(17)	4(2)
C18	65(2)	197(5)	58(2)	-65(3)	19.5(18)	-46(3)
C19	95(3)	215(6)	66(2)	-10(3)	15(2)	-114(4)

Table III-7: Bond Lengths in Å for **III-91b**.

Atom	Atom	Length/Å
Si1	O5	1.6449(17)
Si1	C14	1.859(4)
Si1	C15	1.846(3)
Si1	C16	1.872(3)
O1	C1	1.423(3)
O1	C4	1.450(3)
O2	C1	1.406(3)
O2	C10	1.422(3)
O3	C9	1.205(3)
O4	C8	1.210(3)
O5	C13	1.415(3)
N1	C5	1.466(3)
N1	C8	1.401(3)
N1	C9	1.404(3)
C1	C2	1.513(3)
C2	C3	1.533(3)
C3	C4	1.533(3)
C3	C9	1.523(3)
C4	C5	1.553(3)
C4	C11	1.509(3)

Table III-7 (cont'd)

Atom	Atom	Length/Å
C5	C6	1.495(3)
C5	C13	1.530(3)
C6	C7	1.328(3)
C7	C8	1.488(3)
C7	C12	1.489(3)
C16	C17	1.535(5)
C16	C18	1.535(4)
C16	C19	1.534(6)

Table III-8: Bond Angles in ° for **III-91b**.

Atom	Atom	Atom	Angle/°
O5	Si1	C14	109.58(13)
O5	Si1	C15	103.70(13)
O5	Si1	C16	110.02(12)
C14	Si1	C16	110.77(18)
C15	Si1	C14	110.93(18)
C15	Si1	C16	111.60(15)
C1	O1	C4	111.33(16)
C1	O2	C10	113.84(18)
C13	O5	Si1	126.46(14)
C8	N1	C5	111.01(18)
C8	N1	C9	126.95(18)
C9	N1	C5	111.81(17)
O1	C1	C2	106.30(17)
O2	C1	O1	111.67(17)
O2	C1	C2	107.13(18)
C1	C2	C3	101.61(17)
C4	C3	C2	103.59(17)
C9	C3	C2	110.52(18)
C9	C3	C4	105.08(17)
O1	C4	C3	104.42(16)

Table III-8 (cont'd)

Atom	Atom	Atom	Angle/°
O1	C4	C5	108.23(17)
O1	C4	C11	108.55(18)
C3	C4	C5	103.74(17)
C11	C4	C3	116.22(19)
C11	C4	C5	114.95(18)
N1	C5	C4	102.37(16)
N1	C5	C6	102.37(17)
N1	C5	C13	109.52(17)
C6	C5	C4	119.14(18)
C6	C5	C13	109.09(17)
C13	C5	C4	113.21(18)
C7	C6	C5	111.5(2)
C6	C7	C8	109.1(2)
C6	C7	C12	130.3(2)
C8	C7	C12	120.6(2)
O4	C8	N1	126.2(2)
O4	C8	C7	128.1(2)
N1	C8	C7	105.71(19)
O3	C9	N1	125.0(2)
O3	C9	C3	127.6(2)

Table III-8 (cont'd)

Atom	Atom	Atom	Angle/°
O5	C13	C5	110.00(17)
C17	C16	Si1	109.9(2)
C18	C16	Si1	109.7(2)
C18	C16	C17	109.8(3)
C19	C16	Si1	108.5(3)
C19	C16	C17	109.7(3)
C19	C16	C18	109.2(3)

Table III-9: Hydrogen Fractional Atomic Coordinates ($\times 10^4$) and Equivalent Isotropic Displacement Parameters ($\text{\AA}^2 \times 10^3$) for **III-91b**. U_{eq} is defined as 1/3 of the trace of the orthogonalised U_{ij} .

Atom	x	y	z	U_{eq}
H1	11670	2000	908	38
H2A	12753	2283	2001	40
H2B	11280	1154	1976	40
H3	9240	3581	2668	36
H6	5171	8129	994	40
H10A	12523	4004	94	65
H10B	13126	5688	279	65
H10C	10779	5999	316	65

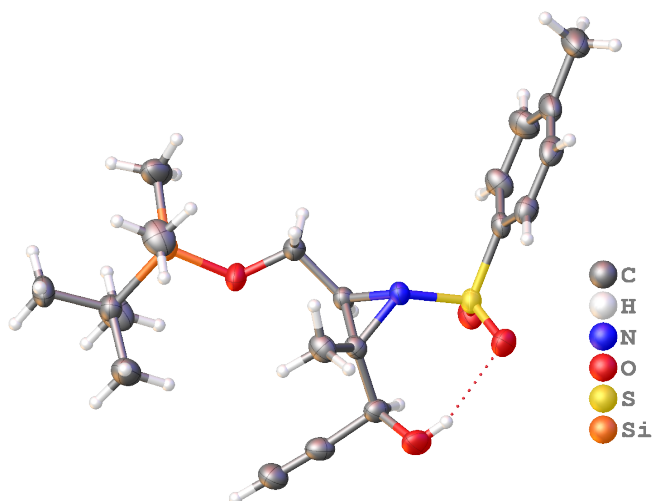
Table III-9 (cont'd)

Atom	x	y	z	U_{eq}
H11A	5450	4184	1608	54
H11B	5772	3958	2353	54
H11C	7193	2290	1893	54
H12A	8335	9987	105	76
H12B	7303	11687	585	76
H12C	5914	10883	270	76
H13A	4877	9013	2370	39
H13B	4116	7350	2269	39
H14A	7693	9564	3115	123
H14B	6629	10330	3802	123
H14C	5308	10885	3202	123
H15A	7581	4644	4127	105
H15B	7834	6296	4476	105
H15C	9193	5539	3822	105
H17A	1649	9264	3232	162
H17B	2017	10946	3525	162
H17C	326	10200	3870	162
H18A	4295	8171	4921	159
H18B	1877	9285	4925	159
H18C	3348	10326	4608	159

Table III-9 (cont'd)

Atom	x	y	z	U_{eq}
H19B	1495	6756	4384	166
H19C	3883	5489	4401	166

III-7-3-2 Crystal data for (–)-III-25 (BB817D)



Experimental. Single colorless plate-shaped crystals of (–)-III-25 (BB817D) were used as received. A suitable crystal (0.46×0.32×0.05) mm³ was selected and mounted on a nylon loop with paratone oil on a Bruker APEX-II CCD diffractometer. The crystal was kept at $T = 173(2)$ K during data collection. Using **Olex2**,⁷⁰ the structure was solved with the XT structure solution program, using the Intrinsic Phasing solution method. The model was refined with version of **XL**⁷¹ using Least Squares

Compound	BB817D
Formula	C ₂₀ H ₃₁ NO ₄ SSi
$D_{calc.}/\text{g cm}^{-3}$	1.194
μ/mm^{-1}	0.218
Formula Weight	409.61
Color	colorless
Shape	plate
Size/mm ³	0.46×0.32×0.05
T/K	173(2)
Crystal System	orthorhombic
Flack	-0.02(2)
Parameter	
Hooft	-0.02(2)
Parameter	
Space Group	$P2_12_12_1$
$a/\text{\AA}$	10.307(2)
$b/\text{\AA}$	12.283(3)
$c/\text{\AA}$	17.991(4)
$\alpha/^\circ$	90

minimisation.

Crystal Data. $C_{20}H_{31}NO_4SSi$, $M_r = 409.61$, orthorhombic, $P2_12_12_1$ (No. 19), $a = 10.307(2) \text{ \AA}$, $b = 12.283(3) \text{ \AA}$, $c = 17.991(4) \text{ \AA}$, $\alpha = \beta = \gamma = 90^\circ$, $V = 2277.7(8) \text{ \AA}^3$, $T = 173(2) \text{ K}$, $Z = 4$, $Z' = 1$, $\mu(\text{MoK}\alpha) = 0.218$, 43882 reflections measured, 5640 unique ($R_{int} = 0.0420$) which were used in all calculations. The final wR_2 was 0.0993 (all data) and R_1 was 0.0372 ($I > 2(I)$).

$\beta/^\circ$	90
$\gamma/^\circ$	90
$V/\text{\AA}^3$	2277.7(8)
Z	4
Z'	1
Wavelength/ \AA	0.710730
Radiation type	MoK α
$\Theta_{min}/^\circ$	2.007
$\Theta_{max}/^\circ$	28.441
Measured Refl.	43882
Independent	5640
Refl.	
Reflections	5095
Used	
R_{int}	0.0420
Parameters	255
Restraints	0
Largest Peak	0.310
Deepest Hole	-0.217
GooF	1.050
wR_2 (all data)	0.0993

Structure Quality Indicators

Reflection:

d min (Mo)	0.75	I/ σ	25.0	R _{int}	4.20%	complete	98%
------------	------	-------------	------	------------------	-------	----------	-----

Refinement:

Shift	0.000	Max Peak	0.3	Min Peak	-0.2	Goof	1.050		-0.02(2)
-------	-------	----------	-----	----------	------	------	-------	--	----------

A colorless plate-shaped crystal with dimensions 0.46×0.32×0.05 mm³ was mounted on a nylon loop with paratone oil. Data were collected using a Bruker APEX-II CCD diffractometer equipped with an Oxford Cryosystems low-temperature device, operating at $T = 173(2)$ K.

Data were measured using ω of -0.50° per frame for 200.84 s using MoK $_{\alpha}$ radiation (sealed tube, 50 kV, 40 mA). The total number of runs and images was based on the strategy calculation from the program **COSMO** (BRUKER, V1.61, 2009). The actually achieved resolution was $\Theta = 28.441$.

Cell parameters were retrieved using the **SAINT**⁷² software and refined using **SAINT**⁷² on 9967 reflections, 23 % of the observed reflections. Data reduction was performed using the **SAINT**⁷² software which corrects for Lorentz polarisation. The final completeness is 100.00 out to 28.441 in Θ . A multi-scan absorption correction was performed using SADABS-2014/5 (Bruker,2014/5) was used for absorption correction. wR_2 ⁷³ was 0.0660 before and 0.0554 after correction. The Ratio of minimum to maximum transmission is 0.9136. The $\lambda/2$ correction factor is 0.00150. The absorption coefficient μ of this material is 0.218 mm⁻¹ at this wavelength ($\lambda = 0.71073\text{\AA}$) and the minimum and maximum transmissions are 0.6813 and 0.7457. SADABS-2014/5

(Bruker,2014/5) was used for absorption correction. wR_2^{73} was 0.0660 before and 0.0554 after correction. The Ratio of minimum to maximum transmission is 0.9136. The $\lambda/2$ correction factor is 0.00150.

The structure was solved in the space group $P2_12_12_1$ (# 19) by Intrinsic Phasing using the XT (Sheldrick, 2015) structure solution program. The structure was refined by Least Squares using version 2014/6 of **XL**⁷¹ incorporated in **Olex2**.⁷⁰ All non-hydrogen atoms were refined anisotropically. Hydrogen atom positions were calculated geometrically and refined using the riding model, except for the Hydrogen atom on the oxygen atom which was found by difference Fourier methods and refined isotropically.

There is a single molecule in the asymmetric unit, which is represented by the reported sum formula. In other words: Z is 4 and Z' is 1.

The Flack parameter was refined to -0.02(2). Determination of absolute structure using Bayesian statistics on Bijvoet differences using the Olex2 results in -0.02(2). Note: The Flack parameter is used to determine chirality of the crystal studied, the value should be near 0, a value of 1 means that the stereochemistry is wrong and the model should be inverted. A value of 0.5 means that the crystal consists of a racemic mixture of the two enantiomers.

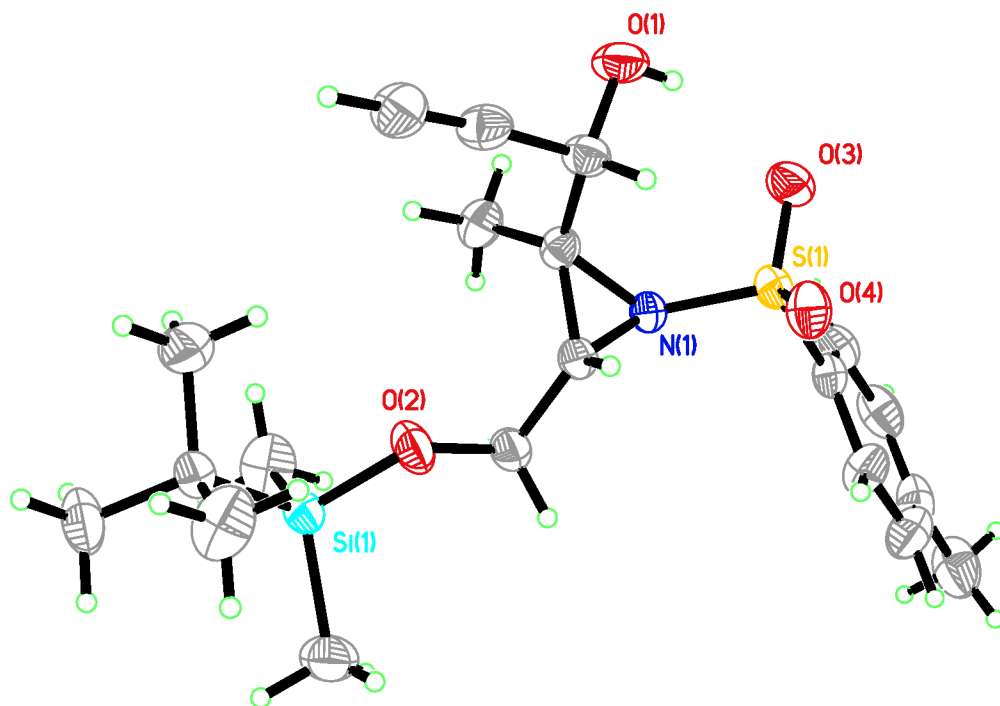


Figure III-34. X-ray structure of (-)-III-25 (view 1).

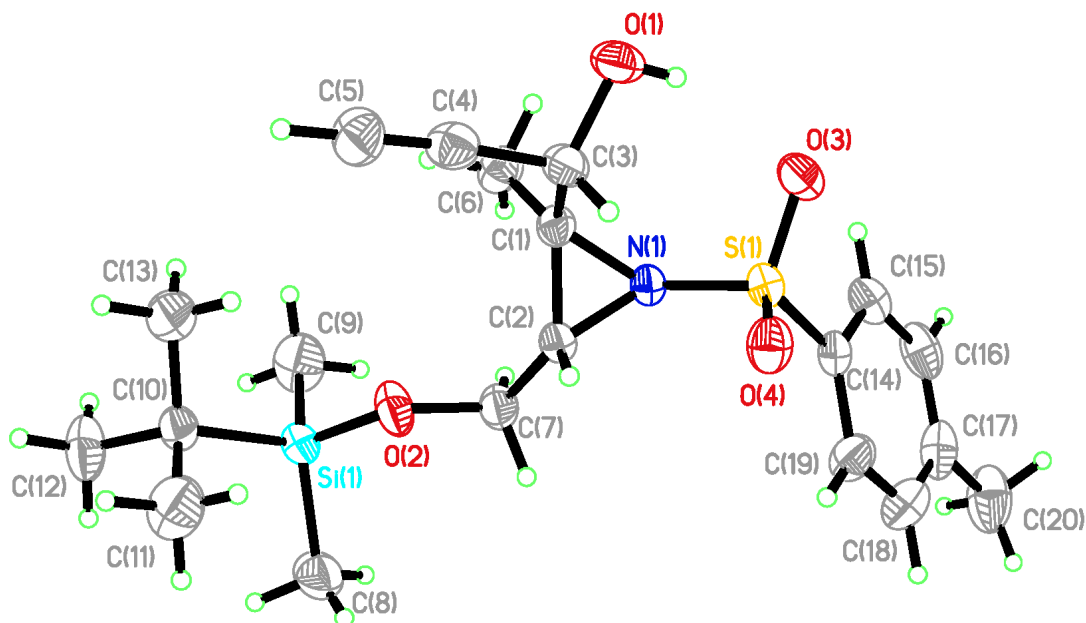


Figure III-35: The Model has Chirality at C1 (Chiral SPGR) S Verify; The Model has Chirality at C2 (Chiral SPGR) S Verify; The Model has Chirality at C3 (Chiral SPGR) S Verify.

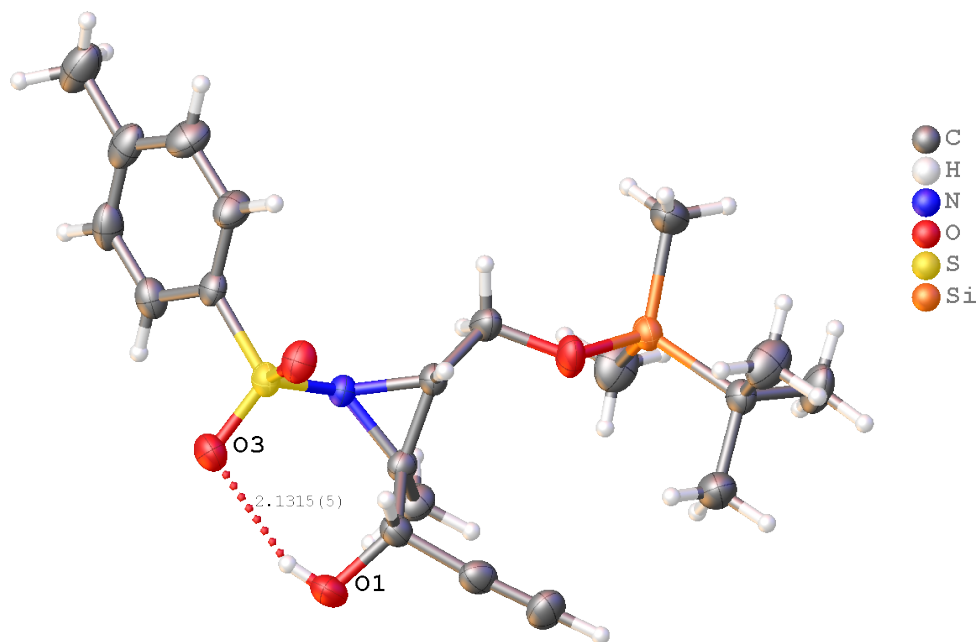


Figure III-36: The following hydrogen bonding interactions with a maximum D-D distance of 2.9 Å and a minimum angle of 120 ° are present in **(-)-III-25**: O1–O3: 2.865 Å.

Table III-10: Fractional Atomic Coordinates ($\times 10^4$) and Equivalent Isotropic Displacement Parameters ($\text{\AA}^2 \times 10^3$) for **(-)-III-25**. U_{eq} is defined as 1/3 of the trace of the orthogonalised U_{ij} .

Atom	x	y	z	U_{eq}
S1	828.6(5)	6886.9(5)	4781.5(3)	29.27(14)
Si1	5881.5(7)	5337.9(5)	2770.5(4)	30.61(16)
O1	429.0(18)	4081.6(17)	4822.9(13)	44.0(5)
O2	4872.6(17)	5517.8(16)	3472.8(11)	41.2(4)
O3	-385.9(17)	6311.0(15)	4848.5(11)	41.4(4)
O4	1622.2(18)	6996.9(16)	5431.6(10)	38.5(4)
N1	1616.0(18)	6305.4(15)	4079.7(11)	27.4(4)

Table III-10 (cont'd)

Atom	x	y	z	U_{eq}
C1	2001(2)	5125.6(18)	4083.4(13)	27.8(5)
C2	3003(2)	5993.0(19)	4150.1(13)	28.3(5)
C3	1748(2)	4458(2)	4789.7(15)	32.6(5)
C4	2615(3)	3501(2)	4781.9(15)	37.8(5)
C5	3375(3)	2779(2)	4767.9(18)	47.0(7)
C6	1730(3)	4554(2)	3359.2(14)	38.3(6)
C7	3886(2)	6318(2)	3517.2(15)	35.2(5)
C8	6873(3)	6589(2)	2629(2)	55.2(8)
C9	4948(4)	5015(3)	1911.7(18)	56.2(8)
C10	6914(2)	4152(2)	3075.2(14)	33.1(5)
C11	7723(4)	4472(3)	3752.3(19)	58.3(9)
C12	7836(3)	3807(3)	2447.9(18)	53.8(8)
C13	6056(3)	3185(2)	3284(2)	53.9(8)
C14	521(2)	8191.0(19)	4413.2(12)	29.4(5)
C15	-561(2)	8341(2)	3964.5(14)	37.1(6)
C16	-817(3)	9376(2)	3693.2(15)	43.3(6)
C17	-11(3)	10251(2)	3855.4(15)	44.2(7)
C18	1065(3)	10074(2)	4305.9(16)	47.4(7)
C19	1340(3)	9046(2)	4588.7(16)	39.7(6)
C20	-280(4)	11368(3)	3534(2)	62.0(9)

Table III-11: Anisotropic Displacement Parameters ($\times 10^4$) **(–)III-25.** The anisotropic displacement factor exponent takes the form: $-2\pi^2[h^2a^{*2} \times U_{11} + \dots + 2hka^* \times b^* \times U_{12}]$

Atom	U_{11}	U_{22}	U_{33}	U_{23}	U_{13}	U_{12}
S1	25.2(3)	31.9(3)	30.8(3)	-1.1(2)	3.4(2)	3.6(2)
Si1	25.7(3)	33.6(3)	32.6(3)	-0.5(2)	3.0(3)	1.5(3)
O1	31.3(9)	36.6(10)	64.1(13)	9.2(10)	4.3(9)	-7.0(8)
O2	33.2(9)	45.3(11)	45.2(10)	5.9(9)	13.2(8)	11.4(8)
O3	29.4(8)	42.2(10)	52.7(11)	2.3(9)	8.7(8)	-0.5(8)
O4	40.7(9)	43.3(10)	31.4(8)	-2.6(7)	-1.6(7)	8.9(8)
N1	24.6(9)	26.0(9)	31.5(9)	-1.1(8)	2.6(8)	3.5(7)
C1	26.1(10)	26.4(11)	31.1(11)	0.1(9)	-1.9(9)	2.9(9)
C2	23.9(10)	27.3(11)	33.7(11)	-0.3(9)	1.8(9)	2.5(9)
C3	27.0(11)	32.2(12)	38.5(12)	4.5(10)	0.3(10)	-1.5(9)
C4	37.1(12)	34.5(12)	41.6(13)	9.8(11)	-3.5(11)	-2.6(11)
C5	46.8(15)	39.4(14)	54.9(16)	11.9(12)	1.4(14)	7.6(12)
C6	42.7(14)	34.4(13)	38.0(13)	-5.3(10)	-5.8(11)	2.2(11)
C7	33.5(12)	29.4(12)	42.8(13)	3.9(10)	10.8(10)	3.8(10)
C8	39.4(15)	40.2(16)	86(2)	13.1(15)	7.9(16)	-2.0(13)
C9	58.7(19)	64(2)	46.4(16)	-4.5(15)	-16.0(14)	11.4(16)
C10	29.3(11)	33.0(12)	36.8(12)	-1(1)	5.1(10)	2.9(10)
C11	64(2)	55.6(19)	55.5(19)	-5.2(15)	-21.7(16)	12.4(16)
C12	54.7(18)	53.3(18)	53.3(17)	6.8(14)	20.5(15)	23.5(15)

Table III-11 (cont'd)

Atom	U_{11}	U_{22}	U_{33}	U_{23}	U_{13}	U_{12}
C13	46.3(16)	37.7(15)	78(2)	7.0(14)	10.0(15)	1.2(13)
C14	27.8(11)	30.0(11)	30.3(11)	-3.5(9)	3.6(8)	6.8(9)
C15	28.3(12)	48.1(15)	34.8(12)	1.3(11)	0.9(9)	3.6(10)
C16	34.0(13)	59.1(17)	36.9(13)	10.8(12)	2.8(11)	16.1(13)
C17	53.8(17)	42.8(15)	36.0(13)	2.3(12)	11.1(12)	18.6(13)
C18	59.6(18)	33.2(13)	49.4(15)	-6.1(11)	-0.9(14)	2.3(13)
C19	41.8(14)	34.1(13)	43.2(14)	-7.4(11)	-9.0(11)	3.7(11)
C20	75(2)	52.0(18)	58.9(19)	15.3(16)	17.9(18)	25.6(17)

Table III-12: Bond Lengths in Å for (–)-III-25

Atom	Atom	Length/Å
S1	O3	1.4428(19)
S1	O4	1.4336(19)
S1	N1	1.6622(19)
S1	C14	1.762(2)
Si1	O2	1.6512(18)
Si1	C8	1.864(3)
Si1	C9	1.863(3)
Si1	C10	1.886(3)

Table III-12 (cont'd)

Atom	Atom	Length/Å
O1	C3	1.437(3)
O2	C7	1.417(3)
N1	C1	1.503(3)
N1	C2	1.486(3)
C1	C2	1.489(3)
C1	C3	1.535(3)
C1	C6	1.506(3)
C2	C7	1.511(3)
C3	C4	1.477(3)
C4	C5	1.183(4)
C10	C11	1.528(4)
C10	C12	1.535(4)
C10	C13	1.528(4)
C14	C15	1.388(3)
C14	C19	1.384(4)
C15	C16	1.387(4)
C16	C17	1.390(4)
C17	C18	1.391(4)
C17	C20	1.514(4)
C18	C19	1.390(4)

Table III-13: Bond angles in ° for (–)-III-25.

Atom	Atom	Atom	Angle/°
O3	S1	N1	106.05(11)
O3	S1	C14	108.71(11)
O4	S1	O3	118.23(12)
O4	S1	N1	112.43(10)
O4	S1	C14	108.89(12)
N1	S1	C14	101.13(10)
O2	Si1	C8	109.85(14)
O2	Si1	C9	109.75(14)
O2	Si1	C10	103.68(10)
C8	Si1	C10	111.55(13)
C9	Si1	C8	110.21(17)
C9	Si1	C10	111.62(14)
C7	O2	Si1	126.02(16)
C1	N1	S1	122.69(15)
C2	N1	S1	121.07(16)
C2	N1	C1	59.75(14)
N1	C1	C3	118.29(19)
N1	C1	C6	113.37(19)
C2	C1	N1	59.57(14)
C2	C1	C3	115.71(19)

Table III-13 (cont'd)

Atom	Atom	Atom	Angle/°
C2	C1	C6	122.1(2)
C6	C1	C3	115.8(2)
N1	C2	C1	60.68(14)
N1	C2	C7	116.53(19)
C1	C2	C7	123.1(2)
O1	C3	C1	111.6(2)
O1	C3	C4	108.4(2)
C4	C3	C1	108.3(2)
C5	C4	C3	175.7(3)
O2	C7	C2	106.93(19)
C11	C10	Si1	109.93(19)
C11	C10	C12	108.6(2)
C11	C10	C13	108.6(3)
C12	C10	Si1	110.44(18)
C13	C10	Si1	110.21(18)
C13	C10	C12	108.9(2)
C15	C14	S1	118.95(19)
C19	C14	S1	119.61(18)
C19	C14	C15	121.4(2)
C16	C15	C14	118.6(3)

Table III-13 (cont'd)

Atom	Atom	Atom	Angle/°
C16	C17	C18	118.5(3)
C16	C17	C20	120.7(3)
C18	C17	C20	120.8(3)
C19	C18	C17	121.2(3)
C14	C19	C18	118.8(3)

Table III-14: Hydrogen fractional atomic coordinates ($\times 10^4$) and equivalent isotropic displacement parameters ($\text{\AA}^2 \times 10^3$) for **(-)-III-25**. U_{eq} is defined as 1/3 of the trace of the orthogonalised U_{ij} .

Atom	x	y	z	U_{eq}
H1	20(30)	4610(30)	4850(20)	51(10)
H2	3382	6084	4658	34
H3	1939	4914	5237	39
H5	3985	2200	4757	56
H6A	831	4295	3355	58
H6B	2320	3933	3305	58
H6C	1863	5062	2946	58
H7A	3393	6350	3045	42
H7B	4270	7044	3613	42
H8A	7671	6402	2361	83

Table III-14 (cont'd)

Atom	x	y	z	U_{eq}
H8B	7096	6905	3113	83
H8C	6375	7120	2339	83
H9A	4432	4356	1992	84
H9B	5551	4897	1498	84
H9C	4369	5624	1793	84
H11A	8274	5096	3627	87
H11B	8269	3857	3902	87
H11C	7145	4669	4163	87
H12A	7330	3613	2006	81
H12B	8346	3176	2609	81
H12C	8421	4411	2328	81
H13A	5508	3382	3709	81
H13B	6604	2563	3418	81
H13C	5506	2989	2860	81
H15	-1114	7747	3846	45
H16	-1560	9489	3390	52
H18	1622	10665	4423	57
H19	2077	8933	4897	48
H20A	-6	11385	3012	93
H20B	203	11918	3815	93

Table III-14 (cont'd)

Atom	Atom	Atom	Atom	Atom
H20C	-1211	11523	3565	93

Table III-15: Hydrogen bond information for (–)-III-25.

D	H	A	d(D-H)/Å	d(H-A)/Å	d(D-A)/Å	D-H-A/deg
O1	H1	O3	0.78(4)	2.13(4)	2.865(3)	158(3)

REFERENCES

REFERENCES

1. Wood, J. L., TOTAL SYNTHESIS Welwitindolinone is well worth it. *Nature Chemistry* **2012**, 4 (5), 341-343.
2. Reddy, L. R.; Fournier, J. F.; Reddy, B. V. S.; Corey, E. J., New synthetic route for the enantioselective total synthesis of salinosporamide A and biologically active analogues. *Organic Letters* **2005**, 7 (13), 2699-2701.
3. Feling, R. H.; Buchanan, G. O.; Mincer, T. J.; Kauffman, C. A.; Jensen, P. R.; Fenical, W., Salinosporamide A: A highly cytotoxic proteasome inhibitor from a novel microbial source, a marine bacterium of the new genus *Salinospira*. *Angew Chem Int Edit* **2003**, 42 (3), 355.
4. Gulder, T. A. M.; Moore, B. S., Salinosporamide Natural Products: Potent 20 S Proteasome Inhibitors as Promising Cancer Chemotherapeutics. *Angew Chem Int Edit* **2010**, 49 (49), 9346-9367.
5. Shibasaki, M.; Kanai, M.; Fukuda, N., Total synthesis of lactacystin and salinosporamide A. *Chem-Asian J* **2007**, 2 (1), 20-38.
6. Groll, M.; Huber, R.; Potts, B. C. M., Crystal structures of salinosporamide A (NPI-0052) and B (NPI-0047) in complex with the 20S proteasome reveal important consequences of beta-lactone ring opening and a mechanism for irreversible binding. *J Am Chem Soc* **2006**, 128 (15), 5136-5141.
7. Reddy, L. R.; Saravanan, P.; Corey, E. J., A simple stereocontrolled synthesis of salinosporamide A. *J Am Chem Soc* **2004**, 126 (20), 6230-6231.
8. Reddy, L. R.; Fournier, J. F.; Reddy, B. V. S.; Corey, E. J., An efficient, stereocontrolled synthesis of a potent omuralide-salinosporin hybrid for selective proteasome inhibition. *J Am Chem Soc* **2005**, 127 (25), 8974-8976.
9. Endo, A.; Danishefsky, S. J., Total synthesis of salinosporamide A. *J Am Chem Soc* **2005**, 127 (23), 8298-8299.
10. Mulholland, N. P.; Pattenden, G.; Walters, L. A. S., A concise total synthesis of salinosporamide A. *Organic & Biomolecular Chemistry* **2006**, 4 (15), 2845-2846.
11. Ma, G.; Nguyen, H.; Romo, D., Concise total synthesis of (+/-)-salinosporamide A, (+/-)-cinnabaramide A, and derivatives via a bis-cyclization process: Implications for a biosynthetic pathway? *Organic Letters* **2007**, 9 (11), 2143-2146.

12. Nguyen, H.; Ma, G.; Romo, D., A(1,3)-strain enabled retention of chirality during bis-cyclization of beta-ketoamides: total synthesis of (-)-salinosporamide A and (-)-homosalinosporamide A. *Chemical Communications* **2010**, 46 (26), 4803-4805.
13. Satoh, N.; Yokoshima, S.; Fukuyama, T., Total Synthesis of (-)-Salinosporamide A. *Organic Letters* **2011**, 13 (12), 3028-3031.
14. Takahashi, K.; Midori, M.; Kawano, K.; Ishihara, J.; Hatakeyama, S., Entry to heterocycles based on indium-catalyzed Conia-ene reactions: Asymmetric synthesis of (-)-salinosporamide A. *Angew Chem Int Edit* **2008**, 47 (33), 6244-6246.
15. Caubert, V.; Masse, J.; Retailleau, P.; Langlois, N., Stereoselective formal synthesis of the potent proteasome inhibitor: salinosporamide A. *Tetrahedron Letters* **2007**, 48 (3), 381-384.
16. Struble, J. R.; Bode, J. W., Formal synthesis of salinosporamide A via NHC-catalyzed intramolecular lactonization. *Tetrahedron* **2009**, 65 (26), 4957-4967.
17. Margalef, I. V.; Rupnicki, L.; Lam, H. W., Formal synthesis of salinosporamide A using a nickel-catalyzed reductive aldol cyclization-lactonization as a key step. *Tetrahedron* **2008**, 64 (34), 7896-7901.
18. Momose, T.; Kaiya, Y.; Hasegawa, J.; Sato, T.; Chida, N., Formal Synthesis of Salinosporamide A Starting from D-Glucose. *Synthesis-Stuttgart* **2009**, (17), 2983-2991.
19. Ling, T. T.; Macherla, V. R.; Manam, R. R.; McArthur, K. A.; Potts, B. C. M., Enantioselective total synthesis of (-)-salinosporamide A (NPI-0052). *Organic Letters* **2007**, 9 (12), 2289-2292.
20. Fukuda, T.; Sugiyama, K.; Arima, S.; Harigaya, Y.; Nagamitsu, T.; Omura, S., Total synthesis of salinosporamide A. *Organic Letters* **2008**, 10 (19), 4239-4242.
21. Joensuu, P. M.; Murray, G. J.; Fordyce, E. A. F.; Luebbers, T.; Lam, H. W., Diastereoselective nickel-catalyzed reductive aldol cyclizations using diethylzinc as the stoichiometric reductant: Scope and mechanistic insight. *J Am Chem Soc* **2008**, 130 (23), 7328-7338.
22. Mosey, R. A.; Tepe, J. J., New synthetic route to access (+/-) salinosporamide A via an oxazolone-mediated ene-type reaction. *Tetrahedron Letters* **2009**, 50 (3), 295-297.
23. Kulshrestha, A., Ph.D., Michigan State University, 2011.

24. Schomaker, J. M.; Geiser, A. R.; Huang, R.; Borhan, B., Tetrasubstituted pyrrolidines via a tandem aza-Payne/hydroamination reaction. *J Am Chem Soc* **2007**, *129* (13), 3794-+.
25. Thakur, V. V.; Sudalai, A., N-bromoamides as versatile catalysts for aziridination of olefins using chloramine-T. *Tetrahedron Letters* **2003**, *44* (5), 989-992.
26. Kulshrestha, A.; Schomaker, J. M.; Holmes, D.; Staples, R. J.; Jackson, J. E.; Borhan, B., Selectivity in the Addition Reactions of Organometallic Reagents to Aziridine-2-carboxaldehydes: The Effects of Protecting Groups and Substitution Patterns. *Chem-Eur J* **2011**, *17* (44), 12326-12339.
27. Nyasse, B.; Grehn, L.; Ragnarsson, U., Mild, efficient cleavage of arenesulfonamides by magnesium reduction. *Chemical Communications* **1997**, (11), 1017-1018.
28. Nicolaou, K. C.; Snyder, S. A.; Longbottom, D. A.; Nalbandian, A. Z.; Huang, X., New Uses for the Burgess Reagent in Chemical Synthesis: Methods for the Facile and Stereoselective Formation of Sulfamidates, Glycosylamines, and Sulfamides. *Chemistry – A European Journal* **2004**, *10* (22), 5581-5606.
29. Grieco, P. A.; Gilman, S.; Nishizawa, M., Organoselenium chemistry. A facile one-step synthesis of alkyl aryl selenides from alcohols. *The Journal of Organic Chemistry* **1976**, *41* (8), 1485-1486.
30. Nakamura, T.; Matsuyama, H.; Kamigata, N.; Iyoda, M., Synthesis of macrocyclic dilactones by cyclization of sulfonium salts. *The Journal of Organic Chemistry* **1992**, *57* (14), 3783-3789.
31. Overman, L. E.; Sato, T., Construction of epidithiodioxopiperazines by directed oxidation of hydroxyproline-derived dioxopiperazines. *Organic Letters* **2007**, *9* (25), 5267-5270.
32. Blaszykowski, C.; Dhimane, A. L.; Fensterbank, L.; Malacria, M., N-silyl-tethered radical cyclizations: A new synthesis of gamma-amino alcohols. *Organic Letters* **2003**, *5* (8), 1341-1344.
33. Duffault, J. M.; Tellier, F., A new route to the synthesis of bicyclo[3.3.2]nonene by radical cyclisation. *Synthetic Commun* **1998**, *28* (13), 2467-2481.
34. Godula, K.; Sames, D., C-H bond functionalization in complex organic synthesis. *Science* **2006**, *312* (5770), 67-72.
35. Wang, D.-H.; Yu, J.-Q., Highly Convergent Total Synthesis of (+)-Lithospermic Acid via a Late-Stage Intermolecular C–H Olefination. *J Am Chem Soc* **2011**, *133* (15), 5767-5769.

36. Davies, H. M. L., Recent Advances in Catalytic Enantioselective Intermolecular C–H Functionalization. *Angewandte Chemie International Edition* **2006**, 45 (39), 6422-6425.
37. Davies, H. M. L.; Beckwith, R. E. J., Catalytic Enantioselective C–H Activation by Means of Metal–Carbenoid-Induced C–H Insertion. *Chemical Reviews* **2003**, 103 (8), 2861-2904.
38. Davies, H. M. L.; Manning, J. R., Catalytic C–H functionalization by metal carbenoid and nitrenoid insertion. *Nature* **2008**, 451, 417.
39. Hinman, A.; Du Bois, J., A stereoselective synthesis of (-)-tetrodotoxin. *J Am Chem Soc* **2003**, 125 (38), 11510-11511.
40. Ye, T.; Mckervery, M. A., Organic-Synthesis with Alpha-Diazocarbonyl Compounds. *Chemical Reviews* **1994**, 94 (4), 1091-1160.
41. Knorr, R., Alkylidenecarbenes, alkylidenecarbenoids, and competing species: Which is responsible for vinylic nucleophilic substitution, [1+2] cycloadditions, 1,5-CH insertions, and the Fritsch-Buttenberg-Wiechell rearrangement? *Chemical Reviews* **2004**, 104 (9), 3795-3849.
42. Wardrop, D. J.; Bowen, E. G., A formal synthesis of (+)-lactacystin. *Chemical Communications* **2005**, (40), 5106-5108.
43. Taber, D. F.; Christos, T. E.; Neubert, T. D.; Batra, D., Cyclization of 1,1-disubstituted alkenes to cyclopentenones. *Journal of Organic Chemistry* **1999**, 64 (26), 9673-9678.
44. Grainger, R. S.; Owoare, R. B., Selective 1,5-alkylidenecarbene insertion reactions on [3.2.1] oxabicyclic ethers: A new approach toward the AB ring system of ingenol. *Organic Letters* **2004**, 6 (17), 2961-2964.
45. Zahel, M.; Keßberg, A.; Metz, P., A Short Enantioselective Total Synthesis of (-)-Englerin A. *Angewandte Chemie International Edition* **2013**, 52 (20), 5390-5392.
46. Nicolaou, K. C.; Dong, L.; Deng, L. J.; Talbot, A. C.; Chen, D. Y. K., Synthesis of functionalized maoecrystal V core structures. *Chemical Communications* **2010**, 46 (1), 70-72.
47. Dagoneau, D.; Xu, Z.; Wang, Q.; Zhu, J., Enantioselective Total Syntheses of (-)-Rhazinilam, (-)-Leucomidine B, and (+)-Leuconodine F. *Angewandte Chemie International Edition* **2016**, 55 (2), 760-763.

48. Molander, G. A.; Hahn, G., Lanthanides in Organic-Synthesis .2. Reduction of Alpha-Heterosubstituted Ketones. *Journal of Organic Chemistry* **1986**, 51 (7), 1135-1138.
49. Smith, A. B.; Dunlap, N. K.; Sulikowski, G. A., Cuprate Additions to 5-Methoxycyclopentenones - a Novel Stereoelectronic Effect. *Tetrahedron Letters* **1988**, 29 (4), 439-442.
50. Castro, J.; Sorensen, H.; Riera, A.; Morin, C.; Moyano, A.; Pericas, M. A.; Greene, A. E., Asymmetric Approach to Pauson-Khand Bicyclization - Enantioselective Formal Synthesis of Hirsutene. *J Am Chem Soc* **1990**, 112 (25), 9388-9389.
51. White, J. D.; Somers, T. C., Total Synthesis of (+/-)-2-Desoxystemodinone - a Novel Hydroxyl-Assisted, Intramolecular Ene Reaction. *J Am Chem Soc* **1987**, 109 (14), 4424-4426.
52. Holton, R. A.; Crouse, D. J.; Williams, A. D.; Kennedy, R. M., A Mild Method for the Reductive Desulfurization of Alpha-Phenylthio and Alpha-Phenylsulfinyl Carbonyl-Compounds. *Journal of Organic Chemistry* **1987**, 52 (11), 2317-2318.
53. Nicolaou, K. C.; Kang, Q.; Ng, S. Y.; Chen, D. Y. K., Total Synthesis of Englerin A. *J Am Chem Soc* **2010**, 132 (23), 8219-8222.
54. Mino, T.; Masuda, S.; Nishio, M.; Yamashita, M., Synthesis of Lactones by Baeyer–Villiger Oxidation with Magnesium Monoperphthalate Hexahydrate. *The Journal of Organic Chemistry* **1997**, 62 (8), 2633-2635.
55. Mycock, D. K.; Glossop, P. A.; Lewis, W.; Hayes, C. J., A formal synthesis of (+)-lactacystin from 4-hydroxyproline. *Tetrahedron Letters* **2013**, 54 (1), 55-57.
56. Šarek, J.; Klinot, J.; Džubák, P.; Klinotová, E.; Nosková, V.; Křeček, V.; Kořínková, G.; Thomson, J. O.; Janošťáková, A.; Wang, S.; Parsons, S.; Fischer, P. M.; Zhelev, N. Z.; Hajdúch, M., New Lupane Derived Compounds with Pro-Apoptotic Activity in Cancer Cells: Synthesis and Structure–Activity Relationships. *J Med Chem* **2003**, 46 (25), 5402-5415.
57. Travis, B. R.; Narayan, R. S.; Borhan, B., Osmium Tetroxide-Promoted Catalytic Oxidative Cleavage of Olefins: An Organometallic Ozonolysis. *J Am Chem Soc* **2002**, 124 (15), 3824-3825.
58. Travis, B. R.; Sivakumar, M.; Hollist, G. O.; Borhan, B., Facile Oxidation of Aldehydes to Acids and Esters with Oxone. *Organic Letters* **2003**, 5 (7), 1031-1034.
59. Yan, J.; Travis, B. R.; Borhan, B., Direct Oxidative Cleavage of α - and β -Dicarbonyls and α -Hydroxyketones to Diesters with KHSO₅. *The Journal of Organic Chemistry* **2004**, 69 (26), 9299-9302.

60. Kawasaki, M.; Shinada, T.; Hamada, M.; Ohfuné, Y., Total synthesis of (-)-kaitocephalin. *Organic Letters* **2005**, 7 (19), 4165-4167.
61. Pellissier, H., Recent Developments in Asymmetric Aziridination. *Adv Synth Catal* **2014**, 356 (9), 1899-1935.
62. Antilla, J. C.; Wulff, W. D., Catalytic asymmetric aziridination with arylborate catalysts derived from VAPOL and VANOL ligands. *Angew Chem Int Edit* **2000**, 39 (24), 4518-+.
63. Moragas, T.; Churcher, I.; Lewis, W.; Stockman, R. A., Asymmetric Synthesis of Trisubstituted Aziridines via Aza-Darzens Reaction of Chiral Sulfinimines. *Organic Letters* **2014**, 16 (24), 6290-6293.
64. Huang, L.; Wulff, W. D., Catalytic Asymmetric Synthesis of Trisubstituted Aziridines. *J Am Chem Soc* **2011**, 133 (23), 8892-8895.
65. Hashimoto, T.; Nakatsu, H.; Yamamoto, K.; Watanabe, S.; Maruoka, K., Asymmetric Trisubstituted Aziridination of Aldimines and Ketimines using N- α -Diazoacyl Camphorsultams. *Chemistry – An Asian Journal* **2011**, 6 (2), 607-613.
66. Hashimoto, T.; Nakatsu, H.; Yamamoto, K.; Maruoka, K., Chiral Brønsted Acid-Catalyzed Asymmetric Trisubstituted Aziridine Synthesis Using α -Diazoacyl Oxazolidinones. *J Am Chem Soc* **2011**, 133 (25), 9730-9733.
67. Deiana, L.; Dziedzic, P.; Zhao, G. L.; Vesely, J.; Ibrahim, I.; Rios, R.; Sun, J. L.; Cordova, A., Catalytic Asymmetric Aziridination of α,β -Unsaturated Aldehydes. *Chem-Eur J* **2011**, 17 (28), 7904-7917.
68. Sevvana, M.; Vijayan, V.; Zweckstetter, M.; Reinelt, S.; Madden, D. R.; Herbst-Irmer, R.; Sheldrick, G. M.; Bott, M.; Griesinger, C.; Becker, S., A ligand-induced switch in the periplasmic domain of sensor histidine kinase CitA. *J Mol Biol* **2008**, 377 (2), 512-523.
69. Campbell, N. E.; Sammis, G. M., Single-Electron/Pericyclic Cascade for the Synthesis of Dienes. *Angewandte Chemie International Edition* **2014**, 53 (24), 6228-6231.
70. Dolomanov, O. V.; Bourhis, L. J.; Gildea, R. J.; Howard, J. A. K.; Puschmann, H., OLEX2: a complete structure solution, refinement and analysis program. *J Appl Crystallogr* **2009**, 42, 339-341.
71. Sheldrick, G. M., A short history of SHELX. *Acta Crystallogr A* **2008**, 64, 112-122.
72. *Software for the Integration of CCD Detector System Bruker Analytical X-ray Systems*, Bruker axs: Madison, WI, after 2013.

73. Derecka, K.; Sheldrick, E. L.; Wathes, D. C.; Abayasekara, D. R. E.; Flint, A. P. F., A PPAR-independent pathway to PUFA-induced COX-2 expression. *Mol Cell Endocrinol* **2008**, *287* (1-2), 65-71.

Chapter IV:
Diastereoselective halonium initiated spiroketalization;
towards the total synthesis of Obtusin

IV-1 Introduction; structural features of spiroketal moiety

A large number of structurally diverse bioactive natural products found in insects, plants, bacteria and marine sources contain a spiroketal moiety. Spiroketal are often the source of bioactivity for molecules bearing this functionality.² Furthermore, the advantageous pharmacophoric properties of this functional group for drug discovery have led to an interest in the study and synthesis of spiroketals.²⁻¹⁰

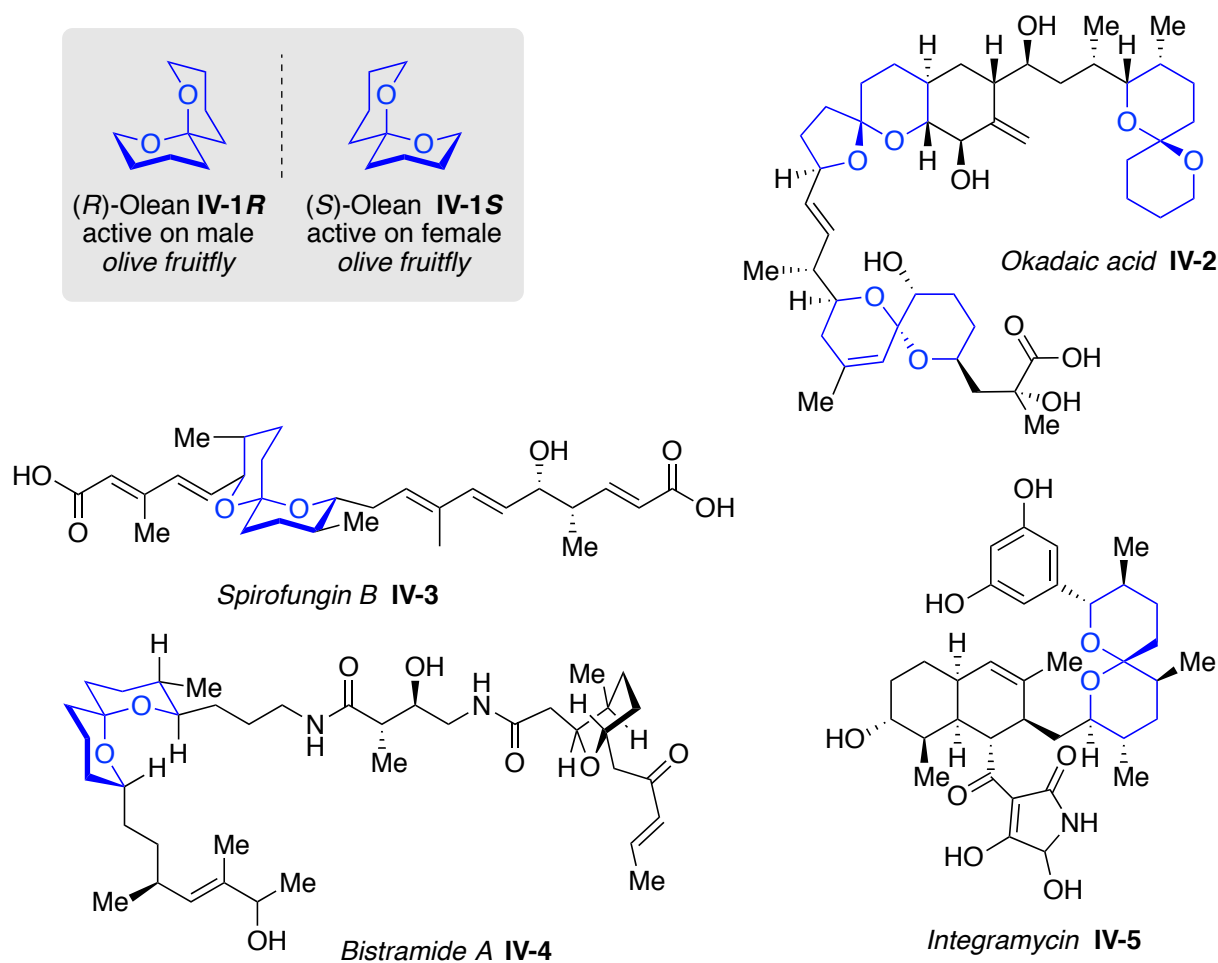


Figure IV-1. Spiroketal moiety embedded in the structure of natural products.

Most spiroketal frameworks found in natural products belong to the 6,6-, 5,6- or 5,5-spiroketal structural categories (Figure IV-1). In fact, the simplest 6,6-spiroketal, Olean **IV-1**, is the female-produced sex pheromone of the olive fruit fly.¹⁰ Okadaic acid **IV-2**,

Spirofungin **IV-3**, Bistramide A **IV-4** and Integramycin **IV-5** are just a few examples of natural products that contain spiroketal moieties in their highly functionalized skeletons (Figure IV-1). From the structural standpoint, spiroketals are members of the acetal containing molecules in which the carbon bearing the two carbon-oxygen single bonds (acetal carbon) is in the junction of two rings.

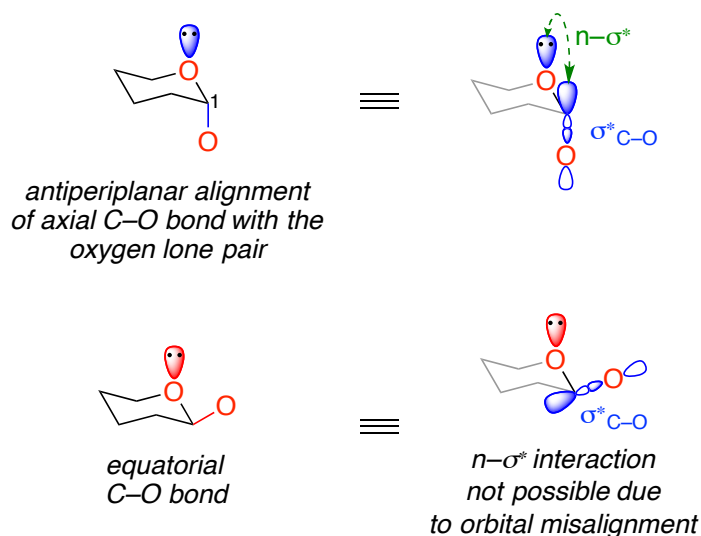


Figure IV-2. Anomeric effect, principle and structural requirements.

The structural feature of spiroketals leads to its special reactivity as the result of the anomeric effects. The term “anomeric effect” refers to the tendency of an electronegative group at the anomeric center (C_1) of a pyranose ring to occupy an axial rather than an equatorial position, despite unfavorable steric repulsions (Figure IV-2). As illustrated in Figure IV-2, anomeric stabilization finds its origin in the interaction between one of the lone pairs on the oxygen atom and the σ^* orbital of the C–O bond. The antiperiplanar alignment of the interacting orbitals can take place when a group is the axial position. The extent of anomeric stabilization is estimated to be in the range of 1.4 – 2.4 kcal/mol. Nonetheless the steric parameter or other molecular forces can obscure the anomeric

stabilization. In a 6,6-spiroketal framework four different arrangements can be identified with regards to the number of anomeric stabilization. As such, one structure with two anomeric interactions, two forms with one anomeric relationship and one with no anomeric alignments are possible (Figure IV-3). The structure with two anomeric relationships is the thermodynamic spiroketal if the anomeric stabilizations are not compromised by other steric parameters.³

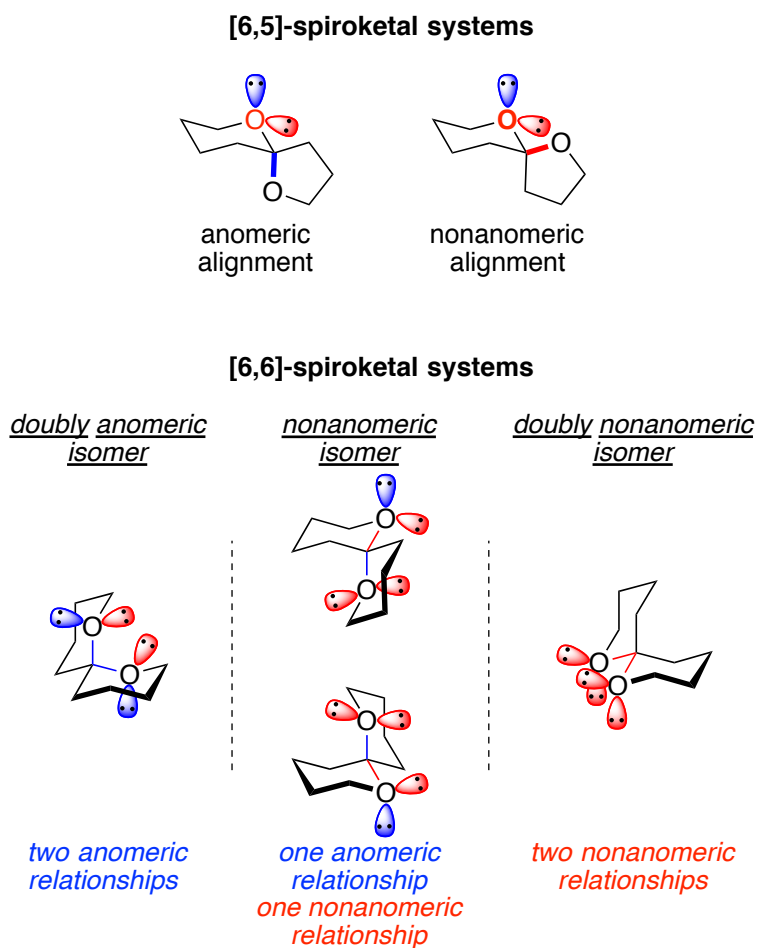


Figure IV-3. The anomeric arrangements in 6,5- and 6,6-spiroketal frameworks.

Not surprisingly, the biochemical applications and structural architecture of spiroketals have attracted vast synthetic efforts over the past few decades. To date, several elegant strategies towards stereoselective construction of these carbocyclic cores

have been reported.²⁻⁴ However, the synthesis of halogenated spiroketal still remains ill explored.¹¹⁻¹⁵ Encouraged by our endeavors in halofunctionalization of olefins, we set out to develop an efficient and robust procedure to access halogenated spiroketals in a diastereoselective fashion.

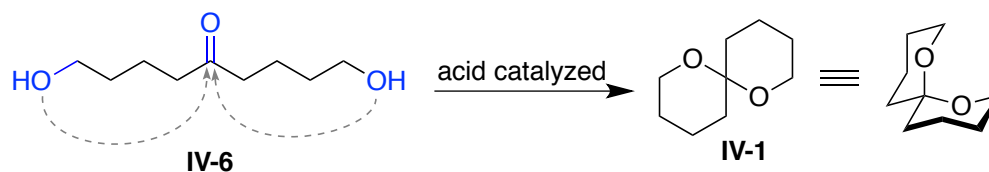
IV-2 Chemical synthesis of spiroketals

The anomeric carbon of the spiroketal moiety is at the ketone oxidation level; hence, the most general approach to access these motifs involves acid catalyzed acetal formation by a pendant diol onto the incipient ketone in **IV-6** (Figure IV-4a).² In this acetalization reaction, the most stable spiroketal product, which is usually the double anomeric spiroketal, can be readily obtained. Since most of the naturally occurring compounds contain a double anomeric spiroketal moiety, the aforementioned acid catalyzed dehydration approach has been extensively utilized to access numerous natural products. Furthermore, the selectivity of the acid catalyzed spiroketalization can be changed by the stereo-defined functionalities along the acyclic chain of the dihydroxy ketone.³ As illustrated in Figure IV-4b, Schreiber has demonstrated that beta diketone **IV-7** with three epimerizable stereocenters can lead to the formation of spiroketal **IV-8** with complete diastereoselectivity.¹⁶ In this reaction the stereodefined centers (highlighted in blue in **IV-7**), determine the course of the reaction. The methyl on the alpha position to carbonyl can be epimerized to give access to a single diastereomer **IV-8**.

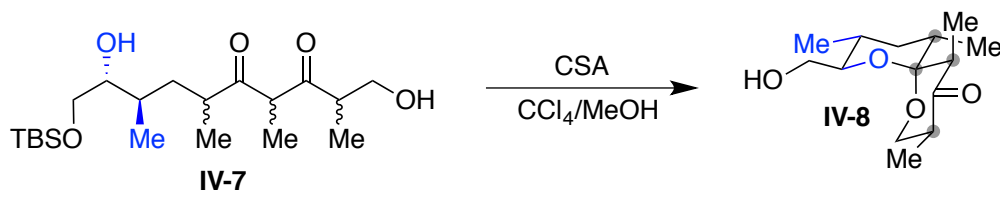
Another approach that allows control over the stereoselectivity in the cyclization event, involves protonation of a dihydropyranyl moiety **IV-9**, leading to the oxocarbenium

intermediate (**IV-10**) followed by interception of this intermediate by a tethered alcohol. In this strategy, the well-defined behaviors of oxonium embedded in a six-membered ring (axial attack) guides the trajectory of the incoming alcohol nucleophile to furnish spiroketal formation (Figure IV-4c).²⁻³

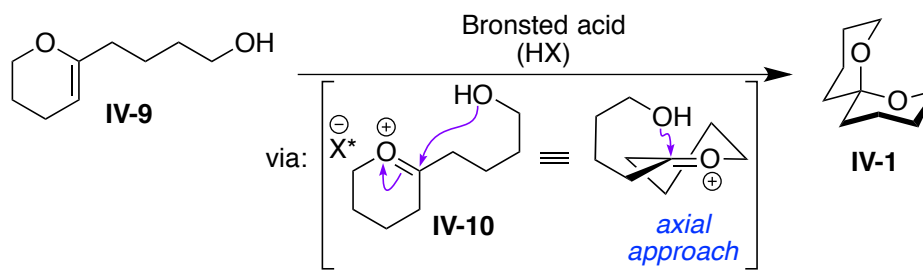
a. general spiroketalization reaction of keto-diols



b. Schreiber's dynamic diastereoselective spiroketalization



c. spiroketalization via protonation of DHP core



d. our approach, halonium initiated spiroketalization

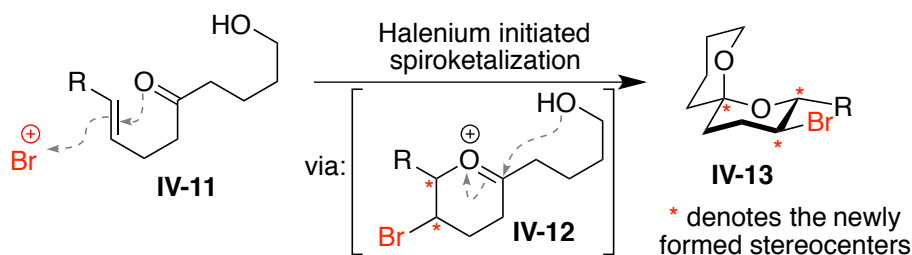


Figure IV-4. Different approaches to access the spiroketal moiety.

We envisioned arriving at a similar oxonium intermediate **IV-12** via activation of an olefin with a halonium, and using a ketone as the nucleophile in **IV-11** (Figure IV-4d). The

well-defined behaviors of the oxonium embedded in **IV-12** would then lead to the diastereoselective formation of spiroketal **IV-13**. The latter oxacrbinium intermediate embedded in a six-membered ring has been utilized by a few researchers to successfully develop enantioselective syntheses of spiroketals. In this respect, List and coworkers have reported the first direct synthesis of spiroketals in a catalytic enantioselective manner via protonation of dihydropyranyl **IV-9** (Figure IV-5).¹⁰ They employed the Brønsted acid catalyst **IV-14**, which contains a highly constrained binding pocket to give rise to the desired enantioselectivity during the spiroketalization event. The latter methodology gives access to various spiroketal frameworks with high enantioselectivity.

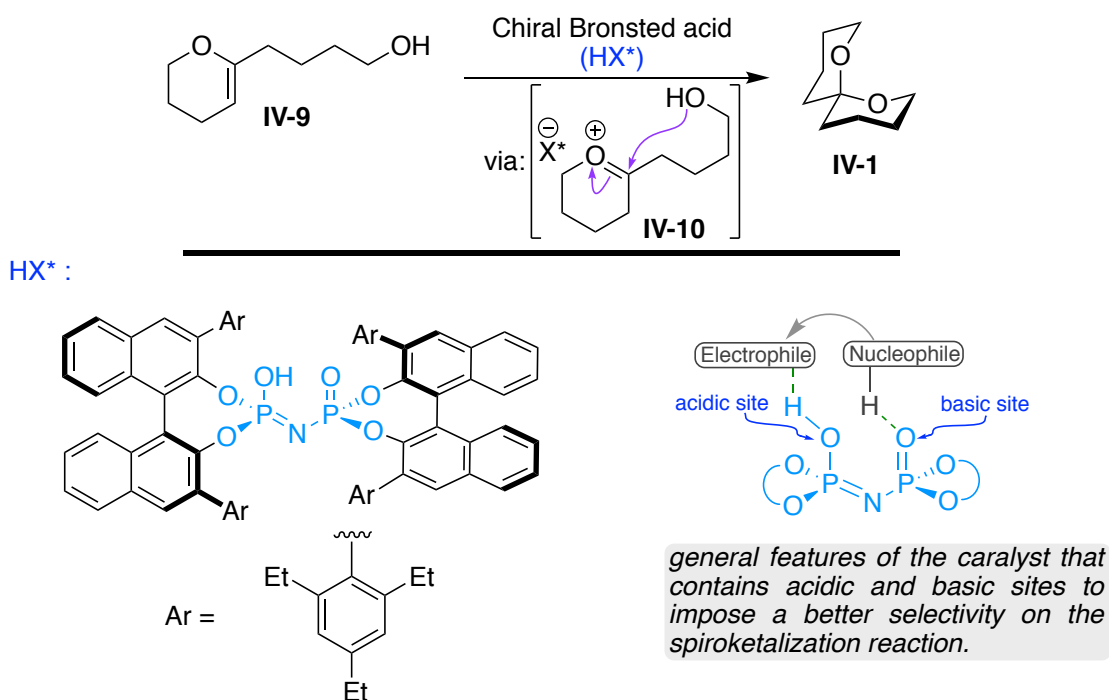


Figure IV-5. List's approach to access the spiroketal moiety in an enantioselective fashion.

In a seminal report, the Nagorny group has used a similar dihydropyranyl moiety as a precursor for enantioselective spiroketalization utilizing a BINOL-based chiral phosphoric acid (Figure IV-6).¹⁷ In their procedure, a tertiary alcohol intercepts the oxocarbenium

intermediate *en route* to the spiroketal formation (Figure IV-6). They have further investigated the mechanism of their spiroketalization reaction as well as the origin of the selectivity through experimental and computational studies. Their results revealed a highly diastereoselective *syn*-selective protonation and nucleophilic addition mechanism in the course of spiroketalization (Figure IV-6).¹⁸

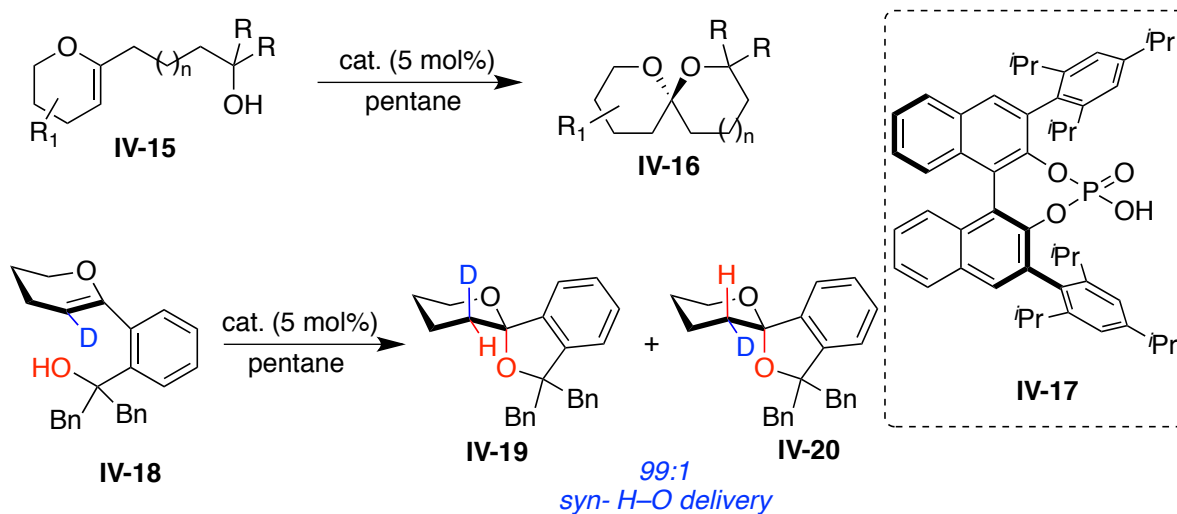


Figure IV-6. Nagorny's approach to access spiroketals in an enantioselective fashion.

Another elegant strategy to forge the spiroketal framework is reported recently by Carreira and coworkers.¹⁹ In this orthogonal approach, the hydroxyketone derivative **IV-22** undergoes formation of π -allyl complex in the presence of iridium-(P, olefin) complex (Figure IV-7). The ketone which is in equilibrium with its hemiacetal moiety via the pendent hydroxyl group, exposes a nucleophile for interception of the metal-allyl complex, consequently forming the spiroketal framework. The chirality of the phosphoramidite based ligands determine the face selectivity of asymmetric allylic substitution. Mutarotation of the equilibrating hemiacetal intermediate provides a mechanism to set the

stereochemistry on the acetal center under the influence of the chiral ligand (Figure IV-7).

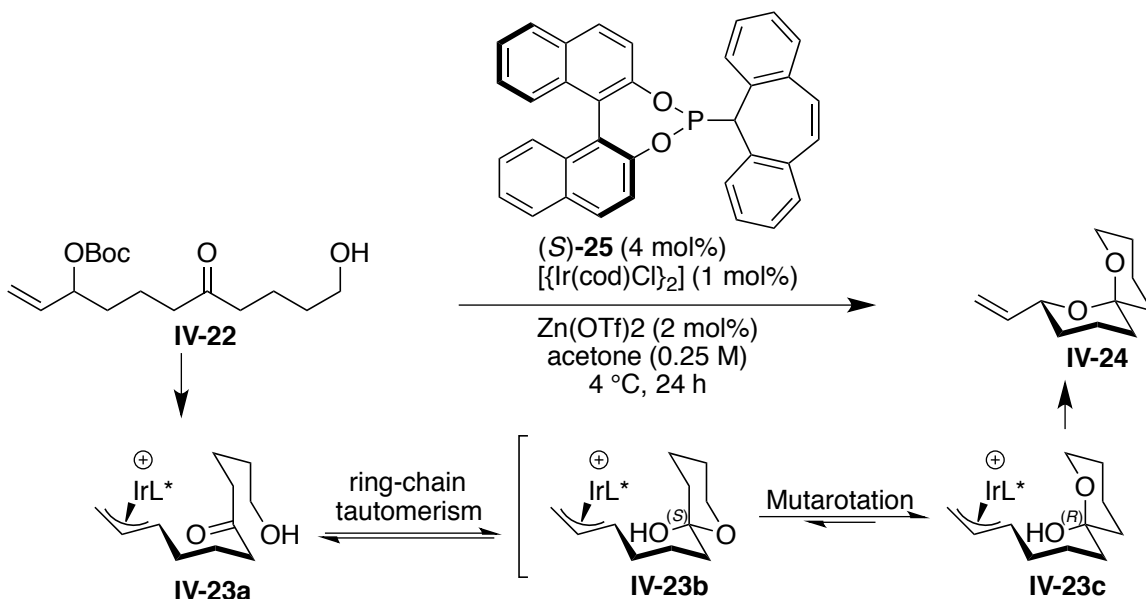


Figure IV-7. Carreira's approach to access spiroketals in an enantioselective fashion.

Despite excellent advances in the spiroketalization reaction, synthesis of halogenated spiroketals is not well explored. Halogenated natural products are frequently encountered. In fact, more than 5000 halogenated natural products had been discovered as of 2011.²⁰ Some of these halogenated natural products contain the spiroketal moiety in their skeleton (Figure IV-8).²¹ A robust and diastereoselective synthesis of halogenated spiroketals can provide a route towards the total synthesis of these compounds.

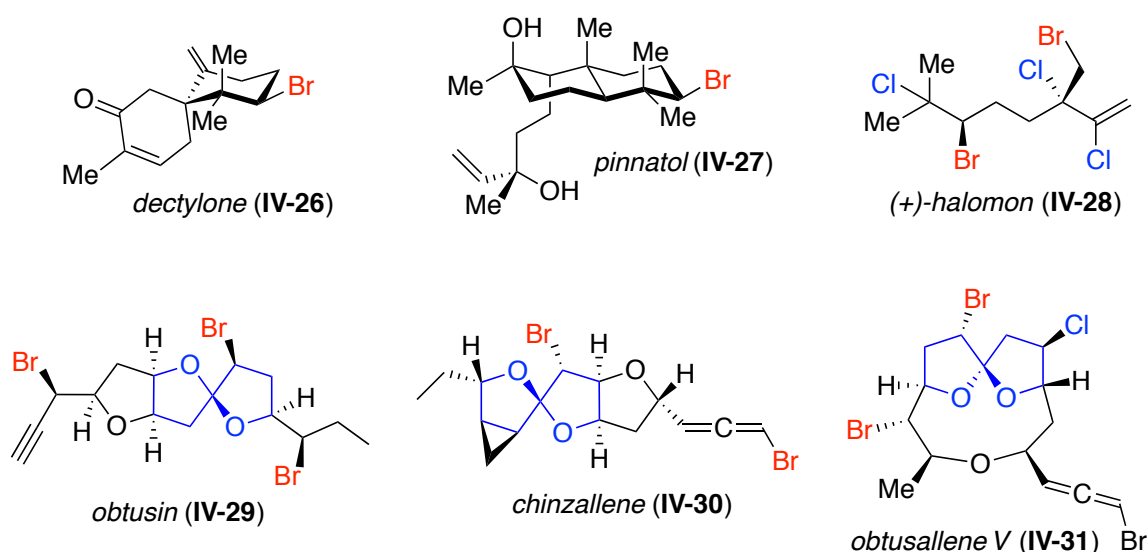


Figure IV-8. Examples of halogenated natural products. The halogenated spiroketals are highlighted in blue.

IV-3 Development of halenium initiated spiroketalization

Our approach for the synthesis of halogenated spiroketals stems from our group's interest in the halofunctionalization of olefins. So far, we have disclosed several methodologies for functionalization of olefins.^{1, 22-25} These reactions are generally initiated by an active halenium source that adds to olefins, initiating further functionalization (Figure IV-9). Enantioselective chlorofunctionalization of the unsaturated carboxylic acids **IV-32** that leads to the synthesis of chiral chlorolactones **IV-33** was our introductory methodology to this field.²⁴ This report stands as the first asymmetric chlorofunctionalization of olefin that was empowered by the unique catalytic effect of the dimer cinchona alkaloid chiral catalyst [DHQD₂PHAL].²⁶ In a similar strategy, the halofunctionalization of unsaturated amides gave access to chiral halogenated oxazoline products.²²⁻²³ Our mechanistic studies led to the interrogation of the face selectivity of the halenium and the nucleophile addition via extensive deuterium labeling experiments. In this investigation, the relative and absolute selectivity of the incoming halenium and

nucleophile were investigated. These studies revealed that *syn* or *anti* addition across the olefin depends on the nature of the nucleophile and all halocyclization reactions investigated, the chloronium face selectivity was the same.²³

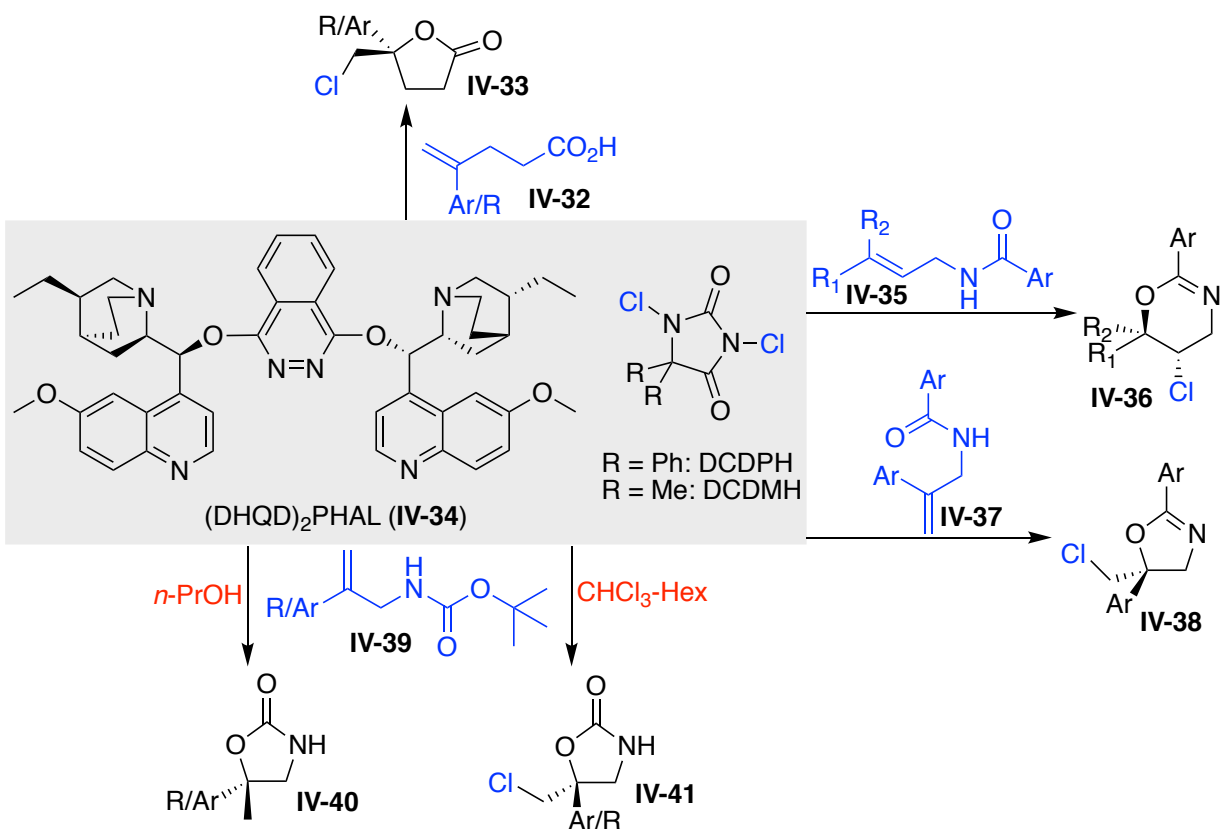
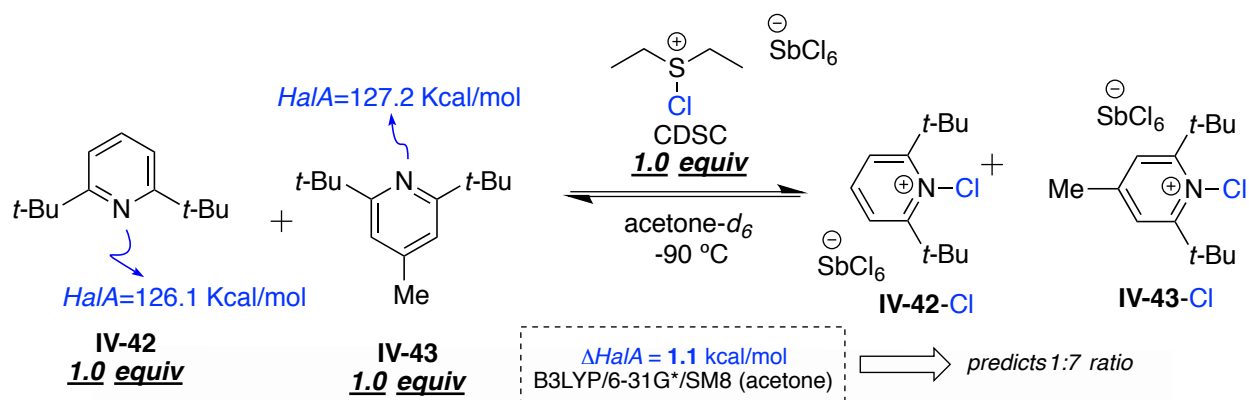


Figure IV-9. Some of the developed methodologies by our group in the field of halofunctionalization of olefins.

During the development of halofunctionalization reactions, we realized the need to introduce a parameter that define the affinity of various functional groups for absorbing a halogen. Therefore, a new scale that defines the thermodynamic tendency of a given nucleophile to capture the halonium ion was introduced.¹ The halonium affinity (HalA) scale ranks various acceptors (olefins for instance) embedded in a molecule based on their ability to stabilize a “free halonium ion”, thus providing a mean for prediction of the path of reactions and product distributions.



integral ratio of **A-Cl**:**B-Cl** = 12:88 ~ 1:7.3

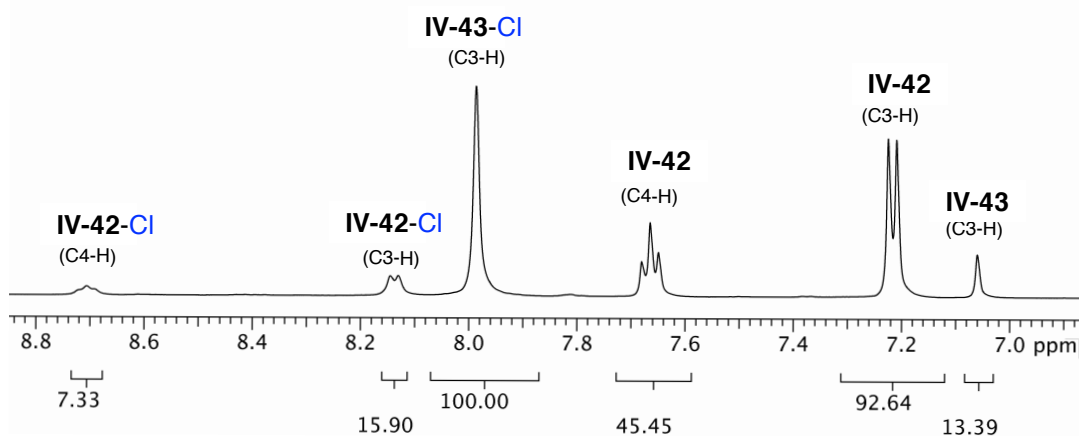


Figure IV-10. Experimental validation of the halenium affinity (HalA).¹

The direct implication of the halenium affinity can be experimentally monitored.¹ It was noted that when equimolar ratio of two pyridines with different halenium affinities are subjected to a competitive reaction with one equivalent of chlorenium ion, the distribution of the chlorinated pyridines can be observed with H-NMR at low temperature (Figure IV-10). The ratio of the two pyridinium products is in agreement with the predicted ratio from the computationally calculated HalA values. In this study the pyridine with a methyl group at the para position **IV-43** has higher tendency to capture the chlorenium leading to **IV-43-Cl**. This provides a predictive tool for the course of a reaction, as well as it can be

utilized to design new reactions and interrogate the mechanism of halogenation reactions.

Parametrization of the affinity of olefins for halenium capture led to a revised mechanistic understanding of halofunctionalization of olefins. In the classical assumptions the role of the nucleophile in the halofunctionalization of olefins is neglected. However, empowered by the HalA, our group was able to demonstrate that the halenium affinity of an olefin can dramatically affect the role pendent nucleophile in the course of the reaction.²⁷ We noted a direct and strong correlation between the rate of halofunctionalization and the strength of the nucleophile (Figure IV-11). Thus, the nucleophile is involved in the halenium capture by the olefin. We proposed nucleophile-assisted alkene activation (NAAA), in which the preorganization of the olefin with the tethered nucleophile facilitates the halofunctionalization reaction.²⁷ As such, a stronger nucleophile (carboxylate anion in this instance) exposes a more reactive olefin for halofunctionalization reaction (Figure IV-11).

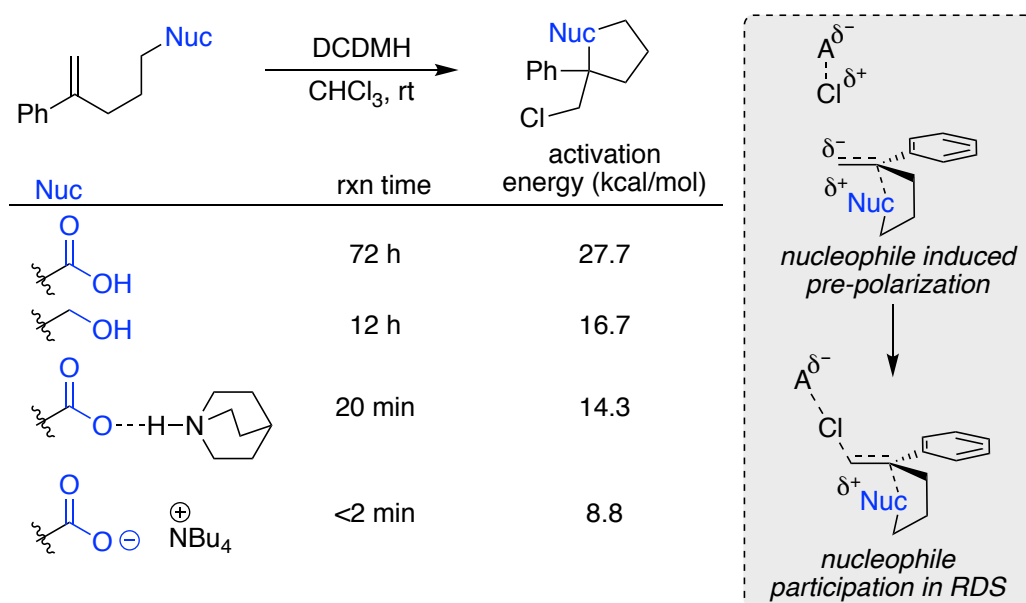


Figure IV-11. The effect of nucleophile on the olefin halofunctionalization, demonstration of nucleophile-assisted alkene activation (NAAA).²⁷

IV-4 Development of mono and di-brominated spiroketalization reaction

We sought to investigate the halofunctionalization with a ketone as the tethered nucleophile. The latter reaction would result in formation of oxocarbinium species that can lead to spiroketals if intercepted by a tethered alcohol moiety. Ketone **IV-11** bearing both alcohol and olefin was envisioned to undergo halonium (bromenium) capture with the aid of the ketone functioning as a weak nucleophile (Figure IV-12). The latter event exposes a oxocarbenium intermediate that can be intercepted by the tethered alcohol to furnish the spiroketal. This would result in the generation of three stereocenters, nonetheless, with complete diastereoselectivity control (Figure IV-12).

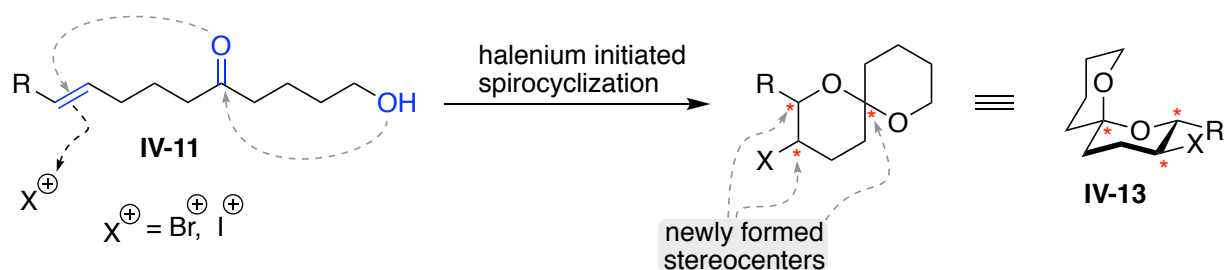


Figure IV-12. Our approach to access halogenated spiroketals.

Ketone **IV-44** was synthesized and subjected to the reaction with the bromenium source (Figure IV-13). To our surprise, we isolated spiroketal **IV-45** only as a minor product. The major product of the reaction was identified as the macrocycle **IV-46** structure was confirmed by X-ray crystallography (Figure IV-14). Despite the fact that synthesis of the macro-cyclic side product is not the main aim of our program, the current methodology can potentially be tuned to access this class of molecules that are challenging to synthesized by the known methods.²⁸⁻³¹ The product distribution of this reaction points to the fact that the ketone is most likely in a pre-equilibrium with the its hemiacetal **IV-44a** and **IV-44b**. Hemiacetal **IV-44a/b** exposes two nucleophilic oxygens

that can act as a nucleophile for interception of the activated olefin via the bromonium ion.

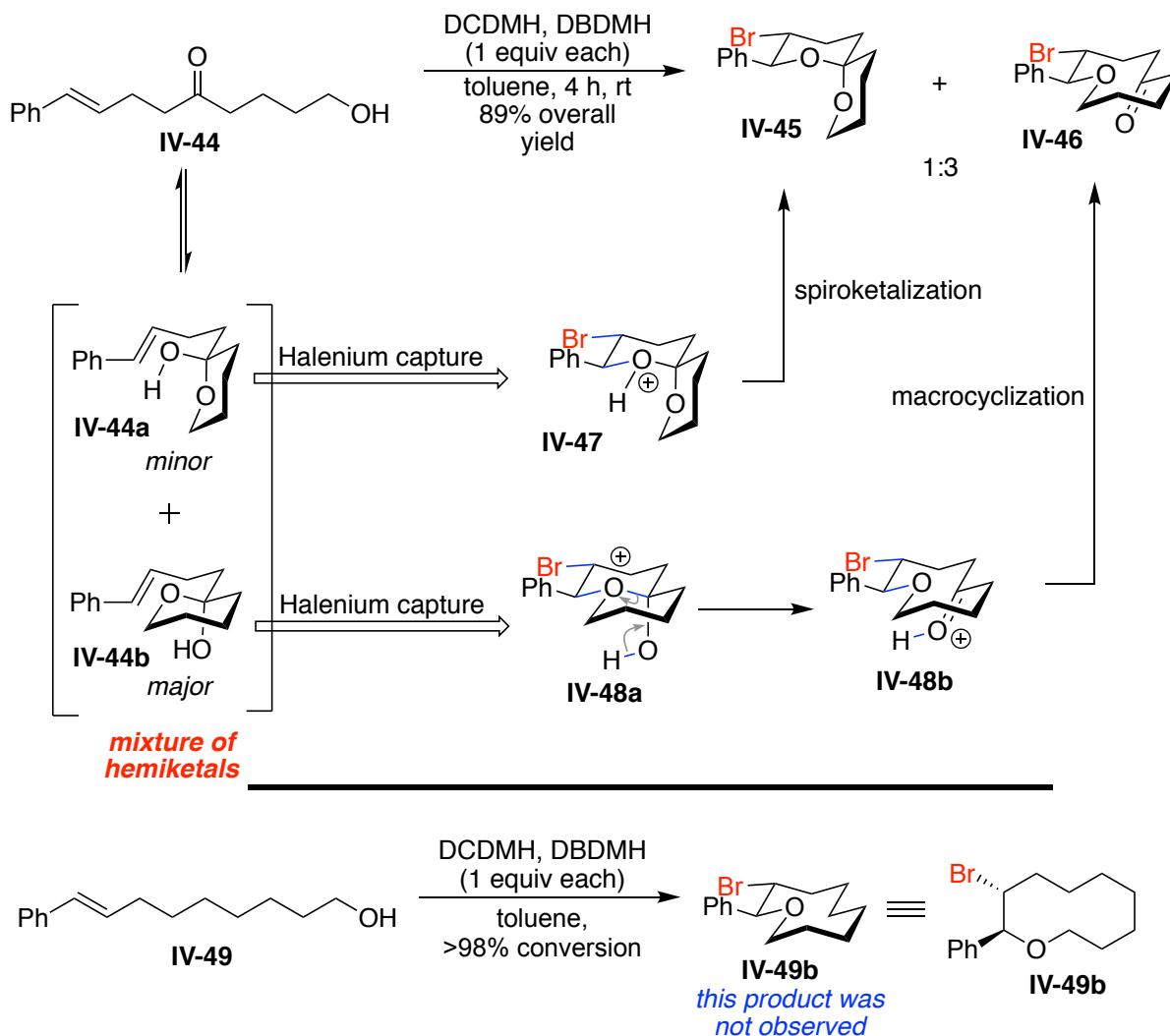


Figure IV-13. Bromo spiroketalization of ketone tethered to an unprotected alcohol.

In such a manner, if the hydroxyl group of the equilibrating hemiacetal **IV-44a** acts as the nucleophile, bromo spiroketal **IV-45** would form as product of the reaction. However, if the other oxygen of hemiacetal, which is imbedded in the six membered ring in **IV-44b** is the nucleophile, macrocyclic **IV-46** will form. To confirm that macrocycle **IV-46** originates from hemiacetal intermediate **IV-44a/b**, unsaturated alcohol **IV-49** was

synthesized and subjected to the same reaction conditions, however, macrocycle **IV-49b** was not obtained. The only difference between the alcohol and the keto-alcohol is the presence of the ketone moiety on the alkyl chain of keto-alcohol **IV-44** (Figure IV-13). The ketone functionality in **IV-44** can provide a route to facilitate the entropically less favorable pathway that leads to macrocycle **IV-46**. The presence of the equilibrating hemiacetal reduces the entropic barrier in comparison to the direct macrocyclization of **IV-49**. Presence of the hemiacetal is in agreement with Carreira's report shown in Figure IV-7. In order to circumvent this side product, we sought to protect the tethered alcohol, to prevent the formation of hemiacetal intermediates that lead to the macrocyclic product.

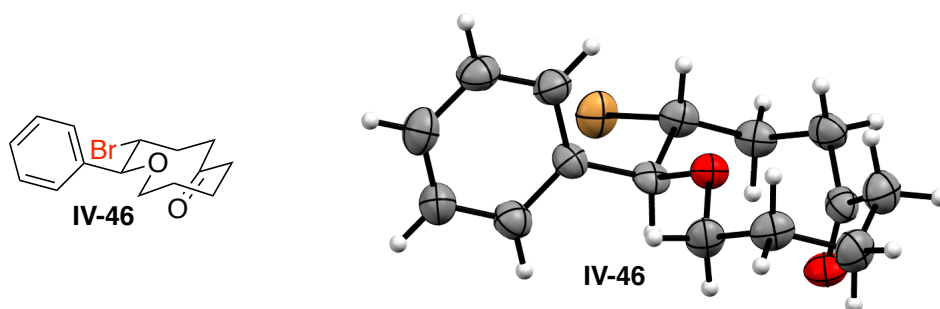


Figure IV-14. X-ray crystal structure of macrocyclic **IV-46**.

In pursuit of the appropriate agent, various protecting groups were screened. Most of the protecting groups did not allow the protected alcohol to form a spiroketal (Figure IV-15). When alcohol in **IV-50** was protected with MOM group, low conversion of the ketone to the spiroketal **IV-45** was observed. Employing THP as a protecting group improved the conversion of the reaction and the spiroketal was isolated in excellent yield and diastereoselectivity (Figure IV-15). Addition of ethanol was crucial for this reaction as it facilitates removal of the THP group from intermediate **IV-51**, furnishing spiroketal formation.

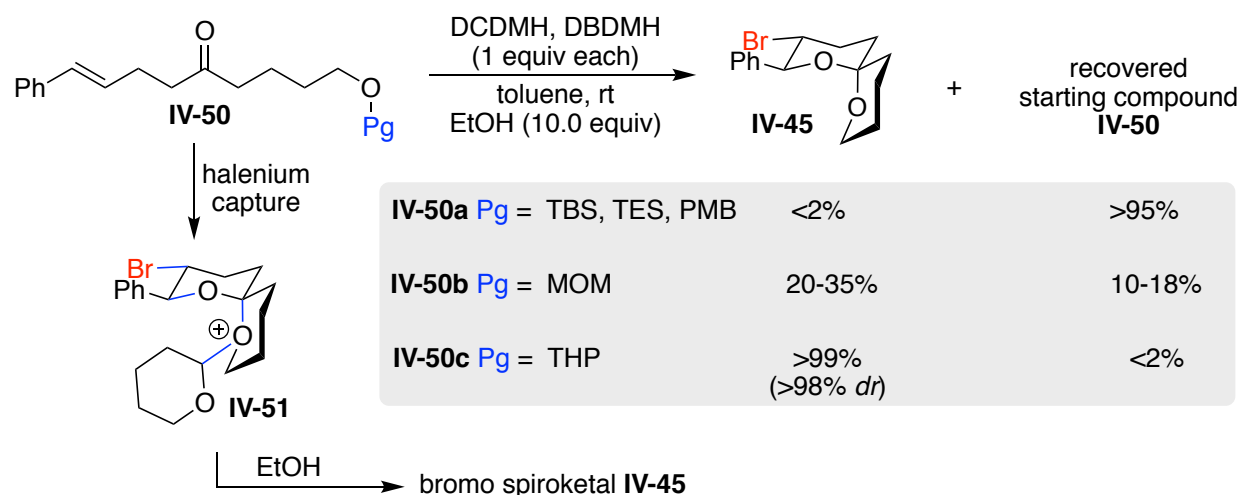


Figure IV-15. Bromo spiroketalization of ketone with a protected tethered alcohol.

This result was justified by the fact that the ketone is a weak nucleophile, thus it is incompetent to aid in the halo-functionalization of the olefin. However, introduction of an alcohol can improve the nucleophilicity of the ketone towards halo-functionalization of olefin. Of note, the putative NAAA pathway facilitated by the hydroxyl of the hemiacetal activates the olefin more than the parent ketone. The protection of the alcohol is required in order to avoid macrocyclization, as discussed above. The latter experimental results are in full agreement with the computationally obtained halonium affinities of the olefin in the presence of a ketone engaged as a hemiacetal with the pendent hydroxyl, in its free and protected forms (Figure IV-16).

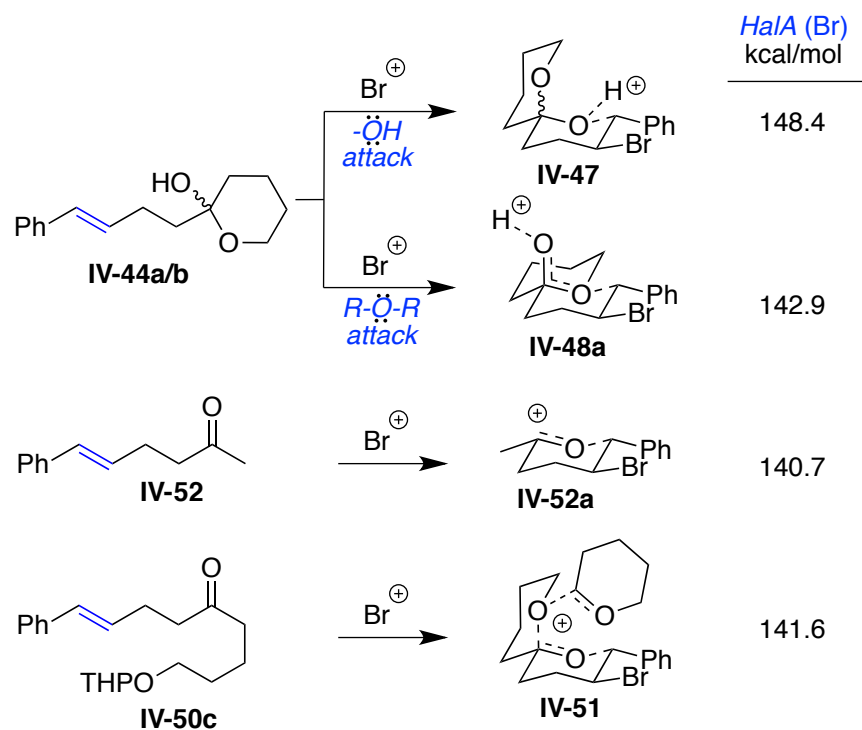


Figure IV-16. Computed *HalA* values for ketones bearing different groups.

As illustrated in Figure IV-16, ketone bearing a free alcohol, which is in equilibrium with its hemiacetal form, exposes two nucleophilic oxygens for halofunctionalization of the olefin. **IV-47** and **IV-48a** have higher *HalA* value as compared to methyl ketone **IV-52**. The methyl ketone that shows the lowest *HalA* value resembles substrates with protecting groups such as TES, TBS and PMB (Figure IV-15) that were incompetent to furnish spiroketalization. Ketone with THP as the alcohol's protecting group showed higher *HalA* as compared to the methyl ketone yet lower than **IV-47** and **IV-48a**. These data are in full agreement with the experimental results depicted in Figure IV-13 and IV-15. It must be noted that prototypical reagents such as N-bromosuccinimide and 1,3-dibromo-5,5-dimethylhydantoin, proved to be slow and less efficient for this transformation. Hence, we resorted to a more active bromonium source *e. i.* 3-bromo-1-chloro-5,5-

dimethylhydantoin, which was generated in situ by combining equimolar amounts of DBDMH and DCDMH.

To demonstrate the generality of this reaction, keto-alkenols shown in Table IV-1, incorporating the tetrahydropyranyl protection were subjected to the optimized conditions. Table IV-1 summarizes the results of halenium atom initiated cascade spiroketalizations that furnished the substituted 3-halo-1,7-dioxaspiro[5,5]undecanes (**45**, **53-60**) in a diastereoselective fashion. Modulating the electronic or steric profile of the substituents attached to the olefins in Table IV-1 did not make any significant difference to the overall reaction outcome. The corresponding [6,6]-spiroketals were obtained in excellent yields and diastereoselectivity. The relative stereochemistry in these halogenated spiroketals was established unequivocally by the crystal structure of product **IV-54** and NOESY analysis of **IV-45** (Figure IV-17).

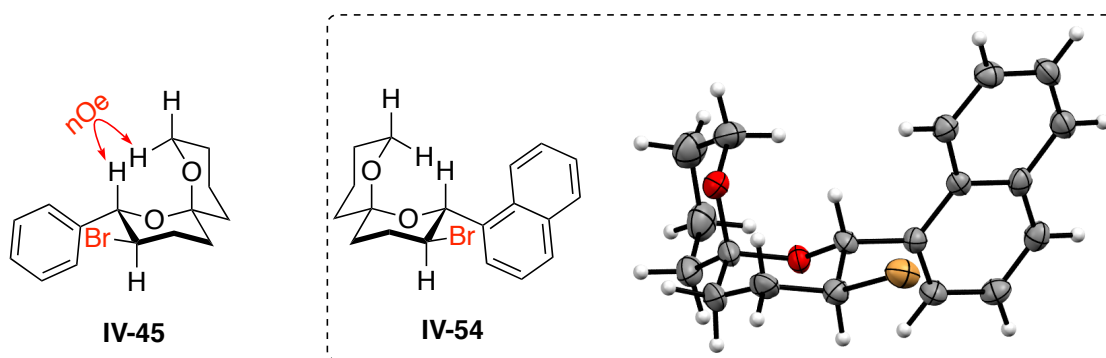


Figure IV-17. X-ray crystal structure of product **IV-54** and NOESY of **IV-45**.

As with the bromenium source, an efficient diastereoselective cascade spiroketalization could also be initiated using N-iodosuccinimide as an iodonium source (entry 2, Table IV-1). Several attempts to initiate the corresponding fluorofunctionalization led only to products of α -fluorination of the ketone, whereas chlorofunctionalization using

trichloroisocyanuric acid gave a complex mixture of undesired alcohol oxidation products resulting from the *in situ* oxidative deprotection of the -OTHP group.

Table IV-1. Substrate scope for halenium atom initiated diastereoselective spiroketalization.

entry ^a	R ¹	R ²	product	Yield ^b	<i>dr</i> ^c
1 ^d	Ph	H	IV-45	>99%	>98:2
2 ^e	Ph	H	IV-45-I	82%	>98:2
3	<i>β</i> -naphthyl	H	IV-53	93%	>98:2
4	<i>α</i> -naphthyl	H	IV-54	88%	>98:2
5	<i>p</i> -CH ₃ -C ₆ H ₄	H	IV-55	87%	>98:2
6 ^f	<i>o</i> -CH ₃ -C ₆ H ₄	H	IV-56	86%	>98:2
7 ^g	<i>p</i> -CH ₃ O-C ₆ H ₄	H	IV-57	65%	>98:2
8	<i>p</i> -F-C ₆ H ₄	H	IV-58	84%	>98:2
9	<i>p</i> -Ph-C ₆ H ₄	H	IV-59	83%	>98:2
10	Ph	CH ₃	IV-60	77%	>98:2

[a] Reactions were performed using 0.1 mmol of substrate. [b] Isolated yields. [c] *dr*s were estimated by ¹H NMR (500 MHz) analysis. [d] Reaction was performed on a 1.0 mmol scale. [e] Reaction was performed for 12 h at rt using 1.1 equiv *N*-iodosuccinimide as a halenium source. [f] After 3 h, conc. HCl (~10 mol%) was added and the reaction was continued for another 20 min prior to quench. [g] 1.1 equiv of NBS was employed as the bromenium source.

Substrate **IV-61** that undergoes a [6,5]-spiroketalization via the intermediacy of a similar six-membered oxocarbenium, furnishes the corresponding product as a single diastereomer (Figure 18). In contrast, a [5,5]-spiroketalization of the keto-alkenol **21** results in a 2:1 mixture of diastereomers. The latter observation is due to the skewed framework of [5,5]-spiroketals that unlike the [6,6]-spiroketals, does not benefit fully from the anomeric effect. Hence, during the formation of [5,5]-spiroketals, the diastereomeric transition states are not energetically biased enough to promote a significant product selectivity, without any external aid.

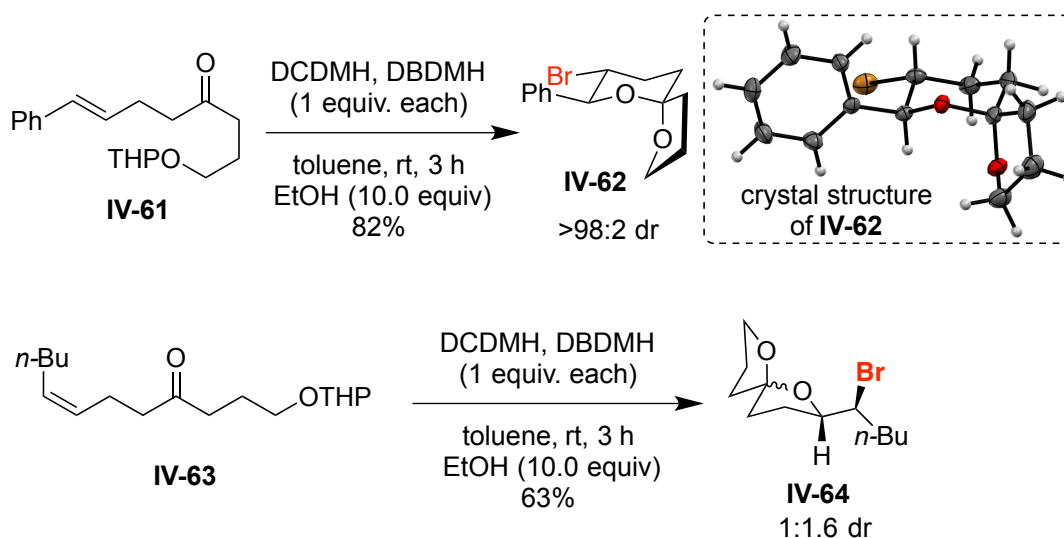


Figure IV-18. Synthesis of 5,6- and 5,5-spiroketal.

We also exploited the stereoelectronics associated with the 6-membered oxocarbenium towards a dual functionalization of the above keto-alkenols. As depicted in Figure IV-19, when ethanol was excluded from the reaction mixture, the oxocarbenium intermediate putatively undergoes α -deprotonation to generate vinyl ether **IV-61**. This intermediate can further proceed through bromonium capture leading to dibrominated **IV-62** that eventually furnishes product **IV-64**. The second bromonium is captured from a

pseudo-axial approach that leads to the high diastereoselectivity of the product. This dibromo-spiroketal scaffold is unique to the bioactive natural products derived from the family of *Laurencia obtusa* and others.^{13, 32-34}

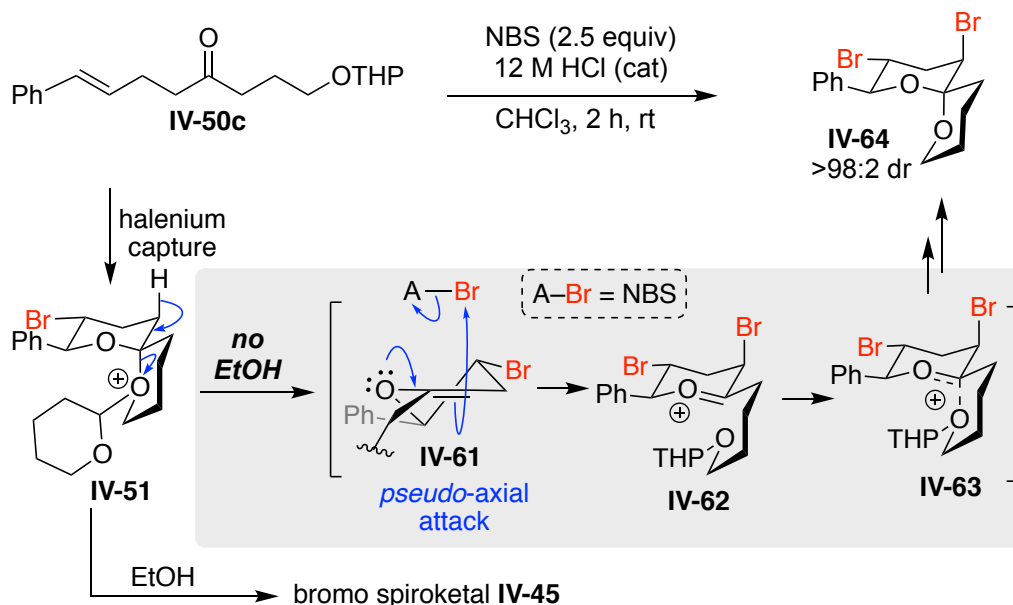


Figure IV-19. Dibromospiroketal formation by excluding ethanol from the reaction mixture.

Table IV-2 summarizes the results for a handful of keto-alkenols that were subjected to the optimized conditions for di-bromospiroketalization. Catalytic amount of HCl was necessary to furnish the desired transformation. Acid can potentially activate N-bromosuccinimide for the latter transformation. Moderate to excellent yields were obtained with various substituted keto-alkenols. As in the monobromo-spiroketalization, the sterics and electronics of the substituted olefins did not have a significant effect on the overall outcome. The relative stereochemistry was established by the crystal structure of **IV-67** (Figure IV-20). The [6,5]-spiroketalization was equally efficient as the [6,6]-spiroketalization (compare entries 1 and 2, Table IV-2), however the [5,5]-ketalization was less selective owing to the skewed stereoelectronics of the oxocarbenium embedded in

a 5-membered ring (entry 9).

Table IV-2. Diastereoselective dibromo spiroketalization

entry ^a	R ¹	R ²	(n, m)	product	Yield ^b	<i>dr</i> ^c
1 ^d	Ph	H	(2, 2)	IV-64	87%	>98:2
2 ^e	Ph	H	(1, 2)	IV-65	73%	>98:2
3	<i>β</i> -naphthyl	H	(2, 2)	IV-66	88%	>98:2
4	<i>α</i> -naphthyl	H	(2, 2)	IV-67	61%	>98:2
5	<i>p</i> -CH ₃ -C ₆ H ₄	H	(2, 2)	IV-68	74%	>98:2
6 ^f	<i>o</i> -CH ₃ -C ₆ H ₄	H	(2, 2)	IV-69	85%	>98:2
7 ^g	<i>p</i> -F-C ₆ H ₄	H	(2, 2)	IV-70	65%	>98:2
8	<i>p</i> -Ph-C ₆ H ₄	H	(2, 2)	IV-71	59%	>98:2
9	H	<i>n</i> -Bu	(1, 1)	IV-72	88%	2:1
10	CH ₃	CH ₃	(2, 2)	IV-73	70%	1:1

[a] Reactions were performed using 0.1 mmol of substrate. [b] Isolated yields. [c] *dr*'s were estimated by ¹H NMR (500 MHz) analysis. [d] Reaction was performed on a 1.0 mmol scale. [e] Reaction was performed for 12 h at rt using 1.1 equiv *N*-iodosuccinimide as a halonium source. [f] After 3 h, conc. HCl (~10 mol%) was added and the reaction was continued for another 20 min prior to quench. [g] 1.1 equiv of NBS was employed as a bromonium source.

The [6,6]-spiroketalization of the tri-substituted olefin in 19 furnished a 1:1 diastereomeric mixture as the energetics of the two conformers (ring flipping) in the corresponding enol-ether intermediate (similar to **IV-61** in Figure IV-19) are not biased due to the presence of the gem-dimethyl substitution.

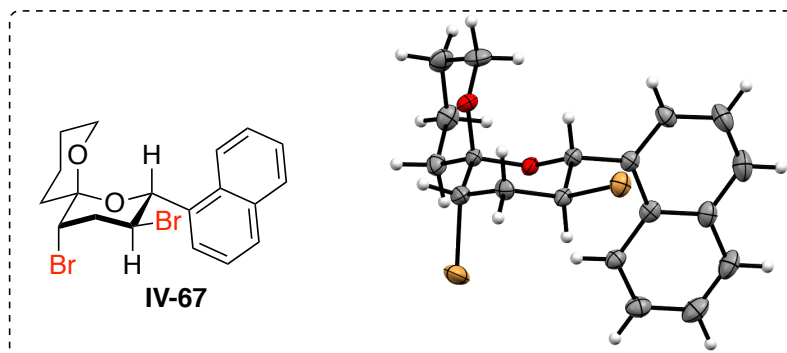


Figure IV-20. X-ray crystal structure of dibromo-spiroketal **IV-67**.

In summary, we have demonstrated the application of Halenium Affinity (HaIA) as a guiding tool towards modulation of nucleophilic strength, leading to a diastereoselective spiroketalization. Unaided ketones were found to be inefficient nucleophiles towards olefin activation; however, the tethered alcohol provided a handle to modulate the ketone's nucleophilic strength. Calculation of the HaIA values revealed the effect of tethered alcohol on the halogen affinity of the olefin. THP protected tethered alcohol proved to be optimal for the spiroketalization reaction. Additionally, the spiroketalization was rerouted to give access to the dibrominated spiroketals in a diastereoselective manner.

IV-5 Towards the total synthesis of Obtusin

IV-5-1 Introduction

With the successful development of bromo spiroketalization, especially the diastereoselective dibromo spiroketalization, we sought to utilize this methodology to access Obtusin **IV-74**, a natural product isolated in 1979 from the Mediterranean alga *Laurencia obtusa*.³³⁻³⁴ From the structural standpoint, Obtusin contains eight contiguous stereocenters and a skeleton featuring three five-membered ether rings, two of which are part of a spiroketal moiety (Figure IV-21). This molecule poses a synthetic challenge and its chemical synthesis has not been reported thus far. Our strategy towards Obtusin takes advantage of the crucial rule of protecting groups to access the desirable selectivity in forging the skeleton of this molecule. We will begin with a molecule from chiral pool followed by sequential diastereoselective synthetic steps towards obtaining the target.

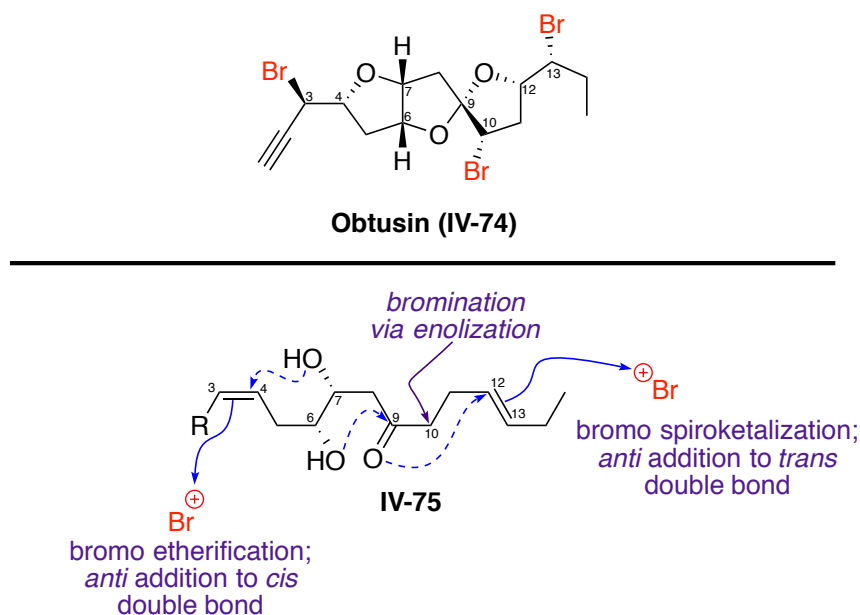


Figure IV-21. Structure of Obtusin and its proposed biogenesis.

Our retrosynthetic approach to Obtusin is inspired by the proposed biosynthesis of this molecule. Obtusin can be unraveled to the linear polyketide structure **IV-75** (Figure 22).³⁵ The stereochemistry at the chiral centers indicates *anti* addition across a *trans* C12-C13 double bond and a *cis* C3-C4 double bond. Based on our retrosynthetic approach, **IV-76** can be obtained from **IV-77** using our dibromo spiroketalization. A bromo etherification reaction can be envisioned to construct the THF ring in **IV-77** from the linear carbon chain of **IV-75**. The carbon chain skeleton of **IV-75** with the central chiral diol will originate from the addition of the appropriate carbon chains to the chiral diepoxide **IV-78** (Figure 22).

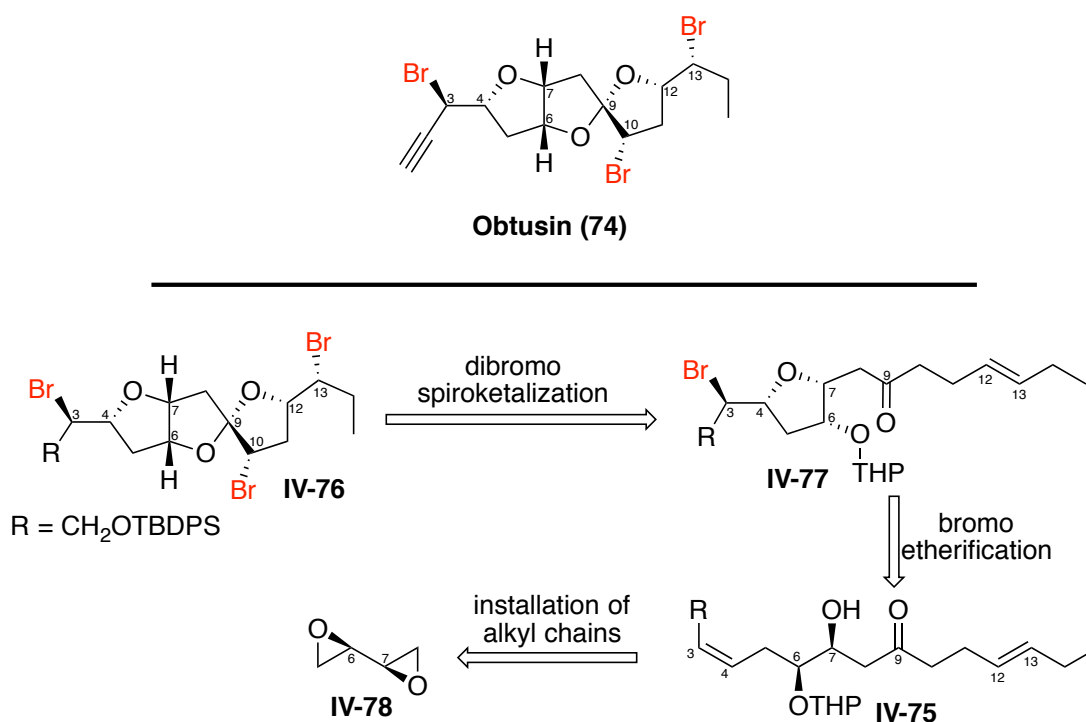


Figure IV-22. Retrosynthetic approach to access Obtusin featuring dibromo-spiroketalization and bromo-etherification steps.

IV-5-2 Progress towards the total synthesis of Obtusin

As illustrated in Figure IV-23, our synthesis of Obtusin commences with enantio-pure diepoxide **IV-78** that contains the correct stereochemistry on the central di-carbinol centers (C6 and C7). Synthesis of diepoxide **IV-78** is reported and amenable to multi gram scale starting from *D*-(–)-tartaric acid.³⁶⁻³⁷ As illustrated in Figure IV-23, *D*-(–)-tartaric acid is converted to the enantio-enriched diepoxide **IV-78** in five steps with high overall yield.³⁶⁻³⁷ This epoxide is the lynchpin for installation of the rest of the carbon atoms of the natural product. To this end, a sequential selective opening of the diepoxide was planned. Alkynyl anion of **IV-79**, as the surrogate for the *cis* olefin, was added to diepoxide **IV-78**.³⁸ Mono-epoxide **IV-80** was isolated in moderate yield. Competing diol formation that originated from double addition of the alkynyl anion to the diepoxide **IV-78** was the unavoidable side product in this reaction. The alkyne functionality in **IV-80** was then partially reduced to the corresponding *cis* double bond in **IV-81** in nearly quantitative yield. The optimization of the reduction reaction showed that longer reaction time would result in the formation of a complex mixture (possibly over reduced product). Thus, a 30-minute reaction time was identified as optimal where the reduction is complete and side product formation is minimal. The alcohol of **IV-81** was then protected as a THP. As outlined in the previous section, this protecting group is essential for the dibromo spiroketalization reaction. This protection led to a separable 2:1 diastereomeric mixture. The major diastereomer was carried in the following steps to avoid complications in NMR assignment, although the stereochemistry is inconsequential, as it is not present in the final target (Figure IV-23).

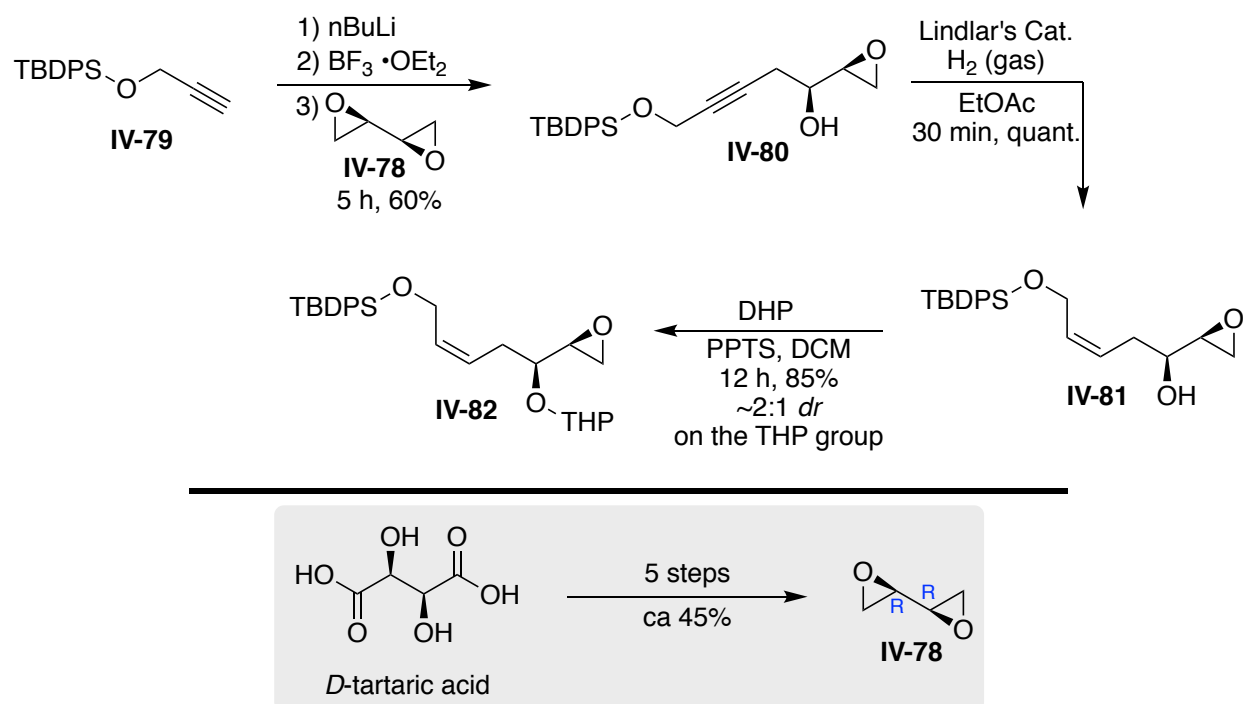


Figure IV-23. Installation of the *cis* olefin, access to epoxy alcohol **IV-91**.

We then turned our attention to opening of the epoxide in **IV-82** in order to install the ketone moiety along with introducing the rest of the alkyl chain (Figure IV-24). Our first was to use dithiane **IV-83**. However, under various reaction conditions, the target alcohol **IV-84** was not formed. We realized that the reaction of dithiane with epoxide **IV-82** requires addition Lewis acids (such as $\text{BF}_3 \cdot \text{Et}_2\text{O}$) to catalyze the reaction. Nonetheless, using Lewis acids to facilitate the latter transformation resulted in the removal of the dithiane group and formation of other side products. We next took a different approach for opening of this epoxide as a path for installation of the ketone moiety, namely, to use a nitrile as the nucleophile. Epoxide **IV-82** was readily reacted with potassium cyanide in methanol, yielding alcohol **IV-86** in good yield (Figure IV-24).³⁹

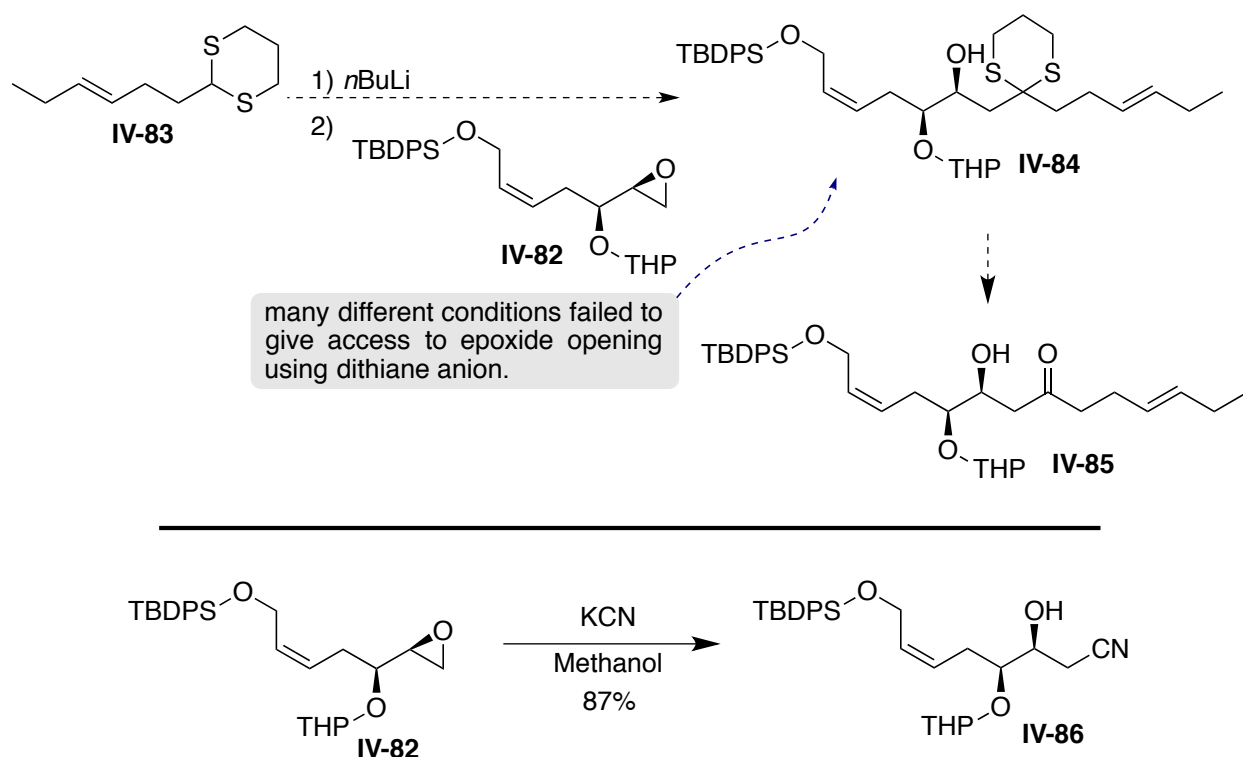
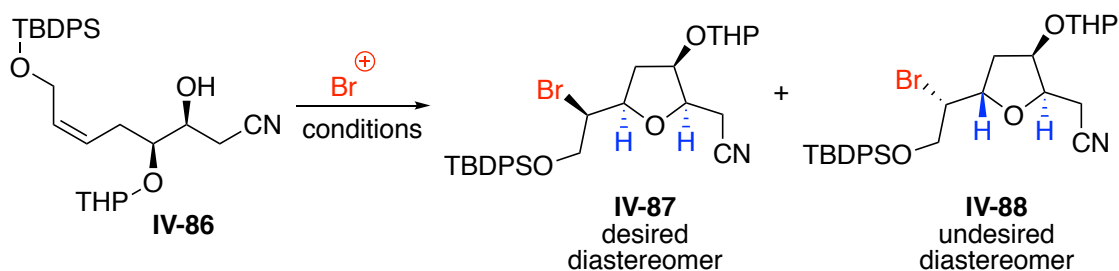


Figure IV-24. Installation of the ketone surrogate, towards bromo-etherification reaction.

With **IV-86** in hand, bromo-etherification of the *cis* olefin was targeted. As illustrated in Table IV-3, bromo etherification of **IV-86** resulted in the formation of diastereomeric tetrahydrofuran rings **IV-87** and **IV-88**. The latter result stems from the opposing face selectivity of the *cis* olefin in the bromo etherification step (*re* face attack leading to **IV-87** while *si* face attack yields **IV-88**). Reaction in DCM as the solvent and 2,4,4,6-tetrabromo-2,5-cyclohexadienone (TBCO) as the bromine source led to the formation of undesired diastereomer **IV-88** as the major diastereomer (>20:1 *dr*), (entry 1, Table IV-3).

Table IV-3: Bromo etherification of alcohol **IV-86**.



entry ^a	solvent	conversion ^b	<i>dr</i> (IV-96:IV-97) ^c
1	DCM	>99	1:20
2	toluene	>99	1:1.6
3	DMF	>99	1:1.6
4	methanol	>99	1:1.5
5	acetonitrile	>99	1:1.6
6	acetonitrile/TFE (1:1)	>99	1:1.7
7	THF:HMPA (50:1)	>99^d	(1:1)
8	THF:HMPA (50:1) ^e	>99	(1:1)
9	THF:HMPA (50:1) ^f	30	(1:1)
10	THF:HMPA (50:1) ^g	>99	(1:1)

[a] Reactions are performed in 0.1 mmol scale unless otherwise noted. [b] Conversions are estimated from ¹H-NMR using tert-butyl methyl ether as internal standard. [c] Diastereomeric ratios are estimated from ¹H-NMR using tert-butyl methyl ether as internal standard. [d] Isolated yields for **IV-87** and **IV-88** are 45% and 49% respectively. [e] NBS was used instead of TBCO. [f] Reaction was performed at room temperature. [g] Reaction was performed at −78 °C.

Further optimization of the reaction revealed that more polar solvents can improve that ratio of the desired diastereomer. As such, when THF with HMPA as co-solvent was used ~1:1 ratio of the diastereomeric products was isolated. TBCO, a commonly used as a mild bromine source for bromo etherification reaction,⁴⁰⁻⁴¹ gave poor diastereoselectivity and so did other bromine sources such as NBS. (Table IV-3, entry 8). Reactions at different temperatures also did not lead to any improved selectivity for the desired product (entries 9 and 10, Table IV-3).

The relative stereochemistries of the diastereomers **IV-87** and **IV-88** were established using extensive 2D NMR analysis. As illustrated in Figure IV-25, for the desired diastereomer **IV-87**, nOe correlations between hydrogen atoms on both ethereal carbon atoms confirm their *syn* geometry. However, for the undesired diastereomer **IV-88**, nOe between these two hydrogen atoms was not observed, while a series of the other nOe correlations confirmed the illustrated relative stereochemistry.

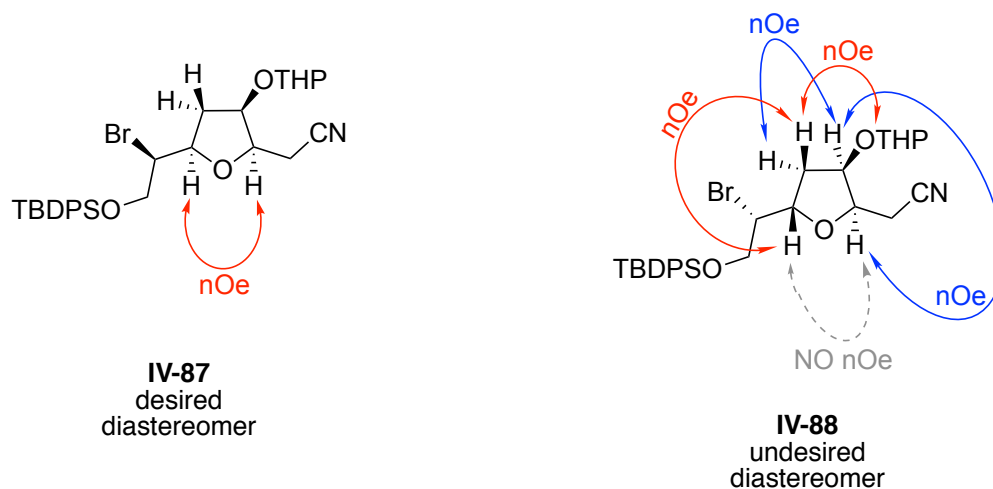


Figure IV-25. Assignment of the relative stereochemistry of the diastereomers **IV-96** and **IV-97**.

With these results in hand, we sought to identify the intrinsic factors that govern the latter selectivity. To better understand the origin of the observed selectivity in this reaction, we turned our attention to the approaches of the nucleophilic oxygen and the bromonium for the reaction with the *cis* olefin. As illustrated in Figure IV-26, since the addition across olefin is *anti*, the face selectivity of the olefin would result in the formation of the two diastereomers (**IV-87** and **IV-88**). In return the face selectivity of the *cis* double bond is dictated by the stereocenters on **IV-86**. Thus, the pre-organized structure **IV-86a** would lead to the desired diastereomer, and **IV-86b** would lead to the undesired diastereomer **IV-88**. In this putative arrangement, the allylic groups on the *cis* double bond would have a pseudo *syn*-pentane interaction with the group on C-7 that is bearing the nucleophilic oxygen atom. This steric repulsion would disfavor **IV-86-a**, and as a result the desired diastereomer will form as the minor product. On the other hand, in **IV-86-b**, which leads to the undesired diastereomer, the bulky allylic group on C-3 points to the opposite side of the groups on C-7 and C-6, thus a facile bromo etherification ensues, leading to **IV-88** as the major product. In order to reverse the intrinsic selectivity, the protecting group on of C-6 oxygen was removed. The hypothesis was that with a smaller group on C-6, the carbon chain may adopt a different conformation as compared to **IV-86**, thus giving access to the desired diastereomer as the major product. To this end, **IV-89** in which the THP group was removed, was subjected to the bromination conditions (dashed box, Figure IV-26). The reaction resulted in a 3:1 diastereomeric ratio in favor of the undesired diastereomer **IV-91** (Figure IV-26).

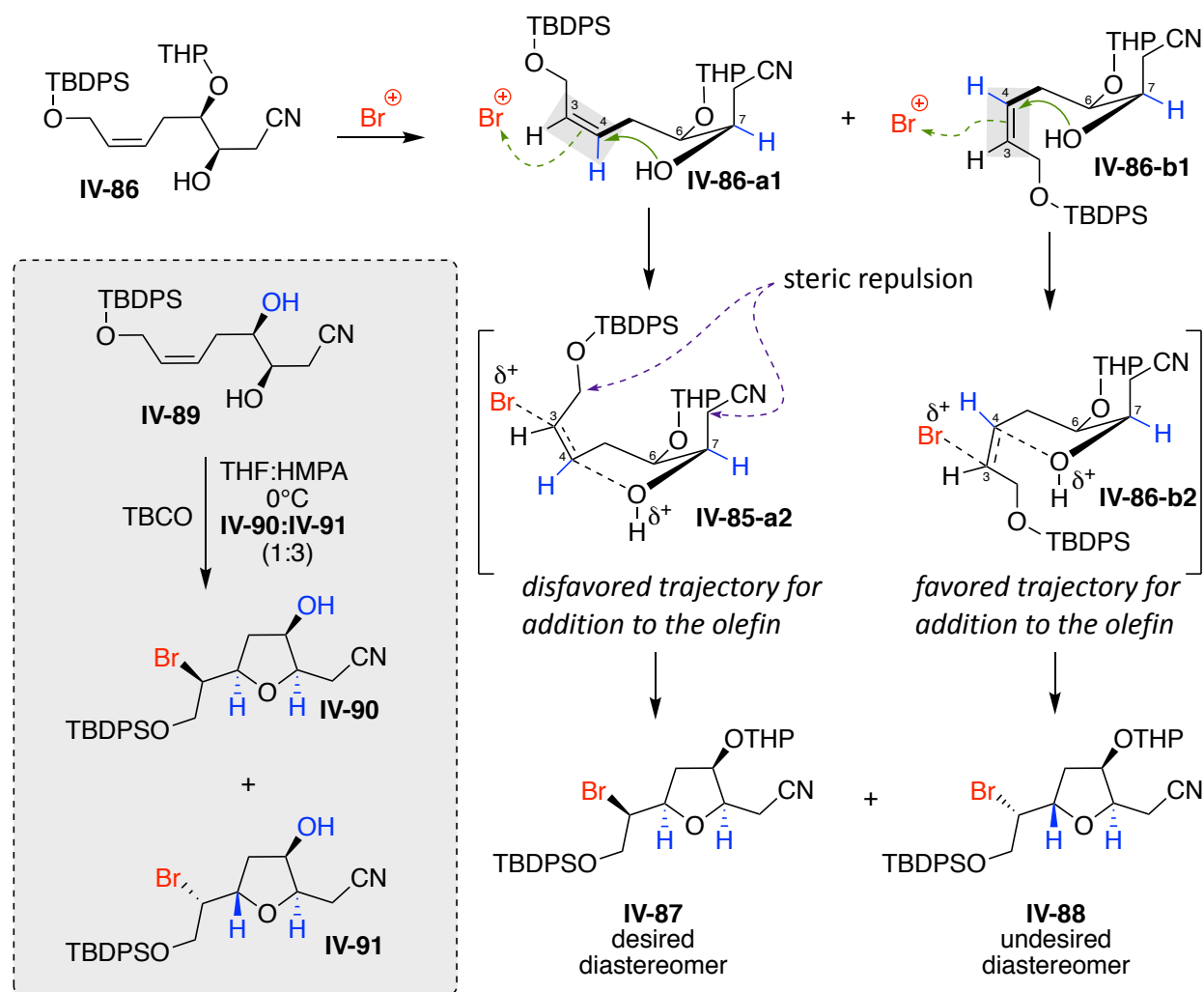


Figure IV-26. On the origin of the diastereoselectivity leading to **IV-87** and **IV-88**.

Since going small on C-6 did not solve the undesired stereochemical problem, we decided to approach the solution in a complete opposite manner. We proposed to impose an artificial bulkiness on the C-7 hydroxyl (the OH involved in the bromo etherification) to disfavor the approach that leads to the undesired diastereomer **IV-88**. We hypothesized a group capable of templating, yet easily removable on this oxygen atom would provide a path to reverse the intrinsic selectivity. The hypothetical group on the nucleophilic oxygen would suffer from a *syn*-pentane interaction with the groups on the allylic position

of the *cis* olefin, thus the approach highlighted in **IV-86-b** would suffer, leading to switch in the diastereoselectivity.

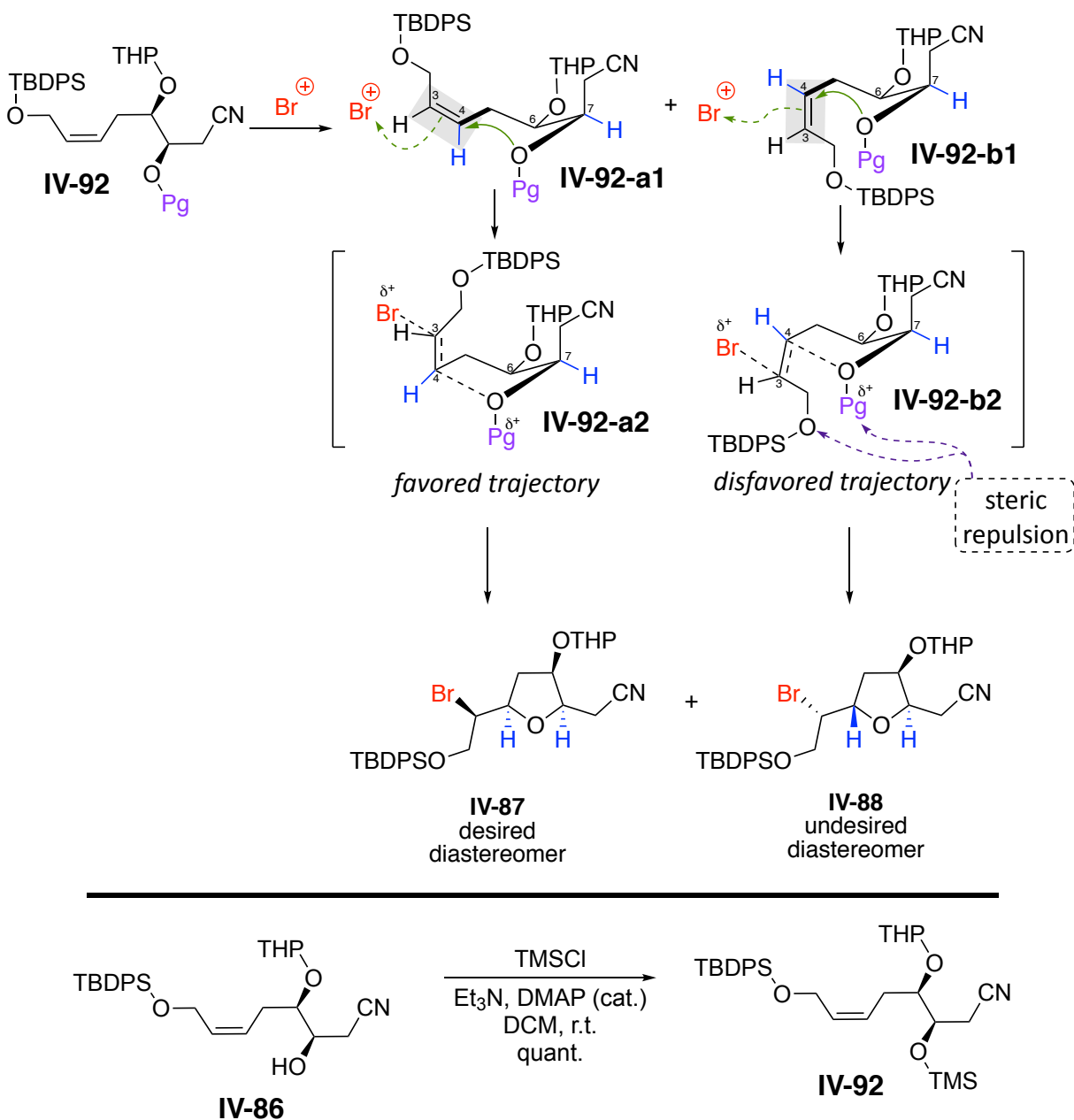
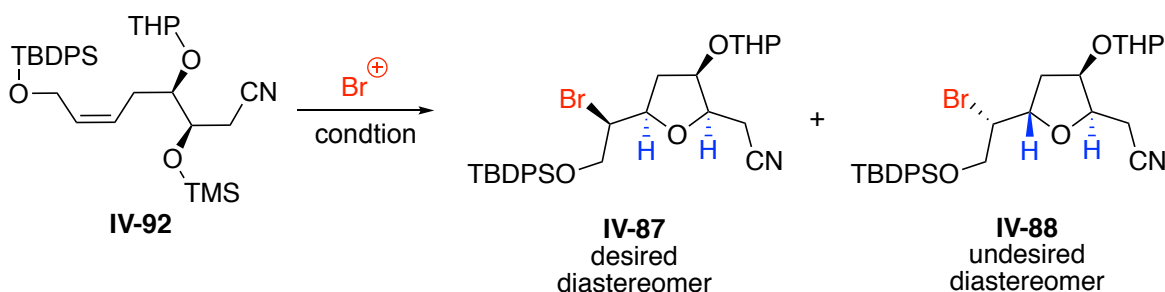


Figure IV-27. Rational design to improve the diastereoselectivity of the bromo-etherification reaction.

To test this hypothesis, trimethylsilyl group as a large, yet easily removable group during the bromo etherification, was chosen (Figure IV-26). Alcohol **IV-86** was reacted with TMSCl to provide the protected alcohol **IV-92** in nearly quantitative yield. With **IV-92**

in hand, bromo etherification was implemented (Figure IV-27). To our delight, employing THF/HMPA as the solvent system leads to the desired diastereomer **IV-87** as the major product with >10:1 selectivity (entry 1, Table IV-4). Of note is that under similar conditions, the unprotected alcohol **IV-86** led to a 1:1 diastereomeric mixture of **IV-87** and **IV-88** (compare entry 7, Table IV-4 with entry 1, Table IV-3). As illustrated in Table IV-4, further optimization of the reaction led to DCM as the solvent of choice, with methanol (10.0 equiv), as the scavenger of TMS group (entry 9). The desired product **IV-87** was isolated in >85% yield along with small amount of the undesired diastereomer (<5%).

Table IV-4: Bromo etherification of protected alcohol **IV-101**.



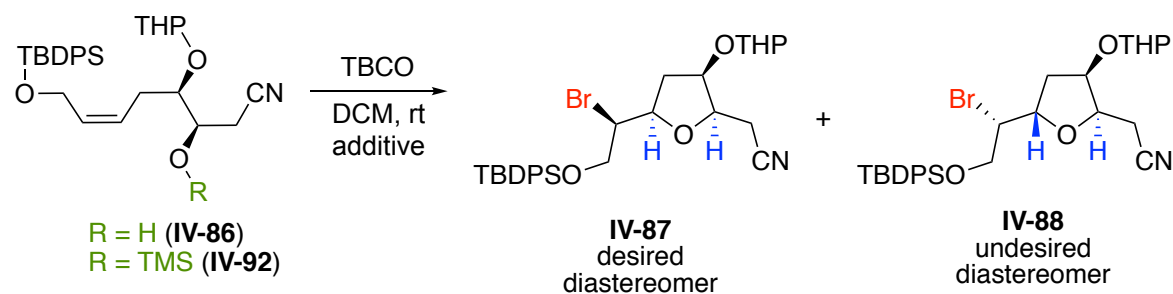
entry ^a	solvent	additive	conversion ^b	dr (IV-96:IV-97) ^c
1	THF	HMPA (2% v:v)	>99 ^d	>10:1
2	DMC	none	25	>10:1
3	THF	none	90	2:1
4	DCM	water (10% v:v)	40	>10:1
5	DCM	MeOH (10% v:v)	>99	14:1
6	chloroform	MeOH (10% v:v)	>99	>15:1
7	DCM	MeOH (10% v:v) ^e	>99	15:1

Table IV-4 (cont'd)

entry ^a	solvent	additive	conversion ^b	<i>dr</i> (IV-96:IV-97) ^c
8	DCM	EtOH (10% v:v)	>99	>10:1
9	DCM	MeOH (10 equiv)	>99	>15:1
10 ^f	DCM	MeOH (10 equiv)	>99 ^g	>15:1

[a] Reactions are performed on a 0.1 mmol scale unless otherwise noted. [b] Conversions are estimated from ¹H-NMR using tert-butyl methyl ether as internal standard. [c] Diastereomeric ratios are estimated from ¹H-NMR using tert-butyl methyl ether as internal standard. [d] Isolated yields for **IV-87** and **IV-88** were 75% and 8%, respectively. [e] Reaction was performed at 0 °C. [f] Reaction was performed on a 1.0 mmol scale. ^g Isolated yields for **IV-87** and **IV-88** were 85% and 4%, respectively

The results of TMS protected and unprotected alcohol for bromo-etherification in DCM highlights the significant effect of the protecting group to improve the *dr*. As depicted in Figure IV-28, the ¹H-NMR traces of the crude reaction mixtures with and without the protecting group on the nucleophilic oxygen atom under similar conditions result in the formation of the opposite diastereomer in nearly exclusive manner.



1. R = H; No additive

IV-87:IV-88 dr: 1:20

2. R = TMS; methanol (10 equiv)

IV-87:IV-88 dr: >15:1

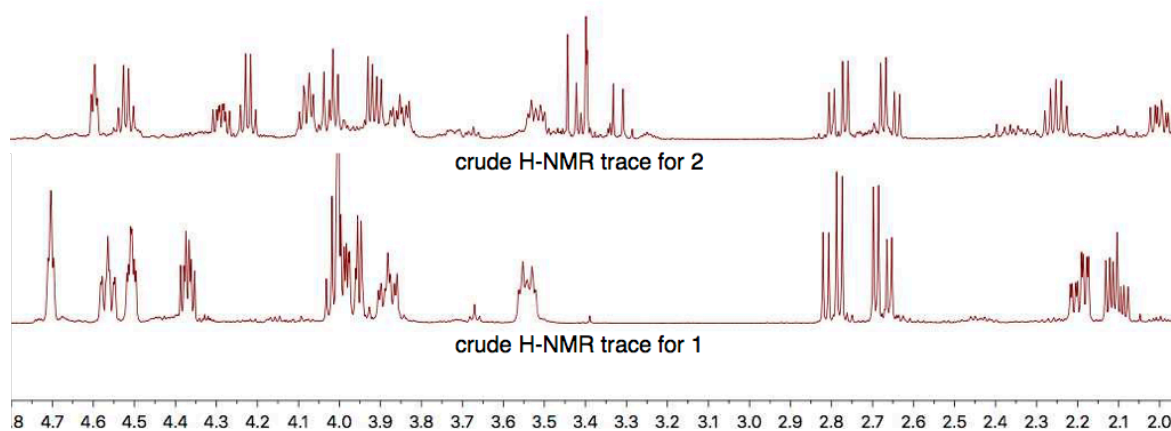


Figure IV-28. Comparison of the bromo-etherification with and without protection group on the nucleophilic oxygen.

With the decorated THF ring **IV-87** in hand, further modification of the nitrile group to install the ketone moiety along with installation of the remaining of the carbon chain to access **IV-93** was pursued. One of our early approaches was to subject the nitrile in **IV-87** to direct nucleophilic addition. For this purpose, *in situ* generated 2-hexenyl lithium was added to **IV-87** at low temperature (Figure 29). The reaction afforded the ketone **IV-93** only in small quantity (<10% yield), returning the nitrile starting material as the major isolated compound. Reaction at higher temperatures or longer reaction times, resulted in complex mixture of products. Products originating from decomposition or degradation of the ring were the major side products of the reaction. Further optimization of this

reaction is necessary to achieve large quantities of ketone **IV 103** in order to implement the key dibromo-spiroketalization.

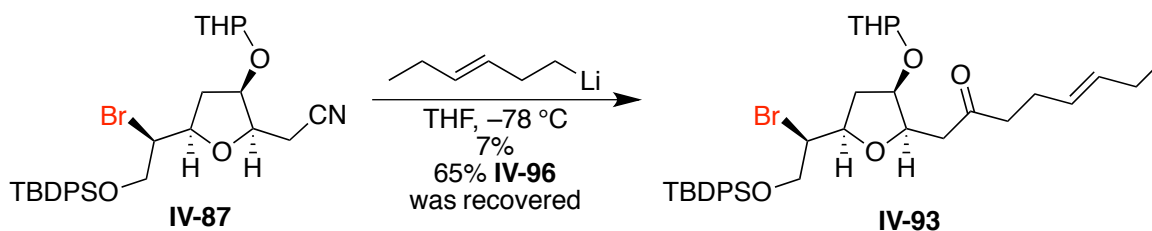


Figure IV-29. Direct addition of alkyl lithium to the nitrile moiety towards installation of the ketone functionality.

Presence of the labile bromide on **IV-87** could be the major issue that hampers the ketone formation. To remedy this issue, the nitrile was converted to the ketone prior to the bromo etherification step. However, the reaction of nitrile **IV-92** with *in situ* generated 2-hexenyl lithium resulted in ketone **IV-94** with only 30% yield (Figure IV-30, top).

In order to improve the yield of ketone formation, an indirect approach was pursued. The nitrile group in **IV-95** was reduced to the corresponding aldehyde **IV-96** followed by addition of 2-hexenyl lithium. The corresponding diastereomeric alcohol was then oxidized to install the ketone functionality leading to **IV-98**. Unfortunately, a complex reaction mixture was observed, hampering the identification of the product. A small fraction of the complex reaction mixture was isolated and identified as the furan derivative **IV-99** (Figure IV-30). This product might have formed under oxidation condition via condensation/dehydration

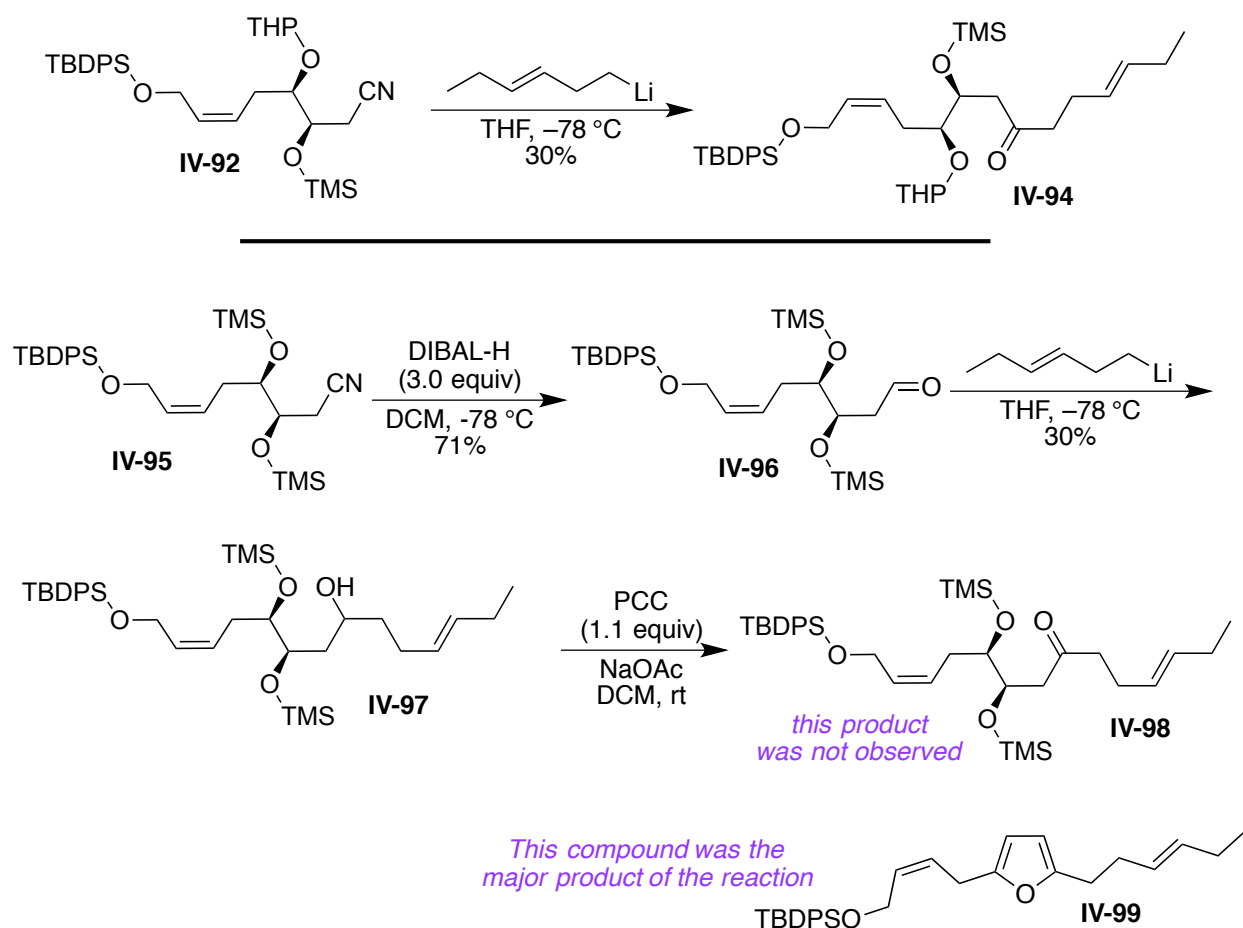


Figure IV-30. Approaches to improve the efficiency of the conversion of nitrile to ketone.

With ketone **IV-94** in hand, the desired bromo functionalization reaction was attempted. However, due to the presence of multiple reactive sites (two double bonds, and nucleophilic oxygen atoms), complex mixture of products was observed. This results assured us that a sequential and stepwise implementation of the bromo etherification and dibromo spiroketalization reactions should be followed in order to minimize the complexity of the synthesis.

Since protection of the epoxy alcohol **IV-81** with the THP protecting group resulted in diastereomeric mixture, a parallel pathway was pursued in which the installation of this protecting group was delayed to a later stage of the synthesis (Figure IV-31). Epoxy

alcohol **IV-81** was subjected to epoxide opening with cyanide to give rise to diol **IV-89** which was immediately protected as TMS ether leading to the di-protected analogue **IV-95** in good yield. Bromo etherification of **IV-95** under optimized condition led to **IV-90** in high yield and excellent diastereoselectivity ($>95:5$ *dr*), after acidic workup of the reaction to remove the TMS group. This alcohol was then protected as a THP acetal (**IV-100**) in high yield as a $\sim 1:1$ diastereomeric mixture on the acetal stereocenter. Future plan is to use this compound to complete the total synthesis of Obtusin.

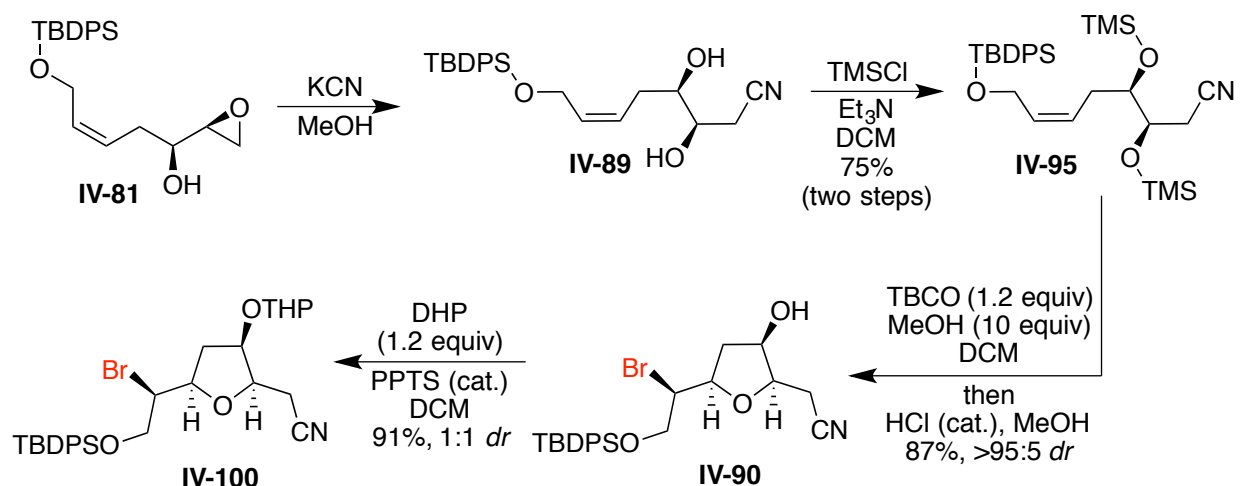


Figure IV-31. A different approach to convert epoxy alcohol **IV-90** to advanced intermediate **IV-109**.

At this point, we believe that the most hopeful strategy is the direct addition of the alkenyl group to the nitrile moiety in **IV-87** or **IV-100** to reveal the desired ketone. There are reported procedures that utilize organo zinc reagents as milder carbon nucleophiles for addition to nitriles. We are considering optimization of the direct addition of the alkyl group to the nitrile to give provide the ketone, setting the stage for the key dibromo spiroketalization.

In summary, we have demonstrated a streamlined synthesis that give access to the advance THF core of Obtusin. During the synthesis we uncovered the key role of the protecting group to control diastereoselectivity of the bromo etherification reaction to that installs the THF core of the natural product. Conversion of the nitrile to the ketone moiety proved to be challenging. Current efforts focus on the optimization of the latter transformation in order to implement the diastereoselective dibromo spiroketalization reaction.

IV-6 Experimental section

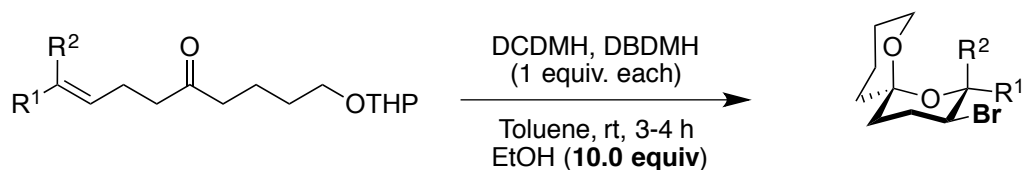
IV-6-1 General remarks:

Molecular sieves (4Å) were dried at 160 °C under 0.25 mtorr vacuum prior to use. Unless otherwise mentioned, solvents were purified as follows. CHCl_3 (amylene stabilized) was purchased from Sigma Aldrich and incubated over 4Å MS for 48 h prior to use. Toluene and CH_2Cl_2 were dried over CaH_2 whereas THF and Et_2O were dried over sodium (dryness was monitored by colorization of benzophenone ketyl radical); they were freshly distilled prior to use. NMR spectra were obtained using a 500 MHz and 600 MHz Varian NMR spectrometers and referenced using the residual ^1H peak from the deuterated solvent. Waters 2795 (Alliance HT) instrument was used for HRMS (ESI) analysis with polyethylene glycol (PEG-400-600) as a reference.

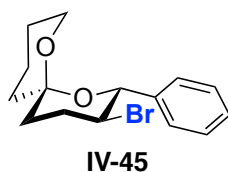
Column chromatography was performed using Silicycle 60Å, 35-75 μm silica gel. Pre-coated 0.25 mm thick silica gel 60 F254 plates were used for analytical TLC and visualized using UV light, iodine, potassium permanganate stain, *p*-anisaldehyde stain or phosphomolybdic acid in EtOH stain.

Halofunctionalization reactions were performed in the absence of light. *N*-chlorosuccinimide (NCS), *N*-bromosuccinimide (NBS), *N*-iodosuccinimide (NIS), 1,3-dichloro-5,5-dimethylhydantoin (DCDMH), and 1,3-dibromo-5,5-dimethylhydantoin (DBDMH) were re-crystallized prior to use. All other commercially available reagents and solvents were used as received unless otherwise mentioned.

IV-6-2 General procedure for bromo spiroketalization of THP-protected keto-alkenols



To the THP-protected keto-alkenol (0.1 mmol) in dry toluene (1 mL) was added dry ethanol (10.0 mmol, 10.0 equiv) and a mixture of 1,3-dibromo-5,5-dimethylhydantoin, DBDMH (1.0 mmol, 1.0 equiv) and 1,3-dichloro-5,5-dimethylhydantoin, DCDMH (1.0 mmol, 1.0 equiv). The reaction mixture was stirred at room temperature and followed by TLC. The initial colorless solution changed to orange, and become clear along with precipitation of hydantoin. This clear solution was the indication for the completion of the reaction, which took 3-4 h. The reaction mixture was diluted with hexanes (2 mL) followed by addition of sodium sulfite (2 ml of a 10% aqueous solution). The organic layer was separated and the aqueous layer was extracted with hexanes (3 x 2 mL). Combined organic extracts were concentrated under reduced pressure at room temperature to give the crude product. Crude ¹H NMR was used to determine the diastereoselectivity of the reaction. The crude product was then purified by column chromatography (silica, ethyl acetate/hexanes = 3%) leading to the pure bromo spiroketal products (65 – 99% average yield).

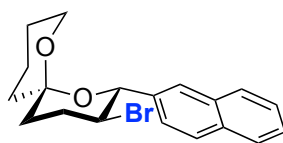


Spiroketalization reaction to produce **IV-45** was performed on a 1.0 mmol of ketone **IV-116**, leading to the **IV-45** in 99% yield (307 mg). Reaction with 0.1 mmol scale yielded a similar result.

^1H NMR (500 MHz, CDCl_3) δ 7.44 – 7.39 (m, 2H), 7.38 – 7.30 (m, 3H), 4.66 (d, J = 10.4 Hz, 1H), 4.00 (ddd, J = 12.0, 10.3, 4.5 Hz, 1H), 3.72 – 3.60 (m, 2H), 2.50 (tdd, J = 12.9, 12.0, 5.0 Hz, 1H), 2.26 (dtd, J = 13.0, 4.5, 2.9 Hz, 1H), 1.82 – 1.63 (m, 4H), 1.63 – 1.54 (m, 1H), 1.52 – 1.41 (m, 3H).

^{13}C NMR (125 MHz, CDCl_3) δ 139.66, 128.31, 128.07, 127.97, 95.98, 76.33, 60.79, 52.39, 37.64, 34.88, 31.25, 25.01, 18.34.

TOF MS ES^+ ($\text{C}_{15}\text{H}_{20}\text{BrO}_2$): Calc. $[\text{M} + \text{H}]^+$: 311.0647, Found $[\text{M} + \text{H}]^+$: 311.0645.

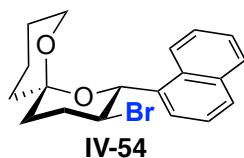


IV-53

Spiroketalization of ketone **IV-132** (35 mg, 0.1 mmol) produced **IV-53** (33.5 mg, 93% yield) as a white foam.

^1H NMR (500 MHz, CDCl_3) δ 7.89 – 7.79 (m, 4H), 7.54 (dd, J = 8.4, 1.7 Hz, 1H), 7.51 – 7.42 (m, 2H), 4.83 (d, J = 10.3 Hz, 1H), 4.12 (ddd, J = 12.1, 10.3, 4.5 Hz, 1H), 3.75 – 3.64 (m, 2H), 2.55 (qd, J = 12.5, 5.5 Hz, 1H), 2.30 (dtd, J = 13.0, 4.4, 3.0 Hz, 1H), 1.87 – 1.78 (m, 2H), 1.75 – 1.66 (m, 2H), 1.62 – 1.55 (m, 1H), 1.53 – 1.42 (m, 3H).

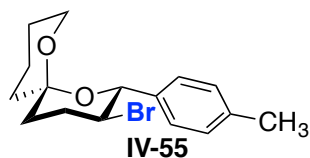
^{13}C NMR (125 MHz, CDCl_3) δ 137.04, 133.40, 132.98, 128.15, 127.89, 127.71, 127.55, 126.04, 125.38, 96.08, 76.56, 60.88, 52.27, 37.70, 34.91, 31.30, 25.02, 18.37.



Spiroketalization of ketone **IV-131** (36 mg, 0.1 mmol) produced **IV-54** (32.8 mg, 88% yield) as a white foam.

^1H NMR (500 MHz, CDCl_3) δ 8.37 (d, J = 8.6 Hz, 1H), 7.85 (dd, J = 16.0, 8.1 Hz, 2H), 7.67 – 7.56 (m, 1H), 7.49 (dq, J = 15.4, 7.4 Hz, 3H), 5.49 (br, 1H), 4.36 (br, 1H), 3.82 – 3.54 (m, 2H), 2.62 (qd, J = 12.1, 7.5 Hz, 1H), 2.34 (dq, J = 12.6, 4.0 Hz, 1H), 1.92 – 1.83 (m, 2H), 1.75 – 1.61 (m, 2H), 1.54 (pd, J = 12.3, 5.8 Hz, 2H), 1.43 (dd, J = 26.1, 9.7 Hz, 2H).

^{13}C NMR (125 MHz, CDCl_3) δ 139.15, 133.76, 131.84, 128.87, 128.84, 125.83, 125.38, 125.21, 96.18, 60.94, 52.47, 37.77, 35.01, 31.56, 24.98, 18.33.

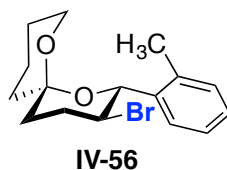


Spiroketalization of ketone **IV-117** (33 mg, 0.1 mmol) produced **IV-55** (28.2 mg, 87% yield) as a white foam.

^1H NMR (500 MHz, CDCl_3) δ 7.30 (d, J = 8.0, 2H), 7.16 (d, J = 8.0 Hz, 2H), 4.63 (d, J = 10.3 Hz, 1H), 4.00 (ddd, J = 12.0, 10.3, 4.5 Hz, 1H), 3.72 – 3.59 (m, 2H), 2.56 – 2.43 (m,

1H), 2.35 (s, 3H), 2.26 (dtd, J = 12.9, 4.4, 2.9 Hz, 1H), 1.81 – 1.62 (m, 4H), 1.60 – 1.41 (m, 4H).

¹³C NMR (125 MHz, CDCl₃) δ 138.0, 136.7, 128.8, 127.8, 95.9, 76.1, 60.74, 52.5, 37.6, 34.8, 31.2, 25.0, 21.2, 18.3 ppm.

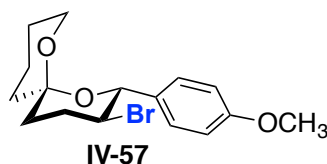


Spiroketalization of ketone **IV-118** (49 mg, 0.15 mmol) produced **IV-56** (39.0 mg, 80% yield) as a white foam.

mp = 47 – 50°

¹H NMR (500 MHz, CDCl₃) δ 7.46 – 7.39 (m, 1H), 7.32 – 7.15 (m, 3H), 5.06 (d, J = 10.4 Hz, 1H), 4.11 (ddd, J = 12.1, 10.4, 4.4 Hz, 1H), 3.76 – 3.63 (m, 2H), 2.59 – 2.52 (m, 1H), 2.51 (s, 3H), 2.29 (dtd, J = 13.0, 4.3, 2.8 Hz, 1H), 1.87 – 1.65 (m, 4H), 1.62 – 1.42 (m, 4H).

¹³C NMR (125 MHz, CDCl₃) δ 138.36, 136.46, 130.14, 127.96, 127.06, 126.11, 95.96, 71.79, 60.72, 53.10, 37.76, 34.95, 31.36, 25.03, 20.22, 18.33.

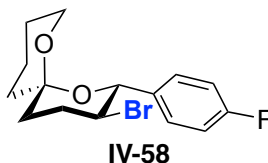


Spiroketalization of ketone **IV-121** (34 mg, 0.1 mmol) produced **IV-57** (25.0 mg, 73% yield) as a white foam.

^1H NMR (500 MHz, CDCl_3) δ 7.33 (d, J = 8.7 Hz, 2H), 6.88 (d, J = 8.6 Hz, 2H), 4.61 (d, J = 10.4 Hz, 1H), 3.99 (ddd, J = 12.0, 10.3, 4.5 Hz, 1H), 3.80 (s, 3H), 3.71 – 3.60 (m, 2H), 2.49 (tdd, J = 12.9, 12.0, 4.9 Hz, 1H), 2.25 (dtd, J = 12.9, 4.4, 2.9 Hz, 1H), 1.80 – 1.62 (m, 4H), 1.60 – 1.42 (m, 4H).

^{13}C NMR (125 MHz, CDCl_3) δ 159.44, 131.98, 129.03, 113.44, 95.98, 75.82, 60.76, 55.20, 52.77, 37.64, 34.87, 31.27, 25.01, 18.34, 14.13.

TOF MS ES^+ ($\text{C}_{16}\text{H}_{22}\text{BrO}_3$): Calc. $[\text{M} + \text{H}]^+$: 341.0752, Found $[\text{M} + \text{H}]^+$: 341.0741.



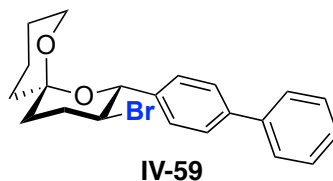
Spiroketalization of ketone **IV-119** (49 mg, 0.15 mmol) produced **IV-58** (41.0 mg, 84% yield) as a white foam.

^1H NMR (500 MHz, CDCl_3) δ 7.43 – 7.34 (m, 2H), 7.09 – 6.99 (m, 2H), 4.64 (d, J = 10.3 Hz, 1H), 3.93 (ddd, J = 12.1, 10.3, 4.5 Hz, 1H), 3.68 (ddt, J = 11.0, 5.0, 1.8 Hz, 1H), 3.64 – 3.57 (m, 1H), 2.49 (tdd, J = 13.1, 12.0, 4.8 Hz, 1H), 2.25 (dtd, J = 13.0, 4.4, 2.8 Hz, 1H), 1.83 – 1.62 (m, 4H), 1.60 – 1.43 (m, 4H).

^{13}C NMR (125 MHz, CDCl_3) δ 162.55 (d, $J_{\text{C-F}}$ = 246.1 Hz), 135.57 (d, $J_{\text{C-F}}$ = 3.3 Hz), 129.55 (d, $J_{\text{C-F}}$ = 8.1 Hz), 114.94 (d, $J_{\text{C-F}}$ = 21.4 Hz), 96.04, 75.63, 60.81, 52.54, 37.59, 34.82, 31.17, 24.96, 18.33.

^{19}F NMR (470 MHz, CDCl_3) δ -113.86 – -113.95 (m).

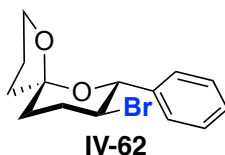
TOF MS ES^+ ($\text{C}_{15}\text{H}_{19}\text{BrFO}_2$): Calc. $[\text{M} + \text{H}]^+$: 329.0552, Found $[\text{M} + \text{H}]^+$: 329.0544.



Spiroketalization of ketone **IV-120** (39 mg, 0.1 mmol) produced **IV-59** (32.0 mg, 83% yield) as a white foam.

^1H NMR (500 MHz, CDCl_3) δ 7.61 – 7.56 (m, 4H), 7.50 – 7.46 (m, 2H), 7.42 (dd, J = 9.3, 5.9 Hz, 2H), 7.34 – 7.31 (m, 1H), 4.71 (d, J = 10.4 Hz, 1H), 4.03 (ddd, J = 10.5, 8.0, 5.1 Hz, 1H), 3.74 – 3.63 (m, 2H), 2.52 (qd, J = 12.7, 5.2 Hz, 1H), 2.32 – 2.26 (m, 1H), 1.83 – 1.71 (m, 3H), 1.71 – 1.65 (m, 1H), 1.61 – 1.43 (m, 4H).

^{13}C NMR (125 MHz, CDCl_3) δ 140.86, 138.67, 128.76, 128.70, 128.36, 127.26, 127.16, 126.86, 96.03, 76.06, 60.83, 52.34, 37.66, 34.88, 31.25, 25.01, 18.37.

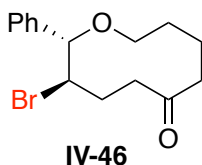


Spiroketalization of ketone **IV-136** (30 mg, 0.1 mmol) produced **IV-63** (24.3 mg, 82% yield) as a white foam.

^1H NMR (500 MHz, CDCl_3) δ 7.40 – 7.28 (m, 5H), 4.82 (d, J = 10.4 Hz, 1H), 4.01 (ddd, J = 11.9, 10.4, 4.6 Hz, 1H), 3.95 (td, J = 8.1, 4.9 Hz, 1H), 3.89 (td, J = 8.1, 6.8 Hz, 1H), 2.54 – 2.45 (m, 1H), 2.38 (dtd, J = 12.7, 4.6, 2.9 Hz, 1H), 2.07 (td, J = 13.6, 4.6 Hz, 1H), 2.03 – 1.92 (m, 2H), 1.88 – 1.78 (m, 2H), 1.76 – 1.67 (m, 1H).

^{13}C NMR (125 MHz, CDCl_3) δ 139.71, 128.31, 128.12, 127.91, 106.14, 77.48, 67.36, 52.06, 37.18, 35.20, 32.71, 23.63.

TOF MS ES⁺ (C₁₄H₁₈BrO₂): Calc. [M + H]⁺: 297.0490, Found [M + H]⁺: 297.0482.

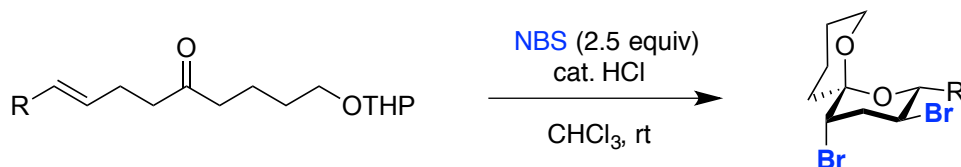


Analytical data for bromo macrocyclic product **IV-46**:

¹H NMR (500 MHz, CDCl₃) δ 7.32 – 7.24 (m, 5H), 4.04 – 3.99 (m 2H), 3.11 – 3.10 (m, 1H), 2.80 (t, J = 10.0, 1H), 2.76 – 2.67 (m, 3H), 2.51 – 2.49 (m, 1H), 2.44 – 2.39 (m, 1H), 2.50 – 2.20 (m, 1H), 2.12 – 2.04 (m, 1H), 1.61 – 1.58 (m, 1H), 1.51 – 1.38 (m, 2H).

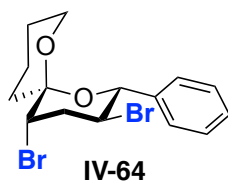
¹³C NMR (125 MHz, CDCl₃) δ 208.15, 139.78, 128.30, 128.15, 127.80, 85.39, 69.49, 55.65, 42.03, 41.97, 32.87, 29.31, 22.07.

IV-6-3 General procedure for dibromo spiroketalization of THP-protected keto-alkenols



To the THP-protected keto-alkenols (0.1 mmol) dissolved in chloroform (amylene stabilized, 1 mL) was added N-bromosuccinimide (44.5 mg, 0.25 mmol, 2.5 equiv) at room temperature. To this mixture was then added concentrated HCl (~10 μL). The reaction was continued to stir at room temperature (protected from light) and was monitored by TLC. After completion of the reaction (~4 h), sodium sulfite (2 mL of 10% aqueous solution) was added to the reaction. The organic layer was separated and the aqueous

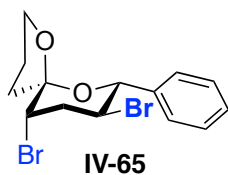
layer was extracted with hexanes (3 x 2 mL). The combined organic extracts were dried over sodium sulfate and concentrated under reduced pressure at room temperature to give the crude product. Crude ^1H NMR was used to determine the diastereoselectivity of the reaction. The crude product was then purified by column chromatography (silica, ethyl acetate/hexanes = 3%) leading to the pure dibromo-spiroketal products.



Dibromo spiroketalization of ketone **IV-116** (31 mg, 0.1 mmol) produced **IV-64** (337 mg product was isolated, 87% yield) as a white foam.

^1H NMR (500 MHz, CDCl_3) δ 7.49 – 7.42 (m, 2H), 7.39 – 7.33 (m, 3H), 4.68 (d, J = 10.5 Hz, 1H), 4.46 (td, J = 11.2, 4.3 Hz, 1H), 4.03 (t, J = 3.2 Hz, 1H), 3.76 (dd, J = 11.7, 3.9 Hz, 1H), 3.65 (td, J = 11.5, 11.1, 2.6 Hz, 1H), 3.11 (ddd, J = 14.2, 11.9, 3.4 Hz, 1H), 2.60 (ddd, J = 14.0, 4.2, 2.9 Hz, 1H), 2.20 (d, J = 13.7 Hz, 1H), 1.65 (td, J = 8.9, 4.5 Hz, 1H), 1.55 (s, 1H), 1.52 – 1.48 (m, 1H), 1.48 – 1.40 (m, 1H), 1.32 (td, J = 13.4, 4.5 Hz, 1H).

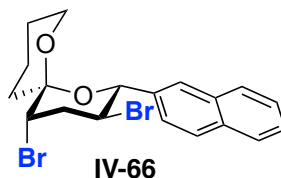
^{13}C NMR (125 MHz, CDCl_3) δ 128.60, 128.18, 128.04, 127.88, 96.29, 88.84, 61.97, 55.17, 48.12, 39.55, 33.86, 24.42, 18.61.



Dibromo spiroketalization of ketone **IV-136** (30 mg, 0.1 mmol) produced **IV-65** (27.3 mg, 73% yield) as a white foam.

^1H NMR (500 MHz, CDCl_3) δ 7.47 – 7.40 (m, 2H), 7.40 – 7.30 (m, 3H), 4.86 (d, J = 10.5 Hz, 1H), 4.45 (ddd, J = 11.8, 10.5, 4.4 Hz, 1H), 4.12 (t, J = 3.1 Hz, 1H), 4.10 – 4.00 (m, 2H), 3.00 (ddd, J = 14.3, 11.9, 3.3 Hz, 1H), 2.69 (ddd, J = 14.2, 4.4, 2.9 Hz, 1H), 2.19 (ddd, J = 12.2, 7.5, 2.8 Hz, 1H), 2.04 – 1.82 (m, 3H).

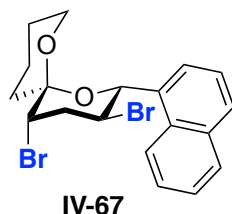
^{13}C NMR (125 MHz, CDCl_3) δ 128.58, 128.21, 128.00, 127.42, 101.53, 77.68, 69.83, 53.24, 47.88, 40.54, 38.36, 23.88.



Dibromo spiroketalization of ketone **IV-132** (35 mg, 0.1 mmol) produced **IV-66** (38.5 mg, 88% yield) as a white foam.

^1H NMR (500 MHz, CDCl_3) δ 7.89 – 7.82 (m, 4H), 7.61 (dd, J = 8.5, 1.9 Hz, 1H), 7.51 – 7.46 (m, 2H), 4.86 (d, J = 10.5 Hz, 1H), 4.65 – 4.54 (m, 1H), 4.07 (t, J = 3.2 Hz, 1H), 3.80 (ddd, J = 10.9, 4.6, 2.2 Hz, 1H), 3.70 (td, J = 11.7, 2.6 Hz, 1H), 3.16 (ddd, J = 14.8, 12.0, 3.4 Hz, 1H), 2.65 (ddd, J = 14.1, 4.4, 2.8 Hz, 1H), 2.24 (dt, J = 13.7, 3.3 Hz, 1H), 1.71 – 1.50 (m, 2H), 1.47 – 1.40 (m, 1H), 1.35 (td, J = 13.4, 4.5 Hz, 1H).

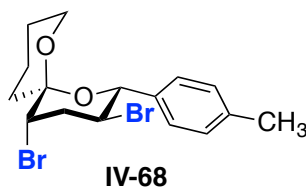
^{13}C NMR (125 MHz, CDCl_3) δ 136.19, 133.51, 132.89, 128.15, 128.10, 127.73, 127.68, 126.19, 126.12, 125.26, 96.36, 76.95, 62.04, 55.20, 47.96, 39.58, 33.86, 24.42, 18.63.



Dibromo spiroketalization of ketone **IV-131** (35 mg, 0.1 mmol) produced **IV-67** (26.7 mg, 61% yield) as a white foam.

^1H NMR (500 MHz, CDCl_3) δ 7.93 – 7.80 (m, 2H), 7.53 (m, 3H), 5.80 – 5.20 (br, 1H), 5.10 – 4.60 (br, 1H), 4.14 (t, J = 3.2 Hz, 1H), 3.84 (d, J = 11.0 Hz, 1H), 3.72 (ddd, J = 13.6, 11.2, 2.6 Hz, 1H), 3.25 (ddd, J = 14.8, 11.7, 3.4 Hz, 1H), 2.71 (ddd, J = 14.1, 4.1, 2.9 Hz, 1H), 2.27 (d, J = 13.8 Hz, 1H), 1.61 – 1.48 (m, 4H), 1.39 (td, J = 13.2, 4.5 Hz, 2H).

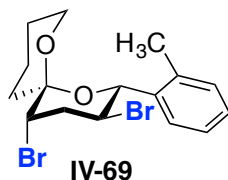
^{13}C NMR (125 MHz, CDCl_3) δ 134.75, 133.27, 128.85, 128.59, 128.37, 125.99, 125.94, 125.50, 125.20, 96.64, 82.47, 62.09, 55.36, 49.49, 40.00, 33.93, 24.39, 18.60.



Dibromo spiroketalization of ketone **IV-117** (33 mg, 0.1 mmol) produced **IV-68** (30.0 mg, 74% yield) as a white foam.

^1H NMR (500 MHz, CDCl_3) δ 7.34 (d, J = 7.8 Hz, 2H), 7.18 (d, J = 7.6 Hz, 2H), 4.65 (d, J = 10.5 Hz, 1H), 4.46 (td, J = 11.3, 4.3 Hz, 1H), 4.03 (t, J = 3.1 Hz, 1H), 3.75 (dd, J = 11.4, 4.4 Hz, 1H), 3.65 (td, J = 11.6, 2.5 Hz, 1H), 3.10 (ddd, J = 14.8, 12.0, 3.4 Hz, 1H), 2.60

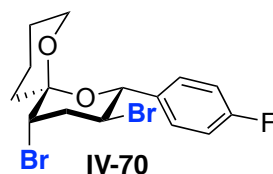
(dt, $J = 14.1, 3.5$ Hz, 1H), 2.35 (s, 3H), 2.22 – 2.15 (m, 1H), 1.65 (tt, $J = 13.9, 4.1$ Hz, 2H), 1.48 (dt, $J = 12.4, 4.2$ Hz, 1H), 1.41 (m, 1H), 1.31 (td, $J = 13.4, 4.5$ Hz, 1H).
 ^{13}C NMR (125 MHz, CDCl_3) δ 138.39, 135.95, 128.92, 127.90, 96.29, 76.49, 61.93, 55.23, 48.26, 39.58, 33.86, 24.43, 21.31, 18.60. ppm.



Dibromo spiroketalization of ketone **IV-118** (33 mg, 0.1 mmol) produced **IV-69** (34.3 mg, 85% yield) as a white foam.

^1H NMR (500 MHz, CDCl_3) δ 7.50 (d, $J = 7.3$ Hz, 1H), 7.27 – 7.20 (m, 2H), 7.16 (d, $J = 7.4$ Hz, 1H), 5.05 (d, $J = 10.6$ Hz, 1H), 4.57 (td, $J = 11.5, 4.1$ Hz, 1H), 4.04 (d, $J = 3.3$ Hz, 1H), 3.81 – 3.73 (m, 1H), 3.66 (td, $J = 11.6, 2.5$ Hz, 1H), 3.12 (ddd, $J = 14.9, 12.0, 3.4$ Hz, 1H), 2.61 (dt, $J = 14.2, 3.6$ Hz, 1H), 2.48 (s, 3H), 2.18 (dd, $J = 13.6, 4.0$ Hz, 1H), 1.72 – 1.57 (m, 2H), 1.41 (d, $J = 13.1$ Hz, 1H), 1.32 (td, $J = 13.5, 4.5$ Hz, 2H).

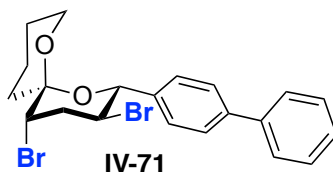
^{13}C NMR (125 MHz, CDCl_3) δ 136.47, 136.36, 130.16, 128.31, 128.25, 126.26, 96.31, 77.20, 61.88, 55.34, 51.75, 39.65, 33.91, 24.43, 20.14, 18.59.



Dibromo spiroketalization of ketone **IV-119** (33 mg, 0.1 mmol) produced **IV-70** (26.5 mg, 65% yield) as a white foam.

^1H NMR (500 MHz, CDCl_3) δ 7.43 (dd, J = 8.6, 5.5 Hz, 2H), 7.08 – 7.01 (m, 2H), 4.66 (d, J = 10.5 Hz, 1H), 4.39 (td, J = 11.3, 4.4 Hz, 1H), 4.02 (t, J = 3.2 Hz, 1H), 3.76 (dd, J = 11.1, 4.5 Hz, 1H), 3.62 (td, J = 11.7, 11.1, 2.7 Hz, 1H), 3.09 (ddd, J = 14.1, 11.9, 3.4 Hz, 1H), 2.59 (ddd, J = 14.1, 4.3, 2.9 Hz, 1H), 2.19 (d, J = 13.7 Hz, 1H), 1.64 (tdt, J = 13.1, 8.3, 4.0 Hz, 1H), 1.49 (dt, J = 12.6, 4.3 Hz, 1H), 1.46 – 1.55 (m, 2H), 1.32 (td, J = 13.3, 4.7 Hz, 1H).

^{13}C NMR (125 MHz, CDCl_3) δ 129.69 (d, $J_{\text{C-F}}$ = 8.4 Hz), 115.10 (d, $J_{\text{C-F}}$ = 21.5 Hz), 96.36, 90.89, 62.03, 55.07, 48.27, 39.48, 33.82, 29.71, 22.70, 18.62.



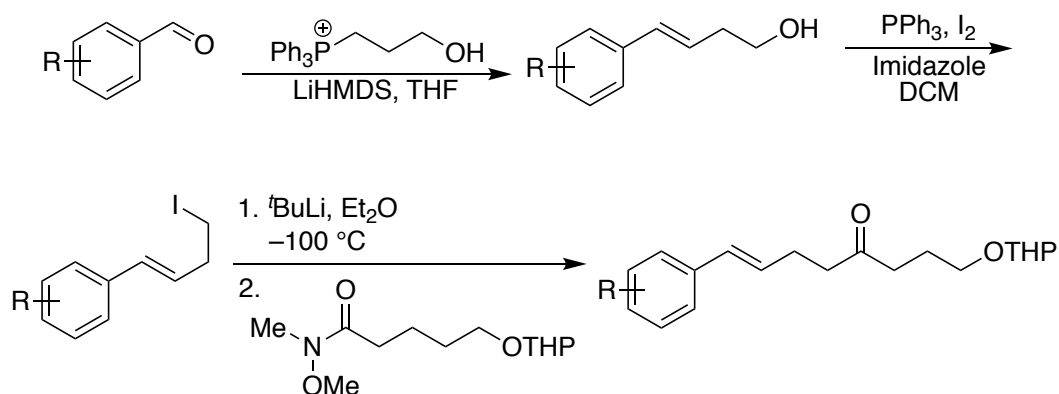
Dibromo spiroketalization of ketone **IV-120** (39 mg, 0.1 mmol) produced **IV-71** (23.0 mg, 59% yield) as a white foam.

^1H NMR (500 MHz, CDCl_3) δ 7.59 (d, J = 8.0 Hz, 4H), 7.53 (d, J = 7.9 Hz, 2H), 7.43 (t, J = 7.6 Hz, 2H), 7.33 (t, J = 7.3 Hz, 1H), 4.74 (d, J = 10.5 Hz, 1H), 4.50 (td, J = 11.1, 4.1 Hz, 1H), 4.05 (d, J = 3.0 Hz, 1H), 3.82 – 3.74 (m, 1H), 3.68 (t, J = 11.4 Hz, 1H), 3.13 (td, J = 12.9, 11.7, 3.3 Hz, 1H), 2.63 (dt, J = 14.3, 3.5 Hz, 1H), 2.22 (d, J = 13.7 Hz, 1H), 1.69 (m, 1H), 1.59 – 1.54 (m, 1H), 1.49 (s, 1H), 1.43 (m, 1H), 1.34 (td, J = 13.4, 4.5 Hz, 1H).

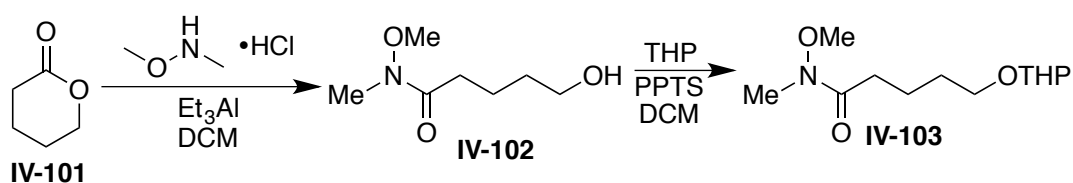
^{13}C NMR (125 MHz, CDCl_3) δ 128.74, 128.44, 127.34, 127.18, 126.98, 96.35, 76.45, 62.02, 55.17, 48.08, 39.56, 33.87, 24.43, 18.65.

IV-6-4 Synthesis of ketones IV-116 to IV-121

These substrates were synthesized according to the following general scheme:



Synthesis of THP-protected Weinreb amide IV-103:



Following a reported procedure,⁴² to a suspension of N,O-dimethyl hydroxyl amine hydrochloride (6.0 g, 61.5 mmol, 3.0 equiv) in dry DCM (60 mL) was added diethyl aluminum (1.0 M in heptane, 60.0 mL, 60.0 mmol) dropwise at -10 °C. After addition was completed, the mixture was stirred at room temperature for 30 min. To this mixture at 0 °C was added a solution of δ-lactone (2.0 g, 20.0 mmol, 1.0 equiv) in DCM (10 mL). The reaction was further stirred at room temperature for 20 h, before it was quenched by careful addition sodium bicarbonate (1.0 M, 100 mL). The aqueous layer was extracted with DCM (5 x 50 mL), and the combined organic extracts were washed with brine, dried over sodium sulfate and concentrated under reduced pressure to give the crude alcohol **IV-102**, which was used in the next step without further purification.

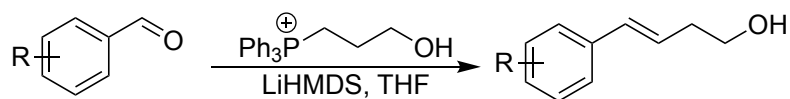
To the crude alcohol (ca. 2.6 g) in anhydrous DCM (100 mL) were added PPTS (100 mg) and DHP (2.0 mL, 22.0 mmol, 1.1 equiv) at 0 °C. The reaction was continued to stirred at room temperature for 12 h. The volatiles were removed under reduced pressure and the crude product was purified on column chromatography (silica, ethyl acetate/hexanes 30%) to yield the pure THP-protected Weinreb amide **IV-103** (2.6 g, 53% yield) as a colorless oil.

^1H NMR (500 MHz, Chloroform-*d*) δ 4.55 (dd, $J = 4.4, 2.8$ Hz, 1H), 3.87 – 3.79 (m, 1H), 3.74 (dt, $J = 9.6, 6.5$ Hz, 1H), 3.65 (s, 3H), 3.51 – 3.42 (m, 1H), 3.38 (dt, $J = 9.7, 6.3$ Hz, 1H), 3.15 (s, 3H), 2.43 (t, $J = 7.5$ Hz, 2H), 1.90 – 1.74 (m, 2H), 1.73 – 1.58 (m, 4H), 1.57 – 1.44 (m, 4H).

^{13}C NMR (126 MHz, CDCl_3) δ 98.77, 69.43, 67.19, 62.23, 61.17, 30.70, 29.41, 25.45, 22.31, 21.44, 19.56, 19.11.

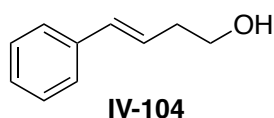
TOF MS ES^+ ($\text{C}_{12}\text{H}_{23}\text{NNaO}_4$): Calc. $[\text{M} + \text{Na}]^+$: 268.1525, Found $[\text{M} + \text{H}]^+$: 268.1548.

Synthesis of but-3-en-1-ol derivatives



Following the reported procedure,⁴³ lithium bis(trimethylsilyl)amide (1.0 M in THF, 14.0 mL, 14.0 mmol) was added at –20 °C to a suspension (3-propan-1-ol) triphenylphosphonium bromide (2.4 g, 6.0 mmol, 1.2 equiv) in dry THF (14.0 mL). The solution was stirred at this temperature for 1 h. To this solution at –20 °C was added aldehyde (5.0 mmol, 1.0 equiv). The reaction was stirred at this temperature for another

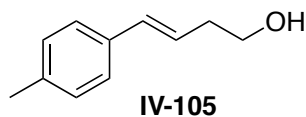
2 h, then allowed to warm up to room temperature and was stirred for 12 h. Saturated ammonium chloride (20 mL) was added to the reaction mixture, the organic layer was separated and the aqueous layer was extracted with ethyl acetate (3 x 20 mL). The combined organic extracts were washed with brine (20 mL), dried over sodium sulfate and concentrated under reduced pressure to yield the crude alcohol that was purified via column chromatography (silica, ethyl acetate/hexanes 10 to 20%) to afford the corresponding pure alcohol.



Following the above procedure, alcohol **IV-104** (350 mg, 47% yield) was synthesized as a colorless oil.

^1H NMR (500 MHz, Chloroform- d) δ 7.37 – 7.32 (m, 2H), 7.31 – 7.26 (m, 2H), 7.23 – 7.16 (m, 1H), 6.49 (dt, J = 15.9, 1.5 Hz, 1H), 6.19 (dt, J = 15.8, 7.1 Hz, 1H), 3.74 (t, J = 6.3 Hz, 2H), 2.48 (dtd, J = 7.6, 6.3, 1.4 Hz, 2H).

^{13}C NMR (126 MHz, CDCl_3) δ : 137.1, 132.7, 128.5, 127.2, 126.1, 126.0, 62.0, 36.3 ppm.

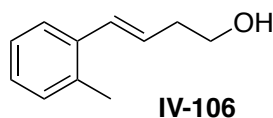


Following the above procedure, alcohol **IV-105** (460 mg, 57% yield) was synthesized as a white solid.

mp = 49 – 51°

^1H NMR (500 MHz, Chloroform-*d*) δ : 7.24 (d, J = 7.9 Hz, 2H), 7.09 (d, J = 7.9 Hz, 2H), 6.45 (d, J = 15.9 Hz, 1H), 6.13 (dt, J = 15.9, 7.2 Hz, 1H), 3.73 (t, J = 6.5 Hz, 2H), 2.46 (td, J = 7.2, 6.5 Hz, 2H), 2.31 (s, 3H), 1.47 (s, 1H) ppm.

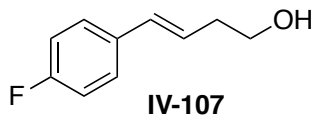
^{13}C NMR (126 MHz, CDCl_3) δ : 137.03, 134.38, 132.73, 129.20, 125.94, 125.15, 62.03, 36.40, 21.15 ppm.



Following the above procedure, alcohol **IV-106** (380 mg, 47% yield) was synthesized as a colorless oil.

^1H NMR (500 MHz, Chloroform-*d*) δ : 7.42 (m, 1H), 7.16 – 7.11 (m, 3H), 6.69 (d, J = 15.5 Hz, 1H), 6.06 (dt, J = 15.5, 7.5 Hz, 1H), 3.75 (t, J = 6.3 Hz, 2H), 2.50 (dt, J = 7.5, 6.3 Hz, 2H), 2.33 (s, 3H), 1.51 (s, 1H).

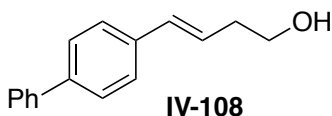
^{13}C NMR (126 MHz, CDCl_3) δ 136.31, 135.02, 130.72, 130.24, 127.59, 127.21, 126.05, 125.43, 62.06, 36.71, 19.84 ppm.



Following the above procedure, alcohol **IV-107** (420 mg, 50% yield) was synthesized as a colorless oil.

^1H NMR (500 MHz, Chloroform- d) δ 7.33 – 7.25 (m, 2H), 7.01 – 6.92 (m, 2H), 6.44 (d, J = 15.7 Hz, 1H), 6.10 (dt, J = 15.8, 7.2 Hz, 1H), 3.74 (t, J = 6.3 Hz, 2H), 2.49 – 2.39 (m, 2H).

^{13}C NMR (126 MHz, cdCl_3) δ 162.08 (d, $J_{\text{C-F}}$ = 246.1 Hz), 133.37 (d, $J_{\text{C-F}}$ = 3.3 Hz), 131.57, 127.50 (d, $J_{\text{C-F}}$ = 8.0 Hz), 126.09 (d, $J_{\text{C-F}}$ = 2.3 Hz), 61.99, 36.32.

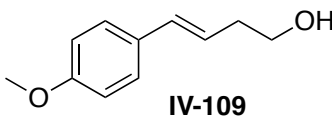


Following the above procedure, alcohol **IV-108** (600 mg, 54% yield) was synthesized as a white solid.

mp = 132–133°

^1H NMR (500 MHz, Chloroform- d) δ 7.60 – 7.56 (d, J = 8.0 Hz, 2H), 7.53 (d, J = 8.0 Hz, 2H), 7.43 – 7.40 (m, 4H), 7.34 – 7.30 (m, 1H), 6.53 (d, J = 15.9 Hz, 1H), 6.28 – 6.20 (dt, J = 15.9, 7.5 Hz, 1H), 3.76 (q, J = 6.0 Hz, 2H), 2.53 – 2.48 (m, 2H), 1.43 (t, J = 5.7 Hz, 1H).

^{13}C NMR (126 MHz, cdCl_3) δ 140.70, 140.01, 136.24, 132.39, 128.76, 127.24, 127.22, 126.89, 126.48, 62.03, 36.49.



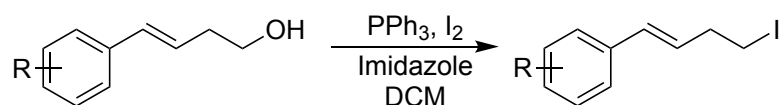
Following the above procedure, alcohol **IV-109** (350 mg, 40% yield) was synthesized as a white solid.

mp = 73–75°

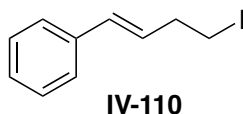
^1H NMR (500 MHz, Chloroform-*d*) δ 7.27 (d, J = 6.5 Hz, 2H), 6.82 (d, J = 6.5 Hz, 2H), 6.43 (d, J = 16.0 Hz, 1H), 6.04 (dt, J = 16.0, 7.2 Hz, 1H), 3.79 (s, 3H), 3.72 (t, J = 6.5 Hz, 2H), 2.45 (td, J = 7.2, 6.5 Hz, 2H), 1.44 (s, 1H).

^{13}C NMR (126 MHz, cdcl_3) δ 158.94, 132.30, 130.01, 127.18, 123.96, 113.92, 62.08, 55.28, 36.40.

Synthesis of homoallylic iodide



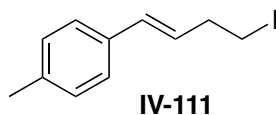
Homoallylic alcohols (~2.5 mmol) from above reactions were dissolved in DCM (~25 mL). To these solutions at room temperature were added triphenyl phosphine (1.2 equiv), iodine (1.2 equiv) and imidazole (1.2 equiv). The reaction mixtures were stirred at room temperature and followed by TLC. The reactions were completed within 1 h, after which water (25 mL) was added to quench the reaction. The organic layer was separated and the aqueous layer was extracted with DCM (3 x 20 mL). The combined organic extracts were washed with brine (20 mL), dried over sodium sulfate and concentrated under reduced pressure to yield the crude alcohol that was purified via column chromatography (silica, ethyl acetate/hexanes 5%) to afford the corresponding pure products.



Following the above procedure, homoallylic iodide **IV-110** (600 mg, 83% yield) was synthesized as a colorless oil.

^1H NMR (500 MHz, Chloroform-*d*) δ 7.39 – 7.33 (m, 2H), 7.29 (dd, J = 8.5, 6.8 Hz, 2H), 7.24 – 7.19 (m, 1H), 6.45 (dt, J = 15.8, 1.5 Hz, 1H), 6.13 (dt, J = 15.8, 7.0 Hz, 1H), 3.23 (t, J = 7.3 Hz, 2H), 2.77 (qd, J = 7.2, 1.4 Hz, 2H).

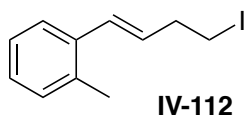
^{13}C NMR (126 MHz, cdCl_3) δ 137.03, 132.26, 130.94, 128.57, 126.99, 126.17, 36.99, 5.06.



Following the above procedure, homoallylic iodide **IV-111** (665 mg, 88% yield) was synthesized as a colorless oil.

^1H NMR (500 MHz, Chloroform-*d*) δ : 7.25 (d, J = 8.5 Hz, 2H), 7.10 (d, J = 8.5 Hz, 2H), 6.42 (d, J = 15.8, 1.5 Hz, 1H), 6.08 (dt, J = 15.8, 7.0 Hz, 1H), 3.22 (t, J = 7.3 Hz, 2H), 2.78 – 2.73 (dtd, J = 7.3, 7.0, 1.5 Hz, 2H), 2.32 (s, 3H) ppm.

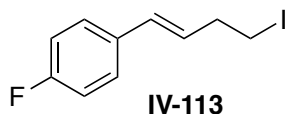
^{13}C NMR (126 MHz, cdCl_3) δ : 137.21, 134.22, 132.08, 129.25, 127.42, 126.04, 37.04, 21.18, 5.23 ppm.



Following the above procedure, homoallylic iodide **IV-112** (500 mg, 85% yield) was synthesized as a colorless oil.

^1H NMR (500 MHz, Chloroform-*d*) δ 7.42 – 7.39 (m, 1H), 7.14 (m, 3H), 6.66 (d, J = 15.6 Hz, 1H), 5.99 (dt, J = 15.6, 7.0 Hz, 1H), 3.25 (t, J = 7.2 Hz, 2H), 2.78 (dt, J = 7.2, 7.0 Hz, 2H), 2.33 (s, 3H) ppm.

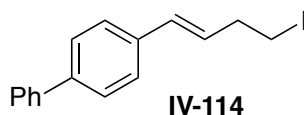
^{13}C NMR (126 MHz, cdCl_3) δ 136.26, 135.21, 130.30, 130.23, 129.80, 127.35, 126.09, 125.60, 37.18, 19.87, 5.40 ppm.



Following the above procedure, homoallylic iodide **IV-113** (610 mg, 93% yield) was synthesized as a colorless oil.

^1H NMR (500 MHz, Chloroform-*d*) δ 7.35 – 7.27 (m, 2H), 7.04 – 6.95 (m, 2H), 6.41 (dt, J = 15.8, 1.4 Hz, 1H), 6.04 (dt, J = 15.8, 6.9 Hz, 1H), 3.22 (t, J = 7.2 Hz, 2H), 2.75 (qd, J = 7.1, 1.4 Hz, 2H).

^{13}C NMR (126 MHz, Chloroform-*d*) δ 162.20 (d, $J_{\text{C-F}}$ = 246.5 Hz), 133.19 (d, $J_{\text{C-F}}$ = 3.3 Hz), 131.10, 128.23 (d, $J_{\text{C-F}}$ = 2.3 Hz), 127.65 (d, $J_{\text{C-F}}$ = 8.1 Hz), 115.47 (d, $J_{\text{C-F}}$ = 21.7 Hz), 36.87, 5.06.

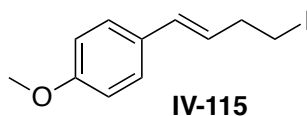


Following the above procedure, homoallylic iodide **IV-114** (850 mg, 98% yield) was synthesized as an off white solid.

mp = 93–95°

^1H NMR (500 MHz, Chloroform-*d*) δ : 7.59 – 7.52 (m, 4H), 7.43 – 7.40 (m, 4H), 7.35 – 7.29 (m, 1H), 6.49 (d, J = 15.8 Hz, 1H), 6.18 (dt, J = 15.8, 7.0 Hz, 1H), 3.24 (t, J = 7.2 Hz, 2H), 2.79 (dt, J = 7.2, 7.0 Hz, 2H).

^{13}C NMR (126 MHz, cdCl_3) δ : 140.70, 140.20, 136.06, 131.82, 128.77, 128.62, 127.28, 126.90, 126.59, 37.04, 5.06 ppm.

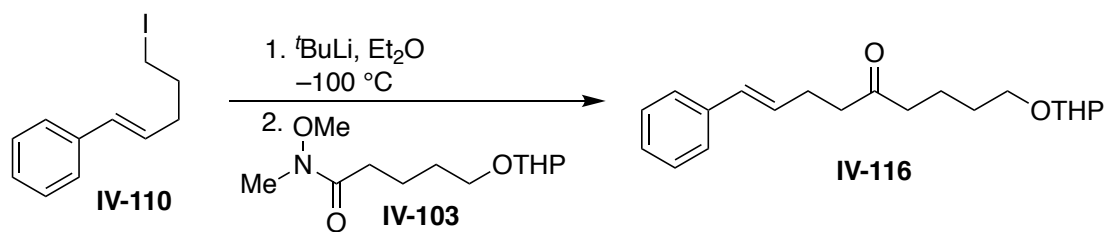


Following the above procedure, homoallylic iodide **IV-115** (500 mg, 94% yield) was synthesized as a colorless oil.

^1H NMR (500 MHz, Chloroform-*d*) δ 7.28 (m, 2H), 6.89 – 6.78 (m, 2H), 6.39 (d, J = 15.8 Hz, 1H), 5.99 (dtd, J = 15.7, 7.0, 0.8 Hz, 1H), 3.79 (s, 3H), 3.21 (td, J = 7.3, 0.8 Hz, 2H), 2.74 (qt, J = 7.2, 1.0 Hz, 2H).

^{13}C NMR (126 MHz, cdCl_3) δ 159.07, 131.65, 129.84, 127.31, 126.29, 113.98, 55.31, 37.08, 5.46.

Synthesis of ketones IV-116 to IV-121



General procedure for synthesis of ketones from the corresponding homoallylic

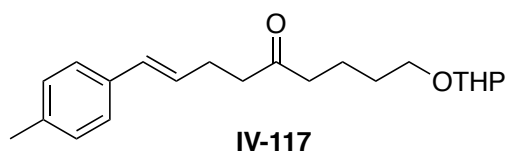
iodide: To a flame dried flask containing diethyl ether (10.0 mL) under argon at $-100\text{ }^{\circ}\text{C}$ (liquid nitrogen in methanol bath) was added ^tBuLi (1.7 M in pentane, 3.0 mL, 5.25 mmol, 2.5 equiv) dropwise. To this solution was added alkyl iodide **IV-110** (560 mg, 2.1 mmol, 1.0 equiv) in diethyl ether (3.0 mL) dropwise at the same temperature. The reaction stirred at this temperature for 30 min. To this solution at $-78\text{ }^{\circ}\text{C}$ was added a solution of the Weinreb amide **IV-103** (514 mg, 2.1 mmol) in diethyl ether (3 mL). The reaction was slowly warmed up to room temperature over 2 h. TLC showed completion of the reaction. Saturated ammonium chloride (10 mL) was added to this solution, the organic layer was separated and the aqueous layer was extracted with ethyl acetate (3 x 10 mL). The combined organic extracts were washed with brine (20 mL), dried over sodium sulfate and concentrated under reduced pressure to yield the crude alcohol that was purified via column chromatography (silica, ethyl acetate/hexanes 10 – 20%) to afford the corresponding pure **IV-116** as a clear oil (510 mg, 82%).

¹H NMR (500 MHz, Chloroform-d) δ 7.31 – 7.28 (m, 2H), 7.28 – 7.24 (m, 2H), 7.19 – 7.13 (m, 1H), 6.39 – 6.35 (m, 1H), 6.17 (dt, $J = 15.8, 6.8\text{ Hz}$, 1H), 4.51 (dd, $J = 4.7, 2.7\text{ Hz}$, 1H), 3.80 (dddd, $J = 11.1, 7.7, 4.3, 2.9\text{ Hz}$, 1H), 3.71 (dt, $J = 9.7, 6.4\text{ Hz}$, 1H), 3.49 – 3.43

(m, 1H), 3.38 (dt, $J = 9.7, 6.1$ Hz, 1H), 2.62 – 2.56 (m, 2H), 2.55 – 2.50 (m, 2H), 2.49 – 2.42 (m, 2H), 1.89 – 1.83 (m, 2H), 1.80 – 1.70 (m, 2H), 1.57 – 1.43 (m, 5H).

^{13}C NMR (126 MHz, cdCl_3) δ 209.79, 137.41, 130.66, 128.99, 128.48, 127.05, 125.98, 98.90, 66.57, 62.45, 42.23, 39.72, 30.69, 27.13, 25.43, 23.94, 19.69.

TOF MS ES^+ ($\text{C}_{20}\text{H}_{28}\text{NaO}_3$): Calc. $[\text{M} + \text{H}]^+$: 339.1936, Found $[\text{M} + \text{H}]^+$: 339.1923.

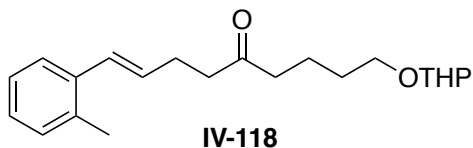


Following the above procedure, ketone **IV-117** (320 mg, 91% yield) was synthesized as a colorless oil.

^1H NMR (500 MHz, $\text{Chloroform-}d$) δ : 7.20 (d, $J = 8.0$ Hz, 2H), 7.07 (d, $J = 8.0$ Hz, 2H), 6.34 (d, $J = 15.7$ Hz, 1H), 6.11 (dt, $J = 15.7, 6.8$ Hz, 1H), 4.54 (dd, $J = 4.4, 2.8$ Hz, 1H), 3.83 (ddd, $J = 11.0, 7.7, 3.2$ Hz, 1H), 3.72 (dt, $J = 9.5, 6.4$ Hz, 1H), 3.51 – 3.43 (m, 1H), 3.36 (dt, $J = 9.6, 6.2$ Hz, 1H), 2.55 (t, $J = 7.5$ Hz, 2H), 2.45 (td, $J = 7.5, 2.2$ Hz, 4H), 2.30 (s, 3H), 1.83 – 1.74 (m, 1H), 1.73 – 1.61 (m, 3H), 1.61 – 1.45 (m, 6H) ppm.

^{13}C NMR (126 MHz, cdCl_3) δ 210.15, 136.77, 134.59, 130.48, 129.15, 127.86, 125.85, 98.84, 67.13, 62.32, 42.63, 42.31, 30.71, 29.21, 27.13, 25.44, 21.12, 20.62, 19.63 ppm.

TOF MS ES^+ ($\text{C}_{21}\text{H}_{30}\text{NaO}_3$): Calc. $[\text{M} + \text{H}]^+$: 353.2093, Found $[\text{M} + \text{H}]^+$: 353.2107.

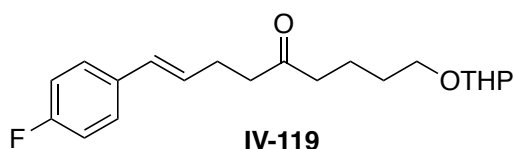


Following the above procedure, ketone **IV-118** (300 mg, 90% yield) was synthesized as a colorless oil.

^1H NMR (500 MHz, Chloroform-*d*) δ 7.36 – 7.34 (m, 1H), 7.14 – 7.08 (m, 3H), 6.58 (d, J = 15.6 Hz, 1H), 6.03 (dt, J = 15.6, 6.8 Hz, 1H), 4.54 (dd, J = 4.4, 2.8 Hz, 1H), 3.83 (ddd, J = 11.0, 7.7, 3.0 Hz, 1H), 3.73 (dt, J = 9.6, 6.4 Hz, 1H), 3.54 – 3.42 (m, 1H), 3.36 (dt, J = 9.6, 6.3 Hz, 1H), 2.60 – 2.54 (m, 2H), 2.53 – 2.43 (m, 4H), 2.30 (s, 3H), 1.85 – 1.73 (m, 1H), 1.73 – 1.61 (m, 3H), 1.63 – 1.45 (m, 6H).

^{13}C NMR (126 MHz, cdCl_3) δ 210.09, 136.52, 134.97, 130.28, 130.15, 128.56, 127.00, 126.00, 125.42, 98.87, 67.15, 62.35, 42.66, 42.38, 30.73, 29.23, 27.48, 25.46, 20.64, 19.81, 19.65.

TOF MS ES^+ ($\text{C}_{21}\text{H}_{30}\text{NaO}_3$): Calc. $[\text{M} + \text{H}]^+$: 353.2093, Found $[\text{M} + \text{H}]^+$: 353.2093.



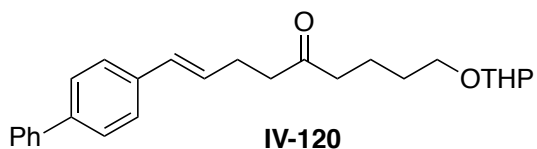
Following the above procedure, ketone **IV-119** (325 mg, 95% yield) was synthesized as a colorless oil.

^1H NMR (500 MHz, Chloroform-*d*) δ 7.30 – 7.20 (m, 2H), 6.99 – 6.91 (m, 2H), 6.34 (dd, J = 15.8, 1.5 Hz, 1H), 6.08 (dt, J = 15.8, 6.9 Hz, 1H), 4.53 (dd, J = 4.5, 2.8 Hz, 1H), 3.83 (ddd, J = 11.0, 7.7, 3.2 Hz, 1H), 3.72 (dt, J = 9.6, 6.4 Hz, 1H), 3.52 – 3.43 (m, 1H), 3.36

(dt, $J = 9.6, 6.3$ Hz, 1H), 2.56 (t, $J = 7.4$ Hz, 2H), 2.50 – 2.39 (m, 4H), 1.84 – 1.74 (m, 1H), 1.73 – 1.62 (m, 3H), 1.62 – 1.45 (m, 6H).

^{13}C NMR (126 MHz, Chloroform- d) δ 210.01, 161.98 (d, $J_{\text{C-F}} = 246.0$ Hz), 133.55 (d, $J_{\text{C-F}} = 3.3$ Hz), 129.52, 128.70 (d, $J_{\text{C-F}} = 2.2$ Hz), 127.41 (d, $J_{\text{C-F}} = 7.7$ Hz), 115.34 (d, $J_{\text{C-F}} = 21.5$ Hz), 98.89, 67.15, 62.38, 42.65, 42.18, 30.73, 29.23, 27.04, 25.46, 20.64, 19.67.

TOF MS ES^+ ($\text{C}_{20}\text{H}_{27}\text{FNaO}_3$): Calc. $[\text{M} + \text{H}]^+$: 357.1842, Found $[\text{M} + \text{H}]^+$: 357.1869.



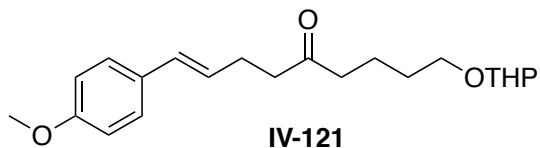
Following the above procedure, ketone **IV-120** (250 mg, 65% yield) was synthesized as an off white solid.

mp = 41– 44°

^1H NMR (500 MHz, Chloroform- d) δ 7.59 – 7.54 (m, 2H), 7.54 – 7.47 (m, 2H), 7.46 – 7.35 (m, 3H), 7.35 – 7.27 (m, 1H), 6.46 – 6.38 (m, 1H), 6.22 (dt, $J = 15.8, 6.8$ Hz, 1H), 4.54 (dd, $J = 4.5, 2.7$ Hz, 1H), 3.83 (ddd, $J = 11.1, 7.6, 3.4$ Hz, 1H), 3.73 (dt, $J = 9.6, 6.4$ Hz, 1H), 3.52 – 3.42 (m, 1H), 3.37 (dt, $J = 9.6, 6.2$ Hz, 1H), 2.63 – 2.54 (m, 2H), 2.53 – 2.43 (m, 3H), 1.85 – 1.74 (m, 1H), 1.74 – 1.63 (m, 3H), 1.63 – 1.42 (m, 6H).

^{13}C NMR (126 MHz, cdCl_3) δ 210.08, 140.75, 139.81, 136.46, 130.25, 129.17, 129.15, 128.77, 128.75, 127.24, 127.19, 127.14, 127.09, 126.98, 126.92, 126.88, 126.46, 126.41, 98.88, 67.17, 62.37, 42.67, 42.24, 30.74, 29.24, 27.20, 25.47, 20.66, 19.66.

TOF MS ES^+ ($\text{C}_{26}\text{H}_{32}\text{NaO}_3$): Calc. $[\text{M} + \text{H}]^+$: 415.2249, Found $[\text{M} + \text{H}]^+$: 415.2264.



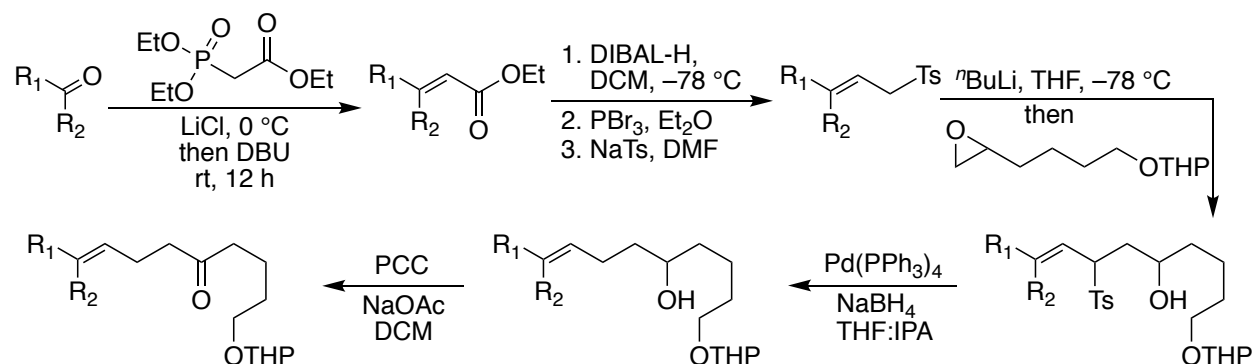
Following the above procedure, ketone **IV-121** (290 mg, 95% yield) was synthesized as a colorless oil.

^1H NMR (500 MHz, Chloroform- d) δ 7.26 – 7.20 (m, 2H), 6.84 – 6.77 (m, 2H), 6.32 (dt, J = 15.8, 1.5 Hz, 1H), 6.02 (dt, J = 15.8, 6.9 Hz, 1H), 4.54 (dd, J = 4.4, 2.8 Hz, 1H), 3.83 (ddd, J = 11.0, 7.5, 3.4 Hz, 1H), 3.77 (s, 3H), 3.72 (dt, J = 9.6, 6.4 Hz, 1H), 3.53 – 3.43 (m, 1H), 3.36 (dt, J = 9.6, 6.2 Hz, 1H), 2.55 (t, J = 7.5 Hz, 2H), 2.43 (tdd, J = 8.0, 7.3, 4.7, 1.5 Hz, 4H), 1.86 – 1.74 (m, 1H), 1.72 – 1.61 (m, 3H), 1.61 – 1.45 (m, 6H).

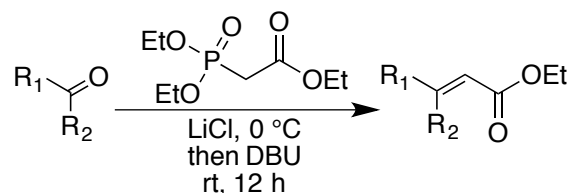
^{13}C NMR (126 MHz, cdCl_3) δ 210.22, 158.79, 130.23, 130.03, 127.08, 126.74, 113.89, 98.87, 67.16, 62.35, 55.27, 42.65, 42.42, 30.73, 29.23, 27.15, 25.46, 20.64, 19.65.

TOF MS ES^+ ($\text{C}_{21}\text{H}_{30}\text{NaO}_4$): Calc. $[\text{M} + \text{H}]^+$: 369.2042, Found $[\text{M} + \text{H}]^+$: 369.2060.

IV-6-5 General procedure for synthesis of ketone IV-131 to IV-133

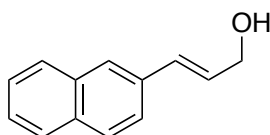


Synthesis of substituted cinnamyl alcohol:



Following a reported procedure,⁴⁴ to a solution of lithium chloride (dried under vacuum, 466 mg, 11 mmol, 1.1 equiv) in dry acetonitrile at $0\text{ }^{\circ}C$, aldehyde or ketone (10.0 mmol, 1.0 equiv) and triethylphosphonoacetate (2.25 g, 10.0 mmol, 1.0 equiv) were added. After 4 min, DBU (1.5 g, 10.0 mmol, 1.0 equiv) was added. The reaction mixture was warmed to room temperature and stirred for 12 h. The reaction mixture was diluted with ethyl acetate (50 mL), washed with saturated ammonium chloride solution and brine. The volatiles were removed under reduced pressure and the resultant crude esters were purified on column chromatography (silica, ethyl acetate/hexanes = 20 – 30%). The resulting esters were reduced with $DIBAL-H$ to yield the allyl alcohols as described below. To a solution of esters (5.0 mmol) in dry DCM (20 mL) at $-78\text{ }^{\circ}C$ was added $DIBAL-H$ (1.0 M in hexane, 10.0 mL, 2.0 equiv). The reaction mixture was warmed to room

temperature over 2 h, upon which TLC showed completion of reaction. The reaction mixtures were quenched by addition of methanol (5.0 mL) at 0 °C. Saturated potassium sodium tartrate solution (20.0 mL) was added to the solution and the mixture was vigorously stirred at room temperature for 2 h. The aqueous layer was extracted with DCM (3 x 30 mL). The combined organic extracts were washed with brine (20 mL), dried over sodium sulfate and concentrated under vacuum to yield the corresponding allyl alcohols.

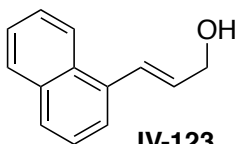


IV-122

Analytical data for alcohol **IV-122**;

^1H NMR (500 MHz, CDCl_3) δ 7.81 – 7.75 (m, 3H), 7.72 (s, 1H), 7.59 (dd, J = 8.6, 1.8 Hz, 1H), 7.48 – 7.39 (m, 2H), 6.77 (dt, J = 15.9, 1.6 Hz, 1H), 6.48 (dt, J = 15.9, 5.7 Hz, 1H), 4.37 (d, J = 5.6 Hz, 2H), 1.46 (s, 1H).

^{13}C NMR (125 MHz, CDCl_3) δ 134.0, 133.5, 133.0, 131.2, 128.8, 128.2, 127.9, 127.6, 126.4, 126.2, 125.9, 123.5, 63.8 ppm.

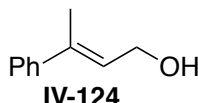


IV-123

Analytical data alcohol **IV-123**;

^1H NMR (500 MHz, CDCl_3) δ 8.11 (d, J = 8.0 Hz, 1H), 7.84 (dd, J_1 = 7.5 Hz, J_2 = 2 Hz, 1H), 7.77 (d, J = 8.0 Hz, 1H), 7.57 (d, J = 7.0 Hz, 1H), 7.51-7.46 (m, 2H), 7.43 (dd, J_1 =

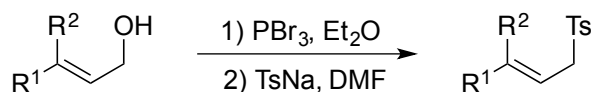
7.5 Hz, J2 = 7.5 Hz, 1H), 7.37 (d, J = 15.5 Hz, 1H), 6.38 (ddd, J1 = 15.5 Hz, J2 = 5 Hz, J3 = 5 Hz, 1H), 4.42 (dd, J1 = 5 Hz, J2 = 1.5 Hz, 2H), 1.66 (br, 1H);
 ^{13}C NMR (125 MHz, CDCl_3) δ 134.4, 133.5, 131.7, 131.1, 128.5, 128.1, 127.9, 126.0, 125.7, 125.5, 123.8, 123.6, 63.9 ppm.



Analytical data for alcohol **IV-124**;

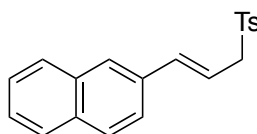
^1H NMR (500 MHz, CDCl_3) δ 7.41 – 7.38 (m, 2H), 7.34 – 7.29 (m, 2H), 7.27 – 7.23 (m, 1H), 5.98 – 5.94 (m, 1H), 4.3 (d, J = 6.5 Hz, 2H), 2.08 – 2.06 (m, 3H), 1.73 (br, 1H).
 ^{13}C NMR (125 MHz, CDCl_3) δ 142.79, 137.73, 128.08, 127.21, 126.45, 125.71, 59.86, 15.95.

General procedure for substituted allyl sulfonyl substrates:



To allyl alcohols (16 mmol) in dry diethyl ether (10 mL) at room temperature was added phosphorous tribromide (6.15 mmol, 0.3 equiv) drop-wise at 0 °C. Reaction was completed in 1 h, as judged by TLC analysis. The reaction mixture was quenched by slow addition sodium bicarbonate (saturated solution, 10 mL). Layers were separated and the aqueous layer was extracted with diethyl ether (3 x 20 mL). The combined organic extracts were washed with brine, dried over sodium sulfate and concentrated under reduced

pressure at 0 °C (protected from light). The resulting crude allyl bromide was quickly reacted with sodium p-toluenesulfinate (1.5 equiv) in DMF (10 mL) at room temperature. The reaction was stirred for 30 h, and then quenched with saturated ammonium chloride (20 mL). The aqueous layer was extracted with ethyl acetate (3 x 20 mL). The combined organic extracts were washed with brine, dried over sodium sulfate and concentrated under reduced pressure. Crude allyl sulfonyl products were purified by crystallization from ethyl acetate.

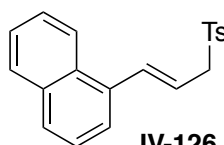


IV-125

Analytical data for sulfonyl **IV-125**;

^1H NMR (500 MHz, CDCl_3) δ 7.75-7.79 (m, 5H), 7.63 (s, 1H), 7.48 (d, $J = 8.5$ Hz, 1H), 7.42-7.47 (m, 2H), 7.30 (d, $J = 7.5$ Hz, 2H), 6.53 (d, $J = 16.0$ Hz, 1H), 6.21 (ddd, $J_1 = 16.0$ Hz, $J_2 = 7.5$ Hz, $J_3 = 7.5$ Hz, 1H), 3.97 (d, $J = 7.5$ Hz, 2H), 2.41 (s, 3H).

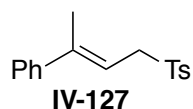
^{13}C NMR (125 MHz, CDCl_3) δ 144.7, 139.0, 135.4, 133.3, 133.28, 133.21, 129.7, 128.5, 128.3, 128.0, 127.6, 127.0, 126.4, 126.3, 123.2, 115.5, 60.6, 21.6 ppm. IR (film) 3052, 2959, 2917, 1652, 1596, 1510, 1406, 1314 (s), 1288, 1151, 1136 (s), 1085, 963, 812, 752, 724 cm^{-1} .



IV-126

Analytical data for sulfonyl **IV-126**;

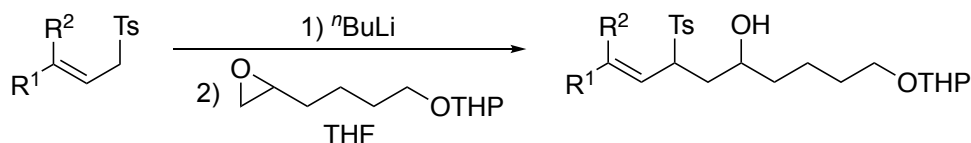
^1H NMR (500 MHz, CDCl_3) δ 7.81 (d, J = 8.0 Hz, 1H), 7.77 (d, J = 8.5 Hz, 3H), 7.66 (d, J = 8.5 Hz, 1H), 7.48-7.40 (m, 4H), 7.31 (d, J = 8.0, 2H), 7.05 (d, J = 15.0 Hz, 1H), 6.11 (ddd, J_1 = 15.0 Hz, J_2 = 7.5 Hz, J_3 = 7.5 Hz, 1H), 4.03 (d, J = 7.5 Hz, 2H), 2.42 (s, 3H); ^{13}C NMR (125 MHz, CDCl_3) δ 144.7, 136.7, 135.2, 133.5, 133.4, 130.7, 129.7, 128.7, 128.6, 128.5, 126.1, 125.9, 125.5, 124.2, 123.4, 118.7, 60.7, 21.6 ppm. IR (film) 3047, 2976, 2925, 1595, 1508, 1398, 1316 (s), 1292, 1148 (s), 1088, 967, 799, 778, 726, 669 cm^{-1} .



Analytical data for sulfonyl **IV-127**;

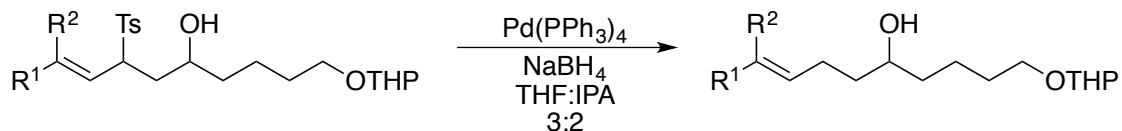
^1H NMR (500 MHz, CDCl_3) δ 7.76 – 7.74 (m, 2H), 7.31 – 7.24 (m, 7H), 5.71 – 5.69 (td, J = 8.0, 1.5 Hz, 1H), 3.97 (d, J = 8.0 Hz, 2H), 2.42 (s, 3H), 1.69 (d, J = 1.5 Hz, 1H). ^{13}C NMR (125 MHz, CDCl_3) δ 144.65, 144.34, 142.24, 135.69, 129.67, 128.51, 128.33, 127.83, 125.81, 113.40, 56.72, 21.63, 15.98.

General procedure for synthesis of substituted sulfonyl alcohol substrates:



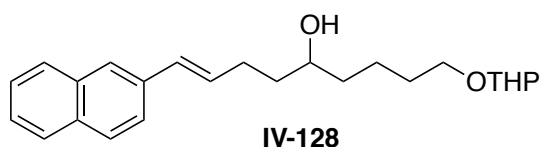
In a typical procedure, allyl sulfonyl substrates (2.0 mmol) were dissolved in dry THF (3 mL) under argon. To this solution at $-78\text{ }^\circ\text{C}$ was added $n\text{BuLi}$ (1.8 M in hexane, 1.2 mL, 2.1 mmol, 1.05 equiv) dropwise. The reaction was stirred at this temperature for 5 min, then it was warmed to room temperature and stirring was continued for another 10 min. To this mixture at $-78\text{ }^\circ\text{C}$ was added neat THP-protected epoxy alcohol (420.2 mg, 2.1 mmol, 1.05 equiv) via syringe over 5 minutes. The reaction mixture was warmed to room temperature and was followed by TLC. After completion of the reaction ($\sim 1\text{ h}$), saturated ammonium chloride (10 mL) was added to the mixture. The aqueous layer was extracted with ethyl acetate (3 x 10 mL). The combined organic extracts were washed with brine, dried over sodium sulfate and concentrated under reduced pressure. The crude mixture was purified via column chromatography yielding a $\sim 1:1$ diastereomeric mixture which was subjected to the next step without further separating the diastereomers.

General procedure for detosylation of substituted sulfonyl alcohol substrates:



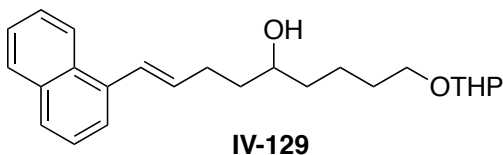
Diastereomeric sulfonyl alcohol (1.5 mmol) was dissolved in a mixture of THF:IPA (3:2, 20 mL) under an argon atmosphere. To this mixture at room temperature was added

tetrakis(triphenylphosphine)palladium (86 mg, 0.075 mmol, 0.05 equiv). The reaction mixture was placed in an ice bath at 0 °C. To this cold mixture sodium borohydride (582 mg, 15.0 mmol, 10.0 mmol) was added in a few portions. The reaction was stirred at room temperature for 12 h, then it was quenched at 0 °C by careful addition of water (10 mL). The aqueous layer was extracted with ethyl acetate (3 x 20 mL). The combined organic layers were washed with brine (20 mL), dried over sodium sulfate and concentrated under reduced pressure. The crude product was purified via column chromatography yielding alcohol products in good yield.



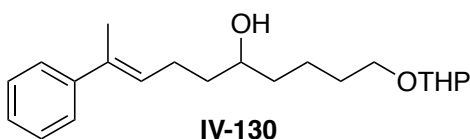
Analytical data for alcohol **IV-128**:

¹H NMR (500 MHz, CDCl₃) δ 7.78 – 7.73 (m, 3H), 7.65 (d, J = 1.6 Hz, 1H), 7.55 (dd, J = 8.5, 1.8 Hz, 1H), 7.44 – 7.37 (m, 2H), 6.60 – 6.53 (m, 1H), 6.35 (dt, J = 15.8, 6.9 Hz, 1H), 4.55 (dd, J = 4.6, 2.8 Hz, 1H), 3.89 – 3.81 (m, 1H), 3.77 – 3.66 (m, 2H), 3.54 – 3.43 (m, 2H), 3.39 (dtd, J = 9.7, 6.4, 1.5 Hz, 1H), 2.38 (m, 2H), 1.88 – 1.75 (m, 2H), 1.73 – 1.37 (m, 12H).



Analytical data for alcohol **IV-129**:

^1H NMR (500 MHz, CDCl_3) δ 8.14 – 8.07 (m, 1H), 7.83 – 7.79 (m, 1H), 7.75 – 7.70 (m, 1H), 7.53 (dt, $J = 7.1, 1.0$ Hz, 1H), 7.50 – 7.38 (m, 3H), 7.21 – 7.10 (m, 1H), 6.23 (dt, $J = 15.5, 6.9$ Hz, 1H), 4.58 – 4.51 (m, 1H), 3.89 – 3.82 (m, 1H), 3.79 – 3.65 (m, 2H), 3.52 – 3.44 (m, 1H), 3.38 (m, 1H), 2.55 – 2.32 (m, 2H), 1.81 (qt, $J = 8.7, 2.5$ Hz, 1H), 1.75 – 1.39 (m, 14H).

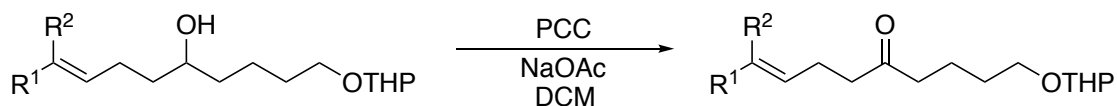


Analytical data for alcohol **VI-130**:

^1H NMR (500 MHz, CDCl_3) δ 7.36 – 7.34 (m, 2H), 7.29 – 7.26 (m, 2H), 7.20 – 7.18 (m, 1H), 5.78 (t, $J = 7.5$ Hz, 1H), 4.56 (m, 1H), 3.86 – 3.83 (m, 1H), 3.77 – 3.72 (m, 1H), 3.66 (m, 1H), 3.50 – 3.47 (m, 1H), 3.41 – 3.37 (m, 1H), 2.34 – 2.27 (m, 2H), 2.04 (s, 3H), 1.81 – 1.78 (m, 1H), 1.71 – 1.66 (m, 1H), 1.63 – 1.43 (m, 12H).

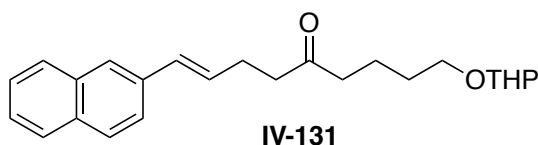
^{13}C NMR (126 MHz, cdcl_3) δ 143.81, 135.15, 128.12, 127.88, 126.52, 125.56, 98.92, 71.46, 67.48, 62.37, 37.31, 37.14, 30.75, 29.66, 25.46, 25.06, 22.40, 19.66, 15.78.

General procedure for oxidation of the alcohol substrates into olefinic ketones:



The olefinic alcohol (1.0 mmol) was dissolved in DCM (5 mL) in a 20 mL screw-top vial. To this solution at room temperature were added pyridinium chlorochromate (323.4 mg,

1.5 mmol, 1.5 equiv) and sodium acetate (24.6 mg, 0.3 mmol, 0.3 equiv). The reaction was stirred at this temperature until TLC showed complete consumption of the alcohol (ca. 1 h). The crude mixture was diluted with ethyl acetate and the precipitates were removed by passing the mixture through celite. Volatiles were removed and the resulting crude ketone was purified via column chromatography (ethyl acetate/hexanes = 20%).

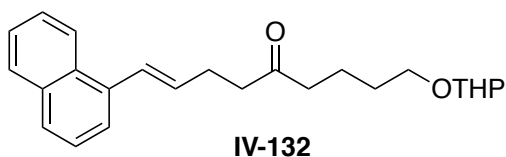


Analytical data for ketone **IV-131**:

^1H NMR (500 MHz, CDCl_3) δ 7.77 – 7.72 (m, 3H), 7.65 (d, J = 1.6 Hz, 1H), 7.53 (dd, J = 8.5, 1.8 Hz, 1H), 7.44 – 7.37 (m, 2H), 6.54 (d, J = 15.8 Hz 1H), 6.31 (dt, J = 15.8, 6.8 Hz, 1H), 4.54 (dd, J = 4.4, 2.8 Hz, 1H), 3.83 (ddd, J = 11.1, 7.6, 3.2 Hz, 1H), 3.73 (dt, J = 9.6, 6.4 Hz, 1H), 3.49 – 3.44 (m, 1H), 3.37 (dt, J = 9.7, 6.2 Hz, 1H), 2.61 (dd, J = 8.2, 6.8 Hz, 2H), 2.55 – 2.49 (m, 2H), 2.46 (td, J = 7.3, 3.7 Hz, 2H), 1.79 (qd, J = 8.0, 3.7 Hz, 1H), 1.68 (dddd, J = 12.6, 9.1, 5.7, 2.4 Hz, 3H), 1.62 – 1.45 (m, 6H).

^{13}C NMR (125 MHz, CDCl_3) δ 210.04, 134.82, 133.58, 133.27, 132.69, 130.76, 129.39, 128.04, 127.80, 127.57, 126.12, 125.54, 123.41, 98.84, 67.12, 62.32, 42.63, 42.20, 30.69, 29.20, 27.21, 25.42, 20.62, 19.62.

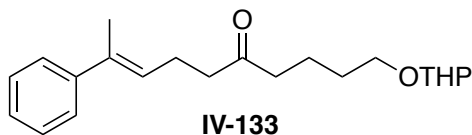
TOF MS ES^+ ($\text{C}_{24}\text{H}_{30}\text{NaO}_3$): Calc. $[\text{M} + \text{H}]^+$: 389.2093, Found $[\text{M} + \text{H}]^+$: 389.2119.



Analytical data for ketone **IV-132**:

^1H NMR (500 MHz, Chloroform- d) δ 8.13 – 8.07 (m, 1H), 7.85 – 7.81 (m, 1H), 7.75 (d, J = 8.0 Hz, 1H), 7.54 – 7.51 (m, 1H), 7.49 (td, J = 8.0, 1.5 Hz, 2H), 7.44 – 7.40 (m, 1H), 7.15 (d, J = 15.5 Hz, 1H), 6.20 (dt, J = 15.5, 6.6 Hz, 1H), 4.55 (dt, J = 5.7, 2.7 Hz, 1H), 3.84 (td, J = 8.3, 3.9 Hz, 1H), 3.75 (dt, J = 9.6, 6.4 Hz, 1H), 3.54 – 3.45 (m, 1H), 3.38 (dt, J = 9.8, 6.4 Hz, 1H), 2.71 – 2.64 (m, 2H), 2.65 – 2.58 (m, 2H), 2.51 (t, J = 7.3 Hz, 2H), 1.85 – 1.77 (m, 1H), 1.74 – 1.66 (m, 3H), 1.66 – 1.44 (m, 6H).

TOF MS ES^+ ($\text{C}_{24}\text{H}_{30}\text{NaO}_3$): Calc. $[\text{M} + \text{H}]^+$: 389.2093, Found $[\text{M} + \text{H}]^+$: 389.2121.

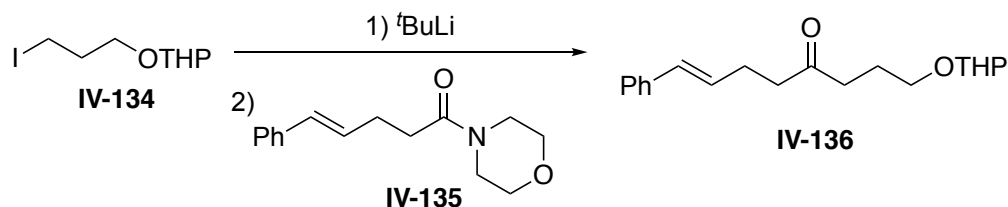


Analytical data for ketone **IV-133**:

^1H NMR (500 MHz, Chloroform- d) δ 7.36 – 7.32 (m, 2H), 7.29 – 7.24 (m, 2H), 7.20 – 7.18 (m, 1H), 5.67 (t, J = 6.5 Hz, 1H), 4.54 (m, 1H), 3.84 – 3.80 (m, 1H), 3.74 – 3.70 (m, 1H), 3.49 – 3.46 (m, 1H), 3.38 – 3.33 (m, 1H), 2.53 (t, J = 6.5 Hz, 2H), 2.46 – 2.43 (m, 4H), 2.02 (s, 3H), 1.80 – 1.76 (m, 1H), 1.70 – 1.63 (m, 3H), 1.60 – 1.51 (m, 6H).

^{13}C NMR (126 MHz, cdCl_3) δ 210.36, 143.61, 135.80, 128.14, 126.65, 126.46, 125.59, 98.85, 67.13, 62.32, 42.61, 42.35, 30.71, 29.22, 25.44, 23.12, 20.64, 19.62, 15.79.

IV-6-6 Procedure for the synthesis of THP-protected keto alkenols IV-136

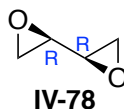


To a flame dried round bottom flask (10 mL) containing dry diethyl ether (4 mL) at $-100\text{ }^{\circ}\text{C}$ (liquid nitrogen-methanol bath) was added ^tBuLi (1.7 M solution in pentane, 1.5 mL) dropwise. The THP protected alkyl iodide **IV-134** (1 mmol) in dry diethyl ether (1 mL) was added over 5 min. The reaction was stirred at $-100\text{ }^{\circ}\text{C}$ for 10 min, then slowly brought to room temperature and kept at that temperature for 10 min. After this period of time (~ 30 min), the reaction mixture was placed in to a liquid nitrogen-methanol bath ($-100\text{ }^{\circ}\text{C}$) and a solution of the corresponding morpholine amide **IV-135** (0.5 mmol) dry ether (1 mL) was added over 5 min. The reaction mixture stirred at $-78\text{ }^{\circ}\text{C}$ and was monitored by TLC. After complete consumption of the amide starting material, the reaction was quenched at $-78\text{ }^{\circ}\text{C}$ with NaCl solution (sat.). The organic phase was separated and the aqueous layer was washed with ethyl acetate (3 x 5 mL). The combined organics were concentrated under reduced pressure to yield the crude product. Column chromatography of the crude mixture (ethyl acetate/hexanes = 20%) led to the isolation of the pure THP-protected keto alkenol **IV-136** (80 mg, 60% yield) as a clear oil.

^1H NMR (500 MHz, Chloroform- d) δ 7.37 – 7.25 (m, 4H), 7.25 – 7.15 (m, 1H), 6.48 – 6.36 (m, 1H), 6.20 (dt, J = 15.8, 6.8 Hz, 1H), 4.54 (dd, J = 4.7, 2.7 Hz, 1H), 3.88 – 3.79 (m, 1H), 3.73 (tt, J = 8.6, 6.3 Hz, 1H), 3.53 – 3.45 (m, 1H), 3.41 (dt, J = 9.7, 6.1 Hz, 1H), 2.66 – 2.58 (m, 2H), 2.58 – 2.52 (m, 2H), 2.52 – 2.46 (m, 2H), 1.94 – 1.86 (m, 2H), 1.83 – 1.76 (m, 1H), 1.73 – 1.65 (m, 2H), 1.59 – 1.48 (m, 4H).

^{13}C NMR (126 MHz, cdCl_3) δ 209.70, 137.31, 130.57, 128.89, 128.39, 126.96, 125.89, 98.80, 66.47, 62.36, 42.14, 39.63, 30.60, 27.04, 25.34, 23.85, 19.60.

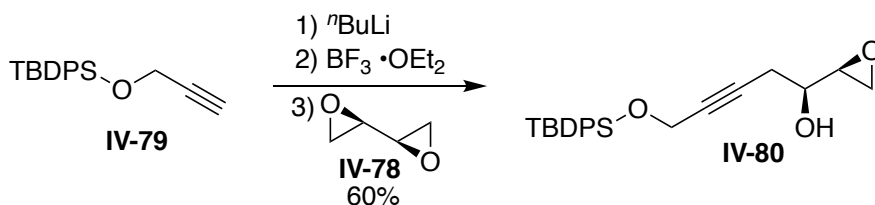
IV-7 Experimental date for the synthesis of Obtusin



Synthesis of Diepoxide IV-78: Following the reported procedure,³⁶⁻³⁷ 7.5-gram **IV-78** as a clear oil (solidifies at $-20\text{ }^{\circ}\text{C}$ to a white solid) was synthesized from *D*-tartaric acid.

^1H NMR (500 MHz, CDCl_3) δ 2.89 – 2.84 (m, 2H), 2.80 (m, 2H), 2.71 (m, 2H).

^{13}C NMR (125 MHz, CDCl_3) δ 77.3, 77.0, 76.7, 51.1, 44.3.



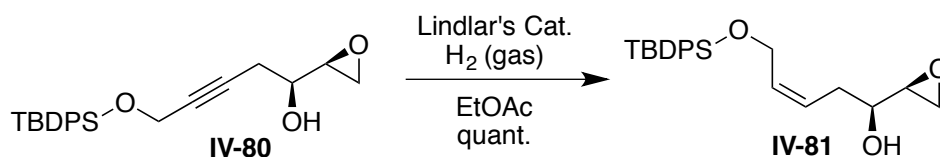
Synthesis of epoxy alcohol IV-80: Following a reported procedure,³⁸ to **IV-79** (1.0 equiv, 10.0 mmol, 2.9 g) in dry THF (90 mL) at $-78\text{ }^{\circ}\text{C}$ $^n\text{BuLi}$ (2.0 M in hexanes, 1.0 equiv, 10.0 mmol, 5 mL) was added dropwise and the reaction was stirred at this temperature for 30 min. To this mixture, was added $\text{BF}_3 \cdot \text{OEt}_2$ (1.0 equiv, 10.0 mmol, 1.3 mL), followed by rapid addition of **IV-78** (1.0 equiv, 10.0 mmol, 860 mg) in dry THF (10 mL) at $-78\text{ }^{\circ}\text{C}$. The reaction was stirred at this temperature for 5 h, before it was quenched by addition of saturated aqueous NH_4Cl (50 mL). Layers were separated and the aqueous layer was extracted with ethyl acetate (3 x 50 mL). The combined extracts were washed with brine (50 mL), dried over sodium sulfate and concentrated under reduced pressure. The crude

residue was purified via column chromatography (silica, ethyl acetate = 20 – 30%) to give pure epoxy alcohol **IV-80** as a clear oil (2.2 g, 60%).

^1H NMR (500 MHz, CDCl_3) δ 7.72 – 7.64 (m, 4H), 7.44 – 7.34 (m, 5H), 4.31 (t, J = 2.2 Hz, 2H), 3.56 (ddd, J = 10.5, 7.5, 4.4 Hz, 1H), 3.05 (td, J = 4.2, 2.7 Hz, 1H), 2.77 (dd, J = 4.9, 4.1 Hz, 1H), 2.71 (dd, J = 4.9, 2.7 Hz, 1H), 2.53 – 2.40 (m, 2H), 1.03 (s, 9H).

^{13}C NMR (125 MHz, CDCl_3) δ 135.59, 133.16, 129.83, 129.81, 129.79, 127.69, 127.68, 81.16, 80.50, 72.20, 70.88, 69.41, 64.69, 53.95, 52.80, 44.86, 26.68, 26.67, 25.07, 24.27, 19.15.

TOF MS ES^+ ($\text{C}_{23}\text{H}_{29}\text{O}_3\text{Si}$): Calc. $[\text{M} + \text{H}]^+$: 381.1886, Found $[\text{M} + \text{H}]^+$: 381.1875.



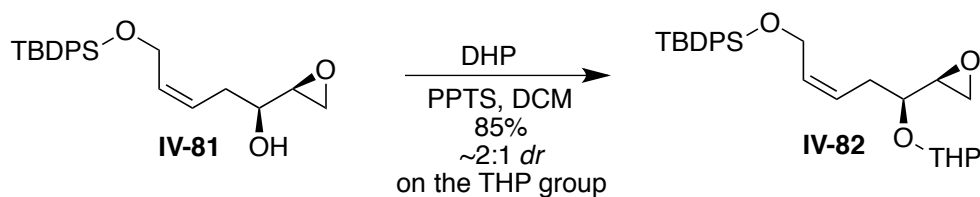
Synthesis of **IV-81**: To epoxy alcohol **IV-80** (900 mg, 2.4 mmol) in ethyl acetate (100 mL) was added Lindlar's catalyst (100 mg) at room temperature. The reaction flask was placed under vacuum and backfilled with hydrogen gas (balloon) three times. The reaction was stirred vigorously at room temperature for 30 min, upon which ^1H NMR showed complete consumption of starting material. The mixture was passed through a pad of celite to remove the insoluble material and the crude was used in the following step without further purification. A small sample of the crude was passed through a plug of silica to afford the pure alcohol **IV-81**.

^1H NMR (500 MHz, CDCl_3) δ 7.72 – 7.68 (m, 4H), 7.47 – 7.38 (m, 6H), 5.81 (dtt, J = 11.0, 6.3, 1.5 Hz, 1H), 5.55 (dtt, J = 10.9, 7.7, 1.6 Hz, 1H), 4.30 – 4.17 (m, 2H), 3.45 (qd, J =

6.3, 4.5 Hz, 1H), 2.93 (td, $J = 4.3, 2.7$ Hz, 1H), 2.75 (dd, $J = 5.0, 4.1$ Hz, 1H), 2.68 (dd, $J = 5.0, 2.7$ Hz, 1H), 2.30 – 2.23 (m, 2H), 1.98 (d, $J = 6.1$ Hz, 1H), 1.05 (s, 10H).

^{13}C NMR (125 MHz, CDCl_3) δ 135.59, 135.56, 133.56, 133.54, 132.30, 129.67, 129.55, 127.69, 127.68, 127.66, 127.65, 127.61, 125.66, 70.54, 59.97, 54.69, 44.79, 32.78, 26.77, 19.13.

TOF MS ES^+ ($\text{C}_{23}\text{H}_{31}\text{O}_3\text{Si}$): Calc. $[\text{M} + \text{H}]^+$: 383.2042, Found $[\text{M} + \text{H}]^+$: 383.2039.



Synthesis of THP protected epoxy alcohol IV-91: To alcohol **IV-81** (1.53 g, 4.0 mmol) in dry DCM (20 mL) at 0 °C were added 3,4-dihydro-2H-pyran (DHP, 1.1 equiv, 4.4 mmol, 0.41 mL) and PPTS (0.1 equiv, 0.4, 100 mg). The reaction was stirred for 12 h, allowing it to warm up to room temperature. Solvent was removed under reduced pressure and the crude product was purified using column chromatography (silica, ethyl acetate/hexanes = 5, to 10%) to give two diastereomers (1.6 g, 85% combined yield).

Data for the less polar diastereomer (F1):

^1H NMR (500 MHz, CDCl_3) δ 7.70 – 7.61 (m, 4H), 7.44 – 7.32 (m, 6H), 5.71 (dtt, $J = 11.1, 6.1, 1.6$ Hz, 1H), 5.50 (dtt, $J = 11.0, 7.5, 1.7$ Hz, 1H), 4.89 (dd, $J = 4.5, 2.8$ Hz, 1H), 4.29 – 4.23 (m, 2H), 3.78 (ddd, $J = 11.3, 8.4, 3.3$ Hz, 1H), 3.41 (dddd, $J = 10.8, 4.9, 3.9, 1.4$ Hz, 1H), 3.31 (q, $J = 6.8$ Hz, 1H), 2.84 (ddd, $J = 7.1, 4.2, 2.7$ Hz, 1H), 2.62 (dd, $J = 4.9,$

4.2 Hz, 1H), 2.37 (dd, $J = 4.8, 2.7$ Hz, 1H), 2.30 – 2.14 (m, 2H), 1.82 – 1.64 (m, 2H), 1.58 – 1.41 (m, 5H), 1.02 (s, 10H).

^{13}C NMR (125 MHz, CDCl_3) δ 135.54, 133.69, 133.68, 131.67, 129.60, 127.64, 125.53, 97.29, 76.45, 62.43, 60.29, 54.55, 43.54, 31.08, 30.72, 26.78, 26.76, 25.40, 19.40, 19.13.

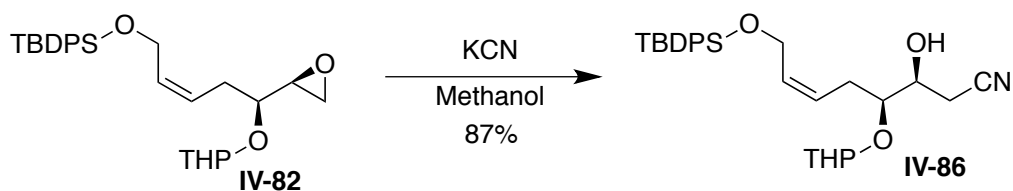
TOF MS ES^+ ($\text{C}_{28}\text{H}_{39}\text{O}_4\text{Si}$): Calc. $[\text{M} + \text{H}]^+$: 467.2618, Found $[\text{M} + \text{H}]^+$: 467.2611.

Data for the more polar diastereomer (F2):

^1H NMR (500 MHz, CDCl_3) δ 7.70 – 7.63 (m, 4H), 7.44 – 7.34 (m, 6H), 5.70 (dtt, $J = 12.3, 6.1, 1.6$ Hz, 1H), 5.44 (dtt, $J = 11.0, 7.6, 1.7$ Hz, 1H), 4.61 (dd, $J = 4.3, 2.9$ Hz, 1H), 4.24 (dd, $J = 6.3, 1.7$ Hz, 2H), 3.92 (ddd, $J = 11.5, 8.1, 3.4$ Hz, 1H), 3.48 – 3.42 (m, 1H), 3.35 (q, $J = 6.3$ Hz, 1H), 2.97 (ddd, $J = 6.2, 4.1, 2.7$ Hz, 1H), 2.68 (dd, $J = 5.0, 4.1$ Hz, 1H), 2.55 (dd, $J = 5.0, 2.7$ Hz, 1H), 2.19 – 2.11 (m, 2H), 1.77 (tdd, $J = 15.9, 8.4, 4.3$ Hz, 1H), 1.68 – 1.59 (m, 1H), 1.58 – 1.44 (m, 4H), 1.02 (s, 9H).

^{13}C NMR (125 MHz, CDCl_3) δ 135.60, 135.57, 135.55, 133.67, 131.90, 129.64, 127.67, 125.32, 97.39, 76.53, 62.37, 60.21, 54.00, 44.54, 30.64, 29.71, 26.79, 25.34, 19.46, 19.15.

TOF MS ES^+ ($\text{C}_{28}\text{H}_{39}\text{O}_4\text{Si}$): Calc. $[\text{M} + \text{H}]^+$: 467.2618, Found $[\text{M} + \text{H}]^+$: 467.2614.

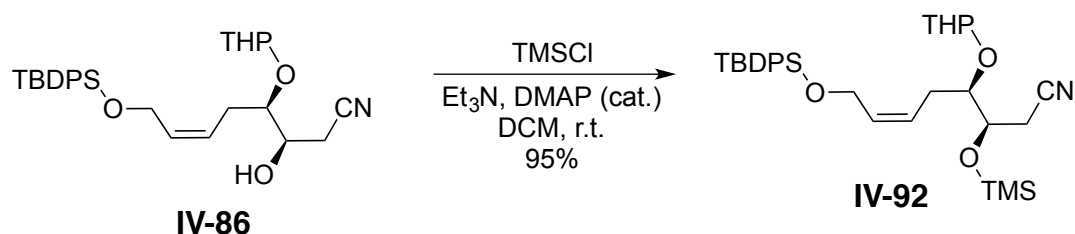


Synthesis of nitrile IV-95: To epoxide **IV-82** (200 mg, 0.4 mmol) in methanol (10 mL), potassium cyanide (10.0 equiv, 4.0 mmol, 260 mg) was added at room temperature. Stirring was continued for 48 h upon which TLC showed complete consumption of epoxide **IV-82**. Saturated ammonium chloride (20 mL) was added to the reaction mixture and the aqueous layer was extracted with ethyl acetate (3 x 20 mL). The combined organic extracts were washed with brine (50 mL), dried over sodium sulfate and concentrated under reduced pressure. The crude residue was purified via column chromatography (silica, ethyl acetate = 20 – 30%) to give nitrile **IV-86** as a clear oil (170 mg, 87%).

^1H NMR (500 MHz, CDCl_3) δ 7.69 – 7.64 (m, 4H), 7.45 – 7.35 (m, 6H), 5.83 – 5.64 (m, 1H), 5.43 (dt, J = 10.8, 7.6, 1.6 Hz, 1H), 4.38 (dd, J = 7.3, 2.5 Hz, 1H), 4.27 – 4.21 (m, 1H), 4.23 – 4.14 (m, 1H), 3.99 (d, J = 4.2 Hz, 1H), 3.92 (dtd, J = 11.5, 3.7, 1.4 Hz, 1H), 3.70 (tdd, J = 6.0, 4.9, 4.2 Hz, 1H), 3.54 (dt, J = 7.5, 5.5 Hz, 1H), 3.46 (dddd, J = 11.5, 8.3, 5.7, 3.1 Hz, 1H), 2.56 (dd, J = 16.8, 4.9 Hz, 1H), 2.40 (ddd, J = 16.7, 6.1, 0.8 Hz, 1H), 2.18 – 2.05 (m, 2H), 1.82 – 1.73 (m, 1H), 1.73 – 1.65 (m, 1H), 1.52 – 1.37 (m, 5H), 1.03 (s, 9H).

^{13}C NMR (125 MHz, CDCl_3) δ 135.59, 135.57, 135.55, 135.48, 133.51, 133.50, 132.17, 129.71, 127.73, 127.71, 127.70, 127.67, 127.62, 125.33, 117.48, 100.88, 80.76, 68.71, 65.35, 60.02, 31.11, 29.42, 26.78, 24.92, 22.45, 21.23, 19.13.

TOF MS ES^+ ($\text{C}_{29}\text{H}_{40}\text{NO}_4\text{Si}$): Calc. $[\text{M} + \text{H}]^+$: 494.2727, Found $[\text{M} + \text{H}]^+$: 494.2722.



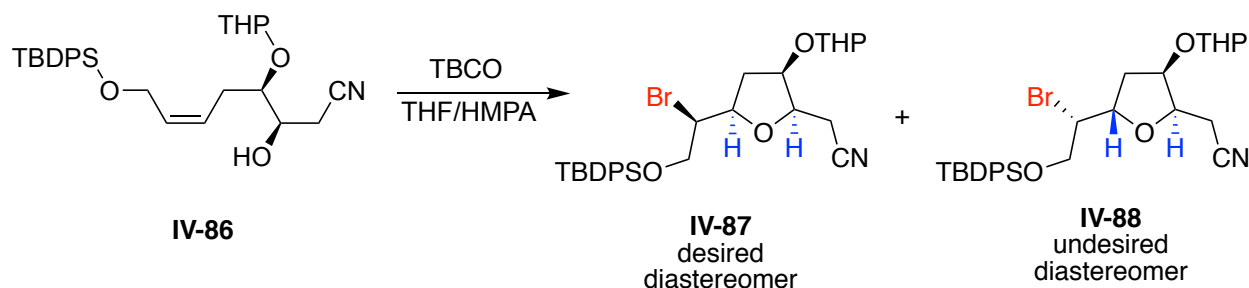
Synthesis of IV-101: Alcohol **IV-95** (7.5 mg, 0.015) was dissolved in dry DCM (1 mL), and to this solution at 0 °C were added triethyl amine (3.0 equiv, 0.045 mmol, 7 μ L), DMAP (1 mg) and trimethylsilyl chloride (3.0 equiv, 0.045 mmol, 6 μ L). After stirring at this temperature for 30 min, TLC showed completion of reaction. Solvent was removed under reduced pressure, and the crude product was passed through a plug of silica (basified with triethyl amine) Ethyl acetate in hexanes (5%) was used as eluent to provide the pure product in >95% yield (8 mg product was isolated). Note, TMS can fall off if the silica is not basified with triethyl amine.

^1H NMR (500 MHz, CDCl_3) δ 7.69 – 7.62 (m, 4H), 7.43 – 7.33 (m, 6H), 5.72 – 5.63 (m, 1H), 5.40 (dddd, J = 9.4, 7.7, 6.3, 3.7 Hz, 1H), 4.41 (dd, J = 5.9, 2.7 Hz, 1H), 4.24 – 4.19 (m, 2H), 4.13 – 4.08 (m, 1H), 3.80 (dt, J = 10.6, 4.8 Hz, 1H), 3.46 – 3.38 (m, 2H), 2.58 (dd, J = 16.6, 3.1 Hz, 1H), 2.27 (dd, J = 16.6, 9.3 Hz, 1H), 2.18 – 2.11 (m, 1H), 1.88 (dt, J = 15.7, 8.7 Hz, 1H), 1.78 – 1.68 (m, 1H), 1.60 (ddd, J = 12.7, 6.2, 2.9 Hz, 1H), 1.50 – 1.35 (m, 4H), 1.02 (s, 9H), 0.10 (s, 9H).

^{13}C NMR (125 MHz, CDCl_3) δ 135.57, 133.67, 131.71, 129.64, 129.63, 127.67, 127.65, 126.45, 119.06, 101.01, 79.61, 70.51, 63.83, 60.23, 30.83, 26.79, 26.69, 25.19, 21.13, 20.45, 19.15, 0.17, 0.08.

TOF MS ES⁺ (C₃₂H₄₈NO₄Si₂): Calc. [M + H]⁺: 566.3122, Found [M + H]⁺: 566.3119.

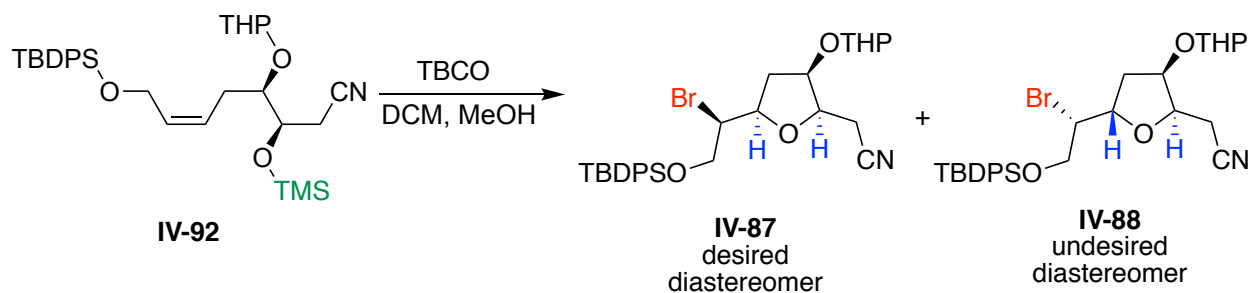
General procedure for the bromo-etherification of alcohol IV-95 (Table IV-3):



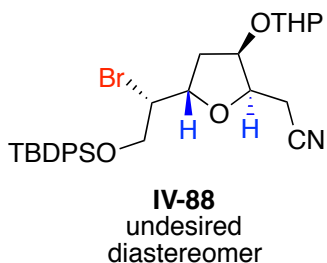
To alcohol **IV-95** (0.06 mmol, 30 mg) in THF (1 mL) and HMPA (40 μ L) was added TBCO (1.2 equiv, 0.07, 30 mg) at room temperature. The reaction was stirred at this temperature and monitored by TLC. After 30 min, TLC showed complete consumption of alcohol **IV-95**. Aqueous sodium thiosulfate (10%, 1 mL) was added to the reaction mixture and the aqueous layer was extracted with ethyl acetate (3 x 2 mL). The combined organic extracts were washed with brine (2 mL), dried over sodium sulfate and concentrated under reduced pressure. ¹H NMR analysis of the crude mixture showed ~1:1 ratio of diastereomers. The crude residue was purified via column chromatography (silica, ethyl acetate = 10 – 20%) to give both diastereomers (15 mg, 45% **IV-96** and 17 mg, 49% **IV-97** were isolated; 94% combined yield).

General procedure for the bromo-etherification of TMS-protected alcohol IV-101

(Table IV-4):



To TMS-protected alcohol **IV-101** (0.5 mmol, 280 mg) in anhydrous DCM (50 mL) were added methanol (10.0 equiv, 5.0 mmol, 0.2 mL) and TBCO (1.2 equiv, 0.6, 246 mg) at room temperature. The reaction was stirred at this temperature and monitored by TLC. After 1 h, TLC showed complete consumption of **IV-101**. The solvent was removed under reduced pressure and ^1H NMR analysis of the crude mixture showed >15:1 ratio of diastereomers. The crude residue was purified via column chromatography (silica, ethyl acetate = 10 – 20%) to give both diastereomers (240 mg, 85% **IV-96** and 10 mg, 4% **IV-97** were isolated; 89% combined yield).

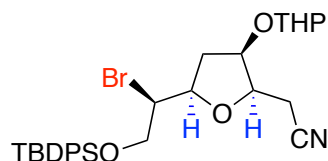


Data for the less polar diastereomer (undesired diastereomer IV-88):

^1H NMR (500 MHz, CDCl_3) δ 7.69 – 7.61 (m, 4H), 7.46 – 7.32 (m, 6H), 4.71 – 4.65 (m, 1H), 4.54 (ddd, J = 8.8, 6.5, 2.2 Hz, 1H), 4.49 (td, J = 4.7, 2.1 Hz, 1H), 4.35 (ddd, J = 6.9, 6.1, 4.2 Hz, 1H), 4.02 – 3.92 (m, 3H), 3.90 – 3.83 (m, 1H), 3.57 – 3.48 (m, 1H), 2.78 (dd, J = 16.5, 7.0 Hz, 1H), 2.70 – 2.61 (m, 1H), 2.18 (ddd, J = 13.5, 6.5, 2.1 Hz, 1H), 2.08 (ddd, J = 13.7, 9.0, 5.0 Hz, 1H), 1.81 (tdd, J = 9.2, 7.5, 6.3, 4.0 Hz, 1H), 1.77 – 1.68 (m, 1H), 1.55 (pd, J = 9.3, 7.5, 5.6 Hz, 4H), 1.04 (s, 9H).

^{13}C NMR (125 MHz, CDCl_3) δ 135.59, 135.53, 135.52, 133.09, 132.86, 129.85, 127.78, 127.77, 127.74, 96.00, 78.18, 76.24, 74.63, 65.36, 62.70, 58.10, 35.34, 30.64, 26.77, 25.23, 19.28, 18.67.

TOF MS ES^+ ($\text{C}_{29}\text{H}_{38}\text{BrNO}_4\text{SiNa}$): Calc. $[\text{M} + \text{Na}]^+$: 594.1651, Found $[\text{M} + \text{Na}]^+$: 594.1675.



IV-87
desired
diastereomer

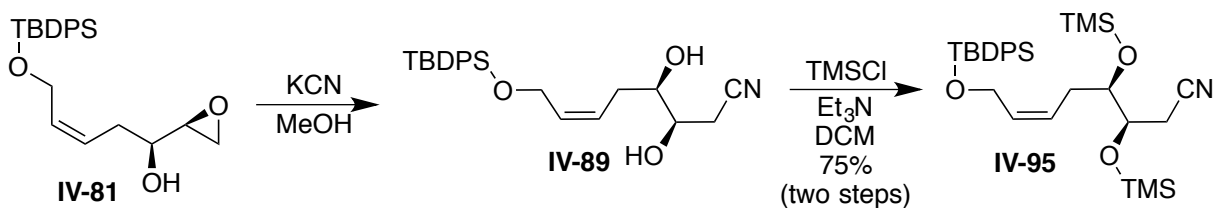
Data for the more polar diastereomer (desired diastereomer IV-87):

^1H NMR (500 MHz, CDCl_3) δ 7.69 – 7.62 (m, 4H), 7.47 – 7.33 (m, 6H), 4.56 (t, J = 3.7 Hz, 1H), 4.49 (q, J = 6.1 Hz, 1H), 4.26 (ddd, J = 8.5, 6.9, 4.6 Hz, 1H), 4.19 (q, J = 6.1 Hz, 1H), 4.05 (dt, J = 6.6, 5.1 Hz, 1H), 3.99 (dd, J = 10.9, 6.6 Hz, 1H), 3.88 (dd, J = 10.9, 5.4 Hz, 1H), 3.82 (ddd, J = 11.5, 7.9, 3.4 Hz, 1H), 3.49 (dt, J = 10.8, 4.7 Hz, 1H), 2.75 (dd, J = 16.7, 6.2 Hz, 1H), 2.63 (dd, J = 16.6, 6.4 Hz, 1H), 2.22 (dt, J = 13.3, 6.7 Hz, 1H), 1.97 (ddd, J = 13.6, 8.5, 5.7 Hz, 1H), 1.76 (td, J = 13.1, 11.1, 5.1 Hz, 1H), 1.64 (td, J = 9.1, 2.9 Hz, 1H), 1.59 – 1.43 (m, 4H), 1.04 (s, 9H).

^{13}C NMR (125 MHz, CDCl_3) δ 135.60, 135.59, 135.53, 135.52, 133.02, 132.79, 129.87, 127.79, 127.77, 96.70, 77.12, 76.56, 74.09, 65.28, 62.81, 56.40, 34.42, 30.44, 26.78, 25.21, 19.36, 19.28.

TOF MS ES^+ ($\text{C}_{29}\text{H}_{38}\text{BrNO}_4\text{SiNa}$): Calc. $[\text{M} + \text{Na}]^+$: 594.1651, Found $[\text{M} + \text{Na}]^+$: 594.1674.

Synthesis of di-TMS-protected diol **IV-95**:

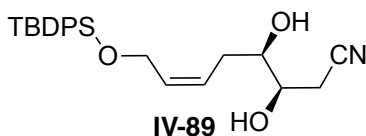


Epoxy alcohol **IV-81** (100 mg, 0.26 mmol) was reacted with potassium cyanide according to the procedure described above for the synthesis of **IV-86**. The crude alcohol was reacted with TMSCl (3.0 equiv, 0.78 mmol, 104 μL) and triethyl amine (3.0 equiv, 0.78 mmol, 121 μL) in the presence of DMAP (5 mg) in DCM (5 mL) at 0 °C. After completion of the reaction (20 min), the crude product was purified with column chromatography (silica basified with Et_3N , ethyl acetate/hexanes 5%). **IV-95** was purified as a clear oil (108 mg, 75% yield).

^1H NMR (500 MHz, CDCl_3) δ 7.77 – 7.60 (m, 4H), 7.48 – 7.34 (m, 6H), 5.72 (dtt, $J = 11.1$, 6.2, 1.5 Hz, 1H), 5.49 – 5.37 (m, 1H), 4.30 – 4.19 (m, 2H), 3.81 (ddd, $J = 8.8$, 4.4, 3.4 Hz, 1H), 3.52 (ddd, $J = 8.6$, 4.4, 3.5 Hz, 1H), 2.56 (dd, $J = 16.6$, 3.4 Hz, 1H), 2.28 – 2.20 (m, 1H), 2.20 – 2.10 (m, 1H), 1.90 – 1.77 (m, 1H), 1.05 (s, 10H), 0.13 (s, 9H), 0.07 (s, 9H).

^{13}C NMR (125 MHz, CDCl_3) δ 135.57, 135.56, 133.70, 133.69, 131.60, 129.62, 127.67, 127.66, 126.71, 118.91, 74.01, 71.60, 60.26, 28.73, 26.79, 20.71, 19.15, 0.29, 0.15.

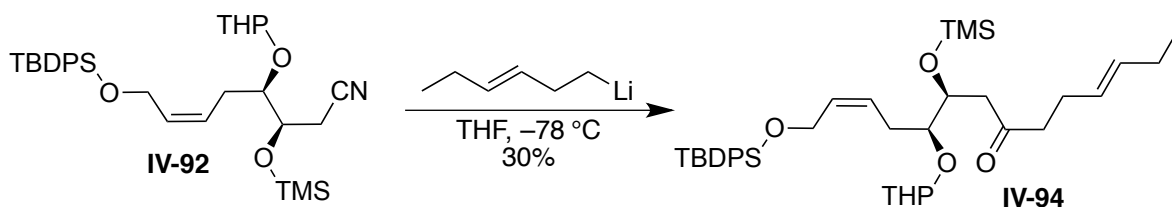
TOF MS ES^+ ($\text{C}_{30}\text{H}_{48}\text{NO}_3\text{Si}_3$): Calc. $[\text{M} + \text{H}]^+$: 554.2942, Found $[\text{M} + \text{H}]^+$: 554.2940.



This diol was purified from a reaction of epoxide **IV-81** and potassium cyanide as specified above. The crude diol was purified with column chromatography (silica, ethyl acetate/hexane = 30 – 40%) leading to pure diol **IV-89**.

^1H NMR (500 MHz, CDCl_3) δ 7.74 – 7.65 (m, 4H), 7.46 – 7.33 (m, 65H), 4.33 (t, J = 2.2 Hz, 2H), 3.81 (qd, J = 6.3, 2.7 Hz, 1H), 3.58 (qd, J = 6.1, 2.8 Hz, 1H), 2.61 – 2.48 (m, 2H), 2.48 – 2.36 (m, 2H), 2.14 (d, J = 6.2 Hz, 1H), 1.03 (s, 9H).

^{13}C NMR (125 MHz, CDCl_3) δ 135.61, 135.59, 133.17, 133.12, 129.90, 129.88, 127.75, 127.74, 117.27, 82.03, 80.42, 70.52, 68.75, 52.72, 26.64, 24.29, 22.79, 19.13.



Synthesis of ketone IV-94: To a flame dried flask containing diethyl ether (4.0 mL) under argon at $-100\text{ }^\circ\text{C}$ (liquid nitrogen in methanol bath) was added $t\text{BuLi}$ (1.7 M in pentane, 0.42 mL, 0.7 mmol, 7.0 equiv) dropwise. To this solution, alkyl iodide (63 mg, 0.3 mmol, 3.0 equiv) in diethyl ether (2.0 mL) was added dropwise at the same temperature. The reaction was stirred at this temperature for 30 min. To this solution at $-78\text{ }^\circ\text{C}$ was added a solution of the nitrile **IV-92** (56 mg, 0.1 mmol) in diethyl ether (2 mL), and the reaction was stirred at for 3 h. Saturated sodium bicarbonate (10 mL) was added to this solution at $-78\text{ }^\circ\text{C}$ to quench the reaction while allowing it to warm up to room temperature. The aqueous layer was extracted with ethyl acetate (3 x 5 mL), and the combined organic

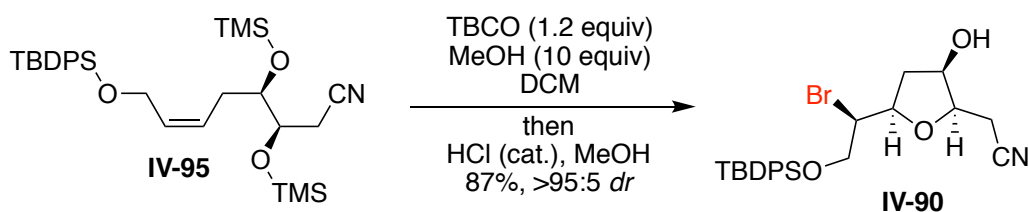
¹H NMR (500 MHz, CDCl₃) δ 7.72 – 7.60 (m, 4H), 7.44 – 7.32 (m, 6H), 5.73 – 5.62 (m, 1H), 5.56 (dt, J = 10.6, 7.2, 1.6 Hz, 1H), 5.44 (dt, J = 15.1, 6.1, 1.3 Hz, 1H), 5.30 – 5.38 (m, 1H), 4.63 – 4.59 (m, 1H), 4.28 (dd, J = 6.7, 5.2 Hz, 2H), 3.83 (ddd, J = 11.1, 8.2, 2.9 Hz, 1H), 3.55 (ddd, J = 8.4, 4.5, 3.4 Hz, 1H), 3.41 – 3.34 (m, 1H), 2.44 – 2.38 (m, 4H), 2.30 – 2.14 (m, 3H), 2.02 – 1.89 (m, 3H), 1.68 (dq, J = 8.5, 5.4, 4.9 Hz, 1H), 1.60 (td, J = 9.3, 3.1 Hz, 1H), 1.51 – 1.40 (m, 4H), 1.03 (s, 9H), 0.01 (s, 9H).

359

the reaction followed by addition of saturated potassium sodium tartrate solution (3.0 mL). The reaction was stirred vigorously at room temperature for 2 h. The aqueous layer was extracted with DCM (3 x 5 mL), and the combined organic extracts were washed with brine, dried over sodium sulfate and concentrated under reduced pressure. The crude aldehyde was purified via column chromatography (silica, ethyl acetate/hexanes 3%) yielding the pure aldehyde (40.0 mg, 71%) as a clear oil.

^1H NMR (500 MHz, CDCl_3) δ 9.70 (q, J = 2.2 Hz, 1H), 7.74 – 7.60 (m, 4H), 7.44 – 7.29 (m, 6H), 5.74 – 5.60 (m, 1H), 5.49 – 5.31 (m, 1H), 4.23 (d, J = 6.1 Hz, 2H), 4.09 (dtd, J = 8.5, 4.3, 2.0 Hz, 1H), 3.49 (dq, J = 5.7, 3.1, 2.4 Hz, 1H), 2.57 (ddt, J = 16.0, 4.4, 2.0 Hz, 1H), 2.36 (ddt, J = 16.1, 8.2, 2.4 Hz, 1H), 2.20 (t, J = 10.9 Hz, 1H), 1.85 (dt, J = 15.6, 8.2 Hz, 1H), 1.02 (s, 9H), 0.03 (s, 18H).

^{13}C NMR (125 MHz, CDCl_3) δ 201.49, 135.56, 133.78, 131.26, 129.57, 127.63, 127.33, 74.61, 70.17, 60.37, 45.78, 29.02, 26.80, 19.16, 0.30, 0.23.



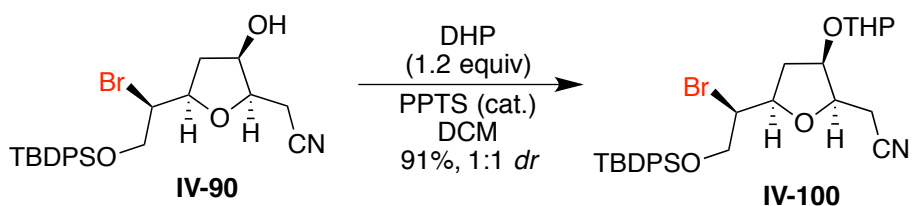
Synthesis of IV-99: To the nitrile **IV-95** (1.2 g, 2.1 mmol) in dry DCM (30 mL) were added TBCO (969 mg, 2.37 mmol, 1.1 equiv) and methanol (0.86 mL, 10.0 equiv) at room temperature. After stirring at this temperature for 2 h, TLC indicated completion of the reaction. The volatiles were removed under reduced pressure. The residue was dissolved

in methanol (50 mL). To this solution at room temperature was added HCl (conc. 2 drops, ~ 50 μ L). After 5 min, solvent was removed under reduced pressure and the crude was purified via column chromatography (silica, ethyl acetate/hexanes 20%) to yield the pure product **IV-90** (900 mg, 88%) as a clear oil.

^1H NMR (500 MHz, CDCl_3) δ 7.64 (tdd, $J = 7.8, 2.3, 1.1$ Hz, 4H), 7.46 – 7.33 (m, 6H), 4.35 (ddd, $J = 8.9, 5.9, 2.8$ Hz, 1H), 4.29 (td, $J = 7.6, 7.2, 3.3$ Hz, 1H), 4.11 – 4.04 (m, 1H), 4.03 – 3.95 (m, 2H), 3.92 (tdd, $J = 6.6, 3.5, 0.8$ Hz, 1H), 2.74 – 2.63 (m, 2H), 2.47 (ddd, $J = 15.0, 9.0, 6.5$ Hz, 1H), 2.36 (d, $J = 9.8$ Hz, 1H), 1.97 (ddd, $J = 14.5, 6.0, 1.8$ Hz, 1H), 1.05 (d, $J = 0.8$ Hz, 9H).

^{13}C NMR (125 MHz, CDCl_3) δ 135.60, 135.52, 132.89, 132.68, 129.96, 127.84, 117.57, 78.52, 76.05, 71.81, 65.04, 57.77, 38.72, 26.81, 19.29, 18.04.

TOF MS ES^+ ($\text{C}_{24}\text{H}_{31}\text{NO}_3\text{SiBr}$): Calc. $[\text{M} + \text{H}]^+$: 488.1257, Found $[\text{M} + \text{H}]^+$: 488.1247.



Synthesis of IV-109: To a solution of alcohol **IV-90** (100 mg, 0.2 mmol) in dry DCM (10 mL) at 0 °C were added 3,4-dihydro-2H-pyran (DHP, 1.1 equiv, 4.4 mmol, 21 μ L) and PPTS (5 mg). The reaction was stirred for 12 h while allowing it to warm up to room temperature. Solvent was removed under reduced pressure, and the crude product was purified via column chromatography (silica, ethyl acetate/ hexanes = 10%) to yield to the

inseparable diastereomeric mixture of **IV-100** (104 mg, 85% combined yield of two diastereomers).

The following NMR data are for both diastereomers:

^1H NMR (500 MHz, CDCl_3) δ 7.64 (tt, $J = 8.3, 1.6$ Hz, 8H), 7.49 – 7.33 (m, 12H), 4.65 (dd, $J = 4.3, 2.7$ Hz, 1H), 4.56 (t, $J = 3.6$ Hz, 1H), 4.49 (q, $J = 6.1$ Hz, 1H), 4.41 (q, $J = 6.5$ Hz, 1H), 4.29 – 4.16 (m, 4H), 4.05 (p, $J = 5.2$ Hz, 2H), 3.98 (ddd, $J = 11.0, 8.8, 6.5$ Hz, 2H), 3.90 (ddd, $J = 19.2, 10.9, 5.4$ Hz, 2H), 3.80 (dddd, $J = 19.3, 11.4, 7.9, 2.9$ Hz, 2H), 3.49 (dt, $J = 11.0, 5.5$ Hz, 2H), 2.75 (dd, $J = 16.6, 6.2$ Hz, 1H), 2.68 – 2.55 (m, 3H), 2.34 (dt, $J = 13.3, 6.7$ Hz, 1H), 2.22 (dt, $J = 13.3, 6.7$ Hz, 1H), 2.10 (ddd, $J = 13.2, 9.0, 6.5$ Hz, 1H), 1.97 (ddd, $J = 13.7, 8.5, 5.7$ Hz, 1H), 1.80 – 1.65 (m, 4H), 1.65 – 1.43 (m, 10H), 1.04 (s, 18H).

^{13}C NMR (125 MHz, CDCl_3) δ 135.62, 135.61, 135.54, 133.02, 132.83, 132.79, 129.88, 129.86, 127.79, 127.78, 127.75, 118.14, 117.69, 100.57, 96.69, 77.87, 77.12, 76.56, 75.97, 65.36, 65.28, 62.81, 56.68, 56.41, 36.66, 34.42, 30.44, 30.39, 26.78, 25.26, 25.21, 19.51, 19.37, 19.33, 19.29

REFERENCES

REFERENCES

1. Ashtekar, K. D.; Marzijarani, N. S.; Jaganathan, A.; Holmes, D.; Jackson, J. E.; Borhan, B., A New Tool To Guide Halofunctionalization Reactions: The Halenium Affinity (*HalA*) Scale. *Journal of the American Chemical Society* **2014**, *136* (38), 13355-13362.
2. Perron, F.; Albizati, K. F., Chemistry of spiroketals. *Chemical Reviews* **1989**, *89* (7), 1617-1661.
3. Aho, J. E.; Pihko, P. M.; Rissa, T. K., Nonanomeric spiroketals in natural products: Structures, sources, and synthetic strategies. *Chemical Reviews* **2005**, *105* (12), 4406-4440.
4. Wilsdorf, M.; Reissig, H. U., Simple, but Challenging: Recent Developments in the Asymmetric Synthesis of Spiroketals. *Angew Chem Int Edit* **2012**, *51* (38), 9486-9488.
5. Ireland, R. E.; Daub, J. P., Macrolide total synthesis. The synthesis of spiro ketal intermediates and their cleavage into open-chain derivatives. *The Journal of Organic Chemistry* **1983**, *48* (8), 1303-1312.
6. Ireland, R. E.; Thaisrivongs, S.; Dussault, P. H., An approach to the total synthesis of aplysiatxin. *Journal of the American Chemical Society* **1988**, *110* (17), 5768-5779.
7. Kocienski, P.; Yeates, C., A new synthesis of 1,7-dioxaspiro[5.5]undecanes. Application to a rectal gland secretion of the olive fruit fly (*Dacus oleae*). *Tetrahedron Letters* **1983**, *24* (36), 3905-3906.
8. Sun, Z. K.; Winschel, G. A.; Borovika, A.; Nagorny, P., Chiral Phosphoric Acid-Catalyzed Enantioselective and Diastereoselective Spiroketalizations. *Journal of the American Chemical Society* **2012**, *134* (19), 8074-8077.
9. Zhu, L.; Song, L.; Tong, R., Diastereoselective Reductive Ring Expansion of Spiroketal Dihydropyranones to cis-Fused Bicyclic Ethers. *Organic Letters* **2012**, *14* (23), 5892-5895.
10. Coric, I.; List, B., Asymmetric spiroacetalization catalysed by confined Brønsted acids. *Nature* **2012**, *483* (7389), 315-319.
11. Brucher, O.; Bergstrasser, U.; Kelm, H.; Hartung, J.; Greb, M.; Svoboda, I.; Fuess, H., Controlling 6-endo-selectivity in oxidation/bromocyclization cascades for

- synthesis of aplysiapyranoids and other 2,2,6,6-substituted tetrahydropyrans. *Tetrahedron* **2012**, *68* (34), 6968-6980.
12. de Greef, M.; Zard, S. Z., Unified, Radical-Based Approach for the Synthesis of Spiroketal. *Organic Letters* **2007**, *9* (9), 1773-1776.
 13. Kusumi, T.; Uchida, H.; Inouye, Y.; Ishitsuka, M.; Yamamoto, H.; Kakisawa, H., NOVEL CYTOTOXIC MONOTERPENES HAVING A HALOGENATED TETRAHYDROPYRAN FROM APLYSIA-KURODAI. *Journal of Organic Chemistry* **1987**, *52* (20), 4597-4600.
 14. Paterson, I.; Anderson, E. A.; Dalby, S. M.; Lim, J. H.; Maltas, P., The stereocontrolled total synthesis of spirastrellolide A methyl ester. Fragment coupling studies and completion of the synthesis. *Organic & Biomolecular Chemistry* **2012**, *10* (30), 5873-5886.
 15. Tanaka, K.; Harada, N., A novel spiroketalization reaction of 1,7-dihydroxyhepta-2,5-diyne-4-ones. *J. Chem. Soc.-Perkin Trans. 1* **2002**, (6), 713-714.
 16. Totah, N. I.; Schreiber, S. L., Thermodynamic Spiroketalization as an Efficient Method of Stereochemical Communication. *Journal of Organic Chemistry* **1991**, *56* (22), 6255-6256.
 17. Sun, Z.; Winschel, G. A.; Borovika, A.; Nagorny, P., Chiral Phosphoric Acid-Catalyzed Enantioselective and Diastereoselective Spiroketalizations. *Journal of the American Chemical Society* **2012**, *134* (19), 8074-8077.
 18. Khomutnyk, Y. Y.; Arguelles, A. J.; Winschel, G. A.; Sun, Z. K.; Zimmerman, P. M.; Nagorny, P., Studies of the Mechanism and Origins of Enantioselectivity for the Chiral Phosphoric Acid-Catalyzed Stereoselective Spiroketalization Reactions. *Journal of the American Chemical Society* **2016**, *138* (1), 444-456.
 19. Hamilton, J. Y.; Rossler, S. L.; Carreira, E. M., Enantio- and Diastereoselective Spiroketalization Catalyzed by Chiral Iridium Complex. *Journal of the American Chemical Society* **2017**, *139* (24), 8082-8085.
 20. Wang, B.-G.; Gloer, J. B.; Ji, N.-Y.; Zhao, J.-C., Halogenated Organic Molecules of Rhodomelaceae Origin: Chemistry and Biology. *Chemical Reviews* **2013**, *113* (5), 3632-3685.
 21. Zhou, Z.-F.; Menna, M.; Cai, Y.-S.; Guo, Y.-W., Polyacetylenes of Marine Origin: Chemistry and Bioactivity. *Chemical Reviews* **2015**, *115* (3), 1543-1596.
 22. Yousefi, R.; Whitehead, D. C.; Mueller, J. M.; Staples, R. J.; Borhan, B., On the Chlorenium Source in the Asymmetric Chlorolactonization Reaction. *Organic Letters* **2011**, *13* (4), 608-611.

23. Yousefi, R.; Ashtekar, K. D.; Whitehead, D. C.; Jackson, J. E.; Borhan, B., Dissecting the Stereocontrol Elements of a Catalytic Asymmetric Chlorolactonization: Syn Addition Obviates Bridging Chloronium. *Journal of the American Chemical Society* **2013**, *135* (39), 14524-14527.
24. Whitehead, D. C.; Yousefi, R.; Jaganathan, A.; Borhan, B., An Organocatalytic Asymmetric Chlorolactonization. *Journal of the American Chemical Society* **2010**, *132* (10), 3298-3300.
25. Jaganathan, A.; Garzan, A.; Whitehead, D. C.; Staples, R. J.; Borhan, B., A Catalytic Asymmetric Chlorocyclization of Unsaturated Amides. *Angew Chem Int Edit* **2011**, *50* (11), 2593-2596; *Angew. Chem.* **2011**, *123*, 2641-2644.
26. Zhelyaskov, V.; Broderick, M.; Raphaelovitz, A.; Davies, B., Automated piezoelectric nanopositioning systems - Long travel ranges and accurate angular movement create new opportunities in biomedical manipulation systems. *Ieee Circuits Device* **2006**, *22* (6), 75-78.
27. Ashtekar, K. D.; Vetticatt, M.; Yousefi, R.; Jackson, J. E.; Borhan, B., Nucleophile-Assisted Alkene Activation: Olefins Alone Are Often Incompetent. *Journal of the American Chemical Society* **2016**, *138* (26), 8114-8119.
28. Crimmins, M. T.; Choy, A. L., Asymmetric aldol-ring-closing metathesis strategy for the enantioselective construction of six- to nine-membered oxygen heterocycles. *Journal of Organic Chemistry* **1997**, *62* (22), 7548-7549.
29. Crimmins, M. T.; Emmitte, K. A., Asymmetric total synthesis of (-)-isolaurallene. *Journal of the American Chemical Society* **2001**, *123* (7), 1533-1534.
30. Izuchi, Y.; Koshino, H.; Hongo, Y.; Kanomata, N.; Takahashi, S., Synthesis and Structural Revision of Phomopsin B, a Novel Polyketide Carrying a 10-Membered Cyclic-Ether Ring. *Organic Letters* **2011**, *13* (13), 3360-3363.
31. Ko, C.; Hsung, R. P.; Al-Rashid, Z. F.; Feltenberger, J. B.; Lu, T.; Yang, J.-H.; Wei, Y.; Zifcsak, C. A., A Stereoselective Intramolecular Halo-Etherification of Chiral Enamides in the Synthesis of Halogenated Cyclic Ethers. *Organic Letters* **2007**, *9* (22), 4459-4462.
32. Norte, M.; Fernandez, J. J.; Ruano, J. Z., 3 NEW BROMO ETHERS FROM THE RED ALGA LAURENCIA-OBTUSA. *Tetrahedron* **1989**, *45* (18), 5987-5994.
33. Howard, B. M.; Fenical, W.; Arnold, E. V.; Clardy, J., OBTUSIN, A UNIQUE BROMINE-CONTAINING POLYCYCLIC KETAL FROM THE RED MARINE ALGA LAURENCIA-OBTUSA. *Tetrahedron Letters* **1979**, (31), 2841-2844.

34. Gonzalez, A. G.; Martin, J. D.; Norte, M.; Perez, R.; Rivera, P.; Ruano, J. Z.; Rodriguez, M. L.; Fayos, J.; Perales, A., X-RAY STRUCTURE DETERMINATION OF NEW BROMINATED METABOLITES ISOLATED FROM THE RED SEAWEED LAURENCIA-OBTUSA. *Tetrahedron Letters* **1983**, 24 (38), 4143-4146.
35. Scheuer, P. J., *Marine Natural Products: Chemical and Biological Perspectives*. Elsevier: 2012.
36. Eugene A. Mash, K. A. N., Shawne Van Deusen, and Susan B. Hemperly, 1,4-DI-O-ALKYL THREITOLS FROM TARTARIC ACID: 1,4-DI-O-BENZYL-L-THREITOL. *Org. Synth.* **1990**, 68, 92.
37. Michael A. Robbins, P. N. D., and Taeboem Oh, *SYNTHESIS OF CHIRAL NON-RACEMIC DIOLS FROM (S,S)-1,2,3,4-DIEPOXYBUTANE: (2S,3S)-DIHYDROXY 1,4-DIPHENYLBUTANE* **1999**, 76, 101.
38. Trost, B. M.; Ashfeld, B. L., Coupling of alkenes and alkynes: Synthesis of the C1-C11 and C18-C28 fragments of miyakolide. *Organic Letters* **2008**, 10 (10), 1893-1896.
39. Behrens, C. H.; Ko, S. Y.; Sharpless, K. B.; Walker, F. J., Selective Transformation of 2,3-Epoxy Alcohols and Related Derivatives - Strategies for Nucleophilic-Attack at Carbon-1. *Journal of Organic Chemistry* **1985**, 50 (26), 5687-5696.
40. Braddock, D. C.; Bhuva, R.; Millan, D. S.; Perez-Fuertes, Y.; Roberts, C. A.; Sheppard, R. N.; Solanki, S.; Stokes, E. S. E.; White, A. J. P., A biosynthetically-inspired synthesis of the tetrahydrofuran core of obtusallenes II and IV. *Organic Letters* **2007**, 9 (3), 445-448.
41. Martin, T.; Soler, M. A.; Betancort, J. M.; Martin, V. S., Biomimetic-type synthesis of halogenated tetrahydrofurans from Laurencia. Total synthesis of trans-(+)-deacetylkumausyne. *Journal of Organic Chemistry* **1997**, 62 (6), 1570-1571.
42. Crich, D.; Dudkin, V., Confirmation of the connectivity of 4,8,12,16,20-pentamethylpentacosylphosphoryl beta-D-mannopyranoside, an unusual,beta-mannosyl phosphoisoprenoid from Mycobacterium avium, through synthesis. *Journal of the American Chemical Society* **2002**, 124 (10), 2263-2266.
43. Zeng, X.; Miao, C.; Wang, S.; Xia, C.; Sun, W., Asymmetric 5-endo chloroetherification of homoallylic alcohols toward the synthesis of chiral [small beta]-chlorotetrahydrofurans. *Chemical Communications* **2013**, 49 (24), 2418-2420.
44. Bouziane, A.; Hérou, M.; Carboni, B.; Carreaux, F.; Demerseman, B.; Bruneau, C.; Renaud, J.-L., Ruthenium-Catalyzed Synthesis of Allylic Alcohols: Boronic Acid as a Hydroxide Source. *Chemistry – A European Journal* **2008**, 14 (18), 5630-5637.